Multidrug resistance afforded by the MtrD efflux transporter protein from *Neisseria gonorrhoeae*

By

Mohsen Chitsaz

Thesis
Submitted to Flinders University
for the Degree of Doctor of Philosophy

Molecular Microbiology

College of Science and Engineering
06/09/2024

TABLE OF CONTENTS

TABLE OF CONTENTS ..... **I**
LIST OF FIGURES ..... **VIII**
LIST OF TABLES ..... **XI**
ABSTRACT ..... **XIII**
DECLARATION ..... **XV**
ACKNOWLEDGEMENTS ..... **XVI**
CONTRIBUTIONS ..... **XVII**
PUBLICATIONS ..... **XVIII**
CHAPTER 1 GENERAL INTRODUCTION **1**

1.1 Overview of *Neisseria gonorrhoeae* 3
1.1.1 Gonorrhoea: a sexually transmitted infection 3
1.1.2 *N. gonorrhoeae*: classification 5
1.1.3 Growth, metabolism, and pathogenesis 5
1.1.4 Antimicrobial resistance 7
1.1.4.1 Mechanisms of antimicrobial resistance 8
1.1.4.1.1 Beta-lactam resistance 8
1.1.4.1.2 Macrolide resistance 9
1.1.4.1.3 Quinolone resistance 9
1.1.4.1.4 Sulfonamide resistance 10
1.1.4.1.5 Tetracycline resistance 10
1.1.4.1.6 Spectinomycin and gentamicin resistance 11
1.1.4.1.7 Decreased influx and increased efflux 11
1.2 Permeability barrier of Gram-negative bacteria 12
1.3 Efflux proteins 14
1.3.1 The ABC superfamily 18
1.3.1.1 The *N. gonorrhoeae* MacAB export proteins 20
1.3.2 The MFS 23
1.3.2.1 The *E. coli* MdfA protein 26
1.3.2.2 The *N. gonorrhoeae* MFS FarAB-MtrE system 30
1.3.3 The MATE family 31
1.3.3.1 The *V. cholerae* NorM protein 34
1.3.3.2 The *N. gonorrhoeae* NorM protein 36

1.3.4 The SMR family 38
1.3.5 The PACE and AbgT families 46
1.3.5.1 The MtrF protein 48
1.3.6 The RND superfamily 48
1.3.6.1 The membrane fusion protein family 49
1.3.6.1.1 The AcrA protein 50
1.3.6.2 The outer membrane factor family 52
1.3.6.2.1 The TolC protein 53
1.3.6.3 The RND transporters 55
1.3.6.4 The *E. coli* AcrAB-TolC efflux system 58
1.3.6.4.1 The *E. coli* AcrB protein 58
1.3.6.4.2 The *E. coli* AcrZ protein 86
1.3.6.4.3 Exploring the structural and functional mechanism of the complete tripartite RND systems 88
1.3.6.4.4 Expression of *acrAB* and *tolC* 89
1.3.6.4.5 Inhibition of the AcrAB-TolC pump 90
1.4 The *N. gonorrhoeae* multiple transferable resistance (*mtr*) system 93
1.4.1 Genetic organisation of the *mtr* locus 97
1.4.2 Regulation of the *mtr* efflux system 99
1.4.3 The MtrR protein 102
1.4.4 The MtrC protein 105
1.4.5 The MtrE protein 106
1.4.6 The MtrD protein 107
1.4.6.1 Crystal structures of the MtrD protein 107
1.4.6.2 Proton translocation and efflux energisation 109
1.4.6.3 Drug binding sites of the MtrD protein 110
1.4.6.4 N917-P927 loop region 111
1.5 Scope of this thesis 112

CHAPTER 2 MULTIDRUG RESISTANCE IN *NEISSERIA GONORRHOEAE*: IDENTIFICATION OF FUNCTIONALLY IMPORTANT RESIDUES IN THE MTRD EFFLUX PROTEIN AND ELUCIDATION OF ITS FUNCTIONALLY ROTATING MECHANISM 115

2.1 Preface 117
2.2 Abstract 117
2.3 Importance 118
2.4 Introduction 118
2.5 Results 121
2.5.1 A highly discriminating *N. gonorrhoeae* strain for *in situ* analysis of MtrD activity 121
2.5.2 Function can be restored in the *N. gonorrhoeae* KH15Δ*mtrD*Δ*norM* derivative by reinsertion of *mtrD* 126
2.5.3 Spontaneous uptake of progesterone identified from MD simulations 128
2.5.4 Docking of substrates to MtrD 128
2.5.5 Site-directed mutagenesis identified six residues involved in MtrD-mediated resistance 137
2.6 Discussion 141
2.7 Materials and Methods 144
2.7.1 Bacterial strains, plasmids, and growth conditions 144
2.7.2 Molecular biology methods 146
2.7.3 Construction of unmarked *mtrD* and *norM* single and *mtrD*/*norM* double deletion strains 147
2.7.4 Cloning of *mtrD* into pGCC4 and recombination into the neisserial chromosome 149
2.7.5 Site-directed mutagenesis 150
2.7.6 Western blotting 150
2.7.7 MIC analyses 151
2.7.8 Molecular dynamics simulations 151
2.7.9 Docking studies 152

CHAPTER 3 COORDINATION OF SUBSTRATE BINDING AND PROTONATION IN THE *NEISSERIA GONORRHOEAE* MTRD EFFLUX PUMP CONTROLS THE FUNCTIONALLY ROTATING TRANSPORT MECHANISM 154

3.1 Preface 156
3.2 Abstract 156
3.3 Introduction 157
3.4 Results and Discussion 159
3.4.1 Characterisation of the MtrD proton relay network 159
3.4.2 Comparison of the MtrD symmetric and asymmetric structures 162
3.4.3 Protonation of a single MtrD monomer activates extrusion gate opening 169
3.4.4 Conformational switching to asymmetric MtrD requires coordinated protonation and substrate binding in two separate monomers 172
3.4.5 Relay network protonation drives the TM helix rotation in MtrD 177
3.5 Conclusions 181
3.6 Materials and Methods 183
3.6.1 System details: simulation-set-up 183
3.6.2 Coarse grained simulations 184
3.6.3 Back-mapping and atomistic simulations 184
3.6.4 Construction and functional analysis of an MtrD site-directed mutant 186
3.6.5 Data analysis 187
3.6.5.1 Visual analysis and graphical rendering of protein structures 187
3.6.5.2 Validation of pre- and post-simulation protein structures 187
3.6.5.3 Distance and density calculations 187

CHAPTER 4 A UNIQUE SEQUENCE IS ESSENTIAL FOR EFFICIENT MULTIDRUG EFFLUX FUNCTION OF THE MTRD PROTEIN OF *NEISSERIA GONORRHOEAE* 189

4.1 Preface 192
4.2 Abstract 192
4.3 Importance 192
4.4 Introduction 193
4.5 Results 196

4.5.1 Removal of N917-P927 significantly reduced MtrD-mediated resistance. 196
4.5.2 Integrity of the N917-P927 sequence is required for efficient efflux activity of the MtrD protein 202
4.5.3 Four residues in the N917-P927 region play an important role in MtrD activity 206
4.5.4 Structural analysis and dynamics of the N917-P927 region 209
4.5.5 Deletion of the N917-P927 region alters progesterone uptake 215
4.6 Discussion 216
4.7 Materials and Methods 219
4.7.1 Bacterial strains, plasmids and growth conditions 219
4.7.2 Molecular biology methods 222
4.7.3 Site-directed mutagenesis 222
4.7.4 Western blot analyses 222
4.7.5 Minimum inhibitory concentration analyses 223
4.7.6 MD simulations 223

CHAPTER 5 ESTABLISHMENT OF AN *ESCHERICHIA COLI*-BASED HOST-VECTOR SYSTEMS FOR OVEREXPRESSION, PURIFICATION AND FUNCTIONAL ANALYSIS OF THE *NEISSERIA GONORRHOEAE* MTRD PROTEIN 225

5.1 Introduction 226
5.2 Material and Methods 228
5.2.1 Buffers and solutions 228
5.2.2 Culture media 228
5.2.3 Plasmids, bacterial strains and growth conditions 228
5.2.4 Bacterial antimicrobial sensitivity assays 230
5.2.4.1 Disc diffusion method 230
5.2.4.2 Micro-broth dilution 231
5.2.5 Molecular biology methods 237
5.2.5.1 Plasmid DNA extraction 237
5.2.5.2 Chromosomal DNA extraction 237
5.2.5.3 Polymerase chain reaction 237
5.2.5.4 DNA agarose gel electrophoresis 237
5.2.5.5 Purification of DNA samples 238

5.2.5.6 Assessment of quantity and quality of DNA samples 238
5.2.5.7 DNA sequencing 238
5.2.5.8 Restriction digestion cloning 238
5.2.5.9 Making calcium competent *E. coli* cells 239
5.2.5.10 Transformation of chemically competent *E. coli* cells 239
5.2.5.11 Electrocompetent *E. coli* cells 240
5.2.5.12 Transformation of electrocompetent *E. coli* cells 240
5.2.6 Protein methods 241
5.2.6.1 Preparation of *E. coli* membrane fractions and whole-cell lysates 241
5.2.6.2 Protein quantification 242
5.2.6.3 SDS PAGE gel electrophoresis 242
5.2.6.4 Coomassie blue staining 242
5.2.6.5 Protein transfer to PVDF membranes 243
5.2.6.6 Immunostaining 243
5.2.6.7 Batch style protein purification 243
5.3 Results 244
5.3.1 Deletion of the *acrAB* region from *E. coli* BL21(DE3) and DH5α strains 244
5.3.2 Cloning of the *mtrD* gene into the pBluescript SK (+) vector 249
5.3.2.1 Construction of an *mtrD* clone in pBluescript II 249
5.3.2.2 Expression of the recombinant MtrD protein from pBluescript-*mtrD*$_{His6}$ 250
5.3.2.3 Antibiotic resistance capacity of *E. coli* strains expressing the MtrD protein in pBluescript-*mtrD*$_{His6}$ 250
5.3.3 Cloning of the entire *mtrCDE* operon into pBluescript and expression in various *E. coli* host strains 254
5.3.3.1 Construction of the recombinant *mtrCDE* operon in pBluescript II vector 254
5.3.3.2 Expression of recombinant MtrCDE from the pBluescript-*mtrCDE*$_{His6}$ plasmid 255
5.3.3.3 Antibiotic resistance capacity of *E. coli* strains expressing MtrCDE efflux proteins from the pBluescript-*mtrCDE*$_{His6}$ plasmid 258
5.3.4 Cloning of *mtrD* into the pGCC4 shuttle vector and expression in *E. coli* 259

5.3.4.1 Construction of the pGCC4-*mtrD*$_{His6}$ plasmid 260
5.3.4.2 Expression of MtrD from pGCC4-*mtrD*$_{His6}$ 260
5.3.4.3 Antibiotic resistance capacity of *E. coli* BW25113(DE3) Δ*acrB* carrying the pGCC4-*mtrD*$_{His6}$ plasmid 261
5.3.5 Cloning of the *mtrD* gene into the pET21a vector 262
5.3.5.1 Construction of an *mtrD* clone in pET21a expression vector 262
5.3.5.2 Expression of MtrD protein from the pET21a-*mtrD*$_{His6}$ plasmid 263
5.3.6 Purification of recombinant MtrD protein 263
5.3.7 Cloning of the *mtrC*, *mtrD* and *mtrE* genes into pETDuet1 vector individually and in combinations 268
5.3.7.1 Construction of the pETDuet-*mtrC* clone 268
5.3.7.2 Construction of the pETDuet-*mtrCE* plasmid 269
5.3.7.3 Construction of the pETDuet-*mtrCE-mtrD* plasmid 270
5.3.7.4 *E. coli* strains carrying the pETDuet-*mtrCE-mtrD* plasmid give resistance to MtrD substrates. 273
5.3.8 Construction of a bank of truncated *mtrD* clones to facilitate *mtrD* site-directed mutagenesis 277
5.4 Discussion 279

CHAPTER 6 DISCUSSION AND CONCLUSION 284

6.1 Using the MtrD protein of *Neisseria gonorrhoeae* as a strategy to address AMR 285
6.2 Construction of a panel of isogenic *N. gonorrhoeae* derivatives for screening MtrD substrates and inhibitors 287
6.3 Identification of functionally important residues in the MtrD efflux protein 290
6.4 Coordination of substrate binding and protonation 292
6.5 Significance and impact of the N917-P927 region in MtrD 293
6.6 Optimising overexpression of MtrD and MtrCDE in *E. coli* 297
6.7 Purification of MtrD protein 300
6.8 Summary 300

CHAPTER 7 APPENDICES 302

7.1 Appendix A: Abbreviations 303
7.2 Appendix B: Paper 1: The role played by drug efflux pumps in bacterial multidrug resistance. 307

7.3 Appendix C: Paper 2: Multidrug resistance in *Neisseria gonorrhoeae*: identification of functionally important residues in the MtrD efflux protein....321
7.4 Appendix D: Paper 3: Coordination of substrate binding and protonation in the *Neisseria gonorrhoeae* MtrD efflux pump controls the functionally rotating transport mechanism. 336
7.5 Appendix E: Paper 4: A unique sequence is essential for efficient multidrug efflux function of the MtrD protein of *Neisseria gonorrhoeae*....352

REFERENCES 369

LIST OF FIGURES

Figure 1.1 Schematic illustration of the seven families/superfamilies of multidrug transport proteins. 16
Figure 1.2: NorM-NG structure overview. 38
Figure 1.3: Structural representation of MexA periplasmic adaptor protein. 51
Figure 1.4: Structure representation of TolC and its periplasmic entrance. 54
Figure 1.5: AcrB structural characteristics and secondary elements. 60
Figure 1.6: The depiction of the AcrB transporter's structure highlights crucial structural attributes and key residues. 64
Figure 1.7: The depiction of the *N. gonorrhoeae* MtrD efflux pump illustrates its structural arrangement. 108
Figure 2.1: An example Western blot showing expression levels of the recombinant WT MtrD and seven MtrD mutants. 127
Figure 2.2: Progesterone binding in monomer B of the MtrD trimer shown as a (A) side view and (B) top view. 130
Figure 2.3: Interactions of progesterone with MtrD. 131
Figure 2.4: MtrD docked to crystal violet and ET. 133
Figure 2.5: MtrD docked to nonoxynol-9 and cholic acid. 134
Figure 2.6: MtrD docked to rifampin. 135
Figure 2.7: MtrD docked to PAβN. 136
Figure 2.8: Protein sequence alignment of MtrD, AcrB and MexB. The sequence alignment is shown up to MtrD residue 715. 138
Figure 3.1: Asymmetric structure of MtrD and proposed transport cycle. 158
Figure 3.2: Protein expression of D405C MtrD mutant. 161
Figure 3.3: MtrD structural overview. 163
Figure 3.4: Coarse-grain simulations RMSD analysis. 166
Figure 3.5: The apo MtrD homotrimer (System 1) simulation across 3 × 250 ns simulations. 168
Figure 3.6: The distance distributions of functionally relevant residue pairs in different MtrD binding configurations from (A) System 2 and (B) System 3. 171
Figure 3.7: TMD rotation in deprotonated monomers. 172

Figure 3.8: The distance distributions of functionally relevant residue pairs in the MtrD binding configurations from (A) System 4 and (B) System 5. 174
Figure 3.9: Time-correlation of proton relay network, extrusion gate and binding cleft distances. 175
Figure 3.10: The extrusion gate distance of each MtrD monomer is an output of conformation....176
Figure 3.11: Protonation of a single monomer in MtrD causes rotation of TM domains....179
Figure 3.12: Rotation of TM domain helices does not occur in apo-MtrD simulations....180
Figure 4.1: Protein sequences of selected members of RND proteins of the HAE1 family. 196
Figure 4.2: Secondary structure of the MtrD protein. 197
Figure 4.3: Western blot image showing expression of constructed MtrD mutants.203
Figure 4.4: Secondary structure of the MtrD protein in complex with Amp (PDB ID 6VKS). 208
Figure 4.5: MD simulations showing the position of MtrD within the membrane. .210
Figure 4.6: Representative MD simulation snapshot of the position and orientation of the TMS 9 and N917-P927 region in relation to the *N. gonorrhoeae* membrane surface. 211
Figure 4.7: MD simulation analysis of interactions between the N917-P927 region and the MtrD periplasmic domain....212
Figure 4.8: Representative snapshot of the position and orientation of the TMS 9 and N917-P92 regions from MD simulations in relation to the *N. gonorrhoeae* membrane surface. 214
Figure 4.9: MD simulations of PRO flooding of the Δ(N917-P927) mutant of MtrD. 216
Figure 5.1: Map of the pBluescript-*mtrD*$_{His6}$ construct. 251
Figure 5.2: WB analysis demonstrating expression of MtrD in *E. coli* strains. 252
Figure 5.3: WB analysis demonstrating expression of MtrD or MtrE in *E. coli* strains. 253
Figure 5.4: Map of the pBluescript-*mtrCDE*$_{His6}$ construct. 259
Figure 5.5: WB analysis demonstrating the expression of the MtrE protein in *E. coli* DH5α. 261
Figure 5.6: The expression of MtrD protein in different *E. coli* strains. 264

Figure 5.7: Purification of the MtrD protein from membrane fractions of *E. coli* BL21(DE3)/pET21a-*mtrD*His6 cells expressing MtrD.....266
Figure 5.8: SDS-PAGE analysis of MtrD protein purification. 267
Figure 5.9: The map of pETDuet-*mtrC1* plasmid. 269
Figure 5.10: Map of pETDuet-*mtrCE* plasmid generated using SnapGene program.....271
Figure 5.11: Map of the pETDuet-*mtrCE-mtrD* plasmid generated using the SnapGene program. 272
Figure 5.12: The expression of MtrC protein in *E. coli* BL21(DE3) Δ*acrAB* carrying pETDuet-*mtrC* plasmid. 274

LIST OF TABLES

Table 2.1: Antimicrobial resistance profiles of *N. gonorrhoeae* strains for 11 compounds.[a] 123
Table 2.2: Antimicrobial resistance profiles of *N. gonorrhoeae* strains for an additional 11 compounds[a] 124
Table 2.3: Antimicrobial resistance profiles of *N. gonorrhoeae* strains for 11 more compounds[a] 125
Table 2.4: Residues belonging to binding pockets of MtrD and AcrB. 132
Table 2.5: *N. gonorrhoeae* KH15Δ*mtrD*Δ*norM* strain expressing MtrD derivatives..... 140
Table 2.6: Bacterial strains and plasmids used in this study. 145
Table 2.7: Oligonucleotides used in this study..... 148
Table 2.8: Docking parameters used. 153
Table 3.1 *Neisseria gonorrhoeae* KH15Δ*mtrD*Δ*norM* strain expressing MtrD derivatives..... 160
Table 3.2 MtrD trimer structures and their global/local conformational characteristics. 164
Table 3.3: RND transport residue pairs used to determine conformation states of MtrD during MD simulations of this publication. 165
Table 3.4 List of MtrD trimeric binding configurations and numbering of simulations..... 167
Table 3.5 Inter-monomeric distances (PN2-PC2) for RND asymmetric transporter structures and MtrD MD simulations. 178
Table 4.1: Oligonucleotides used in this study..... 199
Table 4.2: Antimicrobial resistance of *N. gonorrhoeae* strain KH15Δ*mtrD*Δ*norM* expressing MtrD derivatives..... 204
Table 4.3: Bacterial strains and plasmids used in this study. 220
Table 5.1: Buffers and solutions used in this study..... 229
Table 5.2: Plasmids used in this study 231
Table 5.3 Bacterial strains used in this study. 234
Table 5.4: Oligonucleotides used in this study..... 246
Table 5.5: Antibiotic susceptibility of *E. coli* strains with the *acrAB* region removed. 248

Table 5.6: Antibiotic susceptibility of *E. coli* strains expressing MtrD alone or the whole MtrCDE efflux system from various constructs. 256
Table 5.7: Antibiotic susceptibility of *E. coli* strains expressing pETDuet-*mtrCE-mtrD* plasmid. 275

ABSTRACT

The rise of antimicrobial resistance poses a significant threat to global public health, demanding urgent action. *Neisseria gonorrhoeae*, a sexually transmitted bacterium, has developed resistance to multiple compounds resulting in multidrug and extensively drug-resistant strains. The MtrD protein in *N. gonorrhoeae*, a member of the RND transporter family, plays a crucial role in this characteristic. This PhD thesis focuses on characterising the MtrD protein to gain insights into the corresponding mechanism and identify potential drug targets.

The study began by developing a mutagenesis system specific to *N. gonorrhoeae* for analysing MtrD activity. A panel of *N. gonorrhoeae* strains was constructed to screen MtrD substrates and compounds that can potentially inhibit the systems. Using this panel, several new MtrD substrates were identified. A recombinant wild-type MtrD clone, and a cysteine-less MtrD variant were also created, enabling site-directed mutagenesis and resistance profiling to be performed.

To understand the substrate pathway and binding sites of MtrD, molecular dynamics simulations and molecular docking studies were conducted. These investigations provide insights into the interactions between MtrD and its substrates, identifying key residues involved in drug binding. Notably, conserved phenylalanine residues were found to play a critical role in substrate binding, similar to their counterparts in other RND efflux pumps. Functional roles of these residues were explored and confirmed through the site-directed mutagenesis developed in this study shedding light on the structure-function relationship of MtrD.

Through additional molecular dynamics simulation studies, we illustrated that protonation within the transmembrane domain induces a transition from a symmetric to an asymmetric configuration of the trimer, thereby activating allosteric couplings that regulate MtrD efflux. Our findings demonstrate that MtrD employs a functional rotation mechanism similar to that described in AcrB.

One of the unique structural characteristics of the MtrD protein, the N917-P927 region, was investigated. We demonstrated that this region is crucial for MtrD activity and may have implications for drug design and resistance mechanisms.

Studying the function of the MtrD protein is challenging due to the fastidious nature of the bacterium. To overcome these limitations, an optimised system for overexpressing MtrD by itself or in combination with the other proteins in the *mtr* operon, the MtrCDE, was developed for expressing in *Escherichia coli* using a variety of expression vectors and *E. coli* strains. However, expressing MtrD in *E. coli* strains with native efflux systems could yield conflicting results. To address this, the *acrAB* region encoding a homologous efflux system was deleted from *E. coli* strains, resulting in hyper-susceptibility to hydrophobic antimicrobials. Furthermore, the *mtrD* gene was cloned into the pET21a vector, allowing for high-yield production of MtrD protein in *E. coli*. Batch-style purification of the MtrD protein from this system yielded substantial quantities of high-quality protein, suitable for various downstream investigations.

To streamline the creation of *mtrD* gene variants, a modified pBluescript II vector was developed, facilitating the construction of site-directed mutants. The expanded multiple cloning site in this vector allowed for efficient cloning of *mtrD* gene fragments, simplifying the generation of *mtrD* mutants and enhancing our understanding of MtrD and other RND transporters' efflux mechanisms.

Overall, this PhD thesis provides valuable insights into the structure, function, and role of MtrD in antibiotic resistance. The findings contribute to our understanding of AMR mechanisms in *N. gonorrhoeae* and offer a foundation for future research in combating drug resistance in this pathogen. Furthermore, understanding the distinct features of MtrD among RND efflux pumps can guide the development of targeted drugs and inhibitors.

DECLARATION

I affirm that this dissertation is composed entirely of original work, acknowledging any materials or ideas previously submitted for academic credentials elsewhere. Furthermore, I declare that, to the best of my understanding, it does not include any content previously published or authored by another individual, except where appropriately cited within the text.

Mohsen Chitsaz

ACKNOWLEDGEMENTS

I extend my deepest gratitude to my supervisor, Professor Melissa Brown, for her invaluable guidance, unwavering support, and continuous encouragement throughout the duration of my doctoral research. I am also indebted to the members of her laboratory for their collaboration and assistance.

I would like to express my heartfelt appreciation to my adjunct supervisor, Professor Megan O'Mara, for her expertise in molecular dynamics simulations and her generous mentorship. I am sincerely grateful for her contributions to my research and the insights shared by members of her laboratory.

To my beloved wife, Dr. Maryam Bazargan, I owe a debt of gratitude beyond measure. Her unwavering support, understanding, and encouragement have been the cornerstone of my journey through academia. Her love and belief in me have been a constant source of strength and inspiration.

I also want to acknowledge my sons, Emin and Reza Chitsaz, whose love and understanding have been a source of motivation during challenging times. My granddaughters, Ella, Tiana, and Zoe, have brought immeasurable joy to my life. I cherish every moment spent with them and express my deepest love and gratitude, with a special mention to my beloved Ella.

Their unwavering support and love have been the driving force behind my pursuit of knowledge and academic achievements. I am forever grateful for their presence in my life.

CONTRIBUTIONS

The research conducted during my doctoral studies benefitted significantly from the innovative work carried out by Professor Megan O'Mara's group in the field of molecular dynamics simulations. Specifically, their development of a simulation method for MtrD has been instrumental in advancing our understanding of this transporter's interactions with substrates and elucidating its dynamic behaviour. By leveraging this innovative approach, my research has been able to delve into the intricate functional mechanisms of MtrD, shedding light on key aspects of its role in AMR.

PUBLICATIONS

Paper 1: **Chitsaz, M.** and Brown, M. H. (2017) "The role played by drug efflux pumps in bacterial multidrug resistance." Essays in Biochemistry, 61, 127-139. (Appendix **B**)

Paper 2: **Chitsaz M.**, Booth, L., Blyth M., O'Mara M. L., Brown M. H., (2019) "Multidrug resistance in *N. gonorrhoeae*: identification of functionally important residues in the MtrD efflux protein." *mBio* 10:6, e02277-19. (Appendix **C**).

Paper 3: Fairweather, S. J., Gupta, V., **Chitsaz, M.**, Booth, L., Brown, M. H., O'Mara, M. L. (2021). "Coordination of substrate binding and protonation in the *Neisseria gonorrhoeae* MtrD efflux pump controls the functionally rotating transport mechanism." ACS Infectious Diseases, 7, 1833−1847. (Appendix **D**).

Paper 4: **Chitsaz M.**, Gupta V., Harris B., O'Mara M. L., Brown M. H., (2021) A unique sequence is essential for efficient multidrug efflux function of the MtrD protein of *N. gonorrhoeae*. *mBio* **12**:4, e01675-21. (Appendix **E**).

CHAPTER 1

GENERAL INTRODUCTION

Declaration by candidate

A part of the work presented in this chapter has been published by Chitsaz, M. and Brown, M. H. (2017) "The role played by drug efflux pumps in bacterial multidrug resistance." Essays in Biochemistry, 61, 127-139. The quality and extent of contributions of the candidate and co-authors to this paper are given below. The printed version of this paper can be found in Chapter 7 (Appendix **B**).

Name	**Quality of contribution**	**Contribution extent (%)**
Mohsen Chitsaz (candidate)	Conceptualisation, reviewing literature, writing, editing and revision of the manuscript	90
Melissa Brown (co-author)	Conceptualisation, editing and revision of draft and final manuscript	10

The undersigned hereby certify the above declaration correctly reflects the quality and extent of the candidate and co-author contribution to the paper published from this work.

Candidate signature		18/04/2024
Supervisor signature		18/04/2024

1.1 Overview of *Neisseria gonorrhoeae*

Neisseria gonorrhoeae, commonly known as the gonococcus, is a Gram-negative diplococcus bacterium that is responsible for the sexually transmitted infection, gonorrhoea (Unemo et al., 2019b). It is an obligate human pathogen, meaning that it only infects humans and cannot survive outside the human body for long periods of time (Qian et al., 2024).

1.1.1 Gonorrhoea: a sexually transmitted infection

The historical sexually transmitted infection (STI), gonorrhoea, continues to be a main public health concern worldwide with an estimated global annual incidence of 82 million cases among adults (Rowley et al., 2019, Satterwhite et al., 2013, Unemo et al., 2019b, WHO, 2021). The global incidence of gonorrhoea has markedly risen over the past two decades (Peters et al., 2022). *N. gonorrhoeae* typically infects mucus membranes of the urogenital tract resulting in urethritis in men, and cervicitis in women (Barlow and Phillips, 1978, Edwards et al., 2000, Unemo et al., 2019b). However, it can also infect the rectum, pharynx, and conjunctiva (Bro-Jorgensen and Jensen, 1973, Klein et al., 1977, McCormack et al., 1977, Unemo, 2020). If left untreated or undetected, gonorrhoea can lead to serious complications, such as pelvic inflammatory disease in women and epididymitis in men. Gonorrhoea can also increase the risk of acquisition or transmission of other STIs, including human immunodeficiency virus (HIV) (Fleming and Wasserheit, 1999, Gerbase and Zemouri, 2020, Holmes et al., 1971, World Health Organisation (WHO). 2012). Additionally, gonorrhoea can cause systemic infections such as dermatitis-migrating arthritis-tenosynovitis syndrome, endocarditis, monoarticular septic arthritis, perihepatitis, or meningitis (Holmes et al., 1971, Kerle et al., 1992, Qian et al., 2024).

Gonorrhoea is a leading cause of ophthalmia neonatorum, an acute purulent conjunctivitis that affects new-borns. This infection can be acquired from an infected mother during passage through the birth canal and can result in blindness, joint infection, or a life-threatening blood infection in the baby (Laga et al., 1989, Qian et al., 2024).

Currently, there is no vaccine available for gonorrhoea, and treatment and control of the infection relies on effective antibiotic therapy, prevention, diagnosis, sexual contact notification, and epidemiological surveillance (Williams et al., 2024). Nonetheless, the effectiveness of antibiotic therapy is increasingly compromised by drug resistance in *N. gonorrhoeae*, as the bacterium has developed or acquired resistance to various anti-gonococcal antibiotics, including penicillins (PENs), sulfonamides, tetracyclines, fluoroquinolones, macrolides (such as azithromycin – [AZM]), and cephalosporins (including the extended-spectrum cephalosporin (ESC), ceftriaxone – [CRO]) (Allan-Blitz et al., 2024, Unemo et al., 2019a, Unemo et al., 2019b, World Health Organisation (WHO). 2012). Reports highlighting the emergence and dissemination of *N. gonorrhoeae* strains with high-level resistance to AZM and reduced susceptibility or resistance to CRO are of notable concern (Day et al., 2022, Pleininger et al., 2022, Smolarchuk et al., 2018, Tang et al., 2023), as these two antibiotics are recommended as the first-line treatment for dual therapy against gonorrhoea (Allan-Blitz et al., 2024, Workowski et al., 2021).

The increasing prevalence of antibiotic-resistant gonorrhoea is a major concern for public health globally (Allan-Blitz et al., 2024). In the United States, e.g., the number of gonorrhoea cases increased by 67% from 2013 to 2017, particularly among specific groups such as men who have sex with men. Similarly, in Australia, there has been a steady increase in the number of reported gonorrhoea infections since 2010, along with a rise in antibiotic resistance rates (CDC, 2017a, CDC, 2017b, Lahra et al., 2022, Unemo et al., 2019b).

The Australian Gonococcal Surveillance Program (AGSP) reported decreased susceptibility or resistance rates to antibiotics such as CRO, AZM, PEN, ciprofloxacin (CIP), tetracycline (TET), streptomycin, and gentamicin (GEN). Notably, the rate of resistance to AZM has doubled since 2020, reaching 8.4% in 2021 (Lahra et al., 2022). The COVID-19 pandemic has also had an impact on the reporting of gonorrhoea infections, with a decline in the number of notifiable infections and clinical isolates from 2020 onwards

coinciding with public health measures (Cole et al., 2022, Lahra et al., 2022, Stevens et al., 2015).

Thus, the increasing prevalence of antibiotic-resistant gonorrhoea is a significant concern for global public health. New strategies are needed to prevent and control the spread of gonorrhoea, including the development of new treatments and the implementation of effective prevention and control measures. In the upcoming sections, the discussion will shift towards exploring the biological, physiological, virulence properties, and antimicrobial resistance (AMR) mechanisms of *N. gonorrhoeae*.

1.1.2 *N. gonorrhoeae*: classification

N. gonorrhoeae is a pathogen that belongs to the family Neisseriaceae in the class Betaproteobacteria. The genus Neisseria contains over 23 species, including human-restricted, animal-restricted, and species isolated from mucous membranes of both humans and animals. Among these species, *N. gonorrhoeae* is closely related to *N. meningitides*, another human pathogen that colonizes the upper respiratory tract and can cause fatal septicaemia. *N. gonorrhoeae* shares many genes involved in pathogenicity and virulence with commensal *Neisseria* species such as *N. lactamica*, but these non-pathogenic species do not typically cause pathology due to differences in gene regulation and lack of capacity to induce inflammation based on polymorphonuclear leukocytes (Adeolu and Gupta, 2013, Frost et al., 2024a, Liu et al., 2015, Seifert, 2019, Tønjum and van Putten, 2017, Unemo et al., 2019b).

1.1.3 Growth, metabolism, and pathogenesis

N. gonorrhoeae, a fastidious bacterium, relies on specific nutrients such as glucose, glutamine, thiamine, phosphate, iron, and carbon dioxide for growth, acquiring amino acids like cysteine from the host (Kellogg et al., 1963, Morse, 1979, Spence et al., 2008). The bacterium actively seeks iron as a crucial nutrient during infection, regulated by the ferric uptake regulator (Fur) (Liyayi et al., 2023, Płaczkiewicz et al., 2023, Walker et al., 2023). Fur plays a pivotal role in modulating the adaptation of *N. gonorrhoeae* to the host by controlling iron acquisition mechanisms. The bacterium has evolved strategies to cope

with iron scarcity, showcasing its ability to overcome challenges posed by the host's immune system (Cornelissen and Hollander, 2011, Jackson et al., 2010, Rohde and Dyer, 2003).

To manage stresses during infection, *N. gonorrhoeae* modifies its lipooligosaccharide (LOS), utilises lactate over glucose as a carbon source, engages in anaerobic respiration with nitrite, and exploits efflux pump systems (Cole, 2012, Li et al., 2010, Parsons et al., 1988, Seib et al., 2006, Shafer et al., 2016, Unemo et al., 2019b). Its adaptation to the human host involves a complex regulatory network, including transcriptional regulators, two-component systems, translational regulation through small RNAs, and clonal variation through phase variation, genetic heterogeneity, and natural competence for DNA transformation (Baarda et al., 2018, Biswas et al., 1977, Clark et al., 1987, Cole, 2012, Criss and Seifert, 2012, Davidsen et al., 2004, Fudyk et al., 1999, Gangaiah et al., 2017, Hamilton and Dillard, 2006, Johnston et al., 2014, Koomey, 1998, Laskos et al., 2004, Lorenz and Wackernagel, 1994, Nóbrega et al., 2016, Quillin and Seifert, 2018, Snyder et al., 2007, Spencer-Smith et al., 2016, Steinmoen et al., 2002, Woods et al., 1989). Infection initiation in urogenital tracts involves attachment mechanisms using surface structures like the type IV pili, opacity protein, porin protein PorB, and LOS (Edwards and Apicella, 2004, Harvey et al., 2000, Ketterer et al., 2016, Quillin and Seifert, 2018). Biofilm formation can make the bacterium impervious to immune responses and antibiotics (Craig et al., 2004, Dietrich et al., 2011, Higashi et al., 2007, Kirn et al., 2000, Maier et al., 2002, Merz et al., 2000, Seib et al., 2017, Skerker and Berg, 2001, Srikhanta et al., 2009). The bacterium's pathogenicity is facilitated by homologous recombination, enabling genetic diversity and antigenic variation crucial for pathogenesis and antibiotic resistance (Aas et al., 2002, Cacciapuoti et al., 1978, Callaghan et al., 2017, Cehovin et al., 2013, Chen and Dubnau, 2004, Chen et al., 2008, Goodman and Scocca, 1988, Hamilton and Dillard, 2006, Hebeler and Young, 1976, Helm and Seifert, 2009, Kowalczykowski, 2008, Kowalczykowski, 2015, Kroll et al., 1998, Mehr and Seifert, 1998, Obergfell and Seifert, 2015, Radding, 1981, Saier, 2000, Stein, 1991, Story and Steitz, 1992). *N. gonorrhoeae* demonstrates phenotypic variations, including phase and antigenic variations

affecting major surface structures like type IV pilus, opacity proteins, and LOS (Cahoon and Seifert, 2009, Danaher et al., 1995, Dehio et al., 1998, Kline et al., 2007, Lo et al., 2009, Palmer et al., 2016, Prister et al., 2020, Quillin and Seifert, 2018, Sadarangani et al., 2011, Seifert, 2018, Song et al., 2000, Stern et al., 1986, Swanson, 1978, Wetzler et al., 1992, Zhang et al., 2013).

In summary, *N. gonorrhoeae* employs diverse adaptive mechanisms, including genetic variation, to withstand environmental changes, evade host immunity, cause infections, and resist antimicrobials. Understanding these mechanisms is vital for developing effective strategies against gonococcal infections, including addressing AMR. Subsequently, AMR mechanisms in gonococci will be discuss.

1.1.4 Antimicrobial resistance

AMR in *N. gonorrhoeae* has become an urgent and severe health problem (Allan-Blitz et al., 2024, Cole et al., 2022, Unemo et al., 2017, Unemo and Shafer, 2014, Wi et al., 2017). This bacterium has developed resistance to multiple classes of antibiotics, and multiple drug-resistant strains are currently being reported in many countries worldwide (Tagliabue and Rappuoli, 2018, Thomas et al., 2019a). The current recommended empirical treatment for suspected gonorrhoea infection is the ESC CRO (Fifer et al., 2020, St Cyr et al., 2020). However, there have been reports of gonococcal strains showing decreased susceptibility or full resistance to CRO in various countries (Golparian et al., 2023b, Merrick et al., 2022, Van Hal et al., 2023). An illustrative example of the impact of AMR is the global emergence and dissemination of a CRO-resistant strain (FC428) (Tang et al., 2023). This strain carries mutations in the mosaic *penA* gene, significantly compromising the therapeutic effectiveness of CRO treatment worldwide (Tang et al., 2023). Instances of treatment failure with CRO have also been documented (Eyre et al., 2018, Pleininger et al., 2022). Previously, AZM in combination with CRO was recommended as the first-line dual therapy regime and used for the treatment of gonorrhoea until 2018 when it was removed from the regimen due to an increase in the proportion of isolates resistant to AZM (Unemo et al., 2020). Mathematical modelling based on AMR surveillance data predicts that

by 2030, ≥ 5% resistance to CRO could be reached, highlighting the need for new first-line antimicrobials for the treatment of gonorrhoea (Riou et al., 2023).

1.1.4.1 Mechanisms of antimicrobial resistance

N. gonorrhoeae exhibits a formidable array of AMR mechanisms, engaging with various strategies against most antimicrobials used in treatment. These mechanisms predominantly involve enzymatic modification or destruction of antimicrobials, target modification, reduced influx of antimicrobials, and increased efflux of antimicrobials (Unemo and Shafer, 2014).

1.1.4.1.1 Beta-lactam resistance

Beta-lactam antibiotics, such as PENs and cephalosporins, are bactericidal antimicrobials that work by binding to PEN binding proteins (PBPs) and interfering with the formation of peptidoglycan cross-links in the bacterial cell wall (Lewis and Bush, 2015). Resistance to β-lactam antibiotics in *N. gonorrhoeae* can result from either plasmid- or chromosome-mediated mechanism. Gonococcal strains with high level PEN resistance often carry plasmids with $bla_{\text{TEM-1}}$ gene encoding a TEM-1 type β-lactamase that efficiently hydrolyses PEN and many cephalosporins (Elsener et al., 2023, Elwell et al., 1977). Chromosomal resistance, on the other hand, arises from mutations in the chromosome that modify the target PBPs, combined with resistance determinants that increase efflux and decrease influx of PEN, leading to clinical-level resistance. The primary lethal target protein for β-lactam antibiotics is transpeptidase 2 (PBP2), encoded by the *penA* gene (Powell et al., 2009, Tapsall, 2009). PEN-resistant gonococci typically possess 5 to 9 mutations in the *penA* gene, and mosaic *penA* genes have been identified conferring resistance to both PENs and ESCs (Tang et al., 2023, Unemo and Shafer, 2014). The *ponA* gene encodes another β-lactam target protein, PBP1, which has a minor effect on PEN resistance (Powell et al., 2009). Additionally, specific mutations that enhance efflux through the overexpression of the MtrCDE efflux pump system and reduce influx through decreased permeability of the outer membrane (OM) channel porin PorB1 can further raise PEN MICs (Shafer and Folster, 2006, Thakur et al., 2018, Tomberg et al., 2010).

Cephalosporins have a 7-amino cephalosporanic acid nucleus with a β-lactam ring attached to a dihydrothiazine ring. Substitutions in the β-lactam ring produce cephalosporins with varying antibacterial activities and pharmacokinetics (Lewis and Bush, 2015). In gonococci, cephalosporin resistance can be attributed to mutations in PBPs, decreased influx and increased efflux (Atzori et al., 2019, Gianecini et al., 2019, Thomas et al., 2020, Tomberg et al., 2010). As mentioned in the previous section, the current recommended empirical treatment for gonorrhoea is a single dose of the ESC, CRO (St Cyr et al., 2020). However, it is crucial to note that *N. gonorrhoeae* has developed resistance to this antibiotic, and strains with reduced susceptibility or resistance to CRO are internationally distributed (Day et al., 2022, Lahra et al., 2022, Nakayama et al., 2016, Pleininger et al., 2022, Tang et al., 2023, Tapsall, 2009, Terkelsen et al., 2017). The development of resistance to CRO, as well as other cephalosporins, is a complex process involving multiple mechanisms (Riou et al., 2023).

1.1.4.1.2 Macrolide resistance

Macrolide antibiotics like erythromycin (ERY) and AZM inhibit protein synthesis by binding to the 50S ribosomal subunit. Macrolide resistance in gonococci can result from rRNA methylase-associated modification of 23S rRNA, specific mutations in 23S rRNA, or overexpression of efflux pumps, particularly the MtrCDE system (Retsema et al., 1987, Roberts et al., 1999, Shafer, 2018, Thomas et al., 2020, Wadsworth et al., 2018a, Zarantonelli et al., 1999).

1.1.4.1.3 Quinolone resistance

The term "quinolone" classifies a group of compounds, including nalidixic acid, quinazolines, and isothiazoquinolones. Quinolones target two vital bacterial enzymes, DNA helicase and DNA topoisomerase IV, essential for DNA replication and transcription regulation. These antibiotics are categorised into four generations, with the third-generation quinolones being commonly used in clinical practice (Tang and Zhao, 2023).

The quinolone CIP was once recommended for the treatment of gonorrhoea and widely employed from the mid- to late 1980s (Unemo and Shafer, 2014). However, resistance quickly emerged, leading to treatment failures reported in various regions by 1990 (Unemo and Shafer, 2014). Due to escalating resistance, the use of fluoroquinolones as the first-line empirical treatment for gonorrhoea was abandoned in many countries during the mid- to late 1990s (Unemo and Shafer, 2014). In 2007, the Centers for Disease Control and Prevention (CDC) removed fluoroquinolones from the recommended treatment regimens for gonorrhoea altogether (CDC, 2007).

Quinolone resistance arises from mutations that alter drug uptake, efflux, and the structure of drug, thereby diminishing its effectiveness (Tang and Zhao, 2023). Additionally, plasmid-mediated mechanisms significantly contribute to the development of quinolone resistance (Tang and Zhao, 2023). These resistance mechanisms pose a substantial challenge in combatting infections including gonorrhoea and underscore the importance of prudent antibiotic use and the search for alternative treatment options.

1.1.4.1.4 Sulfonamide resistance

Sulfonamides are antimicrobials that hinder the production of folic acid in bacteria. They obstruct bacterial dihydropteroate synthase (DHPS) enzymes by competing with *p*-aminobenzoic acid. Gonococcal resistance to sulfonamides can be caused by the overproduction of *p*-aminobenzoic acid or by mutations in the *folP* gene, which encodes the target DHPS enzymes. Mutations in *folP* lead to enzymes with reduced sensitivity to the antibiotic (Tapsall, 2005).

1.1.4.1.5 Tetracycline resistance

Tetracyclines inhibit protein synthesis by binding to the 30S ribosomal subunit. Gonococcal resistance arises from plasmid-mediated mutations in the *tetM* gene, encoding TetM protein, or chromosomal mutations modifying 30S ribosomal proteins, decreasing influx, and increasing efflux of tetracycline (Morse et al., 1986, Unemo and Shafer, 2014).

1.1.4.1.6 Spectinomycin and gentamicin resistance

Spectinomycin resistance results from a single nucleotide polymorphism in 16S ribosomal RNA (C1192U) (Galimand et al., 2000). Currently, there are no reported clinical isolates of *N. gonorrhoeae* with GEN resistance, despite its use in certain countries as front-line therapy; however, concerns exist about potential future development (Holley et al., 2022). Spontaneous mutants with low-level resistance have mutations in the *fusA2* gene, that encodes the elongation factor G, and high-level resistance involves mutations in the *fusA* and *ubiM* genes (Holley et al., 2022). Furthermore, a specific FusA mutation (M520I) has been associated with high-level resistance (Golparian et al., 2023a). It has been suggested that while these mutations may impose a fitness cost on the bacterium during infection, compensatory mutations that alleviate this fitness cost could emerge and promote GEN resistance (Golparian et al., 2023a).

1.1.4.1.7 Decreased influx and increased efflux

Gram-negative bacteria, including *N. gonorrhoeae*, have an OM that serves as an important permeability barrier, preventing antimicrobials from reaching their targets in the cell. To overcome this barrier, certain antibiotics such as PENs, TETs, and ESCs must pass through OM channels formed by porin proteins. Each strain of *N. gonorrhoeae* expresses one of two mutually exclusive forms of porins, PorB1a and PorB1b, with mutations in PorB1b resulting in decreased antimicrobial entry (Nikaido, 1994, Olesky et al., 2006).

In addition to OM barriers, *N. gonorrhoeae* can also acquire resistance by eliminating the efficacy of multiple antimicrobials through mutations in or overexpression of multidrug resistance (MDR) transport proteins. Efflux pumps, which are a type of MDR transport protein, are responsible for recognising and exporting toxic drugs from within the cell. *N. gonorrhoeae* possesses several efflux pump systems, with the MtrCDE system being the major one (Shafer et al., 2010).

The interplay between the OM barrier and efflux pumps plays a crucial role in determining the level of drug accumulation within the bacterial cell, ultimately

leading to the expression of toxic effects. To provide a comprehensive understanding of drug translocation in the context of efflux transporter proteins, it is essential to also explore the structure and function of the OM. Therefore, the next section will briefly discuss the permeability barrier of Gram-negative bacteria, further contributing to the overall understanding of AMR in *N. gonorrhoeae*.

1.2 Permeability barrier of Gram-negative bacteria

Gram-negative bacteria exhibit intrinsic resistance to various antimicrobial compounds, including many antibiotics effective against Gram-positive organisms (Zgurskaya and Rybenkov, 2020). This innate resistance is attributed to the unique structure of the Gram-negative envelope, which consists of two membranes, the inner membrane (IM) and the OM, with the periplasmic space in between (Hancock, 1997, Li et al., 2015, Masi et al., 2017, Nikaido, 1989, Rybenkov et al., 2021). The Gram-negative envelope acts as a selective barrier, enabling uptake of essential solutes while differentiating toxic substances, including clinical antibiotics (Hancock, 1997, Nikaido, 1989). This selective barrier plays a crucial role in the development of acquired resistance to multiple antibiotics (Mulani et al., 2019, Unemo et al., 2016, Zgurskaya and Rybenkov, 2020, Zhang et al., 2023a).

The OM, an asymmetric bilayer with specific protein species, plays a vital role in this resistance, with variations in chemical composition affecting permeability across different Gram-negative species (Hancock, 1997, Zgurskaya and Rybenkov, 2020). The composition of the OM, particularly lipopolysaccharides (LPS) in enterobacteria, contributes to its barrier properties (Galdiero et al., 2012, Hancock, 1997, Nikaido, 2003). Notably, *N. gonorrhoeae* lacks the O antigen, expressing LOS instead (Hancock, 1997, Schneider et al., 1982, Schneider et al., 1984). Outer membrane proteins (OMPs), include porin proteins that can form water-filled channels, facilitate nutrient influx and OM channel proteins such as TolC that are used by certain efflux pumps to expel toxic compounds to the cell exterior environment (Kojima and Nikaido, 2013, O'Shea and Moser, 2008, Vergalli et al., 2020).

The OM's exclusion property hinders the easy entry of hydrophobic or lipophilic antibiotics into the cell, but they can still diffuse, albeit slowly, across the OM and are possibly subject to efflux (Hancock, 1997, Silver, 2016). This type of antibiotics such as benzylpenicillin can diffuse across the CM and the lipid bilayers rather rapidly (Kojima and Nikaido, 2013, Li et al., 1994).

Small hydrophilic molecules are prevented from entering the cell by the CM, but they can enter the periplasm through the OM, and they are not likely subject to efflux (Silver, 2016). Clinically important antibacterial drugs can diffuse across the CM because they have some degree of hydrophobicity, with the exception of the aminoglycosides, whose uptake involves two energy-dependent but non-carrier-dependent steps, and fosfomycin, which uses transporters. The diffusion through the CM of Gram-negative bacteria favours neutral lipophilic compounds (Nikaido, 1994, Silver, 2016).

In Gram-negative bacteria, drug resistance is often linked to the lack of, or reduced expression of major porins (Vergalli et al., 2020). The regulation of general porin proteins involves various mechanisms, including transcriptional regulators responsible for chemical stress responses, two-component systems, and extracytoplasmic function sigma factors (Vergalli et al., 2020). Understanding the regulation of porin proteins is crucial for controlling antibiotic susceptibility and resistance.

Alterations in porin structure and function can impact antibiotic susceptibility and resistance in Gram-negative bacteria, including *N. gonorrhoeae*. The major OMP from *N. gonorrhoeae*, originally known as Protein I (PI), can function as a nonspecific porin (Carbonetti et al., 1988, Jones et al., 2023, Sparling et al., 1975). This protein is now referred to as PorB, which exists in two major variants, PorB1A and PorB1B (Garvin et al., 2008). For example, a mutation called *penB* in the gonococcal porin, analogous to loop 3 of the *E. coli* OmpF porin, has been associated with reduced susceptibility of *N. gonorrhoeae* to hydrophilic antibiotics like PEN and TET (Gill et al., 1998, Guymon et al., 1978, Olesky et al., 2002).

Polycationic antimicrobial compounds, such as polymyxins and natural polycationic peptides and aminoglycosides, use a third mechanism of entry through the OM called self-promoted uptake (Hancock, 1997, Huang and Hancock, 1996, Krishnamoorthy et al., 2016). Some bacteria, such as *P. aeruginosa* and *Acinetobacter baumannii*, with highly resistant OMs and deficient porin pathways, require additional resistance mechanisms like β-lactamase production or active efflux (Hancock, 1997).

The composition of the OM, specifically the structure of LOS in *N. gonorrhoeae*, significantly influences susceptibility to antimicrobial compounds. Active efflux and porin proteins in the OM are critical components of the selective barrier in Gram-negative bacteria, including *N. gonorrhoeae*. The subsequent section will delve into efflux transport proteins, detailing their connection to the bacterial cell envelope barrier and their role in AMR.

1.3 Efflux proteins

Drug efflux is a significant mechanism of drug resistance, characterised by the ability of cells to recognise and remove toxic compounds from within the cell to the external medium before they can reach their intended targets (Holmes et al., 2016). Drug efflux mechanisms involve energy-dependent transport proteins, which are located in the CM (Brawley et al., 2022). The web-based Transporter Classification Database (TCDB: http://www.tcdb.org) provides an extensive classification framework for membrane transport proteins, both importers and exporters (Saier et al., 2021). Drug efflux transporters can be grouped into the following seven families/superfamilies based on protein sequence homology, overall protein structure, energy source, substrate specificity and other properties. These families are: (i) the ATP-binding cassette (ABC) superfamily, members of which are primary active transporters that use the free energy of ATP hydrolysis to energise efflux; (ii) the resistance-nodulation division (RND) superfamily; (iii) the major facilitator superfamily (MFS); (iv) the multidrug and toxic compound extrusion (MATE) family; (v) the small multidrug resistance (SMR) family; (vi) the proteobacterial antimicrobial compound efflux (PACE) family and (vii) the *p*-aminobenzoyl-

glutamate transporter (AbgT) family (Figure 1.1) (Dashtbani-Roozbehani and Brown, 2021, Garcia et al., 2022). The latter six groups are secondary active transporters that couple efflux with an ion electrochemical membrane gradient as an energy source (Delmar and Yu, 2016, Hassan et al., 2015, Paulsen et al., 1996b, Paulsen et al., 2000).

Drug efflux pumps are present in all organisms. In bacteria, they play a key role not only in drug resistance but also in the movement of pathogenicity factors, e.g., by modulation of biofilm formation and possibly other physiological processes (Henderson et al., 2021, Zgurskaya et al., 2022). They can also interact synergistically with other AMR mechanisms, the cumulative effects of which can result in AMR of clinical importance (Section 1.1.4.1 and 1.2) (Shafer and Folster, 2006, Yao et al., 2016). Many efflux transporters can accommodate an extremely wide range of antimicrobial compounds (MDR efflux pumps), while others only export a specific substrate and its closely related derivatives. Both types are found in Gram-positive and Gram-negative bacteria and can contribute to clinical resistance (Garcia et al., 2022, Zgurskaya et al., 2021).

Certain efflux transporters operate independently, while others function as multi-component systems (Alav et al., 2021, Murakami et al., 2020). The multi-component systems involve two additional proteins to create a functional tripartite system. In Gram-negative bacteria, these tripartite systems consist of an inner-membrane protein (IMP), a periplasmic adaptor protein (PAP) from the membrane fusion protein (MFP) family, and an outer membrane channel protein from the outer membrane protein family (OMF) (Murakami et al., 2020). This arrangement empowers Gram-negative bacteria to efficiently export compounds across the OM (Benz et al., 1993, Fralick, 1996, Paulsen et al., 1997). Proteins within the OMF family, such as the *E. coli* TolC, collaborate with RND, ABC, and MFS transporters to facilitate the export process.

In Gram-negative bacteria, RND transporters cooperate with singular efflux transporters to remove substances (Tal and Schuldiner, 2009). For example, the two *A. baumannii* RND transporters, AdeABC and AdeIJK, have been shown to remove tigecycline (TGC) from the periplasm that is accumulated in

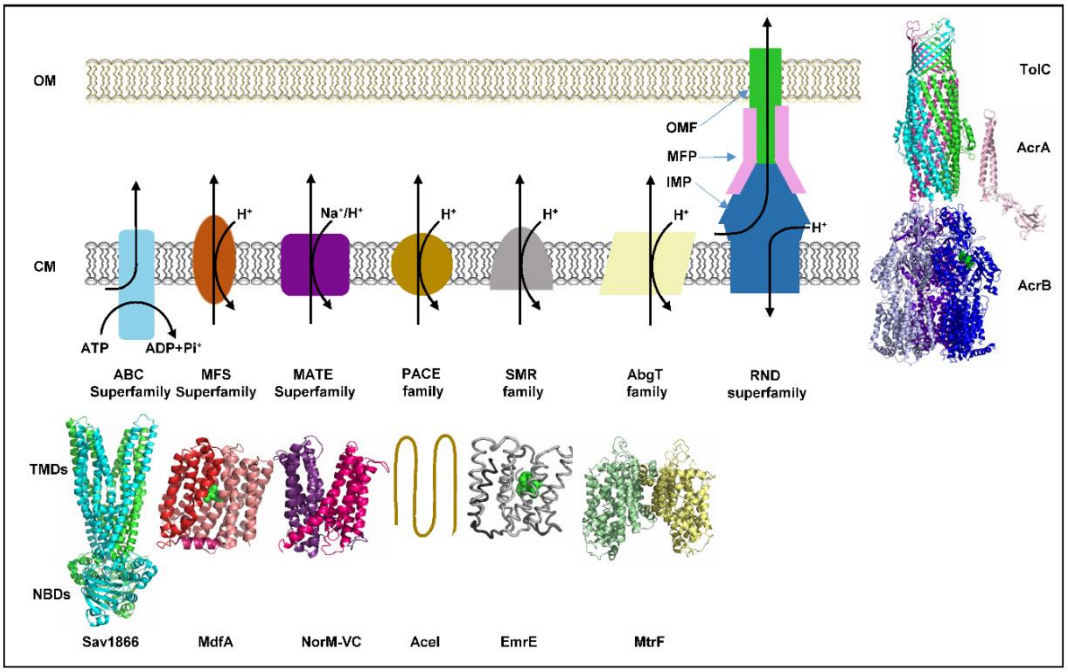

Figure 1.1 Schematic illustration of the seven families/superfamilies of multidrug transport proteins.

Each transporter group is shown by a distinct shape and highlighted with a different colour. Where available, a crystal structure of the functional unit or monomer of a representative protein of each group is shown in a similar colour to the schematic diagram. The crystal structure of *S. aureus* Sav1866 (pdb: 2HYD) representing a functional unit of the ABC transporter is shown. Five singlet system secondary active transporter families/superfamilies: MFS, MATE, PACE, SMR, and AbgT are shown by oval, rectangle, circle, chord, and parallelogram shapes, respectively. Crystal structures of the *E. coli* MFS MdfA (pdb 4ZOW), *V. cholerae* MATE NorM (NorM_VC) (pdb: 3MKT), *E. coli* SMR EmrE (pdb: 3B5D), and *N. gonorrhoeae* AbgT MtrF (pdb: 4R1I) representative transport proteins are shown. A diagram containing four TMS representing the PACE family AceI transporter is also shown. The multicomponent RND superfamily system is shown by a diagram containing the CM-bound, MFP and OMF components, each highlighted by a different colour. Crystal structures of the *E. coli* AcrB (pdb: 2DRD) representing the integral CM protein, AcrA (pdb: 2F1M) the MFP, and TolC (pdb: 2VDE) the OMF of an RND efflux system, are shown.

this compartment by the singlet transporter TetA, and extrude it to the external medium (Dashtbani-Roozbehani and Brown, 2021, Foong et al., 2020). This collaborative interplay between singular and multicomponent transporters enables the export of a diverse range of substrates, including antibiotics, ultimately contributing to MDR (Dashtbani-Roozbehani and Brown, 2021, Foong et al., 2020, Schuldiner, 2018).

In response to the rising threat of AMR linked to efflux mechanisms, inhibiting efflux pumps has emerged as a key strategy (Alenazy, 2022). Efflux pump inhibitors (EPIs) are being developed as effective tools to counter AMR, reviving certain antibiotics and expanding their spectrum to encompass Gram-negative bacteria naturally resistant to antibiotics targeting Gram-positive bacteria (Compagne et al., 2023, Douafer et al., 2019, Lomovskaya and Watkins, 2001). EPIs have shown a significant ability to reduce the frequency of AMR mutant development. Efflux inhibition not only combats resistance but also provides additional benefits, such as decreasing bacterial resistance to innate immune response mediators (also efflux pump substrates) and attenuating the virulence of Gram-negative bacteria (Baugh et al., 2014).

Numerous EPIs have been identified and characterised, including verapamil, reserpine, phenylalanine arginine β-naphtylamide (PAβN), previously called (MC-207,110), 1-(1-naphtylmethyl)-piperazine (NMP), D13-9001, and MBX2319 (Edgar and Bibi, 1999, Erickson et al., 1996, Holler et al., 2012, Lomovskaya et al., 2001, Mahamoud et al., 2007, Renau et al., 1999, Scherman and Henry, 1984, Spoelstra et al., 1994, Tsuruo et al., 1981). Some inhibitors are specific to certain efflux pumps, while others inhibit the efflux activity of multiple proteins. For example, PAβN is a wide-spectrum RND efflux pump inhibitor that was described in 1999, active against all three known *P. aeruginosa* efflux pumps (MexAB-OprM, MexCD-OprJ, and MexEF-OprN), the *E. coli* AcrAB-TolC, and *A. baumannii* AdeABC systems. (Renau et al., 1999). This will be discussed further in Section 1.3.6.4.5. Each family or superfamily of the known MDR efflux systems in bacteria is described in the following sections, provided with examples from *N. gonorrhoeae* or other well-studied

efflux proteins from other bacteria. The impact of efflux transport systems on AMR will also be discussed.

1.3.1 The ABC superfamily

ABC transporters represent one of the largest superfamilies of proteins known involving transport proteins that act as either importers or exporters (Feng et al., 2020, Gorecki and McEvoy, 2020, Ho et al., 2018, Okada and Murakami, 2023, Van Veen, 2016, Wang et al., 2020a). Members of this superfamily translocate a wide range of substrates including, sugars, amino acids, lipids, and antimicrobial compounds (Swier et al., 2016). This substrate diversity reflects the numerous physiological roles that ABC transporters play in the cell, e.g., nutrient uptake, removal of waste and toxic products, and export of cellular components such as cell wall polysaccharides (Rees et al., 2009). LmrA from *Lactobacillus lactis* is a well-described ABC MDR efflux pump that exports a wide variety of substrates including antibiotics, toxic ions, lipids, antimicrobial peptides and antiseptics (Poelarends et al., 2002). The *E. coli* MacB (macrolide-specific ABC-type efflux carrier) protein, another ABC MDR efflux pump, which similar to RND pumps, functions together with its cognate MFP MacA and the OM channel TolC, to confer resistance to macrolides (Kobayashi et al., 2001, Okada and Murakami, 2023). The *E. coli* HlyB protein is also a member of the ABC transporter that uses its cognate MFP HlyD and the OM channel TolC protein for extruding α-haemolysin (HlyA) to the external medium (Blight and Holland, 1994). The orthologous MacAB pump of *N. gonorrhoeae* has also been shown to export multiple substrates including macrolides (Rouquette-Loughlin et al., 2005). Clinical isolates of *N. gonorrhoeae*, such as H041, the first documented case of a gonococcal strain causing a third-generation cephalosporin resistant infection, have shown extensive resistance to ESCs and the macrolide AZM and inactivation of MacAB renders the bacterium clinically susceptible to AZM according to MIC breakpoints indicating the key role of this pump in AZM resistance (Golparian et al., 2014). Another important example of ABC transporters is the ABCG2 transporter which is constitutively expressed in many mammalian tissues and also known as the breast cancer resistance protein, capable of expelling anti-

cancer drugs and its dysfunction linked with several human disorders. Cryo-EM structures of this protein has provided clinically important information, e.g., that substrates of this transporter are flat, circular and hydrophobic molecules providing insights into designing inhibitor molecules (Shvarev et al., 2022).

Solving the crystal structure of the *S. aureus* Sav1866 protein, which can transport structurally-unrelated substrates such as ethidium (ET), tetraphenylphosphonium and Hoechst 33342, marked one of the major steps in understanding ABC transporters at a structural and functional level (Dawson and Locher, 2007) (Figure 1.1). ABC transporters have a basic organisation of two transmembrane domains (TMDs) that contain the substrate translocation pathway and two nucleotide-binding domains (NBDs), which bind and hydrolyse ATP (Dawson and Locher, 2007, Ford and Beis, 2019). NBDs are highly conserved among ABC superfamily proteins and contain several motifs characteristic of this group of transporters. These include: the Walker A and B motifs, present in many nucleotide-binding proteins; motif C, specific to the ABC superfamily; and the stacking aromatic D-, H-, and Q-loops and conserved sequences in loop regions that communicate conformational changes from the NBDs to the TMDs (Rees et al., 2009, Wilkens, 2015). The functional unit of mammalian ABC transporters is a dimer, with each monomer containing two domains (TMD and NBD) contained in a single polypeptide (Ford and Beis, 2019). In bacterial transporters, however, each monomer is considered as a half transporter that is formed by the fusion of one TMD and one NBD which are formed by separate polypeptides. In most ABC transporters, a functional transport complex is a homodimer, with each monomer containing 6 α-helical transmembrane segments (TMS) spanning the inner membrane, and 12 TMS in total per functional unit. Most ABC transporters follow this two-times-six TMS paradigm, albeit exceptions exist (George and Jones, 2013). The structure of Sav1866 showed for the first time that TMD and NBD domains are connected via transmembrane helices and nucleotide binding is associated with dimerisation (Dawson and Locher, 2007).

A general model, referred to as conformational coupling, was proposed as the functional mechanism of ABC transporters (Ford and Beis, 2019, Van

Veen, 2016). This model, however, has several exceptions (Locher, 2016). In this model, ATP-dependent conformational changes in the NBDs drive rearrangements of the TMS that enforces the link between transport and ATP hydrolysis and results in a transport mechanism often referred to as “alternating access” (Ford and Beis, 2019, Van Veen, 2016). This mechanism explains how the transport protein undergoes conformational changes in which a central binding site located within a TMD is exposed alternately to the inside (inward-facing), or the outside (outward-facing) of the cell, but never simultaneously to both sides allowing the binding site alternating accessibility to each side of the membrane (Van Veen, 2016). The current structural evidence obtained from several bacterial ABC transporters including Sav1866 (Dawson and Locher, 2007), the lipid A and lipopolysaccharide transporter MsbA (Ward et al., 2007), BmrA from *Bacillus subtilis* and McjD from *E. coli* (Choudhury et al., 2014), indicate that these ABC exporters adopt an inward-facing conformation in the absence of nucleotide or when bound to ADP, and that they progress via an ATP-bound occluded transition state into the ATP-bound outward-facing conformation. Finally, the transporter is reset to the inward-facing conformation by dissociation of the NBD dimer mediated by ATP hydrolysis (Van Veen, 2016). An outward only mechanism has also been proposed (Locher, 2016). This mechanism has been described for translocation of lipid-linked oligosaccharides (LLO) by the *Campylobacter jejuni* ABC transporter Pg1K (Locher, 2016, Perez et al., 2015). While the Pg1K flippase has been shown to adopt both inward and outward facing conformations, only outward facing conformation is involved in flipping LLO (Locher, 2016, Perez et al., 2015). This mechanism does not involve large separation of NBDs, in contrast to alternating access mechanism. This mechanism is also thought to be favourable for export of large molecules such as proteins and long polysaccharides (Locher, 2016, Perez et al., 2015). The MacAB efflux transporter from the ABC superfamily is described below.

1.3.1.1 The *N. gonorrhoeae* MacAB export proteins

The MacAB-TolC complex is an ABC-type transporter machine that is present in *E. coli* and other Gram-negative bacteria (Okada and Murakami, 2023). This system is known to remove various substances, such as macrolide antibiotics, OM glycolipids, protoporphyrins (including protoporphyrin IX, which is produced inside bacteria when haem homeostasis is disturbed), lipopeptides (like the cyclic lipopeptide that causes haemolytic activity of *Pseudomonas entomophila*), and virulence factors (such as heat-labile enterotoxin II) (Cho and Kang, 2012, Kobayashi et al., 2001, Okada and Murakami, 2023, Turlin et al., 2014, Vallet-Gely et al., 2010, Yamanaka et al., 2008). There is also evidence suggesting that rough core lipopolysaccharide may be a physiological substrate of MacAB-TolC, indicating a potential role in OM maintenance (Lu and Zgurskaya, 2013). Although structural information is lacking, genetic and drug resistance aspects of the homologue of *E. coli* MacAB efflux pump in *N. gonorrhoeae* have been characterised. This section describes the genetics and functional information available for the *N. gonorrhoeae* MacA-MacB efflux system, while the *E. coli* MacAB-TolC system is used to describe structural features.

Analysis of the *N. gonorrhoeae* FA1090 genome sequence identified homologues of the *E. coli* MacA and MacB proteins (Kobayashi et al., 2001, Rouquette-Loughlin et al., 2005). Cooperating with the MFP MacA and the multifunctional OM channel TolC, the integral membrane protein, MacB, has been characterised to have four TMS, a different feature from typical ABC transporters that usually have six TMS, and one NBD. It uses ATP hydrolysis to expel macrolides with 14- and 15-membered lactones such as ERY and AZM but not 16-membered ones (Kobayashi et al., 2001). MacB also has a periplasmic domain (PD) formed between TMS 1 and TMS 2 and is thought to capture some substrates, e.g., heat-labile enterotoxin II from the periplasm, which is another distinct feature of MacB (Kobayashi et al., 2001). MacA and MacB of *N. gonorrhoeae* strain FA19 share 35.1% and 51.1% protein sequence identity with the MacA and MacB proteins of *E. coli*, respectively (Rouquette-Loughlin et al., 2005). The putative NBD of the *N. gonorrhoeae*

MacB protein has been shown to be identical with that of the *E. coli* MacB protein with only one residue difference (Rouquette-Loughlin et al., 2005). In *N. gonorrhoeae* the *macA* and *macB* genes form a single transcriptional unit with their promoter located upstream of *macA* (Rouquette-Loughlin et al., 2005). Cloning and expression of the entire *macAB* sequence in an *E. coli* strain that lacks expression of the AcrA and AcrB proteins has shown that the MacAB transporter system of *N. gonorrhoeae* functionally recognises and expels both ERY and AZM. In wild-type (WT) *N. gonorrhoeae* strains such as FA19, the level of macrolide resistance given by the *macAB* system has been shown to be overshadowed by the activity of MtrCDE, which is also known to be capable of exporting of macrolide antibiotics and has been shown to play a prominent role in development of resistance to macrolides in gonococci (Hagman et al., 1995, Rouquette-Loughlin et al., 2005, Shafer et al., 2001, Zarantonelli et al., 1999). When a guanine (G) is replaced with a thymine (T) nucleotide in the near-consensus -10 sequence of the *macAB* promoter of *N. gonorrhoeae* BR54 strain, it leads to its overexpression. This mutation has demonstrated a remarkable resistance to ERY and AZM despite the strain originally producing a non-functional MtrCDE efflux pump and being super-susceptible to macrolides. This underscores the role of MacAB efflux system in modulating macrolide susceptibility levels in gonococci (Rouquette-Loughlin et al., 2005). The authors concluded that *N. gonorrhoeae* utilises both the MtrCDE and MacAB efflux systems to develop resistance to macrolides and mutations in the promoter region that controls transcription of *macAB* can influence resistance (Rouquette-Loughlin et al., 2005).

The quaternary structure of the *E. coli* MacAB-TolC efflux pump reveals a well-organised efflux machine spanning the cell envelope with specific stoichiometry (Fitzpatrick et al., 2017, Okada and Murakami, 2023). The assembly consists of three TolC, six MacA, and two MacB units. MacB, forming a homodimer, exhibits three domains: NBD, TMD, and PD. The TMD contains four transmembrane segments (TMS 1-4), and the periplasmic loop between TMS 1 and TMS 2 extends into a PD, subdivided into periplasmic N-terminus (PSN) and C-terminus (PSC) subdomains. Notably, the PSN shares structural similarity with the PN and PC subdomains of RND pumps like AcrB, while PSC

shows no such resemblance (Fitzpatrick et al., 2017, Okada and Murakami, 2023). An identified opening between the periplasmic extensions of TMS 1 and TMS 2 in MacB, termed the portal, is proposed as an entry point for large substrates. The MFP MacA bridges the OM channel TolC and the IM dimer of MacB, creating a continuous conduit (Du et al., 2015a, Fitzpatrick et al., 2017). The four domains of MacA include the α-helical hairpin (HP) domain, also known as helix-loop-helix (HLH) in AcrA, for engaging TolC, the lipoyl (LIP) and β-barrel (BB) domains forming a one-way valve, and the membrane proximal (MP) domain contributing to MacB interaction (Fitzpatrick et al., 2017, Okada and Murakami, 2023). The interaction between MacA and TolC is suggested to directly open the TolC channel at its periplasmic end (Fitzpatrick et al., 2017, Lu and Zgurskaya, 2013, Yamanaka et al., 2008). MacB operates through an outward-only mechanism, capturing large substrates from the periplasm via the portal, initiating ATP hydrolysis-induced conformational changes, reducing substrate binding affinity, and expelling the substrate to the exterior (Fitzpatrick et al., 2017, Perez et al., 2015). This mechanism distinguishes MacB from other ABC transporters, emphasising its unique substrate uptake from the periplasm (Fitzpatrick et al., 2017, Okada and Murakami, 2023).

1.3.2 The MFS

MFS transporters are found ubiquitously in the membranes of all types of living organisms and compose the largest superfamily of secondary transporters (Pao et al., 1998, Saier et al., 1999). These proteins utilise power in the electrochemical gradients of either protons and/or sodium ions to transport amino acids, sugars, peptides and drugs, among others, and can act as symporters, uniporters, or antiporters. This superfamily is currently composed of 105 recognised subfamilies (Law et al., 2008, Reddy et al., 2012, Saier et al., 1999, Wang et al., 2020b). Many drug and multidrug transporters are classified within the MFS superfamily, with three drug/H^+ antiporter (DHA) families, i.e. DHA1, DHA2, and DHA3, comprised exclusively of efflux transporters (Paulsen et al., 1996b, Saier et al., 1999). DHA1 and DHA3 families contain transport proteins that display 12 TMS and include several

well-characterised MDR transporters such as MdfA of *E. coli*, LmrP of *Lactococcus lactis* and NorA of *S. aureus* (Debruycker et al., 2020a, Debruycker et al., 2020b, Edgar and Bibi, 1997, Naroditskaya et al., 1993, Ubukata et al., 1989). In contrast, members of the DHA2 family such as QacA/QacB, and EmrB, contain 14 TMS (Lomovskaya and Lewis, 1992, Paulsen et al., 1996a). It is believed that the most abundant MFS transporters, i.e. 12-TMS proteins, have arisen from a single 2-TMS HP that triplicated, giving rise to a protein with 6 TMS which through a duplication event resulted in the formation of 12-TMS proteins (Reddy et al., 2012). Several superfamily and family specific amino acid sequences (motifs) within MFS transporters have been identified (Paulsen et al., 1996b). High conservation of these sequences/motifs within MFS members indicates that they are possibly involved in structural or functional roles. Motifs A and B are known as the MFS-specific motifs, and are common in symporters and antiporters while also conserved in both 12- and 14- TMS families and other families (Paulsen et al., 1996b). Structural analysis of the MFS transporter YjaR demonstrated that residues contained in motif A sense and respond to protonation inside the central cavity (Jiang et al., 2013). Motif C, also known as antiporter motif, is specific for antiporters and found in both 12- and 14- TMS families (Paulsen et al., 1996b, Varela et al., 1995). Exclusive to either 12- or 14-TMS families, motifs D to G have also been identified in MFS transporters (Paulsen et al., 1996b).

Analyses of MFS transporters, including structures of MDR exporters EmrD, LmrP, MdfA, QacA and NorA have resulted in the following postulations: i) MFS transporters generally function as monomers; ii) they have a common structural architecture called the MFS-fold which comprises a 12 TMS core forming two domains (N- and C-domains), each consisting of bundles of six consecutive TMS organised into a pair of inverted “3+3” repeats; iii) the N- and C-domains are related by a pseudo-twofold symmetry axis in the membrane plane and are linked by a long cytoplasmic loop or by two TMS; and iv) a membrane-embedded central cavity is present between these two domains, thus forming the substrate-transport pathway (Abramson et al., 2003b, Debruycker et al., 2020a, Huang et al., 2003, Yan, 2015). In EmrD this central

cavity is quite large and surrounded by hydrophobic and aromatic side-chains (Yin et al., 2006). This is in line with the MdfA structure (Figure 1.1) which also possesses a central cavity of hydrophobic residues (Heng et al., 2015). In EmrD the loops connecting TMS 4 and 5, and TMS 10 and 11 protrude into the cytoplasm, and it is believed they play a role in substrate recognition and capture (Yan, 2015, Yin et al., 2006). The presence of a lipid within the binding cavity of LmrP has been suggested to offer a flexible hydrophobic element, enabling adaptation to diverse substrates, thereby contributing to the broad specificity observed in LmrP and potentially other multidrug transporters (Debruycker et al., 2020a). In NorA, a member of the DHA12 subfamily encoded by all methicillin-resistant *S. aureus* (MRSA), synthetic antigen-binding fragments (Fabs) have been shown to inhibit NorA by inserting a Fab loop into the substrate-binding pocket of NorA, targeting indispensable residues. Peptide mimics of the Fab loop show potent NorA inhibition, synergising with norfloxacin to halt MRSA growth, providing a class of peptide inhibitors that do not require membrane permeability to block antibiotic efflux in MRSA (Brawley et al., 2022).

Alternating access is the widely accepted mechanism of MFS substrate translocation, similar to that proposed for other transport proteins (Abramson et al., 2003a, Kazmier et al., 2017, Ward et al., 2007, Yardeni et al., 2020). Analyses of crystal structures of MFS transporters in multiple conformations (inward-open (C_{in}), occluded, and outward-open (C_{out})) have enabled the elucidation of details of alternating access and energy coupling mechanisms of MFS substrate transport translocation (Abramson et al., 2003b, Dang et al., 2010, Debruycker et al., 2020a, Huang et al., 2003). These analyses suggested that the translocation pathway of the substrate follows the interface between the two six-helices, with the substrate binding pocket located halfway into the membrane (Du et al., 2015b). A rocker-switch type movement mechanism involving successive and concerted conformational changes of the two halves of the protein between C_{in}, occluded and C_{out} states alternately generate a pathway of access to either surface of the membrane (Huang et al., 2003). The transport coupling of MFS proteins occurs through sequential

binding/releasing of substrate/counter-ion and this varies between family members (Du et al., 2015b, Yan, 2015).

Multiple MFS efflux transporters can be found in Gram-negative bacteria (Wang et al., 2020b, Yardeni et al., 2020). In *E. coli* K-12, e.g., 70 MFS proteins have been identified, 15 of which may be considered drug efflux transporters (Reddy et al., 2012). Some of these are present as tripartite systems, as in a similar fashion to the RND systems they use their cognate adaptor protein and the TolC channel. In *E. coli*, e.g., EmrB (occurring with the cognate adaptor EmrA), and EmrY (with EmrK) are believed to be involved in the efflux of uncouplers and other substrates (Lomovskaya and Lewis, 1992). In contrast, MdfA is a singlet pump that has been studied extensively (Li et al., 2015). This Chapter provides detailed explanations of two MFS efflux transporters: MdfA, a widely studied multidrug resistant antiporter, and FarB, a transporter found in *N. gonorrhoeae*.

1.3.2.1 The *E. coli* MdfA protein

The MdfA protein is an MDR efflux pump encoded on the *E. coli* chromosome (Edgar and Bibi, 1997). This 410 amino-acid-protein provides resistance to various unrelated compounds, including lipophilic compounds like tetraphenylphosphonium (TPP), EtBr, daunomycin, rhodamine 6G (R6G), TET, rifampin (RIF), puromycin, and benzalkonium (BC), as well as several clinically important antibiotics such as CHL, ERY, fluoroquinolones, and aminoglycosides like neomycin and kanamycin (Kan) (Edgar and Bibi, 1997). In some cases, MdfA is also responsible for MDR in *E. coli* strains isolated from hospitalised patients due to overexpression of *mdfA* carried on conjugative plasmids (Wang et al., 2013). Furthermore, MdfA orthologs have been identified in various pathogenic bacterial species (Lewinson et al., 2004).

MdfA, a substrate/H^+ antiporter, utilises the PMF to transport its substrates (Edgar and Bibi, 1997). The transport mechanism of MdfA has been found to be ΔpH-dependent for monovalent cations, but electrogenic for uncharged compounds such as CHL (Lewinson et al., 2003). MdfA has been suggested to have a role in pH homeostasis by acting as a Na^+ or K^+-dependent proton

antiporter, which enables *E. coli* to grow at an alkaline pH of 9.5 (Lewinson et al., 2004). For multidrug/proton antiport, it has been proposed that there is an indirect competition between substrate and proton where both compete for binding to MdfA, and two acidic residues (E26 and D34) have been identified as important in this competition (Fluman et al., 2012). In contrast to other antiporters such as the Na^+/H^+ antiporter NhaA, where similar substrates use a common binding site, MdfA has been shown to have separate binding sites for proton and substrate (e.g., TPP) but with a competitive nature of binding (Fluman et al., 2012, Padan et al., 2009). MdfA exchanges a single proton for a single monovalent substrate, while translocating divalent cations has been suggested to be energetically unfavourable (Fluman et al., 2014). However, MdfA is able to export divalent cations such as chlorhexidine (CH) that have a unique structural architecture by adopting a processive-like mode of action, involving the exchange of two protons for one substrate molecule, thus expanding the substrate spectrum of multidrug transporters (Fluman et al., 2014). These findings suggest that MdfA is structurally flexible and can recognise dissimilar substrates through its conformationally sensitive multidrug binding pocket in a similar manner (Fluman et al., 2009).

In 2015, three crystal structures of MdfA in C_{In} conformation were reported, all of which were bound to ligands at high resolution (Heng et al., 2015). These structures represented the first of their kind for an MFS antiporter protein in complex with compounds, and were obtained using a MdfA(Q131R) mutant (Heng et al., 2015). The ligands included the substrate CHL, and substrate analogues deoxycholate (Dxc) and n-dodecyl-N,N-dimethylamine-N-oxide (LDAO) (Heng et al., 2015). Despite differences in ligand structure, all three protein structures were almost identical and revealed details of the MFS antiporter architecture (Heng et al., 2015). MdfA confirmed as consisting of 12 TMS, with TMS 1-6 forming the N-domain and TMS 7-12 forming the C-domain (Heng et al., 2015). A 12-residue amphipathic helix (α_{6-7}) connected these two domains (Heng et al., 2015). MdfA was also found to have four pseudo-symmetrical repeats of three helices, with the first helix of each repeat (TMS 1, 4, 7, and 10) forming the central substrate-binding cavity (Heng et al., 2015). The second helix of each repeat (TMS 2, 5, 8, and 11) was long and curved

and referred to as rocker helices, while the third helix of each repeat (TMS 3, 6, 9, and 12) was shorter and straighter, and referred to as support helices (Heng et al., 2015). The two previously identified proton-titratable residues (E26 and D34) were found inside the central cavity and served as potential protonation sites (Heng et al., 2015). The central cavity was large, with an area of approximately 3000 $Å^3$, and was hydrophobic in nature, consistent with the hydrophobic substrates that MdfA transports (Edgar and Bibi, 1997, Heng et al., 2015).

At the apex of the central cavity where D34 resides, all three ligands bind using their polar or positively charged groups, while residues from the hydrophobic cavity wall interact with the hydrophobic parts of these ligands. Twelve residues within this cavity, including Y30, N33, and D34 from the MFS motif D, were found to contribute to the binding of CHL. These residues come from the cavity helices (TMS 1, 4, and 7) and rocker helices (TMS 2 and 5) and are mostly conserved among MdfA orthologs (Heng et al., 2015). It has been suggested that the hydrophobic residues lining the side walls of the substrate-binding cavity in MdfA are a similar feature to the substrate recognition mechanism of poly-specific multidrug-binding proteins of the soluble QacR/TetR (tetracycline resistance) repressor family (Alguel et al., 2007, Grkovic et al., 2003, Schumacher et al., 2001).

The mechanism of the transport cycle of MdfA has been proposed based on crystal structure analysis and biochemical experiments (Heng et al., 2015). The conformational change of the transporter is suggested to be more dependent on the protonation status of titratable residues, particularly D34, than substrate binding mode (Heng et al., 2015, Lu et al., 2013a). The C_{In} and C_{Out} states of MdfA are thermodynamically favoured by the interaction between protonation site(s) and membrane potential (Heng et al., 2015, Lewinson et al., 2003). Deprotonation of D34 upon substrate binding triggers the C_{In} to C_{Out} conformational change in electrogenic transport, while binding of a positively charged substrate induces deprotonation of D34 in electroneutral transport (Heng et al., 2015). The protonation and membrane potential interaction are

considered the major driving force for conformational changes in MdfA and other proton motive force-driven antiporters (Heng et al., 2015).

The MdfA transporter undergoes conformational changes in its N- and C-domains in the membrane when transitioning from the C_{in} state to the C_{out} state (Nagarathinam et al., 2018). The TMS 5 region exhibits significant deviations as a kink and twist before motif C of the transporter. The N-domain hydrophobic core involves a hydrophobic cluster near the periplasmic face and a residue R112 that exhibits small rearrangements. The cytoplasmic loop of the C-domain reorganises to accommodate closure of the transporter from the cytoplasm (Nagarathinam et al., 2018). MD simulations indicate that the C_{out} state can transition to an occluded conformation in which both cytoplasmic and periplasmic entrances are closed when D34 is protonated (Nagarathinam et al., 2018). The single-molecule fluorescence resonance energy transfer (smFRET) analysis reveals that the detergent solubilised MdfA is in equilibrium between its two major conformational states (C_{In} and C_{out}) in the absence of any substrate (Zhu et al., 2019). Addition of the electroneutral substrate CHL stabilises the C_{In} conformation, while binding of the electrogenic substrate TPP+ stabilises the C_{out} conformation and increases the transport rate (Zhu et al., 2019). The substrate-responsive lateral gate that is open to the inner leaflet of the CM and closes upon drug binding has been identified (Zhu et al., 2019). The electrostatically asymmetric rim of MdfA plays an important role in multidrug recognition, conformational behaviour, and transport activity of this antiporter (Zomot et al., 2018). The deviation of MdfA from the canonical alternating access mechanism of drug transport by MFS transporters suggests that large-scale conformational changes are not induced by the substrate TPP or by protonation (Yardeni et al., 2020).

This review of the literature on the MdfA protein serves to provide a comprehensive understanding of multidrug efflux mechanisms. The MdfA protein, identified as a member of the MFS superfamily transporter, showcases the intricate interplay between substrate binding, protonation, and conformational changes. By elucidating its structural flexibility and substrate recognition capabilities, this research sheds light on how multidrug efflux

operates within the context of the MFS superfamily transporters. Furthermore, it holds broader implications for comprehending bacterial efflux transporters, including RND pumps like the MtrD protein in *N. gonorrhoeae*. By utilising the insights gained from the MdfA protein research, this section aims to enhance our understanding of the multidrug resistance mechanisms utilised by the MtrD protein in *N. gonorrhoeae*, thus contributing to a more profound comprehension of bacterial efflux transport and its significance in addressing antibiotic resistance.

1.3.2.2 The *N. gonorrhoeae* MFS FarAB-MtrE system

Miller et al., examined how different fatty acids (FAs) affect the growth, oxygen consumption, and *in vitro* reduced nicotinamide adenine dinucleotide oxidase activity of *N. gonorrhoeae* (Miller et al., 1977). Saturated FAs had an inhibitory effect on growth, and the level of inhibition increased as the FA chain length increased, up to palmitic acid (PA) (C16) (Miller et al., 1977). In 1983, McFarland discovered that certain clinical strains exhibited resistance to long-chained FAs but remained susceptible to other hydrophobic antimicrobials (HAs) such as ERY, Triton X-100 (TX-100), and crystal violet (CV). Previous research had already established a connection between resistance to these compounds and specific mutations in the *mtr* locus within gonococci (Maier et al., 1975, McFarland et al., 1983, Sparling et al., 1975). These strains were suggested to have a mechanism independent of *mtr* to resist long-chained FAs (Shafer et al., 2001). Interestingly, the long-chained FAs such as PA, oleic acid, and linoleic acid are part of innate mucosal defence (Fischer, 2020, Mahlapuu et al., 2016, Morse et al., 1982, Porter et al., 2015, Sierra et al., 2017, Unemo et al., 2019b).

The *farAB* locus, which has been ascribed responsible for resistance to FAs, was identified and named in 1999 (Lee and Shafer, 1999). It consists of two genes, *farA* and *farB*, that are organised in tandem and separated by 23 bp, forming a single transcriptional unit (Lee and Shafer, 1999). The FarA MFP, encoded by *farA*, contains 394 amino acids and has a molecular weight of 42.5 kDa (Lee and Shafer, 1999). It shows a strong similarity to EmrA and EmrK of *E. coli*, VceA of *V. cholerae*, and EmrA of *Haemophilus influenzae*, especially

in the C-terminus region of these proteins (Lee and Shafer, 1999). The *farB* gene encodes the FarB CM-bound antiporter protein, which contains 504 amino acids and has a molecular weight of 54.8 kDa (Lee and Shafer, 1999). FarB belongs to the MFS superfamily of transporter proteins and is predicted to have 14 TMS topology (Lee and Shafer, 1999). It is similar to the *E. coli* EmrB and the *Vibrio cholerae* VceB efflux transporter proteins (Colmer et al., 1998, Lee and Shafer, 1999, Lomovskaya and Lewis, 1992).

Similar to other multicomponent systems, FarB is believed to form a tripartite efflux pump system utilising the MFP FarA and the OM channel MtrE. Mutational analyses of FA19 strain derivatives have revealed that MtrE functions as the partner protein for the Far system, forming a pathway for extruding substrates into the external environment (Delahay et al., 1997, Lee and Shafer, 1999). Additionally, the *farAB* operon expression is positively regulated by the MtrR protein (Johnson and Shafer, 2015, Lee and Shafer, 1999). This regulation has been shown to be indirect and occur via the direct transcriptional repressor of *farAB*, FarR which is itself subject to repression by MtrR (Lee et al., 2003, Lee and Shafer, 1999).

Collectively, the gonococcal response to the presence of HAs, including toxic FAs, in their environment is mediated by the *far*- and *mtr*-encoded efflux pumps. These two efflux systems seem to operate independently. The autoregulatory activity of FarR can also upregulate the *far* operon by supressing its own expression. This mechanism of MtrR regulation of two efflux pump operons in opposite ways possibly harmonies gonococci response when confronting toxic FAs, e.g., during faecal infection, ensuring that detrimental effects of overproduction of efflux pumps is minimised (Lee et al., 2003).

In addition to shedding light on the intricate mechanisms of efflux pumps in *N. gonorrhoeae*, the insights gained from studying the *N. gonorrhoeae* MFS FarAB-MtrE system hold significant implications for our understanding of AMR in this pathogen. The intricate interplay between the *far*- and *mtr*-encoded efflux pumps, regulated by transcriptional factors like MtrR and FarR, underscores the adaptable nature of *N. gonorrhoeae* in countering the challenges posed by toxic FAs and HAs.

1.3.3 The MATE family

MATE proteins are found in all kingdoms of living organisms, contributing to a variety of fundamental biological processes (Brown et al., 1999, Huang et al., 2021, Ito et al., 2010, Kar et al., 2022, Maron et al., 2010, Omote et al., 2006, Rogers et al., 2009, Yonezawa and Inui, 2011, Zhang et al., 2014). Discovered over 20 years ago, the MATE family comprises more than 1000 transport proteins that can be categorised into three main groups, the NorM, DNA damage-inducible protein F (DinF), and eukaryotic subfamilies, which are further subdivided into 14 subfamilies (Brown et al., 1999, Hvorup et al., 2003, Morita et al., 1998, Omote et al., 2006, Saier, 2023). Bacterial MATE transporters are grouped in family 1 represented by *Vibrio parahaemolyticus* NorM as the prototypic MATE transporter (Kaatz et al., 2005, Morita et al., 2000, Morita et al., 1998). Eukaryotic MATE transporters are grouped in family two and include yeast and fungi, plant, animals, and protozoan MATEs (Masuda et al., 2006, Morita et al., 2009, Otsuka et al., 2005a, Takanashi et al., 2014, Tanihara et al., 2007, Thompson et al., 2009). Other bacterial MATEs and archaebacterial MATEs are classified in family 3 (Brown et al., 1999, Omote et al., 2006). Plants possess a considerably greater quantity of MATE genes compared to microorganisms and animals (Upadhyay et al., 2019). A highly conserved sequence “GKFGXP” has been identified in the members of family 1 (previously cluster 1) (Miyamae et al., 2001). These transporters use the membrane gradient of Na^+, H^+, or both, as an energy source for driving export of cationic compounds (Brown et al., 1999). Examples of H^+-driven MATE transporters are human MATE1 and human MATE2 antiporters, whereas the bacterial MATE transporters, NorM from *N. gonorrhoeae* (NorM_NG), *V. cholerae* (NorM_VC), and *V. parahaemolyticus* (NorM_VP) are examples that harness the energy stored in Na^+ electrochemical gradient for driving efflux (He et al., 2010, Masuda et al., 2006, Morita et al., 1998, Otsuka et al., 2005b, Rouquette-Loughlin et al., 2003). NorM_VP was the first MATE protein identified (Morita et al., 1998). When expressed in *E. coli* NorM_VP confers resistance to norfloxacin (NOR) and CIP, as well as structurally unrelated compounds ET, Kan, and streptomycin (Morita et al., 1998). Other MATE members, including NorM_NG, *E. coli* YdhE, and *S. aureus* MepA

proteins have been well characterised, with extensive substrate profiles identified (Kaatz et al., 2005, Long et al., 2008, McAleese et al., 2005). MATE protein substrates are typically cationic and polyaromatic, although they show chemically distinct structures (Lu et al., 2013a). Plant MATE transporters play a crucial role in accumulating diverse metabolites within organelles, notably vacuoles, facilitating xenobiotic detoxification, aluminium tolerance, disease resistance, iron homeostasis, regulation of cell and organ size and hormone transport (Upadhyay et al., 2019). Conversely, human MATE transporters are expressed in the brush-border membrane of the kidney, aiding in the elimination of cationic drugs from the body (Kusakizako et al., 2020).

Most proteins within the MATE family typically consist of 400-550 amino acids, featuring 12 TMS (Saier et al., 2009). They exhibit approximately 45% similarity suggesting the presence of shared structural and functional characteristics (Saier et al., 2009). Despite the common 12 TMS architecture among MATE transporters, their topology differs from that of other transporters including MFS (Kusakizako et al., 2020). Mammalian MATE transporters possess an additional helix, TMS 13, on the C-terminus side (Lu, 2016). MATE transporters function as antiporters that couple substrate export to inwardly-directed Na^+ or H^+ gradients (Kuroda and Tsuchiya, 2009). Crystal structures from various transporter families, including the MATE family, along with biophysical studies have supported the fundamental elements of the alternating access mechanism (Claxton et al., 2021, Drew and Boudker, 2016, Jia et al., 2020). These structures have captured different predicted conformational states and revealed the relative positions of substrate and ion binding sites. Most crystal structures of the MATE family have exhibited a C_{out} conformation, indicating that these C_{out} intermediates are energetically favoured in crystal lattice formation (Claxton et al., 2021). Simulations have shown water penetration in the central cavity in the C_{out} conformation of multiple MATE representatives, reaching into the middle of the lipid bilayer (Krah et al., 2020, Leung et al., 2014, Zakrzewska et al., 2019).

Unlike the other well-studied antiporters such as EmrE (Section 1.3.4), the ion and substrate binding sites in NorM transporters do not overlap, suggesting

a departure from the classical exchange mechanism (Claxton et al., 2021, Schuldiner, 2014). This leads to a proposed allosteric mechanism of “indirect competition”, where global changes in protein structure induce ion-substrate competition to promote efflux (Claxton et al., 2021). In DinF transporters from *Pyrococcus furiosus* (PfMATE), and the structure of the H^+-coupled transporter from *Bacillus halodurans* (DinF-Bh), crystal structure analysis implies a direct competition mechanism, where protonation of D40 is suggested to facilitate substrate release from the C_{out} state into the extracellular milieu through the C-terminus crevice (Lu et al., 2013a, Tanaka et al., 2013). A C_{in} conformation from PfMATE and a predicted C_{in} conformation from NorM-NG support the presence of a rocker switch mechanism (Radchenko et al., 2016). Hydrogen-deuterium exchange mass spectrometry (HDX-MS) revealed that the *Pseudomonas stutzeri* (NorM-PS) transporter adopts a C_{out} conformation upon substrate binding, with specific changes in deuterium uptake along specific periplasmic helices (Eisinger et al., 2018, Nie et al., 2016). DEER spectroscopy in PfMATE confirmed an C_{out}/C_{in} conformational switch, driven by H^+ and substrate binding (Claxton et al., 2018). The cytoplasmic gate of PfMATE, modulated by E163, suggests a release mechanism upon protonation (Jagessar et al., 2020). Overall, the conservation of key residues and mechanistic insights across MATE transporters, including eukaryotic members, highlights shared principles in alternating access mechanisms (Claxton et al., 2021).

1.3.3.1 The *V. cholerae* NorM protein

With a unique topology, NorM_VC was the first member of the MATE family whose cation-bound crystal structures were solved with and without substrate (rubidium) (Figure 1.1) (He et al., 2010). Like other MATE transporters, these crystal structures unveil a membrane-spanning protein comprised of two sets of 6-TMS bundles (TMS 1-6 and TMS 7-12), creating a V-shaped large internal cavity accessible from the extracellular space (C_{out}) (Claxton et al., 2021, He et al., 2010). These two halves of the protein exhibit an intramolecular two-fold symmetry, suggesting their origin from gene duplication events (Brown et al., 1999, He et al., 2010, Kusakizako et al., 2020, Omote et al., 2006). Connecting

these two halves is a cytoplasmic loop, reminiscent of what is observed in MFS transporters (Section 1.3.2) (Brown et al., 1999, Omote et al., 2006). The first helix of each segment (TMS 1 and TMS 7) is preceded by an extended helical region originating from the inner membrane leaflet (He et al., 2010, Kusakizako et al., 2020). In contrast to MFS transporters, the symmetrical helices TMS 1 (N-terminus) and TMS 7 (C-terminus) establish packing interactions with helices in the opposite lobe within the inner membrane leaflet (Claxton et al., 2021, Kusakizako et al., 2020). Furthermore, an extra helix following TMS 12 is situated beneath the cytoplasmic side of TMS 11 (He et al., 2010). Within the lipid bilayer of the cell membrane, two distinct substrate passages are present on opposite sides of the protein, opening towards the outer leaflet (He et al., 2010, Kusakizako et al., 2020). These passages facilitate the extrusion of substrates to the external environment. Residues lining the internal cavity exhibit considerable conservation and are contributed by all TMSs, except for TMS 3 and TMS 9, which are situated at the periphery in this conformation (He et al., 2010, Kusakizako et al., 2020). In addition, the monocation (Na^+), a lighter analogue of rubidium (Rb^+), binding site with 9 amino acids implicated in the binding was identified in the internal cavity suggesting that the C_{out} conformation favours high affinity binding of monocations such as Na^+, and low affinity binding for substrates (He et al., 2010, Kusakizako et al., 2020). Notably, this topology differs fundamentally from that observed in MFS transporters (Claxton et al., 2021, He et al., 2010). Residues E255 and D371, lining the internal cavity within the C-terminal half of the protein, have been proposed to play a crucial role in cation recognition, binding, and the transport cycle in NorM-VC (He et al., 2010). HDX-MS indicates that these residues are crucially engaged in substrate recognition and the substrate binding site might be situated in close proximity to these residues (Eisinger et al., 2018). The electrostatic milieu provides a conducive setting for the binding of the substrate and counter cation within the pocket (Kusakizako et al., 2020). These structural insights have revealed that unlike proteins from the RND transport family, which employ a periplasmic domain for substrate binding, MATE transporters, along with other MDR transporters from ABC, MFS, SMR, PACE, and AbgT families, possess poly-specific drug binding sites comprised of TMS

embedded within the lipid bilayer (He et al., 2010, Kusakizako et al., 2020). Despite significant primary sequence divergence, the common theme of proteins from these transporter families appears to involve the capture and expulsion of substrates directly from the inner to the outer membrane leaflet through portals that face the lipid bilayer (Claxton et al., 2021, He et al., 2010). More information on how MATE antiporters achieve multidrug recognition of structurally diverse compounds and how they couple antimicrobial agents' efflux with influx of counter ions come from NorM_NG crystal structures explained in the next section.

1.3.3.2 The *N. gonorrhoeae* NorM protein

The *norM* gene spans 1380 bp and encodes a 459-amino-acid efflux MATE transporter that belongs to family 1 (Rouquette-Loughlin et al., 2003). The NorM_NG transporter has been demonstrated to give resistance to various antimicrobials, including ET, ACR, 2-N-methylellipticinium, berberine, and fluoroquinolones (Rouquette-Loughlin et al., 2003). It has been demonstrated that the presence of a positively charged moiety on NorM substrates, such as CIP and NOR (at physiological pH), is crucial for recognition by NorM_NG (Rouquette-Loughlin et al., 2003). Expression of NorM_NG in the heterologous host *E. coli* has shown elevated resistance to the antimicrobial compounds just mentioned and R6G, CV, TPP, doxorubicin, novobiocin (NOV), and the fluoroquinolone enoxacin (Long et al., 2008). Additionally, a study by Long et. al. revealed that NorM_NG functions as a Na^+/drug antiporter, while efflux is also influenced by the integrity of PMF of the CM (Bay and Turner, 2009, Long et al., 2008).

The crystallographic study of NorM_NG yielded four structures complexed with different substrates; ET, R6G, TPP, and Cs+ (a Na^+ congener), all exhibiting an extracellular-facing, Na^+-free, and drug-bound state (Lu et al., 2013b). The 12-TMS antiporter forms a chalice-shaped complex, with two similarly folded N and C-terminal domains connected by 11 intracellular and extracellular loops, resembling other MATE transporters (Lu et al., 2013b). A drug-binding central cavity is formed between the N- and C-terminal domains (Lu et al., 2013b). Notably, the architecture of the central cavity and charge

distribution favour cationic substrates over hydrophobic compounds (Lu et al., 2013b). An opening flanked by loops L3-4 and L9-10 provides a passage for Na^+ and drug entry (Lu et al., 2013b). Residues D41, D355, and D356 confer electrostatic interactions within the drug binding site, while charge-dipole interactions and limited hydrophobic interactions contribute to substrate binding (Lu et al., 2013b). Mutagenesis experiments pinpoint D41, F265, Q284, D355, and D356 as crucial for drug transport (Lu et al., 2013b). The N- and C-domains are separated by intracellular Loop L6-7, and the central cavity, with its bottom located about halfway through the membrane bilayer, is shielded from the cytoplasm. The central cavity is formed with many conserved or semiconserved residues and has an excess of negative charges and relatively limited hydrophobic residues, which explains why the transporter prefers cationic substrates and shows reduced affinity for hydrophobic compounds (Lu et al., 2013b). An opening to the periplasmic side is seen in the structure flanked by loops L3-4 and L9-10 that may facilitate entry of Na^+ and exit of drugs (Figure 1.2) (Erkens et al., 2011, Lu et al., 2013b).

The proposed antiport mechanism involves Na^+ triggering conformational changes that lead to drug release (Lu et al., 2013b). Interestingly, crystallisation of NorM_NG with Cs^+ revealed an alternate conformation where both a drug and a counterion can bind simultaneously, deviating from conventional antiport mechanisms (Lu et al., 2013b). The antiport function is believed to rely on Na^+-induced rearrangements of transmembrane helices, causing substrate release (Lu et al., 2013b). Notably, DinF-Bh MATE transporter proposes a different antiport mechanism where H^+ and substrate compete for binding (Lu et al., 2013a). This antiport mechanism was supported by the observation that protonation of D41 leads to substrate extrusion in a PfMATE transporter (Tanaka et al., 2013). Functional analyses also suggest that NorM_NG alternates between extracellular- and intracellular-facing conformations during substrate export (Lu, 2016, Radchenko et al., 2016).

In summary, the NorM MATE transporter proteins exhibit remarkable resistance to antimicrobials through their complex structure and functional mechanisms. The interplay between conformational changes, ion

coordination, and substrate recognition sheds light on the intricate workings of this transporter family.

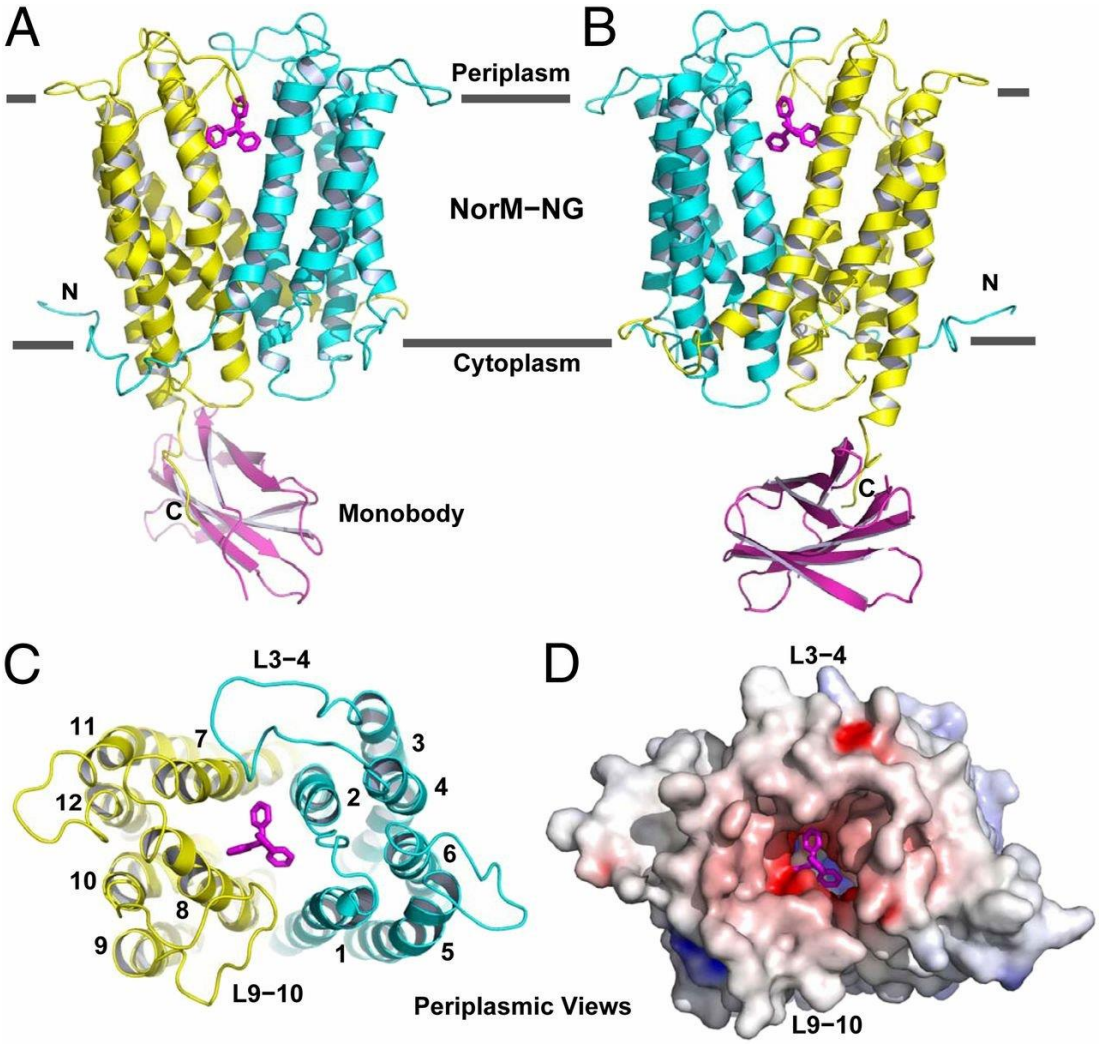

Figure 1.2: NorM-NG structure overview.

(A and B) Representation of the NorM-NG monobody complex structure, observed from the membrane plane. The monobody is depicted as a magenta ribbon, with the bound TPP illustrated as magenta sticks. (C) Illustration displaying the arrangement of TMSs in NorM-NG, observed from the periplasmic side. (D) Surface visualisation of NorM-NG from the periplasmic side. Adapted from Lu et al., 2013b**,** with permission from the Proceedings of the National Academy of Sciences (PNAS).

1.3.4 The SMR family

The SMR family of transporters, known for their compact size and multifunctional role in bacterial resistance, has garnered significant attention. This section of the thesis searches into the nuances of SMR family transporters, examining their classification, structural characteristics, transport mechanisms, and broader implications in the context of bacterial resistance.

The SMR family encompasses a group of compact transport proteins distinguished by their concise amino acid sequences, typically consisting of 100-150 amino acids and forming four TMSs (Bay et al., 2007, Burata et al., 2021, Burata et al., 2022, Chung and Saier, 2001, Macdonald et al., 2020, Paulsen et al., 1996c). These integral membrane proteins play a pivotal role in conferring bacterial resistance against a diverse range of compounds (Bay et al., 2007). Among the substances they can expel are biocides, such as quaternary ammonium compounds (QAC), also called quaternary cationic compounds (QCC); lipophilic aromatic compounds like DNA intercalating dyes, limited antibiotics, as well as potentially toxic metabolic by-products and polyamine compounds (Gillings, 2017, Kermani et al., 2020, Pal et al., 2015). Additionally, certain SMR members act as glycolipid flippases (Burata et al., 2022). In general, the proteins of the SMR family facilitate the transport of positively-charged solutes across the membrane utilising the bacterial PMF to achieve substrate transportation in a 2:1 H^+:substrate antiport manner (Chung and Saier, 2001, Grinius et al., 1992, Macdonald et al., 2020, Paulsen et al., 1996c, Schuldiner et al., 2001, Yerushalmi and Schuldiner, 2000b). Additionally, the lipophilicity of a drug determines its potential as an SMR substrate (Macdonald et al., 2020). Furthermore, research findings have consistently demonstrated that the SMR transporters commonly exhibit a notable functional promiscuity as a general characteristic (Jurasz et al., 2021, Kermani et al., 2020).

The genes encoding SMR proteins are frequently found on mobile gene arrays, such as class I integrons and MDR plasmids, providing bacteria with a selective advantage, promoting adaptation, and driving the spread of resistance genes among bacteria (Bay and Turner, 2009, Lewis, 1994,

Littlejohn et al., 1991, Lyon and Skurray, 1987, Paulsen and Skurray, 1993, Paulsen et al., 1996c, Purewal, 1991, Sasatsu et al., 1989, Yerushalmi et al., 1995). Consequently, this adaptation can lead to the concurrent selection of genes that confer resistance to clinical antibiotics (Kermani et al., 2020, Pal et al., 2015, Wales and Davies, 2015).

The SMR family, previously recognised as having the smallest membrane transport proteins until the discovery of the PACE transporter family, is a part of the larger Drug/Metabolite Transporter (DMT) superfamily consisting of 44 known families (Hassan et al., 2013, Jack et al., 2001, Paulsen et al., 1996c, Saier, 2023, Yen et al., 2010). The family can be divided into three distinct subfamilies: the small multidrug proteins (SMPs), paired small multidrug resistance (PSMRs), and suppressors of *groEL* mutations (SUGs) (Bay et al., 2007). Each subfamily serves unique roles in bacterial resistance mechanisms and other roles (Bay et al., 2007).

The SMP subfamily, represented by *E. coli* EmrE, imparts resistance to a broad spectrum of lipophilic cationic compounds (Bay and Turner, 2016, Paulsen et al., 1996c). Deletion of the *emrE* gene has been shown to influence *E. coli* biofilm formation, pH, and the osmotic stress response in addition to resistance to toxic compounds (Bay et al., 2017, Matsumura et al., 2011, Nishino et al., 2009). Other SMP members, including *A. baumannii* AbeS, *P. aeruginosa* EmrE, *S. aureus* QacC (also called Smr), and *Mycobacterium tuberculosis* Smr contribute to broad drug resistance by forming functional homooligomers (Bay and Turner, 2016). SMP members carried by mobile genetic elements, e.g., the *S. aureus* QacC transporter, are commonly identified as Qac efflux pumps due to their capacity to grant resistance against such harmful compounds (Bay and Turner, 2016, Paulsen et al., 1995). Homologous to suppressor of *groEL* mutation protein E of *E. coli* (Eco-SugE), the SUG subfamily, similar to SMP, confers resistance to a limited range of QCCs (Bay et al., 2007, Chung and Saier, 2002, Greener et al., 1993). However, its members show diverse heritability and potential involvement in bacterial protein folding (Bay and Turner, 2016). It's worth noting that the latter role was not confirmed in subsequent studies discussed later in this section.

The PSMR subfamily, distinctive in its requirement for simultaneous expression of two SMR gene copies for drug resistance, encompasses a diverse range of members with unique insertion orientations and roles (Bay et al., 2007, Kikukawa et al., 2007, Kikukawa et al., 2006, Zhang et al., 2007). Phylogenetic analysis reveals that PSMR members evolved from gene duplication events, as observed with *B. subtilis* EbrAB and *E. coli* MdtIJ/YdgEF (Bay and Turner, 2009, Paulsen et al., 1996c).

A recent study has revealed that SMR transporters can be categorised into four distinct functional subtypes: guanidinium exporters (Gdx), quaternary ammonium cation exporters (Qac), polyamine transporters, and glycolipid flippases (Burata et al., 2022). While the two major subtypes, Gdx and Qac, do not overlap in terms of physiological roles, they do export a common subset of hydrophobic cationic compounds (Kermani et al., 2018). Additionally, they exhibit high sequence identity and similarity (Kermani et al., 2020). These four functional subtypes are elaborated below.

The Gdx subtype of SMR proteins, although common in bacterial genomes, was initially characterised with incomplete understanding (Bay and Turner, 2016, Kermani et al., 2018). Originally linked to the chaperone GroEL (Greener et al., 1993), these proteins were later recognised for their role in guanidinium ion (Gdm^+) export rather than GroEL interactions (Kermani et al., 2018). Gdx proteins are involved in the export of Gdm^+, a small byproduct of nitrogen metabolism, known since the late 1800s, but these proteins also transport hydrophobic guanidinium compounds (Kermani et al., 2020, Kermani et al., 2018, Nelson et al., 2017). Nevertheless, Gdx transporters prevent the export of naturally occurring guanidinium-substituted metabolites (Kermani et al., 2020). Co-localisation of genes for Gdx members with horizontal gene transfer elements suggests their involvement in drug resistance (Slipski et al., 2019). The crystal structures of a protein from *Clostridales* oral taxon 876 (Gdx-Clo) provided insights into the SMR family's structural features, including the antiparallel topology wherein the two monomers (also called subunits A and B) are assembled as an asymmetric homodimer with a spacious aqueous cavity opened to one side of the membrane (Kermani et al., 2020). Each dimer

subunit consists of two distinct lobes (labelled as Lobe 1 and Lobe 2), separated by a conserved GIG motif serving as a fulcrum in TMS 3. Within the cavity, there are two highly conserved glutamates, also called central glutamates, (E13 in each subunit) that serve as binding sites for substrate and proton molecules (Kermani et al., 2020, Muth and Schuldiner, 2000, Saleh et al., 2018, Yerushalmi and Schuldiner, 2000b).

The mechanism of transport through antiparallel SMR proteins entails a conformational exchange between the two distinct monomers (Kermani et al., 2020, Wu et al., 2019, Yerushalmi and Schuldiner, 2000a). This action seals the substrate binding site on one membrane side while simultaneously unveiling an identical site on the opposing side (Dutta et al., 2014, Kermani et al., 2020, Morrison et al., 2012). This process is facilitated by the antiparallel dual topology, rendering the C_{in} and C_{out} conformations indiscernible (Kermani et al., 2020). Notably, TMS 3 features two GxxAxxG helical packing motifs, with G_{64}IG at the midpoint of the helix acting as a pivot between the N- and C-terminal domains (Kermani et al., 2020). This pivotal region, conserved as G_{64}VG in EmrE, contributes to the conformational exchange observed in Gdx transporters (Kermani et al., 2020). Also, T63 before GIG can bond with the main chain, impacting helix shape; mutating the equivalent EmrE serine disrupts conformational dynamics (Wu et al., 2019). Furthermore, an additional mechanism known as the "tyrosine switch," involving Y59, also contributes to this conformational exchange (Kermani et al., 2020). The details of the tyrosine switch mechanism will be discussed in the context of the Qac subtype.

The crystal structure of Gdx-Clo complexed with phenylGdm$^+$ substrate reveals insights into SMR protein substrate binding, with $E13_B$ (E13 from subunit B) coordination and a stack of conserved hydrogen bond donors and acceptors ($W62_B$, $S42_B$, and $W16_B$) stabilising $E13_B$ (Kermani et al., 2020). W62 and S42's conservation is linked to substrate specificity, while $E13_A$ and universally conserved Y59 are crucial for phenylGdm$^+$ translocation, involving guanidinium group competition for $E13_A$ and displacement of $Y59_B$ to initiate transport motion (Brill et al., 2015, Kermani et al., 2020, Rotem et al., 2006, Vermaas et al., 2018).

The structure also revealed a membrane portal, suggesting substrate access from the membrane interior (Kermani et al., 2020). This portal could be significant in addressing environmental challenges posed by hydrophobic guanidinium compounds like biocides and pharmaceuticals in wastewater and runoff (Kermani et al., 2020). The Qac subtype of SMR transporters is known for its role in bacterial multidrug resistance and resistance to common antiseptics (Kermani et al., 2020, Macdonald et al., 2020, Pal et al., 2015, Paulsen et al., 1996b, Wales and Davies, 2015). As observed in proteins of the SMP subfamily, the Qac subtype includes promiscuous exporters that confer resistance against antiseptic QACs and a variety of structurally diverse polyaromatic cationic compounds, such as ET (Bay et al., 2007, Paulsen et al., 1996b, Russell, 2002). They are linked to multidrug resistance gene arrays and have exhibited dynamic associations with resistance genes over time (Gillings, 2017, Russell, 2002, Zhu et al., 2017).

The well-studied EmrE variant from *E. coli*, as previously mentioned, is a bacterial multidrug exporter representative of this subtype (Kermani et al., 2022). It has been the subject of numerous studies by various laboratories, with the aim of analysing its biochemical and structural complexities (Korkhov and Tate, 2008, Morrison and Henzler-Wildman, 2014). Its antiparallel architecture, helical connectivity, and protein fold were established through low-resolution electron microscopy (Ubarretxena-Belandia et al., 2003). The latest high-resolution crystallographic analyses of EmrE in the presence of different substrates, as well as in its apo form, have unveiled its structural characteristics and binding mechanisms (Kermani et al., 2022). This arrangement exhibits significant structural resemblance to Gdx-Clo, albeit with distinct variations in the hydrogen bonding network within the substrate-binding site (Kermani et al., 2022). Notable differences in subunit packing are evident (Kermani et al., 2022). Both monomers A and B adopt dissimilar structures, differing in the orientation of their lobes around the conserved GVG motif in helix 3. This architecture aligns with the proposed conformational exchange of two distinct monomers (Morrison et al., 2012). The central glutamates in the binding pocket (E14 in EmrE), the tyrosine switch (involving Y60), the GXG fulcrum, and the hydrophobic portal are shared features with

the Gdx subtype (Kermani et al., 2022, Muth and Schuldiner, 2000, Saleh et al., 2018, Schuldiner et al., 2001, Yerushalmi and Schuldiner, 2000b). Additionally, S64, akin to T63 in Gdx, is positioned immediately before the GVG fulcrum, forming hydrogen bonds between subunit sidechains, potentially pivoting conformational changes in the transport cycle (Kermani et al., 2022).

The sidechain movement and hydrogen bonding interactions influence substrate transport by EmrE in comparison to Gdx-Clo. The crystal structures of EmrE with various substrates reveal that despite considerable structural differences among the substrates, EmrE accommodates them through sidechain rearrangements without significant backbone conformational changes (Kermani et al., 2022). Unlike Gdx-Clo, EmrE does not rely on a rigid hydrogen bond network to stabilise its substrate binding site. This flexibility allows the central glutamate residues (E14) and key aromatic sidechains (Y60, and W63) to adopt different rotamers, enabling EmrE to adjust to a diverse range of substrates (Kermani et al., 2022). This dynamic behaviour supports the ability of EmrE to transport a variety of chemically distinct compounds as previously identified in multiple studies (Korkhov and Tate, 2008, Morimyo et al., 1992, Purewal et al., 1990, Yerushalmi et al., 1995). Additionally, EmrE exhibits malleability at the portal formed by transmembrane helices, allowing it to accommodate substrates with hydrophobic alkyl tails (Kermani et al., 2022). This suggests that hydrophobic substituents of substrates can extend out of the binding site into the membrane, further contributing to the polyspecificity of substrate transport (Burata et al., 2022).

The "tyrosine switch" mechanism, as previously mentioned in the context of Gdx transporters in this section, plays a crucial role in the substrate transport processes of the Gdx and EmrE transporters (Burata et al., 2022, Kermani et al., 2022, Kermani et al., 2020). In both proteins, a conserved tyrosine (Y60 in EmrE and Y59 in Gdx-Clo) is strategically positioned within the binding pocket to interact with substrates. However, the specific interactions and consequences of the movement of this tyrosine differ between the two transporters. In Gdx-Clo, the tyrosine forms hydrogen bonds with surrounding residues in a stacked network, helping to stabilise the binding pocket and

facilitating substrate specificity (Kermani et al., 2020). In contrast, in EmrE the tyrosine participates in cross-subunit interactions, interacting with glutamate residues critical for substrate coordination (Kermani et al., 2022), adopting different rotamers to accommodate various substrates, allowing for a more flexible binding pocket (Kermani et al., 2022). This "tyrosine switch" mechanism thus exemplifies how similar structural elements can be employed differently in these transporters to achieve substrate transport versatility (Burata et al., 2022).

Polyamine transporters play a crucial role in bacterial physiology, facilitating the movement of polyamines such as spermidine, putrescine, and cadaverine (Burata et al., 2022, Higashi et al., 2008). These compounds have diverse functions within bacteria, acting as synthetic precursors, contributing to cell wall structure, offering protection against oxidative stress, regulating translation processes, and even inducing the expression of virulence genes (Barbagallo et al., 2011, Hirao et al., 2000, Shah and Swiatlo, 2008). Additionally, polyamines can initiate the formation of biofilms and enable swarming behaviour (Patel et al., 2006). However, an excessive buildup of polyamines can lead to toxicity (Fukuchi et al., 1995). To prevent this, specific SMR transporters act as "safety valves," exporting polyamines and maintaining their intracellular levels at a manageable range (Burata et al., 2022). These transporters, known as MdtIJ, form heterodimers and share similarities with the Qac and Gdx subtypes (Burata et al., 2022).

Within the SMR family, certain members function as glycolipid flippases, such as *arnE* and *arnF*, which are part of biosynthetic operons modifying lipid A within the outer membrane with L-Ara4N, thus reducing interactions with polymyxin antibiotics (Burata et al., 2022, Yan et al., 2007). In Salmonella, an SMR transporter aids the transfer of undecaprenyl phosphate aminoarabinose, conveying L-Ara4N from the cytoplasmic to the periplasmic leaflet, contributing to polymyxin resistance (Gunn et al., 1998). These SMRs potentially exhibit broader substrate specificity. Unlike other SMRs, lipid transport SMRs replace a central glutamate with an asparagine residue (Burata et al., 2022). Their mechanism may not depend on proton coupling but rather involve facilitated

diffusion along concentration gradients. They might retain a membrane portal similar to other SMRs and preserve the tyrosine switch despite limited sequence similarity (Burata et al., 2022).

In this section, the intricacies of SMR family transporters have been explored, shedding light on their structural characteristics and transport mechanisms, which have implications for bacterial resistance. The clinical significance of SMR-mediated resistance is linked to bacterial growth states, biofilm formation, and virulence. Efforts to combat SMR-mediated resistance involve peptide-based inhibitors that disrupt multimer formation, showing potential for future therapeutic strategies against these pumps(Ovchinnikov et al., 2018). Understanding these proteins has contributed to our knowledge of general transport mechanisms, despite the absence of homologues in *Neisseria*.

An understanding is crucial as we confront broader challenges of AMR, as seen with the MtrD transporter in *N. gonorrhoeae*. These insights highlight the urgency of tackling resistance and emphasise the need for innovative strategies in the face of evolving bacterial threats.

1.3.5 The PACE and AbgT families

In the last few years two new secondary-active drug transporter families have been identified: the PACE family and the antimetabolite transporters forming the AbgT family (Figure 1.1). The inaugural member of the PACE family, AceI (Figure 1.1), emerged during a transcriptomic investigation in *A. baumannii* following exposure to the biocide CH (Hassan et al., 2013). Subsequent research has indicated that AceI-mediated resistance is exclusive to CH as confirmed by gene inactivation analysis, which underscored its role in intrinsic resistance of *A. baumannii* to CH (Mackie et al., 2014) (Tucker et al., 2014). This protein comprises four TMSs, with both N- and C-termini located in the cytoplasm (Hassan et al., 2013). The direct transport of CH by AceI was demonstrated through the analysis the purified protein and substrate (Bolla et al., 2020).

AceR, a member of the LysR family of regulators, serves as the direct activator of the *aceI* gene in response to CH (Bolla et al., 2020, Liu et al., 2018). Diamines such as putrescine and cadaverine have been identified as potential physiological substrates of AceI (Hassan et al., 2021). The efflux of these diamines and CH has been shown to be driven by an electrochemical gradient of protons in intact *A. baumannii* cells, with the E15 residue suggested to play a role in this proton-coupled transport (Hassan et al., 2018, Hassan et al., 2019).

Bioinformatic analyses and subsequent functional assays have revealed AceI homologues in a wide range of species, predominantly in *Proteobacteria*, and some in *Actinobacteria*. Moreover, the substrates of these transporters have expanded to encompass other synthetic biocides including BC, proflavine, ACR and DQ (Hassan et al., 2013, Hassan et al., 2018, Henderson et al., 2021). Members of the PACE family are compact membrane proteins, typically consisting of approximately 150 residues, and they contain two tandem bacterial transmembrane pair (BTP; Pfam accession number PF05232) domains (Hassan et al., 2018). Preliminary studies have suggested that functional units of PACE family proteins exist as multimers, most likely as tetramers (Hassan et al., 2018).

The AbgT family is the latest group of MDR transporters and is illustrated by the MtrF MDR protein found in *N. gonorrhoeae* (Figure 1.1) (Su et al., 2015). The family normally consists of proteins that function as importers, like the AbgT (YdaH) protein in *E. coli* (Prakash et al., 2003), which is involved in the uptake of *p*-aminobenzoyl-glutamate, a precursor of folic acid biosynthesis (Carter et al., 2007, Hussein et al., 1998). However, the MtrF protein, which is necessary for high-level hydrophobic AMR in *N. gonorrhoeae*, is the first efflux transporter identified in the AbgT family and works in conjunction with the MtrCDE RND efflux system (Veal and Shafer, 2003). YdaH from *Alcanivorax borkumensis*, a marine bacterium that solely relies on oil hydrocarbons as its source of carbon and energy, was also identified as a member of the AbgT family (Delmar and Yu, 2016). Both MtrF and YdaH form dimers with unique architectures different from all other families of transporters, with each

monomer containing 9 TMS and two HPs, forming a bowl-shaped structure with a solvent-filled basin extending from the cytoplasm midway through the membrane bilayer (Delmar and Yu, 2016). Structural analyses combined with biochemical studies suggest that both MtrF and YdaH are efflux pumps that export sulphonamide antimetabolites, thereby producing resistance (Delmar and Yu, 2016). In the next section, the *N. gonorrhoeae* MtrF protein will be discussed in more detail.

1.3.5.1 The MtrF protein

The *N. gonorrhoeae* MtrF protein comprises 522 amino acids and exhibits a 38% identity with the *E. coli* AbgT protein (Su et al., 2015). MtrF has been found to contribute to the high-level resistance of gonococci to various HAs, such as ERY and TX-100, when working together with the gonococcal MtrCDE efflux pump complex (Folster and Shafer, 2005, Shome et al., 2021, Veal and Shafer, 2003).

The MtrF crystal structure was established at 3.95 Å resolution and exhibited unique architecture, with two MtrF molecules forming a dimer (Su et al., 2015). This MtrF dimer is bowl-shaped with a basin filled with water molecules extending from the cytoplasm to the midpoint of the CM (Su et al., 2015). Each subunit of the transporter includes nine TMSs and two HPs, with HP1 and HP2 being relatively short helices that span only half of the lipid bilayer. The dimer structure of MtrF can be divided into the inner and outer cores. TMS 1, 2, 5, 6, and 7 make up the inner core of MtrF, creating a frame-like structure that houses the outer core while also contributing to the protein's dimerisation. TMS 3, 4, 8, 9, as well as HP1 and 2, make up the outer core of MtrF, creating a channel that spans approximately from halfway across the CM to the periplasmic space (Delmar and Yu, 2016, Su et al., 2015). The combination of structural data and functional analysis suggested that MtrF is an antibiotic efflux pump that exports sulphonamide drugs from the cell, providing bacterial resistance to this class of antimetabolites (Delmar and Yu, 2016).

1.3.6 The RND superfamily

RND transporters constitute a three-component system, including an inner membrane IMP, a PAP or MFP, and OM channel protein from the OMF family. Together, they form a functional tripartite efflux complex that spans the inner membrane, periplasm, and outer membrane, facilitating the transport of substrates from the periplasm out of the cell (Figure 1.1) (Du et al., 2014, Nikaido, 2011, Nikaido, 2018). This feature is evident in various systems, including the *E. coli* AcrAB-TolC, *P. aeruginosa* MexAB-OprM, *C. jejuni* CmeABC, and *A. baumannii* AdeIJK RND efflux pumps (Darby et al., 2023, Lin et al., 2002, Sharifi et al., 2021, Sugawara and Nikaido, 2014). In the following sections, the components of an RND transporter will be explored, using the well-studied tripartite system AcrA-AcrB-TolC as an example.

1.3.6.1 The membrane fusion protein family

Proteins in the MFP family act as adaptors, linking the primary transporter in the CM of Gram-negative bacteria to an OMF protein. In collaboration with an MFP and OMF, the primary transporter expels molecules across both membranes without equilibration with periplasmic solutes (Higgins et al., 2004, Zgurskaya et al., 2009). Typically, 350-500 residues, MFPs likely span the CM or anchor via a lipoyl moiety (Higgins et al., 2004). They form phylogenetic subfamilies based on the CM transport system (MFS, RND, or ABC) they interact with (Higgins et al., 2004, Yoneyama et al., 2000). In Gram-positive bacteria, MFP homologs aid in exporting bacteriocins and competence peptides via ABC-type transporters (e.g., *Streptococcus pneumoniae* Spr0693), existing in full-length or truncated forms (Harley et al., 2000, Yang et al., 2018).

Structural analyses of MFPs including *P. aeruginosa* MexA (Figure 1.3), *E. coli* AcrA, and *Cupriavidus metallidurans* ZneB reveal an elongated configuration with distinct domains, facilitating interactions with conserved OMPs and diverse inner membrane proteins (De Angelis et al., 2010, Higgins et al., 2004, Mikolosko et al., 2006, Symmons et al., 2009). A hexameric model has been proposed for the adapter protein, engaging in an intermeshing cogwheel manner with the outer membrane factor (Xu et al., 2011). This

supports an adapter-bridging model for the tripartite pump assembly employed by Gram-negative bacteria.

Additional information about MFPs will be examined in the following section dedicated to the AcrA protein.

1.3.6.1.1 The AcrA protein

In *E, coli* AcrA serves as the PAP, assembling with AcrB and TolC into a tripartite pump system (Alav et al., 2022, Shi et al., 2019). Early research on the physical interactions between these proteins proposed that AcrA to play an active role in the AcrAB-TolC efflux process (Aires and Nikaido, 2005, Husain et al., 2004, Tikhonova and Zgurskaya, 2004, Zgurskaya and Nikaido, 2000).

The structure of AcrA and MexA is characterised by an elongated, sickle-shaped configuration, consisting of four domains (Mikolosko et al., 2006, Symmons et al., 2009). These domains include a MP domain located at one end, a BB, a centrally positioned LIP domain, and a coiled-coil HP or HLH situated at the opposite end of the molecule (Figure 1.3) (Akama et al., 2004b, Higgins et al., 2004, Symmons et al., 2009).

The flexibility of AcrA has been proposed to be essential for the assembly and overall dynamics of the pump, as indicated by the HPs substantial length and conformational flexibility at the base of AcrA's HLH domain observed in captured crystal structures, suggesting a hinge-like characteristic (Mikolosko et al., 2006, Zgurskaya et al., 2015). New research indicates that AcrA plays a vital and dynamic role in both the assembly of pumps and the expulsion of substrates (Alav et al., 2021). Recognising this significance has prompted the consideration of MFPs as promising targets for addressing antibiotic resistance driven by efflux mechanisms (Abdali et al., 2017, Alav et al., 2021).

The structural determination of the complete AcrAB-TolC pump revealed the formation of a hexameric ring of AcrA within the tripartite pump, connecting AcrB and TolC (Du et al., 2014, Wang et al., 2017). This arrangement reveals two distinct conformational states of AcrA protomers, namely protomers I and II, arranged alternately around the ring. The MP and BB domains establish

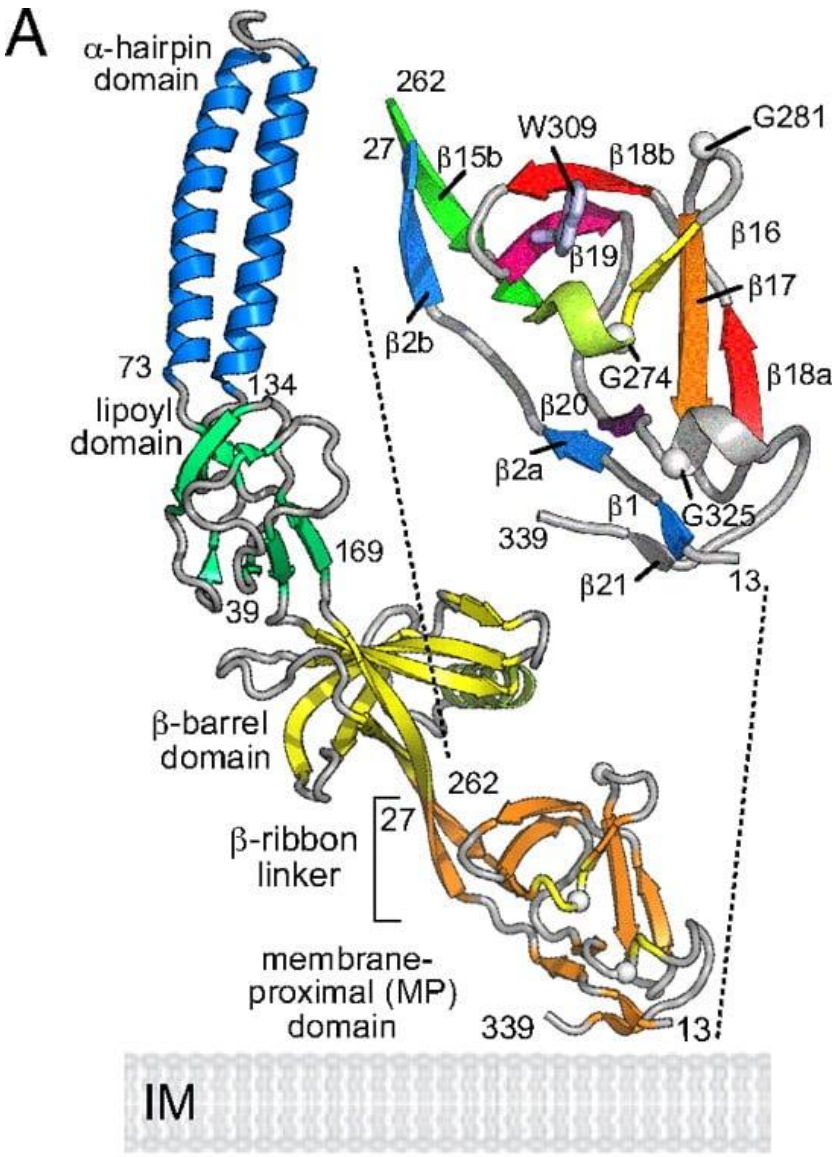

Figure 1.3: Structural representation of MexA periplasmic adaptor protein.

(A) MexA adaptor protein is comprised of four distinct domains: α-hairpin (blue), lipoyl (green), β-barrel (yellow), and MP β-roll (orange). Adapted from Symmons et al., 2009, with permission from the Proceedings of the National Academy of Sciences (PNAS).

contact with AcrB, featuring unique interactions between adjacent AcrA protomers and a single AcrB protomer (Du et al., 2014). Protomer-I interacts with the DC, PC1, and PC2 subdomains of AcrB, whereas protomer-II is in contact with the DN and PN2 subdomains. Meanwhile, the HLH domains engage in tip-to-tip interactions with the periplasmic helices of TolC (Du et al., 2014). The quaternary structure of the pump showcases the assembly of BB

and LIP domains into two rings, while HLH domains collectively create a channel (Du et al., 2014). Complementary computational studies have disclosed that the dimeric configuration of MexA represents the minimal unit required to assemble with its cognate partner proteins, forming a functional complex. This conclusion is supported by the observation that the G72S substitution at the LIP domain hinders the dimerisation of AcrA and impedes the formation of a stable tripartite assembly (Cacciotto et al., 2022). These findings clarify the crucial role of the multidomain structure of the AcrA protein, characterised by high intrinsic flexibility, in establishing a fully functional tripartite efflux pump.

AcrA also plays a part in scrutinizing the entry of substances into AcrB (Alav et al., 2022). Using mutagenesis, the previously reported "binding box" model of protein-protein interaction between AcrA and AcrB, identified the importance of specific amino acids in the binding box for substrate preference and selection (Alav et al., 2022). A mutation in AcrA (K366D) caused a growth defect in the presence of several substrates (Alav et al., 2022). The K366 amino acid is located near the proposed entrance of substrate tunnels, suggesting that it may affect substrate access and kinetics (Alav et al., 2022). The available data provides hints to the possible mechanism of the K366 action, suggesting that it may play a role in sensing the substrate-occupied state of the PAP, leading to TolC engagement and channel opening (Alav et al., 2022).

1.3.6.2 The outer membrane factor family

Proteins belonging to the OMF family collaborate with primary CM transporters from the MFS, ABC superfamily, and RND superfamily, along with a MFP. This collaborative complex enables the transport (export) of various solutes (such as heavy metal cations, drugs, oligosaccharides, and proteins) across the two membranes of Gram-negative bacterial cells in a single energy-coupled step. OMF proteins likely form homotrimeric 12-stranded β-barrel-type pores in the outer membrane, facilitating the passage of solutes pumped out of the cytoplasm or cytoplasmic membrane in response to the energy-coupled export process catalysed by the CM permease. In some instances, the

complex of primary transporter, MFP, and OMF forms transiently in response to substrate binding. However, in another case involving AcrA and TolC, the interaction appears to be substrate independent.

Further details regarding OMF proteins will be explored in the upcoming section dedicated to the TolC protein.

1.3.6.2.1 The TolC protein

Enterobacteriaceae, such as *E. coli*, exclusively possess a singular OMF protein known as TolC (Kuo et al., 2024, Webber et al., 2022). TolC has been demonstrated to play a crucial role in the expulsion of antibiotics and metabolites, acid tolerance, virulence, and maintenance of cell membrane integrity (Zgurskaya et al., 2011).

In 2000, the crystal structure of the TolC protein was solved at 2.1 Å resolution (Koronakis et al., 2000) and not long after that of the *P. aeruginosa* homologue, OprM (Akama et al., 2004a). Analysis of these structures revealed a tightly woven trimeric configuration, consisting of three domains: a β-barrel domain measuring 40 Å, embedded in the OM and composed of 12 β-sheets (four per monomer); an α-helical coiled-coil domain comprising 12 α-helices spanning approximately 100 Å into the periplasm; and an α/β equatorial domain (Figure 1.4). This 140 Å long continuous solvent accessible conduit, the channel-tunnel, crosses both OM and periplasmic space (Koronakis et al., 2000). In the crystal structures this tunnel is tightly closed at the periplasmic (proximal) end by tightly packed coiled helices, inner H7/H8, and outer H3/H4, forced by a network of hydrogen bonds, particularly by a ring of D371 and D374 residues (Figure 1.4) (Andersen et al., 2002b). The closed state likely to prevent substrate exchange between the cell environment and the periplasm (Bavro et al., 2008).

The TolC closed state entrance was suggested to undergo transition to the open state when TolC is recruited by the IM transporter and the adaptor protein (Bavro et al., 2008, Koronakis et al., 2000, Pei et al., 2011, Thanabalu et al., 1998, Tikhonova et al., 2011, Weeks et al., 2010). This transition was also suggested to be dependent on interaction with AcrA in an energy dependent

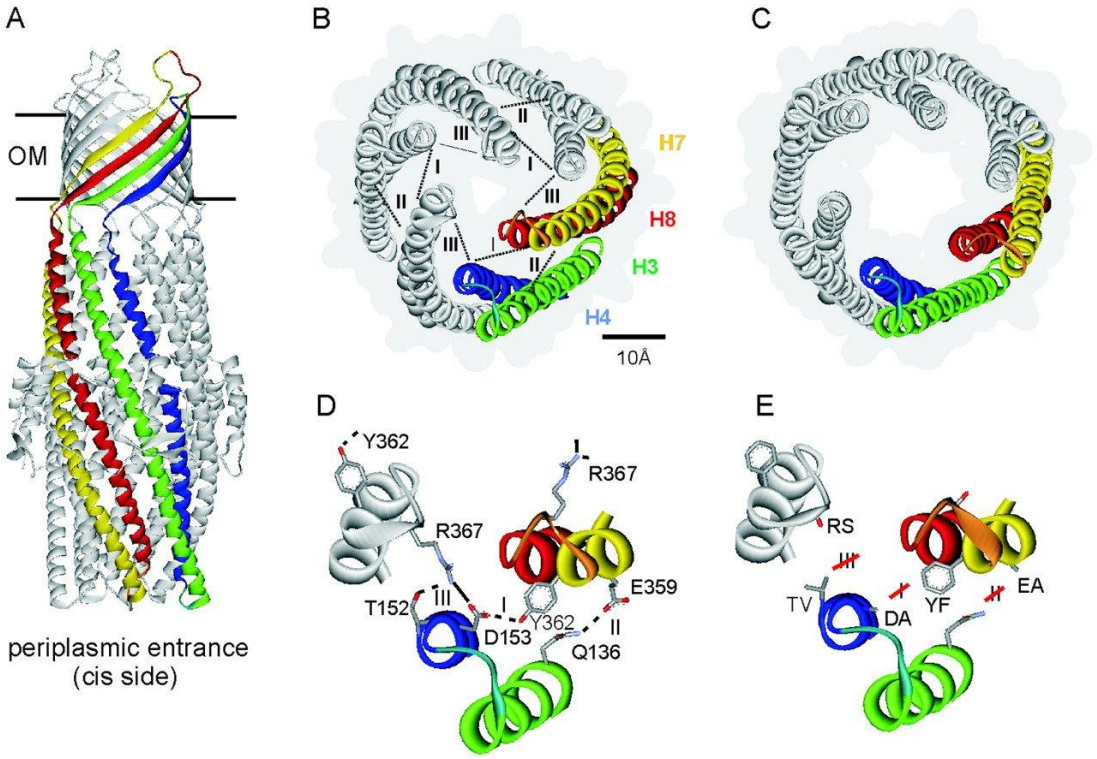

Figure 1.4: Structure representation of TolC and its periplasmic entrance.

(A) The TolC protein consists of a β-barrel domain embedded in the OM, an α-helical domain spanning the periplasmic space, and an α/β equatorial domain. (B) Depicts the closed state of the entrance as viewed from the periplasmic side. (C) Illustrates the modelled open state of the entrance. (D) Zooms in on the circular network at the tunnel entrance, displaying the residues critical for intra-monomer (I and II) and intermonomer (III) connections. Adapted from Andersen et al., 2002a, with permission from the Proceedings of the National Academy of Sciences (PNAS). Copyright (2002) National Academy of Sciences, U.S.A.

conformational change manner (Gerken and Misra, 2004, Weeks et al., 2010). Consistent with these suggestions, studies have demonstrated that MexAB is essential for the opening of OprM (Glavier et al., 2020, Verchere et al., 2015). In this mechanism of TolC allosteric opening, an iris-like movement of the inner coiled-coil α-helices (H7/H8) realigns the inner coiled-coil with the outer coils (H3/H4) resulting in the pore opening in a twist-to-open transition (Figure 1.4) (Andersen et al., 2002a, Koronakis et al., 2000, Krishnamoorthy et al., 2013).

This mechanism of opening was also supported by leaky variants of the TolC protein (Bavro et al., 2008, Pei et al., 2011).

Close end-to-end fitting of the AcrB-TolC complex is believed to initiate the expansion of the periplasmic end of TolC while it is not sufficient for full dilation of the inner constriction (Bavro et al., 2008, Pei et al., 2011). Opening of the TolC channel has been suggested likely to be the final step in the transport cycle of the AcrAB-TolC system that causes dissociation of the complex (Krishnamoorthy et al., 2013, Tikhonova et al., 2011).

After exploring the MFP and OMF proteins, we now delve into examining the RND transporters, the IM component of a tripartite RND efflux system in the next section.

1.3.6.3 The RND transporters

Belonging to the RND superfamily, these RND transporters represent a large ubiquitous group of proteins that are found in prokaryotes, eukaryotes and archaea (Nikaido, 2018, Tseng et al., 1999). Of the ten recognised phylogenetic families within this superfamily one, the hydrophobe/amphiphile efflux 1 (HAE1) family, cluster 2.A.6.2 in the tcdb (http://www.tcdb.org), contains well-characterised, Gram-negative bacterial-specific, (Saier, 2023). Included in RND superfamily are transporters involved in; protein secretion, e.g, SecDF of *E. coli* and of *Thermus thermophilus* (Tsukazaki, 2018, Tsukazaki et al., 2011), extrusion of lipids and other compounds such as anti-tuberculosis drugs, e.g., the MmpLs proteins from *Mycobacterium tuberculosis* (Zhang et al., 2019), and export of metal or heavy metals (the HME family transporters) such as the CnrA protein of *Cupriavidus* (*Ralstonia*; *Alcaligenes*) *metallidurans* (Tibazarwa et al., 2000), the *E. coli* CusA (Long et al., 2010, Moseng et al., 2021) and the *Pseudomonas putida* CzcA1 (Liu et al., 2021) transporters. Examples of RND transporters in humans are the Niemann–Pick C1 (NPC1) protein which is involved in cholesterol transport (Li et al., 2017, Scott and Ioannou, 2004) and protein patched homolog 1 (PTCH1) that is involved in the Hedgehog signalling which is central in embryonic development and tissue regeneration (Qi et al., 2019, Taipale et al., 2002).

Extensive reviews have emphasised the significance of RND transporters in the resistance and physiology of Gram-negative bacteria (Alav et al., 2021, Colclough et al., 2020, Li et al., 2015, Neidig et al., 2023, Nikaido, 2018, Poole, 2004, Zwama and Nishino, 2021). These transporters exhibit specificity mainly for hydrophobic and amphiphilic compounds, catalysing export of a wide spectrum of compound including detergents, antibiotics, dyes, bile salts, FAs, biocides, isoflavenoids, and aliphatic and aromatic organic solvents (Alav et al., 2021, Gervasoni et al., 2022, Rosenberg et al., 2000, Seeger et al., 2006, Tseng et al., 1999). However, some RND transporters, e.g., the *E. coli* AcrD, and the *P. aeruginosa* MexY efficiently extrude aminoglycosides that have multiple positive charges and are highly hydrophilic (Lau et al., 2014, Rosenberg et al., 2000, Zhang et al., 2023c).

RND family proteins significantly contribute to the inherent MDR observed in Gram-negative bacteria due to their constitutive expression (Neidig et al., 2023, Nikaido, 1996, Poole, 2004, Sulavik et al., 2001, Zwama and Nishino, 2021). This empowers Gram-negative bacterial strains equipped with these efflux pumps to thrive in certain natural habitats saturated with harmful substances. For instance, *E. coli* expressing the AcrB efflux pump demonstrates the capability to endure and proliferate in the human large intestine, which is rich in bile salts and FAs (Anes et al., 2015, Henderson et al., 2021). Additionally, AcrB enables *E. coli* to survive in the presence of antimicrobial peptides, which are involved in the defence mechanisms of the human host (Blair et al., 2022). Furthermore, the overexpression of RND pumps has been associated with MDR in various Gram-negative bacteria, including clinical strains of *E. coli*, *K. pneumoniae*, *Salmonella enterica* serovar Typhimurium, *P. aeruginosa*, *Campylobacter jejunei*, *A. baumannii*, *N. gonorrhoeae* and others (Buckley et al., 2006, Hagman et al., 1995, Maness and Sparling, 1973, Piddock, 2006a, Poole and Srikumar, 2001, Warner et al., 2008, Yao et al., 2016, Yoon et al., 2016, Zwama and Nishino, 2021). For example, the primary factor behind carbapenem (imipenem [IPM] and meropenem [MEM]) resistance is the overexpression of MexXY-OprM efflux pump of *P. aeruginosa* (Petrova et al., 2019). Additionally, RND transporters play important roles in survival, fitness and metabolism of bacterial cells

(Piddock, 2006b, Wang-Kan et al., 2021, Zgurskaya et al., 2022). Apart from over-expression, alterations in the amino acids within the RND pumps themselves, leading to enhanced drug efflux efficiency, has also been associated with MDR, and are causing additional concern (Wadsworth et al., 2018a, Zwama and Nishino, 2022).

Beyond conferring resistance against various antibiotic classes, RND transporters also contribute to the pathogenesis and virulence of several bacterial pathogens. For instance, the *E. coli* AcrAB-TolC pump influences the survival of adherent-invasive *E. coli* strain LF82 within macrophages (Fanelli et al., 2023). Additionally, AcrAB has been demonstrated to specifically contribute to the invasion of epithelial cells by *Shigella flexneri* (Coluccia et al., 2023). Some Gram-negative bacteria possess multiple RND transporters. For instance, *P. aeruginosa* has several RND pumps, such as MexAB-OprM, MexXY-OprM/OprA, MexVW-OprM, MexPQ-OpmE, MexCD-OprJ and MexEF-OprN (Kobylka et al., 2020, Seeger et al., 2008, Zgurskaya et al., 2022). These transporters enable the bacterium to expel antibiotics commonly used in clinical practice, including fluoroquinolones, TET, CHL, and some β-lactams (Li et al., 2015, Poole and Srikumar, 2001). *E. coli* is another example that possesses several RND transporters, including characterised members such as AcrAB-TolC, AcrAD-TolC, AcrEF-TolC, MdtABC-TolC, and MdtEF-TolC, from the HAE1 family, and CusBAC from the HME family (Klenotic et al., 2021, Kobylka et al., 2020, Li et al., 2015, Poole and Srikumar, 2001, Seeger et al., 2008). *A. baumannii* represents another example, featuring three RND efflux pumps, namely AdeABC, AdeFGH, and AdeIJK (Zgurskaya et al., 2022). In contrast, *N. gonorrhoeae* possesses only one RND transporter, the MtrCDE system (Ayala et al., 2022).

The AcrB protein in *E. coli*, the IMP of the AcrAB-TolC system, stands out as the extensively studied exemplar among all RND-type efflux transporters. In the upcoming section, we will delve into a detailed discussion of this efflux pump, emphasising the distinctive features of RND transporters. Additionally, other RND pumps will be addressed as needed to elucidate the characteristics of these transporters.

1.3.6.4 The *E. coli* AcrAB-TolC efflux system

The AcrAB-TolC is the main efflux system in *E. coli*, *Enterobacteriaceae* and *Salmonella Typhimurium* (Andersen et al., 2015). In *E. coli* it is encoded by three genes. Two of these genes, *acrA* and *acrB*, are located in a single operon known as the *acrAB* locus on the chromosome (Dinh et al., 1994, Ma et al., 1993, Ma et al., 1995). AcrA is a periplasmic lipoprotein of 397 amino acids that belongs to the MFP family and is anchored to the IM via its N-terminal 24-residue peptide (Dinh et al., 1994, Ma et al., 1993, Ma et al., 1995). AcrB is an integral membrane protein of 1049 amino acids (Ma et al., 1993), that shares 65% identity and 88% similarity with the *Burkholderia pseudomallei* BpeB protein (Kato et al., 2023). The third gene, *tolC*, is situated in a separate locus on the chromosome and its product, TolC, is a 52 kDa multifunctional OM channel protein required for α-haemolysin secretion and the expression of multiple-antibiotic-resistance (Mar) phenotype in *E. coli* (Fralick, 1996, Morona et al., 1983, Wandersman and Delepelaire, 1990). TolC also operates with transporter proteins of the MFS and ABC families (Paulsen et al., 1997) to form a conduit through which the transporters can expel a wide range of toxic compounds directly to the external medium without passing the periplasm (Figure 1.1) (Nikaido, 2000, Zgurskaya and Nikaido, 1999).

The central role of the AcrB protein as the active transporter in an efflux system will be further elaborated in the subsequent section.

1.3.6.4.1 The *E. coli* AcrB protein

The AcrB protein has been extensively studied using diverse methods, including X-ray crystallography, single-particle cryo-electron microscopy with nanodiscs, sm-FRET imaging, MD simulations, molecular docking, site-directed mutagenesis, and biochemistry techniques such as fluorescent compound efflux assays, among others (Doerr, 2016, Su et al., 2017). The Protein Data Bank currently contains over 166 structures of the AcrB protein (Burley et al., 2021). The subsequent sections will explore the structural intricacies of the AcrB protein.

1.3.6.4.1.1 Conserved architecture of AcrB and related RND transporters

RND efflux pumps exhibit significant topological similarity, typically featuring 12 TMS and two large hydrophilic PD positioned between TMS 1 and 2 and TMS 7 and 8 (Fujihira et al., 2002, Tseng et al., 1999). The N-terminal half of these RND transporters shares homology with the C-terminal half, suggesting an internal gene duplication event in the past, similar to what is observed in MFS family proteins (Tseng et al., 1999).

In 2002, the initial X-ray crystal structure of an RND transporter, AcrB, was reported without a bound substrate (Murakami et al., 2002). This structure unveiled a homotrimer with a mushroom-like appearance and exhibited a pseudo three-fold symmetry, featuring identical conformations across all three protomers. The mushroom-like trimer was characterised by two main regions: the headpiece projecting into the periplasm, also known as the PD, and the TM region (Figure 1.5). The PD headpiece consists of two distinct regions, including an upper area featuring an opening that forms a funnel-like shape, known as the TolC docking domain, also called inner membrane-distal region, and a lower area forming a central pore, which remained closed in this crystal structure, also known as periplasmic porter (pore) domain (PPD) and inner membrane-proximal region (Figure 1.5) (Murakami et al., 2002). The PD headpiece is stabilised by an interlocking arrangement involving three HP structures, each contributed from one protomer, that fits into the TolC docking domain (Figure 1.5) (Murakami et al., 2002).

The TM domains of the three protomers in AcrB protein form a ring-like structure called the central cavity (CC), spanning the IM and extending towards the bottom of the PD headpiece. The TM domain of each protomer comprises 12 α-helices organised into two pseudo-symmetric sets of six helices (six N-terminal and six C-terminal), connected by an additional α-helix (Iα) situated parallel to the CM surface. Both the N-terminal TMS 2 helix and its corresponding C-terminal TMS 8 helix are long and extend upwards into the

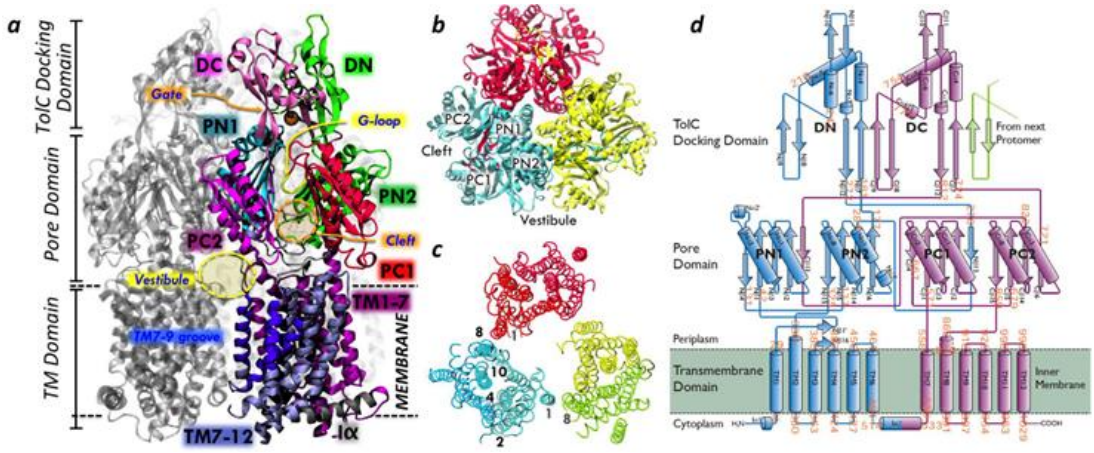

Figure 1.5: AcrB structural characteristics and secondary elements.

A) Depiction of the AcrB asymmetric homotrimer structure in a side view, with the A protomer represented in solid ribbons and distinct colours highlighting its main domains and subdomains, while the other monomers are displayed in transparent ribbons. B) Overhead view of the PD of AcrB, featuring the three protomers (A in cyan, B in yellow, and C in red), with the TM domain removed for clarity. C) Overhead view of the TM domain of AcrB, with the same colour scheme as in B, emphasising the symmetry between the TM1-6 (darker colours) and TM7-12 moieties (lighter colours). Key helices involved in the proton-relay network and transmission of allosteric conformational changes to/from PD are labelled in black in the A protomer, while helices 1 of A and C protomers and 8 of protomer B indicated in grey. D) Illustration of subdomains and secondary structural elements within a protomer of AcrB. Figure adapted from Ruggerone et al., 2013, with permission from the Bentham Science Publisher.

periplasmic region. In comparison TMS 2, the top of TMS 8 is distorted compromising the symmetry (Figure 1.5) (Murakami et al., 2002).

Four distinct secondary structures, comprising PN1, PN2, PC1, and PC2, are recognisable in each porter domain (Figure 1.5). Specifically, the PN1 and PN2 subdomains span the polypeptide region between TMS 1 and TMS 2, while the PC1 and PC2 subdomains encompass the polypeptide region between TMS 7 and TMS 8 (Figure 1.5) (Murakami et al., 2002). With all four subdomains arranged in a clockwise direction, the second helix of PN1 from

each protomer contributes to the formation of the central pore. This central pore starts at the funnel-like structure in the TolC docking domain and leads to the central cavity (Murakami et al., 2002).

The PC1 and PC2 subdomains create a deep cleft of approximately 40 Å in length perpendicular to the membrane plane (Figure 1.5) (Murakami et al., 2002). Subsequently revealed in asymmetric structures (to be described in the following section) of numerous HAE1-type RND transporters, the PC1/PC2 cleft exhibits the flexibility to be either open or closed, creating an entrance for substrates to enter the pump from the periplasm (Kato et al., 2023, Lyu et al., 2022, Morgan et al., 2021, Sennhauser et al., 2009b, Yao et al., 2016, Zhang et al., 2023a, Zhang et al., 2021). Three openings called vestibules exist at the membrane-periplasmic space boundary between each PN2 and PC2 subdomain. These vestibules connect the CC to the PD at the IM/PD interface, are suggested to allow drugs to diffuse from the periplasm and the outer leaflet of the IM to the narrow central pore (Murakami et al., 2002).

The TolC docking region consists of two subdomains, DN and DC (Figure 1.5). The DN subdomain has an elongated HP protruding approximately 35 Å, while the DC subdomain features a hook-like structure. The DN subdomain is coordinated and interlocked with the neighbouring protomer's hook-like structure, thereby stabilising the trimeric assembly This TolC docking domain with protomer-protomer interlocking feature has been suggested to also function as a hinge allowing the TM domains to associate or dissociate as seen in AdeB (Morgan et al., 2021, Murakami et al., 2002).

A groove exists in the membrane-exposed surface of the TM domain, which is formed by TMS 7 and TMS 8 and extends throughout the entire membrane-embedded region. The top of TMS 8 links this groove to the CC, while TMS 9 contributes to the formation of the shallow bottom part of the groove. This groove was proposed to facilitate the movement of substrates from the IM (Eicher et al., 2012, Murakami et al., 2002).

The protomer conformation in the symmetric trimer of AcrB was subsequently identified as the resting state in the transport cycle (Murakami,

2008, Su et al., 2006). A resting-state symmetric structure has also been reported for other HAE1-RND type proteins, such as CmeB, MtrD, and CusA (Bolla et al., 2014, Long et al., 2010, Su et al., 2017, Zhang et al., 2023a). Additionally, RND pumps exhibiting trimeric symmetric structures, characterised by the three protomers adopting an extraction (E) conformation, specifically the EEE configuration, have been documented (to be described in the following section) (Morgan et al., 2021).

The initial structure of AcrB revealed a homotrimeric three-dimensional architecture with various substructural features. Subsequent research unveiled that this AcrB-like arrangement is preserved among diverse RND transporters, encompassing the *E. coli* AcrD and CusA, the *P. aeruginosa* MexB, the *A. baumannii* AdeB, the *C. jejuni* CmeB, and the *N. gonorrhoeae* MtrD transporters (Bolla et al., 2014, Moseng et al., 2021, Su et al., 2019, Su et al., 2017, Tsutsumi et al., 2019, Zhang et al., 2023c).

1.3.6.4.1.2 The dynamic conformations of AcrB and related RND transporters

The crystal structures of AcrB, solved independently by three different laboratories between 2006 and 2007, significantly advanced our understanding of the structure and function of RND pumps. These trimeric structures were notably asymmetric, revealing that each protomer had a unique conformation that differed slightly from those of the other two neighbouring protomers (Murakami et al., 2006, Seeger et al., 2006, Sennhauser et al., 2007). In these asymmetric structures, a spacious substrate binding site, surrounded by β-sheets of PN1, PN2, PC1, and PC2, was identified in the PPD of each protomer (Figure 1.6). Only one protomer was found to bind to a substrate molecule (Murakami et al., 2006, Seeger et al., 2006, Sennhauser et al., 2007). The analysis of asymmetric structures revealed three functional states in drug export: access/loos (A/L), binding/tight (B/T), and extrusion/open (E/O) (Figure 1.6) (Murakami et al., 2006, Seeger et al., 2006). The A protomer awaits substrate binding with an upright central helix and no bound substrate. In the B protomer, the central helix from the next

protomer closes the exit to the funnel, containing a substrate bound in the deep pocket within the porter domain. The E protomer exhibits an open exit to the funnel, and possible drug entrances via the periplasm and the IM both closed enabling the expulsion of the substrate into the TolC channel.

In these asymmetric structures, only one conformation (the A protomer of Murakami or the L protomer of Seeger) closely resembled the symmetric AcrB protomer model identified by Murakami et al. in 2002 (Murakami et al., 2006, Seeger et al., 2006, Sennhauser et al., 2007).

Examination of the asymmetric structures revealed additional noteworthy and significant structural characteristics within AcrB. These encompass: 1) the proximal drug-binding pocket (PBP), also known as access pocket (AP), 2) the deep drug-binding pocket (DBP), also known as distal pocket (DP), 3) the flexible G-loop (also known as gate loop), 4) the F-loop, 5) the hoisting loop, 6) the presence of four substrate translocation channels, and 7) the hydrophobic pit within the DBP (Figure 1.6). Elaboration on these structural features will be provided in the subsequent sections.

Similar functionally rotating structures have been reported for other HAE1-RND type transporters. Examples include MexB, the *B. pseudomallei* BpeB, BpeF transporters, and resistance-enhancing CmeB variant (RE-CmeB) of the WT CmeB protein from *C. jejuni*, MtrD, AdeB, and AdeJ, all of which exhibit a comparable asymmetric fold as described in AcrB (Kato et al., 2023, Lyu et al., 2022, Morgan et al., 2021, Sennhauser et al., 2009b, Yao et al., 2016, Zhang et al., 2023a, Zhang et al., 2021). However, certain HAE1-RND type proteins differ from this asymmetric fold described. For example, WT CmeB from *C. jejuni* strain NCTC 11168 adopts both symmetric, and asymmetric structural folds. In the symmetric structure, all three protomers were in the resting state conformation where the PC1/PC2 cleft is closed in all three protomers. In the asymmetric trimer, the three protomers represent the B, E, and resting conformations, with the PC1/PC2 cleft open in the B protomer and closed in the other two protomers. Direct conformational dynamics analysis using sm-

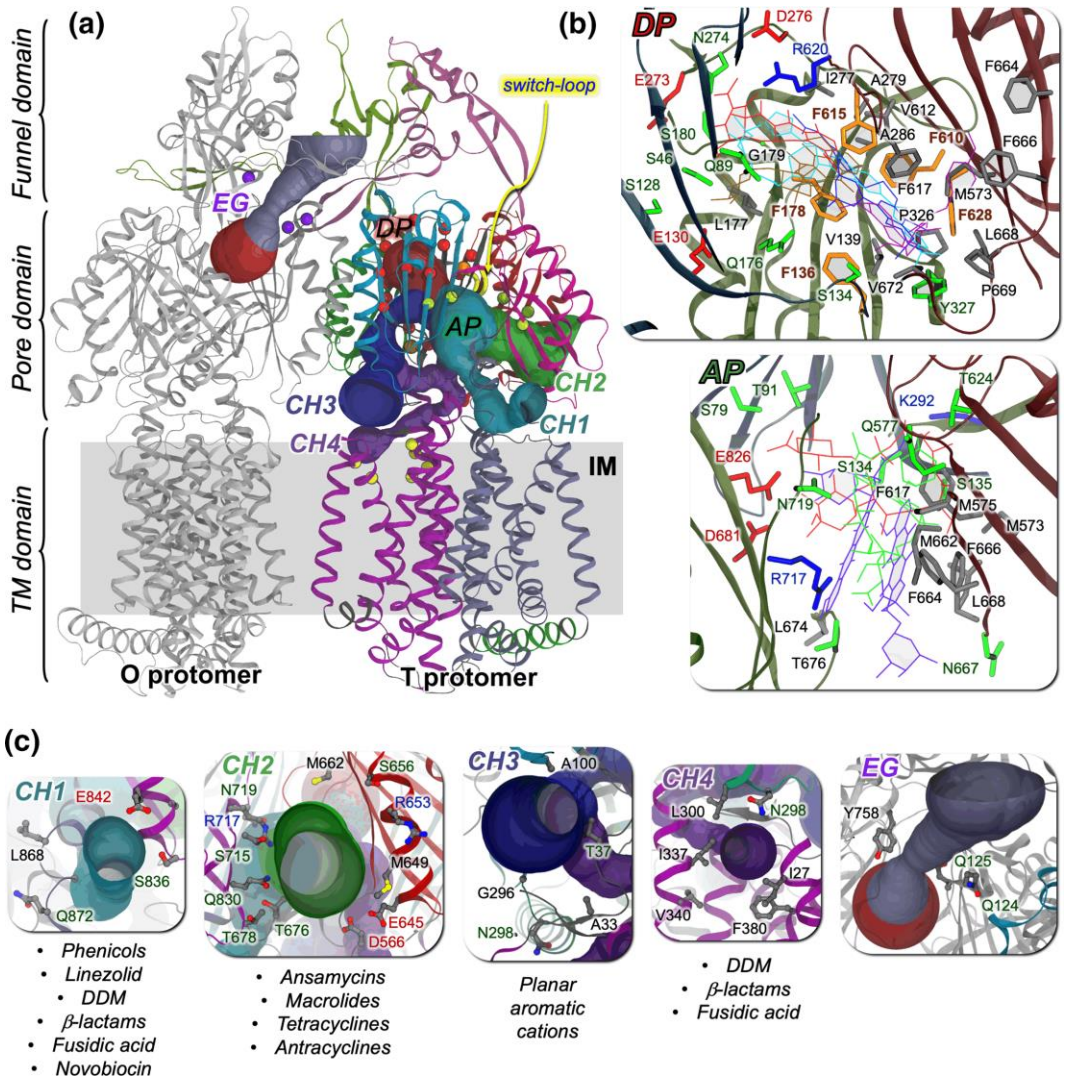

Figure 1.6: The depiction of the AcrB transporter's structure highlights crucial structural attributes and key residues.

(a) Structure of the AcrB transporter (PDB ID: 4D×5 - (Eicher et al., 2012)) is depicted, illustrating four potentially functional entry channels (CH1–CH4) within the T protomer. Additionally, the EG opening towards the funnel domain in the O protomer is indicated. C_α atoms of residues forming the multifunctional sites AP (PBP), DP (DBP), HT, and S1/2 are represented as green, red (orange), and yellow spheres, respectively. (b) Residues outlining the DBP and PBP are depicted. Phenylalanines delineating the HT are shown in orange. Co-crystallised antibiotics and inhibitors within each site are depicted as sticks, coloured according to the molecule. (c) Residues forming the entrances of transport channels CH1–CH4 and the bottleneck of the EG are represented as sticks, with colours corresponding to atom types. The substrate specificities of each channel are reported for AcrB. Figure adapted from Athar et al., 2023. Reproduced under the terms of the Creative Commons Attribution license.

FRET of this transporter led to the proposal that in the CmeB transporter, each protomer functions unsynchronised and independent of each other (Su et al., 2017). Building on this discovery, the ET-bound asymmetric structures of AdeB have been observed to engage ET molecules in two protomers (Morgan et al., 2021). Specifically, one ET molecule binds at the entrance of the PC1/PC2 cleft entrance in the A protomer, while two ET molecules bind at the DBP in the B protomer. Furthermore, within the ET-bound asymmetric AdeB structures, three distinct trimeric protomer configurations have been identified, namely $T_{(transient)}$EE, resting-EB, and BEA (Morgan et al., 2021). These observations led the authors to propose a parallel with CmeB, suggesting that each protomer within AdeB operates independently to bind and export substrate (Morgan et al., 2021). A comparable pattern of B, E, and resting conformation among the three protomers of CmeB has also been observed in both apo and GEN-bound asymmetric structures of AcrD. Drawing an analogy to the proposed efflux mechanism of CmeB, it has been suggested that in AcrD, each protomer cycles asynchronously and independently through three different conformational states to facilitate the extrusion of GEN (Zhang et al., 2023c). This different efflux mechanism can potentially extend to other RND pumps such as AcrB, MexB, and MtrD. Additionally, structural analysis identified that the majority of AdeB trimers are in the O state without apparent transport channels or antibiotic binding sites (Ornik-Cha et al., 2021). However, approximately 10% of the protomers adopt a conformation where three transport channels lead to the closed substrate binding pocket. This analysis reports a previously undescribed protomer conformation, namely L*, presumed to be the first conformational state in a transport cycle, in which three substrate entry channels may permit the entry of drugs into the efflux pump (Ornik-Cha et al., 2021).

Symmetric trimeric configurations in the BBB state have also been identified in the *B. pseudomallei* BpeF and the *K. pneumoniae* OqxB transporters with three protomers in the B state conformation (Bharatham et al., 2021, Kato et al., 2023). These two HAE1-RND proteins share a significant amino acid homology, with a 60% identity and 80% similarity. In both structures, each protomer was observed to bind two DDM molecules in the DBP. This binding

pattern is proposed to result from induced fit, influenced by the detergent added during the purification and crystallisation processes (Kato et al., 2023).

Interestingly, asymmetric structures have been observed in HAE1-RND type proteins even in the absence of any bound substrate. Notable examples of such structures include the RE-CmeB and Kp-AcrB proteins (Zhang et al., 2023a, Zhang et al., 2023b). In Kp-AcrB, both apo and ligand-bound structures depict the three protomers in different conformations. However, in apo-Kp-AcrB, the three protomers adopt E, A, and B conformations, respectively, in a clockwise direction. This is in contrast to the three protomers in the ligand-bound Kp-AcrB structure, which assume E, B, and A conformations, respectively, also in a clockwise direction (Zhang et al., 2023b). Moreover, a distinct asymmetric structure has been identified in both apo- and GEN-bound-AcrD, with the three protomers adopting B, A, and resting states. This conformation contrasts with the asymmetric structures of AcrB and other HAE1 RND type transporters, where the three protomers adopt A, B, and E conformations (Zhang et al., 2023c).

Shifting from the overarching structural insights of AcrB and HAE1-RND type transporters, the discussion now turns to the specifics of drug binding sites and substrate pathways. The previously explored asymmetric structures, highlighting distinctive conformations in each protomer, underscore the dynamic nature of RND pumps during drug export. The upcoming section will delve into the molecular intricacies of drug recognition and translocation, providing a nuanced exploration of the factors contributing to the observed polyspecificity and functional adaptability in these transporters.

1.3.6.4.1.3 Drug recognition and substrate pathway

Genetic studies have revealed that substrate discrimination takes place in the PD, rather than the TMD (Eda et al., 2003, Elkins and Nikaido, 2002, Tikhonova et al., 2002, Yu et al., 2005). The drug-bound asymmetric structures of AcrB and other HAE1-RND transporters revealed two voluminous substrate binding pockets in the PD (Eicher et al., 2012, Nakashima et al., 2011, Zhang et al., 2023a, Zhang et al., 2023b).

1.3.6.4.1.3.1 The proximal drug-binding pocket

Found in the A protomer, the PBP resides within the lateral periplasmic cleft between the PC1 and PC2 subdomains (Figure 1.6) (Eicher et al., 2012, Nakashima et al., 2011). Various residues in AcrB, such as S46, S79, Q89, T91, S128, E130, S134, S135, K292, M573, M575, Q577, F617, T624, M662, F664, F666, E673, L674, T676, D681, R717, N719, and L828, have been identified as contributors to this site, engaging in interactions with diverse drugs (Eicher et al., 2012, Kato et al., 2023, Nakashima et al., 2011, Vargiu and Nikaido, 2012). Several of these residues exhibit high conservation across other HAE RND transporters (Lyu et al., 2020, Morgan et al., 2022, Murakami et al., 2006, Su et al., 2019, Zhang et al., 2023a). Different subsets of these residues bind to specific substrates, with some residues overlapping when interacting with structurally different substances (Zhang et al., 2023a). Substrate binding in this pocket predominantly occurs through aromatic stacking and polar interactions (Eicher et al., 2012, Nakashima et al., 2011).

1.3.6.4.1.3.2 The distal drug-binding pocket

Adjacent to the proximal site, within the deep recesses of the porter domain and surrounded by PN1, PN2, PC1, and PC2 β-sheets of each protomer, lies another drug binding pocket termed the DBP (Figure 1.6) (Eicher et al., 2012, Murakami et al., 2006, Nakashima et al., 2011, Seeger et al., 2006, Sennhauser et al., 2007). In the asymmetric co-crystal structures of AcrB, as elucidated by Murakami et al., doxorubicin or minocycline were exclusively observed to bind to this pocket in the B protomer (Murakami et al., 2006). The DBP is linked to the funnel-like opening through an exit gate (EG) (Figure 1.6), formed by the residues Q124, Q125, and Y758 (Sennhauser et al., 2007). The capacious DBP encompasses several hydrophobic, polar, and charged residues, including S46, Q89, S128, E130, F136, V139, Q176, L17, F178, S180, E273, N274, D276, I277, G290, Y327, F572, M573, F609, F610, V612, F615, F617, R620, F627, F628 and F665, suggesting their involvement in diverse interactions with substrate molecules (Eicher et al., 2012, Husain and

Nikaido, 2010, Kato et al., 2023, Murakami et al., 2006, Nakashima et al., 2011, Seeger et al., 2006, Sennhauser et al., 2007).

Similar to PBP, different subsets of residues in this pocket were found to bind to structurally different substrates, while some residues overlap in interaction with different substrates (Zhang et al., 2023a). Importantly, several of these residues are highly conserved among AcrB, Kp-AcrB, MtrD, MexB, CmeB, RE-CmeB, AdeB, and AdeJ (Lyu et al., 2020, Morgan et al., 2022, Murakami et al., 2006, Su et al., 2019, Zhang et al., 2023a, Zhang et al., 2023b). For example, Q176, conserved as glutamine among AcrB, MexB, OqxB, and AdeB, has been shown to increase binding energy to cefotaxime, enhancing recognition within DBP and resulting in increased efflux efficiency in *Salmonella* strains bearing the Q176K mutation in AcrB acquired through exposure to cefotaxime (Trampari et al., 2023, Zwama and Nishino, 2022). Despite the hydrophobic nature of DBP, hydrogen-bound interactions, possibly mediated by water processes, may also contribute to drug binding at this site. Notably, a predominantly hydrophobic DBP has been identified in the *K. pneumoniae* OqxB transporter (Bharatham et al., 2021, Li et al., 2019). This site includes negatively charged residues (E50, D87, and E184) and positively charged residues (R48, R157, and R774), predicted to be involved in H-bound interactions (Bharatham et al., 2021, Li et al., 2019). Targeted MD simulations have demonstrated that the AcrB pump employs water molecules to extrude substrates, as water molecules flow from the binding pocket to the exit gate during the extrusion state. This observation suggests that the directionality of substrate movement is facilitated by a stream of water, and the presence of water flattens the electrostatic interaction energy profile between the protein environment and the drug allowing for unobstructed passage of the substrate (Schulz et al., 2011). A subsequent study by these researchers demonstrated that doxorubicin translocation, driven by protein conformational changes, facilitated the development of a structured water layer in the transport channel of AcrB (Vargiu et al., 2018b). This enabled constant substrate hydration, promoting smooth diffusion over a free energy profile. These findings provide insights into polyspecific transport mechanisms by HAE1-RND transporters (Vargiu et al., 2018b).

The DBP has been divided into two subsites referred to as the groove and the cave. These subsites are suggested to facilitate the binding of various substrates. In a computational docking analysis, 30 compounds, including TET, NOV, RIF, and ERY, predominantly bind to a narrow groove in the upper part of the DBP (termed "groove binding") (Takatsuka et al., 2010). Another group, including NMP, ET, and CHL, primarily binds to the lower part of the DBP (termed "cave binding"). A third group, including PAβN, TX-100, cephaloridine, linezolid, and CIP, binds to both the narrow groove and the cave subdomains (Takatsuka et al., 2010). Imai et al., also demonstrated the existence of two 'multifunctional sites' (MSs) capable of binding aromatic, hydrophobic, and polar groups within the groove and cave sub-pockets (Imai et al., 2011). Intriguingly, a subsequent study found that although Takatsuka et al. did not explicitly state it, the compounds favouring binding to the groove are HMM, whereas those preferring the cave are LMM compounds (Atzori et al., 2020). This investigation also revealed that HMM carbapenems tend to bind to the groove, while LMM carbapenems prefer to bind to the cave, illustrating the polyspecific substrate-binding nature of AcrB and, more broadly, HAE1-RND transporters, which occurs through the utilisation of multifunctional sites within a drug-binding pocket (Atzori et al., 2020).

The existence of specific sites in the DBP provides intriguing insights into how the presence of one substrate can enhance the efflux of another substrate in AcrB. Quantitative analysis has demonstrated that the simultaneous presence of benzene, a solvent, or CHL in the test environment can enhance the efflux of nitrocefin. MD simulations support this concept by revealing that nitrocefin binds to the upper part, the groove area, while benzene binds to the bottom part, the cave area, within the DBP. Given that AcrB rapidly expels benzene, it consequently accelerates the efflux of nitrocefin (Kinana et al., 2016, Kinana et al., 2013).

Instances also exist where drug binding extends across both the PBP and DBP. An examination of crystal structures of RE-CmeB, bound with ERY, hydrolysed AMP and CHL, demonstrates that the binding of these antibiotics encompasses both PBP and DBP (Zhang et al., 2023a). Furthermore, analysis

of asymmetric structures of BpeB has uncovered a distinctive binding mode of the n-undecyl-β-D-maltoside (UDM) detergent molecule in the B protomer. This binding mode stands apart from all other detergent-bound RND transporters. Notably, the interaction of UDM involves residues from the lower G-loop and the HT (both features are described later in this section) located at the PBP-DBP interface. Further scrutiny of these structures has also revealed the presence of a second UDM molecule bound to the DBP like the ET-bound structures of AdeB (Kato et al., 2023, Morgan et al., 2021).

1.3.6.4.1.3.3 The hydrophobic trap

Within the DBP of AcrB, MexB, and other HAE1-RND type transporters, a hydrophobic pit or trap (HT) is established between PN1–PC1 at the bottom of DBP, highlighting a significant preservation of aromatic amino acid residues such as F136, F610, F615, F617, and F628 in AcrB (Figure 1.6) (Aron and Opperman, 2018, Ruggerone et al., 2013, Sjuts et al., 2016, Zgurskaya et al., 2021). Site-directed mutagenesis has shown that these phenylalanine amino acids are crucial for drug efflux by AcrB (Bohnert et al., 2008, Bohnert et al., 2011). Furthermore, MD simulations have elucidated the details of how the F610A mutation impairs efflux by AcrB (Vargiu et al., 2011).

The HT is critical for recognition and binding of several drugs, and more strongly, inhibitors (Aron and Opperman, 2018, Nakashima et al., 2013). An in-silico study categorising AcrB substrates as good or bad revealed that bad substrates are highly stable in the HT and PBP, while good substrates show low interaction with the HT. Additionally, binding of good substrates induces the displacement of TMS 8, causing a transition between the B and E states and an intermediate state (Malvacio et al., 2019). Molecular docking and MD simulations investigating poor and good substrates in AcrB revealed that cefepime, a good substrate despite lower hydrophobicity than ceftazidime, prefers binding to the HT (Atzori et al., 2019). Conversely, ceftazidime, a poor substrate, prefers binding outside the HT. The study emphasizes that surface complementarity between a substrate, cefepime, and AcrB, rather than the substrate's intrinsic hydrophobicity, is crucial for inducing allosteric

conformational changes required for drug efflux (Atzori et al., 2019). In alignment with these results, it has been previously shown that MEM, a recognised substrate of MexB, exhibits higher affinity to the DBP compared to IPM, a poor MexB substrate, with both compounds weakly interacting with the PBP (Collu et al., 2012, Masuda and Ohya, 1992, Pournaras et al., 2005). Furthermore, the hydration properties of the non-pharmacophore region of these compounds were identified as a potential determinant influencing their distinct binding behaviours (Collu et al., 2012). Consistently, a subsequent study employing MD simulations and free energy calculations to rationalise interactions between carbapenems and AcrB found that, except for IPM, all studied carbapenems, including MEM, displayed a relatively higher affinity for the DBP. This study also highlighted a preference for hydrophilic surface matching within the DBP for carbapenem antibiotics (Atzori et al., 2020). According to Ruggerone et al., distinctions in substrate binding strengths to the HT in AcrB may contribute to their ability to instigate allosteric structural changes in both the TMD and the periplasmic domain PD, facilitating substrate efflux (Ruggerone et al., 2013). The authors also propose that this phenomenon could be applicable to other HAE1-RND transporters (Athar et al., 2023, Ruggerone et al., 2013).

In a recent study investigating quinolone antibiotic competition, the HT's role in drug binding was clarified (Vergalli et al., 2022). Using a whole-cell efflux competition assay, the study quantitatively measured quinolone binding affinities and analysed efflux efficacy. Some quinolones efficiently competed, enhancing bacterial killing activities of some others. Rosoxacin particularly inhibited efflux of various fluoroquinolones, including norfloxacin, by tightly binding to the HT in the DBP and impeding norfloxacin binding through creating a steric hindrance (Vergalli et al., 2022). These findings have implications for developing drugs or inhibitors targeting RND pumps.

1.3.6.4.1.3.4 The Switch-loop

The PBP and DBP pockets in AcrB are separated by an HP-like loop situated between the PC1 and PC2 subdomains (Ababou and Koronakis, 2016, Eicher et al., 2012, Müller et al., 2017, Nakashima et al., 2011). This HP-like loop, common to Kp-AcrB, MtrD, CmeB, RE-CmeB, AdeB, and AdeJ (Lyu et al., 2020, Morgan et al., 2022, Murakami et al., 2006, Su et al., 2019, Zhang et al., 2023a, Zhang et al., 2023b), comprising eleven amino acid residues (^{613}NGFGFAGRGQN^{623}), or six amino acid residues (^{615}FGFAGR^{620}) according to different references, is referred to as the switch-loop or gate-loop (G-loop) (Figure 1.5 and Figure 1.6), with the F617 residue positioned at the tip (Eicher et al., 2012, Nakashima et al., 2011, Zwama and Yamaguchi, 2018). The switch-loop assumes distinct conformations in the A and B protomers, playing a role in directing the substrate path from the PBP in the A conformation to the DBP in the B conformation (Vargiu and Nikaido, 2012). The flexibility of the G-loop was supported by site-directed mutagenesis and crystallographic studies, that revealed that restricting the flexibility of the G-loop diminishes the transporter's capability to complete the extrusion cycle. Additionally, it results in reduced pump activity due to the obstruction of the substrate pathway caused by proline substitutions and the impact of the bulky phenylalanine residue at position 617 (Cha et al., 2014, Nakashima et al., 2011). Furthermore, this loop may be interacted with by substrates or inhibitors of AcrB. For example, mutagenesis of G616 has shown that this residue is implicated in macrolide binding to AcrB (Wehmeier et al., 2009).

Typically, high molecular mass drugs (HMMDs), such as Ery, exhibit binding affinity to the PBP and a looser binding to the DBP, whereas LMMDs, like doxorubicin, tend to bind loosely to the PBP and more firmly to the DBP (Murakami et al., 2006, Nakashima et al., 2011). Nakashima et al. supported this proposition in the same study through mutagenesis of residues located at different drug binding sites (Nakashima et al., 2011). MD simulation studies also suggest that the existence of various binding sites is, to some extent, influenced by the size of the substrate (Vargiu and Nikaido, 2012). However, cryo-EM structures of Kp-AcrB and MtrD reveal Ery binding to the DBP in the

B protomer, diverging from the findings of Nakashima et al. (Lyu et al., 2020, Zhang et al., 2023b). Furthermore, in the AcrB ortholog MexB, it has been demonstrated that HMMD compounds like lauryl maltose neopentyl glycol bind to the DBP in the B protomer, differing from original proposals (Nakashima et al., 2011, Sakurai et al., 2019, Zwama and Yamaguchi, 2018). This aligns with the functional rotation theory, suggesting that properties beyond size may influence substrate recognition by AcrB (Murakami et al., 2006, Seeger et al., 2006, Sennhauser et al., 2007). Differences in substrate selectivity between AcrB and its close homologue AcrD, as well as between MexB and its homologue MexY, also emphasise that characteristics other than size influence substrate selectivity (Kobayashi et al., 2014, Rosenberg et al., 2000). AcrB and AcrD share common substrates, such as most β-lactam antibiotics, owing to their amphiphilic nature. Nevertheless, AcrB transports lipophilic macrolides and tetracyclines, a task AcrD cannot accomplish. Conversely, AcrD handles hydrophilic aminoglycosides, which AcrB cannot transport (Kobayashi et al., 2014, Lau et al., 2014, Masuda et al., 2000). Comparative analysis of the physiochemical properties of the PBP and DBP of AcrB and AcrD revealed differences (Zwama and Yamaguchi, 2018). Notably, the lipophilicity index of the PBP and DBP of AcrB is higher compared to that in the corresponding pockets in AcrD, creating a favourable environment for binding its hydrophobic substrates. The DBP of AcrB exhibited the highest hydrophobicity, indicating its role as a hydrophobicity selectivity filter (Ramaswamy et al., 2017, Zwama and Yamaguchi, 2018). Additionally, distinct large electrostatic negative environment in the PBP of AcrB play a crucial role in recognising mono-cationic compounds. However, this becomes disadvantageous for hydrophilic polycationic compounds such as aminoglycosides because of the high lipophilicity exhibited by this pocket in AcrB (Ramaswamy et al., 2017). Moreover, AcrB exhibits an electrostatic funnel with a negative gradient from the periplasm to the centre of the PBP, potentially facilitating the extended recognition of positively charged compounds, aligning with the mono-cationic nature of various AcrB substrates (Ramaswamy et al., 2017). It is believed that this feature is essential for initial substrate recruitment by AcrB. Specific features, such as the flip conformations

of the T676-loop and the lipophilic bridge created by F617 of the G-loop, unique to AcrB (not in AcrD), are key contributors to the recognition and transport function of these pumps (Ramaswamy et al., 2017, Zwama and Yamaguchi, 2018). Moreover, the broader distribution of multifunctional sites in the DBP of AcrB, as compared to that in the DBP of AcrD, enhances the polyspecificity of AcrB toward hydrophobic and aromatic compounds, surpassing that of AcrD (Ramaswamy et al., 2017).

1.3.6.4.1.3.5 The central cavity

The large CC of AcrB was initially thought to be the site of drug entry and binding based on the first *R32* symmetric structure (Murakami et al., 2002). Subsequent symmetric structures of AcrB bound to four different ligands (R6G, ET, DQ, and CIP) revealed that these compounds bind to the wall of the CC located at the top of the CC above the CM surface (Yu et al., 2003). Various subsets of residues interact with different drugs, and hydrophobic interactions between the contributing residues of the CC and the bound compounds are dominant (Yu et al., 2003). Contributing residues are mainly F664, F666, E673, and R717. It was suggested that drugs are taken up via vestibules to the CC and from there through the central pore to the funnel at the top of the PD (Yu et al., 2003). To open the closed central pore in their structures, Q109 was changed to alanine, resulting in solved structures with five diverse ligands. Analyses reveal ligands binding to both the CC wall and the cleft between PC1 and PC2 subdomains (Yu et al., 2005). However, a review argues that binding of these substrates in the CC appears to be peripheral and loose and that interactions with the phospholipids need to be taken into account when defining this binding site (Ruggerone et al., 2013). Despite this argument, additional support for the hypothesis that the CC is a substrate-binding site for some substrates comes from the analysis of the structure of the AcrB and AcrD pumps. Linezolid, a crucial anti-Gram-positive bacterial agent, was identified binding to the CC in a cocrystallography study using symmetrical R32 crystals of AcrB and linezolid. It was observed to bind to the wall of the upper portion of the CC near residues A385 and F386 in each protomer of the symmetric trimer (Hung et al., 2013). Cryo-EM structures of AcrD with GEN bound

revealed that AcrD is capable of capturing aminoglycosides from the CC, with negatively charged residues located in the ceiling of this cavity playing a critical role in shuttling drugs for extrusion (Zhang et al., 2023c). GEN binding takes place in the E protomer and involves residues such as D99, D101, and E102 (Zhang et al., 2023c). It is believed that GEN is guided by four additional charged residues (R130, K131, D174, and D176) located in the central pore above the CC toward the bottom of the funnel in the DC domain. Subsequently, it exits AcrD through the exit site formed by Q125 and Y756 (Zhang et al., 2023c).

AcrB bound to fusidic acid, an anti-Gram-positive bacterial agent, reveals an additional drug binding site situated in the groove between TMS 1 and 2 in the TMD (Oswald et al., 2016). This site likely captures lipophilic and cocarboxylated substrates, including OXA, cloxacillin, dicloxacillin, and piperacillin, from β-lactam antibiotics in the outer leaflet of the IM, akin to the previously identified TMS 7/TMS 8 groove in the same protomer (Oswald et al., 2016). The suggested mechanism involves the upward motion of TMS 2 toward the periplasmic porter domain in response to protonation events during functional rotation cycling, facilitating the displacement of the bound molecule from the initial binding site at the TMS 1/TMS 2 groove to the DBP through the PN2/PC1 interface pathway (Oswald et al., 2016, Tam et al., 2020). Interestingly, in the pursuit of comprehending the cooperative kinetics of AcrB when multiple drugs present, a study utilising a drug cocktail of Ery, OXA, linezolid, and FUS in co-crystallization of WT AcrB revealed an additional FUS binding site deep within the TMD. This site is surrounded by TMS 2, TMS 4, and TMS 10-12, situated near the triad of proton relay (D407, D408, and K940). Named the deep TMD binding pocket (TMD-BP), analysis of this structure, along with other FUS-bound structures under varying crystallisation conditions, suggests that this new mode of FUS binding is allosteric. Consequently, it is proposed that TMD-BP functions as an allosteric site (Tam et al., 2021).

1.3.6.4.1.3.6 The drug entrance channels

The drug binding pockets are connected to the outside of the protein via four channels with entrances to the periplasm or the outer leaflet of the IM (Figure 1.6). AcrB utilises these pathways to take up drugs from the periplasm or the outer leaflet of the IM. Channel 1 (CH1) (Figure 1.6), leading to the PBP, is situated in the vicinity of the vestibule and opens to the inner membrane, specifically to the groove formed between TMS 7/TMS 8 (Nakashima et al., 2011). It is noteworthy that Murakami et al. later designated the vestibules initially observed in the symmetric structure as CH1 (Figure 1.5) (Kato et al., 2023). In many AcrB structures, a molecule of dodecyl β-D-maltoside (DDM) binds at the entrance of the CH1 to the TMS 7/TMS 8 groove of the A protomer (Eicher et al., 2012, Nakashima et al., 2011, Tam et al., 2021, Tam et al., 2020). An intermediate structure of AcrB (between A and B) unveiled the entrapment of DDM within a tunnel formed between TMS 8 and PC2 located at PBP, in close proximity to the F-loop. This interaction involves several residues of PBP, the F-loop, and the tilted TM8, suggesting that the substrate is directed through CH1 via the suggested peristaltic motion rather than through diffusion (Tam et al., 2021). The process begins with initial binding at the TM7/TM8 groove, followed by peristaltic movement to the DBP (Tam et al., 2020). DDM export supports the idea that substrates partitioned in the membrane likely enter the pump through CH1 (Murakami et al., 2006, Nakashima et al., 2011, Seeger et al., 2006, Sennhauser et al., 2007). Systematic substitution of residues lining CH1, those facing the TMS 7/TMS 8 groove, and the CH1 entrance revealed that CH1 serves as the primary transport pathway for LMM and low polar surface area (LPSA) substrates such as DDM, β-lactams, fusidic acid, and novobiocin. Conversely, HMM polyaromatic cationic compounds like ERY may use alternative pathways through AcrB, potentially through CH2 (Figure 1.6) (Tam et al., 2021). Furthermore, mutational analysis has revealed that the F-loop may contribute to drug translocation not only via CH1 but also through CH4 (to be described later in this section) (Tam et al., 2021). It is noteworthy to mention here that the N-terminal end of TMS 8, referred to as the hoisting loop or convertible TM section, is a region where a coil-to-helix transition occurs. It is evident that this

coil-to-helix transition of the hoisting loop is involved in the opening and closing of CH1 (Kobylka et al., 2020).

Leading to the proximal pocket, CH2 opens to the periplasm at the lower external depression formed between PC1 and PC2, expected to be the main route for gathering substrates present in the periplasm. CH2 is present in both A and B protomers. In MD simulations, it has been demonstrated that CH1 is involved in gathering hydrophobic drugs with relatively LMM, while CH2 plays a role in collecting hydrophilic drugs with relatively HMM (Yao et al., 2013). In AcrB this external cleft or entrance is surrounded by residues F664, F667, L668, R717, and L828 (Husain and Nikaido, 2010, Vargiu and Nikaido, 2012). All CH2 entrance residues in AcrB are conserved as identical residues in Kp-AcrB (Zhang et al., 2023b). In the *C. jejuni* RE-CmeB protein, the entrance of CH2, involves residues Y658, L660, R710, and D823 (Zhang et al., 2023a). Notably, among these residues, R710 (R717 in AcrB) is conserved across RE-CmeB, AcrB, AcrD, MtrD and MexB (Lyu et al., 2022, Morgan et al., 2021, Murakami et al., 2006, Sennhauser et al., 2009b, Zhang et al., 2023a). It has been suggested that CH2 entrance residues play a crucial role in drug selectivity and specificity (Schuster et al., 2016, Zhang et al., 2023a, Zhang et al., 2023b). For example, R717 in AcrB has been demonstrated to reduce steric barriers associated with AZM passage via CH2 when mutated to leucine, leading to clinical-level resistance to AZM (Lyu et al., 2022, Morgan et al., 2021, Murakami et al., 2006, Sennhauser et al., 2009b, Trampari et al., 2023, Zhang et al., 2023a).

A flexible F-loop, identified in AcrB, Kp-AcrB, RE-CmeB, MtrD, AdeB, and AdeJ, connects the CH2 entrance to the PBP (Lyu et al., 2020, Morgan et al., 2021, Morgan et al., 2022, Su et al., 2019, Zhang et al., 2023a, Zhang et al., 2023b). In both AcrB and Kp-AcrB, this flexible loop is composed of residues ^{669}PAIVELGT^{676} and connects the PC1 and PC2 subdomains (Ec-AcrB numbering) (Tam et al., 2021, Zhang et al., 2023b). Certain residues within the F-loop contribute to the formation of the bottom of the PBP (Schuster et al., 2016, Zhang et al., 2023a). The prevailing belief is that drugs recognised by the CH2 entrance are guided by the F-loop to reach and bind to the PBP

(Zhang et al., 2023b). Subsequently, the drug molecule will pass through the G-loop to access the DBP before being expelled by the pump (Zhang et al., 2023b). Some of the residues in the loop have also been found to play a critical role in drug selectivity, such as I670 in AcrB (Schuster et al., 2016). Moreover, the F-loop has been suggested to play an important role in drug transport from both CH1 and CH4 (Tam et al., 2021).

CH3 opens to the central cavity, connecting the DBP directly to the CC by passing the PBP and the switch-loop (Figure 1.6) (Nakashima et al., 2011). This channel is observed in the T protomer. Cationic substrates, such as ET with a planar aromatic structure, prefer CH3 to CH1 and CH2, and the efflux of such compounds has been shown not to compete with substrates that use CH1 and CH2 (Zwama et al., 2018). Molecular docking studies have identified that chlorpromazine, an antipsychotic drug, binds directly below the CH3 domain in both the *E. coli* and Salmonella enterica AcrB transporters (Grimsey et al., 2020). Referred to as CH4, the groove formed between TMS 1 and TMS 2 orients membrane-localised substrates, such as carboxylated drugs and hydrophobic β-lactams, from their initial binding site at the TMS 1/TMS 2 groove to the DBP at the PD (Figure 1.6) (Tam et al., 2020). It has been suggested that these substrates are transported independently via both CH1 and CH4 (Tam et al., 2020).

The latest structures of ET-bound AdeB, characterised by asymmetry, reveal the binding of multiple ET molecules at distinct sites within a single protomer, including the entrance of the periplasmic cleft, the DBP, and the HT. This finding underscores the plasticity and flexibility inherent in AdeB, providing compelling evidence that supports the existence of a substrate extrusion pathway in RND pumps, particularly in the context of the drug efflux mechanism (Morgan et al., 2021).The presence of several expansive drug-binding pockets, specifically DBP and PBP, in AcrB, each housing multiple drug-binding sites utilising unique sets of residues to engage with a variety of structurally diverse antimicrobials, offers valuable understanding into the versatile nature of RND pumps. Furthermore, these drug binding sites exhibit flexibility and overlap, featuring an abundance of polar and aromatic residues.

These characteristics allow them to bind substrate molecules at various locations and orientations, reinforcing the pumps' polyspecific nature. Specifically, this pertains to the HAE1 type RND transporters and MDR in Gram-negative bacteria (Kato et al., 2023, Zgurskaya et al., 2021, Zhang et al., 2023a). The proposed mode of multisite multiple drug binding in AcrB differs from the typically accepted conformational selection and induced fit modes in enzymology (Vogt et al., 2014). Instead, it is believed to align with principles elucidated by crystallographic studies of QacR and MtrR, which are soluble regulators of the multidrug efflux proteins QacA and MtrD, respectively (Beggs et al., 2021, Beggs et al., 2019, Schumacher et al., 2001).

Moreover, the use of multiple channels, accessing distinct cellular environments where drugs with varying physiochemical characteristics are compartmentalised, amplifies ability of AcrB to accommodate and transport structurally different substrates. These attributes of AcrB elucidate the polyspecific nature of the HAE1 RND transporters (Kato et al., 2023, Zhang et al., 2023a).

An alternative explanation for the promiscuity of AcrB is provided by the multisite-drug-oscillation hypothesis. Experimental evidence demonstrates that drug efflux by AcrB is an efficient process (Matsumoto et al., 2011). However, the question of how this efficient drug elimination aligns with the seemingly low binding affinity of certain drugs, as predicted by co-crystal structures, has led to the multisite-drug-oscillation hypothesis (Yamaguchi et al., 2015). According to this hypothesis, drug molecules oscillate within a large binding pocket. In this mechanism, even if the affinity for each individual site is low, the overall binding efficiency within the pocket may be high (Yamaguchi et al., 2015). The dynamic nature of multiple binding sites, driven by spatial changes in internal cavities due to peristaltic motions, is crucial for preventing drug entrapment in a single site and facilitating smooth efflux through multisite drug oscillation (Marsh, 2015, Ramaswamy et al., 2017).

Having explored the detailed structural characteristics of drug binding sites and substrate pathways in the *E. coli* AcrB protein, we will now delve into the fascinating realm of proton translocation and the mechanisms that energise

the efflux process. While AcrB's structure provides the foundation, understanding its functional dynamics adds a crucial layer to our comprehension of RND pumps.

1.3.6.4.1.4 Proton translocation and efflux energisation

Proton translocation and the energisation of efflux in RND transporters represent a complex interplay of molecular mechanisms essential for bacterial survival in hostile environments. These intricate processes have been extensively studied to decipher the strategies bacteria employ to expel harmful substances and confer MDR.

As described previously (Section 1.3.6.3), substrate efflux by RND transporters is catalysed via an H^+ antiport mechanism (Okusu et al., 1996, Paulsen et al., 1996b, Thanassi et al., 1997, Zgurskaya and Nikaido, 1999). Functional assays employing a reconstituted MexAB-OprM system in liposomes has demonstrated an effective drug transport, with a notable correlation with a proton gradient (Verchere et al., 2015).

An amino acid network involving residues D407 and D408 on TMS 4, K940 on TMS 10, and R971 and T978 on TMS 11 contributes to the formation of a proton relay network in the TMD, suggesting a mechanism for proton translocation in AcrB (Guan and Nakae, 2001, Su et al., 2006, Takatsuka and Nikaido, 2006). Analysis of the initial symmetric AcrB structure revealed that K940 forms two ion pairs, one with D407 and another with D408 (Murakami et al., 2002). In the asymmetric structures of AcrB, the two ion pairs were observed in the A and B protomers. However, in the E protomer, which showed the largest conformational alteration, these ion pairs are not present, and instead the side chain of K940 reorients away from D408 and forms a salt bridge with D407, stabilised by the hydrogen bonding of T978 on TMS 11, causing the twisting of TMS 4 and TMS 10 (Murakami et al., 2006, Seeger et al., 2006, Sennhauser et al., 2007). This substantial movement in the TMD was proposed to drive simultaneously a sequence of conformational changes in the PD that lead to the closure of the entrances, the opening of the EG, and the compression of the DBP (all seen in E conformation), ultimately propelling

the bound substrate into the lumen of the TolC channel (Murakami et al., 2006, Seeger et al., 2006, Sennhauser et al., 2007).

Coupling of drug export in PD and proton translocation in TMD was elucidated in a study by Eicher et al (Eicher et al., 2014). Within the porter domain, each protomer contains two structural repeats, PN1/PC2 and PN2/PC1, with PN1/PC2 remaining rigid throughout the ABE cycle and PN2/PC1 changing conformation during the A to T and T to E states. In the TMD, each protomer contains two structural repeats, R1 (the six N-terminal helix bundle) and R2 (the six C-terminal helix bundle). R1 and R2 undergo concerted motions during the ABE cycle, with R1 and R2 switching between an engaged state in the A and B conformations and a disengaged state in the E conformation. Residues, D407, D408, K940, and R971, control the positioning of the repeats relative to each other. Proton relay across the membrane has been observed, with D924 and E346 residues binding two protons at the periplasmic side in the A and B state, and D407 and D408 binding the protons in the E state. The disengagement and engagement of the R1 and R2 repeats are consistent with the proposed protonation state of D407 and D408 during the B to E transition and the deprotonation state during the E to A transition, respectively. Two remote alternating-access conformational phases have been suggested to couple drug export in the porter domain with proton uptake in the TMD, with each cycle enabled by two types of collective motions of two structural repeats that are coupled by two adjoining alpha-helices (TMS 2 and TMS 8) projecting from the membrane (Eicher et al., 2014).

Seeger et al's research identified D408 as the critical residue with a p*Ka* of 7.4 for binding and releasing protons at physiological pH (Seeger et al., 2009). It has been suggested that the E protomer has both D407 and D408 protonated, while in the B conformation, they are deprotonated. The A protomer may have protonated D408 and deprotonated D407 or both deprotonated (Seeger et al., 2009). Transition from B to E alters the local environment of D407 and D408, increasing their p*Ka* values and promoting proton binding from the periplasm. Additionally, R971 was proposed to play a pivotal role in the pathway from the triad to the cytoplasm (Seeger et al., 2009).

These findings were consistent with the findings of all-atom MD simulations and observations from the asymmetric structures (Yamane et al., 2013). Structural changes in the porter domain, indicative of the transition from E to A state in protomer E, were observed during the simulation of D407 deprotonated and D408 deprotonated for all three protomers, representing a step in the functional rotation cycle of AcrB. Analyses suggested that the deprotonation of only D408 leads to a structural transition from E to A, implying a proton translocation stoichiometry of one proton per complete functional cycle of one AcrB protomer (Yamane et al., 2013, Yue et al., 2017). A proposed exchange mechanism suggested that in the B state, the core triad has access to the periplasm via a water or proton channel, adopting an outward-facing conformation that facilitates proton transfer from the periplasm. Conversely, in the E state, the core triad gains access to the cytoplasm via a water or proton channel, accepting an inward-facing conformation allowing the release of protons into the cytoplasm (Yue et al., 2017). MD simulations revealed that in protomers A and B, the continuously hydrated TMD core region containing residues D407, D408, and K940 has access to periplasmic and cytoplasmic bulk water. However, in protomer E, such access is absent, indicating an asymmetric distribution of TMD water (Fischer and Kandt, 2011). The study identified three potential proton transfer channels connecting the TMD interior to bulk water—one cytoplasmic and up to three periplasmic channels in protomers A and B (Fischer and Kandt, 2011). Consistent with these findings, a continuous water pathway in the TMD linking cytoplasmic water to the titratable triad has been identified in the *Mycobacterium tuberculosis* MmpL3 protein illustrating a putative route for proton translocation (Li et al., 2023).

Free energy calculations revealed atomic details of the intricate connection between proton translocation in the TMD and functional rotation, with Matsunaga et al.'s study proposing that protonation of D408 in the TMD of the B protomer initiates the functional rotation in trimeric AcrB (Matsunaga et al., 2018). The suggested mechanism involves an energy-consuming B to E state transition that links TMD and PD, where protonation of D408 in the B state induces a vertical shear motion in the TMD, regulating water access and PD motion (Matsunaga et al., 2018). The extension of TMS 8 acts as a transmitter,

initiating rigid body motion in the PN2/PC1 tandem, opening EG, and shrinking DBP. During E to A transition, the PD of the E protomer relaxes towards A, possibly driven by cooperativity between protomers without systematic couplings with the TMD (Matsunaga et al., 2018). These findings align with a previous study indicating that protonation of D408 in the E state stabilises the asymmetric structure of AcrB, and deprotonation of D408 induces the opening of the entrance and closing of the EG, leading to the transition from E to A state (Jewel et al., 2017).

Building on the insights gained from proton translocation, the subsequent section will delve into the specific details of the efflux mechanism employed by AcrB, shedding light on its crucial role in multidrug resistance.

1.3.6.4.1.5 Drug efflux mechanism of the *E. coli* AcrB protein

The efflux mechanism of AcrB was originally proposed based on its symmetric crystal structure (Murakami et al., 2002). When AcrB interacts with a substrate, it recruits TolC to create a direct path from inside the cell to the outside. Drug molecules travel through the CH1, and vestibules to reach the CC, where they can be transported through TolC to the outside (Murakami et al., 2002). However, with the advent of the asymmetric structures in 2006, a three-step functional rotation mechanism for the efflux function of AcrB was proposed (Murakami et al., 2006, Sennhauser et al., 2007). This mechanism outlines that conformational changes in the three protomers are interdependent, with each protomer of the trimer sequentially cycling through three different conformations, each corresponding to a functional state in drug transport. Yamaguchi and Pos summarised the drug efflux mechanism (Kobylka et al., 2020, Yamaguchi et al., 2015, Zwama and Yamaguchi, 2018). In the A state, assumed to be the resting state and ready for substrate uptake, the PBP expands between PC1 and PC2, while the DBP contracts between PC1 and PN2. Conversely, in the B state, the PBP shrinks, and the DBP expands due to the separation of the PC1 and PN2 subdomains (Nakashima et al., 2011). In both the A and B functional states, the entrance from the periplasm is open, and in the B state, entrances from both the periplasm and the outer leaflet of the IM are open, allowing potential substrates to access the

uptake channels. However, the exit to the central pore and top funnel remains closed in both A and B states due to the inclination of the central helix from the E protomer, preventing the bound substrate from moving out (Murakami et al., 2006).

HMMDs initially bind to the PBP along with the CH2 pathway in the A state, but they cannot move deeper into the DBP because the space underneath the G-loop is too narrow in this state (Nakashima et al., 2011). The G-loop facilitates accommodation of HMMDs in the PBP and plays an important role in efflux mechanism of AcrB (Ababou and Koronakis, 2016, Eicher et al., 2012, Müller et al., 2017, Nakashima et al., 2011, Tam et al., 2021). The transition from the A to B state leads to the expansion and activation of the DBP. This happens as PC1 and PN2 separate, also causing the PBP to contract, and the G-loop to swing away. This movement facilitates the deeper penetration of HMMDs, allowing them to pass through the G-loop. (Cha et al., 2014, Nakashima et al., 2011). The binding and translocation mode of HMMDs has found support through the analysis of AcrB structures in the intermediate state during the transition from A to B (Tam et al., 2021). During the A stage, LMMDs, such as doxorubicin, can access the DBP by slipping underneath the switch-loop after being loosely positioned in the PBP (Zwama and Yamaguchi, 2018). Moreover, LMW and LPSA substrates initially bind to the groove formed by TMS 7/TMS 8 or TMS 1/TMS 2, interacting with residues in either the CH1 or CH2 pathways. They then proceed to move towards and interact with the PBP and the F-loop. During the transition from the A to B state, these substrates shift their position to interact with residues at the DBP mediated by G-loop (Tam et al., 2021). In the case of cationic substrates with a planar aromatic structure, they initially bind to the CC and, through interaction with residues in the CH3 pathway, move to bind to the DBP during the transition from the A to B state bypassing the PBP (Zwama et al., 2018). In the B state, LMMDs or HMMDs are attached to the now active DBP. The binding of drugs at the DBP stabilises the B state, inducing a downward shift in TMS 2 and a slight TMD displacement, facilitating proton accessibility from the periplasmic side in the TMD (Kobylka et al., 2020). Despite the initial assumption that HMMDs are not tightly bound to the DBP and are instead occluded within the

DBP due to an inability to move past the G-loop, later crystal structures of HMMDs demonstrated that they are indeed bound to the DBP (Yamaguchi et al., 2015, Zhang et al., 2023b). In both A and B states, the PC1/PC2 cleft is open, but it is wider in the A state.

The shift from the E to A state occurs as a result of proton release to the cytoplasm, triggering conformational changes in the PN1 and PC2 subdomains. This leads to the closing of the EG and the opening of the PC1/PC2 cleft, ultimately restoring the system to its initial A state. Therefore, during functional rotation the substrates undergo transportation from the entrance to the PBP, then to the DBP, and ultimately to the funnel-like exit through the peristaltic motion of the AcrB porter domain (Seeger et al., 2006). Evidence supporting the functional rotation mechanism and interdependence of both the subdomains within a protomer and individual protomers is derived from a covalently linked trimer of AcrB (Takatsuka and Nikaido, 2009). In this arrangement, a single protomer is inactivated either by a mutation in the proton relay network or by disulphide cross-linking of the PC1/PC2 cleft (Takatsuka and Nikaido, 2009). Additionally, site-directed cross-linking, achieved by introducing cysteine at interfaces of moving subdomains, contributes to this evidence (Seeger et al., 2006).

The proposed drug export mechanism of AcrB and allosteric coupling among the trimer's three protomers have also received support from several MD simulations studies. It has been demonstrated that the thermodynamically stable form of the trimer is the BEA structure, with a substrate molecule bound to the B protomer. Conversely, substrate dissociation stabilises the resting symmetric AAA structure, which represents an off-pathway state (Yao et al., 2010). This implies that when AcrB substrates are scarce, the trimer transitions into the AAA state, similar to the initially symmetric structure reported by Murakami (Murakami et al., 2002, Yao et al., 2010). In the resting state, AcrB can avoid energy loss by refraining from translocating protons. Symmetric resting states have also been reported for MtrD, CmeB, and CusA (Bolla et al., 2014, Long et al., 2010, Su et al., 2017). Additionally, these analyses have revealed that protonation in the TMD of the B protomer, which contains a

bound substrate, triggers the B to E change in this protomer. This change coincides with the completion of alterations in the two other protomers (the E to A change in the extrusion protomer via deprotonation and the A to B change in the access protomer through substrate binding to the porter domain), resulting in substrate export towards the exit tunnel to the TolC channel. This dynamic has been suggested to be the possible scenario of AcrB function, consistent with the proposed functional rotation mechanism of efflux (Yao et al., 2010). This MD simulations study has also suggested that completing a full functional cycle is not essential for the bond drug export alone, but it is necessary for the next cycle (Yao et al., 2010). Consistent with these findings, MD simulations demonstrated displacement of doxorubicin through translocation pathway during the B to E transition (Schulz et al., 2010, Zuo et al., 2015).

The discovery of intermediate states supports the functional rotation theory. In BpeB, the A protomer exhibits a hybrid A-B state with closures in CH1 and CH2, resembling the E state of AcrB and MexB. Additionally, in the TMD, it shows an extrusion conformation akin to the E state of AcrB and MexB (Kato et al., 2023). This suggests the occluded conformation of the A protomer of BpeB as the initial intermediate state transitioning from extrusion to access (Kato et al., 2023). The functional rotation mechanism in AcrB mirrors ATP synthesis F_1F_0 ATPase, with coordinated conformational changes among protomers (Boyer, 1997, Murakami et al., 2006). Trimerisation in AcrB compensates for entropy loss, essential for functional rotation (Mishima et al., 2015). Cryo-EM structures of AcrB revealed protein-lipid interactions impacting its active mechanism, facilitating conformational changes during drug extrusion (Qiu et al., 2018). Protein-lipid interactions differ among the three protomers and facilitate inter-protomer communication signals during drug extrusion (Qiu et al., 2018).

1.3.6.4.2 The *E. coli* AcrZ protein

AcrZ, formerly known as YbhT, is a small protein in *E. coli* identified for its role in enhancing resistance to specific antibiotics that are substrates of AcrB. (Fontaine et al., 2011, Hemm et al., 2008, Hobbs et al., 2012, Moussatova et

al., 2008). This 49-amino-acid protein is highly conserved among enterobacteria and other Gram-negative species but is absent from *Neisseria* (Fontaine et al., 2011, Hemm et al., 2008, Hobbs et al., 2012, Moussatova et al., 2008). The expression of AcrZ is coregulated with the *acrAB* operon by transcriptional factors that regulate cellular responses to antibiotics, detergents, redox cycling drugs, and other stresses. This suggests the significance of AcrZ in the efflux activity of AcrB (Hobbs et al., 2012). AcrZ has been shown to affect specificity of drug export of AcrB as Δ*acrZ* strains of *E. coli* are hypersensitive to some but not all of the AcrB substrates. Examples include CHL and TET antibiotics. AcrZ forms a hydrophobic TMS and interacts with the AcrAB-TolC efflux pump via the concave surface of the TMD of AcrB (Hobbs et al., 2012, Wang et al., 2017). The interaction between these two proteins has been confirmed by mass spectrometry (Chorev et al., 2018).

Cryo-EM analysis of AcrB and AcrBZ in saposin A discs containing *E. coli* lipids, with or without supplemented cardiolipin, revealed that AcrZ, in combination with cardiolipin modulates AcrB efflux activity toward CHL (Du et al., 2020). Similar to the previous observation of a well-organised lipid bilayer in the CC region of AcrB, a well-organised lipid bilayer is observed in AcrBZ structures (Du et al., 2020, Qiu et al., 2018). Conformational changes in PC1/PC2, PN2, TMS 2, and TMS 8 regions have been identified in AcrZ-bound AcrB, with significant bending around the P16 position of AcrZ crucial for interaction with AcrB and drug efflux (Du et al., 2020). AcrZ and cardiolipin together enhance CHL efflux by AcrB, inducing changes in entry channels, gating loop, and the drug-binding pocket. MD simulations highlight that cardiolipin prefers interaction with the AcrBZ complex due to increased contact surface resulting from AcrZ binding (Du et al., 2020). The study proposes collaborative allosteric modulation of AcrB by AcrZ and lipids, suggesting broader implications for membrane protein regulation (Du et al., 2020).

It is noteworthy to mention that an earlier study revealed the interaction between AcrB and another relatively small TM protein named YajC (Törnroth-Horsefield et al., 2007). This interaction was found to induce a specific rotation in the porter domain, as observed in the co-crystal structure with AcrB. *E. coli*

cells lacking YajC were found to exhibit modestly increased sensitivity to certain β-lactam antibiotics, excluding CHL or TET (Hobbs et al., 2012, Törnroth-Horsefield et al., 2007). While intriguing, the similarities and differences between AcrZ and YajC are yet to be explained.

1.3.6.4.3 Exploring the structural and functional mechanism of the complete tripartite RND systems

The complete structures of the AcrAB-TolC, and MexAB-OprM pumps have been identified (Daury et al., 2016, Du et al., 2014, Tsutsumi et al., 2019). These structures suggest a 3:6:3 stoichiometric assembly of the components (Daury et al., 2016, Du et al., 2014). In 2017, cryo-EM structures of the complete AcrAB-TolC were resolved in three states: without a substrate, in the presence of puromycin (a known AcrB substrate), and bound to MBX3132 (a potential AcrB inhibitor) (Sjuts et al., 2016, Wang et al., 2017). In the apo structure, TolC is closed at the periplasmic end, AcrA dimers show a gap at interfaces, and AcrB adopts a symmetric state (AAA), representing a resting state (Wang et al., 2017). In the structures solved in the presence of puromycin or bound to MBX3132, TolC is fully opened through tip-to-tip interactions with AcrA, forming a sealed channel, and AcrB adopts different asymmetric states in the presence of puromycin, and AcrB bound to MBX3132 depicts a TTT state, altogether representing a transport-activated state (Wang et al., 2017).

An allosteric mechanism for drug transport by AcrAB-TolC has been proposed based on these structural findings (Glavier et al., 2020, Wang et al., 2017). With substrates like puromycin, the periplasmic end of TolC undergoes an iris-like dilation resulting in full opening, and AcrB assumes asymmetric conformations, presumably gearing up for drug efflux. Quaternary structural changes in AcrB, transitioning from apo to transport-active state, are transmitted to TolC via AcrA, which seals the pump channel (Glavier et al., 2020, Lopez et al., 2017, Wang et al., 2017). AcrA also has been suggested to enforce directionality of substrate transport in RND transition states (Alav et al., 2021, Glavier et al., 2020). Additionally, cryo-EM structures of the MexA-MexB-OprM complex have suggested a similar allosteric mechanism of drug transport (Alav et al., 2021, Glavier et al., 2020, Tsutsumi et al., 2019). Long-

distance communication among the IMP AcrB, the MFP AcrA, and the OMF TolC has been elucidate through a comparative analysis of resting and transport-active states utilising difference distance matrices, along with insights from evolutionary couplings data and buried surface area measurements (Webber et al., 2022). These analyses have revealed that substrate binding by the IMP initiates quaternary-level conformational changes in the MFP. These changes prompt the OMP to transition from a closed to an open state, accompanied by a notable increase in the interface area between MFP subunits and between OMPs and MFPs. This observation implies that the transport-ready state of the pump resides at a more favourable energy level than the resting state (Webber et al., 2022).

New trimeric assembly configurations provide insights into conformational communications between IMP AdeB and MFP AdeA (Morgan et al., 2021). Six AdeB populations were identified: AdeB-I, AdeB-II, AdeB-III without bound ET; and AdeB-ET-I, AdeB-ET-II, AdeB-ET-III with bound ET. Apo structures (AdeB-I, AdeB-II, AdeB-III) exhibit an EEE conformation with closed entrances and evident extrusion channels. They differ in TMD arrangements: AdeB-I as a trimeric TMD, AdeB-II as a dimer plus monomer, and AdeB-III as a monomer plus monomer plus monomer. It has been suggested that switching between these configurations may impact AdeB-AdeA protein-protein interactions at the periplasmic docking domain of AdeB, facilitating drug extrusion in the PD domain, akin to membrane fusion proteins CusA and AcrA in CusAB and AcrAB-TolC complexes (Du et al., 2014, Morgan et al., 2021, Su et al., 2011).

1.3.6.4.4 Expression of *acrAB* and *tolC*

The expression of *acrAB* and *tolC* in *E. coli* is regulated at both local and global levels. Although located in separate locations on the chromosome, their expression is frequently regulated by common mechanisms involving repressors, activators, two-component systems, and small RNAs. The *acrR* gene, divergently transcribed from *acrAB*, directly represses *acrAB* and its own expression (Ma et al., 1996). AcrR, which belongs to the TetR/QacR family of transcriptional regulators, functions as a dimeric-two-domain molecule, with the N-terminal region containing the helix-turn-helix containing DNA-binding

domain and the C-terminal region forming the dimerisation and multidrug-binding domain (Li et al., 2007, Peters et al., 2011). AcrR, however, does not entirely inhibit the expression of *acrAB*, allowing constitutive expression of the transporter and thus intrinsic MDR. In addition to AcrR, two other proteins, AcrS and SdiA, are involved in the regulation of *acrAB*. AcrS, a direct repressor of the AcrEF pump, also represses the expression of other multidrug transporter genes, including *acrAB* (Hirakawa et al., 2008). SdiA, the quorum sensing receptor, positively controls the expression of *acrAB*, possibly by acting as a minor activator (Rahmati et al., 2002). Three global regulators, MarA, SoxS, and Rob, positively control the expression of *acrAB* and *tolC* (Alekshun and Levy, 1997, Barbosa and Levy, 2000, Kwon et al., 2000, McMurry et al., 1998). In addition, the two-component system EvgAS regulates the expression of both *acrAB* and *tolC*, and the PhoPQ two-component system regulates the expression of *tolC* (Eguchi et al., 2003). Furthermore, the small RNA RyeB has been demonstrated to be involved in controlling *acrAB* expression. The existence of multiple regulatory systems controlling the expression of RND pumps at both local and global levels facilitates the adaptation of bacteria hosting these systems to various environmental conditions (Li et al., 2015).

1.3.6.4.5 Inhibition of the AcrAB-TolC pump

Numerous classes of EPIs have been identified to impede AcrAB-TolC activity and enhance antibiotic efficacy. Examples include PAßN, NMP, pyridopyrimidines, pyranopyridines from the MBX series, 2H-benzo[h]chromene derivatives (WK2) and nordihydroguaretic acid derivatives (Bohnert and Kern, 2005, Lomovskaya et al., 2001, Nakashima et al., 2013, Opperman et al., 2014, Vargiu et al., 2014, Wang et al., 2021, Wang et al., 2020c). Unfortunately, certain EPIs have been shown to possess acute toxicity and to accumulate persistently in tissue cells (Lomovskaya and Bostian, 2006, Lomovskaya et al., 2001). Additionally, some have exhibited off-target activity, such as NMP (Bolla et al., 2011). Consequently, no EPIs have received approval for clinical use to date, underscoring the challenges associated with developing universal or targeted EPIs and medications capable of overcoming efflux pumps (Bolla et al., 2011).

While no RND inhibitor has progressed to clinical use as of yet, studying them has yielded valuable insights into their activities and mechanisms for inhibiting efflux. Examples of RND inhibitor series will be briefly discussed here, followed by a brief discussion about their interactions with RND transporters and mechanisms of inhibition.

PAβN, for instance, has demonstrated the ability to potentiate the activities of certain antibiotics, including fluoroquinolones, macrolides, CHL, and RIF, but not aminoglycosides and β-lactams (Cortez-Cordova and Kumar, 2011, Mamelli et al., 2003, Schweizer, 2012, Zechini and Versace, 2009). However, a drawback of PAβN is its observed cytotoxicity as demonstrated in a murine model (Renau et al., 2003, Sun et al., 2014). Furthermore, it has membrane permeabilization effect on Gram-negative bacteria, such as *P. aeruginosa*, even at levels below those used in combination studies (Lamers et al., 2013, Lomovskaya et al., 2001, Matsumoto et al., 2011).

NMP and arylpiperazines constitute another group of inhibitors capable of reversing multidrug resistance in *E. coli* by impacting the AcrAB-TolC and AcrEF-TolC (Bohnert and Kern, 2005). NMP (14, 1-(1-naphthylmethyl)-piperazine) stands out as one of the most potent inhibitors in this group, boosting the activity of several antibiotics in *E. coli* overexpressing AcrAB-TolC and partially reversing resistance in *A. baumannii* (Pannek et al., 2006).

D13-9001, with a pyridopyrimidine core, is a specific inhibitor of MexB and AcrB binding to MexB and AcrB in the HT and inhibiting drug efflux by MexB and AcrB, respectively (Nakashima et al., 2013, Yoshida et al., 2007). However, it does not inhibit MexY. D13-9001 is highly water soluble, is minimally transported by efflux transporters, and exhibits almost no antibiotic activity (Nakashima et al., 2013).

The MBX compounds, specifically pyranopyridines, were initially described in 2014 as AcrAB-TolC efflux pump inhibitors in *E. coli* (Opperman et al., 2014). MBX2319, identified as a CIP potentiator, demonstrated the ability to enhance the activity of several families of AcrB substrate antibiotics (Opperman et al., 2014). Co-crystal structures of pyranopyridines revealed that MBX2319 binds

to the HT in the AcrB T protomer (Opperman et al., 2014, Sjuts et al., 2016). At present, the optimisation of pyranopyridine derivatives is ongoing, with MBX3796 and MBX4191 being the latest lead compounds in the optimisation process (Moir et al., 2021).

WK2, characterised by a 2H-benzo[h]chromene core, is an AcrB inhibitor that enhances the activity of several antibiotics (Guo et al., 2023, Wang et al., 2021). Without disrupting the bacterial outer membrane or causing toxicity in *Caenorhabditis elegans* at concentrations that inhibit efflux, some derivatives of this pharmacophore have shown a promising scaffold for further AcrB inhibitor discovery (Guo et al., 2023, Wang et al., 2021).

As part of the TXA series, TXA09155 has been developed to treat MDR *P. aeruginosa* infections in burn victims or cystic fibrosis patients (Zhang et al., 2022). It inhibits the efflux of several antibiotics, including fluoroquinolones, tetracyclines, and β-lactams, in *P. aeruginosa* strains overexpressing MexAB-OprM or MexYZ-OprM (Blankson et al., 2019, Zhang et al., 2022).

Pyridylpiperazine compounds have been recently described as AcrB inhibitors, enhancing antibiotic activity in *E. coli* (Plé et al., 2022). BDM88855 and its derivatives act as allosteric efflux-pump inhibitors, uniquely binding to the transmembrane domain (Plé et al., 2022). BDM91288, another member of this group, has been shown to enhance antibiotic activity against *K. pneumoniae* and reverse clinically relevant antibiotic resistance mediated by AcrAB-TolC overexpression. Cryo-EM confirms the binding of BDM91288 to the transmembrane region of *K. pneumoniae* AcrB, validating its mechanism of action (Vieira Da Cruz et al., 2024).

Two additional groups of RND inhibitors have also been described. Biogenic chalcones, such as ZINC000004695648 and ZINC000014762506, represent a group of compounds identified through computer-aided discovery approaches as stable hits against AcrB (Rathod et al., 2023). Furthermore, NSC-33353-derived compounds, a distinct group of RND inhibitors, act as MFP AcrA inhibitors, boosting the activity of antibiotics like NOV and ERY (Abdali et al., 2017, Darzynkiewicz et al., 2019).

AcrB inhibitors, like substrates, typically contain one or more hydrophobic moieties (Ornik-Cha et al., 2021, Zwama and Nishino, 2021). D13-9001 and the MBX series (MBX2329, MBX2931, MBX3132, MBX3135) have been identified to interact extensively with the hydrophobic face of the DBP including HT, involving key residues like F136, F178, I277, A279, Y327, F610, V612, F615 and F628 (Moir et al., 2021, Nakashima et al., 2013). This contrasts with substrate binding in terms of the intensity and multiplicity of interactions. Inhibitor-HT interactions involve strong π-π stacking with F178, F615, and F628 (Moir et al., 2021, Nakashima et al., 2013). High-affinity inhibitor-DBP interactions are assumed to competitively inhibit substrate binding through steric hindrance (Compagne et al., 2023). Additionally, inhibitor binding likely prevents the T-O transition, preventing conformational changes in other protomers (Compagne et al., 2023). Compared to inhibitors, substrate recognition is more flexible and dynamic, emphasising a gradual distinction between substrates and competitive inhibitors. Notably, certain substrates, like berberine, can also act as competitive inhibitors, depending on the specific efflux pump properties (Morita et al., 2016). Furthermore, inhibitor binding is influenced by the spatial characteristics of an efflux pump, as demonstrated by mutagenesis studies on MexB. Mutating positions 139, 277, 279, and 612 to the bulky amino acid tryptophan has rendered MexB insensitive to the inhibitor ABI-PP (Yamasaki et al., 2022).

Having thoroughly examined the intricacies of the *E. coli* AcrB transporter, a pivotal HAE1-RND type transporter and foundational prototype in understanding RND pump-mediated MDR, the focus will now transition to an exploration of the *N. gonorrhoeae* MtrD transporter. This shift will enhance our understanding of diverse aspects within the broader context of the thesis.

1.4 The *N. gonorrhoeae* multiple transferable resistance (*mtr*) system

The foundation of our understanding of antibiotic resistance in *N. gonorrhoeae* (gonococcus) lies in the pioneering work of P.F. Sparling, who first identified a common resistance mechanism in a laboratory-derived strain of the bacterium (Maness and Sparling, 1973). This mechanism, known as the *mtr* system (multiple transferrable resistance), demonstrated resistance to various hydrophobic antimicrobials (HAs), including antibiotics such as PEN, ERY, RIF, TET, as well as dyes like ET and acridine orange (Maness and Sparling, 1973).

In the early studies, Sparling and colleagues linked a single mutation at the *ery* locus to low-level resistance, and they discovered class mutations designated as *env* that influenced cell envelope properties (Sarubbi et al., 1975, Sparling et al., 1975). Later, a clinical isolate revealed the existence of the *mtr* locus, responsible for multiple transferrable resistance, and *penB*, which gave low-level resistance to specific antibiotics (Sparling et al., 1975). Notably, mutations at *penA*, *mtr*, and *penB* had an additive effect on resistance, and the coexistence of *mtr* and *penB* mutations demonstrated higher resistance levels (Sparling et al., 1975). The molecular basis of *mtr*-mediated resistance was associated with alterations in the OM, impacting the penetration of various compounds into the cell (Maness and Sparling, 1973). Subsequent studies linked *mtr* mutations to structural changes in the cell envelope, providing the first direct evidence of the association between antibiotic resistance and cell envelope modifications (Guymon et al., 1978).

Mtr mutations were proposed to arise in environments rich in toxic hydrophobic compounds, such as FAs and bile salts, providing selective pressure favouring *mtr* mutants with increased resistance to HAs (Morse et al., 1982). Clinical studies supported this, showing higher prevalence among rectal isolates from men who have sex with men, where *mtr* strains exhibited resilience to inhibition by faecal lipids (Morse et al., 1982, Zarantonelli et al., 1999). Further investigations revealed the impact of the *mtr* system on

gonococcal susceptibility to antibacterial peptides, emphasising its role in evading host defences (Blair et al., 2022, Shafer et al., 1998).

The significance of the *mtr* system extended to antibiotic susceptibility, as evidenced by reduced susceptibility to AZM and ERY due to *mtrR* mutations (Zarantonelli et al., 1999, Zarantonelli et al., 2001). Additional research identified the collaboration of the *PorIB* OMP and the MtrCDE efflux pump in conferring resistance to PEN and TET (Olesky et al., 2006, Shafer and Folster, 2006, Veal et al., 2002). Moreover, the overexpression of the *mtrCDE* efflux pump had broader consequences, influencing cellular transcription patterns beyond drug efflux. Enhanced expression of the *ccpR* gene, contributing to resistance against oxidative stresses, was observed in strains with *mtrCDE* overexpression, showcasing the global impact of drug efflux gene overexpression in bacteria (Ohneck et al., 2015).

In summary, the *mtr* system in *N. gonorrhoeae* plays a pivotal role in mediating resistance to a spectrum of antibiotics and impacts the bacterium's overall response to environmental challenges. Its multifaceted contributions underscore the complex interplay between genetic factors and antibiotic resistance mechanisms in this clinically significant pathogen. The MtrCDE efflux system is the sole RND pump in *N. gonorrhoeae* and stands as a promising target for innovative antimicrobial approaches. Clinical strains, notably BR87 and BR54, showcase hypersusceptibility to HAs due to small deletions in their *mtrC* or *mtrD* genes (Veal et al., 1998). In vivo studies in female mice affirm the role of the MtrCDE system in enhancing gonococcal survival in the genital tract, suggesting its prowess against natural host defence components (Jerse et al., 2003). Contrary to traditional views, an *mtrR* mutant strain displays heightened fitness in a mouse model, indicating a fitness advantage conferred by its antibiotic resistance (Warner et al., 2007). Further exploration into extensively drug-resistant clinical isolates, such as H041, reinforces the critical role of MtrCDE, as its inactivation significantly enhances susceptibility to various antibiotics, presenting a valuable strategy against multidrug resistance (Golparian et al., 2014, Ohnishi et al., 2011a).

Species within the genus *Neisseria* often share adaptive allelic variation, with commensal species frequently transferring resistance to *N. gonorrhoeae*, as supported by experimental evolution studies revealing convergence on mutations within ribosomal components or the *mtrRCDE* efflux pump for AZM-based selection, and *mtrRCDE*, *penA*, and *rpoB* for penicillin selection (Frost et al., 2024a, Rouquette-Loughlin et al., 2018b, Shafer, 2018). Observations by Wadsworth et al. suggest that gonococci with mosaic-like sequences in *mtrD* display strong linkage disequilibrium and epistatic effects, likely enhancing the activity of the MtrD multidrug efflux pump (Wadsworth et al., 2018a).

Amino acid changes in the MtrD transporter can result from spontaneous mutations or horizontal gene transfer. Highly efficient DNA repair mechanisms of *N. gonorrhoeae* facilitate gene transfer and recombination, enhancing its infectivity and resistance to host defences. Interspecies recombination, particularly the acquisition of AZM resistance and *mtr* locus mosaics, has been well-documented (Grad et al., 2016). Commensal *Neisseria* species serve as a reservoir for AMR alleles, including mosaic *mtr* alleles, which influence AZM and other MtrD substrates (Goytia and Wadsworth, 2022). An *in vitro* evolutionary study demonstrated the development of resistance to antibiotics like AZM and PEN in commensal *Neisseria* species, suggesting that interspecies DNA exchange in the oropharyngeal site through recombination can lead to the acquisition of mosaic *mtrRCDE* alleles in pathogenic *N. gonorrhoeae* from commensal *Neisseria* species (Frost et al., 2024b, Goytia and Wadsworth, 2022, Raisman et al., 2022).

Wadsworth and colleagues identified a mechanism underlying low-level resistance to MtrD substrates, including AZM, in certain U.S. gonococcal isolates collected through the Gonococcal Isolate Surveillance Project (GISP). Genomic sequencing of these isolates revealed mosaic-like sequences within the *mtr* locus, specifically involving the *mtrR* gene, the overlapping *mtrR*/*mtrC* promoter region, and the *mtrD* gene. These mosaic alleles, likely originating from *N. meningitidis* and *N. lactamica*, contain several nucleotide changes. The study highlighted the mtrR/*mtrC* promoter region and the *mtrD* gene as

key hotspots for mutations, driven by the acquisition of these mosaic alleles. Moreover, the research demonstrated epistasis between the mosaic *mtrR* and *mtrD*, which collectively reduced susceptibility to AZM by increasing the expression of the *mtrCDE* operon and enhancing the function of the MtrD efflux pump (Wadsworth et al., 2018b). Notably, a nucleotide change (T to G) in the -35 hexamer sequence of the mosaic *mtrCDE* promoter, along with two amino acid substitutions (S821A and K823E) in mosaic *mtrD*, were identified as the mechanistic basis for low-level resistance in strains with a mosaic *mtr* locus (Rouquette-Loughlin et al., 2018b, Shafer, 2018).

Further examples of mosaic-like alleles in the *mtr* locus have been reported. For instance, the clonally spreading strain ST9363 bears a mosaic *mtr* locus associated with low-level AZM resistance (MIC 2–4 µg/mL) (Gernert et al., 2020, Thomas et al., 2019b). The clonal spread of NG-MAST genogroup G12302 strains, which carry the mosaic-like *mtr* locus, has also been directly linked to low-level AZM resistance (Banhart et al., 2021). Mosaic *mtrD* and *mtrR* promoter 2 loci, along with mutations in the 23S rRNA AZM binding site, have been implicated in high-level AZM resistance in strains from the internationally spreading NG-MAST genogroup G12302, which had sustained transmission in Argentina from 2018 to 2022 (Gianecini et al., 2023). Although rare, mosaic *mtrD* has been reported to contribute to reduced AZM resistance, with only one isolate from South Africa carrying a mosaic *mtrD* with S812A and K823E substitutions during a 2015–2020 survey (Kakooza et al., 2023).

Non-mosaic *mtrD* mutations at MtrD drug binding site residues have also been linked to AZM nonsusceptibility, including R714H, L, and C changes, as well as K823E and N mutations. Most of these gonococcal strains also harbour *mtrR* promoter mutations (Grad et al., 2016, Harris et al., 2018, Ma et al., 2020a). In the U.S., amino acid changes in the *mtrD* gene, resulting from the acquisition of mosaic alleles from other *Neisseria* species or single nucleotide polymorphisms (SNPs), were identified in *N. gonorrhoeae* isolates in 2019. These changes include simultaneous S821A and K823E substitutions, indicative of mosaic *mtrD*, or a single K823E substitution from SNP events. Combinations of these mutations, along with mosaic *mtrR*, *mtrR* promoter

mutations, and 23S rRNA gene mutations, have been reported to contribute to various elevated MIC levels to AZM (Reimche et al., 2023).

1.4.1 Genetic organisation of the *mtr* locus

The genetic organisation of the *mtr* locus in *N. gonorrhoeae* has been meticulously examined, particularly in the antibiotic-sensitive strain FA19 (Hagman et al., 1995, Pan and Spratt, 1994). Spanning 6793 base pairs, this locus comprises four coding sequences (CDS), with *mtrC*, *mtrD*, and *mtrE* forming a single transcriptional unit or operon. The fourth gene, *mtrR*, is positioned 250 base pairs upstream of *mtrC*, transcribed divergently (Hagman et al., 1995, Pan and Spratt, 1994). The *mtrR* gene encodes MtrR, a 210-amino acid protein, that shares similarities with transcriptional regulators like the TET repressor family, AcrR, and AcrS proteins in *E. coli*, and LuxR in *Vibrio harveyi* (Brow et al., 1985, Ma et al., 1996, Ma et al., 1994, Swartzman et al., 1992).

The overlapping promoter regions of *mtrR* and *mtrC* have been identified, revealing -10, -35 sequences and the transcription start sites. A 13 bp inverted repeat sequence, with a single base pair deletion associated with high-level HA resistance in CH95 strain, is present in these promoters (Hagman et al., 1995, Shafer et al., 1995). Homology studies established similarities between the *mtr* region and the *acrAB* region of *E. coli* (Dinh et al., 1994, Ma et al., 1993, Ma et al., 1995, Pan and Spratt, 1994).

Deletion or missense mutations in *mtrR* increases resistance to HAs, indicating its role in responding to toxic faecal lipids in various environments (Pan and Spratt, 1994). Mutations in the *mtrR* promoter region, particularly the single base pair deletion in the inverted repeat sequence, lead to elevated MtrC production and heightened HA resistance (Shafer et al., 1995). Complete inactivation of *mtrR* results in less resistance compared to clinical rectal isolates with single base pair deletion in the inverted repeat sequence in the promoter region (Pan and Spratt, 1994). A common mutation at codon 45 (G45 to D) affects the helix-turn-helix domain of MtrR (Shafer et al., 1995).

The first gene in the *mtrCDE* operon, *mtrC*, encodes a the MtrC lipoprotein a member of the MFP family of proteins (Hagman et al., 1995, Hess et al.,

1986, Kobayashi et al., 2001, Lomovskaya and Lewis, 1992, Nies et al., 1989, Pan and Spratt, 1994, Poole et al., 1993, Saier et al., 1994). Inactivation of *mtrC* in FA19 and highly resistant strain KH8, renders them hypersusceptible to HAs, underscoring the significance of the *mtrCDE* system in HA protection (Hagman et al., 1995, Pan and Spratt, 1994).

Situated 12 base pairs downstream from the translational stop codon of *mtrC*, the second gene within the *mtrCDE* operon is *mtrD* (Hagman et al., 1995). With a length of 3204 base pairs, *mtrD* encodes the MtrD integral membrane protein with an anticipated molecular mass of approximately 114 kDa (Hagman et al., 1995).

The third gene, *mtrE*, encodes the MtrE lipoprotein an OMF family protein. Knocking out *mtrE* in strain FA19 confirmed its role in MDR via an active efflux mechanism (Delahay et al., 1997).

A fourth Mtr protein, MtrF, has been identified as crucial for exporting high levels of HAs in resistant gonococci strains (Folster and Shafer, 2005, Shafer et al., 2001). MtrF shares similarities with hypothetical proteins in other bacteria and exhibits amino acid identity with the AbgT protein from *E. coli* (Section 1.3.5.1) (Hussein et al., 1998, Shafer et al., 2001). The *mtrF* gene is divergently transcribed from the *mtrCDE* operon, and its expression is MtrR-dependent (Veal and Shafer, 2003). The involvement of MtrF in glutamine uptake and phase variation of the DNA methyltransferase ModA13 adds additional layers to the complexity of the *mtr* system (Friedrich et al., 2007, Sunkavalli et al., 2022).

1.4.2 Regulation of the *mtr* efflux system

The regulatory landscape of the *mtr* efflux system in *N. gonorrhoeae* mirrors the complexity observed in the *E. coli* AcrAB-TolC efflux pump. In response to environmental cues, intricate networks of negative and positive transcriptional regulators orchestrate the expression of efflux pump genes (Shafer et al., 2001). These regulators react to signals such as antimicrobial agents, environmental stress, and nutrient availability, reflecting the adaptability of the bacterium. The MtrR-dependent pathway, a trans-acting mechanism, involves

the transcriptional repressor MtrR, which specifically binds to the *mtrC* promoter, downregulating the *mtrCDE* operon (Hagman and Shafer, 1995).

Conversely, positive regulation comes into play through the MtrA protein, activated when gonococci encounter HAs (Rouquette et al., 1999). This induction, independent of MtrR, amplifies the expression of the *mtrCDE* operon, enhancing resistance to these agents (Rouquette et al., 1999). The interaction between MtrA and the *mtrCDE* promoter reveals a nuanced mechanism, where the presence of the effector TX-100 heightens the affinity of MtrA for the promoter (Zalucki et al., 2012).

Further investigations highlighted the involvement of the TonB-ExbB-ExbD complex in inducible resistance, adding a layer of complexity to the energy requirements beyond constitutive pump activity (Rouquette-Loughlin et al., 2002). The iron-repressed regulator MpeR emerged as a key link between antimicrobial efflux and iron transport, influencing gonococcal susceptibility by modulating the expression of *mtrCDE* (Mercante et al., 2012). As gonococci enter the late logarithmic growth phase, a critical juncture marked by declining free iron levels due to bacterial consumption, MpeR comes into play. It represses *mtrR*, unleashing increased expression of the *mtrCDE* efflux pump operon directly and under iron limitation. This dynamic interplay between genetic and physiological factors, particularly the availability of iron, shapes the expression of the *mtr* efflux system, thereby impacting the susceptibility levels of gonococci to efflux pump substrates (Mercante et al., 2012). The integration of these regulatory elements showcases the sophisticated strategies employed by *N. gonorrhoeae* to navigate and adapt to a diverse range of environmental challenges, providing crucial insights for developing effective antimicrobial strategies.

Regulation through MtrR impacts *farAB* expression, evident in higher levels in MtrR-positive FA19 compared to MtrR-negative KH15, influencing resistance to long-chained FAs. This contrasts with hydrophobic antimicrobial trends regulated by *mtrCDE*. MtrR regulates *farAB* by potentially activating transcription or indirectly through *farR* repression, part of the MarR family. The FarAB efflux pump, regulated oppositely to MtrCDE by MtrR, minimises

specific FA effects during infection. This dual regulation underscores the intricate control of MtrR over diverse efflux pump systems (Johnson and Shafer, 2015, Lee et al., 2003, Shafer et al., 2001).

Furthermore, integration host factor (IHF) has been identified as necessary for the FarR-mediated repression of the FarAB efflux pump. FarR was discovered to repress FarAB by binding to three sites, designated A, B, and C, in the sequence upstream of *farAB*. Additionally, IHF binds to the B site, implying a model where the expression of the *farAB*-encoded efflux pump in *N. gonorrhoeae* is regulated by the DNA binding activities of both FarR and IHF (Lee et al., 2006).

Beyond *trans*-acting mechanisms, gonococcal resistance to HAs involves *cis*-acting elements. Deletion of one base pair in the13-base pair inverted repeat sequence within the *mtrR* gene promoter reduces the *mtrR* promoter gap, suppressing *mtrR* but increasing *mtrC* transcription (Hagman and Shafer, 1995, Shafer et al., 2001). Another *cis*-acting mechanism involves a TT dinucleotide insertion in the *mtrR* promoter of a clinically resistant strain (Shafer et al., 2001, Zarantonelli et al., 2001). In meningococci, distinct regulatory schemes include insertion elements such as the Correia element in the *mtrCDE* promoter region and IHF-mediated transcriptional and post-transcriptional regulation via the Correia element (Rouquette-Loughlin et al., 2004). Additionally, a mutation (*mtr120*) 120 bp upstream of *mtrC* start codon in strain MS11 yields a new, highly active promoter, contributing to increased AMR (Ohneck et al., 2011). These *cis*-acting mechanisms underscore the adaptability of gonococci in altering regulatory dynamics to boost AMR.

The regulatory influence of MtrR extends beyond the *mtr* efflux system. Its pivotal role extends to genes (namely, *ponA*, and *pilQ*) involved in PEN susceptibility, impacting overall AMR (Folster et al., 2007, Johnson and Shafer, 2015). The comprehensive control exerted by MtrR spans over 69 genes, including direct repression of *rpoH*, influencing gonococcal susceptibility to hydrogen peroxide and ERY (Folster et al., 2009, Johnson and Shafer, 2015). Furthermore, MtrR activates *glnE*, contributing to the intricate balance of gonococcal physiology (Folster et al., 2009, Johnson and Shafer, 2015). The

regulatory prowess of MtrR extends to genes like *gdhR*, crucial for glucose catabolism and amino acid transport, emphasising its significance in *N. gonorrhoeae* fitness during infection (Rouquette-Loughlin et al., 2017). Ectopic expression of a WT *mtrR* copy enhances antimicrobial susceptibility, revealing its potential therapeutic utility in combating gonococcal infections (Chen et al., 2019). The broad gene control exerted by MtrR stands in contrast to the 'local-only' or 'proximal' transcriptional control observed in numerous multidrug-binding transcription regulators, including MexR, CmeR, QacR, AcrR, and TtgR (Alguel et al., 2007, Routh et al., 2009, Schumacher et al., 2001, Schumacher et al., 2002, Su et al., 2007, Wilke et al., 2008).

N. gonorrhoeae, akin to other bacteria, utilises complex regulatory networks involving negative and positive transcriptional regulators to adjust efflux pump gene expression in response to environmental factors, maintaining a delicate equilibrium between survival advantages in antimicrobial conditions and energy conservation during normal growth. The following section will delve into the structural features the MtrR protein as the primary regulator of the mtr system.

1.4.3 The MtrR protein

MtrR is a member of the TetR/QacR family of transcriptional regulators (TFR), characterised by a dimeric-two-domain structure (Cuthbertson and Nodwell, 2013). Their N-terminal region houses the helix-turn-helix (HTH) DNA-binding site, while the C-terminal region forms the dimerisation and multidrug-binding domain (Cuthbertson and Nodwell, 2013, Hoffmann et al., 2005, Li et al., 2007, Peters et al., 2011). DNA-recognition and induction mechanisms have been elucidated on the structural characteristics of a few TFR members, such as *E. coli* TetR, *S. aureus* QacR, *Streptomyces antibioticus* SimR, and *Pseudomonas putida* TtgR (Alguel et al., 2007, Le et al., 2011, Orth et al., 2000, Routh et al., 2009, Schumacher et al., 2001, Schumacher et al., 2002). A comparison of HTH motifs revealed the highest sequence homology between MtrR and TetR/QacR HTH motifs among these well-studied TFRs (Beggs et al., 2021).

The 2019 resolution of the crystal structure of MtrR revealed an asymmetrical two-dimer arrangement, with each subunit within a dimer comprising nine α helices (α1-α9) (Beggs et al., 2019). In each subunit of the functional homodimer, MtrR has an N-terminal DNA binding domain and a C-terminal dimerisation/ligand-binding domain. The N-terminal domain features a three-helix bundle (α1 to α3) with a canonical HTH motif (Cuthbertson and Nodwell, 2013). In the HTH motif, α3 serves as the "recognition helix. In the C-terminal domain, six α-helices (α4 to α9) constitute the dimerisation and ligand-binding region, forming a multidrug-binding pocket. The dimer interface is primarily composed of hydrophobic residues within a four-helix bundle (α8 and α9 of each subdomain). The MtrR-ligand-binding site's lateral walls (α4, α5, α7, and α8) and the "floor" (α6) are detailed, with a potential drug entry portal resembling that of *P. putida*'s TtgR. The cavity includes over 20 hydrophobic or aromatic amino acids, and the binding pocket incorporates six positively charged and two negatively charged residues (Beggs et al., 2019).

In the drug-binding region, each protomer binds a molecule of N-cyclohexyl-3-aminopropanesulfonic acid (CAPS) from the crystallisation reagent (Beggs et al., 2019). Fluorescence polarization (FP)-based DNA binding assays reveal that CAPS mimics physiological MtrR inducers, inducing the MtrR structure (Beggs et al., 2019). Structural, biophysical, and biochemical data suggest that chenodeoxycholate (CDCA) and taurodeoxycholate (TDCA), chemical analogues of CAPS, are physiological inducers of MtrR, possibly binding to distinct locations in the multidrug-binding pocket (Beggs et al., 2019). These collective findings suggest that MtrR follows the characteristic fold of the TetR family, recognising and binding to inducers such as bile salts in its binding pocket (Cuthbertson and Nodwell, 2013). This induction leads to the derepression of *mtrCDE*, which contributes to the organism's defence against the detrimental effects of cytotoxic compounds by expelling them into the extracellular milieu (Beggs et al., 2019, Hoffmann et al., 2005).

MtrR structures bound to *mtrCDE* and *rpoH* operators revealed DNA recognition mechanisms (Beggs et al., 2021). In both crystal structures, a functional MtrR homodimer binds to the respective 21-mer operator sites,

displaying identical residues contacting the DNA for each subunit. α3 and α3' insert into adjacent major grooves of B-DNA. Residues in the recognition helices, turn of the HTH motif, and amino terminus of helix α1, engaged with the DNA bases. Stabilisation of α3 within the major groove involves 'positioning' helix α2, T43, and Y48 forming hydrogen bonds with the phosphate backbone. Critical residues T43, R44, G45, Y48, and W49 contact DNA bases, unveiling a consensus recognition sequence, 5'-MCRTRCRN4YGYAYGK-3 (Beggs et al., 2021). Furthermore, DNA binding assays employing FP-based assays with MtrR derivatives, in which each important residue was replaced with alternative amino acids, substantiated the crucial role of the identified MtrR-DNA contacts for precise, high-affinity binding to both the *mtrCDE* and *rpoH* operators. The DNA recognition processes of MtrR for its *rpoH* and *mtrCDE* target operators were additionally confirmed in vivo by introducing these mutants into FA19, leading to increased resistance against ERY and PMB, recognised substrates of MtrD (Beggs et al., 2021). In this context, certain critical residues identified in either the DNA-binding or inducer-binding regions have been consistently isolated in clinical isolates resistant to HA, such as G45D and H105Y (Chen et al., 2014, Ezewudo et al., 2015). Considering these structural insights into DNA recognition, *in silico* modelling of these point mutations has elucidated the mechanisms affecting DNA or inducer binding and, consequently, influencing drug resistance (Beggs et al., 2021). Moreover, according to this research by Beggs et al., the Y48 residue exhibits the most significant similarity in protein–DNA contacts across diverse TFRs (Beggs et al., 2021).

Investigation into the binding affinity of MtrR for *rpoH* and *mtrCDE* operators uncovered that MtrR demonstrated a higher binding affinity for *rpoH*. According to the observed different binding affinity of MtrR for its cognate operators, the authors suggested that low cytotoxin concentrations derepress the multidrug efflux transporter, while the oxidative stress response system controlled by *rpoH* remains tightly down-regulated by MtrR; induction of MtrR from the *rpoH* operator occurs at higher threshold cytotoxin concentrations, responding to stresses, and accumulating bile salts may sequentially induce *mtrCDE* and

then *rpoH* in the bacterial cytosol under oxidizing conditions (Beggs et al., 2021).

Structural analysis of MtrR-DNA complexes and the ‘induced’ MtrR structure reveals conformational changes upon DNA binding and MtrR induction. Notably, the DNA-binding domain (α1–α3) undergoes substantial motion, exhibiting a 20° rotation downward towards the MtrR dimer centre in the DNA-bound conformation. This shift, coupled with a 21° slope in α1, results in a closer centre-to-centre distance between the recognition helices of the HTH motifs in the dimer-bound DNA complex (37 Å) compared to the induced dimeric form (45 Å). This conformational change aligns with the capability of the recognition helices, α3 and α3', to seamlessly fit into successive major grooves of the B-DNA. Other changes involve a 3.0 Å translation and 22° rotation of α4, bringing it closer to α5, and a 6° rotation of α7 to accommodate the shift of the HTH motifs in the DNA-bound form (Beggs et al., 2021). According to the authors' analysis, the induction mechanism of MtrR closely resembled that of QacR, involving a loop-to-helix transition of residues 119–123 linked to movement of α7, rotation of the DNA-binding domains, rotation and translation of α4, and expansion of the ligand-binding pocket upon ligand binding, resulting in increased centre-to-centre distance of the recognition helices (α3-α3′) incompatible with binding to B-DNA (Beggs et al., 2021). Additionally, very recently it was demonstrated that MtrR binds hormonal steroids including progesterone (PRO), β-estradiol, testosterone and ethinyl estrogen, thereby reducing its affinity to its cognate DNA, increasing *mtrCDE* expression, and boosting AMR (Hooks et al., 2024).

1.4.4 The MtrC protein

MtrC, an MFP, is a multidomain protein in *N. gonorrhoeae*, and similar to AcrA, it comprises a MP domain, a LPI domain, a HLH domain, and a BB domain arranged in a string-like fashion (Alav et al., 2022, Blair et al., 2022, Janganan et al., 2011b, Marshall and Bavro, 2020). Consistent with the importance of MtrC in drug resistance, genome analyses across a global collection of clinical *N. gonorrhoeae* isolates identified that *mtrC* loss-of-

function mutations are linked with increases in antibiotic susceptibility and cervical infections (Ayala et al., 2022, Ma et al., 2020b).

MtrC exhibits a robust interaction with MtrE and MtrD, while the latter two proteins display weak mutual interaction, implying that MtrC binding plays a crucial role in stabilising the tripartite complex (Janganan et al., 2011b). Cross-linking studies revealed that the α-helical HP domain of MtrC binds to both interprotomer and intraprotomer grooves on the surface of MtrE, resembling the AcrA HP–TolC interaction observed previously (Janganan et al., 2011a, Lobedanz et al., 2007, Symmons et al., 2009). Despite the absence of an experimental structure for MtrC, computational simulations indicate that the binding of the MtrC adapter protein is essential to maintain the MtrE channel in a fully open conformation (Tamburrino et al., 2017). This suggests that MtrC/MtrE binding events serve as crucial regulators of MtrE function, potentially serving as targets for novel efflux pump inhibitors (Tamburrino et al., 2017).

1.4.5 The MtrE protein

The structure of MtrE has been resolved (Lei et al., 2014) and shown to be similar to TolC from *E. coli* (Koronakis et al., 2000). MtrE forms an elongated homotrimeric channel-tunnel that contains three domains: a 12-stranded β-barrel domain embedded in the OM, a large *α*-helical barrel domain extending down to the periplasm reaching the peptidoglycan layer, and an equatorial domain which is mostly unstructured. The interior surfaces of MtrE form a continuous channel in an open conformational state. Like the TolC channel, an aspartate ring (containing six aspartates, D402 and D405 of each protomer of MtrE) exists at the entrance of the periplasmic tunnel of MtrE, which presumably acts as a selectivity gate for the channel (Lei et al., 2014). It has been shown that the aspartate ring of MtrE can be blocked by large cations such as hexamminecobalt (III) complex (Janganan et al., 2013). The structure of TolC indicates that its interior surfaces are highly electronegative (Koronakis et al., 2000). However, the internal surfaces of MtrE have no extensive charged patches (Lei et al., 2014). Mutagenesis studies identified that residues N198, E434 and Q441, located in the proximal, middle, and distal end of the intra-

protomer groove of MtrE, are important for the MtrCDE efflux pump function as their mutation made the cells hypersensitive to a range of antibiotics (Janganan et al., 2011b).

1.4.6 The MtrD protein

Structural and functional characterisation of MtrD not only advances our understanding of this crucial bacterial AMR mechanism but also offers valuable insights that are essential for a comprehensive comprehension of MDR mechanisms utilised by RND transporters and other efflux transporters contributing to MDR in pathogenic bacteria. This section will delve into the structural and functional characteristics of MtrD, the IM component of the MtrCDE pump system.

1.4.6.1 Crystal structures of the MtrD protein

In 2014, the three-dimensional structure of apo MtrD was elucidated using the A protomer of AcrB (PDB: 2DHH) as a molecular replacement template (Bolla et al., 2014). The crystal structure, resolved at 3.53 Å and encompassing 97% of the amino acids (residues 2–493 and 508–1040) in the final model, revealed the typical HAE1-RND type fold of a homotrimer. This structure consists of 12 TMS helices and a large PD, further subdivided into six subdomains like other RND proteins (Section 1.3.6.4.1.1 and Figure 1.7) (Bolla et al., 2014).

The trimeric organisation, and creation of an external cleft between PC1 and PC2 are the same as other HAE1-RND transporters (Section 1.3.6.4.1.1 and Figure 1.7) (Bolla et al., 2014). Despite the structural similarity to the A protomer of AcrB, notable differences exist between these two transporters, evidenced by a high root mean square difference (RMSD) of 7.6 Å over 1,000 C_α atoms upon superimposition (Bolla et al., 2014).

Insights into drug efflux mechanisms by MtrD were gained through cryo-EM analyses of a K823E derivative bearing a mosaic-like sequence associated with elevated AZM resistance found in *N. gonorrhoeae* strain CR.103 (Lyu et al., 2020, Rouquette-Loughlin et al., 2018b, Shafer, 2018, Wadsworth et al.,

2018a). Two cryo-EM structures were reported, bound deeply in the PD with hydrolysed, Amp or ERY, at resolutions of 3.02 Å and 2.72 Å, respectively. In contrast to the symmetric crystal structure of MtrD (Bolla et al., 2014), these two structures are asymmetric timers with distinct monomers displaying

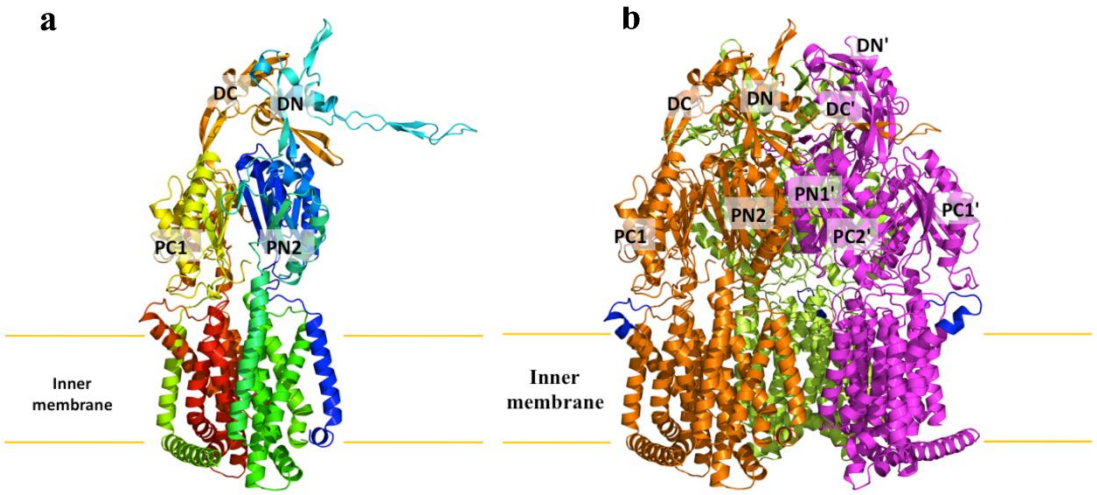

Figure 1.7: The depiction of the *N. gonorrhoeae* MtrD efflux pump illustrates its structural arrangement.

(a) Displayed is a ribbon diagram of a MtrD protomer observed in the membrane plane. The molecule is colour-coded along a spectrum from blue (N-terminus) to red (C-terminus), with labelled sub-domains DN, DC, PN2, PC1, and PC2. PN1 is positioned behind PN2, PC1, and PC2.
(b) Demonstrated is a ribbon diagram of the MtrD trimer seen in the membrane plane, with each subunit distinguished by a unique colour. Residues 917–927, exclusive to MtrD, constituting the upper segment of TM9 and the connecting loop between TM9 and TM10, are highlighted in blue. Adapted from Bolla et al., 2014. Reproduced under the terms of the Creative Commons Attribution license.

different conformational states as described in Section 1.3.6.4.1.2 (Lyu et al., 2020, Murakami et al., 2006, Sennhauser et al., 2009b). Only one Amp or ERY molecule was found to bind in the DBP of the B protomer of MtrD (Lyu et al., 2020), suggesting a similar functional rotation mechanism for MtrD identified in other HAE1-RND type transporters (Lyu et al., 2020, Murakami et al., 2006, Seeger et al., 2006).

The cryo-EM structures of MtrD in complex with a novel cationic antibiotic-sensitising peptide (CASP), cyclic peptide colistin, and linear human cationic antimicrobial peptide LL-37, provided further insights into drug recognition and efflux mechanisms (Lyu et al., 2022). In all three peptide-bound structures MtrD adopted the canonical asymmetric configuration of the HAE1-RND transporters, with bound peptide found in the B protomer. LL-37 utilised a very spacious binding site involving 31 residues across the entrance, the F-loop, PBP, G-loop, DBP and hydrophobic trap. In contrast, CASP and colistin, both cyclic peptides, primarily localised at the DBP, resembling canonical antibiotic binding modes for these pumps. Interestingly, CASP sensitised three bacillus shaped Gram-negative bacteria including *E. coli*, *P. aeruginosa*, and *Salmonella enterica* serovar Typhimurium to novobiocin, a substrate of MtrD, but not *N. gonorrhoeae* and *N. subflava*, which have a coccobacillary shape. CASP's potential as an adjuvant for antibiotic treatment in Gram-negative infections previously hindered by RND transporters was proposed. The difference in the ability of CASP to sensitise different bacteria was attributed to variations in the permeability barrier of outer membranes between rod-shaped bacilli and coccoid-shaped *Neisseria* (Lyu et al., 2022).

1.4.6.2 Proton translocation and efflux energisation

The initial MtrD symmetric trimer revealed a possible proton-relay network encompassing charged residues D405 and D406 of TMS 4 and K948 of TMS 10, and it was proposed that these residues undergo protonation and deprotonation during the transport cycle (Bolla et al., 2014). The subsequent high quality cryo-EM structures (Amp- and ERY-bound) allowed a more detailed understanding of proton transfer within the proton-relay network (Lyu et al., 2020). Two additional residues (N949, TMS 10 and T985, TMS 11) were identified to participate in proton transfer according to these substrate-bound structures (Lyu et al., 2020). K948 was designated as the "proton sweeper" and plays a crucial role in sweeping protons from the periplasm to the cytoplasm. In the A state, K948 and D406 closely interact with each other, while in the B state, D405 moves closer to K948, allowing for additional hydrogen binding. This movement of D405 was postulated to be the result of

a major allosteric shift triggered by binding a drug molecule in the PD causing a shift in the protomer to the B conformation. To advance the transport cycle, MtrD was assumed to switch to the E form, where K948 points towards N949 and T985, forming hydrogen bonds with both. It was suggested that the hydrogen bonding network's dynamic change could facilitate the transfer of protons from the periplasm to the cytoplasm, creating the PMF that energises the drug efflux process. K948 is probably accountable for transferring protons from D405 to N949 or T985, enabling the transfer process to proceed. D406 helps stabilise different transient states by interacting with K948 during the proton translocation process (Lyu et al., 2020).

1.4.6.3 Drug binding sites of the MtrD protein

The structures of MtrD bound to Amp and ERY revealed the substrate binding sites partially overlapped with both substrates binding at the DBP in the B protomer (Lyu et al., 2020). These structures identified residues F658, I660, V662, P664, S711, R714, E823, and S825 to surround the entrance of the periplasmic cleft in MtrD and it was suggested that they may contribute to substrate specificity and selectivity drawing evidence from homologous AcrB and MexB transporters (Lyu et al., 2020). Among these residues, R714 is conserved as an arginine in CmeB, AcrB, MtrD, MexB and AdeB transporters, and in AcrB, its equivalent residue R717 has been demonstrated to lead to clinical-level resistance to AZM when mutated to leucine (Lyu et al., 2022, Morgan et al., 2021, Murakami et al., 2006, Sennhauser et al., 2009a, Trampari et al., 2023, Zhang et al., 2023a). Intriguingly, an unbiased, long time scale MD simulation of MtrD bound to AZM revealed the spontaneous diffusion of AZM through the periplasmic cleft. This study demonstrated that the peristaltic motions of the periplasmic cleft facilitate substrate transport by MtrD, suggesting the potential existence of multiple transport pathways for macrolides within the periplasmic cleft of MtrD (Ammerman et al., 2021).

Despite the absence of drug binding to the PBP in structures solved by Lyu et al., the researchers successfully identified this putative extensive drug-binding pocket and its contributing residues based on homology to the AcrB site (Lyu et al., 2020, Nakashima et al., 2011). A flexible F-loop

(^{665}PPILELGN^{672}) connects the entrance of the periplasmic cleft and the putative PBP of MtrD. The conserved isoleucine I677 of the F-loop is essential for drug selectivity based on comparison to the AcrB model (Lyu et al., 2020, Schuster et al., 2016).

The DBP is extensive and involves aromatic, hydrophobic, polar, and positively charged residues, facilitating Amp or ERY binding through aromatic stacking, hydrophobic, and electrostatic interactions. Key residues involved in these interactions include S134, I139, R174, L175, F176, E271, S275, T277, Y325, F568, M570, V607, F610, F612, and F623 (Lyu et al., 2020). Most of these interactions are shared between MtrD-Amp and MtrD-ERY. Among these residues, eleven are conserved between MtrD and AcrB, indicating their vital role in drug recognition (Vargiu and Nikaido, 2012). Furthermore, a hydrophobic patch similar to that observed in the AcrB distal site was identified in the DBP of MtrD, consisting of the residues F176, V607, and F610, and it was proposed to be crucial for interacting with drugs and possibly inhibitors (Lyu et al., 2020, Vargiu and Nikaido, 2012). It was concluded that the ability of the periplasmic binding cleft to accommodate both Amp and ERY highlights the MtrD efflux pump's effectiveness in binding and extruding a wide range of antimicrobial compounds (Lyu et al., 2020).The structures of MtrD bound to Amp and ERY also revealed a gate G-loop, akin to that observed in AcrB, composed of the sequence ^{609}GFSFSGS^{615}. The glycine residues within this sequence are considered essential for providing flexibility, facilitating the transfer of the bound drug from the PBP to DBP (Cha et al., 2014, Eicher et al., 2012, Lyu et al., 2020, Nakashima et al., 2011).

The cryo-EM structures of the MtrD-Amp and MtrD-Ery complexes also reveal a consistent anchoring of phosphatidylethanolamine (PE) lipids, with at least 17 PE lipids in the Amp-bound structure and 23 PE lipids in the Ery-bound structure oriented similarly within the large central cavity of the MtrD trimer. This includes specific interactions at protomer-protomer interfaces and the conservation of a PE-binding site observed in the AdeB multidrug efflux pump (Lyu et al., 2020, Su et al., 2019).

1.4.6.4 N917-P927 loop region

One of the most intriguing aspects of the secondary structure of MtrD is found in TMS 9. Unlike other known RND transporters, MtrD possesses an extended region that protrudes into the periplasm, contributing to the PD (Bolla et al., 2014). This area, consisting of residues 917-927, includes an α-helix extending from the upper portion of TMS 9 to the loop that connects TMS 9 and TMS 10 (Bolla et al., 2014). Based on protein sequence alignment, it appears that these extra residues are unique to MtrD and are not present in other homologous RND proteins. Consequently, this segment represents a distinct characteristic of the MtrD pump that sets it apart from other RND pumps. The way in which the elongated helix and loop are positioned in the upper part of TMS 9, along with the periplasmic cleft created by PC1 and PC2, implies that these added structural characteristics could enhance the capacity of the pump to efficiently transport substrates from the outer layer of the inner membrane to the multidrug binding site located in the PD.

1.5 Scope of this thesis

N. gonorrhoeae is the causative agent of gonorrhoea, a sexually transmitted disease. It is a successful human pathogen that has developed resistance to antibiotics used for its treatment, in addition to host-derived antimicrobials, enabling it to colonise and establish infection. Unfortunately, strains of *N. gonorrhoeae* resistant to clinically important antibiotics, such as CRO and AZM, have emerged, significantly reducing treatment options for gonorrhoea.

MtrD, the sole RND transporter protein and primary efflux pump in gonococci, plays a pivotal role in conferring resistance to a broad spectrum of HAs, including antibiotics. Previous studies have provided valuable insights into the substrate pathways and binding sites of RND proteins, such as AcrB, through co-crystallography and MD simulations (Alav et al., 2022, Kobylka et al., 2020, Murakami et al., 2020, Ornik-Cha et al., 2021, Sakurai et al., 2019, Tam et al., 2021, Tam et al., 2020). However, limited information is available regarding the interactions between MtrD and its substrates, with only a handful of compounds co-crystallised with MtrD thus far (Lyu et al., 2022, Lyu et al.,

2020). Although *E. coli* AcrB has been a prototype for studying RND transporters, differences within these transporters necessitate focused research on individual proteins to comprehend the molecular mechanisms driving drug resistance. Moreover, a detailed understanding of mechanisms utilised by MtrD to mediated AMR is a crucial initial step in addressing AMR and developing strategies to inhibit this protein.

Our hypothesis posits that MtrD employs both proximal and distal substrate binding sites, akin to those described in its homologue AcrB. To test this, *in silico* methods, including MD simulations and molecular dockings, were employed using PRO as a known MtrD substrate. Importantly, at the time of this study, only a symmetric structure of MtrD without a bound substrate was available.

Chapter 2 addressed this hypothesis and additionally explored which amino acids within the putative MtrD drug binding pockets interact with substrates from different chemical classes, elucidating their roles in drug recognition and extrusion. A particular focus was on understanding the roles played by amino acids equivalent to the phenylalanine residues in AcrB (F136, F178, F610, F615, F617, and F628) in MtrD drug recognition. Despite the absence of a structure of MtrD with a bound substrate during this study, MD simulations, molecular docking, and site-directed mutagenesis were employed to gain insights for analysing both the WT and site-directed mutants of MtrD in *N. gonorrhoeae*.

As MtrD belongs to the HAE1-RND family of transporters, known for expelling a broad range of substrates, Chapter 2 investigated whether MtrD can handle additional compounds beyond those identified as its substrates. This involved generating various *N. gonorrhoeae* efflux gene knockout strains and using them to examine several compounds, evaluating their susceptibility to MtrD efflux.

The functionally rotating transport mechanism is widely accepted in AcrB for drug transport. Chapter 3 aimed to elucidate this mechanism in MtrD through MD simulations and site-directed mutagenesis experiments. This included

identifying proton relay network residues and transitioning from the symmetric to asymmetric conformation of MtrD using combinations of protonation of titratable residues in the TMD with and without bound PRO in the putative drug biding sites, providing insights into the drug transport mechanism in MtrD.

Chapter 4 shifted the focus to a unique sequence of 11 amino acids (N917 to P927) in MtrD, absent in homologous proteins. Hypothesising that this region facilitates substrate recognition and binding, MD simulations, site-directed mutagenesis, and resistance profiling were employed to explore its role in MtrD-mediated MDR.

Recognising limitations in using *N. gonorrhoeae* for functional analyses, Chapter 5 aimed to establish an *E. coli* host and vector system. This system allows optimal overexpression of active MtrD protein and includes a modified pBluescript vector facilitating cloning of the *mtrD* gene for site-directed mutagenesis.

Overall, the study utilised a wide range of *in silico* and experimental approaches and analyses to generate a wealth of information on the *N. gonorrhoeae* MtrD-mediated drug resistance features. The results provide new insights into the mechanisms used by *N. gonorrhoeae* and other Gram-negative bacteria to avoid antibiotics used for treatment or persist in the presence of natural host-derived antimicrobials during infection.

CHAPTER 2

MULTIDRUG RESISTANCE IN *NEISSERIA GONORRHOEAE*: IDENTIFICATION OF FUNCTIONALLY IMPORTANT RESIDUES IN THE MTRD EFFLUX PROTEIN AND ELUCIDATION OF ITS FUNCTIONALLY ROTATING MECHANISM

Declaration by candidate

The quality and extent of contributions of the candidate and co-authors to this work was as follows:

Name	Quality of contribution	Contribution extent (%)
Mohsen Chitsaz (candidate)	Conceptualisation, data curation, methodology, performance of experiments, writing, editing and revision of the manuscript	75
Lauren Booth (co-author)	Conceptualisation, data curation, methodology, performance of MD simulations	5
Mitchell Blyth (co-author)	Conceptualisation, data curation, methodology, performance of MD simulations, writing, editing and revision of the manuscript	10
Megan O'Mara (co-author)	Conceptualisation, data curation, editing and revision of draft and final manuscript	5
Melissa Brown (co-author)	Conceptualisation, data curation, editing and revision of draft and final manuscript	5

The undersigned hereby certify the above declaration correctly reflects the quality and extent of the candidate and co-author contribution to this work.

Candidate signature		18/04/2024
Supervisor signature		18/04/2024

2.1 Preface

The information provided in this chapter has been published by Chitsaz M., Booth, L., Blyth M., O'Mara M. L., Brown M. H., (2019) "Multidrug resistance in *N. gonorrhoeae*: identification of functionally important residues in the MtrD efflux protein." *mBio* **10**:6, e02277-19. The printed version of this paper can be found in Chapter 7 (Appendix **C**).

2.2 Abstract

A key mechanism that *N. gonorrhoeae* uses to achieve MDR is the expulsion of structurally different antimicrobials by the MtrD multidrug efflux protein. MtrD resembles the homologous *E. coli* AcrB efflux protein with several common structural features, including an open cleft containing putative access and deep binding pockets proposed to interact with substrates and a proton relay-network proposed to be responsible for proton translocation needed for substrate efflux through the MtrCDE system. A highly discriminating *N. gonorrhoeae* strain, with the MtrD and NorM multidrug efflux pumps inactivated, was constructed and used to confirm and extend the substrate profile of MtrD to include 14 new compounds. The structural basis of substrate interactions with MtrD was interrogated by a combination of long-timescale MD simulations and docking studies together with site-directed mutagenesis of selected residues. Of the MtrD mutants generated, only one (S611A) retained a WT resistance profile, while others (F136A, F176A, I605A, F610A, F612C, and F623C) showed reduced resistance to different antimicrobial compounds. Docking studies of eight MtrD substrates confirmed that many of the mutated residues play important nonspecific roles in binding to these substrates. Long-timescale MD simulations of MtrD with its substrate PRO showed the spontaneous binding of the substrate to the access pocket of the binding cleft and its subsequent penetration into the deep binding pocket, allowing the permeation pathway for a substrate through this important resistance mechanism to be identified. By conducting a range of MD simulations and mutagenesis experiments, the specific arrangement of substrate binding and protonation states within the proton relay network that

facilitates the shift from the symmetric to the asymmetric structure of MtrD was determined. This involved analysing the interconnectedness of key local regions responsible for regulating conformational alterations among the access, binding, and extrusion states. These findings, which provide a detailed understanding of the interaction between MtrD and substrates and elucidate the mechanism of allosteric coupling that enables the transition to the asymmetric conformation of MtrD, broaden our comprehension of the efflux mechanisms employed by RND transporters. Additionally, they can serve as a foundation for the rational design of antibiotics and inhibitors.

2.3 Importance

With over 78 million new infections globally each year, gonorrhoea remains a frustratingly common infection. Continuous development and spread of antimicrobial-resistant strains of *N. gonorrhoeae*, the causative agent of gonorrhoea, have posed a serious threat to public health. One of the mechanisms in *N. gonorrhoeae* involved in resistance to multiple drugs is performed by the MtrD MDR efflux pump. This study demonstrated that the MtrD pump has a broader substrate specificity than previously proposed and identified a cluster of residues important for drug binding and translocation. Additionally, a permeation pathway for the MtrD substrate PRO actively moving through the protein was determined, revealing key interactions within the putative MtrD drug binding pockets. Identification of functionally important residues and substrate-protein interactions of the MtrD protein is crucial to develop future strategies for the treatment of multidrug-resistant gonorrhoea. Through this study, we also gain molecular-level understanding of the interplay between substrate binding sites and protonation states that regulate the shift from the symmetric to the asymmetric conformations of MtrD. These insights shed light on the functional rotation mechanism employed by MtrD.

2.4 Introduction

The emergence of MDR in bacteria is a global health problem that severely compromises effective treatment options, and efflux of antibiotics by membrane-bound transport proteins has been implicated as a key mechanism.

In particular, in Gram-negative pathogens RND multidrug efflux systems are the first line of defence for the cell. RND efflux systems are an inducible simultaneous MDR mechanism that act against a broad spectrum of antibiotics and other antimicrobial agents. These tripartite protein complexes span the bacterial inner and OMs to provide a continuous drug efflux pathway.

The sexually transmitted pathogen *N. gonorrhoeae* is unique amongst Gram-negative bacteria in that it contains a single RND efflux system to promote survival: MtrCDE (Hagman et al., 1997, Maness and Sparling, 1973). The MtrD efflux protein is embedded in the inner membrane and exports drugs from the periplasm and inner membrane to the MtrE OM channel. MtrD contains the substrate binding sites and transduces the electrochemical energy required for drug export via a H^+/substrate antiporter mechanism (Janganan et al., 2013). MtrD and MtrE are anchored together by the periplasmic MtrC to enable substrate efflux from the bacterium.

MtrD shares 48.9% sequence identity with the homologous *E. coli* RND exporter, AcrB, which has provided the structural basis for our understanding of RND exporters to date. It is well established that homologous proteins share common structural features. However, the unique amino acid sequence of each protein allows recognition and efflux of a distinct set of compounds, required for survival of that specific bacterial species in its particular environment. Similar to AcrB, MtrD effluxes a wide spectrum of compounds including detergents, antibiotics, dyes, bile salts, FAs, biocides, steroidal hormones, and aliphatic and host-derived cationic antimicrobial peptides (Hagman et al., 1995, Shafer et al., 1998). Given that gonococci commonly infect mucosal sites bathed in fluids containing a number of these compounds, MtrCDE contributes to bacterial virulence as well as AMR, enhancing colonization and disease development (Hagman et al., 1995, Jerse et al., 2003).

In 2014, the crystal structure of MtrD was resolved to 3.53 Å revealing a similar architecture to the homologous AcrB and MexB structures (Bolla et al., 2014). Each MtrD monomer shows two pseudo-symmetric halves and contains two domains: a TMD, which is organized into 12 transmembrane α-helices

embedded in the CM, and a large PD that can be subdivided into a porter and a docking domain. The porter domain is composed of four sub-domains, i.e., PN1, PN2, PC1 and PC2. In MtrD, PN1 makes up the central pore and stabilises the trimeric organization, while PC1 and PC2 create a substrate binding cleft along the pseudo-symmetric axis between the two halves of the porter domain. The docking domain is formed of two sub-domains, DN and DC, that are likely to interact with MtrE in the OM (Bolla et al., 2014, Lei et al., 2014).

Structures of AcrB bound to various substrates have identified two multidrug-binding sites within the binding cleft of the porter domain: the proximal (access) and distal (deep) binding pockets, which are separated by a so-called ‘switch loop’ (Murakami et al., 2006, Nakashima et al., 2011). It is postulated that substrates first enter the access pocket of the binding cleft, then permeate into the deep binding pocket. The AcrB deep binding pocket is rich in phenylalanine residues and many residues that have been identified as crucial to the export process (F136, F178, F610, F615, F617 and F628) are highly conserved between MexB and MtrD suggesting they play important and possibly similar roles in MtrD.

To date, MtrD, has not been co-crystallized with substrate. It is noteworthy to mention that this study was completed before a structure of MtrD bound to a substrate was resolved and published. Thus, the residues that comprise the MtrD substrate binding site(s), and whether the substrate binding residues common to RND proteins also play a role in MtrD efflux has not been ascertained. In this study, a site-directed mutagenesis system specific for analysing the MtrD export protein in its natural host was established and using this system 14 new MtrD substrates were identified. Furthermore, the roles of F136, F176, I605, F610, S611, F612 and F623 in MtrD-mediated MDR were experimentally explored. To characterize the structural basis of substrate interactions with MtrD, a combination of long-timescale MD simulations and docking studies was used. Long timescale MD simulations of PRO show the spontaneous binding of PRO to the access pocket of the binding cleft and its subsequent permeation past the switch loop and into the deep binding pocket.

Docking studies of PRO, N-9, AZM, RIF, ET, CV, cholic acid (CHO) and the RND pump inhibitor PAβN indicate that several key residues play important non-specific roles in the efflux of these substrates.

2.5 Results

2.5.1 A highly discriminating *N. gonorrhoeae* strain for *in situ* analysis of MtrD activity

An expression and integration system was established in a *N. gonorrhoeae* host to analyse the function of WT MtrD and construct a set of isogenic mutants. This has the advantage that it produces both cognate partner proteins of MtrD, i.e. MtrC and MtrE, allowing assembly of the active tripartite MtrCDE system in the neisserial membrane. This ensures that alterations in spectrum and/or levels of resistance are solely due to manipulation of MtrD. The well characterised antibiotic sensitive strain *N. gonorrhoeae* FA19 was selected as the background strain (Sarubbi et al., 1974). As an initial step, three isogenic FA19 derivatives (FA19Δ*mtrD*, FA19Δ*norM*, and FA19Δ*mtrD*Δ*norM*) were created using overlap extension PCR (Vallejo et al., 1994). The NorM_NG efflux pump is known to expel a number of cationic toxic compounds, such as CIP, ET and acriflavine (ACR); the latter two compounds are substrates common with MtrD (Rouquette-Loughlin et al., 2003). Thus, to remove any contribution that the unrelated NorM_NG multidrug efflux pump has in the assessment of MtrD function, MtrD derivatives were constructed in a strain in which *norM* was also deleted from the chromosome. To achieve a high Discrimination for antimicrobial susceptibility assessments of MtrD, the isogenic FA19 derivate, KH15 was also employed. This strain of *N. gonorrhoeae* has a single bp deletion in the *mtrR* promoter that results in upregulation of the *mtrCDE* system and consequential increased levels of resistance (Hagman et al., 1995). Hence, two KH15 isogenic derivatives (KH15Δ*mtrD* and KH15Δ*mtrD*Δ*norM*) were also constructed using the same overlap extension PCR methodology. Sequencing of the complete *mtrRCDE* region of KH15Δ*mtrD* and KH15Δ*mtrD*Δ*norM* strains confirmed deletion of the *mtrD* gene and ensured integrity of the *mtrR/C* promoter region as well as the *mtrC* and the *mtrE* genes. Resistance profiles of the resulting strain set were

determined to 33 compounds, which included two known RND pump inhibitors (Table 2.1, Table 2.2, and Table 2.3).

Deletion of *mtrD* and *norM* from FA19 resulted in a (1.5- to 32-fold) reduction of the MICs for 25 of 31 of the tested compounds (Table 2.1, Table 2.2, and Table 2.3), and 29 of 31 compounds showed reduced (1.5-fold to >256-fold) MIC levels in the KH15 strain background. Sodium dodecyl sulphate (SDS), Tween 80 (TW-80), CA, and CRO showed a decrease in resistance only in the KH15 background, probably due the higher level of *mtrCDE* expression in this strain than in strain FA19 (Table 2.1 and Table 2.3). In fact, a 4-fold or greater reduction in MICs was observed for 20 of 31 tested compounds for the KH15 derivatives, while this level of reduction in MICs in the FA19 background was observed for only nine compounds. These data suggested that KH15Δ*mtrD*Δ*norM* can function as a good discriminative background strain for conducting analyses of *mtrD* mutants.

No change in resistance profiles was observed for the antibiotics TET and GEN in strains with either *mtrD*, *norM*, or both inactivated (Table 2.2). Although TET has previously been identified as an MtrD substrate, this can be observed only in strains with concomitant mutations in multiple genes, including *mtrR*; these were not present in our background strain (Sarubbi et al., 1975, Shafer and Folster, 2006, Sparling et al., 1975).

In addition to antimicrobial compounds, *N. gonorrhoeae* KH15 and derivatives were tested against two known RND pump inhibitors, PAβN and NMP, for their resistance capacities. These assays showed decreased resistance of KH15Δ*mtrD* and KH15Δ*mtrD*Δ*norM* cells to PAβN and NMP with an 8-fold and 4-fold reduction in MICs, respectively (Table 2.3). Deletion of *norM* from the KH15Δ*mtrD* strain did not result in a further decrease of MIC for either compound. Thus, inactivation of *mtrD* in KH15 produced a decrease in resistance to 31 compounds, confirming the broad spectrum of antimicrobials that can be handled by this protein (Table 2.1, Table 2.2, and Table 2.3).

Table 2.1: Antimicrobial resistance profiles of *N. gonorrhoeae* strains for 11 compounds.[a]

	MIC (µg/ml)										
	Detergent					Antibiotic					
Strain or mutant	**N-9[b]**	**TX-100**	**SDS**	**TW-80**	**CHAPS**	**RIF**	**NOV**	**ERY**	**AZM**	**CRO**	**OXA**
FA19	64	128	16	64	2048	0.03	0.25	0.25	0.125	0.0005	0.50
FA19Δ*mtrD*	16	32	16	64	1024	0.008	0.03	0.06	0.03	0.0005	0.06
FA19Δ*norM*	64	128	16	64	2048	0.03	0.25	0.25	0.125	0.0005	0.50
FA19Δ*mtrD*Δ*norM*	16	32	16	64	1024	0.008	0.03	0.06	0.03	0.0005	0.06
KH15	≥4096	≥4096	32	128	>2048	0.125	1	2	0.50	0.001	4
KH15Δ*mtrD*	16	32	16	64	1024	0.008	0.03	0.06	0.03	0.0005	0.06
KH15Δ*mtrD*Δ*norM*	16	32	16	64	1024	0.008	0.03	0.06	0.03	0.0005	0.06
KH15Δ*mtrD*Δ*norM*(*mtrD*)	≥4096	≥4096	32	128	>2048	0.125	1	ND	ND	0.001	4

[a]All MIC data are representative of three or more independent experiments. Abbreviations: AZM, azithromycin; CHAPS, 3-[(3-cholamidopropyl)dimethylammonio]-1-propanesulfonate; CRO, ceftriaxone; ERY, erythromycin; N-9, nonoxynol-9; ND, not determined; NOV, novobiocin; OXA, oxacillin; RIF, rifampin; TW-80, Tween 80; TX-100, Triton X-100

Table 2.2: Antimicrobial resistance profiles of *N. gonorrhoeae* strains for an additional 11 compounds[a]

	MIC (µg/ml)										
	Antibiotic						CAMP		Dye		
Strain or mutant	CHL	TET	PEN	TGC	CIP	GEN	CST	PMB	ET	CV	ACR
FA19	0.75	0.25	0.024	0.06	0.003	4	200	100	2	1	0.5
FA19Δ*mtrD*	0.5	0.25	0.016	0.03	0.003	4	100	50	0.5	0.125	0.25
FA19Δ*norM*	0.5	0.25	0.024	0.06	0.003	4	200	100	0.25	1	0.25
FA19Δ*mtrD*Δ*norM*	0.5	0.25	0.016	0.03	0.0025	4	100	50	0.06	0.125	0.06
KH15	0.75	0.25	0.060	0.125	0.003	4	400	100	4	2	0.5
KH15Δ*mtrD*	0.5	0.25	0.016	0.03	0.003	4	100	50	0.5	0.125	0.25
KH15Δ*mtrD*Δ*norM*	0.5	0.25	0.016	0.03	0.0025	4	100	50	0.06	0.125	0.06
KH15Δ*mtrD*Δ*norM*(*mtrD*)	>0.75	0.25	0.060	0.125	0.003	4	400	100	0.25	2	0.125

[a]All MIC data are representative of three or more independent experiments. Abbreviations: ACR, acriflavine; CHL, chloramphenicol; CIP, ciprofloxacin; CST, colistin; CV, crystal violet; ET, ethidium; GEN, gentamicin; PEN, benzylpenicillin; PMB, polymyxin B; TET, tetracycline; TGC, tigecycline

Table 2.3: Antimicrobial resistance profiles of *N. gonorrhoeae* strains for 11 more compounds[a]

	MIC (µg/ml)										
	BA	**FA**		**Biocide**					**Hormone**	**EPI**	
Strain or mutant	**CHO**	**CA**	**PA**	**BC**	**CH**	**TR**	**DQ**	**PT**	**PRO**	**NMP**	**PAβN**
FA19	200	12.5	12.5	2	0.25	0.125	4	4	40	ND	ND
FA19Δ*mtrD*	100	12.5	6.25	1	0.125	0.06	2	2	20	ND	ND
FA19Δ*norM*	200	12.5	12.5	2	0.25	0.125	1	1	40	ND	ND
FA19Δ*mtrD*Δ*norM*	100	12.5	6.25	1	0.125	0.06	1	1	20	ND	ND
KH15	400	25	100	4	0.5	0.25	16	8	80	256	512
KH15Δ*mtrD*	100	12.5	6.25	1	0.125	0.06	1	2	20	64	128
KH15Δ*mtrD*Δ*norM*	100	12.5	6.25	1	0.125	0.06	1	1	20	64	128
KH15Δ*mtrD*Δ*norM*(*mtrD*)	400	25	ND	4	0.5	0.25	1	1	80	256	512

[a]All MIC data are representative of three or more independent experiments. Abbreviations: BA, Bile acid; FA, Fatty acid; EI, Efflux inhibitor; BC, benzalkonium; CA, capric acid; CH, chlorhexidine; CHO, cholic acid; DQ, dequalinium; NMP, 1-(1-naphtylmethyl)-piperazine; PA, palmitic acid; PAβN, phenylalanine arginine beta-naphthylamide; PRO, progesterone; PT, pentamidine; TR, triclosan

2.5.2 Function can be restored in the *N. gonorrhoeae* KH15Δ*mtrD*Δ*norM* derivative by reinsertion of *mtrD*

A procedure was established for introduction of *mtrD* derivatives, all containing a sequence encoding six C-terminal histidine residues (*mtrD*$_{His6}$) into the chromosome of the KH15Δ*mtrD*Δ*norM* strain via the pGCC4 (*Neisseria* insertion complementation system [NICS]) shuttle vector. This system allows integration of an *mtrD* determinant into the *N. gonorrhoeae* chromosome between *aspC* and *lctP* and provides cells with a recombinant *mtrD* allele with its expression under *lac* promoter regulation (Mehr and Seifert, 1998). A pGCC4-*mtrD*$_{(His6)}$ clone was constructed and used for recombination of the WT *mtrD* allele into the *N. gonorrhoeae* KH15Δ*mtrD*Δ*norM* chromosome, producing the KH15Δ*mtrD*Δ*norM*(*mtrD*$_{His6}$). At the same time, the pGCC4 empty vector was also recombined to create an isogenic KH15Δ*mtrD*Δ*norM*(NICS) strain that contained all the NICS elements including the ERY resistance determinant present on the pGCC4 vector used for selection, and that could be utilised as a negative/background control. Western blot analysis confirmed expression and localization of the recombinant WT MtrD$_{His6}$ protein within isolated membranes of *N. gonorrhoeae* KH15Δ*mtrD*Δ*norM*(*mtrD*$_{His6}$) cells (Figure 2.1).

Complementation of KH15Δ*mtrD*Δ*norM* with *mtrD*$_{His6}$ fully restored resistance to WT levels for 24 and partially for four compounds (Table 2.1, Table 2.2, and Table 2.3). Partial complementation was seen for ET, ACR, DQ and pentamidine (PT), as the MICs were below those for the parental strain (Table 2.2 and Table 2.3). This was expected as these four compounds are substrates of both the MtrD and NorM_NG multidrug efflux pumps. These data confirmed the MtrCDE system is functional in the KH15Δ*mtrD*Δ*norM*(*mtrD*$_{His6}$) strain, offering a reliable system for analysing incorporated site-directed MtrD mutants. Additionally, these data showed that the histidine-tagged MtrD protein in the KH15Δ*mtrD*Δ*norM*(*mtrD*$_{His6}$) strain provides resistance to a large number of MtrD substrates allowing selection of a range of structurally different compounds for functional analysis of MtrD mutants. From these analyses 11

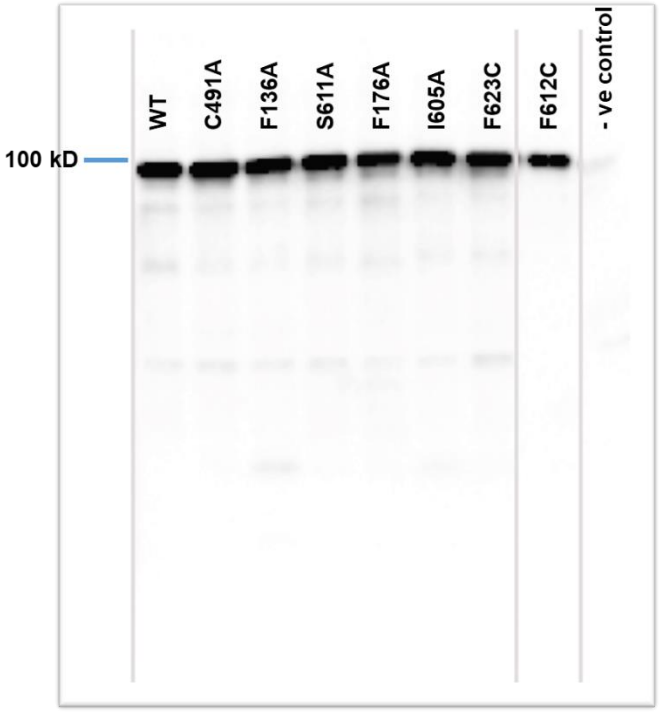

Figure 2.1: An example Western blot showing expression levels of the recombinant WT MtrD and seven MtrD mutants.

Membrane protein samples are of isolated membranes from the KH15ΔmtrDΔnorM strain expressing these MtrD mutant derivatives. The negative (–ve) control is KH15ΔmtrDΔnorM complemented with a NotI digested NICS portion of the pGCC4 vector, lacking the mtrD gene. After transfer to a polyvinylidene difluoride membrane, MtrD proteins were immunologically detected using a rabbit anti-6 his tag antibody that binds to the C-terminal histidine-tag on MtrD.

compounds were chosen as representative compounds for subsequent MIC analysis of MtrD activity due to their high discrimination in MIC analysis and provide examples of a range of antimicrobials from different chemical classes. While both ERY and AZM demonstrated excellent MIC differentiation between the *mtrD* deletion and its respective parental strain, the use of the ERY-resistance cassette present in pGCC4 as a selection marker precluded testing constructed MtrD mutant derivatives against these clinically important antibiotics.

2.5.3 Spontaneous uptake of progesterone identified from MD simulations

To investigate the interaction of MtrD with substrates, spontaneous binding simulations were performed with the substrate PRO. In these simulations, 30 molecules of PRO were randomly placed in the aqueous solution surrounding the MtrD porter and docking domains. In two of the three simulations (representing 700 nanseconds (ns) simulation time), PRO randomly adsorbed to the protein via non-specific interactions. In the remaining 200 ns replicate, a single molecule of PRO entered the access pocket of the binding cleft, straddled the switch loop and interacted with the deep binding pocket in the first 100 ns of the simulation, where it remained for the duration of the analysis. The time-dependent motion of PRO within the binding cleft throughout the simulation is shown in Figure 2.2. In the first 2 ns of the simulation, PRO associated with the outer lip of the binding cleft in an upright orientation. PRO then rotated 90° to interact with the β-sheet residues from PC2 that line the binding cleft (Figure 2.2, bottom panel, red) before moving into the MtrD access binding pocket, where it resided for the first 40 ns of simulation (Figure 2.2, bottom panel, green). After 40 ns of simulation, PRO moved further into the binding cleft, straddling the switch loop before interacting with the deep binding pocket where it remained for the rest of the 200 ns trajectory. Throughout the last 100 ns of simulation, PRO moved freely and changed orientation in the deep binding pocket, residing ~10 Å from the entrance of the binding cleft. From these simulations, 25 binding cleft residues were identified as being within 4 Å of PRO throughout the simulation (Figure 2.3). These residues include four phenylalanines (F174, F610, F612 and F623) that are conserved in both AcrB and MexB (Table 2.4).

2.5.4 Docking of substrates to MtrD

MD simulation studies are a computationally expensive approach to analyze the interaction of MtrD with a range of substrates. Thus, to determine whether a simplified docking approach could give insights into key MtrD residues in contact with substrates, flexible docking studies of PRO were compared with MD simulations. PRO docked into the deep binding pocket of MtrD in several

orientations, as shown in Figure 2.3B, primarily interacting with F623, F612, F610, F176 and F136. A number of these residues were also highlighted in MD simulations; e.g., PRO interacts with F612 for >90% of the simulation time, while F623 and F610 interact with PRO for >50% of the simulation time, and the interaction with F176 persisted for 25% of the simulation time.

Overall, docking studies and MD simulations of PRO binding were in good agreement. Thus, we extended the procedure to dock a further six substrates and one inhibitor into the MtrD access and deep binding pockets. These compounds were the substrates N-9, AZM, RIF, ET, CV, CHO and the inhibitor PAβN. As stated previously, we were unable to test resistance to AZM for the MtrD mutants in our *in vivo* system. Thus, the ability to analyse the interaction of MtrD with AZM through *in silco* docking studies provides an example of the usefulness and versatility of this system. The lowest-energy docked poses revealed a set of common residues that appear to play a role in the binding and/or transport of these compounds (Figure 2.4 to Figure 2.7). Critically, a number of residues (F136, F176, F610, F612 and F623) were found to be implicated in substrate binding and are conserved in both the AcrB and MexB efflux proteins (Figure 2.4 to Figure 2.7). Site-directed mutagenesis was used to confirm their importance in MtrD-mediated resistance.

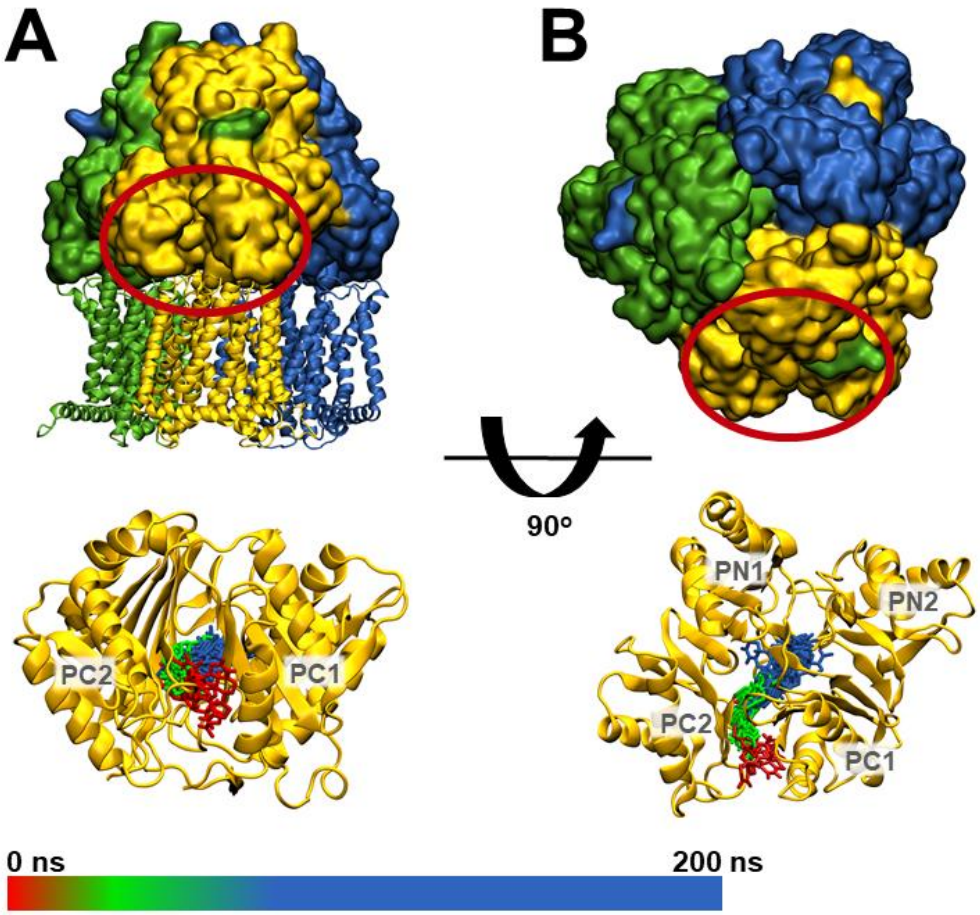

Figure 2.2: Progesterone binding in monomer B of the MtrD trimer shown as a (A) side view and (B) top view.

Monomers A, B, and C of MtrD are coloured green, gold, and blue, respectively. The periplasmic region of monomer B is circled in red. The lower panels show MtrD monomer B with the position of PRO throughout the 200 ns simulation. Snapshots of PRO taken every 10 ns are shown in licorice representation and colored according to simulation time. The scale bar gives the correlation between simulation time and PRO color. The starting position of the PRO molecule at 0 ns is shown in red, and the final position of PRO at 200 ns, straddling the switch loop, is in blue.

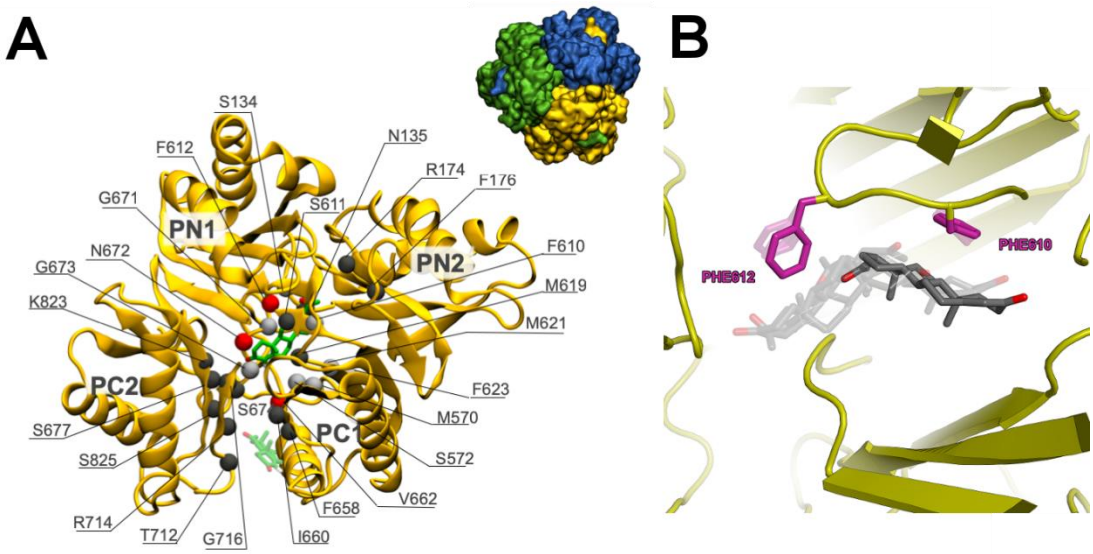

Figure 2.3: Interactions of progesterone with MtrD.

(A) Porter domain of MtrD viewed from the top, illustrating the residues implicated in binding of progesterone. PRO is drawn in liquorice representation at 0 ns (washed out) and 200 ns. The Cα of 25 residues most frequently within 4 Å of PRO are drawn in van der Waals representation and colored as follows: red, >75% frequency; silver, >50% frequency; dark gray, >25% frequency. The inset shows a top view of the MtrD trimer with the periplasmic region of monomer B in gold. (B) The lowest-energy docked poses for PRO in the access and deep pockets. F610 (magenta) plays the largest role in binding and transport of this substrate in the access pocket. F612 (magenta) plays the largest role in binding and transport of this substrate in the deep pocket.

Table 2.4: Residues belonging to binding pockets of MtrD and AcrB.

Region	AcrB Residues	MtrD Residues from alignment[a]
Access Pocket	79, 91, 134, 135, 292, 573, 575, 577, 617, 624, 662, 664, 666, 667, 668, 674, 676, 681, 717, 719, 826	**79, 91, 134, 135, 290, <u>570</u>, 572, 574, <u>612</u>, 619, 658, 660, 662, 663, 664, 670, 672, 678, 714, 716, 823**
Deep Binding Pocket	46, 89, 128, 130, 134, 136, 176, 177, 178, 180, 273, 274, 276, 277, 290, 327, 573, 610, 612, 615, 617, 620, 628	46, 89, 128, 130, **134**, 136, **174** 175, **176**, 178, 271, 272, 274 275, 288, 325, **<u>570</u>**, 605, 607 **610**, **<u>612</u>**, 615, **623**

[a] MtrD residues implicated in binding PRO in MD simulations are shown in bold; residues contributing to both the access and deep binding pockets are underlined.

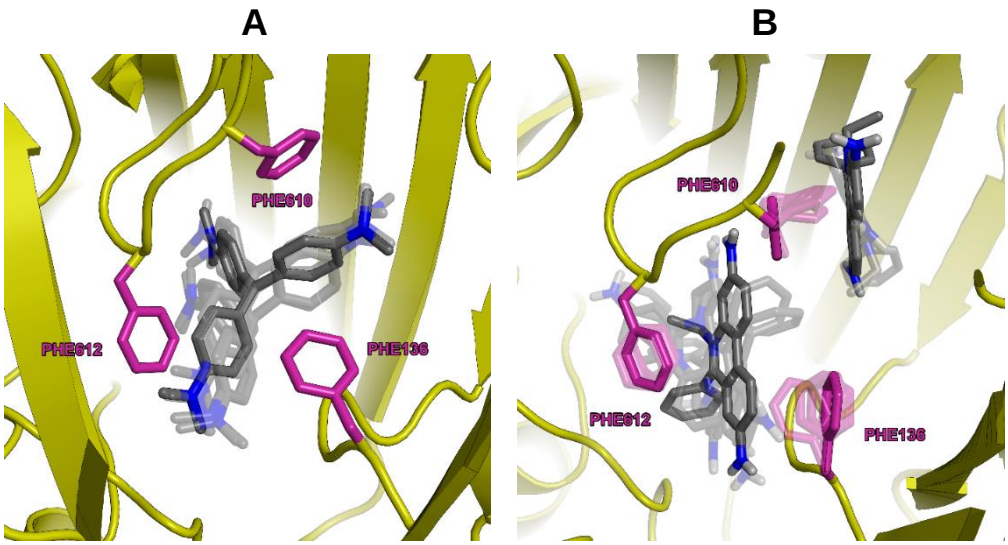

Figure 2.4: MtrD docked to crystal violet and ET.

A) The lowest-energy docked poses for CV. Three residues, F612, F136, and F610 (magenta sticks), form key interactions with CV in all of the lowest energy docked conformations. B) The lowest-energy docked poses for ET. Residues F610, F612 and F136 (magenta sticks) interact with the lowest energy conformations of ET docked to either the access or deep binding pocket of MtrD.

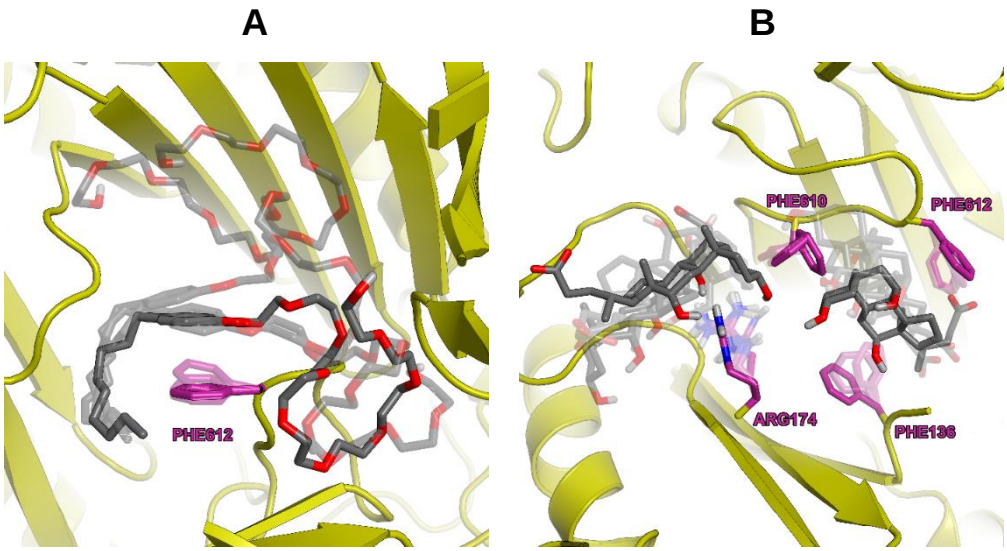

Figure 2.5: MtrD docked to nonoxynol-9 and cholic acid.

A) The lowest-energy docked poses for N-9 in the access pocket. F612 consistently interacts with N-9 in the lowest energy docked poses. B) The lowest-energy docked poses for CHO. Here F610, F612, F136, and R174 (magenta sticks) interact with the lowest energy conformations of CHO docked to either the access or deep binding pocket of MtrD.

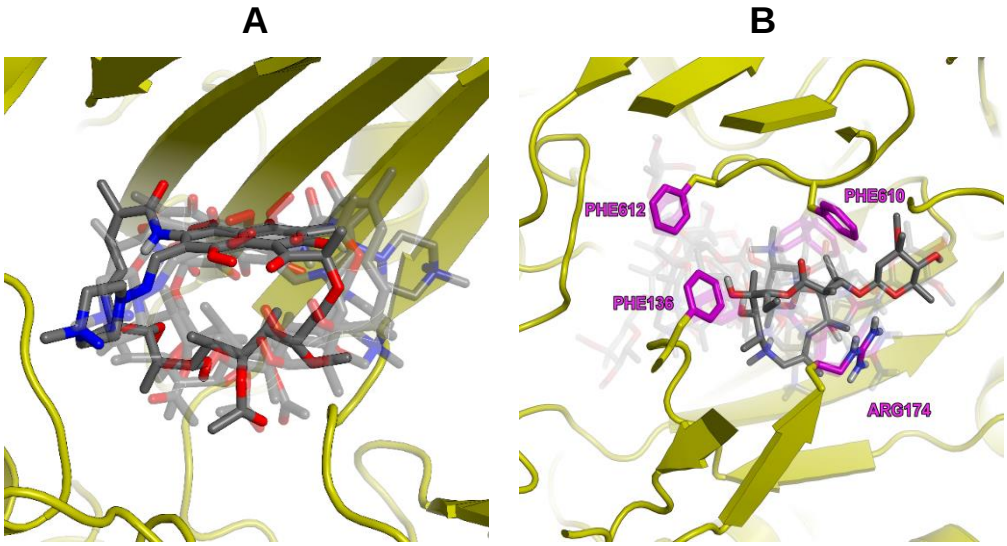

Figure 2.6: MtrD docked to rifampin.

A) The lowest-energy docked poses for rifampin. Docking results suggest that F612 (not shown for clarity) plays a key role in RIF binding. B) The lowest-energy docked poses for AZM. Residues F136, R174, F610 and F612 (magenta sticks) interact with the lowest energy docked poses of AZM.

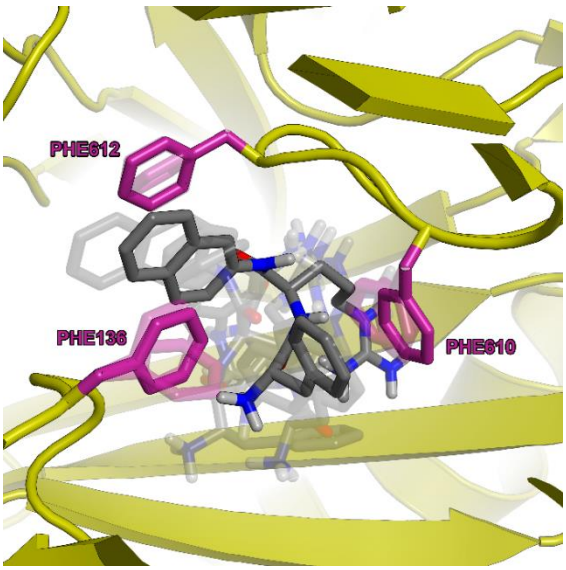

Figure 2.7: MtrD docked to PAβN.

The lowest-energy docked poses for PaβN are shown. Here F610, F612 and F136 (magenta sticks) interact with the lowest energy docked poses of PAβN.

2.5.5 Site-directed mutagenesis identified six residues involved in MtrD-mediated resistance

Detailed knowledge of the interactions between substrates and amino acids that comprise drug binding sites within the porter domain of AcrB have been obtained by a variety of methods (Schuster et al., 2016, Yamamoto et al., 2016, Zwama et al., 2018). Such studies identified, among others, a cluster of six phenylalanine residues (F136, F178, F610, F615, F617 and F628) that contribute to formation of the deep drug-binding pocket and that are involved in substrate binding and recognition (Murakami et al., 2006, Nakashima et al., 2011). In MtrD, five of these phenylalanine residues are conserved (F136, F176, F610, F612 and F623) at similar locations, whereas F610 is an isoleucine in the corresponding position in MtrD (I605) (Figure 2.8). Also included in our set of targets was S611, corresponding to G616 in AcrB (Figure 2.8), which has been identified as playing a role in resistance (Cha et al., 2014, Wehmeier et al., 2009, Zwama et al., 2018). Thus, we were interested to learn whether these residues perform similar roles in the related RND transporter MtrD.

To facilitate later studies on the located/inhibition of substituted residues (Hassan et al., 2006b) we initially generated a cysteine-less variant of the *mtrD*$_{His6}$ clone in pGCC4 (pGCC4-CL*mtrD*$_{His6}$). This produced a MtrD C491A variant in which the sole cysteine residue at position 491 was replaced with alanine. When integrated into the KH15Δ*mtrD*Δ*norM* background, the KH15Δ*mtrD*Δ*norM*(CL*mtrD*$_{His6}$) strain had WT levels of resistance to all tested compounds (Table 2.5), and Western blot expression levels of the CL-MtrD$_{His6}$ protein in neisserial membranes were comparable to the expression level measured for WT MtrD$_{His6}$ (Figure 2.1). As a result, the MtrD mutants described below were constructed in this pGCC4-CL*mtrD*$_{His6}$ derivative. Seven MtrD mutants (F136A, F176A, I605A, F610A, S611A, F612C, and F623C) were generated and individually recombined into the *N. gonorrhoeae* KH15Δ*mtrD*Δ*norM* chromosome. Western blotting of isolated membranes from these bacteria confirmed expression of the MtrD mutant proteins at levels comparable to that determined for the CL-MtrD$_{His6}$ parent (Figure 2.1).

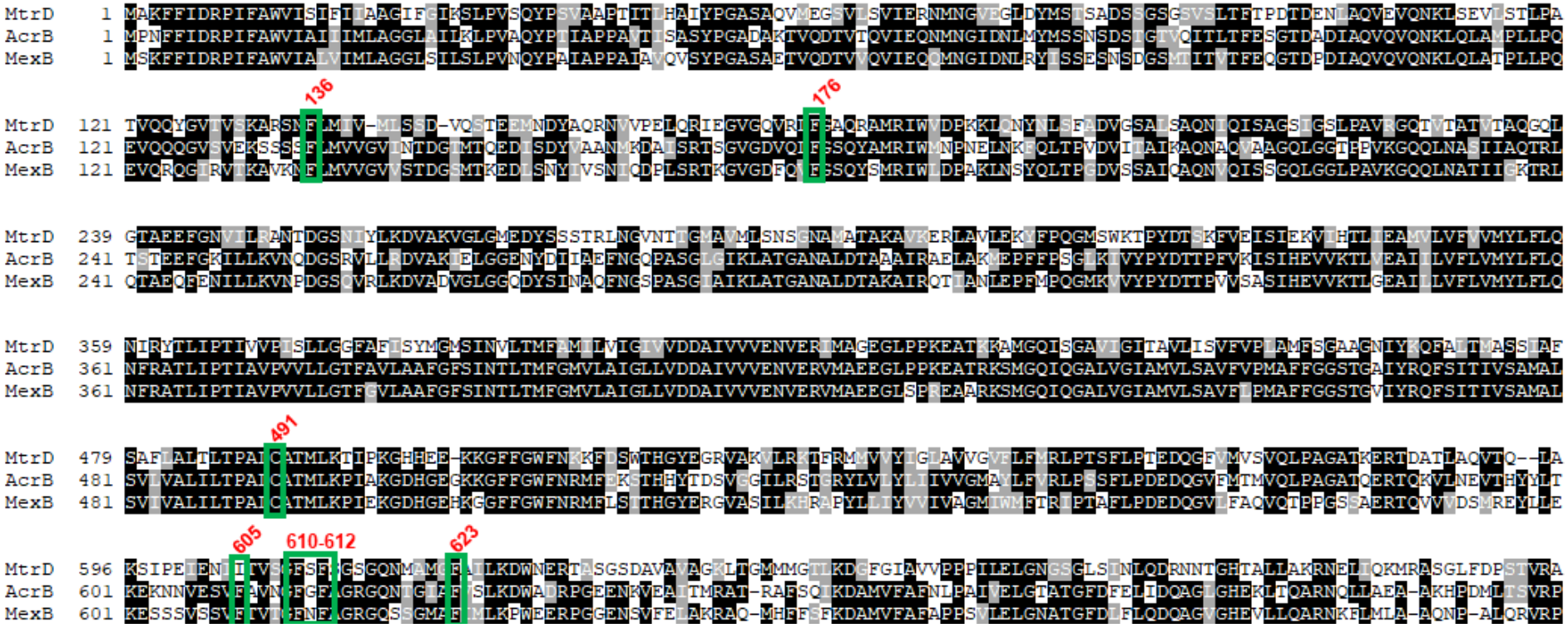

Figure 2.8: Protein sequence alignment of MtrD, AcrB and MexB. The sequence alignment is shown up to MtrD residue 715.

Protein sequence alignment was done using the T-Coffee program and visualized by BoxShade with residue boxes coloured based on % identity. MtrD residues targeted by site-directed mutagenesis are shown within green rectangles with residue number at the top in red. Accession numbers are: MtrD, AAC45560.1; AcrB, P31224; and MexB P52002.

Three MtrD mutants (F176A, F612C and F623C) exhibited reduced resistance to all 11 compounds, indicating a significant and wide-ranging impact on resistance (Table 2.5). No resistance to ET, PMB, PRO and DQ was observed for any of the three mutants, and F623 showed only background levels of resistance to N-9. They did retain a small degree of resistance to the other six compounds, namely, TX-100, RIF, NOV, CV, OXA, and CHO (Table 2.5). It is worth noting that the retention of this small degree of resistance is evidence that the complete loss of resistance that was seen for the group of four substrates, was likely not due to complete misfolding of the mutant protein. These data suggest that F176, F612 and F623 residues play important and widespread roles in MtrD-mediated MDR.

Replacement of residues in MtrD at positions 136, 605 and 610 differentially affected resistance to distinct compounds (Table 2.5). The MtrD F136A mutant showed reduced resistance to five compounds while no changes in MICs were observed for six compounds (Table 2.5). Substitution of I605 with alanine reduced resistance to eight of 11 tested compounds, with the WT resistance profile retained for only 3 compounds (Table 2.5). The effect of substitution of F610 was more limited, as MtrD F610A showed a reduction in resistance only to NOV, which was observed by a consistent 2-fold reduction in MICs for this compound (Table 2.5). The MtrD S611A mutant was the only variant that retained a complete WT resistance profile with no change in MICs for any tested compound (Table 2.5).

Table 2.5: *N. gonorrhoeae* KH15Δ*mtrD*Δ*norM* strain expressing MtrD derivatives

	MIC (μg/ml)[a]										
	Detergent		Antibiotic			CAMP[b]	Dye		BA	Hormone	Biocide
Mutation	N-9	TX-100	RIF	NOV	OXA	PMB	ET	CV	CHO	PRO	DQ
$MtrD_{His6}$[c]	≥4096	≥4096	0.125	1	4	100	0.25	2	400	80	1
CL-$MtrD_{His6}$	≥4096	≥4096	0.125	1	4	100	0.25	2	400	80	1
F136A	≥4096	≥4096	0.03	0.25	2	100	0.25	0.5	200	80	1
F176A	32	128	0.03	0.125	0.5	50	0.06	0.25	200	20	0.5
I605A	32	128	0.03	0.5	1	100	0.125	1	400	80	0.5
F610A	≥4096	≥4096	0.125	0.5	4	100	0.25	2	400	80	1
S611A	≥4096	≥4096	0.125	1	4	100	0.25	2	400	80	1
F612C	32	128	0.016	0.125	0.5	50	0.06	0.25	200	20	0.5
F623C	16	64	0.016	0.125	0.25	50	0.06	0.125	100	20	0.5
- ve control[d]	16	32	0.008	0.03	0.06	50	0.06	0.125	100	20	0.5

[a] All MIC data are representative of three or more independent experiments. [b] Abbreviations: CAMP, cationic antimicrobial peptide; BA, Bile acid; CHO, cholic acid; CV, crystal violet; DQ, dequalinium; ET, ethidium; N-9, nonoxynol-9; NOV, novobiocin; OXA, oxacillin; PMB, polymyxin B; PRO, progesterone; RIF, rifampin; TX-100, Triton X-100; [c] Recombinant WT $MtrD_{His6}$

[d] KH15Δ*mtrD*Δ*norM* strain transformed with pGCC4 empty vector expressing no MtrD [KH15Δ*mtrD*Δ*norM*(NICS) strain]

2.6 Discussion

Antibiotic resistance in *N. gonorrhoeae* is an effective survival strategy as this bacterium has been successful in developing resistance to almost all antibiotics previously or currently used for treatment of gonorrhoea. With the emergence and spread of gonococci strains that have shown resistance to the last options of empirical therapy, AZM and CRO, the problem has become more alarming. The limited discovery of new antibiotics during past 3 decades, particularly of those against Gram-negative bacteria, has intensified this concern. One of the mechanisms of drug resistance utilised by *N. gonorrhoeae* involves efflux pumps that enable the cells to keep interior levels of drugs below toxic levels. Recent reports have highlighted the importance of this mechanism of resistance by showing that *N. gonorrhoeae* can acquire mosaic drug efflux gene sequences from commensal *Neisseria* that can lead to low-level AZM resistance expressed by *N. gonorrhoeae* clinical isolates (Shafer, 2018). Interestingly, the acquired mosaic-like sequence within *mtrD* in these isolates was found to increase MtrD activity, resulting in clinical resistance to AZM in the background of elevated expression of the MtrCDE efflux proteins.

To analyse in detail the MtrD pump component of the MtrCDE efflux system, a site-directed mutagenesis system specific for manipulation and analysis of this protein in its natural host *N. gonorrhoeae* was established. Addition of a histidine tag on the C terminus of MtrD for monitoring expression levels and increasing the versatility of the system did not affect resistance (Table 2.1,Table 2.2, and Table 2.3), making the $MtrD_{His6}$ protein advantageous for studying the effect of mutations on resistance to many important antibiotics, biocides and human-derived antimicrobial peptides. Additionally, the cysteine-less derivative of $MtrD_{His6}$ (CL-$MtrD_{His6}$) retained full activity compared to the corresponding parental $MtrD_{His6}$ protein, providing a reliable site-directed cysteine-scanning mutagenesis system for further analysis of MtrD (Table 2.5).

This study revealed that the MtrD efflux pump possesses an even wider substrate specificity than had previously proposed (Golparian et al., 2014, Hagman et al., 1995, Sparling et al., 1975) with the addition of fourteen new substrates, including detergents (SDS, 3-[(3-cholamidopropyl)dimethylammonio]-1-propanesulfonate (CHAPS), and TW-

80; antibiotics (TGC, NOV, CIP, and PT); biocides (DQ, BC, CH, and TR); and a cationic polypeptide (colistin, CST) as well as two efflux pump inhibitors PAβN and NMP (Tables Table 2.1, Table 2.2, and Table 2.3).

One of the interesting features of RND transporters is that they recognise and export a remarkably broad range of substrates from different chemical classes. This feature has been mainly attributed in AcrB to the existence of multiple pockets with each pocket containing multiple overlapping drug-binding sites within the porter domain as well as several entrances with specificity for different substrates (Nakashima et al., 2013, Yamaguchi et al., 2015, Zwama et al., 2018), similarly to the substrate recognition mechanism first described for the multidrug binding protein QacR (Grkovic et al., 2003, Schumacher et al., 2001). Additionally, the presence of multiple aromatic residues such as phenylalanine in a multisite substrate-binding pocket that can act in a drug-specific manner has been reported previously for both QacR and AcrB (Schumacher et al., 2001). Similar features are apparent in the MtrD poly-specific RND efflux transporter. MD simulations of PRO binding to MtrD identified 25 residues within the binding cleft that are implicated in PRO binding (Table 2.4; see also Figure 2.3A). This was in good agreement with docking results from analysis of PRO, which identified a similar set of residues in contact with PRO, including F176, F610, F612, and F623. Docking studies of a further six compounds also indicated that these five phenylalanine residues form key interactions with substrates in the access and deep binding pockets of MtrD. Mutational analyses of these five phenylalanine residues showed reduced resistance to various MtrD substrates, confirming the integral role that these aromatic residues play in MtrD drug binding and translocation.

PRO binding MD simulations of MtrD, docking analyses of eight compounds and MIC analysis of F176A and F623C mutants showed that these residues, located in the region of MtrD corresponding to the deep binding pocket, have important functional roles in drug binding and resistance. This is similar to what has been ascribed to the homologous residues, F178 and F628 in AcrB, which are involved in binding to drugs and RND efflux pump inhibitors (Bohnert et al., 2008, Husain and Nikaido, 2010, Murakami et al., 2006, Nakashima et al., 2013, Schulz et al., 2010, Sjuts et al., 2016, Takatsuka et al., 2010, Vargiu and Nikaido, 2012, Vargiu et al., 2018a, Vargiu et al., 2014).

F612 is a conserved residue located in the region corresponding to the AcrB switch loop (F617 in AcrB) that projects into the binding cleft cavity between the access and deep binding pockets. During the transition from the access conformation to the binding conformation of AcrB, movement of the switch loop allows high-molecular mass (*Mr*>600 Dalton) substrates to move from the AcrB access pocket to deep binding pocket (Eicher et al., 2012, Nakashima et al., 2011). Spontaneous binding of PRO from MD simulations showed that Cα of F612 was within 4 Å of PRO for >75% of the 200 ns simulation time (Table 2.4 and Figure 2.3A), while docking analyses confirmed that F612 is a contributor to the binding affinity for all eight docked compounds (Figure 2.3B,Figure 2.4 to Figure 2.7). Analysis of cells expressing the F612C MtrD mutant showed a significant reduction in resistance to all 11 tested compounds, confirming the importance of F612 in resistance afforded by MtrD (Table 2.5).

Like the homologous counterparts in AcrB (F136, F610 and F615), F136, I605, and F610 form part of the deep binding pocket and are involved in nonspecific drug binding of MtrD (Figure 2.8) (Ababou and Koronakis, 2016, Bohnert et al., 2008, Murakami et al., 2006, Schulz et al., 2010). Our PRO binding MD simulations showed that Cα of MtrD F610 was within 4 Å of PRO for >50% of the simulation time (Figure 2.3A). Docking analyses identified F136 and F610 as contributors to the binding affinity for various compounds (Figure 2.3B,Figure 2.4 to Figure 2.7), and the data were confirmed by MIC analysis of the corresponding MtrD mutant derivatives, even though the MIC for PRO was unaffected in the F610A mutant. MIC data also suggest that I605, located in the distal region of the deep binding pocket, has a functionally important role in MtrD. However, analysis of the starting MtrD crystal structure and MD trajectories showed that, unlike the corresponding residue in AcrB (F610), I605 did not form part of the solvent-accessible cavity surface of the deep binding pocket in the MtrD crystal structure and thus did not interact with PRO in either MD simulations or docking-based studies. The lack of correlation between the MIC data and the co-crystallography or MD simulations data is not uncommon in studies of these dynamic transporters, which undergo large-scale conformational changes during their transport cycle.

The use of MD simulations of PRO binding in this study was found to be a successful approach for characterisation of MtrD binding to a substrate. The

predictive power of this method comes from a circumstantial finding of this study, which identified K823, located in the access pocket, as interacting with PRO. In a recent study of a *N. gonorrhoeae* clinical isolate possessing a mosaic-like *mtr* efflux pump locus with reduced susceptibility to antimicrobials, mutation of K823 to glutamate (K823E) resulted in a gain-of-function impact on MtrD activity (Rouquette-Loughlin et al., 2018b) suggesting an important functional role for this residue in MtrD drug translocation and confirming our assignment of this residue in substrate binding.

Characterization of antimicrobial efflux mechanisms in bacteria has helped understanding the resources through which bacteria, including *N. gonorrhoeae* are able to develop resistance against toxic compounds present in their environment, including those found naturally and antibiotics used for treatment of infections. In Gram-negative bacteria in particular, characterization of RND efflux pumps, including the gonoccocal MtrCDE system has helped improve understanding the main barrier for accumulation of antibiotics within the cells at toxic levels. The detailed molecular, biochemical, structural and computational studies of RND pumps, including the *N. gonorrhoeae* MtrD protein have provided new insights regarding determinations of operation/efflux mechanisms, substrate pathways, amino acid residues required for drug recognition and binding, and residues that are involved in other mechanisms of efflux operation such as energy coupling or interaction with partner proteins. These studies have also provided new insights regarding how some molecules interact with and inhibit RND pumps. New drugs that by-pass efflux mechanisms are desperately needed for treatment of infections with highly resistant bacterial strains, especially of infections with Gram-negative bacteria. Identification of functionally important residues in MtrD represent a start for efforts aimed at gaining a better understanding of the transport mechanism(s) of the RND family of multidrug transporters and at rationally based designing of antimicrobial drugs or efflux pump inhibitors.

2.7 Materials and Methods

2.7.1 Bacterial strains, plasmids, and growth conditions

The bacterial strains and plasmids used in this study are listed in Table 2.6. Gonococci were grown on GC medium (Difco Laboratories, Detroit, MI) as

previously described (Kellogg et al., 1963). The pGCC4 vector was used as the backbone in which *mtrD* mutants were constructed and then mobilized into *N. gonorrhoeae* (see below). ERY was added into GC plates for selecting *N. gonorrhoeae* transformed with pGCC4 (0.5 µg/ml) or for replica plating for selection of *mtrD* deletions (0.06 µg/ml). Isopropyl-β-D-thiogalactopyranoside (IPTG) was used at a final concentration of 0.5 mM to induce *mtrD* expression in *N. gonorrhoeae* strains containing integrated *mtrD* constructs.

E. coli DH5α (Hanahan, 1983) was used in cloning experiments and for propagation of all pGCC4 vector-based constructs. *E. coli* cells were grown on Luria-Bertani (LB) agar or in LB broth (Oxoid, Thermo Fisher Scientific Australia Pty Ltd) with Kan (40 µg/ml) where required.

Table 2.6: Bacterial strains and plasmids used in this study.

Strain or plasmid	**Relevant genotypes or description**	**S[@]**
Strains		
E. coli		
DH5α	*fhuA2* Δ(*argF-lac*Z)U169 *phoA* *glnV*44 Φ80 Δ(*lacZ*)M15 *gyrA*96 *recA*1 *relA*1 *endA*1 thi-1 hsdR17	a
N. gonorrhoeae		
FA19	Antimicrobial sensitive	b
KH15	As FA19 but *mtrR*-171	c
FA19Δ*mtrD*	As FA19 but Δ*mtrD*	d
FA19Δ*norM*	As FA19 but Δ*norM*	d
FA19Δ*mtrD*Δ*norM*	As FA19 but Δ*mtrD* and Δ*norM*	d
KH15Δ*mtrD*	As KH15 but Δ*mtrD*	d
KH15Δ*mtrD*Δ*norM*	As KH15 but Δ*mtrD* and Δ*norM*	d
KH15Δ*mtrD*Δ*norM*(*mtrD*)	As KH15Δ*mtrD*Δ*norM* but complemented with WT $mtrD_{6his}$	d
Plasmids		
pGCC4	Neisseria insertion complementation system (NICS) vector; *lacI*, P_{lac}, Kan^R, ERY^R	f

Strain or plasmid	Relevant genotypes or description	S[@]
pGCC4-*mtrD*$_{6His}$	*mtrD* cloned into *Pme*I and *Pac*I site of pGCC4 under the control of P_{lac} promoter with a 6His-tag at the C-terminus	d
pGCC4-CL*mtrD*$_{His6}$	Cysteine-less derivative of *mtrD*$_{His6}$ in pGCC4	d
pGCC4-CL*mtrD*$_{His6}$(F136A)	Site-directed F136A MtrD mutant based in pGCC4-CL*mtrD*$_{His6}$	d
pGCC4-CL*mtrD*$_{His6}$(F176A)	Site-directed F176A MtrD mutant based in pGCC4-CL*mtrD*$_{His6}$	d
pGCC4-CL*mtrD*$_{His6}$(I605A)	Site-directed I605A MtrD mutant based in pGCC4-CL*mtrD*$_{His6}$	d
pGCC4-CL*mtrD*$_{His6}$(F610A)	Site-directed F610A MtrD mutant based in pGCC4-CL*mtrD*$_{His6}$	d
pGCC4-CL*mtrD*$_{His6}$(S611A)	Site-directed S611A MtrD mutant based in pGCC4-CL*mtrD*$_{His6}$	d
pGCC4-CL*mtrD*$_{His6}$(F612C)	Site-directed F612C MtrD mutant based in pGCC4-CL*mtrD*$_{His6}$	d
pGCC4-CL*mtrD*$_{His6}$(F623C)	Site-directed F6123C MtrD mutant based in pGCC4-CL*mtrD*$_{His6}$	d

[@]Source or reference: a, (Hanahan, 1983), b, (Sparling et al., 1975); c, (Hagman et al., 1995); d, (This study); f, (Mehr and Seifert, 1998)
[a]Abbreviations: ERY^R, erythromycin resistance; Kan^R, kanamycin resistance.

2.7.2 Molecular biology methods

Chromosomal DNA was isolated from *N. gonorrhoeae* cells using a Wizard genomic DNA purification kit (Promega Co., USA) and plasmid DNA from *E. coli* using an Isolate II Plasmid Mini kit (Bioline, Boston, USA) per the instructions of the manufacturers. Primers used in this study are listed in Table 2.7 and were synthesized by GeneWorks (GeneWorks Pty. Ltd., Australia) or Integrated DNA Technologies. Bioline Velocity DNA polymerase was used in all cloning and mutagenesis procedures and Bioline Mango*Taq*™ DNA polymerase for screening PCRs (Bioline, Boston, MA, USA). All restriction

digestion enzymes and T4 DNA ligase were from New England Biolabs (New England Biolabs Inc., Ipswich, MA, USA). Transformations into *N. gonorrhoeae* or *E. coli* cells were carried as described previously (Dillard, 2011, Hanahan, 1983). All sequencing was performed by Australian Genome Research Facility (AGRF; Australia).

2.7.3 Construction of unmarked *mtrD* and *norM* single and *mtrD*/*norM* double deletion strains

Two unmarked *mtrD* deletion strains (the FA19Δ*mtrD* and KH15Δ*mtrD* strains) were created by overlap extension PCR (Vallejo et al., 1994). Briefly, a 3,150-bp fusion DNA fragment that encompassed the *mtrD* gene was created by PCR using the primers MtrD-Del-F2, MtrD-Ovl-R1, MtrD-Ovl-F2, and MtrD-Del-R2 (Table 2.7) and FA19 chromosomal DNA as the template. This two-step PCR removed *mtrD*, leaving only 177 bp before its stop codon. The PCR-amplified DNA was transformed into the FA19 and KH15 strains, and the resultant colonies were selected by susceptibility to ERY performed by replica plating on GC plates with and without ERY (0.06 µg/ml, 4-fold below MIC for FA19). ERY was used as it is a known substrate of the MtrD protein, and sensitivity to ERY at a concentration below the MIC for FA19 could be used as evidence that for the *mtrD* gene had been removed. Sequencing confirmed the removal of *mtrD* and the integrity of the flanking regions. The same method was used for creating the *N. gonorrhoeae* FA19Δ*norM*, FA19Δ*mtrD*Δ*norM*, and KH15Δ*mtrD*Δ*norM* strains by deleting the *norM* gene from the respective progenitors. The NorM_NG substrate ET (0.25 µg/ml for *norM* only deletion and 0.06 µg/ml for *norM* and *mtrD* double deletion mutants) was used for selecting the *norM* knockout derivatives by replica plating.

Table 2.7: Oligonucleotides used in this study.

Name and purpose[a]	Sequence 5' to 3'
Cloning *mtrD* into pGCC4	
PacI-*mtrD* for	GAGATTAATTAAAGGAAGGCATCGATGGCTAAATT
PmeI-*mtrD* rev	TCTCGTTTAAACTTAATGGTGATGATGGTGATGATATT GTTTATCGTCCG
PCR screening for integration of *mtrD* between *acpC* and *lctP*	
SCRNG1	CGCCTTATGATGCAAATG
MTRDSF5	CCGTATTCTGGGGGATGTTG
Sequencing of *mtrD* in pGCC4	
PGCC4_F2	CCCAGGCTTTACACTTTATGCT
PGCC4-R1.1	GGGGATCCGCTAGCACTAGG
MtrD-SF4.1	GCAGTTGGGTACGGCAGAAG
MtrD-SR4.1	GCTCTGTTCCGTACCGTTTTC
Deleting *mtrD* from the *N. gonorrhoeae* chromosome	
MtrD-Del-F1	CGCGTCAAACAAGTCTTC
MtrD-Del-F2	GGCAAAACCCTTTACATC
MtrD-Ovl-R1	GGTATTTTGCCGATGCCTTCCTTATTTCGCTTC
MtrD-Ovl-F2	GGAAGGCATCGATCGGCACGACCGTATTCTG
MtrD-Del-R2	GGCAAAACCCTTTACATC
Deleting *norM* from the *N. gonorrhoeae* chromosome	
NorM-AF1	GCAGCGAGAATGCTTTTG
NorM-AR	GCAATCAATGCCGTCAAGTGTTCAGTCAATAAAAATG
NorM-BF	GACTGAACACTTGACGGCATTGATTGC
NorM-BR1	CCAATGCCTGTTTATCGTG
Mutagenesis	
C491A-F	CTGACCCTTACCCCTGCGCTAGCAGCCACAATGTTGAAG
C491A-R	CTTCAACATTGTGGCTGCTAGCGCAGGGGTAAGGGTCAG

Name and purpose[a]	Sequence 5' to 3'
F136A-F	CAAGGCGCGTTCCAATGCATTGATGATTGTGATG
F136A-R	CATCACAATCATCAATGCATTGGAACGCGCCTTG
F176A-F	CAGGTCCGCCTGGCTGGGGCGCAACGCGCGATG
F176A-R	CATCGCGCGTTGCGCCCCAGCCAGGCGGACCTG
I605A-F	CGAAATTGAAAACATCGCGACCGTTTCCGGCTTC
I605A-R	GAAGCCGGAAACGGTCGCGATGTTTTCAATTTCG
F610A-F	CGTTTCCGGCGCTAGCTTTTCGGGCAGCGGTCAG
F610A-R	CTGACCGCTGCCCGAAAAGCTAGCGCCGGAAACG
S611A-F	CGTTTCCGGCTTCGCGTTTTCGGGCAGCGGTCAG
S611A-R	CTGACCGCTGCCCGAAAACGCGAAGCCGGAAACG
F612C-F	CGTTTCCGGCTTCAGCTGCTCAGGCAGCGGTCAGAATATG
F612C-R	CATATTCTGACCGCTGCCTGAGCAGCTGAAGCCGGAAACG
F623C-F	CAGAATATGGCGATGGGTTGCGCAATATTGAAAGATTGGAAC
F623C-R	GTTCCAATCTTTCAATATTGCGCAACCCATCGCCATATTCTG

[a]The source of all oligonucleotides listed in this table originated from this research.

2.7.4 Cloning of *mtrD* into pGCC4 and recombination into the neisserial chromosome

To recombine *mtrD* into the chromosome of the *N. gonorrhoeae* Δ*mtrD* knockout strains, the *mtrD* determinant was cloned into the pGCC4 shuttle vector behind the lac promoter. A *Pac*I-*mtrD*-*Pme*I fragment was obtained by PCR amplification using FA19 chromosomal template DNA and PacI-*mtrD*-for and PmeI-*mtrD*-rev primers (Table 2.7). A sequence was also incorporated in the reverse primer, allowing addition of six histidine residues to act as an affinity tag at the C terminus of the protein. The resultant PCR product and vector were digested and cloned with *Pac*I and *Pme*I, producing the *mtrD* clone called pGCC4-*mtrD*$_{(His6)}$.

The *mtrD* derivatives were recombined into KH15Δ*mtrD*Δ*norM* chromosome by transformation as previously described (Dillard, 2011). The pGCC4 empty vector was also integrated into KH15Δ*mtrD*Δ*norM* chromosome, producing a NICS-only recombinant strain that could be utilised as a negative control by employment of the same methodology. KH15Δ*mtrD*Δ*norM* recombinants were selected on GC plates containing ERY (0.5 µg/ml). A single purified transformant colony was subjected to PCR using SCRNG1 and MTRDSF5 primers (Table 2.7) for verification of *mtrD*$_{His6}$ integration between *lctP* and *aspC*.

2.7.5 Site-directed mutagenesis

The QuickChange site-directed mutagenesis method was used to individually replace the selected MtrD residues using the primers listed in Table 2.7. To aid in screening, a silent restriction site was incorporated into each primer pair where possible. Initially, a cysteine-less derivative of MtrD was created by PCR-amplification using C491A-F and C491A-R primers and pGCC4-*mtrD*$_{His6}$ as the template. The PCR cycling conditions were as follows: denaturation at 95°C for 5 min, followed by 30 cycles of 95°C for 20 sec, 55°C for 1 min, 72°C for 8 min 30 sec and then 72°C for 10 min. Subsequent mutants (F136A, F176A, I605A, F610A, S611A, F612C, and F623C) were created using the pGCC4-CL*mtrD*$_{His6}$ construct as the template. Integrity of all constructs was verified by sequencing the whole *mtrD* gene and followed by recombination of the gene into the *N. gonorrhoeae* KH15Δ*mtrD*Δ*norM* chromosome.

2.7.6 Western blotting

Expression of MtrD proteins in KH15Δ*mtrD*Δ*norM* membranes was analysed by Western blotting using anti-6XHis epitope tag (rabbit) antibody and peroxidase-conjugated anti-rabbit IgG (goat) antibody (Rockland) as primary and secondary antibodies, respectively. *N. gonorrhoeae* strains were grown at 37° C to an optical density at 600 nm (OD_{600}) of 0.6 in GC broth containing 0.5 mM IPTG. All membrane isolation and protein experiments were conducted on ice or at 4°C as previously described (Hassan et al., 2006a, Hassan et al., 2009). The total protein content in each sample was quantified using a Bio-Rad DC protein assay kit, and 10-µg samples were resolved on a

10% SDS-PAGE gel and transferred (Hassan et al., 2006a, Hassan et al., 2009). Membranes were scanned with a BioRad ChemiDoc MP imaging system and analysed using Image Lab software 6.0.1 (Bio-Rad). Mutant protein expression levels were compared the WT protein expression level (Figure 2.1).

2.7.7 MIC analyses

MIC analyses of the *N. gonorrhoeae* strains used a previously reported agar dilution method (CLSI, 2012) with modifications. MIC analyses were conducted using solid GC media supplemented with 0.5 mM IPTG and antimicrobial compounds. The MIC was determined as the lowest concentration of the antimicrobial compound required to fully inhibit bacterial growth. All MIC values shown are representative of results from three replicates.

2.7.8 Molecular dynamics simulations

The MtrD crystal structure (PDB identifier [ID]: 4MT1) was used for all simulations (Bolla et al., 2014). The missing residues between residues 494 and 507, 671, and 672 were rebuilt; the N and C termini were capped respectively with acetyl and amine groups, respectively; and the crystallographic symmetry operators were applied to rebuild the trimeric biological assembly (Schrodinger, 2015). The MtrD trimer was embedded in an equilibrated *Neisserial* lipid bilayer containing 80% 1-palmitoyl-2-palmitoleoyl-*sn*-glycero-3-phosphatidylethanolamine (PPoPE) and 20% 1,2-dimyristoyl-sn-glycero-3-phospho-(1'-rac)-glycerol (DMPG) as described previously (Anandan et al., 2017), using the Orientation of Membrane Proteins database to guide the orientation in the membrane (Lomize et al., 2011). Thirty molecules of PRO were inserted randomly in the solvent layer surrounding MtrD. The system was solvated with explicit water and 150 mM NaCl. Counter-ions were added to ensure the overall charge neutrality of the system.

All simulations were performed using GROMACS 2016.1 (Abraham et al., 2015, Van Der Spoel et al., 2005) in conjunction with the GROMOS 54a7 forcefield and a 2-fs timestep (Schmid et al., 2011). The simple point charge (SPC) water model (Berendsen et al., 1981) was used to describe the solvent water. The parameters used for progesterone analyses, DMPE and DMPG, are available from the automated force field topology builder (ATB) (Malde et

al., 2011). All simulations were performed under periodic boundary conditions in a hexagonal prism box. The dimensions of the box were chosen such that minimum distance of the protein to its periodic image was 3.5 nm.

The system was equilibrated over 10 ns, using a series of 2 ns simulations in the NPT (fixed number of atoms N, fixed pressure P, fixed temperature T) ensemble with progressively decreasing position restraint force constants of 500 kJ mol^{-1} nm^{-2}, 100 kJ mol^{-1} nm^{-2}, 50 kJ mol^{-1} nm^{-2}, 20 kJ mol^{-1} nm^{-2} and 0 kJ mol^{-1} nm^2 on the C_α atoms. The temperature of the simulations was maintained at 300 K using a Bussi velocity rescaling thermostat, with a coupling constant of 0.1 ps (Bussi et al., 2007). The pressure coupling was semi-isotropic. The pressure was maintained at 1 bar using a Parrinello-Rahman barostat pressure coupling with a constant of 5 ps. The Particle Mesh Ewald (PME) method (Darden et al., 1993) was used to calculate electrostatic interactions with a cutoff at 1.4 nm. The LINCS algorithm (Hess et al., 1997) was used for bond constraints, and the SETTLE algorithm (Miyamoto and Kollman, 1992) was utilised to constrain waters. Three replicate simulations were performed, each 200 ns in length. To examine how changes in timescale influence the interaction with PRO, the third simulation was extended to 500 ns in total, giving a total combined simulation time of 900 ns for the three replicates.

2.7.9 Docking studies

To identify the molecular interactions underlying the modified resistance profiles of our MtrD mutants, molecular docking of seven diverse MtrD substrates (PRO, N-9, AZM, RIF, ET, CV and CHO and the PAβN inhibitor was performed with AutoDock Vina V.1.1.2. United-atom representations of these substrates (with protonation states appropriate for pH 7.4) were docked to the repaired crystal structure of the MtrD trimer used to initialize the MD simulations reported in this study. AutoDock Tools V.1.5.6 was used to determine two sets of grid parameters centred on the access and deep binding pocket cavities, respectively (Table 2.8). For each substrate, docked poses within the proposed access pocket or deep binding pocket were selected for analysis if the energy of a given pose was within 1 kcal/mol (inclusive) of the lowest-energy pose for a given substrate, with weighted energies obtained

according to the default AutoDock Vina scoring-function. Substrate amide bonds were allowed to rotate during docking. Residues comprising the putative access and deep binding pockets (Table 2.4) were made flexible during the docking procedure centred on the corresponding pocket. To identify residues with the most significant binding interactions, approximate per-residue contributions to the binding affinity and energy breakdowns for each substrate were obtained by systematically removing each residue found within 8 Å of the lowest-scoring docked pose followed by (static) rescoring.

Table 2.8: Docking parameters used.

Parameter	Access Binding Pocket Grid	Deep Binding Pocket Grid
X centre	26.061	25.725
Y centre	-17.867	-8.799
Z centre	40.542	47.640
X points	46	44
Y points	46	44
Z points	46	44
Spacing (Å)	0.375	0.375
Exhaustiveness	12	12

CHAPTER 3

COORDINATION OF SUBSTRATE BINDING AND PROTONATION IN THE *NEISSERIA GONORRHOEAE* MTRD EFFLUX PUMP CONTROLS THE FUNCTIONALLY ROTATING TRANSPORT MECHANISM

Declaration by candidate

The quality and extent of contributions of the candidate and co-authors to this work was as follows:

Name	Quality of contribution	Contribution extent (%)
Mohsen Chitsaz (candidate)	Conceptualisation, data curation, methodology, performance of experiments, writing, editing and revision of the manuscript	25
Stephen J. Fairweather (co-author)	Conceptualisation, data curation, methodology, performance of MD simulations, writing, editing and revision of draft and final manuscript	55
Lauren Booth (co-author)	Conceptualisation, data curation, methodology, performance of MD simulations	3
Vrinda Gupta (co-author)	Conceptualisation, data curation, methodology, performance of MD simulations, writing, editing and revision of the manuscript	7
Megan O'Mara (co-author)	Conceptualisation, data curation, editing and revision of draft and final manuscript	5
Melissa Brown (co-author)	Conceptualisation, data curation, editing and revision of draft and final manuscript	5

The undersigned hereby certify the above declaration correctly reflects the quality and extent of the candidate and co-author contribution to this work.

Candidate signature		18/04/2024
Supervisor signature		18/04/2024

3.1 Preface

The information provided in this chapter has been published by Fairweather, S. J., Gupta, V., Chitsaz, M., Booth, L., Brown, M. H., O'Mara, M. L. (2021). "Coordination of substrate binding and protonation in the *Neisseria gonorrhoeae* MtrD efflux pump controls the functionally rotating transport mechanism." ACS Infectious Diseases, 7, 1833−1847. The printed version of this paper can be located in Chapter 7 (Appendix **D**). This chapter is based on research conducted in 2018 when only the apo structure of MtrD in a symmetric configuration was available, thus requiring consideration of the timeline mentioned herein.

3.2 Abstract

Multidrug resistance is a serious problem that threatens the effective treatment of the widespread sexually transmitted disease gonorrhoea, caused by the Gram-negative bacterium *Neisseria gonorrhoeae*. The drug efflux pump primarily implicated in *N. gonorrhoeae* AMR is the inner membrane transporter MtrD, which forms part of the tripartite Multiple Transferable Resistance (Mtr) CDE efflux system. A structure of MtrD was first solved in 2014 as a symmetrical homotrimer, and then, in 2020, as an asymmetrical homotrimer. Through a series of MD simulations and mutagenesis experiments, we identify the combination of substrate binding and protonation of the proton relay network drives transition from the symmetric to asymmetric conformation of MtrD. We characterise the allosteric coupling between the functionally important local regions that control conformational changes between the access, binding and extrusion states and allow for transition to the asymmetric MtrD conformation. We also highlight a significant rotation of the transmembrane helices caused by protonation of the proton relay network, which widens the inter-monomeric gap that is a hallmark of the rotational transporter mechanism. This is the first analysis and description of the transport mechanism for the *N. gonorrhoeae* MtrD transporter and provides evidence that antimicrobial efflux in MtrD follows the functionally rotating transport mechanism seen in protein homologues from the same transport protein superfamily.

3.3 Introduction

Previous work on the MtrD homologue, AcrB, has provided a working paradigm of the RND transport cycle, in which trimeric RND efflux proteins adopt an asymmetric conformation with each of the three monomers in an ‘access’, ‘binding’ or ‘extrusion’ state (Murakami et al., 2006, Seeger et al., 2006, Sennhauser et al., 2007). Substrate efflux depends on the synchronous cycling of the monomers through these three functional states (Figure 3.1 C) (Jewel et al., 2020, Yao et al., 2010). The transport cycle begins with the spontaneous binding of substrate in the proximal binding pocket of the access state (Figure 3.1 B). During transition from the access to the binding state, substrate permeates along the binding pocket, ending in the distal (or deep) binding pocket (Section 2.5.3). Finally, in the extrusion state, substrate is effluxed from the MtrD DBP, to the MtrE outer membrane channel. These conformational states are coupled to changes in the protonation state of the TMD proton relay network, driven by the proton motive force across the inner membrane.

The proton relay network is highly conserved across all RND transporters and contains a network of titratable residues located on either side of the axis of pseudosymmetry to form a hydrogen bonding network. From structural comparison and sequence homology against AcrB, the MtrD residues D405 and D406 (TM 4), K948 and N949 (TM 10) and T985 (TM 11) form the putative proton relay network (Jewel et al., 2020, Lyu et al., 2020, Su et al., 2006, Takatsuka and Nikaido, 2006, Yamane et al., 2013, Yue et al., 2017). In AcrB protonation of D405 and/or D406 via the periplasmic uptake of protons leads to disengagement of the proton relay network and a global conformational change from the binding to the extrusion conformation (Murakami et al., 2006). Conversely, deprotonation of D405 and/or D406 engages the proton relay network and drives the monomer back into the access conformation.

The asymmetric MtrD cryo-EM structures (PDB ID: 6VKT, 6VKS) (Lyu et al., 2020) each contain an access, binding and extrusion monomer, with substrate bound in the DBP of the binding monomer. In comparison, in the earlier crystal structure (PDB ID: 4MT1), all three monomers are in a symmetric conformation that does not align to the prototypical RND access, binding or extrusion states.

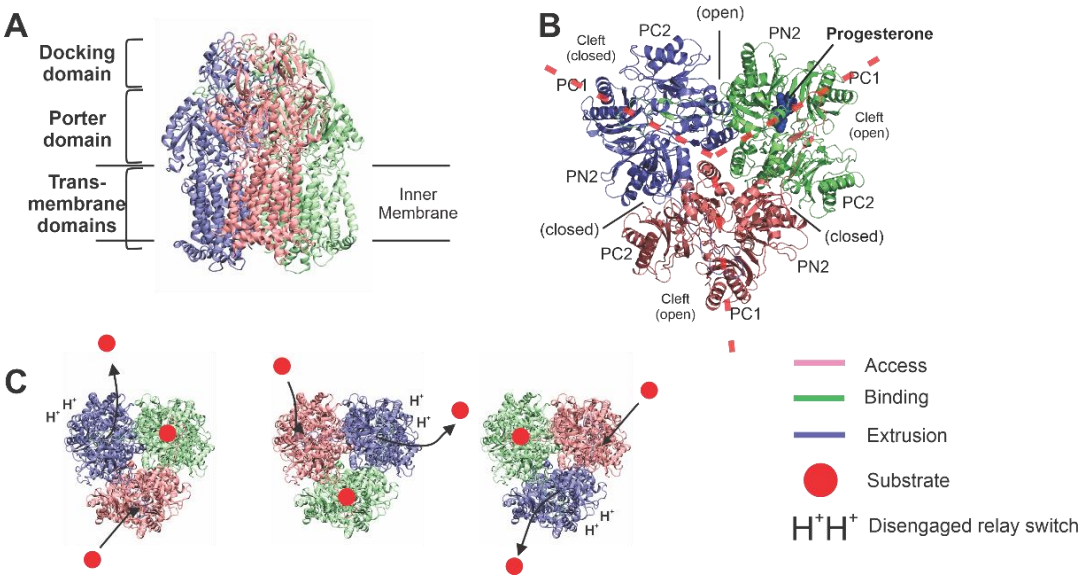

Figure 3.1: Asymmetric structure of MtrD and proposed transport cycle.

(A) Side view and (B) top view of the asymmetric homotrimeric MtrD structure (PDB ID: 6VKT) showing key domains and subdomains, coloured by access, binding or extrusion conformation (transmembrane domains are hidden for clarity). Progesterone (blue VDW rendering) is shown in the binding conformation monomer (green) of the asymmetric structure. The axis of pseudosymmetry through each monomer is shown by a dashed red line. (C) The proposed asymmetric RND transport cycle alternates in a synchronized fashion through the access, binding and extrusion conformations. The substrate binding configuration and protonation state of the three conformations are indicated by the presence of two protons (H+) and substrate (red dot).

Instead, each monomer has a mix of local features characteristic of the binding and extrusion states. A similar hybrid conformation with features from both the binding and extrusion states within the same monomer was also observed in a symmetric structure of the *Acinetobacter baumannii* AdeB RND transporter (Su et al., 2019).

Here, we confirm the identity of the proton relay network residues in MtrD and investigate whether the symmetric MtrD structure will transition into an asymmetric state using a multiscale MD simulation approach. Specifically, we examine whether simulations initiated from the symmetric MtrD structure sample states which correspond to the cryo-EM MtrD access, binding and extrusion conformations. We show the symmetric MtrD homotrimer can only

undergo coordinated conformational switching to the asymmetric state when the protonation state of the proton relay network residues is altered, and substrate is also present in the binding cleft. Protonation at the relay switch is allosterically coupled to conformational changes within the same and adjacent monomers of the MtrD homotrimer. In particular, relay switch protonation instigates a rotation of one half of the TM domain along the axis of pseudosymmetry, an event time-correlated with opening of intramolecular distances between monomers, a feature which is a hallmark of and consistent with the functionally rotating efflux mechanism observed in other RND transporters.

3.4 Results and Discussion

3.4.1 Characterisation of the MtrD proton relay network

The proton relay network of the MtrD homologues AcrB and MexB involves four strictly conserved residues that straddle the longitudinal axis of pseudosymmetry (Murakami et al., 2006, Su et al., 2006, Takatsuka and Nikaido, 2009). In MtrD, the corresponding residues are D405, D406 (TM 4), K948 (TM 10), and T985 (TM 11) (Lyu et al., 2020). These residues are hypothesised to act as a proton relay via the formation of a hydrogen bonding network, where the protonation of D405 and/or D406 leads to the subsequent disengagement of D405 from K948 (Lyu et al., 2020). To confirm the identity of the proton relay network through the impact of charge state on substrate efflux, D405 was mutated to cysteine by site-directed mutagenesis to disrupt the hypothesised proton transfer between D405 and K948 during the transport cycle. A histidine-tagged cysteine-less allele of the *mtrD* gene (CL-*mtrD*$_{his6}$) that has been shown to express fully functional MtrD protein (Section 2.5.5) (CL-MtrD$_{His6}$, referred to as the wild-type) was used as a backbone for constructing the D405C mutant. Analyses were conducted in *N. gonorrhoeae* KH15Δ*norM*Δ*mtrD* cells, which is a highly antimicrobial susceptible strain with both the *mtrD* and *norM* genes (encoding MtrD and NorM efflux pumps, respectively) removed and allows analysis of MtrD mutants in terms of resistance to the transporter substrates (Section 2.5.5). Resistance profiling of MtrD D405C in *N. gonorrhoeae* KH15Δ*norM*Δ*mtrD* showed no resistance to a panel of eleven previously identified MtrD substrates

Table 3.1 *Neisseria gonorrhoeae* KH15Δ*mtrD*Δ*norM* strain expressing MtrD derivatives.

Mutation	MIC (μg/ml)[a]										
	Detergent		Antibiotic			CAMP	Dye		BA	Hormone	Biocide
	N-9	TX-100	RIF	NOV	OXA	PMB	ET	CV	CHO	PRO	DQ
CL-MtrD$_{His6}$ (WT)[b]	≥4096	≥4096	0.125	1	4	100	0.25	2	400	80	1
D405C	16	32	0.008	0.03	0.06	50	0.06	0.125	100	20	0.5
Negative control[c]	16	32	0.008	0.03	0.06	50	0.06	0.125	100	20	0.5

[a] All MIC data is representative of three or more independent experiments. Abbreviations: CAMP, cationic antimicrobial peptide; BA, bile acid; CHO, cholic acid; CV, crystal violet; DQ, dequalinium; ET, ethidium; N-9, nonoxynol-9; NOV, novobiocin; OXA, oxacillin; PMB, polymyxin B; PRO, progesterone; RIF, rifampicin and TX-100, Triton X-100. [b] Cysteine-less MtrD mutant representing wild-type resistance profile. [c] KH15Δ*mtrD*Δ*norM* strain transformed with the NICS section of the pGCC4 vector that expresses no *mtrD* gene.

Protein expression levels of the D405C MtrD mutant present in *N. gonorrhoeae* KH15Δ*norM*Δ*mtrD*/CL-*mtrD*(D405C) were comparable to that of wild-type MtrD (Figure 3.2), indicating that the change in AMR was not due to a reduced amount of MtrD protein in the bacterial membrane but could be attributed to mutation of D405. These findings indicate the D405 residue is crucial for functional efflux in MtrD thereby supporting its key role in the proton relay network.

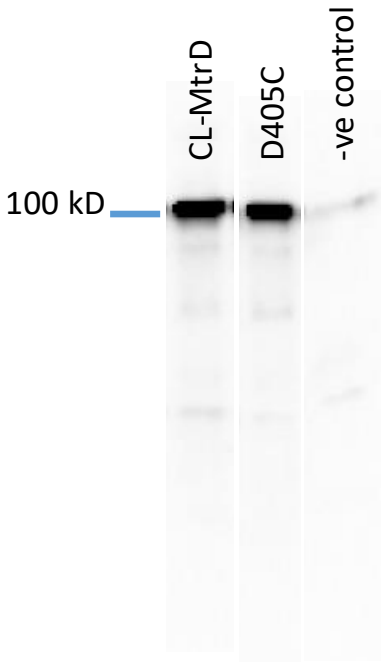

Figure 3.2: Protein expression of D405C MtrD mutant.

Western blot analysis demonstrating expression of MtrD proteins in *N. gonorrhoeae* KH15Δ*norM*Δ*mtrD* cells. Isolated membrane fractions were separated by SDS-PAGE and the blot was probed with an anti-6xHis epitope tag (rabbit) antibody using standard methods (Section 2.7.6). The full-length MtrD protein has a predicted molecular mass of nearly 114 kDa.(Hagman et al., 1997) Expression of MtrD was determined by presence of a protein band at position approximately 100 kDa using protein molecular mass standard (Precision Plus Protein Dual Colour; Bio-Rad), indicated on the left in kDa. CL-MtrD represents expression of the cysteine-less $MtrD_{6His}$ protein (referred to as wild-type). Expression of D405C mutant is shown in the second lane, and -ve control are KH15Δ*norM*Δ*mtrD* cells with no MtrD expression.

(Sections 2.5.1 and 2.5.2), exhibiting a resistance profile similar to that of the negative control expressing no MtrD (Table 3.1). For example, resistance to detergent nonoxynol-9, antibiotics rifampicin and oxacillin, and hormone progesterone was reduced 256-, 16-, 64-, and 4-fold, respectively, compared to that of the wild-type.

3.4.2 Comparison of the MtrD symmetric and asymmetric structures

The 2014 crystal structure of MtrD (PDB ID: 4MT1) was solved at 3.53 Å resolution, with the three monomers adopting a symmetric conformation (Figure 3.3 A) (Bolla et al., 2014). In each monomer the transmembrane proton relay network residues D405/D406 and K948 were disengaged (Figure 3.3 B), the entrance to the binding cleft and the binding pocket were open, and the substrate extrusion gate was closed (Figure 3.3 C). Table 3.2 shows this hybrid conformation differs from the prototypical asymmetric access, binding, and extrusion conformations observed in the MtrD homologues, AcrB, MexB (Eicher et al., 2012, Murakami et al., 2006, Nakashima et al., 2011, Seeger et al., 2006, Sennhauser et al., 2007) and in the MtrD cryo-EM structures, resolved to 2.72 Å (PDB ID: 6VKT) and 3.02 Å (PDB ID: 6VKS) (Lyu et al., 2020). Corresponding residue pair distances in the MtrD binding pocket, PC1-PC2 domains, extrusion gate and proton relay network of the symmetrical hybrid and asymmetric MtrD structures are listed in Table 3.3 below.

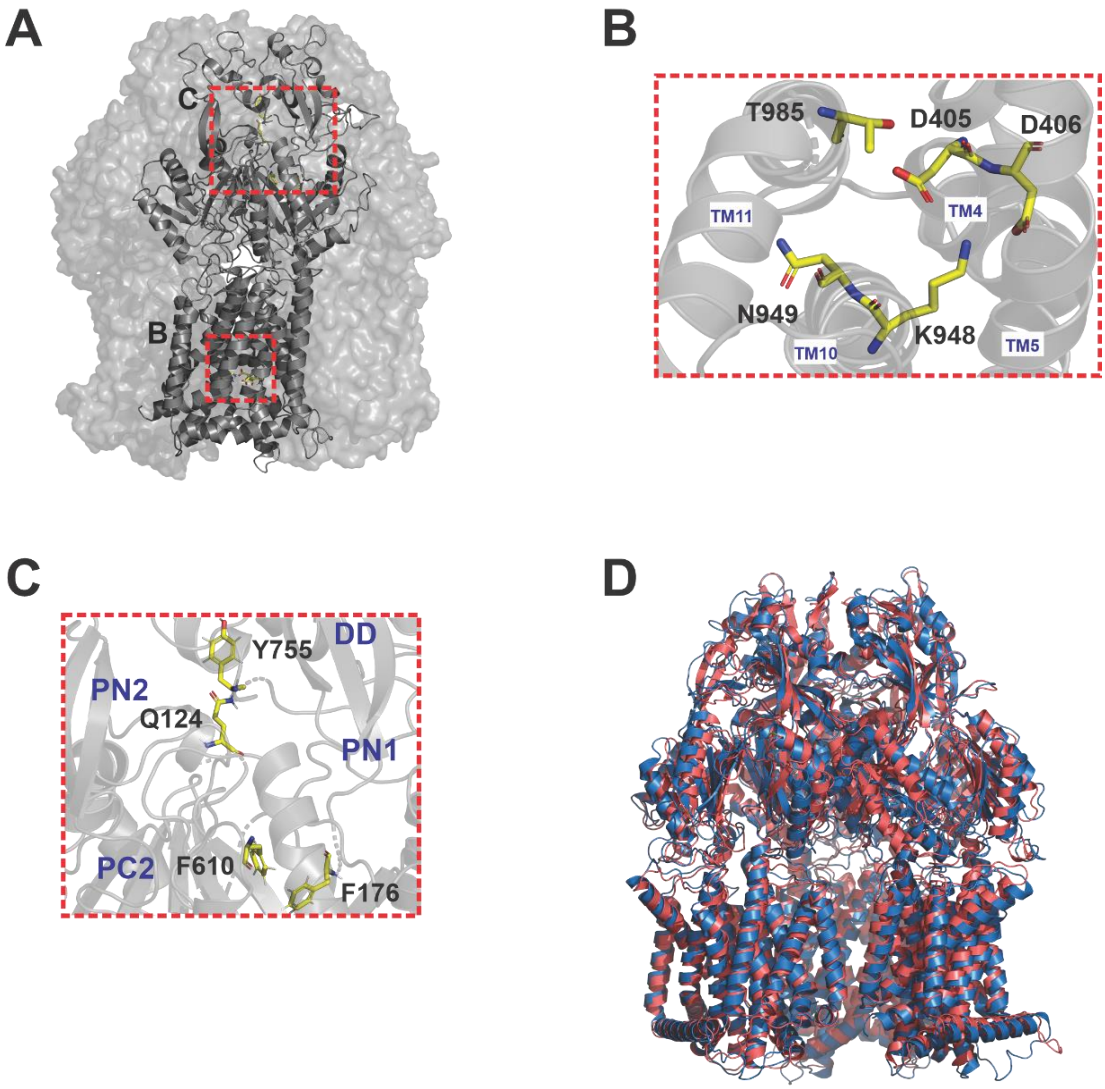

Figure 3.3: MtrD structural overview.

(A) The functional regions of MtrD involved in the conformational transitions needed for the functionally rotating transport mechanism. (B) Close-up view of the proton relay network (D405, D406, K948, K949 and T985) and (C) binding cleft (F176-F610) and extrusion gate (Q124-Y755) residues used in analysis. (D) Alignment between the MtrD symmetric hybrid structure (PDB ID: 4MT1) in pink and asymmetric structure (PDB ID: 6VKS) in blue along the backbone heavy atoms.

Table 3.2 MtrD trimer structures and their global/local conformational characteristics.

Global structural characteristic			**Local conformation characteristic**					
RND Structure (PDB ID)	Trimer Structure	Monomer conformation	Cleft entrance	Deep Binding Pocket	Extrusion Gate	Proton relay network	Substrate present	Ref.
MtrD (4MT1)	Symmetric	Hybrid	Open	Open	Closed	Disengaged	No	(Bolla et al., 2014)
MtrD (6VKS, 6VKT)	Asymmetric	Access	Open	Closed	Closed	Engaged	No	(Lyu et al., 2020)
		Binding	Open	Open	Closed	Engaged	Yes	
		Extrusion	Closed	Closed	Open	Disengaged	No	

Table 3.3: RND transport residue pairs used to determine conformation states of MtrD during MD simulations of this publication.

Local conformation characteristic	Centre of mass residues	'Access' distance (Å)[a]	'Binding' distance (Å)	'Extrusion' distance (Å)
Cleft entrance	PC1-PC2 domains	28.5 ± 1.76	30.09 ± 1.01	24.94 ± 0.25
Binding Pocket	F176-F610	7.14 ± 0.31	10.45 ± 0.35	6.98 ± 0.21
Extrusion Gate	Q124-Y755	5.51 ± 0.32	5.04 ± 0.18	12.15 ± 0.96
Proton relay network	D406-K948	8.42 ± 0.60	7.84 ± 0.31	9.42 ± 0.32
	D405-K948	6.77 ± 0.65	6.58 ± 0.38	7.27 ± 0.20
	K948-N949	4.6 ± 0.19	4.74 ± 0.11	3.87 ± 0.15
	K948-T985	9.11 ± 0.59	10.00 ± 0.29	7.36 ± 0.16

[a] All distance values in angstroms are given as mean ± S.D. from the following RND multidrug efflux proteins: AcrB (PDB ID: 2GIF, 2HRT, 3AOB, 4DX5), MexB (PDB ID: 2V50, 6IIA), MtrD (PDB ID: 6VKS, 6VKT).

Despite these conformational differences, the backbone RMSD between the symmetric MtrD and asymmetric MtrD structures over the whole trimer was less than 2 Å, indicating localised structural rearrangements rather than large-scale conformational changes (Figure 3.3 D). To identify whether the symmetric MtrD structure would spontaneously adopt an asymmetric conformation in coarse-grained MD simulations, triplicate 1 ms coarse-grained MD simulations were performed using the MARTINI 2.2P force-field with Gō potentials used for the protein (aka GoMARTINI) (Poma et al., 2017). In each case, the backbone RMSD was less than 4 Å from the starting MtrD structure, which lies within the thermal noise of simulation (Figure 3.4) (Maiorov and Crippen, 1994). In all simulations, the conformation of MtrD moved away from the symmetric MtrD crystal structure and developed asymmetries across the three monomers. Here, monomer B adopted a prototypical access conformation; whilst monomer A and C were in an intermediate conformation between access and extrusion. It is also important to note that the proton relay network was engaged in all three monomers, consistent with the access conformation, and as would be expected with D405/D406 deprotonated in the

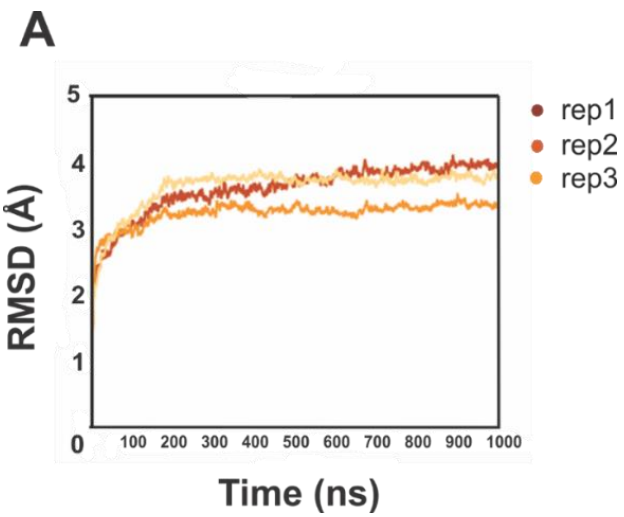

Figure 3.4: Coarse-grain simulations RMSD analysis.

The protein backbone RMSD for the symmetric MtrD trimer (PDB ID: 4MT1) across the 1 ms of GoMARTINI coarse-grained simulations. RMSD values are shown individually for each of the three system replicates. The GoMARTINI forcefield replaces the elastic models of restricted movement with a more physically motivated model that allows for extensive thermal motions and better accuracy of protein dynamics.

coarse-grained model. To further investigate what MtrD conformation would be obtained from an atomistic MD system, the final frame of the coarse-grained replicate 1 trajectory was back-mapped to a united-atom conformation and energy minimised (Wassenaar et al., 2014).

Symmetric structures of AcrB and other RND efflux transporters, in which all three monomers adopt an access conformation in the absence of substrate and any changes to protonation state, have been proposed to represent a resting transporter state (Yamaguchi et al., 2015). To determine whether the back-mapped MtrD would adopt a resting access conformation, simulations of MtrD were performed in the absence of substrate, with the proton relay network of each monomer deprotonated (Table 3.4 System 1, Figure 3.5 2A).

Table 3.4 List of MtrD trimeric binding configurations and numbering of simulations.

Simulation System	Monomer A	Monomer B	Monomer C
System 1	$D405^{-}/D406^{-}$[a]/no substrate	$D405^{-}/D406^{-}$ /no substrate	$D405^{-}/D406^{-}$ /no substrate
System 2	$D405^{H}$[b]$/D406^{H}$/no substrate	$D405^{-}/D406^{-}$ /no substrate	$D405^{-}/D406^{-}$ /no substrate
System 3	$D405^{H}/D406^{H}$/no substrate	$D405^{-}/D406^{-}$ /no substrate	$D405^{-}/D406^{-}$ /progesterone proximal
System 4	$D405^{H}/D406^{H}$/progesterone distal	$D405^{-}/D406^{-}$ /no substrate	$D405^{-}/D406^{-}$ /progesterone proximal
System 5	$D405^{H}/D406^{H}$/no substrate	$D405^{-}/D406^{-}$ /progesterone proximal	$D405^{-}/D406^{-}$ /progesterone distal

[a]$D405^{-}/D406^{-}$ refers to engaged and deprotonated relay network residues.

[b]$D405^{H}/D406^{H}$ refers to a disengaged and protonated relay network.

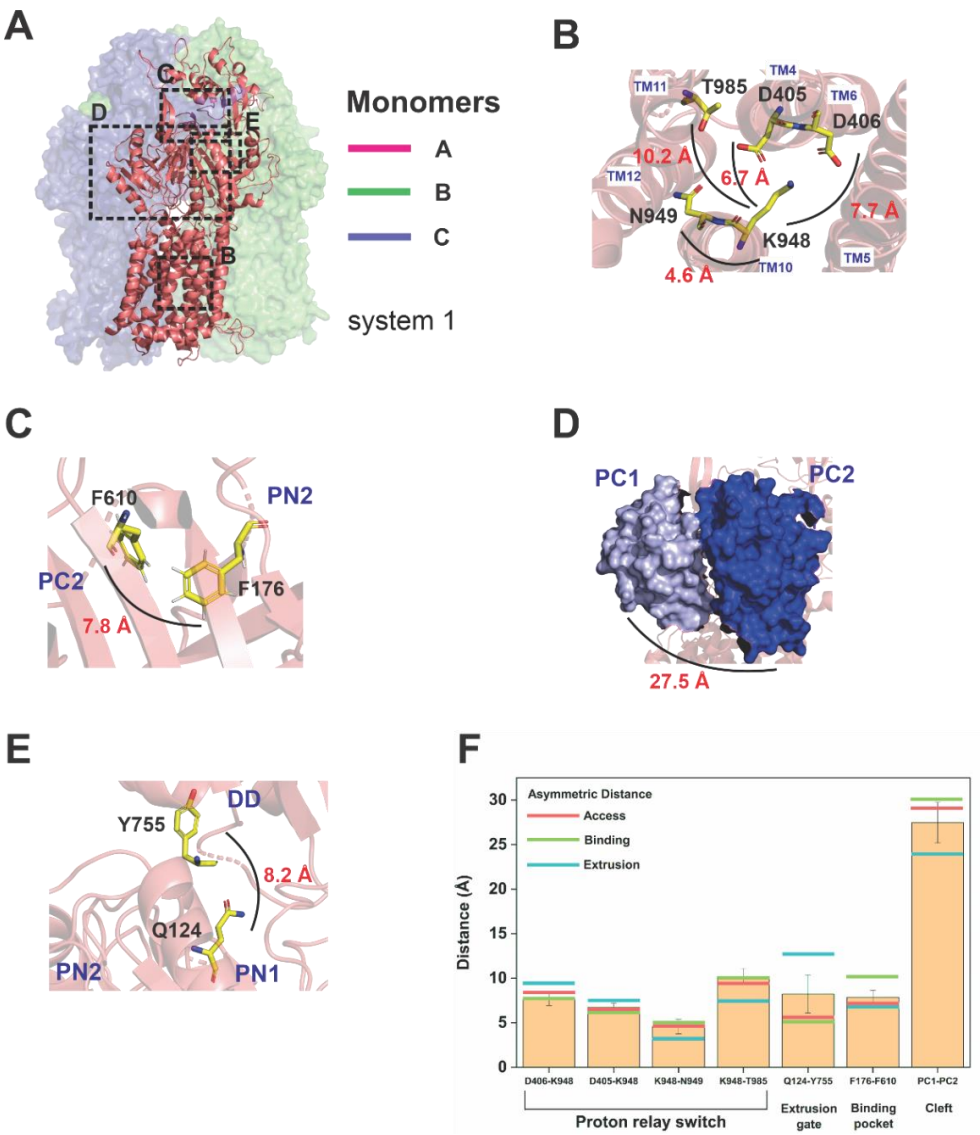

Figure 3.5: The apo MtrD homotrimer (System 1) simulation across 3 × 250 ns simulations.

(A) The back-mapped MtrD homo-trimer. Monomers A, B, and C are coloured pink, green, or blue, respectively. Monomer A is in cartoon, monomers B and C are rendered in transparent surface representation. The post-simulation analysis focused on several regions of monomer A (dashed box inserts), including (B) the proton relay network, (C) the distal binding pocket, (D) the binding cleft entrance between PC1-PC2 sub-domains, and (E) the extrusion gate. (F) Bar graph of the mean distances from the key regions shown in (B) to (D). Error bars show 1 SEM. Mean centre of mass distances were calculated across all three monomers and all three 250 ns simulation repeats. The corresponding distances from the access, binding, and extrusion states of published RND asymmetric structures (Table 3.3) are in red, green and blue, respectively.

In the three replicate simulations, each MtrD monomer adopted an access conformation in 250 ns of simulation, consistent with the symmetric resting state observed for AcrB. Figure 3.5 shows residue pairs in the proton relay network were engaged, as expected with deprotonated D405 and D406 (Fig. 2A). The average centre of mass distances of the binding pockets (Figure 3.5 C) and cleft entrances (Figure 3.5 D) of all three monomers were also consistent with an access conformation. The opening of the extrusion gate of each monomer, given by the distance between Q124 and Y755 (Figure 3.5 E), fluctuated throughout the simulation. The average distances from System 1 are summarized in Figure 3.5 F.

Based on these distance measurements, the conformation of all three MtrD monomers corresponds most closely to the access conformation, albeit with a wider extrusion gate than observed for other RND access state monomers (Lyu et al., 2020, Murakami et al., 2006).

3.4.3 Protonation of a single MtrD monomer activates extrusion gate opening

Many published asymmetric structures of RND efflux pumps contain bound substrate (Lyu et al., 2020, Murakami et al., 2006, Seeger et al., 2006, Sennhauser et al., 2007, Sennhauser et al., 2009b). However, different monomer-specific combinations of substrate binding and protonation have been proposed to synchronise the functionally rotating transport mechanism of AcrB (Jewel et al., 2020, Matsunaga et al., 2018, Wang et al., 2015, Yao et al., 2010, Yue et al., 2017). To characterise the order of events in the transport cycle, we varied the simulation conditions by changing the protonation state of the proton relay network and the location of docked substrate in the different monomers of the MtrD trimer. These different simulation conditions are summarised in Table 3.4.

Systems 2 to 5 examined whether an asymmetric MtrD conformation could be captured within a 500 ns timeframe in triplicate atomistic MD simulations. In Systems 2-5, residues D405 and D406 of the proton relay network were protonated in monomer A. System 3 also contained a single molecule of the substrate progesterone docked into the proximal binding pocket of the adjacent, anticlockwise monomer (monomer C), whilst Systems 4 and 5

contained two molecules of progesterone: one molecule each docked to monomer A and C (System 4) or to monomer B and C (System 5), as shown in Table 3.4. Based on previous structural data, the monomeric conformation of MtrD and its homologues can be characterised by three residue pair distances that accurately represent the discreet access, binding and extrusion conformations of asymmetric structures: K948-T985 in the proton relay network, Q124-Y755 of the substrate extrusion gate, and F176-F610 of the MtrD binding cleft (Fischer and Kandt, 2013, Jewel et al., 2017, Schulz et al., 2010). Distance distributions for these three residue pairs were assessed for each MtrD monomer across the combined 1500 ns of simulation for each system and compared with the prototypical asymmetric structure distances given in Table 3.3.

Initially protonation of D405 and D406 was carried out on monomer A alone (Table 3.4, System 2), with the hypothesis that this would lead to disengagement of the proton relay network and drive conformational transition in monomer A from a resting access-like conformation to an extrusion conformation and induce the overall transition of the protein into a functional asymmetric trimer. In System 2, protonation of monomer A alone induced large changes in pair-wise distances of the proton relay network. The distance distribution for K948-T985 in monomer A shows a wider distance distribution of 8-13 Å which, compared to the other two non-protonated monomers, approaches the fully disengaged distance of 7.36 Å (Figure 3.6 A, LH panel).

The distance distribution displayed three peaks at 12.1, 10, and 8.2 Å, respectively, indicating protonation introduced instability at the relay switch. The extrusion gate Q124-Y755 also occupied two distance distribution peaks; one heavily occupied at 8.6 Å and a second smaller peak at 11.9 Å, which corresponds to the distances present in the extrusion conformation of other RND asymmetric structures. The shift of extrusion gate distance was coupled to a disengagement of the proton relay network in monomer A across all replicate simulations (Figure 3.7 A). In both monomer B (Figure 3.6 A, centre panel) and monomer C (Figure 3.6 A, right panel), the proton relay network and binding cleft distance distributions are consistent with an ‘access/binding’ conformation. However, the extrusion gates of both monomer B and C displayed a broad distance distribution with multiple peaks, which do not

closely align with any of the prototypical access, binding, or extrusion conformations. These results demonstrate protonation of a single MtrD monomer cannot induce complete transition to the MtrD asymmetric conformation but can couple protonation of the relay switch and opening of the extrusion gate within a single monomer.

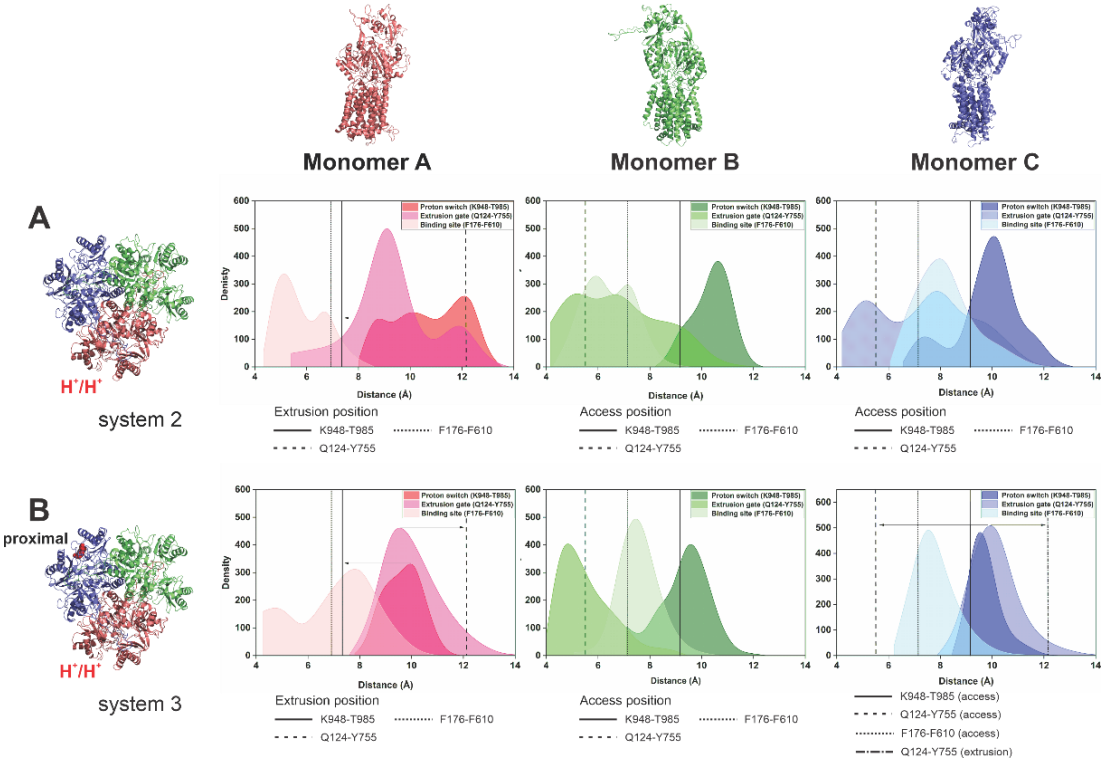

Figure 3.6: The distance distributions of functionally relevant residue pairs in different MtrD binding configurations from (A) System 2 and (B) System 3.

The simulation configuration is displayed by the top-down view of the MtrD homotrimer at the left-hand side. Each panel represents the residue pair centre of mass distance for each monomer of the simulation system (top). The vertical lines represent the measured distances for the asymmetric configurations access, binding, and extrusion from a set of RND asymmetric structures (Table 3.3). The horizontal arrows indicate the distance from the peak distance density for a given residue pair to the vertical lines corresponding to asymmetric structure average.

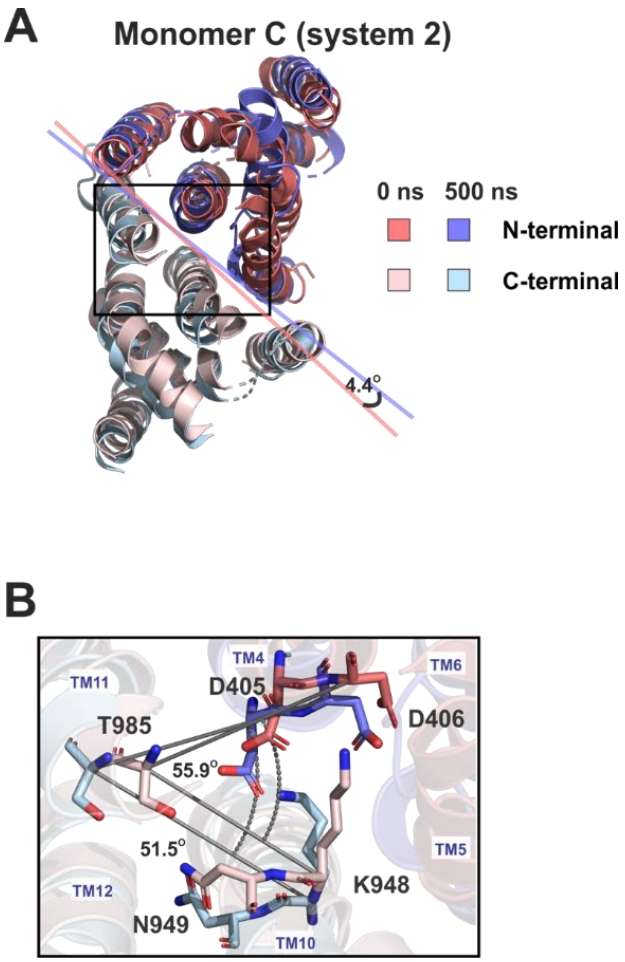

Figure 3.7: TMD rotation in deprotonated monomers.

Deprotonated monomer C of System 2 showed little TM domain helical rotation. The MtrD TM domains forming the proton relay network are viewed from the cytosolic side of the transporter. (A) The Δ D406-T985-K948 C_a angle shows a 4.4° rotation about the pseudosymmetrical axis of the TM domains between the initial (red) and final (blue) frames. (B) Overlay of the initial (red) and final (blue) frames of the proton relay network residues in monomer C of System 2 indicate a change in the Δ D406-T985-K948 C_a angle from 55.9° to 51.5°.

Conformational switching to asymmetric MtrD requires coordinated protonation and substrate binding in two separate monomers

Numerous asymmetric structures of MtrD (Lyu et al., 2020) and other RND transporters (Murakami et al., 2006, Seeger et al., 2006) have been solved with substrate in the binding pocket of one monomer. To investigate whether substrate is required to facilitate a conformational transition to the asymmetric MtrD, in System 3 a single molecule of progesterone was docked in the

proximal binding pocket of monomer C, the monomer anti-clockwise to the protonated monomer A (Figure 3.5 A). In this binding configuration, the proton relay network of monomer A shows a narrower distribution density than System 2, with greater than 98% of K9498-T985 distances occupying a range from 11.0 to 8.0 Å (Figure 3.6 B, left panel). Similar to System 2, the System 3 distance distribution approaches but does not reach the distance observed structurally in the fully disengaged proton relay network state (7.32 ± 0.16 Å, Table 3.3). Likewise, the monomer A extrusion gate distance displays a wider distribution than in the apo-MtrD simulation of System 1, with >95% of distance lying between 8 and 12.5 Å. As with System 2, fluctuations in extrusion gate distance of monomer A were allosterically coupled to fluctuations in the relay switch: the greater the disengagement of the relay switch (smaller distance) the greater the opening of the extrusion gate. However, in contrast to System 2, the degree of fluctuations in both these regions is smaller, indicating the presence of progesterone has stabilised monomer A without allowing for the full transition to the extrusion conformation. The inter-residue distance pairs from monomer B and monomer C were largely stable across all simulations, displaying narrow distance distributions for all key functional regions, corresponding to the prototypical access distances (Figure 3.6 B, centre and right panel). These results show that in the presence of a single bound substrate molecule, the complete transition to an asymmetric conformation of MtrD is not readily sampled in the 500 ns timescale of the simulations. Recent MD work on AcrB has suggested that the conformational transition into an asymmetric functional RND state is accelerated when substrate is simultaneously bound to two monomers of the protein (Jewel et al., 2020, Wang et al., 2015).

To identify whether the docking of PRO to multiple monomers would allow for the full transition to an asymmetric structure, PRO was docked to two adjacent MtrD monomers (Figure 3.8). Residues D405 and D406 of monomer A were again protonated. In System 4, PRO was docked to the proximal binding pocket of monomer C, and to the DBP of the protonated monomer A (Figure 3.8 A). In System 5, PRO was docked to the DBP of monomer C and

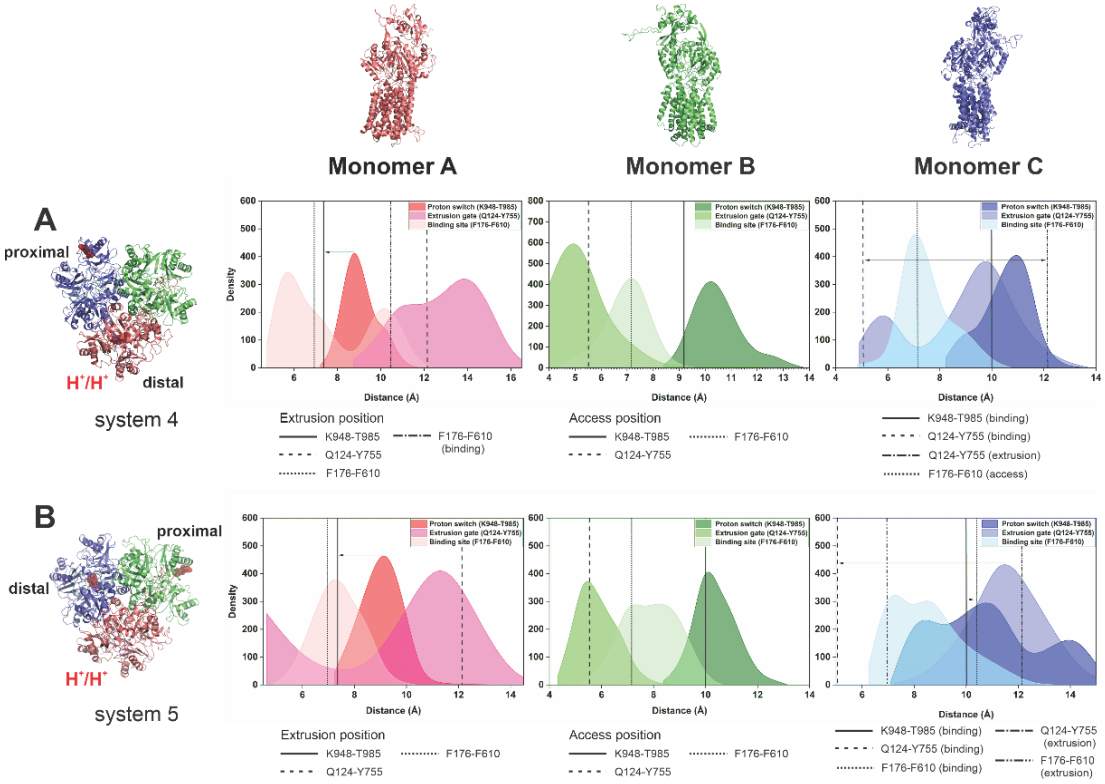

Figure 3.8: The distance distributions of functionally relevant residue pairs in the MtrD binding configurations from (A) System 4 and (B) System 5.

The simulation configuration is displayed by the top-down view of the MtrD homotrimer at the left-hand side. Each panel represents the residue pair centre of mass distance for each monomer of the simulation system (top). The vertical lines represent the measured distances for the asymmetric configurations access, binding and extrusion from a set of RND asymmetric structures (Table 3.3: RND transport residue pairs used to determine conformation states of MtrD during MD simulations of this publication.). The horizontal arrows indicate the distance from the peak distance density for a given residue pair to the vertical lines corresponding to asymmetric structure average.

the proximal pocket of monomer B (Figure 3.8 B). In System 4, the presence of two PRO molecules induced a significant opening in the extrusion gate distance of the protonated monomer A towards a fully open state (Figure 3.8 A and B, left panel). The two peaks of the extrusion gate distance distribution are centred at 10.8 and 13.9 Å, with >90 % of the distances sampled lying between 10 and 15 Å. In addition, the K948-T985 proton relay network distance distribution adopts a single narrower peak at 8.6 Å. For System 5, the extrusion gate and proton relay network distance distribution displayed peaks

at 11.8 and 8.9 Å, respectively. When compared to Systems 1 to 3, the distance distributions sampled in System 4 and 5 represent a large shift towards the extrusion conformation distances of the asymmetric structures in Figure 3.6. Despite this trend, significant differences in the dynamics of monomer A are observed between System 4 and 5. In System 4, the opening of the extrusion gate and near-complete disengagement of the monomer A relay switch is accompanied by the opening of the binding cleft (Figure 3.8 A, left panel). The changes between functionally relevant regions of monomer A in System 4 are coupled (Figure 3.9 A), such that disengagement of the proton relay network accompanies opening of the extrusion gate, as was observed in Systems 2 and 3. Notably, the binding cleft distance distribution contains two peaks, at 5.8 and 10.2 Å, showing System 4 sampled both the closed and open binding cleft conformations in monomer A. In contrast, when PRO was docked into the two non-protonated monomers of System 5, the monomer A binding

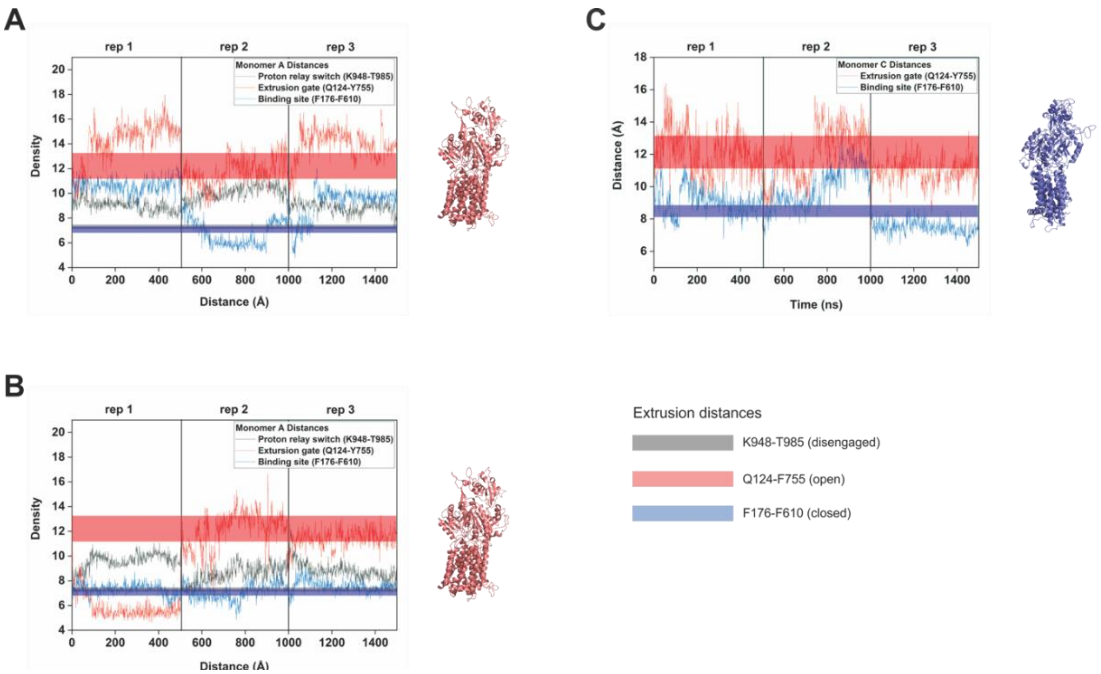

Figure 3.9: Time-correlation of proton relay network, extrusion gate and binding cleft distances.

Coupling between the monomer A and monomer C proton relay network (grey), extrusion gate (red) and binding cleft (blue) distances across the concatenated trajectory of three 500 ns system replicates. (A) Simulation System 4, monomer A, (B) simulation System 5, monomer A and (C) simulation System 5, monomer C.

cleft remained in the closed extrusion conformation (Figure 3.8 B, left panel, Figure 3.9 B).

Overall, System 5 approaches an overall asymmetric MtrD conformation more closely than System 4. For example, in System 4, when PRO is docked at the proximal binding pocket of monomer C, it does not adopt the prototypical MtrD asymmetric 'binding' conformation, but instead adopts a 'hybrid' conformation (Figure 3.8 A, right panel). In contrast, monomer C of System 5 is consistent with the binding conformation (Figure 3.8 B, right panel). In both Systems 4 and 5, monomer B adopts an 'access' conformation (Figure 3.8 A

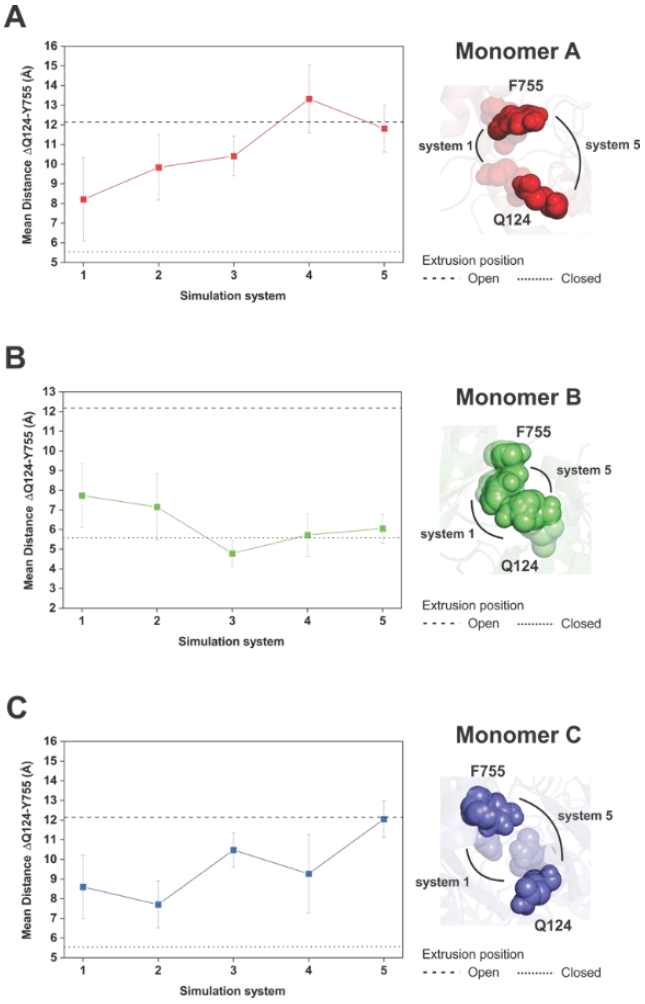

Figure 3.10: The extrusion gate distance of each MtrD monomer is an output of conformation.

The extrusion gate distances across all simulation systems for (A) monomer A (protonated), (B) monomer B, and (C) monomer C. Residues pairs to the right of each figure show a frame representing the average centre of mass distances from simulation System 5.

and B, centre panels) as predicted by the rotational asymmetric model of transport (Figure 3.1 C). These simulations confirm that neither protonation of D405/D406 in the proton relay network, nor the presence of a single substrate molecule alone, is sufficient to induce full extrusion gate opening in MtrD within a 500 ns timescale over replicate simulations. When a single monomer is protonated, the binding of substrate in the two adjacent monomers (System 5) is required for the full transition to the functional asymmetric MtrD structure. Figure 3.10 plots the extrusion gate distance distributions from Systems 1 to 5. Although D405/D406 is always protonated, monomer A only adopted a full open extrusion conformation in System 5 (Figure 3.10. A), where PRO is bound at the proximal binding pocket of monomer B and in the DBP of monomer C.

Here the proximally bound monomer B has a stable closed extrusion gate and adopts the access conformation (Figure 3.10 B). The distally bound monomer C adopts the binding conformation (Figure 3.8 B, right panel), where opening of the binding pocket is coupled to a dynamic transition of the extrusion gate (Figure 3.10 C).

Notably, complete disengagement of the proton relay network was not observed in any of the simulations, despite protonation of the proton relay network titratable aspartate residues. This could be due to one of several reasons. Firstly, complete disengagement of the proton relay network may occur on timescales longer than those simulated in this study. Secondly, there is significant uncertainty of the exact proton stoichiometries involved in RND transporter proton translocation (Eicher et al., 2014, Fischer and Kandt, 2013, Matsunaga et al., 2018, Yamane et al., 2013). Thus, accelerated disengagement of the proton relay network may be driven by a proton stoichiometry not explored in this study.

3.4.4 Relay network protonation drives the TM helix rotation in MtrD

The coupling of local conformational changes in MtrD to the large-scale conformational movements required for the functionally rotating transport cycle has not yet been resolved. Allosteric coupling between the extrusion gate and other regions, particularly between monomers A and C (Figure 3.9), suggests

there is an overall coordination between subunits that must be reflected in these large-scale conformational changes. Other asymmetric RND transporter structures show a widening of the inter-monomeric gap between the PN2 domain of the binding monomer and PC2 domain of the extrusion monomer (Figure 3.1 B) thus TM domain rotation may form a significant step in the functionally rotating transporter mechanism of RND transporters. It has been suggested that this widening occurs due to rotation of one half of protonated monomer's TM domains with respect to the other along the two-fold pseudosymmetrical axis (Figure 3.1 B, red lines) (Eicher et al., 2014, Zhang et al., 2017). In the symmetric MtrD structure, the inter-monomeric gap of 11.86 Å was largely consistent with the distances observed for resting or access conformations observed in other RND transporters (Table 3.5).

Table 3.5 Inter-monomeric distances (PN2-PC2) for RND asymmetric transporter structures and MtrD MD simulations.

MtrD Structure	**PN2-PC2 Distances (Å)**		
	Monomer A-Monomer B (extrusion-access)	**Monomer B-Monomer C (access-binding)**	**Monomer C-Monomer A (binding-extrusion)**
Combined RND asymmetric structures[a]	16.19 ± 1.75	15.40 ± 1.40	31.0 ± 1.90
MtrD (4TM1)	11.86	11.86	11.86
System 1[b]	21.39 ± 2.84	21.31 ± 4.09	18.87 ± 1.73
System 2	21.21 ± 2.26	21.53 ± 2.86	26.98 ± 2.37
System 3	16.07 ± 2.14	20.60 ± 2.50	20.34 ± 2.43
System 4	21.96 ± 3.44	19.08 ± 2.94	20.29 ± 2.59
System 5	18.62 ± 4.24	18.96 ± 3.11	22.50 ± 2.84

[a]calculated using the same structures used for Table 3 calculations.

[b]Inter-monomeric distances from all simulation systems are the mean ± S.D. of 3 × 500 ns repeats for each system, except for System 1 which underwent 3 × 250 ns repeats.

Protonation of D405 and D406 in monomer A (System 2) led to rotation of its TM helices along the pseudosymmetrical axis (Figure 3.11 A), as measured by the angle between C_α atoms of the key proton relay network residues K948, T985 and D406. All three replicate simulations started with a D406-T985-K948 C_α angle between 53.7° and 54.9°. A rapid conformational change occurred in

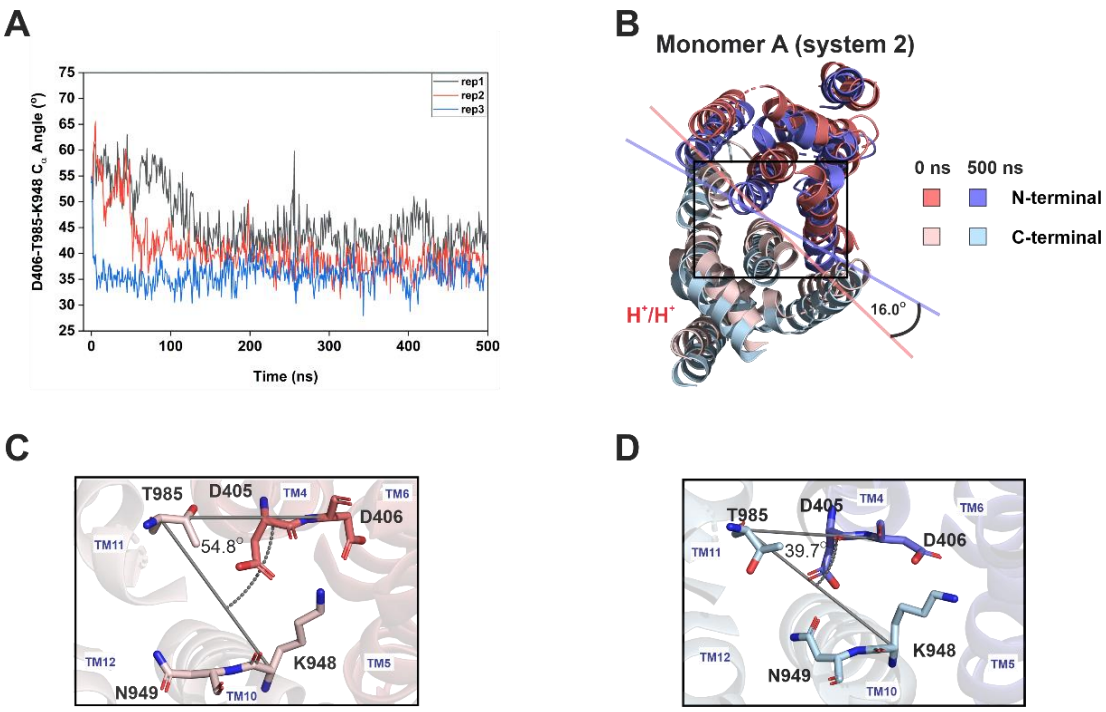

Figure 3.11: Protonation of a single monomer in MtrD causes rotation of TM domains.

(A) The D406-T985-K948 Cα time-resolved angle values in the three replicates of simulation System 2, where only monomer A is protonated. (B) The Δ D406-T985-K948 Cα angle of the second replicate of System 2 shows a 16° rotation about the pseudosymmetrical axis of the TM domains between the (C) initial and (D) last frames.

each replicate simulation (after ~120 ns in replicate 1, ~80 ns for replicate 2 and within the first 5 ns of replicate 3), characterised by a significant narrowing of the D406-T985-K948 Cα angle to stabilise at a mean angle of 43.6° ± 3.5°, 38.8° ± 2.5° and 36.0° ± 2.3° in replicates 1, 2 and 3 respectively, throughout the remaining 400 ns of simulation.

In Figure 3.11 B the initial (pink) and final (blue) frames of System 2 replicate 2 are superimposed to show the helical rotation about the pseudosymmetrical axis, resulting in a 16.0° change of the D406-T985-K948 Cα angle. The initial (pink) and final (blue) conformation of the monomer A relay switch D406-T985-K948 Cα angle is shown in Fig. 6C and 6D, respectively.

In contrast, when D406 and D405 were deprotonated (charged) in all monomers of System 1, the rotation of the TM domain did not change significantly (Figure 3.12 A). The three 500 ns replicate simulations started with

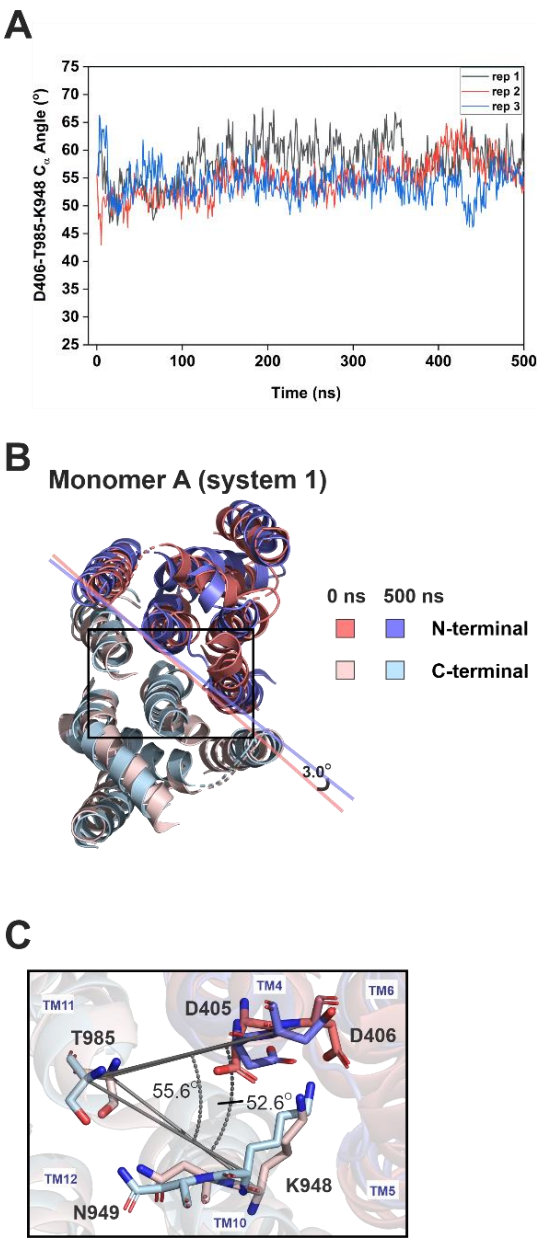

Figure 3.12: Rotation of TM domain helices does not occur in apo-MtrD simulations.

The MtrD TM domains forming the proton relay network are viewed from the cytosolic side of the transporter. (A) The D406-T985-K948 Cα time-resolved angle values in the three replicates of simulation System 1, where no monomers are protonated or have substrate bound. (B) The Δ D406-T985-K948 Cα angle of the second replicate of System 1 shows a (C) 3° rotation about the pseudosymmetrical axis of the TM domains between the initial and last frames.

a D406-T985-K948 Cα angle of between 52.4° and 55.6°, which stabilised to a mean angle of 59.2° ± 2.9°, 55.6° ± 3.1°, 53.8° ± 2.5° across the final 400 ns

of each replicate simulation. Figure 3.12 B and C show that in replicate 2 of System 1 the K948-T985-D406 C_α angle between the starting and final structure changed by only 3° in monomer A, compared to a 16° rotation on protonation of D405 and D406. Similar changes were seen in the deprotonated monomers B and C of System 2, which showed only small helical rotations about the two-fold pseudosymmetrical axis (Figure 3.7 A and B).

The helical rotation observed upon protonation of monomer A in System 2 is time-correlated with a widening of the inter-monomer distance between monomer A and C (Figure 3.12 A). The increase in monomer A to C distance is achieved rapidly following the start of simulations over a similarly rapid helical rotation in the protonated monomer A. The distance between the PC2 domain of protonated monomer A and PN2 domain of monomer C averages at 26.98 ± 2.37 Å across the three simulation replicates of System 2 (Table 3.5, Figure 3.12 B). By contrast, the inter-monomeric distances in apo-MtrD (System 1) range from 21.39 ± 2.84 to 18.87 ± 1.73 (Table 5, Figure 3.12 C). The distances between the unprotonated monomers in System 2 were also smaller. These results suggest that protonation of D406 and D405 in the MtrD relay switch is the probable cause of the TM domain helical rotation in the protonated monomer. We hypothesise that functional rotation of MtrD is driven by protonation leading to helical rotation and subsequent PC2-PN2 gap opening. Both the helical rotation and inter-monomeric gap opening are proposed to be key for the functional rotational transport cycle for MtrD.

3.5 Conclusions

Our results indicate the MtrD inner membrane transporter from *N. gonorrhoeae* follows the functionally rotating transport mechanism identified in other RND inner membrane transporters (Murakami et al., 2006, Seeger et al., 2006, Zwama and Yamaguchi, 2018). We identify the conserved proton relay network in MtrD involves residues D405, D406, K948, N949, and T985. We show that protonation at D405/D406 and substrate binding in adjacent monomers drives asymmetry between monomers. Specifically, we demonstrate rotation of TM helices along the pseudosymmetrical axis and opening of inter-molecular gap between the extrusion and binding monomers is only observed upon protonation of the relay network residues. We have

validated these conclusions through highly conserved distance values from residue pairs in functionally relevant regions of multiple RND inner membrane transporter asymmetric structures (Table 3.3). The recent publication of the asymmetric structures of MtrD allowed for comparison between an inactive or resting symmetric conformation of the transporter and a functionally active one (Lyu et al., 2020).

Specifically, the System 5 simulations most closely approach the average distances observed in other asymmetric RND transporters. System 5 contains a single protonated monomer (relay network disengaged) and the remaining two monomers contain PRO bound either in the distal binding site or the proximal binding site. However, we point out that simulation System 5 has two main differences that do not conform exactly to the static asymmetric RND transporter structures. Specifically, in the ‘binding’ monomer C, the extrusion gate Q124-F755 residue distance is open; and the trimeric MtrD contains two PRO molecules bound in both the binding and access monomers, at the proximal and distal binding sites, respectively. We suggest that these are related molecular events and represent the dynamic nature of the functionally rotating mechanism. Notably, the opening of the Q124-F755 extrusion gate in the ‘binding’ monomer C does not occur in simulations that only include a single substrate molecule (System 3). Simulations involving different substrate stoichiometries and configurations in AcrB have also demonstrated the requirement for two substrates, synchronised in adjacent binding and access monomers, to instigate and accelerate full substrate extrusion (Jewel et al., 2020). The RND asymmetric structures, considered in isolation, suggest that a stable state is sufficient for continual cycling through the tri-conformational mechanism. Our results suggest that time-correlated molecular events such as the binding and efflux of substrate drive the dynamic transitions of the transporter.

The rotation of the TM domains about the pseudosymmetrical axis of the protonated monomer and the subsequent opening of the inter-monomeric distance between the extrusion monomer and adjacent ‘binding’ monomer are key global conformational changes resulting from protonation and which may be associated with substrate exit. Our results confirm, that for MtrD, both events occur only at the site of the protonated monomer, consistent with

previous observations for TM domain rotation in AcrB (Matsunaga et al., 2018). Indeed, thermodynamic calculations from simulations with protonation of AcrB D408 (homologous to D406 in MtrD) show that protonation at the relay network is the critical event for inducing large-scale substrate release and rotational conformational movements in the homotrimer and the larger tripartite RND complex (Matsunaga et al., 2018, Zhang et al., 2017). It is notable, however, that the conformations in the proton relay network we observe in System 2 (in the absence of substrate) whilst instigate the requisite TM helical rotation and inter-molecular distance asymmetries, do not reach the full disengaged 'extrusion' state when compared to the recent asymmetric MtrD structures (Lyu et al., 2020). This is further evidence that a specific configuration and stoichiometry of substrate binding is ultimately required to induce full conformational transitioning.

These results imply that substrate extrusion is the rate-limiting step of the functionally rotating mechanism. The synchronisation between local molecular binding events and large-scale conformational movements implied by the functionally rotating mechanism is a membrane transport paradigm that is being transferred to a wide array of unrelated prokaryotic and eukaryotic solute carrier families (Fairweather et al., 2021). The widespread application for this paradigm highlights the need for continued research into the full and dynamic transport cycle, which will require close collaboration between structural and computational biochemists.

3.6 Materials and Methods

3.6.1 System details: simulation-set-up

The symmetric MtrD crystal structure, resolved to 3.53 Å (PDB ID: 4MT1), was used for all simulations.(Bolla et al., 2014) The missing residues between residues 494 and 507, 671, and 672 were rebuilt; the N- and C-termini were capped with acetyl and amine groups, respectively. Crystallographic symmetry operators were applied to rebuild the trimeric biological assembly as previously described in Section 4.7.6. All simulations were carried out under periodic boundary conditions in a hexagonal prism box with semi-isotropic pressure coupling. The dimensions of the box were chosen such that minimum distance of the protein to its periodic image was 3.5 nm.

3.6.2 Coarse grained simulations

The GROMACS 2016.1 MD engine (Abraham et al., 2015) and the MARTINI2.2P forcefield (De Jong et al., 2013) were used for all coarse-grained simulations. The repaired MtrD homotrimer was converted to a GoMARTINI coarse-grained model using the *go_martinize* package with Gō contacts of 9.414 kJ/mol (Poma et al., 2017). The protein was embedded in a neisserial lipid bilayer containing 1-palmitoyl-2-palmitoleoyl-*sn*-glycero-3-phosphatidylethanolamine (PPoPE) and 20% 1,2-dimyristoyl-sn-glycero-3-phosphoglycerol (DMPG) constructed using a custom version of the *insane* package (Wassenaar et al., 2015). The system was solvated with the MARTINI polarizable water model and a concentration of 150 mM NaCl was added for charge neutralization (Yesylevskyy et al., 2010).

The system was energy minimised using the steepest descent algorithm and equilibrated prior to production simulations. Equilibration was conducted for 5 ns at constant temperature and pressure. The temperature was maintained at 320 K using the Bussi thermostat (Bussi et al., 2007) with a coupling constant of 1.0 ps. The pressure was maintained at 1 bar using a semi-isotropic Berendsen barostat with a compressibility of 3×10^{-4} bar^{-1} and a coupling constant of 12 ps. Following equilibration, coarse-grained simulations were run for the system in triplicate for 1 µs. Temperature was maintained as described above, whilst semi-isotropic Parrinello-Rahman pressure coupling (Parrinello and Rahman, 1980, Parrinello and Rahman, 1981a) was used to maintain a pressure of 1 bar with a compressibility of 3×10^{-4} bar^{-1} and a coupling constant of 12 ps. All simulations were conducted according to the recommended standard MARTINI configuration (De Jong et al., 2016).

3.6.3 Back-mapping and atomistic simulations

Following the coarse-grained simulations, MtrD from the final frame of replicate 1 of the GoMARTINI simulations was back-mapped to united-atom coordinates using the *backward.py* program and protocol (Wassenaar et al., 2014). The protein was energy minimised using the steepest descent algorithm. The VMD cispeptide, chirality and Ramaplot plugins (Schreiner et al., 2011) were used to perform preliminary checks on the back-mapped

structure. *Cis* peptide bonds not found in original MtrD structure were converted to the correct *trans* bonds with the VMD cispeptide plugin (Schreiner et al., 2011).

The resulting MtrD back-mapped structure was used for all subsequent atomistic simulations. Five simulation regimes were carried out, as listed in Table 4. In summary these were: an *apo* regime on the MtrD back-mapped structure with the fixed *cis* peptide bonds but no other changes; protonation of MtrD monomer A only; MtrD protonated in monomer A and PRO in the proximal binding pocket of monomer C; and MtrD protonated in monomer A and PRO in the proximal binding pocket of monomer C or B and DBP of monomer A or C respectively. All simulations used the GROMOS 54a7 forcefield (Schmid et al., 2011) and the GROMACS2016.1 and GROMACS2019.4 MD engines (Abraham et al., 2015). In System 2 to 5, residues D405 and D406 of the proton relay network were protonated in monomer A, as specified in Table 4. In System 3 to 5, PRO was added to the substrate binding cleft of the specified monomer/s from Table 4 via structural alignment to bound PRO from previous PRO flooding simulations (Section 2.7.8).

In all simulations, the protein was embedded in an 80% 1-palmitoyl-2-palmitoleoyl-*sn*-glycero-3-phosphatidylethanolamine (PPoPE), 20% 1,2-dimyristoyl-*sn*-glycero-3-phosphorylglycerol (DMPG) membrane. Each system was solvated with simple point charge (SPC) water, (Berendsen et al., 1981) and 150 mM NaCl was added for charge neutralization. United atom parameters for PPoPE and DMPG were taken from Anandan *et al.* (Anandan et al., 2017) whilst parameters for PRO were obtained from the Automated Topology Builder and Repository (ATB) (Molid: 1305) (Koziara et al., 2014, Malde et al., 2011).

All systems were energy minimised using a steepest descent algorithm and subsequently equilibrated with decreasing restraints on the protein in six sequential 2 ns simulations (1000 kJ mol^{-1} nm^{-2}, 500 kJ mol^{-1} nm^{-2}, 100 kJ mol^{-1} nm^{-2}, 50 kJ mol^{-1} nm^{-2}, 10 kJ mol^{-1} nm^{-2}, and 0 kJ mol^{-1} nm^{-2} protein position restraints). The temperature was maintained at 300 K using the Bussi-Donadio-Parrinello velocity rescale thermostat and a coupling constant of 0.1

ps. Pressure was maintained at 1 bar using semi-isotropic pressure coupling, and in the equilibration simulations the Berendsen barostat was used with a 0.5 ps coupling constant and an isothermal compressibility of $4.5x10^{-5}$ bar^{-1}.

The coordinates from the final frame of each equilibrated system were used as the starting configuration for production simulations, performed in triplicate. All simulations were maintained at a constant temperature of 300K as described above. In production simulations, the pressure was maintained at 1 bar using semi-isotropic pressure coupling with the Parrinello-Rahman barostat using a 5 ps coupling constant and an isothermal compressibility of $4.5x10^{-5}$ bar^{-1}. In System 1, production simulations were run for 250 ns per replicate, whilst Systems 2 to 5 were run for 500 ns per replicate. SETTLE was used to constrain the geometry of water molecules and LINCS was used to constrain the covalent bond lengths of the solute. The electrostatic interactions were calculated using the Particle Mesh Ewald summation, and non-covalent interactions were determined via the Verlet scheme with a 1.4 nm cut-off (De Jong et al., 2016).

3.6.4 Construction and functional analysis of an MtrD site-directed mutant

Construction and functional analysis of site-directed *mtrD* mutants have been described previously (Section 2.7.5). The same methodology was used for construction and analysis of the MtrD D405C mutant in this study. Briefly, a pGCC4-Cl-$mtrD_{His6}$ clone, containing a fully functional histidine-tagged cysteine-less variant of the *mtrD* gene in the pGCC4 neisseria/*E. coli* shuttle vector, was used as template DNA for PCR amplification using the primers D405C F (GGCATCGTGGTCTGTGACGCGATTGTG) and D405C R (CACAATCGCGTCACAGACCACGATGCC). Transformation into *Escherichia coli* DH5α cells, colony screening using restriction enzyme digestion, and sequencing of the whole *mtrD* gene of the identified mutant confirmed the target amino acid change and integrity of the *mtrD* gene. The constructed MtrD D405C variant was reintroduced into the chromosome of the *N. gonorrhoeae* KH15Δ*norM*Δ*mtrD* strain, (Section 2.7.5) a highly susceptible strain for analysis of MtrD pump substrates. The resultant strain, KH15Δ*norM*Δ*mtrD*(D405C), was evaluated for MtrD protein expression by

Western blotting and its resistance profile determined by using a standard agar dilution method (Cockerill et al., 2012) against eleven representative MtrD substrates. To construct appropriate control strains, *N. gonorrhoeae* KH15Δ*norM*Δ*mtrD* was complemented with the recombinant wild-type ($MtrD_{His6}$) and cysteine-less ($CL\text{-}MtrD_{His6}$) alleles of the *mtrD* gene, and with the neisseria insertion complementation system (NICS) section of the pGCC4 vector that does not express *mtrD* and was used as a negative control.

3.6.5 Data analysis

3.6.5.1 Visual analysis and graphical rendering of protein structures

For all graphical analysis of protein structures and simulations and all figure rendering VMD 1.9.3 (Humphrey et al., 1996) and PyMOL2.3.1 (Schrodinger, 2015) were used. RMSD calculations were provided by the Align tool on VMD and the Alignment Plugin on PyMOL. The asymmetric structures of MtrD (PDB ID: 6VKS, 6VKT) were used along with additional RND family structures for comparison and validation of simulation conformations as detailed in Table 3.2 and Table 3.3, in addition to structural alignment with the symmetrical MtrD structure (PDB ID: 4TM1). Alignment between MtrD symmetric and asymmetric structures was carried out using both Pymol and VMD protein backbone least squares RMSD alignment algorithms Align and Multiseq.

3.6.5.2 Validation of pre- and post-simulation protein structures

The MtrD structures after each set of simulations were validated via the protein quality check WhatCheck to assess the quality of the structure (Hooft et al., 1996). WhatCheck provides Z-scores for a set of parameters, indicating the deviation from the average values as derived from a database of structures.

3.6.5.3 Distance and density calculations

Conformational changes within monomers were measured using the inter-residue distances across four key functional monomer regions: the (1) binding cleft entrance; (2) DBP; (3) extrusion gate; and (4) proton relay network. These regions were chosen as they are known to vary distinctly across the three asymmetric monomer conformations (Table 3.2). Distances were measured between the center of mass of the PC1 and PC2 subdomains for the cleft

entrance; F176 and F610 in the DBP; Q124 and Y755 in the extrusion gate; and K948 and T985 of the proton relay network. Distances were measured over the combined trajectories of all three system replicates (1500 ns). Residue groups were chosen based on previously published analysis for the MtrD homologue, AcrB (Fischer and Kandt, 2013, Jewel et al., 2017, Schulz et al., 2010). Density distribution of distances was obtained by binning the distance values for each system.

CHAPTER 4

A UNIQUE SEQUENCE IS ESSENTIAL FOR EFFICIENT MULTIDRUG EFFLUX FUNCTION OF THE MTRD PROTEIN OF *NEISSERIA GONORRHOEAE*

Declaration by candidate

The quality and extent of contributions of the candidate and co-authors to this work was as follows:

Name	Quality of contribution	Contribution extent (%)
Mohsen Chitsaz (candidate)	Conceptualisation, data curation, methodology, performance of experiments, writing, editing and revision of the manuscript	75
Vrinda Gupta (co-author)	Conceptualisation, data curation, methodology, performance of MD simulations, writing, editing and revision of the manuscript	10
Benjamin Harris (co-author)	Data curation, methodology, performance of MD simulations,	5
Megan O'Mara (co-author)	Conceptualisation, data curation, writing, editing and revision of draft and final manuscript	5
Melissa Brown (co-author)	Conceptualisation, data curation, editing and revision of draft and final manuscript	5

The undersigned hereby certify the above declaration correctly reflects the quality and extent of the candidate and co-author contribution to this work.

Candidate signature		18/04/2024
Supervisor signature		18/04/2024

4.1 Preface

The information provided in this chapter has been published by Chitsaz M., Gupta V., Harris B., O'Mara M. L., Brown M. H., (2021) A unique sequence is essential for efficient multidrug efflux function of the MtrD protein of *N. gonorrhoeae*. *mBio* **12**:4, e01675-21. The printed version of this paper can be found in Chapter 6 (Appendix **E**).

4.2 Abstract

AMR in *N. gonorrhoeae* has reached an alarming level, severely impacting the effective treatment of gonorrhoea. Belonging to the RND superfamily of efflux transporters, the MtrD membrane protein of *N. gonorrhoeae* provides resistance to a broad range of antimicrobial compounds. A unique feature of MtrD is an 11-residue sequence (from N917 to P927 [N917-P927]) that connects TMS 9 and 10; this sequence is not present in homologous RND proteins. This study explores the structural and functional roles of the N917-P927 region by means of mutant analysis and MD simulations. We show that N917-P927 plays a key role in modulating substrate access to the binding cleft and influences the overall orientation of the protein within the inner membrane necessary for optimal functioning. Removal of N917-P927 significantly reduced MtrD-mediated resistance to a range of antimicrobials and mutations of three single amino acids impacted MtrD-mediated MDR. Furthermore, MD simulations showed deletion of N917-P927 in MtrD may dysregulate access of the substrate to the binding cleft and closure of the substrate-binding pocket during the transport cycle. These findings indicate that N917-P927 is a key region for interacting with the inner membrane, conceivably influencing substrate capture from the membrane-periplasm interface and thus is essential for full MDR capacity of MtrD.

4.3 Importance

The historical sexually transmitted infection gonorrhoea continues to be a major public health concern with an estimated global annual incidence of 86.9 mil- lion cases. *N. gonorrhoeae* has been identified by the World Health Organization as one of the 12 antimicrobial-resistant bacterial species that poses the greatest risk to human health. As the major efflux pump in

gonococci, the MtrD transporter contributes to the cell envelope barrier in this organism and pumps antimicrobials from the periplasm and IM, resulting in resistance. This study demonstrates that a unique region of the MtrD protein that connects TMS 9 and TMS 10 forms a structure that may interact with the inner membrane positioning TMS 9 and stabilising the protein facilitating substrate capture from the inner membrane-periplasm interface. Analysis of mutants of this region identified that it was essential for MtrD-mediated MDR. Characterization of the structure and function of this unique local region of MtrD has implications for drug efflux mechanisms used by related proteins and is important knowledge for development of antibiotics that bypass efflux.

4.4 Introduction

With an estimated 86 million new cases of gonorrhoeal infections in adults in 2016 caused by *N. gonorrhoeae*, the longstanding disease gonorrhoea remains a serious global public health problem (Wi et al., 2017) primarily due to ability of the bacterium to develop or acquire resistance mechanisms to clinically-relevant antibiotics (Lahra et al., 2018). Export of antibiotics across the cellular membrane via efflux pumps is one of the most efficient mechanisms used by *N. gonorrhoeae*, providing concomitant resistance to multiple antibiotics (Shafer et al., 2010). Gonococci possess five drug efflux pump systems (Prakash et al., 2003, 2016, Su et al., 2015). Of these, the multiple transferrable resistance CDE (MtrCDE) system is the only transporter from the RND superfamily and is the most important efflux-mediated drug resistance mechanism (Hagman et al., 1997, Hagman et al., 1995). Overexpression of MtrCDE imparts clinically significant levels of resistance to many important antibiotics used for treatment, such as β-lactams, and the currently used combined frontline treatment for gonorrhoea of the third generation cephalosporin CRO and macrolides such as AZM (Hagman et al., 1995, Maness and Sparling, 1973, Warner et al., 2008). This can be mediated by *mtrR,* the transcriptional repressor of the *mtrCDE* operon (Beggs et al., 2019, Hoffmann et al., 2005), through mutations in either *mtrR* or its promoter region (Cousin et al., 2003, Lindberg et al., 2007, Shafer et al., 1995, Xia et al., 2000, Zarantonelli et al., 1999) with the structural mechanism recently described (Beggs et al., 2021). Furthermore, MtrCDE enables *N. gonorrhoeae* to persist in the presence of host-derived compounds, such as long-chain FAs,

bile salts, hormones (e.g., PRO) and cationic antimicrobial peptides that are found in human body sites frequently infected by *N. gonorrhoeae*, enhancing the ability of this pathogen to establish an infection or proliferate at mucosal surfaces (Hagman et al., 1997, Shafer et al., 1998).

The MtrD component of the tripartite MtrCDE efflux system is a large protein of 1067 amino acids, that together with its closely related homologues (AcrB from *E. coli* and MexB from *P. aeruginosa*), belongs to the largely Gram-negative bacterial HAE1 family of the RND superfamily (Hagman et al., 1997, Janganan et al., 2013, Saier and Paulsen, 2001, Tseng et al., 1999). The first crystal structure of MtrD revealed a homotrimer with symmetric monomers and an overall structure similar to those of homologous RND drug transporters (Bolla et al., 2014). Each MtrD monomer has pseudosymmetric halves containing two domains: a TMD organised into 12 TMS and a large PD that can be subdivided into a porter domain and an MtrE docking domain (Bolla et al., 2014). The porter domain is composed of four subdomains, PN1, PN2, PC1 and PC2, with three PN1 subdomains (one from each protomer) making up a central pore and stabilising the trimeric organization. PC1 and PC2 create a cleft that opens to the periplasm likely allowing for periplasmic entry of substrates (Bolla et al., 2014).

Recent cryo-EM structures of MtrD in complex with Amp and ERY revealed greater insight into the MtrD substrate translocation pathway and functional mechanism of drug efflux (Lyu et al., 2020). In contrast to the first MtrD apo structure, these substrate-bound trimeric structures, similar to substrate-bound structures of AcrB and MexB (Lyu et al., 2020, Murakami et al., 2006, Seeger et al., 2006, Sennhauser et al., 2007), are asymmetric. Each protomer adopts a distinct conformation resembling a three-step functionally-rotating export cycle, that is comprised of the access (A), binding (B), and extrusion (E) conformations (Lyu et al., 2020, Murakami et al., 2006, Seeger et al., 2006, Sennhauser et al., 2007). We described the functionally rotating transport mechanism of MtrD (Section 3.4.4). As is the case for AcrB and MexB, the substrate permeation pathway through each MtrD protomer contains three possible entrance points, from the IM, the periplasm, or via the central cavity (Murakami et al., 2006, Nakashima et al., 2011, Seeger et al., 2006, Sennhauser et al., 2007). Substrates then pass through the proximal and distal

substrate recognition and binding sites and exit via the funnel-like channel within the MtrE docking domain (Lyu et al., 2020, Murakami et al., 2006, Nakashima et al., 2011, Seeger et al., 2006, Sennhauser et al., 2007). The periplasmic entrance (also known as entrance channel 2 in AcrB) is located in the cleft formed between PC1 and PC2 and leads to the proximal pocket, likely collecting substrates found in the periplasm (Nakashima et al., 2011, Seeger et al., 2006, Yamaguchi et al., 2015). Drugs that are partitioned in the membrane are expected to enter the pump via the IM entrance (also known as lateral entrance or entrance channel 1 in AcrB) that opens to the groove formed in the boundary between the TMD and IM (Murakami et al., 2006, Nakashima et al., 2011, Seeger et al., 2006, Sennhauser et al., 2007). Surrounded by PN1, PN2, PC1 and PC2 β-sheets, the DBP is separated from the proximal pocket by a flexible switch loop or G-loop (Eicher et al., 2012, Nakashima et al., 2011, Vargiu and Nikaido, 2012). These binding pockets are voluminous and formed by many hydrophobic, aromatic, polar and charged residues (Eicher et al., 2012, Lyu et al., 2020, Murakami et al., 2006, Nakashima et al., 2011, Seeger et al., 2006, Sennhauser et al., 2007). In the MtrD cryo-EM structures, Amp and ERY were both found in the DBP and only in the protomer adopting the binding conformation (Lyu et al., 2020).

MtrD shares many, but not all, features with other bacterial HAE1 RND drug exporters (Bolla et al., 2014, Murakami et al., 2006, Sennhauser et al., 2009b). One of the unique features of MtrD is a sequence of eleven amino acids (N917-P927) which is not present in homologous proteins. Using site-directed mutagenesis, MD simulations, and resistance profiling, we explore the role of the N917-P927 region in MtrD-mediated MDR. We found that this unique region is essential for full multidrug efflux and resistance capacity of MtrD as its removal rendered *N. gonorrhoeae* cells susceptible to many antimicrobials, and three individual residues within it in particular are important for drug resistance. In addition, we show that N917-P927 may influence the accessibility of substrates to the proximal binding pocket and stabilization of the protein within the IM required for optimal function. Furthermore, deletion of N917-P927 in MtrD may dysregulate the access of substrate to the binding cleft and the propagation of conformational changes to the substrate binding pocket during the transport cycle.

4.5 Results

4.5.1 Removal of N917-P927 significantly reduced MtrD-mediated resistance.

Bioinformatics analyses revealed that the N917-P927 sequence is unique to the MtrD protein (Figure 4.1). In addition, analyses of whole-genome sequences available in the NCBI database revealed that this 11-amino acid sequence (NLFEGLLGSVP) is 100% conserved among 739 *N. gonorrhoeae* genomes, including the two multidrug-resistant clinical isolates, H041 and F89, that are highly resistant to the extended-spectrum cephalosporins CRO and cefixime (Ohnishi et al., 2011b, Unemo et al., 2012, Zhang et al., 2000). Furthermore, the sequence is also conserved in *mtrD* within other pathogenic and commensal Neisseria species (data not shown). This sequence forms a short α-helix extending from TMS 9 and continues to a loop connecting TMS 9

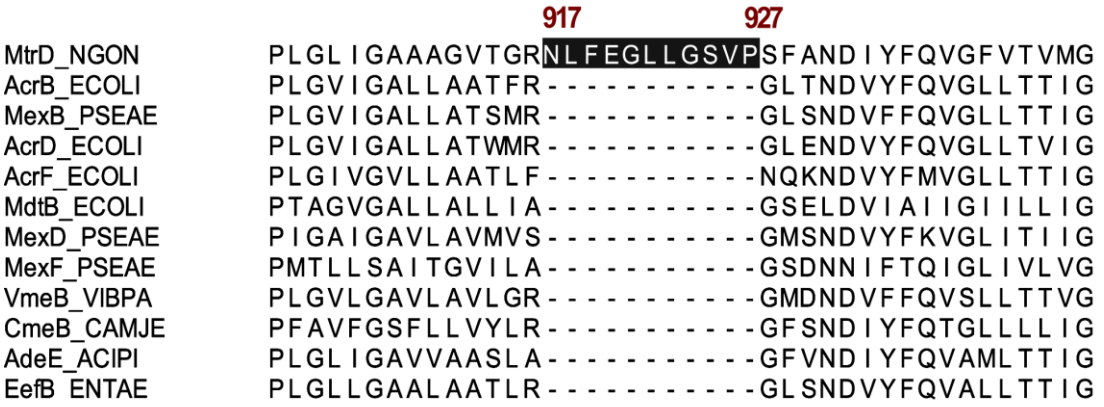

Figure 4.1: Protein sequences of selected members of RND proteins of the HAE1 family**.**

Sequences were taken from the Transporter Classification Database (TCDB) (Ruggerone et al., 2013, Saier, 2023) and are: MtrD of *N. gonorrhoeae* (Q51073), AcrB of *E. coli* (P31224), MexB of *P. aeruginosa* (P52002), AcrD of *E. coli* (P24177), AcrF of *E. coli* (P24181), MdtB of *E. coli* (P76398), MexD of *P. aeruginosa* (Q9HVI9), MexF of *P. aeruginosa* (Q9I0Y8), VmeB of *Vibrio parahaemolyticus* (Q2AAU3), CmeB of *C. jejuni* (AAL74245), AdeE of *Acinetobacter* sp. (Q8GKU1), EefB of *Enterobacter aerogenes* (Q8GC83), TtgB of *Pseudomonas putida* (O52248), TtgH of *P. putida* (Q93PU4). Protein sequence alignment was performed using the NCBI protein blast tool and visualized using Ugene software. The N917-P927 sequence unique to MtrD is outlined in red.

and TMS 10 (Figure 4.2 A-B) positioned directly beneath the binding cleft entrance formed by PC1 and PC2 (Figure 4.2 C). In addition, this region is linked via the N-terminus of TMS 9 to the groove formed between TMS 8 and TMS 9, which has been proposed to facilitate collection of substrates from the outer leaflet of the IM through the IM entrance (entrance 1) in AcrB (Figure 4.2 A-B) (Bolla et al., 2014, Pos, 2009). The spatial arrangement of the N917-P927 region suggests that this local structure may play a role in facilitation of substrate uptake during a functional cycle. Furthermore, the observed high conservation of the N917-P927 sequence suggests that this region of MtrD does not play a substrate-specific interaction that would have evolved under specific antibiotic pressure.

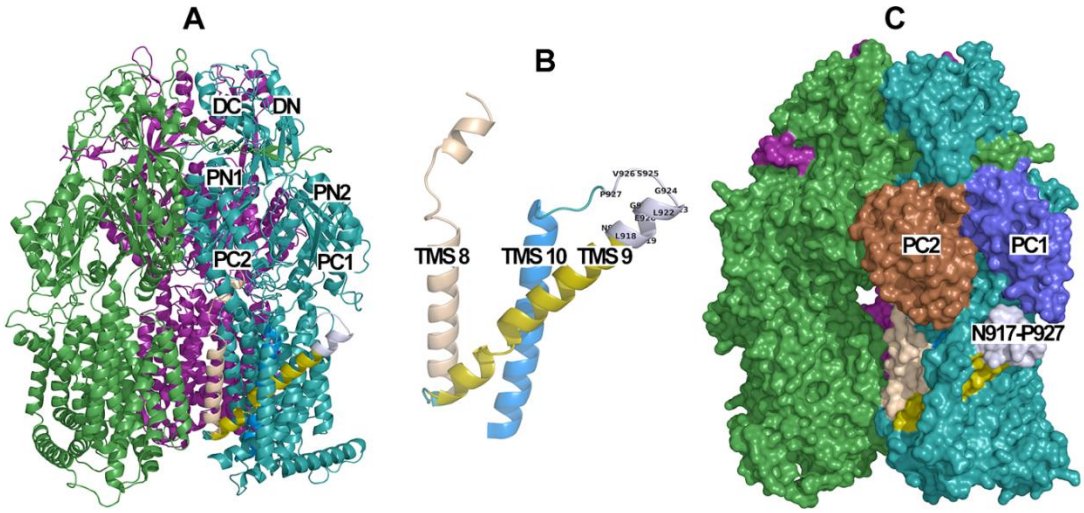

Figure 4.2: Secondary structure of the MtrD protein.

(A) Side view of the cryo-EM structure of the MtrD K823E variant. The three protomers are coloured green (Access), teal (Binding), and magenta (Extrusion). The six subdomains of the porter domain are labelled in the B protomer. (B) Enhanced view of TMS 8 (beige), TMS 9 (gold), TMS 10 (marine blue), and N917-P927 (grey). (C) Surface representation of the K823E MtrD variant. Subdomains PC1 and PC2 in the binding protomer are shown in blue and russet, respectively. Position of the N917-P927 region at the bottom of the cleft opening between PC1 and PC2 is shown in grey.

As an initial step in determining the role of N917-P927, the sequence encoding this region was deleted from *mtrD* by PCR mutagenesis using primers MTRD_LF1 and MTRD_LR1 (Table 4.1) and pGCC4-CL-*mtrD*$_{His6}$ as

template DNA (Section 2.7.5). The use of the pGCC4 vector allows for amplification of *E. coli*-based cloned *mtrD* or derivatives and subsequent integration of these determinants into the chromosome of a *N. gonorrhoeae* strain using the NICS (Mehr and Seifert, 1998). This provides the gonococcal cells with a recombinant *mtrD* allele expressed under *lac* regulation (Mehr and Seifert, 1998) (Section 2.7.5). Thus, the resultant construct, pGCC4-CL-*mtrD*$_{His6}$Δ(N917-P927), was recombined into the chromosome of *N. gonorrhoeae* strain KH15Δ*mtrD*Δ*norM*. This bacterial strain is a derivative of the *N. gonorrhoeae* KH15 strain known to bear a single bp deletion in the coinciding *mtrR* and *mtrC* promoter sequence resulting in upregulation of the *mtrCDE* system and consequential increased levels of resistance to MtrD substrates (Hagman et al., 1995). Since the NorM_NG efflux pump shares some substrates in common with MtrD, the *N. gonorrhoeae* variant KH15Δ*mtrD*Δ*norM* with both the *norM* and *mtrD* efflux pumps deleted was constructed, producing a strain that was shown to be hypersusceptible to a broad range of MtrD-specific substrates (Rouquette-Loughlin et al., 2003) (Section 2.5.1). Expression of recombinant WT *mtrD* from DNA integrated into this strain provided gonococcal cells with a fully functional MtrCDE efflux system mediating high levels of resistance to a broad range of antimicrobial compounds (Section 2.5.1). Integration of the constructed CL-*mtrD*$_{His6}$Δ(N917-P927) mutant produced the strain KH15Δ*mtrD*Δ*norM*-CL-*mtrD*$_{His6}$Δ(N917-P927), which was confirmed by PCR using primers SCRNG1 and MTRDSF5 (Table 4.1). SCRNG1 anneals to a location on the *N. gonorrhoeae* chromosome upstream of and outside the recombination site for the NICS of pGCC4 and MTRDSF5 anneals to the 3' end of *mtrD* 167 bp upstream of its stop codon allowing verification of *mtrD* integration (Section 2.7.4). Western blot analysis confirmed the presence of the MtrD Δ(N917-P927) deletion mutant protein in the membrane of KH15Δ*mtrD*Δ*norM*-CL-*mtrD*$_{His6}$Δ(N917-P927) cells at a level comparable with WT (Figure 4.3). It has been shown previously that addition of a histidine tag on the C terminus of MtrD for monitoring expression levels and increasing the versatility of the system does not affect protein expression and resistance (Section 2.5.2). Therefore, any change in resistance profile of this mutant compared to WT could be attributed to the constructed Δ(N917-P927) deletion. Consequently, the KH15Δ*mtrD*Δ*norM*-*mtrD*$_{His6}$Δ(N917-P927) strain was tested for resistance

against a panel of ten compounds (Table 4.2) using a standard MIC analysis method. These 10 compounds are known MtrD substrates and were selected as they give higher discrimination (≥4-fold difference in MIC) between the WT MtrD and the appropriate negative-control strain (KH15Δ*mtrD*Δ*norM* complemented with the NICS portion of the pGCC4 vector) (Section 2.5.1). While the two macrolide antibiotics ERY and AZM are MtrD substrates with clinical importance, and our previous study has demonstrated excellent MIC differentiation between KH15Δ*mtrD*Δ*norM* and its parental strain KH15, the use of the ERY resistance cassette present in pGCC4 as a selection marker precluded testing constructed MtrD mutant derivatives against these antibiotics (Mehr and Seifert, 1998) (Section 2.5.2). MIC analysis revealed that the deletion of N917-P927 did not totally abrogate but reduced resistance to all ten tested compounds from a minimum of 1.3-fold for CHO to a maximum of >128-fold for N-9 (Table 4.2). These data indicate that the N917-P927 sequence is necessary for complete and efficient activity of the MtrD protein.

Table 4.1: Oligonucleotides used in this study.

Name and purpose	**Sequence 5' to 3'**	**S[@]**
PCR screening for integration of *mtrD* between *aspC* and *lctP*		
SCRNG1	CGCCTTATGATGCAAATG	a
MTRDSF5	CCGTATTCTGGGGGATGTTG	a
Sequencing of *mtrD* in pGCC4		
PGCC4_F2	CCCAGGCTTTACACTTTATGCT	a
PGCC4-R1.1	GGGGATCCGCTAGCACTAGG	a
MtrD-SF4.1	GCAGTTGGGTACGGCAGAAG	a
MtrD-SR4.1	GCTCTGTTCCGTACCGTTTTC	a
Mutagenesis		
MTRD-L F1	GGGCGTAACCGGTCGCTCGTTTGCCAACGACATC	b
MTRD-L R1	GATGTCGTTGGCAAACGAGCGACCGGTTACGCCC	b

Name and purpose	Sequence 5' to 3'	S[@]
DLT92_11Ala_F	CTGCGGGCGTAACCGGGCGCGCTGCAGCTGCAGCCGCGGCTGCAGCTGCAGCCTCGTTTGCCAACGACATC	b
DLT92_11Ala_R	GATGTCGTTGGCAAACGAGGCTGCAGCTGCAGCCGCGGCTGCAGCTGCAGCGCGCCCGGTTACGCCCGCAG	b
DLT92_11Gly_F	CTGCGGGCGTAACCGGGCGCGGTGGAGGTGGAGGTGGGGGTGGAGGTGGAGGCTCGTTTGCCAACGACATC	b
DLT92_11Gly_R	GATGTCGTTGGCAAACGAGCCTCCACCTCCACCCCCACCTCCACCTCCACCGCGCCCGGTTACGCCCGCAG	b
N917C For	GCGTAACCGGGCGCTGCCTGTTTGAAGGACTGTTGG	b
N917C Rev	CCAACAGTCCTTCAAACAGGCAGCGCCCGGTTACGC	b
L918C For	CGTAACCGGGCGCAACTGCTTCGAAGGACTGTTGG	b
L918C Rev	CCAACAGTCCTTCGAAGCAGTTGCGCCCGGTTACG	b
F919C For	CGGGCGCAACCTGTGTGAAGGACTGTTGG	b
F919C Rev	CCAACAGTCCTTCACACAGGTTGCGCCCG	b
E920C For	GGCGCAACCTGTTTTGCGGTCTCTTGGGCAGCGTTC	b
E920C Rev	GAACGCTGCCCAAGAGACCGCAAAACAGGTTGCGCC	b
G921C For	GCAACCTGTTTGAATGTCTTCTGGGCAGCGTTCC	b
G921C Rev	GGAACGCTGCCCAGAAGACATTCAAACAGGTTGC	b

Name and purpose	Sequence 5' to 3'	S[@]
L922C For	GCAACCTGTTTGAAGGATGCTTAGGCAGCGTTCCCTC	b
L922C Rev	GAGGGAACGCTGCCTAAGCATCCTTCAAACAGGTTGC	b
L923C Fw	CAACCTGTTTGAAGGCCTGTGCGGCAGCGTTCCCTCG	b
L923C Rev	CGAGGGAACGCTGCCGCACAGGCCTTCAAACAGGTTG	b
G924C Fw	CAACCTGTTTGAAGGACTGCTCTGCAGCGTTCCCTCGTTTGC	b
G924C Rev	GCAAACGAGGGAACGCTGCAGAGCAGTCCTTCAAACAGGTTG	b
S925C Fw	CCTGTTTGAAGGCCTGTTGGGCTGCGTTCCCTCGT	b
S925C Rev	ACGAGGGAACGCAGCCCAACAGGCCTTCAAACAGG	b
V926C Fw	AGGACTGTTGGGCAGCTGTCCCTCGTTTGCCAAC	b
V926C Rev	GTTGGCAAACGAGGGACAGCTGCCCAACAGTCCT	b
P927C Fw	ACCTGTTTGAAGGACTGTTGGGATCCGTTTGCTCGTTTGCCAACGACATCTAC	b
P927C Rev	GTAGATGTCGTTGGCAAACGAGCAAACGGATCCCAACAGTCCTTCAAACAGGT	b
N917K F	CTGCGGGCGTAACCGGTCGCAAACTGTTTGAAGGACTGTTGG	b
N917K R	CCAACAGTCCTTCAAACAGTTTGCGACCGGTTACGCCCGCAG	b
P927G F	CAACCTGTTTGAAGGACTGTTGGGATCCGTTGGCTCGTTTGCCAACGACATCTAC	b

Name and purpose	Sequence 5' to 3'	S[@]
P927G R	GTAGATGTCGTTGGCAAACGAGCCAACGGAT CCCAACAGTCCTTCAAACAGGTTG	b
N917Q F	GTGCGGCTGCGGGCGTAACCGGTCGACAGC TGTTTGAAGGACTGTTGGGCAGCGTTC	b
N917Q R	GAACGCTGCCCAACAGTCCTTCAAACAGCTG TCGACCGGTTACGCCCGCAGCCGCAC	b
N917S F	GTGCGGCTGCGGGCGTAACCGGGCGATCGC TGTTTGAAGGACTGTTGGGCAGCGTTC	b
N917S R	GAACGCTGCCCAACAGTCCTTCAAACAGCGA TCGCCCGGTTACGCCCGCAGCCGCAC	b

[@]Source or reference: a: (see Section 2.7.3); b: This study

4.5.2 Integrity of the N917-P927 sequence is required for efficient efflux activity of the MtrD protein

To investigate if the length or the specific residue composition of the N917-P927 sequence is an important factor for full function of the MtrD protein, the 11-amino-acid sequence was replaced with all alanines by site-directed mutagenesis using 11Ala F and 11Ala R primers (Table 4.1) and pGCC4-CL-*mtrD*$_{His6}$(ΔN917-P927) as template DNA. The resultant 11 alanine replacement mutant 11A(917-927) was integrated into the chromosome of KH15Δ*mtrD*Δ*norM* strain and PCR using primers SCRNG1 and MTRDSF5 confirmed the existence of this mutant in the chromosome. Using Western analysis, cells expressing *mtrD* mutant, was found to produce protein at a very low level, and MIC assays against TX-100 and OXA showed no resistance, exhibiting a resistance profile similar to that of the negative control (Table 4.2; see also Figure 4.3). Thus, this mutant was not experimentally analysed any further. A second mutant was similarly designed replacing the N917-P927 sequence with a stretch of 11 glycine residues 11G(917-927). However, construction of this mutant was unsuccessful possibly due to lethality. Together, these data indicated that the presence of the protein backbone alone (glycine substitution) or truncated side chains (alanine substitution) is not sufficient to support production of a fully active MtrD variant.

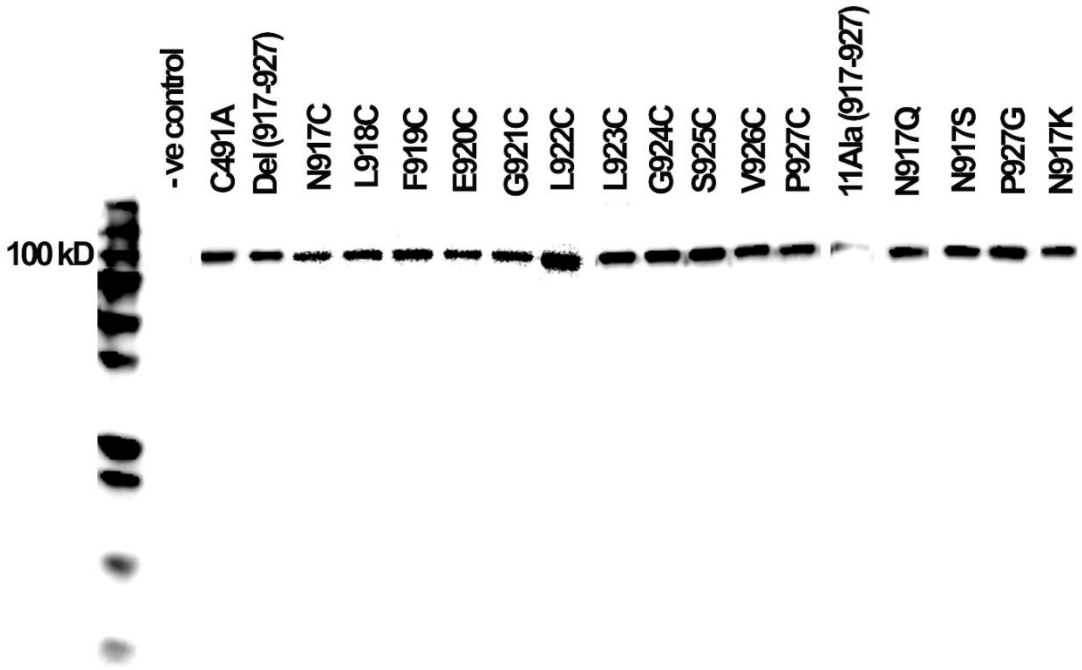

Figure 4.3: Western blot image showing expression of constructed MtrD mutants.

Equal amounts of protein from isolated membranes of N. gonorrhoeae KH15Δ*mtrD*ΔnorM expressing various constructs were separated on a polyacrylamide gel and transferred to a polyvinylidene difluoride membrane. MtrD proteins (identified by a protein band at approximately 100 kDa as the predicted molecular weight was 113.62 kDa) were immunologically detected using a rabbit anti-6His tag antibody that binds to the C-terminal His tag on MtrD. Note that the Western blot image is a combination of multiple individual experiments and includes (from left to right): negative control (-ve), MtrD KH15Δ*mtrD*ΔnorM [NICS], that carries pGCC4 and lacks MtrD; cysteine-less MtrD C491A positive control; 917-927 MtrD deletion derivative; 11 individual cysteine replacement mutants, the 11 alanine replacement MtrD mutant [11 A (917-927)] and four individual amino acid replacement MtrD mutants.

Table 4.2: Antimicrobial resistance of *N. gonorrhoeae* strain KH15Δ*mtrD*Δ*norM* expressing MtrD derivatives.

	MIC (μg/ml)[a]									
	Detergent		Antibiotic			CAMP	Dye		Bile acid	Hormone
Mutation	N-9	TX-100	RIF	NOV	OXA	PMB	ET	CV	CHO	PRO
WT[b]	≥4096	≥4096	0.125	1	4	100	0.25	2	400	80
Δ(N917-P927)	64	128	0.03	0.5	2	50	0.125	1	300	40
N917C	32	64	0.015	0.25	1	50	0.06	0.5	300	40
L918C	≥4096	≥4096	0.125	1	4	100	0.25	2	400	80
F919C	≥4096	≥4096	0.125	1	4	100	0.25	2	400	80
E920C	≥4096	≥4096	0.06	1	4	100	0.25	1	300	80
G921C	≥4096	≥4096	0.125	1	4	100	0.25	2	400	80
L922C	≥4096	≥4096	0.125	1	2	100	0.25	2	400	80
L923C	≥4096	≥4096	0.125	1	4	100	0.25	2	400	80
G924C	32	64	0.015	0.25	2	50	0.06	0.5	200	40
S925C	≥4096	≥4096	0.125	1	4	100	0.25	2	400	80
V926C	≥4096	≥4096	0.125	1	4	100	0.25	2	400	80
P927C	32	64	0.03	0.25	1	50	0.06	0.5	300	40
11Ala	ND	32	ND	ND	0.06	ND	ND	ND	ND	ND

	MIC (μg/ml)[a]									
	Detergent		Antibiotic			CAMP	Dye		Bile acid	Hormone
Mutation	N-9	TX-100	RIF	NOV	OXA	PMB	ET	CV	CHO	PRO
N917K	16	32	0.015	0.06	0.25	50	0.06	0.125	100	40
N917Q	32	64	0.015	0.25	0.5	50	0.06	0.5	200	40
N917S	64	128	0.06	1	2	75	0.125	1	300	80
P927G	≥4096	≥4096	0.125	1	4	100	0.25	2	400	80
-ve control[c]	16	32	0.008	0.03	0.06	50	0.06	0.125	100	20

[a] All MIC data are representative of three or more independent experiments. Abbreviations: CAMP, cationic antimicrobial peptide; CHO, cholic acid; CV, crystal violet; ET, ethidium; N-9, nonoxynol-9; NOV, novobiocin; OXA, oxacillin; PMB, polymyxin B; PRO, progesterone; RIF, rifampin; TX-100, Triton X-100; ND, not determined

[b] Recombinant cysteine-less MtrD variant with a 6-histidine affinity tag at C-terminus (CL-MtrD$_{His6}$)

[c] KH15Δ*mtrD*Δ*norM* strain transformed with pGCC4 empty vector expressing no MtrD [KH15Δ*mtrD*Δ*norM* (NICS) strain].

4.5.3 Four residues in the N917-P927 region play an important role in MtrD activity

As mentioned above, the positioning of the N917-P927 region suggests it has structural and functional roles, e.g., by facilitation of substrate uptake during a functional cycle. Therefore, it was proposed that some residues in this region may be involved in mechanisms that help substrate uptake from the IM and are important for MtrD activity. To identify the functional importance of individual residues within this region, each of the 11 residues was individually substituted with cysteine; cysteine was selected to facilitate later studies on the location/inhibition of substituted residues (Hassan et al., 2006b) and allows characterization of properties such as charge, polarity or hydrophobicity linked to the target residue side-chain. The 11 mutants were generated by site-directed mutagenesis using the primers listed in Table 4.1 and pGCC4-CL-*mtrD*$_{His6}$ as template DNA (Section 2.7.4). All 11 MtrD mutants were expressed in KH15Δ*mtrD*Δ*norM* cells at levels comparable to that of the WT as judged by Western blotting (Figure 4.3), indicating that the amino acid substitutions did not affect MtrD protein stability and membrane insertion. MIC analyses revealed that cells expressing six of the MtrD mutants (L918C, F919C, G921C, L922C, L923C, S925C, and V926C) retained resistance profiles similar to that of the WT with no change in MICs for any of the 10 tested compounds (Table 4.2). In contrast, three MtrD mutants (N917C, G924C and P927C) showed a reduction in resistance to all compounds with the greatest decrease (>128-fold) to the nonionic and amphiphilic surfactant TX-100 and the spermicide N-9 (Table 4.2), demonstrating that these three residues are critical for efficient MtrD-mediated resistance against a broad range of substrates. In addition, mutation of a fourth residue (E920C), affected resistance to RIF, CV and CHO (Table 4.2). These data raised questions about the possible role(s) played by these residues in the MtrD efflux process. Specifically, do they directly bind MtrD substrates or alternatively interact with neighbouring residues to indirectly affect transport function through another mechanism, e.g., by altering the volume of the nearby substrate entrance. To address these questions, we conducted additional site-directed mutagenesis and MD simulations.

To ascertain the role played by N917, and to determine whether there were side-chain requirements/limitations in this position, we aimed to replace the

polar noncharged side chain of asparagine with amino acids of both similar and different side chain properties. N917 was replaced with two polar noncharged residues (glutamine and serine) and the positively charged lysine. In addition, replacement of asparagine with a negatively charged residue (aspartic acid) and an amphipathic and bulky amino acid (tryptophan) was attempted, however construction of these two mutants was unsuccessful. Western blot analyses confirmed expression of N917K, N917Q and N917S protein in membranes of KH15Δ*mtrD*Δ*norM* cells expressing these mutant MtrD proteins at levels comparable to that of WT (Figure 4.3). Assays determined that resistance was not fully maintained by replacing N917 with either glutamine or serine although the N917S derivative mediated higher levels of resistance compared to the original N917C mutation (Table 4.2). These data indicate that side-chain properties of asparagine are required at position 917. The MtrD N917K derivative exhibited reduced resistance to many of the tested compounds even more than that by the N917C mutation, with a resistance capacity for N-9, TX-100, ET, CHO and PMB only at levels comparable with the negative control (Table 4.2).

We hypothesised that both G924 and P927 are residues required for optimal/efficient efflux function of MtrD through providing structural flexibility (glycine) or constraining backbone geometry (proline) within the loop region. Both proline and glycine are associated with a propensity to destabilise α-helices, promoting the formation of unstructured loops. modifying substrate capture from the IM. Interestingly, in the MtrD extrusion protomer, G924 is located at a position that corresponds to a break in the α-helix (Figure 4.4). To test these hypotheses, we designed mutagenesis strategies to create the MtrD mutants G924P and P927G. Construction of the G924P mutant was not successful likely due to lethality in *E. coli* cells, however the MtrD P927G derivative was obtained and shown to be expressed at a level comparable to that of WT (Figure 4.3). MIC analysis of MtrD P927G in KH15Δ*mtrD*Δ*norM* cells indicated that the proline at this position could be replaced by glycine as it retained full resistance capacity (Table 4.2). We postulate that this may be due to the backbone conformational flexibility of glycine, which allows it to adopt backbone dihedral conformations that span the region of the Ramachandran plot occupied by proline (Hollingsworth and Karplus, 2010).

Together these data showed that N917, G924 and P927 play important roles in MtrD-mediated MDR.

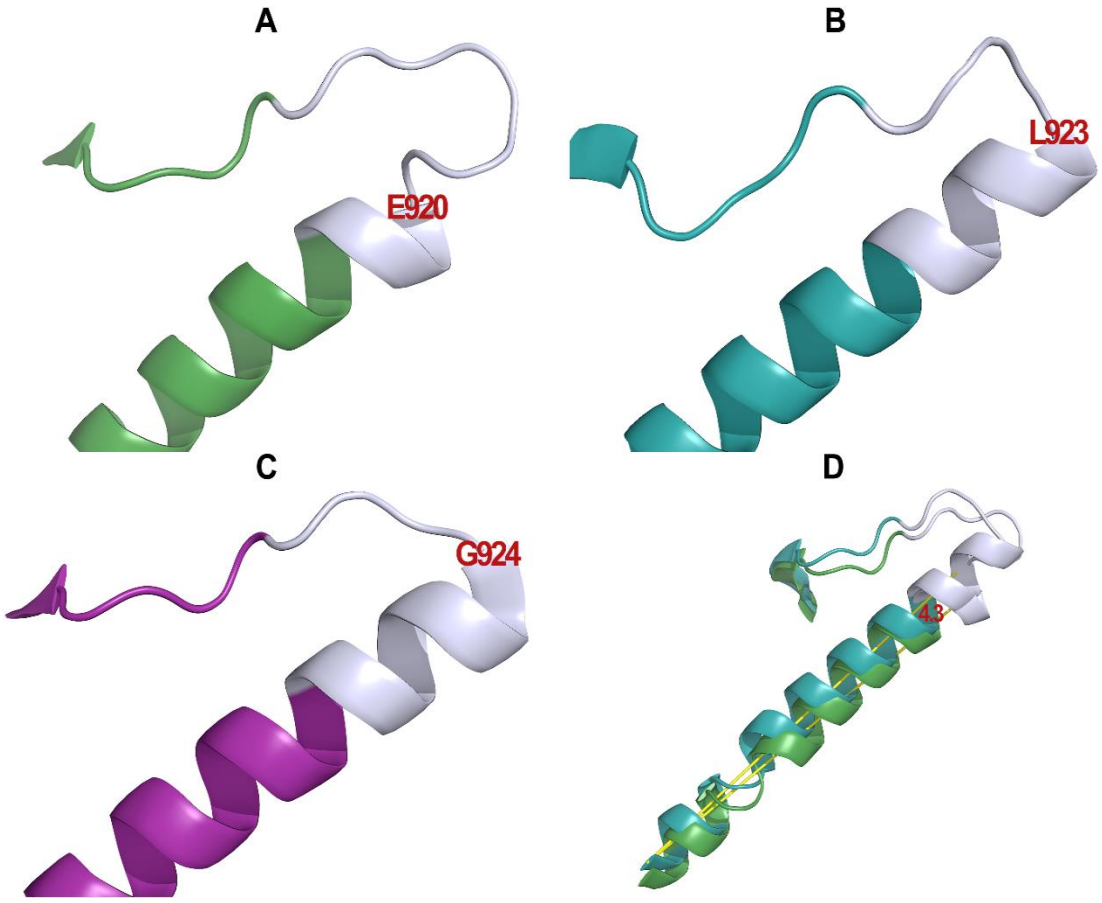

Figure 4.4: Secondary structure of the MtrD protein in complex with Amp (PDB ID 6VKS).

C-terminus of TMS 9 and the N917-P927 is shown in cartoon representation. Each helix is coloured according to its protomer; Access (green), Binding (teal), and Extrusion (magenta). N917-P927 is shown in grey in all pictures. (A) TMS 9 in the A protomer α-helix extends up to E920. (B) TMS 9 in the B protomer extends up to L923 forming two full turn α-helix turn in this region. (C) TMS 9 in the E protomer extends up to G924. (D) Superimposition of the A protomer and the B protomers (RMSD of 1.6 Å). Residues 893 to 935 encompassing TMS 9 are shown in cartoon representation and the 4.3° angle formed between the C-alpha atoms of residues E920 and S893 is illustrated in yellow.

4.5.4 Structural analysis and dynamics of the N917-P927 region

The Amp-bound cryo-EM structure of MtrD (PDB ID: 6VKS) revealed that the conformation of the N917-P927 region at its N-terminus is different in the A, B, and E protomers. In the A protomer the α-helix of TMS 9 is shorter than that in the B and E protomers (Figure 4.4 A-C). In the A protomer the TMS 9 α-helix extends to E920, whilst in the B protomer it extends to L923 and is further extended in the E protomer to G924 (Figure 4.4 A-C). These changes correspond to a change in the overall tilt angle of TMS 9 within the bilayer between these three conformations (Figure 4.4 D).

To better understand the impact of N917-P927 and the orientation of the TMS 9 helix on MtrD function, the Amp-bound cryo-EM structure of MtrD was embedded in a solvated neisserial membrane model (Section 2.7.8) and MD simulations were carried out for 500 ns in triplicate (Figure 4.5 A). MD simulations were also performed on the Δ(N917-P927), 11G(917-927) variants, and an MtrD triple mutant (N917C/G924C/P927C), containing concurrent N917C, G924C and P927C substitutions (Figure 4.5 B and C).

MD simulations of the WT MtrD trimer showed that N917-P927 of the A protomer lay within the membrane, positioned at the periplasmic membrane interface. In comparison, N917-P927 of the B and E protomers extended above the membrane into the periplasm (Figure 4.6 A to C). The amino acid sequence of N917-P927 (NLFEGLLGSVP) is aliphatic, supporting its preferential location at the membrane/water interface.

In replicate 500 ns simulations of WT MtrD, the position and relative orientation of the TMS 9 extension, N917-P927, changed relative to the starting cryo-EM structure. In all three protomers of the cryo-EM structure, N917-P927 did not form close contacts with other regions of the protein. Within the first 50 ns of simulation, N917-P927 formed contacts with residues in the PD, which differed between the A, B and E protomers.

In the A protomer, N917-P927 remained close to the PC1 domain near the membrane interface. In particular, G924 was in close proximity to S635 from the PC1 domain, while P927 was positioned near to A641 (Figure 4.7 A). In the B protomer, N917-P927 interacted with the PC1 domain slightly higher in

the binding pocket than in the A protomer and directly contacts it to form a protein-protein interface (Figure 4.7 B). In all three replicate simulations, the G924-P927 region formed protein-protein contacts in the vicinity of V640, A641 and S635. Compared to the A protomer, the change in position of N917-P927 effectively narrowed the binding cleft entrance and prevented the efficient entry of substrates (Figure 4.7 B). The precise nature of the contacts between G924-P927 and V640, A641 and S635 varied by replicate simulation. Notably, in one replicate simulation, the TMS 9 helical extension reorientated so that 917-927 adopted an elongated conformation in which G924 extends vertically into the

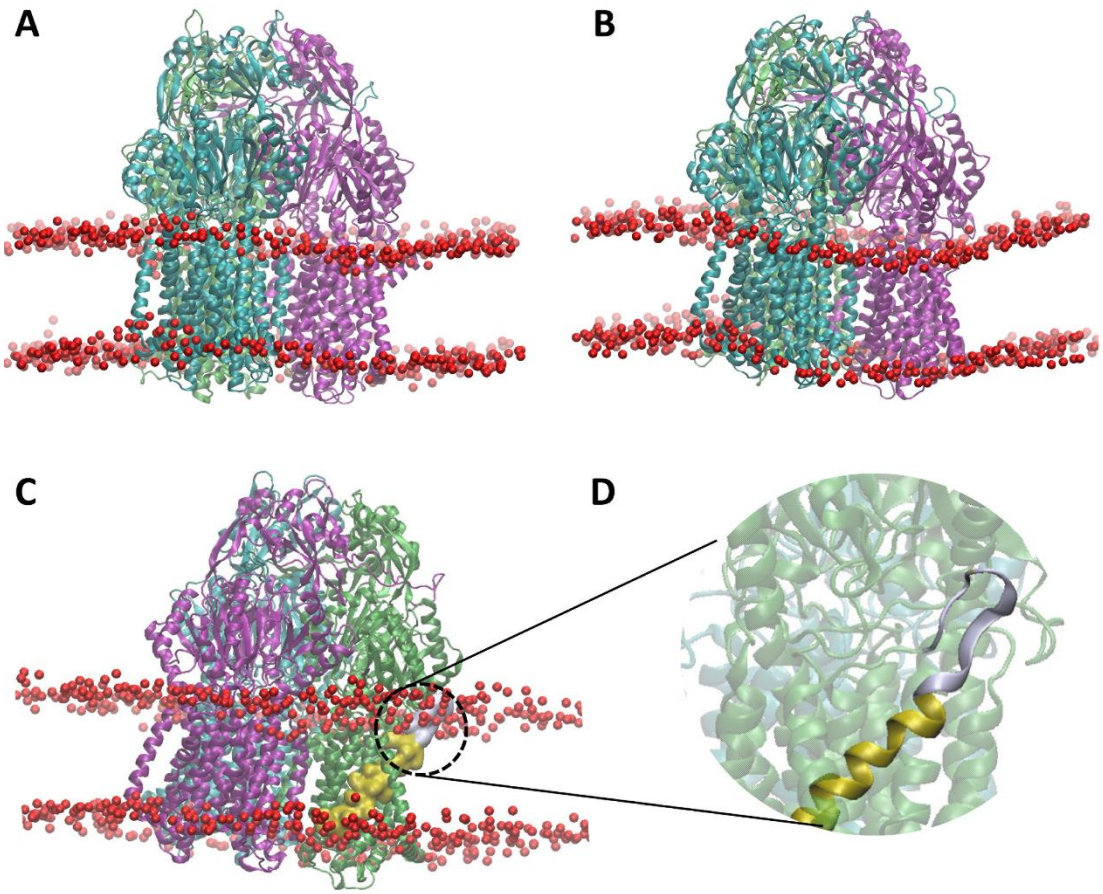

Figure 4.5: MD simulations showing the position of MtrD within the membrane.

The three MtrD protomers are shown in ribbon representation and coloured Access (green), Binding (teal), and Extrusion (magenta). The lipid phosphate head groups of the membrane are shown as red beads. Positions of the WT trimer (A), Δ(N917-P927) trimer (B), and 11G(917-927) trimer (C) within the membrane. (D) Closeup view of the TMS 9 and N917-P927 regions in the Access protomer of the 11G(917-927) MtrD mutant. In panels C and D, TMS 9 is gold and N917-P927 is grey.

base of the binding cleft to form a protein-protein contact with V640. In the remaining two replicate simulations, the conformation is less extreme. In all three replicate simulations, these interactions partially occluded the periplasmic binding cleft entrance. In the E protomer, N917 interacts with F929, while P927 interacts with T830 on the PC2 side of the binding cleft (Figure 4.7 C), protruding into the binding cleft to physically prevent substrate entry from both the periplasm and the IM substrate entrance.

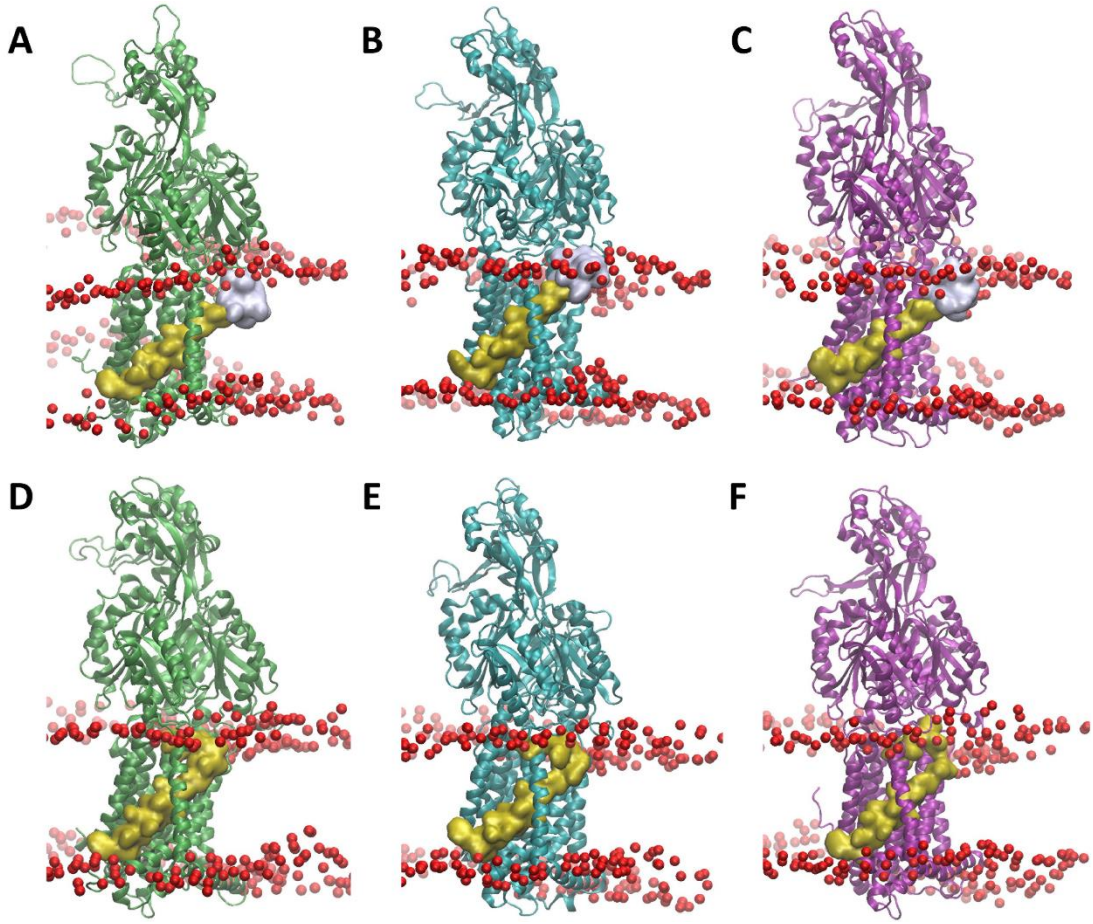

Figure 4.6: Representative MD simulation snapshot of the position and orientation of the TMS 9 and N917-P927 region in relation to the *N. gonorrhoeae* membrane surface.

Position and orientation of TMS 9 and N917-P927 is shown for the Access (green) (A), Binding (teal) (B), and Extrusion (magenta) (C) protomers of the WT MtrD protein and the Access (green) (D), Binding (teal) (E), and Extrusion (magenta) (F) protomers of the Δ(N917-P927) MtrD mutant. TMS 9 is in gold and the N917-P927 region is in grey ribbon representation.

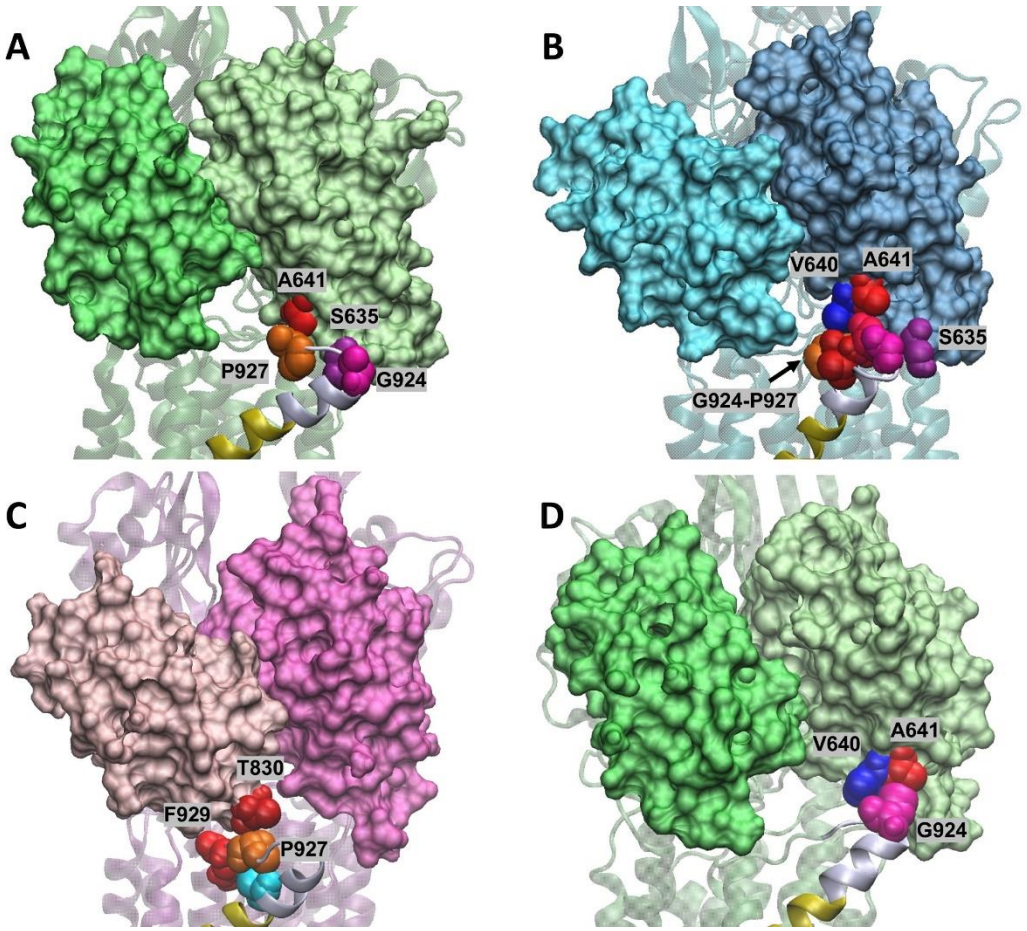

Figure 4.7: MD simulation analysis of interactions between the N917-P927 region and the MtrD periplasmic domain.

Interactions are shown for the Access (green) (A), Binding (teal) (B), and Extrusion (magenta) (C) protomers in the WT MtrD protein and the Access (green) protomer (D) of the N917C/G924C/P927C triple mutant MtrD protein. The PC1 (right) and PC2 (left) domains are shown in surface representation. Interacting residues (labelled on the figure) are shown in Van der Waals (VDW) rendering and are coloured by residue identity. TMS 9 is in gold and the N917-P927 region is in grey ribbon representation.

MD simulations were then performed to assess the impact of the cysteine replacements at positions that were found to be important for MtrD function. Based on the underlying hypothesis that individual mutations within a protein are unlikely to perturb the overall secondary structure, a triple MtrD mutant, containing concurrent N917C, G924C, and P927C mutations (N917C/G924C/P927C) was developed. No steric clashes were observed in

MtrD upon mutation of N917, G924, or P927 to cysteine. MD simulations showed that in contrast to the WT, for the triple mutant both the position and orientation of 917-927 in each protomer fluctuated and protruded above the membrane interface into the periplasm (Figure 4.8 A to C). Interactions between the N917-P927 region and the rest of the protein are most altered in the A protomer of the triple cysteine mutant. In the A protomer, the N917-P927 loop extends to form a HP oriented into the binding cleft. Here G924C interacts with V640 and A641 from the PC1 domain (Figure 4.7D). This interaction extends further into the binding cleft than in simulations of WT MtrD, in which G924 interacts with S635 below the level of V640 and A641. The deeper penetration of G924C into the binding cleft entrance partially occluded the periplasmic entrance to the binding cleft. We hypothesise that this prevented the entry of some substrates through the proposed periplasmic entrance of the mutant MtrD A protomer. In the B protomer of the triple cysteine MtrD mutant, G924C interacts with S635 from the PC1 domain, anchoring N917-P927 at the lower righthand entrance of the binding cleft. This interaction was also observed in the B protomer for the WT simulations but was more persistent throughout the simulations of the triple cysteine mutant. In the E protomer of the triple mutant, N917C formed contacts with F929, while P927C interacted with T830 on the PC2 side of the binding cleft, as was observed in the WT E protomer. We hypothesise that the P927C mutation decreases backbone dihedral angle constraints associated with the presence of proline, resulting in greater backbone mobility. The noticeable alteration in the positioning of the N917-P927 region in the A protomer of the triple cysteine mutant compared to the WT protein suggests the mutated residues N917, G924 and P927 play a key role in controlling substrate entry. The higher positioning of N917-P927 in the binding cleft of the triple cysteine mutant partially occluded the binding cleft entrance, preventing the entry of some substrates in the mutant MtrD A conformation. This restriction in substrate entry supports the decreased resistance profile experimentally observed upon mutation of these residues. Bioinformatics analysis of MtrD proteins in the NCBI database revealed that T830 and N929 are very highly conserved (100% amino acid identity) while S635 (63%), V640 (24%) and A641 (55%) are less conserved within *N. gonorrhoeae* strains. A similar homology trend is seen in MtrD present in strains of the closely related species *N. meningitidis*. The conservation of these

PC1/PC2 domain residues supports the MD simulations and the proposition that they interreact with TMS 9 in MtrD efflux.

Simulations of the Δ(N917-P927) MtrD mutant showed the terminal region of TMS 9 was located at the periplasmic membrane-water interface in the A and B protomers and protruded slightly above the membrane into the periplasm in the E protomer (Figure 4.6 D to F). Simulations of the Δ(N917-P927) MtrD protein, showed TMS 9 and TMS 10 did not associate with the periplasmic entrance to the binding cleft and a greater localised curvature in

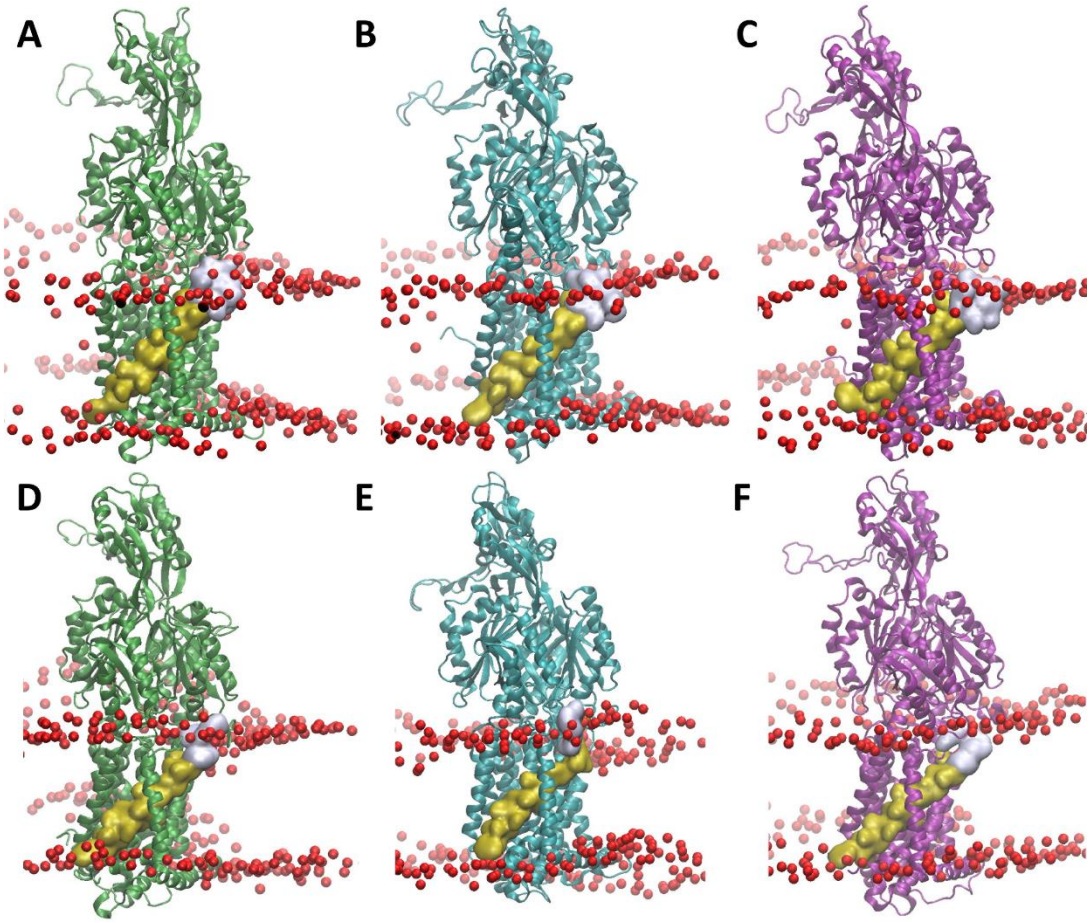

Figure 4.8: Representative snapshot of the position and orientation of the TMS 9 and N917-P92 regions from MD simulations in relation to the *N. gonorrhoeae* membrane surface.

Position and orientation of TMS 9 and N917-P927 is shown for the Access (green) (A), Binding (teal) (B), and Extrusion (magenta) (C) protomers of the N917C/G924C/P927C triple mutant and the Access (green) (D), Binding (teal) (E), and Extrusion (magenta) (F) protomers of the 11G(917-927) mutant. TMS 9 is in gold and the N917-P927 region is in grey ribbon representation.

the membrane around MtrD was observed (Figure 4.5A and B), suggesting that N917-P927 plays a role in the stability and orientation of MtrD within the membrane. Destabilisation of the protein-lipid interface of MtrD upon deletion of N917-P927 supports the hypothesis that this region plays a key role in stabilising MtrD within the membrane.

Simulations of the 11G(917-927) MtrD mutant show the 11G(917-927) region protruded above the membrane into the periplasm in the A and B protomers (Figure 4.8 D and E). In the E protomer, 917-927Gly lay at the periplasmic membrane interface (Figure 4.8 F). Consistent with the mutation to glycine, there was a loss of α-helical secondary structure in 11G(917-927) (Figure 4.5 D) across all three protomers. There was also a noticeable tilting of the 11G(917-927) MtrD mutant within the membrane during the 500-ns replicate MD simulations (C), again indicating a destabilisation in the protein-lipid MtrD interface, as was seen in the Δ(N917-P927) mutant. The overall changes in the localization and stability of N917-P927 between the MtrD mutants may underpin the limited activity of the transporter seen in the MIC analyses.

4.5.5 Deletion of the N917-P927 region alters progesterone uptake

To investigate the interaction of Δ(N917-P927) MtrD mutant with substrates, spontaneous binding simulations were performed with the substrate PRO. To increase the likelihood of observing spontaneous substrate binding, simulations were performed with the symmetric MtrD crystal structure (PDB ID: 4MT1), containing all three protomers in the A conformation, using the same protocol as previously described (Section 2.7.8) (Bolla et al., 2014). Here, 30 molecules of PRO were randomly placed in the solution surrounding the Δ(N917-P927) MtrD porter and docking domains and triplicate 500 ns MD simulations were performed. As observed in our previous simulations (Section 2.7.8 and 4.7.6), PRO adsorbed nonspecifically to the protein and membrane. In two of the three simulations, multiple molecules of PRO entered the binding cleft in the region that would have been occupied by N917-P927 (Figure 4.9) and bound to the proximal binding site. In both simulations, an initial PRO molecule first entered the binding cleft and moved into the proximal binding site before a second PRO molecule entered the binding cleft and formed

stacking interactions with the first PRO in the proximal binding site. No closure of the binding pocket was observed in the timeframe of the simulation. We postulate that deletion of N917-P927 dysregulates the access of substrate to the MtrD binding cleft and the closure of the substrate binding pocket during the transport cycle.

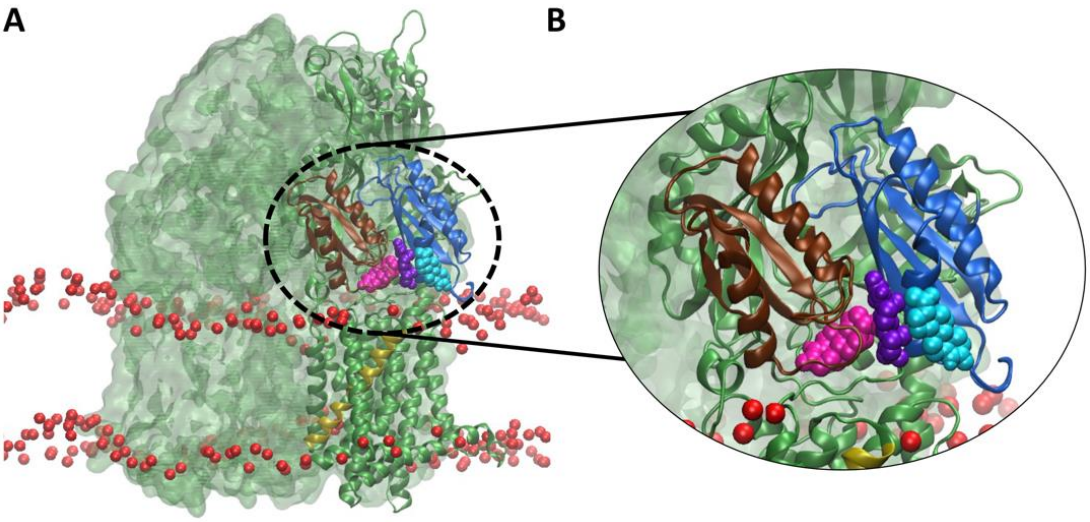

Figure 4.9: MD simulations of PRO flooding of the Δ(N917-P927) mutant of MtrD.

Phosphate groups of the *N. gonorrhoeae* phospholipid inner membrane are shown as red beads. All three MtrD protomers are green, and TMS 9 is gold. The binding cleft of the PC1 domain is dark blue and the PC2 domain is brown. Three PRO molecules (magenta, violet and cyan) within the binding cleft entrance are shown VDW representation. (A) Representative view showing multiple PRO molecules in the MtrD binding cleft after 250 ns of the Δ(N917-P927) PRO flooding simulation. (B) Magnification of the clustered PRO molecules within the MtrD binding cleft.

4.6 Discussion

In this study, we outline important features concerning multidrug export and resistance by the MtrD protein of *N. gonorrhoeae* involving the unique N917-P927 region. MtrD belongs to the RND superfamily of transport proteins, which in Gram-negative bacteria form one of the first line defence mechanisms against toxic chemicals including antibiotics and host-derived antimicrobials. It has been shown that upregulation of MtrD, in synergy with other mechanisms

of resistance, can result in highly drug resistant strains of *N. gonorrhoeae* such as H041 and FC428 (Golparian et al., 2018, Nakayama et al., 2016, Ohnishi et al., 2011b). One of the most interesting findings of this study is that the TMS 9 N917-P927 sequence is a unique dynamic region of MtrD that interacts with the membrane-periplasm interface and modulates drug access to the transporter during a functional cycle. Functional analysis of a set of MtrD mutants demonstrated that the N917-P927 region is essential for functional efflux and drug resistance capacity. In addition, MD simulations identified that this region may contribute to the positioning of the TMS 9 helix and stabilization of the protein within the neisserial IM, further facilitating efficient substrate capture.

Like AcrB, the MtrD substrate range is extremely broad and includes cationic, neutral and anionic compounds (Hagman et al., 1997, Nikaido, 1996). Presence of a hydrophobic domain on the molecule or hydrophobicity *per se* seems to be a common feature of MtrD substrates (Hagman et al., 1997, Nikaido, 1996, Nikaido et al., 1998) and suggests that they interact with the IM-periplasm interface before they are captured and exported by MtrD (Nikaido, 1996). Supporting this, RND transporters of the HAE1 family have been suggested to capture amphiphilic substrate molecules from the outer leaflet of the CM or from the membrane-periplasm interface (Nikaido, 1996, Yao et al., 2013). Indeed, the recent MtrD crystal structures (PDB ID: 6VKS and 6VKT) revealed two entrances; one from a periplasmic cleft and a second that opens to the outer leaflet of IM, both of which have been proposed as routes for hydrophobic substrate capture (Lyu et al., 2020). The periplasmic end of the TMS 9 helix, including its N917-P927 region extension, is located at the membrane-periplasm boundary, such that mutations in this region are expected to impact on protein-lipid interactions in this area. As expected, MD simulations showed that deletion of the extension (ΔN917-P927) and replacement with a string of glycines [11G(917-927)] in MtrD resulted in destabilisation of the protein-lipid interface and altered the positioning of MtrD within the membrane, supporting the hypothesis that this region plays a key role in stabilising MtrD within the membrane. In addition, disturbances in the protein-lipid interface could also influence interactions with MtrD substrates at the membrane-periplasm interface and substrate capture via the IM entrance.

This was supported by the reduced resistance to multiple substrates of *N. gonorrhoeae* cells expressing the Δ(N917-P927) MtrD mutant compared to the WT parent (Table 4.2). Furthermore, MD simulations of this deletion mutant with the substrate PRO revealed that destabilisation of the protein-lipid interface in the region of TMS 9 possibly impacts on substrate access to the binding cleft.

MtrD-mediated resistance to 10 selected substrates was significantly reduced by mutations to N917, G924 and P927. Their altered resistance profile could be attributed to changes in the position and relative orientation of the TMS 9 helix extension (N917-P927) during a transport cycle, as MD simulations of WT MtrD showed that the position and relative orientation of N917-P927 varies in the three protomers and involves interactions between N917, G924 and P927 with amino acids in the PD. These variations would explain how access of hydrophobic substrates to the binding cleft entrance could be facilitated in the access protomer, but efficiently prevented in the binding and extrusion protomers during a functional cycle.

In MD simulations of the N917C/G924C/P927C MtrD variant both the position and orientation of N917-P927 in each protomer fluctuated. In these simulations the interaction between N917-P927 and rest of the protein was most altered in the A protomer. Here, the N917-P927 region partially occluded the periplasmic substrate entrance to the binding cleft indicating that N917, G924 and P927 play a key role in substrate entry. It appears that reduced resistance capacity (Table 4.2) of the individual cysteine mutants (N917C, G924C, and P927C) is a result of altered interactions of these residues with rest of the protein impacting on correct positioning and orientation of N917-P927 in the membrane of *N. gonorrhoeae* thereby limiting substrate access to MtrD. The first 50 ns simulations of WT MtrD revealed these important interactions. Mutations of N917, demonstrated that a positively charged polar amino acid was not tolerated in this position, since cells expressing the MtrD N917K mutant conferred resistance levels for compounds at levels only comparable to the negative control. Further analysis of the N917 asparagine side-chain demonstrated that neither glutamine nor serine (two polar noncharged residues) could compensate for asparagine, indicating that key features of asparagine are required for this position. Analysis of the residue

requirement at position 927 showed that a glycine replacement in the P927G MtrD mutant still produced a fully functional protein. This supports the notion that the proline at 927 plays a structural role linked to MtrD stabilization in the IM and substrate capture from the IM-periplasm interface.

A comprehensive understanding of RND efflux pumps, which are a major contributor of AMR in Gram-negative bacteria, is central for combating bacterial infections including those caused by multidrug resistant strains of *N. gonorrhoeae*. Extensive genetic, biochemical, biophysical, and computational studies have hugely advanced our knowledge of efflux transporter systems and proteins, including the MtrCDE system of *N. gonorrhoeae*. A large body of knowledge already available with respect to the genetic aspects of the *mtrCDE* system (Beggs et al., 2021) availability of crystal and cryo-EM structures of the MtrD protein in apo form and in complex with drugs, has provided insights regarding the mechanisms used by this efflux pump to provide resistance against important antibiotics and other antimicrobials. Limited new antibiotics with activity against multidrug resistant strains of Gram-negative pathogens have been discovered in the past two decades even though they are desperately needed as this important public health problem continues to grow. Characterization of the structural and functional role of the unique N917-P927 region which connects TMS 9 and TMS 10 of MtrD provides insights concerning MDR afforded by this efflux pump. Moreover, it has revealed that subtle differences between RND transporters may have implications for drug efflux mechanisms and as such is important knowledge required to rationally design effective antibiotics or efflux pump inhibitors.

4.7 Materials and Methods

4.7.1 Bacterial strains, plasmids and growth conditions

The bacterial strains and plasmids used in this study are listed in

Table 4.3. The background *N. gonorrhoeae* strain is based on a FA19 derivative, KH15 that overexpresses the MtrCDE complex due to a single-base-pair deletion in the promoter of the *mtrR* gene, whose product, the MtrR protein, negatively controls expression of the *mtrCDE* operon (Beggs et al., 2021, Hagman et al., 1995). KH15Δ*mtrD*Δ*norM* is a derivative of KH15

(Hagman et al., 1995) with the *mtrD* and *norM* genes removed and is a highly discriminating strain for AMR assays (Section 2.7.3). pGCC4-CL-*mtrD*$_{His6}$ is a cysteine-less variant of *mtrD* (MtrD C491A) encoding a 6-histidine affinity tag at the C-terminus (Section 2.7.4). This fully functional *mtrD* derivative was used as a template for generating and mobilizing *mtrD* mutants into *N. gonorrhoeae*. Gonococci were grown on GC medium (Difco Laboratories, Detroit, MI) containing Kellogg's supplements I and II (Kellogg et al., 1963) at 37° C under 5% CO_2 or in GC broth (Difco Laboratories, Detroit, MI) containing Kellogg's supplements I and II and 0.048% (Vol/Vol) sodium bicarbonate at 37° C with shaking. *E. coli* DH5α (Invitrogen, Thermo Fisher Scientific Australia Pty Ltd) was used for propagation of all plasmid constructs and strains were grown on LB agar or in LB broth (Oxoid, Thermo Fisher Scientific Australia Pty Ltd). Antibiotics were added at the following concentrations: KAN, 40 µg/ml and ERY, 0.5 µg/ml. IPTG at a final concentration of 0.5 mM was used to induce *mtrD* transcription in *N. gonorrhoeae* strains harbouring pGCC4 vector constructs (Mehr and Seifert, 1998). Chemicals and antibiotics, if not specified, were from Sigma Chemicals (Sigma-Aldrich Pty Ltd).

Table 4.3: Bacterial strains and plasmids used in this study**.**

Strain or plasmid	Relevant genotypes or description	S[@]
Strains		
E. coli		
DH5αI	*fhuA2* Δ(*argF-lacZ*)U169 *phoA glnV*44 Φ80 Δ(*lacZ*)M15 *gyrA*96 *recA*1 *relA*1 *endA*1 thi-1 hsdR17	a
N. gonorrhoeae		
KH15Δ*mtrD*Δ*norM*	KH15 is a derivative of the antibiotic sensitive strain FA19 with a 1-bp deletion in the *mtrR* promoter	b
Plasmids		
pGCC4	*Neisseria* insertion complementation system (NICS) vector; *lacI*, P_{lac}, Kan^r, Ery^r	c
pGCC4-CL*mtrD*$_{His6}$	Cysteine-less derivative of *mtrD*$_{His6}$ in pGCC4	d

Strain or plasmid	Relevant genotypes or description	S[@]
N917C	N917C MtrD mutant based in pGCC4-CL*mtrD*$_{His6}$	e
L918C	L918C MtrD mutant based in pGCC4-CL*mtrD*$_{His6}$	e
F919C	F919C MtrD mutant based in pGCC4-CL*mtrD*$_{His6}$	e
E920C	E920C MtrD mutant based in pGCC4-CL*mtrD*$_{His6}$	e
G921C	G921C MtrD mutant based in pGCC4-CL*mtrD*$_{His6}$	e
L922C	L922C MtrD mutant based in pGCC4-CL*mtrD*$_{His6}$	e
L923C	L923C MtrD mutant based in pGCC4-CL*mtrD*$_{His6}$	e
G924C	G924C MtrD mutant based in pGCC4-CL*mtrD*$_{His6}$	e
S925C	S925C MtrD mutant based in pGCC4-CL*mtrD*$_{His6}$	e
V926C	V926C MtrD mutant based in pGCC4-CL*mtrD*$_{His6}$	e
P927C	P927C MtrD mutant based in pGCC4-CL*mtrD*$_{His6}$	e
Δ(N917-P927)	917-927 deletion MtrD mutant based in pGCC4-CL*mtrD*$_{His6}$	e
11A(917-927)	11Ala(917-927) insertion MtrD mutant based in pGCC4-CL*mtrD*$_{His6}$	e
11G(917-927)	11Gly(917-927) insertion MtrD mutant based in pGCC4-CL*mtrD*$_{His6}$	e
N917Q	N917Q MtrD mutant based in pGCC4-CL*mtrD*$_{His6}$	e
N917S	N917S MtrD mutant based in pGCC4-CL*mtrD*$_{His6}$	e
N917K	N917K MtrD mutant based in pGCC4-CL*mtrD*$_{His6}$	e

Strain or plasmid	Relevant genotypes or description	S[@]
P927G	P927G MtrD mutant based in pGCC4-CL*mtrD*$_{His6}$	e

[@]Source or reference: a, (Hanahan, 1983); b, (Hagman et al., 1995); c, (Mehr and Seifert, 1998); d, (Section 2.7.4); e, (This study)

4.7.2 Molecular biology methods

Plasmid DNA was isolated from *E. coli* cells using a Bioline Isolate II Plasmid Mini Kit (Bioline Meridian Bioscience, USA). Chromosomal DNA was isolated from *N. gonorrhoeae* cells by the use of a Wizard genomic DNA purification kit (Promega Co., USA). Primers used in this study are listed in Table 3.1 and were synthesized by Integrated DNA Technologies or Sigma-Aldrich. Bioline Velocity DNA polymerase was used in all PCR mutagenesis reactions and Bioline Mango*Taq*™ DNA polymerase for screening PCRs (Bioline, Boston, USA). All restriction digestion enzymes were from New England Biolabs (New England Biolabs Inc, Ipswich, MA, USA). Transformations into *N. gonorrhoeae* or *E. coli* cells were carried as described previously (Dillard, 2011). All sequencing was performed by AGRF.

4.7.3 Site-directed mutagenesis

The QuickChange site-directed mutagenesis method was used to construct *mtrD* mutants in the pGCC4-CL-*mtrD*$_{His6}$ plasmid using the primers listed in Table 4.1. To aid in screening, a silent restriction site was incorporated into each primer pair where possible (Section 2.7.5). Integrity of *mtrD* constructs were verified by sequencing the whole insert and then recombined into the FA19 KH15Δ*mtrD*Δ*norM* chromosome (Section 2.7.2). *N. gonorrhoeae* mutants were assessed for mutant MtrD protein production and their resistance profile.

4.7.4 Western blot analyses

Expression of MtrD mutant proteins in *N. gonorrhoeae* KH15Δ*mtrD*Δ*norM* membranes was determined by Western blotting as previously described, using anti-6xHistidine epitope tag (rabbit) antibody, and peroxidase-conjugated anti-rabbit IgG (goat) (Rockland antibodies and assays) as primary

and secondary antibodies, respectively (Section 2.7.6). Mutant protein expression levels were expressed as a percentage of the WT protein.

4.7.5 Minimum inhibitory concentration analyses

Resistance profiles of the *N. gonorrhoeae* KH15Δ*mtrD*Δ*norM* strain expressing the MtrD mutants were determined by MIC analyses to a selected panel of 10 compounds using standard agar dilution method (Section 2.7.7) (CLSI, 2012) with modifications. MIC analyses were conducted using solid GC medium supplemented with 0.5 mM IPTG and increasing concentrations of antimicrobials (Table 4.2). The MIC was determined as the lowest concentration of the antimicrobial compound required to fully inhibit bacterial growth and was repeated at least three times.

4.7.6 MD simulations

The Amp-bound MtrD cryo-EM structure (PDB ID: 6VKS) was used for the WT and mutant MtrD MD simulations (Bolla et al., 2014). Amp was removed prior to simulations. WT and mutant MtrD simulations were carried out on four protein models: WT, Δ(N917-P927), 11G(917-927), and a triple cysteine-replacement mutant, with concurrent mutation of residues N917, G924 and P927 (N917C/G924C/P927C). All proline residues were assigned a *trans* isomerisation, consistent with the conformation observed in the cryo-EM structures. Protein mutants were generated using the PyMOL Mutagenesis Wizard and SWISS-MODEL (Waterhouse et al., 2018). All simulations were performed using GROMACS2019.4 (Abraham et al., 2015, Lindahl et al., 2019) and the united-atom GROMOS 54a7 forcefield (Schmid et al., 2011). The MtrD protein for each system was embedded in a neisserial IM model, consisting of a 4:1 ratio of 1-palmitoyl-2-palmitoleoyl-*sn*-glycero-3-phosphatidylethanolamine (PPoPE) and DMPG. Systems were oriented in the *x-y* plane of a 18-nm x 18-nm x 19-nm box, solvated with the simple-point-charge water model (Berendsen et al., 1981), and charge neutralized with a physiological concentration of 150 mM NaCl. GROMOS parameters for PPoPE and DMPG were modified from previously published membrane models (Piggot et al., 2011), while parameters for Amp (Molid: 574595) were obtained from the Automated Topology Builder and Repository (ATB) (Koziara et al., 2014, Malde et al., 2011).

All systems were energy minimized using the steepest descent algorithm. Systems were equilibrated in a series of six sequential 2 ns simulations with progressively decreasing position restraints on the protein backbone atoms (force constants of 1,000, 500, 100, 50, 10, and 0 kJ mol^{-1} nm^{-2}). The coordinates from the final equilibration frame were used as the starting coordinates for unrestrained production simulations performed in triplicate for each system. Production simulations were 500 ns for each system.

Simulations were performed using the NPT ensemble, with solute (protein/membrane) and solvent (ions/water) separately coupled to an external temperature bath of 310K. Temperature was held constant with the Bussi thermostat (τ_T = 0.1 ps) (Bussi et al., 2007). Pressure was maintained via semi-isotropic pressure coupling to an external pressure bath at 100,000 Pa. The Berendsen barostat was used for equilibration simulations (τ_P = 0.5 ps and isothermal compressibility = 4.5 x 10^{-10} Pa^{-1}) (Berendsen et al., 1984). Production simulations employed the Parrinello-Rahman barostat (τ_P = 5 ps and isothermal compressibility = 4.5 x 10^{-10} Pa^{-1}) (Parrinello and Rahman, 1981b). Non-covalent interactions were determined via the Verlet scheme with a 1.4-nm cutoff (De Jong et al., 2016). Electrostatic interactions were calculated using Particle Mesh Ewald (Darden et al., 1993), and covalent bonds were constrained using the LINCS algorithm (Hess et al., 1997).

PRO flooding simulations were conducted using the symmetric apo MtrD crystal structure (PDB ID: 4MT1) (Bolla et al., 2014). Flooding simulations were carried out as previously described (Section 2.7.8) though with the protein being changed to a Δ(N917-P927) mutant of the symmetric crystal structure generated using SWISS-MODEL (Waterhouse et al., 2018).

CHAPTER 5

ESTABLISHMENT OF AN *ESCHERICHIA COLI*-BASED HOST-VECTOR SYSTEMS FOR OVEREXPRESSION, PURIFICATION AND FUNCTIONAL ANALYSIS OF THE *NEISSERIA GONORRHOEAE* MTRD PROTEIN

5.1 Introduction

To analyse the function of a bacterial protein it is preferable to do so in its native host so that any required processing or other factors necessary for activity are present. However, *N. gonorrhoeae* as a host has limitations that hinders undertaking some functional analyses. Neisseria itself is a fastidious organism for growth and assaying function, including real time efflux assays, which are common methods for measuring transport activity. Typically, *E. coli* can be used as the host strain when conducting real time efflux assays, including characterising the export mechanisms provided by efflux transporters heterologously expressed in *E. coli*. These assays usually require at least one hour to perform. During this time *E. coli* cells that are suspended in buffer solutions keep viable and stabile (Hassan et al., 2013, Sakurai et al., 2019, Zwama et al., 2018). In contrast, gonococcal cells have been found to lose these attributes quickly when suspended in various buffers and solutions (Elmros et al., 1976, Morse and Bartenstein, 1974). Previous investigations have found limited buffer solutions, e.g., Gey's balanced salt solution with 0.01% BSA were able to maintain viability of *N. gonorrhoeae* suspensions for 25 minutes (Norrod and Williams, 1979). However, this solution includes glucose, which must be omitted for undertaking efflux transport assays. Glucose or formate is used as an efflux pump energiser in transport assays after *E. coli* cells are loaded with substrate in presence of an uncoupler agent such as CCCP (Brown and Skurray, 2001, Lambert and LePecq, 1984, Littlejohn et al., 1992, Tennent et al., 1989).

A challenging aspect of studying MtrD transport activity in *N. gonorrhoeae* is the difficulty in growing gonococci in liquid medium. While *N. gonorrhoeae* has successfully been grown in some specific liquid media, such as GC broth, difficulties in obtaining consistent cell growth still exits. During this study, *N. gonorrhoeae* strains were able to be grown in GC broth, however, efforts for growing *N. gonorrhoeae* strains in liquid cultures for protein overexpression or efflux assay purposes failed multiple times for an unknown reason. This limitation, therefore, hinders overexpression of recombinant MtrD protein in gonococci. *E. coli* has long been used for overexpression of various RND type transport proteins such as AdeB, MexB, and EmhB (Hearn et al., 2006a, Hearn et al., 2006b, Morgan et al., 2021, Nakashima et al., 2013, Su et al., 2019).

Production of sufficient amounts of the MtrD protein is required for undertaking a detailed characterisation, such as reconstitution of the MtrD protein in liposomes for efflux assays; substrate or inhibitor binding assays using surface plasmon resonance (SPR) analysis; crystallography and many other *in vitro* assays. Therefore, alternative methods for conducting analysis of MtrD-mediated transport can be obtained in a heterologous host such as *E. coli* or using purified protein expressed and isolated from *E. coli*.

The focus of this chapter is to establish an *E. coli* host and vector system that allows optimal overexpression of active MtrD protein. *E. coli* has a number of efflux systems, the most important and highly characterised is the AcrAB-TolC pump system (Section 1.3.6.4). Since the *N. gonorrhoeae* MtrCDE system is homologous, it is possible that expression of the MtrD protein in *E. coli* strains possessing their native AcrB could produce conflicting results with functional analyses of MtrD in this background or interfere with purification of MtrD protein. Therefore, deletion of the *acrAB* region from the *E. coli* chromosomes of BL21(DE3) and DH5α strains was attempted. *E. coli* BL21(DE3) strain has been used successfully for expression of many membrane proteins (Debruycker et al., 2020a, Lyu et al., 2020, Miroux and Walker, 1996, Su et al., 2021, Yousefian et al., 2020). For the *in vivo* functional analyses of MtrD the strain *E. coli* DH5α was selected for this purpose as it has been used successfully for other membrane transporter proteins (Hassan et al., 2006b, Hassan et al., 2008, Lv et al., 2020). Multiple iterations of the *mtrCDE* operon, with *mtrD* by itself, together in the *mtrCDE* operon, and as three individual genes, viz., *mtrC*, *mtrD* and *mtrE* in one plasmid, were cloned in several plasmids including pBluescript II, pGCC4, pET21a, and pETDuet1. This chapter provides details of plasmid construction and discusses protein expression and functional analysis of MtrD from constructed plasmids in multiple *E. coli* host strains. Chapters 2, 3 and 4 of this thesis included construction of several *mtrD* mutants using the pGCC4-*mtrD*$_{His6}$ plasmid. This construct is quite a large plasmid of more than 12 Kb in size. The large size of this plasmid posed challenges when constructing *mtrD* mutants using PCR amplification. To overcome this problem, a pBluescript-based modified vector was constructed that enables cloning the 3204 bp *mtrD* as truncated four short sequences facilitating site-directed mutagenesis of the gene.

5.2 Material and Methods

5.2.1 Buffers and solutions

Buffers and solutions used in this study are listed in Table 5.1. All chemicals were of analytical grade and purchased from Sigma-Aldrich unless stated otherwise. Buffers and solutions were prepared from powdered or liquid chemicals according to manufacturers' recommendations. If required, buffers or solutions were sterilised by either autoclaving at 121°C for 15 minutes or filtration through a membrane filter with 0.22 µm pore size (Millipore).

5.2.2 Culture media

Luria-Bertani (LB) broth was prepared by dissolving tryptone (Oxoid, Australia) 1% (w/v), yeast extract (Oxoid, Thermo Fisher Scientific Australia Pty Ltd) 0.5% (w/v), and NaCl 1% (w/v) in the required amount of reverse osmosis (RO) purified water and adjusting the pH to 7.5. To create LB agar, 13 g/L of agar powder was added to LB medium, which was later sterilized through autoclaving (Section 5.2.1). Muller-Hinton medium was prepared as per the guidelines provided by the manufacturer, Oxoid Australia.

5.2.3 Plasmids, bacterial strains and growth conditions

Plasmids used in this study are listed in Table 5.2. Bacterial strains used in this study are listed in Table 5.3. *E. coli* was grown on LB agar or in LB broth (Oxoid, Thermo Fisher Scientific Australia Pty Ltd) unless stated otherwise and incubated at 37° C or at 25° C if a temperature sensitive strain. Broth cultures in tubes were positioned at a 45° angle and incubated with shaking (200 rpm) for better aeration. Where selection was required, antibiotics were added to the media at the following concentrations: Amp (100 µg/ml) and KAN (25 µg/ml).

Table 5.1: Buffers and solutions used in this study**.**

Buffer/solution	Ingredients
12% SDS PAGE gel (House-made)	30% acrylamide/bis solution (Bio-Rad), 1.5 M Tris-HCl (pH 8.8), 10% SDS, 10% APS, and TEMED
12% SDS PAGE stacking gel (House-made)	30% acrylamide/bis solution (Bio-Rad), 1.5 M Tris-HCl (pH 6.8), 10% SDS, 10% APS, and TEMED
APS solution	10% ammonium persulphate
Blocking buffer	10% Skim milk powder in 1X TTBS buffer
Colony lysis solution (1x)	20 mM Tris-HCl (pH 8.5), 2 mM EDTA, 1% Triton X-100
Crushing buffer	20 mM Tris-HCl (pH 7.5), 300 mM NaCl, 10% glycerol
Elution buffer	50 mM phosphate buffer (pH 8.0), 300 mM NaCl, 10% glycerol, 0.1% DDM, 250 mM imidazole
Equilibration and Wash Buffer	50 mM phosphate buffer (pH 8.0), 300 mM NaCl, 10% glycerol, 0.1% DDM, 10 mM imidazole
Membrane suspension buffer	20 mM Tris-HCl (pH 7.5), 300 mM NaCl, 10% glycerol
SDS PAGE running buffer for in house-made gels (10x)	250 mM Tris, 1.92 M glycine (pH 8.3), 1% SDS
SDS PAGE running buffer for pre-cast gels (20x)	1.2 M Tris, 0.8 M tricine, 50 mM sodium bisulphite (The pH should be between 8.2 - 8.3), 2% SDS
SDS sample buffer (4x)	200 mM Tris-HCl (pH 6.8), 4% β-mercaptoethanol, 8% (w/v) SDS, 40% (v/v) glycerol, 0.4% bromophenol blue
Solubilisation buffer	50 mM phosphate buffer (pH 8.0), 300 mM NaCl, 10% glycerol, 2% DDM,

Buffer/solution	Ingredients
TAE buffer (1x)	40 mM Tris, 1 mM EDTA, 20 mM acetic acid
TBS (1x)	50 mM Tris-HCl (pH 7.5), 300 mM NaCl
TFB1 buffer	30 mM potassium acetate, 100 mM rubidium chloride, 10 mM calcium chloride, 50 mM manganese chloride, 15% glycerol, pH 5.8, filter sterilised
TFB2 buffer	10 mM MOPS, 10 mM rubidium chloride, 75 mM calcium chloride, pH 6.5, filter sterilised
Transfer buffer (1x)	25 mM Tris, 192 mM glycine, 20% MeOH (pH 8.3 - 8.8)
TTBS buffer	0.1% Tween 20 in 1 L 1x TBS buffer

5.2.4 Bacterial antimicrobial sensitivity assays

Two methods were employed to measure bacterial sensitivity to a range of compounds, namely the micro-broth dilution method and the disc diffusion method. The micro-broth dilution method was mainly used to determine resistance profiles by measuring MICs. However, due to time constraints, the disc diffusion method was also utilised for resistance profiling (CLSI, 2012, Wiegand et al., 2008).

5.2.4.1 Disc diffusion method

A standard disc diffusion method with Mueller-Hinton (MH) plates supplemented with IPTG (0.5 mM final concentration) was used (Jorgensen and Turnidge, 2015). *E. coli* strains were grown overnight (O/N) in LB broth cultures containing appropriate antibiotic selection, diluted 1:100 in MH broth and grown until the turbidity reached OD_{600}=0.6. If induction of protein expression was required, cultures were cooled to 25° C before the addition of IPTG (0.5 mM, final concentration) and incubated for another 1-2 hours. Bacterial inoculums were prepared by diluting broth cultures to OD_{600}=0.1 in MH broth (equivalent to 0.5 McFarland standard) using a spectrophotometer (Spectronic 200, Thermo Scientific) and used to inoculate MH plates using sterile cotton swabs. Antibiotic discs were placed on the agar using a disc

dispenser at a maximum of five discs per plate. Plates were incubated at 37° C for 20-24 hours before measuring the inhibition zones (mm). Disc diffusion assays were performed at least two times on different days.

5.2.4.2 Micro-broth dilution

The Clinical and Laboratory Standard Institute (CLSI) micro-broth dilution method was used to determine MIC of several antimicrobials for various *E. coli* strains with modifications (CLSI, 2012). Two-fold serial dilutions of the compound of interest were made in a microtiter plate in 50 µl of MH broth. These antimicrobial agents included, with their concentration range: (OXA 0.5-8 µg/ml, ET 1-64 µg/ml, CV 0.5-32 µg/ml, ERY 2-512 µg/ml, NOV 0.5-512 µg/ml). Bacterial suspensions with an OD_{600} = 0.1 were prepared as described in Section 5.2.4.1. Bacterial inoculums were prepared from these cell suspensions by diluting 1:100 in MH broth. These diluted cells suspensions were used to inoculate microtiter plates by addition of 50 µl ($5X10^5$ CFU/ml in a total volume of 100 µl) to each well except for the cavity specified for sterility control, to which 50 µl MH broth was added. Microtiter plates were placed in a humid container and incubated at 37° C without shaking for 20-24 hours. Bacterial growth was assessed by measuring absorbance at 600 nm (endpoint, OD_{600}) using a FLUOstar Omega spectrometer (BMG Labtech, Germany). The MIC was defined as the lowest concentration of the antimicrobial agent that inhibited visible growth of the tested *E. coli* strain.

Table 5.2: Plasmids used in this study

Plasmid	Relevant genotypes or description	S[@]
pKD46	λ Red recombinase expression plasmid; temperature sensitive	a
pKD4	Source of Kan^R gene flanked by FRT sites; used as template for gene disruption	a
pCP20	Expresses the yeast recombinase flippase (FLP) protein that removes resistance marker flanked by FRT sequences; temperature sensitive	a

Plasmid	Relevant genotypes or description	S[@]
pBluescript II SK (+)	Expression vector; Amp^R	b
pBluescript-*mtrD*$_{His6}$	Constructed by cloning *mtrD* from FA19 into pBluescript II SK (+)	c
pBluescript-*mtrCDE*$_{His6}$	Constructed by cloning the *mtrCDE* operon from FA19 into pBluescript II SK (+)	c
pGCC4	Neisseria insertion complementation system (NICS) vector; *lacI*, P_{lac}, Kan^R, ERY^R	d
pGCC4-CL-*mtrD*$_{His6}$	Constructed by cloning *mtrD* into pGCC4 and replacing the sole cysteine of *mtrD* at position 419 with alanine	c
pETDuet-1	Co-expression vector for two target genes; Amp^R	e
pETDuet-*mtrC*	Constructed by cloning *mtrC* into multiple cloning site 1 (MCS1) of pETDuet-1	c
pETDuet-*mtrCE*	Constructed by cloning *mtrC* and *mtrE* as contiguous joint DNA sequence into MCS1 of pETDuet-1	c
pETDuet-*mtrCE-mtrD*	Constructed by cloning *mtrD* into MCS2 of pETDuet-*mtrCE* plasmid	c
pET21a (+)	Expression vector containing T7*lac* promoter and the natural promoter and coding sequence for the LacI repressor (*lacI*) allowing control of the basal level expression of the target gene; Amp^R	f
pET21a-*mtrD*	Constructed by cloning *mtrD* into pET21a (+) vector using *Nde*I and *Xho*I restriction sites	c

Plasmid	Relevant genotypes or description	S[@]

[@]Source or reference: a, (Datsenko and Wanner, 2000); b, (Alting-Mees and Short, 1989); c, (This study); d, (Mehr and Seifert, 1998); e, (Novy et al., 2002); f, (Novagen)

Abbreviations: ERY^R, erythromycin resistance; Kan^R, kanamycin resistance; Amp^R, ampicillin resistance

Table 5.3 Bacterial strains used in this study.

Strain	Relevant genotypes or description	S[@]
E. coli strains		
AG100A	F⁻ *glnX44*(AS), *galK2*(Oc), *rpsL*704(*strR*), *xyl*A5, *mtl*-1, *argE*3(Oc), *thiE*1, *tfr*-3, Δ*acrAB*	a
AG100A/pBluescript II	AG100A strain carrying pBluescript	b
AG100A/pBluescript-*mtrCDE*$_{His6}$	AG100A strain carrying pBluescript-*mtrCDE*$_{His6}$ plasmid	b
BL21(DE3)	F⁻, *lon*-11, *Δ*(*ompT-nfrA*)885, *Δ*(*galM-ybhJ*)884, *λ-DE3* [*lacI, lacUV5*-T7 gene 1, *ind1*, *sam7*, *nin5*], Δ46, [*mal*+]$^{K-12}$(*λS*), *hsdS*10	c
BL21(DE3) Δ*acrAB*	BL21(DE3) strain with *acrAB* region removed	b
BL21(DE3)/pBluescript-*mtrD*$_{His6}$	BL21(DE3) strain carrying pBluescript-*mtrD*$_{His6}$ plasmid	b
BL21(DE3)/pKD46	BL21(DE3) carrying pKD46 and expressing *λ* Red recombinase when induced with arabinose	b
BL21(DE3)/pKD46*acrAB*:FRT-Kan^{R}	BL21(DE3)/pKD46 strain with *acrAB* region replaced with flippase recognition target (FRT)-Kan^{R}	b
BL21(DE3)Δ*acrAB*/pETDuet-1	BL21(DE3)Δ*acrAB* strain carrying pETDuet-1	b
BL21(DE3)Δ*acrAB*/pETDuet-*mtrCE-mtrD*	BL21(DE3)Δ*acrAB* strain carrying pETDuet-*mtrCE-mtrD* plasmid	b
BW25113(DE3)	F⁻, Δ(araD-araB)567, ΔlacZ4787(::rrnB-3), λ-DE3, rph-1, Δ(rhaD-rhaB)568, hsdR514	d

Strain	Relevant genotypes or description	S[@]
BW25113(DE3) Δ*acrB*	BW25113(DE3) strain with *acrB* removed	e
BW25113(DE3)/Δ*acrAB*/pETDuet-1	BW25113(DE3)Δ*acrAB* strain carrying pETDuet-1	b
BW25113(DE3)Δ*acrAB*/pETDuet-*mtrCE-mtrD*	BW25113(DE3)Δ*acrAB* strain carrying pETDuet-*mtrCE-mtrD* plasmid	b
BW25113(DE3)Δ*acrB/*pBluescript-$mtrD_{His6}$	BW25113(DE3)Δ*acrB* strain carrying pBluescript-$mtrD_{His6}$ plasmid	b
BW25113(DE3)Δ*tolC*	As BW25113(DE3) strain but Δ*tolC*	e
BW25113(DE3)Δ*tolC*/pETDuet-1	BW25113(DE3)Δ*tolC* strain carrying pETDuet-1	b
BW25113(DE3)Δ*tolC/*pETDuet-*mtrCE-mtrD*	BW25113(DE3)Δ*tolC* strain carrying pETDuet-*mtrCE-mtrD* plasmid	b
BW25113(Δ*acrB*ΔemrE ΔmdfA::kan)	BW25113 strain with *acrB* and *emrE* genes removed and *mdfA* inactivated	f
BW25113(Δ*acrB*Δ*emrE*Δ*mdfA::kan*)/pBluescript	BW25113 (Δ*acrB* Δ*emrE* Δ*mdfA::kan*) strain carrying pBluescript	b
BW25113(Δ*acrB*Δ*emrE*Δ*mdfA::kan*)/pBluescript-$mtrD_{His6}$	BW25113 (Δ*acrB* Δ*emrE* Δ*mdfA::kan*) strain carrying pBluescript-$mtrD_{His6}$ plasmid	b
C41(DE3)	$F^{–}$, *ompT*, *hsdSB*, (r^{B-} m^{B-}), *gal*, *dcm*, *λ-DE3*	g
C43(DE3)	$F^{–}$, *ompT*, *hsdSB*, (r^{B-} m^{B-}), *gal*, *dcm*, *λ-DE3*	g
C43(DE3)/pBluescript-$mtrD_{His6}$	C43(DE3) strain carrying pBluescript-$mtrD_{His6}$ plasmid	b

Strain	Relevant genotypes or description	S[@]
DH5α	fhuA2 Δ(argF-lacZ)U169 phoA glnV44 Φ80 Δ(lacZ)M15 gyrA96 recA1 relA1 endA1 thi-1 hsdR17	h
DH5α Δ*acrAB*	DH5α strain with *acrAB* region removed	b
DH5α Δ*acrAB*/pBluescript	DH5αΔ*acrAB* strain carrying pBluescript	b
DH5α/pBluescript	DH5α strain carrying pBluescript	b
DH5α/pBluescript-*mtrCDE*$_{His6}$	DH5α strain carrying pBluescript-*mtrCDE*$_{His6}$ plasmid	b
DH5α/pKD46	DH5α carrying pKD46 and expressing *λ* Red recombinase when induced with arabinose	b
DH5α/pKD46 *acrAB*:FRT-Kan^{R}	DH5α strain carrying pKD46 plasmid, with *acrAB* region replaced with FRT-Kan^{R}	b
DH5αΔ*acrAB*/pBluescript-*mtrCDE*$_{His6}$	DH5αΔ*acrAB* strain carrying pBluescript-*mtrCDE*$_{His6}$ plasmid	b
MC33.7	ΔacrABΔtolC	e
MC33.7/pETDuet-1	MC33.7 strain carrying pETDuet-1	b
MC33.7/pETDuet-*mtrCE-mtrD*	MC33.7 strain carrying pETDuet-*mtrCE-mtrD* plasmid	b
N. gonorrhoeae strains		
FA 19	Antimicrobial sensitive strain	i

[@]Source or reference: a, (George and Levy, 1983, Okusu et al., 1996); b, (This study); c, (Studier and Moffatt, 1986); d, (Datsenko and Wanner, 2000); e, (A kind gift from Professor Rietie Venter); f, (Tal and Schuldiner, 2009); g, (Miroux and Walker, 1996); h, (Hanahan, 1983); I, (Sparling et al., 1975)

Abbreviations: Kan^{R}, kanamycin resistance

5.2.5 Molecular biology methods

5.2.5.1 Plasmid DNA extraction

The *E. coli* strain carrying plasmid of interest was grown O/N in LB broth supplemented with appropriate selection antibiotic (Section 5.2.3). Depending on the copy number, 1 to 5 ml of O/N culture was used for plasmid extraction using the Isolate II Plasmid Mini Kit (Bioline, Boston, MA, USA) as per manufacturer's protocols.

5.2.5.2 Chromosomal DNA extraction

Five to ten millilitres of *E. coli* O/N cultures (Section 5.2.3) were used for isolation of chromosomal DNA. The Wizard genomic DNA purification kit (Promega Co., USA) was used as per manufacturer's recommendations.

5.2.5.3 Polymerase chain reaction

Velocity Taq DNA polymerase (Bioline, USA) was used for all PCR amplifications that required a high-fidelity product such as for cloning and Sanger sequencing (Sections 5.3 1-8). Mango Taq DNA polymerase (Bioline, USA) or Econo Taq DNA polymerase (Lucigen, USA) were used for screening purposes, such as colony PCR screening (Sections 5.3 1-8). For colony PCR screening, individual well-isolated colonies were suspended in 50-100 µl colony lysis solution (Table 5.1) and incubated at 90° C for 10 minutes; 5 µl of each colony lysate was used as template. All PCR reactions were setup as per manufacturer's recommendations. Typical cycling conditions included initial denaturation at 95° C for 5 minutes followed by 30 cycles of: denaturation at 95° C for 20 seconds; annealing at 55° C for 30 seconds; extension at 72° C for 1 minute/kb; followed by 1 cycle of final extension at 72° C for 5 minutes. Target DNA amplification was analysed by agarose gel electrophoresis (Section 5.2.5.4).

5.2.5.4 DNA agarose gel electrophoresis

Agarose gel electrophoresis was used for resolving DNA fragments in experimental samples such as PCR and restriction digestion following standard methods (Russell and Sambrook, 2001). Agarose gels, using biotechnology grade agarose (Amresco, USA) were prepared in 0.5X TAE buffer (Table 5.1) at various concentrations depending on the size of DNA

fragment; <1 kb, 2% and fragments between 1 to >10 kb, 1% agarose gels were prepared. Blue/Orange Loading Dye, 6X (Promega, USA) was added to DNA samples at 1X final concentration before loading in gel wells and electrophoresis in 0.5X TAE buffer (Table 5.1). DNA fragments were resolved at 100 volts until the dye front (orange G) reached bottom half of the gel. Agarose gels were stained in Gel Red (Biotium) for at least five minutes and de-stained for at least 15 minutes using RO water before being visualised using a Gel Doc EZ system (Bio-Rad, USA).

5.2.5.5 Purification of DNA samples

DNA fragments isolated by agarose gel electrophoresis, PCR products, restriction enzymes digestion products, and DNA fragments treated with shrimp alkaline phosphatase were purified using ISOLATE II PCR and Gel Kit (Bioline, USA) or Wizard® SV Gel and PCR Clean-Up System (Promega, USA) according to manufacturers' instructions.

5.2.5.6 Assessment of quantity and quality of DNA samples

The concentration of DNA in samples was measured using a NanoDrop One Microvolume UV Spectrophotometer (Thermo Scientific) by absorbance reading at 260 nm (A_{260}). Good quality DNA samples with a purity ratio of 1.7-2.0 both for A_{260}/A_{280} and A_{260}/A_{230} indicating no protein or salt contamination, respectively, were used for sensitive down-stream applications.

5.2.5.7 DNA sequencing

The AGRF (Australia) performed all Sanger sequencing. For sequencing plasmids, typically 750 ng DNA and 1 µl primer (10 µM) in a 12 µl total volume of MQ water was submitted. Sequencing results were analysed using Sequencher program (Gene Codes corporation, USA).

5.2.5.8 Restriction digestion cloning

All restriction endonuclease enzymes, T4 DNA ligase and shrimp alkaline phosphatase were purchased from New England Biolabs (NEB, USA). All restriction digestion reactions were setup in 50 µl total volume and incubated as per manufacturer's recommendations. Restriction digestion reactions were heat inactivated as per manufacturer's instructions and column cleaned before ligation (Section 5.2.5.5). For cloning purposes, DNA fragments were isolated

by agarose gel electrophoresis followed by excision and column purification (Sections 5.2.5.4 and 5.2.5.5). Vectors digested with a single enzyme and DNA fragments digested with restriction enzymes that produce blunt ends were treated with shrimp alkaline phosphatase, heat inactivated, and column cleaned before ligation (Section 5.2.5.5). Ligation reactions using T4 DNA ligase were setup at either 1:3 or 1:5 ratios (vector:insert) and incubated either O/N at 4°C or at room temperature (RT) for 3 hours before transformation into *E. coli* cells.

5.2.5.9 Making calcium competent *E. coli* cells

The *E. coli* strain of interest was streaked onto a LB agar plate and grown O/N at 37° C. One well isolate colony was transferred into 5 ml LB broth and grown at 37°C with shaking (200 rpm) for 2 hours serving as a seed culture. The seed culture was transferred into 100 ml pre-warmed (37° C) LB broth and grown at 37° C with shaking (200 rpm) until the turbidity reached OD_{600}=0.4. The culture flask was put on ice for 15 minutes swirling occasionally before cells were transferred into pre-chilled centrifuge tubes and pelleted at 3,735 g for 10 minutes at 4° C. Cells were gently resuspended in 0.4 volumes of ice-cold TFB1 buffer (Table 5.1) and incubated on ice for 5 minutes. Cells were harvested by centrifugation at 3,735 g for 10 minutes and the pellet resuspended in 0.015 volumes of TFB2 buffer (Table 5.1) and incubated on ice for 20-30 minutes. Aliquots of 50 µl of cells were placed in pre-chilled 1.5 ml tubes and stored at -80° C.

5.2.5.10 Transformation of chemically competent *E. coli* cells

Transformation of *E. coli* cells was carried using the heat shock method as described previously with modifications (Hanahan, 1983). Chemically competent *E. coli* cells (Section 5.2.5.9), from -80° C storage, were thawed on ice. Plasmid DNA (10-100 ng) or 10 µl of ligation reaction (Section 5.3.5.1, and 5.3.7.1-2) mix was mixed with ice-cold cells and incubated on ice for 30 minutes. The cells were given a heat-shock by placing the tubes in a water bath set at 42° C for 45 seconds and were recovered on ice for 2 minutes. Cell recovery was continued by addition of 950 µl of LB broth and incubation at 37° C in a shaking incubator for 1 hour or at 25° C for 1.5 hour for temperature-sensitive plasmids. Recovered cells (100 µl) were plated on LB agar containing

appropriate antibiotic selection and incubated O/N at 37° C or 25° C for temperature-sensitive plasmids. Isolated single colonies were purified for further assessments. When blue-white screening was required, transformed cells were plated onto LB agar plates containing ampicillin (100 µg/ml), IPTG (0.2 mM final concentration) and X-gal (50 µg/ml final concentration).

5.2.5.11 Electrocompetent *E. coli* cells

A single isolated colony of the *E. coli* strain of interest was transferred into 5 ml of LB broth containing appropriate antibiotic selection and grown O/N at 37° C with shaking (200 rpm) or at 25° C if temperature sensitive, e.g., *E. coli* strains that contained pKD46 plasmid. The O/N culture was diluted into 50 ml of LB broth at a 1:100 ratio and incubation with shaking continued until the culture reached OD_{600} = 0.4. Cells were spun down at 3,735 g for 10 minutes at 4° C and the pellet was gently resuspended in 15 ml ice-cold Milli-Q water. Cells were pelleted and washed with ice-cold MQ water once again as described in the previous step. Cells were pelleted at 3,735 g for 10 minutes at 4° C, and the supernatant was decanted. Cells were resuspended in the residual liquid, aliquoted into 200 µl samples in 1.5 ml pre-chilled tubes and kept on ice for using on the same day within 1 hour.

5.2.5.12 Transformation of electrocompetent *E. coli* cells

Transformation of electrocompetent *E. coli* cells was accomplished by electroporation. Approximately 2 µg of purified DNA was mixed with one aliquot (200 µl) of electrocompetent *E. coli* cells immediately before electroporation and transferred into a pre-chilled 0.2 ml electroporation cuvette (Bio-Rad, USA). Cells were electroporated using a Gene Pulser II machine (Bio-Rad, USA) with parameters set at 2.5 kV, 200 Ω and 25 µF. Cells were immediately transferred into 5 ml LB broth pre-warmed to 37° C and recovered for 1 hour by incubation at 37° C with shaking before plating on LB agar containing appropriate antibiotic selection. Plates were incubated O/N at 37° C or at 25° C if temperature sensitive and single colonies were purified for further analyses.

5.2.6 Protein methods

5.2.6.1 Preparation of *E. coli* membrane fractions and whole-cell lysates

The *E. coli* strain of interest was cultured in 5 ml LB broth containing appropriate antibiotic selection and grown O/N at 37° C with shaking (200 rpm). The O/N seed culture was diluted 1:50 into 200 ml LB broth containing the same antibiotic selection and incubated at 37° C with shaking (200 rpm) until it reached OD_{600}=0.6. The culture was cooled down to 25° C and *E. coli* cells were induced by addition of IPTG (0.5 mM at final concentration), and incubation at 25° C was continued for another 3-6 hours. All following steps were performed at 4° C and cells and protein samples were kept on ice unless stated otherwise. Cells were harvested by centrifugation at 3750 x g for 10 minutes using Beckman Coulter Avanti J-26 XPI centrifuge and JLA-16.250 fixed-angle rotor (Beckman Coulter, USA). Cells were washed once with 1X TBS buffer, pH 7.5 (Table 5.1). Cells were then resuspended in 30 ml of crushing buffer (Table 5.1) and disrupted by one passage through a Multi Shot Cell Disrupter (Constant Systems Ltd) at 30,000 psi (Constant Systems Ltd, UK). Cell debris was removed by centrifugation (27,000 x g for 30 minutes) using a Beckman Coulter Avanti J-26 XPI centrifuge (Beckman Coulter, USA). The pellet (bacterial membranes) collected by ultracentrifugation at 125,000 x *g* for 1 hour using Optima™ L-100 XP Ultracentrifuge (Beckman Coulter, USA) was suspended in 300 µl of membrane suspension buffer (Table 5.1). Unless used straight away, the isolated membrane fractions were kept at -80° C.

To prepare whole cell lysates, the *E. coli* strain of interest was cultured in 5 ml LB broth containing appropriate antibiotic selection and grown O/N at 37° C with shaking (200 rpm). The O/N culture was diluted 1:50 into 20 ml LB broth containing the same antibiotic selection and incubated at 37° C with shaking (200 rpm) until it reached OD_{600}=0.6. The culture was cooled down to 25° C and the *E. coli* cells were induced by addition of IPTG (0.5 mM at final concentration), and incubation at 25° C was continued for another 3-6 hours. Whole cell lysates were prepared by collecting cells from 1 ml aliquots of broth cultures by centrifugation at 16,110 *x g* for 1 minute. Supernatant was removed and the cell pellet resuspended in 200 µL of 2x reducing sample buffer and incubated at 37° C for 30 minutes before loading in SDS PAGE gels (Table

5.1). Ten µL of each sample was used for analysing proteins in SDS PAGE gels for the purpose of WB analysis.

5.2.6.2 Protein quantification

The total protein concentration in the membrane fractions (Section 5.2.6.1) was quantified using a detergent compatible colorimetric protein assay kit (Bio-Rad, USA) according to the manufacturer's recommendations. This kit uses a modified Lowry assay method. A 96 well microtiter plate was used for performing the assays and known concentrations of bovine serum albumin were used for establishment of a standard curve. Each assay was performed in three replicates, test plates were scanned for absorbance measurement at 650 nm using a FLUOstar Omega spectrometer (BMG Labtech, Germany).

5.2.6.3 SDS PAGE gel electrophoresis

Membrane fractions were separated using both house-made and pre-cast (Bio-rad) SDS PAGE gels (Table 5.1). Membrane samples were mixed with SDS sample buffer (1X final concentration) and diluted with MQ water to final concentration of 1 mg/ml total protein. Diluted membrane samples were incubated at 37° C for 15-30 minutes before loading on the SDS PAGE gel. Precision Plus Protein Dual Colour (Bio-Rad) was used as an indicator of protein molecular size and 7.5 µl was loaded in first well. Proteins (10 µg total protein) were resolved by running the SDS PAGE gel at 80 V for 30 minutes and electrophoresis continued at 150 V until the dye front reached the bottom of the gel. Gels were transferred to PVDF membranes for WB analysis (Amersham™ Hybond® P Western blotting membranes) as described in Section 5.2.6.5 or stained using Coomassie brilliant blue (Section 5.2.6.4).

5.2.6.4 Coomassie blue staining

Coomassie brilliant blue staining and de-staining solutions were prepared as described previously (Table 5.1) (Sambrook and Russell, 2001). SDS PAGE gels (Section 5.2.6.3) were incubated in Coomassie blue staining solution at RT at least for 4 hours with slow shaking on an orbital shaker. They were then transferred to de-staining solution and left with slow shaking at RT until protein bands were brightly visible on the gels. Gels were either scanned using a digital scanner or imaged using a Gel Doc™ EZ Gel Imager (Bio-Rad, USA).

5.2.6.5 Protein transfer to PVDF membranes

Gels that were used for WB analysis were immersed in transfer buffer (Table 5.1) for equilibration and assembled with a polyvinylidene fluoride (PVDF) membrane by sandwiching between two absorbent papers sitting on sponge layers from both sides. The assembled transfer gel was placed in a gel tank within a gel holder with the membrane facing the anode and the tank filled with the same transfer buffer and ran O/N at 30 mA to allow all proteins to migrate onto the membrane.

5.2.6.6 Immunostaining

The PVDF membrane containing the transferred proteins was removed from the gel transfer assembly and washed once with 1x TTBS buffer (Table 5.1) for 5 minutes. It was then placed on a slow shaking rocker and (i) incubated in 50 ml blocking buffer (Table 5.1) at RT for 1 hour, (ii) washed with 1x TTBS buffer, (iii) incubated in 20 ml 1x TTBS buffer containing 1:5000 dilution of anti-6xHis epitope tag (rabbit) antibody (Rockland, Gilbertsville, USA) for 2 hours, (iv) washed three times with TTBS buffer, and (v) incubated in 20 ml 1x TTBS buffer containing 1:10,000 dilution of peroxidase-conjugated anti-rabbit IgG (goat) antibody (Rockland, Gilbertsville, USA) for 1 hour. For visualisation of protein size markers, 4 µl Precision Protein StrepTactin-HRP conjugate (Bio-Rad) was added to the previous solution, and unstained Precision Plus Protein standards (Bio-Rad) was used in SDS PAGE gel as per manufacturer's protocol. After the final incubation the membrane was washed five times with 1x TTBS buffer. Washed membrane was incubated at RT for 5 minutes after addition of 2 ml Clarity Western ECL substrate mix (1:1 ratio) (Bio-Rad) on the top of the membranes. The membrane was imaged using The ChemiDoc™ MP imaging system (Bio-Rad).

5.2.6.7 Batch style protein purification

Immobilized metal-ion affinity chromatography (IMAC) was used for purification of the MtrD protein as described below (Bornhorst and Falke, 2000). *E. coli* membrane fractions (Section 5.2.6.1) were solubilized in 4 volumes of solubilization buffer (Table 5.1) by incubation at 4°C for 2 hours with slow shaking using a rotary shaker. Insoluble material was removed by centrifugation at 16,110 *x g* for 30 minutes using an Eppendorf 5415 C

Microcentrifuge (Eppendorf, Germany). In a fresh 1.5 ml tube, 100 µL HIS-Select^{R} HF Nickel Affinity Gel (50% slurry, Sigma) was centrifuged at 5000 *x g* for 1 minute and the supernatant removed. The affinity gel was equilibrated and washed once with 4 volumes of equilibration/wash buffer (Table 5.1) and brought back to the original volume using the same buffer after the supernatant removed. The solubilised and clarified membrane proteins solution was incubated with 0.05 volumes of the washed and equilibrated affinity gel at 4°C for 30 minutes with slow rotary shaking. The bond affinity gel was washed four times in 20 volumes of the same wash buffer and wash solutions were saved. Proteins were eluted by addition of 100 µl of elution buffer (Table 5.1) to the washed affinity gel and incubation at 4° C for 20 minutes, and the eluate was saved. The elution step was repeated once again, and the eluate saved. Fifty µl of each of the initial solubilised and cleared membrane proteins solution, the saved wash solution from the first wash step, the first and second eluates were mixed with SDS-PAGE sample buffer and MQ water (to final concentration of 1X sample buffer) and incubated at 37° C for 15-30 minutes before loading on SDS-PAGE gels. Equal volume of each sample was loaded on a 1% house-made SDS PAGE gel and proteins were resolved by electrophoresis (Section 5.2.6.3).

5.3 Results

5.3.1 Deletion of the *acrAB* region from *E. coli* BL21(DE3) and DH5α strains

The bacteriophage λ Red recombinase-based gene inactivation method was used in this study (Datsenko and Wanner, 2000) to remove genes that may confound results and to make a hypersensitive transporter mutant for expression analyses. In this procedure, the sequence of the gene of interest is replaced with a selectable antibiotic resistance gene amplified by PCR using specific primers. These primers include in their sequences extensions homologous to sites adjacent to the gene of interest. Additionally, they incorporate sequences that anneal to short flippase recognition target (FLP recognition target; FRT) sequences flanking an antibiotic resistance gene in a plasmid that is used as the template DNA. This recombination system comprises three genes (*γ*, *β*, *exo*), whose products mediate homologous

recombination and promote a greatly enhanced rate of recombination in *E. coli* (Murphy, 1998).

E. coli BL21(DE3) and *E. coli* DH5α cells were transformed (Section 5.2.5.10) with the pKD46 plasmid (GenBank: AY048746.1) giving rise to *E. coli* BL21(DE3)/pKD46 and *E. coli* DH5α/pKD46 strains (Table 5.3). These strains express bacteriophage λ Red recombinase when induced with arabinose.

A Kan^R gene was used to replace the complete *acrAB* region on the chromosomes of the *E. coli* BL21(DE3)/pKD46 and DH5α/pKD46 strains. Forward and reverse primer sequences for amplification of the Kan^R gene from the pKD4 plasmid (GenBank: AY048743) were adopted from Hayashi and co-workers with a modification in the reverse primer to match the reference sequences (GenBank: CP001509.3, and GenBank: U00096.3) used in this study (Hayashi et al., 2016). The forward primer (MCdel*acrAB*-FRT-Kan-F) sequence contains a 50-nucleotide homologous extension for the sequence immediately upstream of the start codon of the *acrA* gene and a 20-nucleotide priming sequence that anneals to the sequence 408 bp upstream of the start codon of the Kan^R gene on the pKD4 plasmid (Table 5.2). The sequence of the reverse primer (MCdel*acrAB*-FRT-Kan-R) contains a 50-nucleotide homologous extension for the sequence 49 bp downstream from the stop codon of the *acrB* gene and a 20 bp priming sequence that anneals to the site 253 bp downstream from the stop codon of the Kan^R gene on the pKD4 plasmid (Table 5.4). Thus, the FRT-Kan^R fragment was PCR amplified using MCdel*acrAB*-FRT-Kan-F and MCdel*acrAB*-FRT-Kan-R primers and pKD4 as template DNA resulting in an *acrAB*:FRT-Kan^R DNA fragment of 1597 bp (Section 5.2.5.3). In order to increase the yield of the *acrAB*:FRT-Kan^R DNA fragment and remove unspecific bands, this PCR product was amplified again using a pair of nested primers (MCdel*acrAB*-Nested-F and MCdel*acrAB*-Nested-R) and the previous step PCR product as the template DNA (Table 5.4). The resultant PCR product (1597 bp) was transformed into *E. coli* BL21(DE3)/pKD46 and *E. coli* DH5α/pKD46 cells by electroporation (Section 5.2.5.11) and plated onto Kan (25 µg/ml) LB agar. Transformants were screened for loss of resistance to ERY and NOV, two AcrB substrates by patching onto agar plates containing ERY (8 and 16 µg/ml) and another series of agar plates containing NOV (16 and 32 µg/ml). Two representative

transformants that showed loss of resistance to ERY and NOV were subjected to MIC analysis for these two antibiotics. MIC analysis showed that the *E. coli* BL21(DE3)/pKD46 Δ*acrAB*-FRT-Kan^R and *E. coli* DH5α/pKD46 Δ*acrAB*-FRT-Kan^R representative strains lost resistance to ERY and NOV compared to their parental strains indicating deletion of the *acrAB* region from their chromosomes (Table 5.5).

The *E. coli* BL21(DE3)/pKD46 Δ*acrAB*-FRT-Kan^R and *E. coli* DH5α/pKD46 Δ*acrAB*-FRT-Kan^R strains were then transformed with the pCP20 plasmid in order to remove the Kan^R gene by a mechanism described by (Datsenko and Wanner, 2000). The transformed cells were grown on LB agar plates containing no antibiotic at 37° C in order to cure pKD46 and pCP20 plasmids and a single representative colony from each transformation was inoculated on both Amp and Kan plates.

Table 5.4: Oligonucleotides used in this study.

Name and purpose	**Sequence 5' to 3'**	**S[@]**
Deletion of *acrAB* from the chromosome of *E. coli* BL21(DE3) and DH5α		
MCdel*acrAB*-FRT-Kan-F	TTAACTTTTGACCATTGACCAATTT GAAATCGGACACTCGAGGTTTACA TGTGTAGGCTGGAGCTGCTTC	a
MCdel*acrAB*-FRT-Kan-R	TCGTATGAGATCCTGAGTTGGTGG TTCAATTACTCCTTAATGTTCGTAG GATGGGAATTAGCCATGGTCC	a
MCdel*acrAB*-Nested-F	TTAACTTTTGACCATTGAC	a
MCdel*acrAB*-Nested-R	TCGTATGAGATCCTGAGTTG	a
Check-del-*acrAB*-F	GCAGTGAACCAGAATAGC	a
Check-del-*acrAB*-R	GGATTATTAAATCTATTAG	a
Cloning of *mtrD* into pBluescript II		
mtrD-F1	GAGACTGCAGAGGAAGGCATCGA TGGCTAAATTC	a
mtrD-R1	GAGAGGATCCTTAATGGTGATGAT GGTGATGATATTGTTTATCGTCCG	a
Cloning of *mtrCDE* into pBluescript II		

Name and purpose	Sequence 5' to 3'	S[@]
mtrCDE-F1	GAGACTGCAGGATAGGATAAATAATGGCTTTTTATGC	a
mtrCDE-R1	GAGAGGATCCTTAATGGTGATGATGGTGATGTTTGCCGGTTTGGGTATC	a
Cloning of *mtrD* into pET21a(+)		
MCNdeI-*mtrD* F	GAGACATATGGCTAAATTCTTTATCGACCGCCCCATTTTCG	a
MCXhoI-*mtrD* R	TCTCCTCGAGATATTGTTTATCGTCCGAACCGGTTATACCCG	a
Cloning of *mtrC* into MCS-1 of pETDuet-1		
MCBamHI-*mtrC*-F	GAGAGGATCCGGCTTTTTATGCTTCTAAGGCGATGCGTGC	a
MCEcoRI-*mtrC*-SD-R	GAGAGAATTCTAATAATTCCTCTTATTTCGCTTCAGAAGCAGG	a
Cloning of the *mtrE* into MCS-1 of pETDuet-1		
MCEcoRI-*mtrE*-ATG F	GAGAGAATTCATGAATACTACATTGAAAACTACC	a
MCHindIII-*mtrE* R	TCTCAAGCTTTTTGCCGGTTTGGGTATCCCGTTTCAATCCGC	a
Cloning of *mtrD* into MCS-2 of pETDuet-1		
NdeI-*mtrD* F	GAGACATATGGCTAAATTCTTTATCGACCGCCCCATTTTCG	a
MCKpnI-*mtrD* R	TCTCGGTACCATATTGTTTATCGTCCGAACCG	a
Addition of new cloning sites with MCS of pBluescript II		
BsiWIFseI F	GATCCCGTACGGGCCGGCCG	a
BsiWIFseI R	AATTCGGCCGGCCCGTACGG	a
MCSpBSK F	GAGAGGATCCTTAATTAAGACGTCCCTGCAGGCGTACGGGCCGGCCGAATTCGAGA	a

Name and purpose	Sequence 5' to 3'	S[@]
MCSpBSK R	TCTCGAATTCGGCCGGCCCGTAC GCCTGCAGGGACGTCTTAATTAAG GATCCTCTC	a
Sequencing primers		
pET Upstream	ATGCGTCCGGCGTAGA	c
T7 terminator	GCTAGTTATTGCTCAGCGG	c
DuetDown1	GATTATGCGGCCGTGTACAA	c
DuetUp2	TTGTACACGGCCGCATAATC	c
M13 Fw	GTAAAACGACGGCCAGT	a
mtrCDE-SF4.1	GCAGTTGGGTACGGCAGAAG	a
mtrCDE-SR4.1	GCTCTGTTCCGTACCGTTTTC	a
M13 Rev	CAGGAAACAGCTATGAC	a
mtrCDE-SF2	CTGCGCCGGCAGATAGCCG	a
mtrCDE-SR2	CGGCTGCGCGCGGCATGGGC	a

@Source or reference: a, (Hayashi et al., 2016); b, (This study); c, (Novy et al., 2002);

Table 5.5: Antibiotic susceptibility of *E. coli* strains with the *acrAB* region removed.

	MIC (µg/ml)	
Strains	**ERY**	**NOV**
BL21(DE3)	128	128
DH5α	64	256
BL21(DE3)/pKD46 Δ*acrAB*-FRT-Kan^{R}	16	≤16
DH5α/pKD46 Δ*acrAB*-FRT-Kan^{R}	16	≤16

No growth of the bacteria on both antibiotic plates confirmed the loss of the pKD46 and pCP20 plasmids. PCR amplification using Check-del-*acrAB*-F and Check-del-*acrAB*-R primers and chromosomal DNA from the resulting transformants (*E. coli* BL21(DE3)Δ*acrAB* and *E. coli* DH5αΔ*acrAB*) as template showed a reduction in the amplicon size corresponding to the

deletion of the *acrAB* region (Sections 5.2.5.2, 5.2.5.3 and 5.2.5.4, and Table 5.4). Sequencing these PCR products verified removal of the *acrAB* region producing the strains *E. coli* BL21(DE3) Δ*acrAB* and *E. coli* DH5α Δ*acrAB* (Section 5.2.5.7). These *acrAB* deletion strains were used for analyses of the recombinant MtrD and MtrCDE constructs described in this chapter.

5.3.2 Cloning of the *mtrD* gene into the pBluescript SK (+) vector

The plasmid pBluescript SK (+) has been used successfully for cloning and expression of many genes (Chen and Seifert, 2014, Hassan et al., 2009). For example, it has been used for cloning, expression and functional analysis of the *qacA* gene from *S. aureus* in an *E. coli* heterologous host (Hassan et al., 2009). This vector possesses an extensive polylinker with 21 unique restriction enzyme recognition sites and allows for blue-white screening of transformation colonies when it is present in an appropriate host strain containing *lacZ*ΔM15 on an F´ episome such as *E. coli* DH5α (Alting-Mees and Short, 1989). Additionally, cloning of a gene of interest into pBluescript II downstream from the T7 promoter allows controlled expression of the inserted gene in λ-DE3 lysogenised *E. coli* strains such as BL21(DE3) by induction with IPTG.

5.3.2.1 Construction of an *mtrD* clone in pBluescript II

The *mtrD* gene spans 3204 bp (1106197-1109400) on the chromosome of *N. gonorrhoeae* FA19 (Genbank: CP_012026). The *mtrD* gene was PCR amplified using the primers *mtrD*-F1 and *mtrD*-R1 and the *N. gonorrhoeae* FA19 chromosome as template (5.2.5 and Table 5.3 and Table 5.4). The cloning was designed to insert *mtrD* downstream from the T7 promoter of pBluescript using *Pst*I and *Bam*HI restriction sites of the vector and the native *mtrD* ribosome binding site (RBS). At the same time a six-histidine residue (His6) affinity tag before the stop codon of the gene facilitating detection and purification was incorporated. The PstI-*mtrD*$_{His6}$-BamHI fragment (3254 bp) that was PCR amplified, was ligated into pBluescript after it was digested with the same enzymes, and then transformed into *E. coli* DH5α. (Section 5.2.5). Blue-white screening of the transformation product resulted in several white colonies potentially bearing the clone of interest. White colonies were screened by PCR (Section 5.2.5) using M13 F and M13 R primers to confirm

the insertion of *mtrD* into pBluescript. A representative plasmid was selected and the whole insert was sequenced using M13 F, *mtrCDE*-SF4.1, *mtrCDE*-SR4.1, and M13 R primers to verify the integrity of *mtrD*. This resulted in the creation of the pBluescript-*mtrD*$_{His6}$ construct (Section 5.2.5; Table 5.2, and Table 5.4; and Figure 5.1). This construct was subsequently analysed for the MtrD protein expression and resistance capacity of *E. coli* strains carrying the plasmid.

5.3.2.2 Expression of the recombinant MtrD protein from pBluescript-*mtrD*$_{His6}$

Expression of *mtrD* from the pBluescript-*mtrD*$_{His6}$ plasmid was analysed in five different *E. coli* strains including BL21(DE3), C43(DE3), BL21(DE3) Δ*acrAB*, BW25113(DE3) Δ*acrB*, and BW25113 (Δ*acrB* Δ*emrE* Δ*mdfA::kan*) (Table 5.3). Each strain was transformed with pBluescript-*mtrD*$_{His6}$ or pBluescript and grown in 200 ml batch cultures under non-induced and induced conditions (Sections 5.2.5 and 5.2.6). Cellular membranes isolated from each culture, or whole cell lysates, were assessed by WB for recombinant MtrD protein expression (Sections 5.2.5 and 5.2.6). All five strains carrying pBluescript-*mtrD*$_{His6}$ expressed the recombinant MtrD protein (Figure 5.2: WB analysis demonstrating expression of MtrD in *E. coli* strains.), with expression from λ-DE3 lysogenised strains significantly higher than that from non λ-DE3 lysogenised strains (Figure 5.2: WB analysis demonstrating expression of MtrD in *E. coli* strains.). Expression under IPTG-induced conditions from λ-DE3 lysogenised strains was slightly higher compared with that from under non-induced conditions (Figure 5.2).

5.3.2.3 Antibiotic resistance capacity of *E. coli* strains expressing the MtrD protein in pBluescript-*mtrD*$_{His6}$

To evaluate the resistance capacity of the MtrD protein, the MIC of *E. coli* strains carrying pBluescript-*mtrD*$_{His6}$ was analysed (5.2.4.2). These *E. coli* strains included; BL21(DE3) Δ*acrAB*, BW25113(DE3) Δ*acrB*, and BW25113 (Δ*acrB* Δ*emrE* Δ*mdfA::kan*). In each set of MIC experiments both the strain carrying the pBluescript-*mtrD*$_{His6}$ plasmid and the same strain carrying the empty vector pBluescript were assessed in parallel. MIC tests were conducted under both IPTG induced and non-induced conditions for those strains that carry λ-DE3 bacteriophage (5.2.4.2). MIC assays showed there wasn't an

increase in resistance to ERY (an MtrD representative substrate) for any of the *E. coli* strains carrying pBluescript-*mtrD*$_{His6}$ compared to the same strains carrying the empty vector in either of the conditions indicating a lack of MtrD activity (Table 5.6). Instead, under IPTG induced conditions MIC of ERY was

Figure 5.1: Map of the pBluescript-*mtrD*$_{His6}$ construct.

The recombinant *mtrD* gene is coloured brown with the direction of transcription shown and has 3222 nucleotides encoding the recombinant MtrD protein of 1073 amino acids with a calculated molecular size of 114.7 kDa. The map was generated using SnapGene. The T7 promoter, *Pst*I and *Bam*HI sites, *mtrD*-F1, *mtrD*-R1, M13 forward and M13 reverse primers, ampicillin resistance (*bla* or Amp^R), open reading frame (ORF) and its promoter, and pUC origin of replication (ori), are labelled.

decreased for strains carrying pBluescript-*mtrD*$_{His6}$ compared to the strains carrying the empty vector.

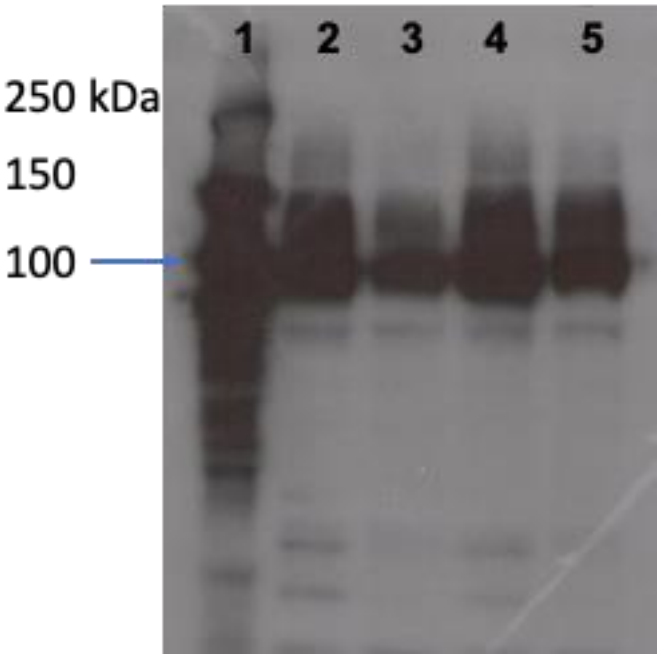

Figure 5.2: WB analysis demonstrating expression of MtrD in *E. coli* strains.

Membrane fractions (10 µg total protein) obtained from *E. coli* cells carrying pBluescript-*mtrD*$_{His6}$ were separated by 12% SDS-PAGE, transferred to a PVDF membrane, and probed with a 1:5000 dilution of anti-6xHis epitope tag (rabbit) antibody (Section 5.2.6). The full-length MtrD protein has a predicted molecular mass of ~114 kDa (Hagman et al., 1997), therefore expression of MtrD was determined by presence of a protein band at position approximately 100 kDa indicated on the left in kDa. Loading details are: 1) Precision Plus Protein Dual Colour; Bio-Rad; 2) BL21(DE3) carrying pBluescript-*mtrD*$_{His6}$ and induced with IPTG; 3) BL21(DE3) carrying pBluescript-*mtrD*$_{His6}$; 4) C43(DE3) carrying pBluescript-*mtrD*$_{His6}$ and induced with IPTG; 5) C43(DE3) carrying pBluescript-*mtrD*$_{His6}$.

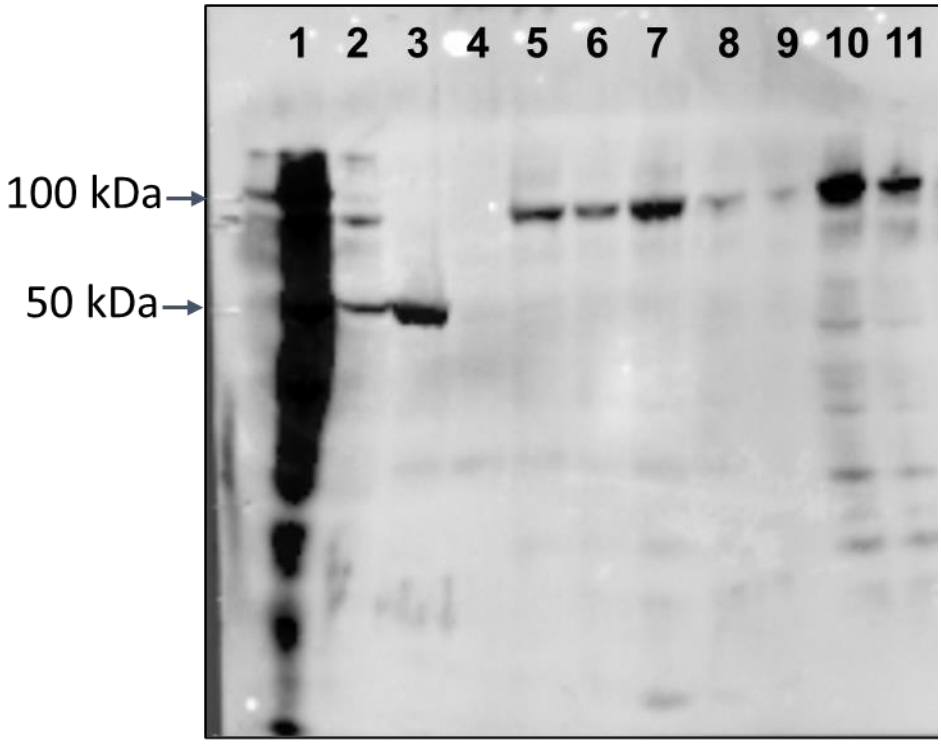

Figure 5.3: WB analysis demonstrating expression of MtrD or MtrE in *E. coli* strains.

Membrane fractions (10 µg total protein), or whole-cell lysates (10 µl) from *E. coli* cells were separated using SDS-PAGE, transferred to a PVDF membrane, and probed with a 1:5000 dilution of anti-6xHis epitope tag (rabbit) antibody (Section 5.2.6). The full-length MtrD protein has a predicted molecular mass of approximately 114 kDa while the MtrE protein has a mass of 50.4 kDa (Delahay et al., 1997, Hagman et al., 1997). Loading details are: 1) Precision Plus Protein Dual Colour; Bio-Rad; 2) DH5α-Δ*acrAB* carrying pBluescript-*mtrCDE*$_{His6}$; 3) AG100A carrying pBluescript-*mtrCDE*$_{His6}$; 4) BW25113 (Δ*acrB* Δ*emrE* Δ*mdfA::kan*) carrying pBluescript-*mtrCDE*$_{His6}$; 5) BL21(DE3) *ΔacrAB* carrying pBluescript-*mtrD*$_{His6}$ induced with IPTG; 6) BL21(DE3) *ΔacrAB* carrying pBluescript-*mtrD*$_{His6}$; 7) BW25113(DE3) *ΔacrB* carrying pBluescript-*mtrD*$_{His6}$ induced with IPTG; 8) BW25113(DE3) *ΔacrB* carrying pBluescript-*mtrD*$_{His6}$; 9) BW25113 (Δ*acrB* Δ*emrE* Δ*mdfA::kan*) carrying pBluescript-*mtrD*$_{His6;}$ 10) BW25113(DE3) Δ*acrB* carrying pGCC4-*mtrD*$_{His6}$ induced with IPTG; 11) BW25113(DE3) Δ*acrB* carrying pGCC4-*mtrD*$_{His6}$.

5.3.3 Cloning of the entire *mtrCDE* operon into pBluescript and expression in various *E. coli* host strains

Expression of the recombinant MtrD protein from the pBluescript-*mtrD*$_{His6}$ plasmid in various *E. coli* strains did not result in any increase in resistance to the MtrD substrate, ERY, as described in the previous section. This lack of MtrD activity may be because the protein is not partnering with the components of the AcrABTolC system, namely, the AcrA adaptor protein or the TolC channel protein, or both to make a functional pump. It is also possible that the expression of MtrD from pBluescript-*mtrD*$_{His6}$ is not optimally controlled, making host cells sick and susceptible to antibiotics. Therefore, the entire *mtrCDE* operon was cloned in the pBluescript II SK (+) vector to enable the expression of all three proteins, namely MtrC, MtrD, and MtrE, of the efflux system from one vector at the same time, as described below.

5.3.3.1 Construction of the recombinant *mtrCDE* operon in pBluescript II vector

The *mtrCDE* operon was PCR amplified using the primers *mtrCDE*-F1 and *mtrCDE*-R1 and FA19 chromosomal DNA as template (Section 5.2.5, and Table 5.3 and Table 5.4). The *mtrCDE* region spans 5910 bp (1104741 to 1110650) on the of FA19 chromosome (Genbank: CP_012026). The cloning was designed to insert the *mtrCDE* operon between *Pst*I and *Bam*HI restriction sites under control of T7 promoter. The *mtrCDE*-F1 primer includes in its sequence a *Pst*I restriction site at the 5'-end immediately before a sequence that corresponds to the putative RBS of the of the *mtrC* gene followed by its start codon (Table 5.4). The *mtrCDE*-R1 primer was designed to incorporate a BamHI restriction site at the 3'-end of the *mtrE* gene (the last gene of the operon) after an incorporated six histidine affinity tag followed by an incorporated stop codon (Table 5.4). The PstI-*mtrCDE*$_{His6}$-BamHI fragment (5961 bp) that was PCR amplified, was ligated into pBluescript after it was digested with the same enzymes, and then transformed into *E. coli* DH5α. After blue-white screening, three white colonies were identified as potentially containing the clone of interest. PCR screening was performed using M13 F and M13 R primers (Section 5.2.5) to confirm the insertion of *mtrCDE* into pBluescript. Linearized plasmids from each of these three transformants were verified to be 8896 bp in size, corresponding to the pBluescript-*mtrCDE*$_{His6}$

construct (Table 5.2 and Section 5.2.5). To confirm the integrity of *mtrCDE* within pBluescript, a representative plasmid was sequenced using the following primers: M13 Fw, *mtrCDE*-SF2, *mtrD*-F1, *mtrCDE*-SF4.1, *mtrCDE*-SR4.1, *mtrD*-R1, *mtrCDE*-SR2, and M13 Rev (Section 5.2.5, and Table 5.4). The sequencing confirmed the presence of *mtrCDE* within pBluescript, resulting in the pBluescript-*mtrCDE*$_{His6}$ construct (Table 5.2, and Figure 5.4)

5.3.3.2 Expression of recombinant MtrCDE from the pBluescript-*mtrCDE*$_{His6}$ plasmid

The expression of the recombinant MtrC, MtrD, and MtrE proteins from the pBluescript-*mtrCDE*$_{His6}$ plasmid was analysed initially in three λ-DE3 lysogenised *E. coli* strains including, BL21(DE3), BW25113(DE3) Δ*acrB*, and BW25113(DE3) Δ*acrAB* (Table 5.3). Each strain was separately transformed with the pBluescript-*mtrCDE*$_{His6}$ plasmid and the pBluescript empty vector. Transformed cells were plated onto LB agar plates containing Amp (100 µg/ml) (Section 5.2.6). While numerous transformant colonies were obtained on the LB agar plates for all three strains transformed with the empty vector, no transformant colonies were obtained on the selection plates for any of the three λ-DE3 lysogenized strains transformed with pBluescript-*mtrCDE*$_{His6}$ after several attempts. These results show that the transformation of pBluescript-*mtrCDE*$_{His6}$ into these λ-DE3 lysogenised *E. coli* strains is lethal and will not produce transformants on a selection plate containing Amp (100 µg/ml).

The expression of recombinant MtrCDE efflux proteins from the pBluescript-*mtrCDE*$_{His6}$ plasmid was subsequently analysed in four non-λ-DE3 lysogenised *E. coli* strains including DH5α, DH5α Δ*acrAB*, AG100A, and BW25113 (Δ*acrB* Δ*emrE* Δ*mdfA::kan*) (Table 5.2). Like in previous analyses, these strains were separately transformed with the pBluescript-*mtrCDE*$_{His6}$ plasmid and pBluescript empty vector, and transformed cells were selected on Amp plates (Section 5.2.5). Transformation of both the pBluescript-*mtrCDE*$_{His6}$ plasmid and the empty vector resulted in numerous transformant colonies on the selection plates. WB analysis confirmed the expression of the MtrE protein within the membranes of DH5α cells (Figure 5.5), and in whole-cell lysates of DH5α Δ*acrAB*, and AG100A cells (Figure 5.3), as determined by presence of a protein band at approximately 50 kDa in WB images (Section 5.2.5, and .

Table 5.6: Antibiotic susceptibility of *E. coli* strains expressing MtrD alone or the whole MtrCDE efflux system from various constructs.

	MIC (µg/ml)				
	OXA		ERY		CV
Strain	**+ IPTG**	**- IPTG**	**+ IPTG**	**- IPTG**	**- IPTG**
BL21(DE3) *ΔacrAB*/pBluescript-*mtrD*$_{His6}$	-	-	≤ 2	4	-
BL21(DE3) *ΔacrAB*/pBluescript	-	-	4	4	-
BW25113(DE3) *ΔacrB*/pBluescript-*mtrD*$_{His6}$	-	-	2	2	-
BW25113(DE3) *ΔacrB*/pBluescript	-	-	2	2	-
BW25113 (Δ*acrB* Δ*emrE* Δ*mdfA::kan*) /pBluescript-*mtrD*$_{His6}$	-	-	-	2	-
BW25113 (Δ*acrB* Δ*emrE* Δ*mdfA::kan*) /pBluescript	-	-	-	2	-
DH5α /pBluescript-*mtrCDE*$_{His6}$	-	-	-	32	2
DH5α /pBluescript	-	-	-	128	8
DH5α Δ*acrAB*/pBluescript-*mtrCDE*$_{His6}$	-	1	-	2	-
DH5α Δ*acrAB*/pBluescript	-	≥ 8	-	2	-
AG100A/pBluescript-*mtrCDE*$_{His6}$	-	2	-	4	-

	MIC (µg/ml)				
	OXA		**ERY**		**CV**
Strain	**+ IPTG**	**- IPTG**	**+ IPTG**	**- IPTG**	**- IPTG**
AG100A/pBluescript	-	≥ 8	-	4	-
BW25113(DE3) *ΔacrB*/pGCC4-*mtrD*$_{6His}$	1	1	≤ 2	16	-
BW25113(DE3) *ΔacrB*/pGCC4	1	1	-	16	-

OXA, oxacillin; ERY, erythromycin; CV, crystal violet; +IPTG, culture induced with IPTG; -IPTG, no IPTG induction; “-“ Not determined

Figure 5.3 and Figure 5.5). The expression of the MtrE protein, which was encoded as the last gene in the *mtrCDE* operon and contained the 6-histidine tag, indicated the expression of the whole operon.

This protein expression required no IPTG induction likely because of a leaky expression of the *mtrCDE* operon from pBluescript as the host strain lacking the T7 polymerase. This was not surprising as leaky expression of the membrane protein, QacA has already been shown from pBluescript (Hassan et al., 2009).

Expression of the MtrCDE efflux pump proteins from the pBluescript-*mtrCDE*$_{His6}$ plasmid was not detected by WB in the whole cells lysate of BW25113 (Δ*acrB* Δ*emrE* Δ*mdfA::kan*) cells transformed with this plasmid (Figure 5.2).

5.3.3.3 Antibiotic resistance capacity of *E. coli* strains expressing MtrCDE efflux proteins from the pBluescript-*mtrCDE*$_{His6}$ plasmid

To assess MtrCDE activity, the resistance capacity of *E. coli* strains carrying the pBluescript-*mtrCDE*$_{His6}$ plasmid was assessed by determining MICs for three representative MtrD substrates, ERY, OXA, and CV, using the agar dilution method (Section 5.2.4). These *E. coli* strains included DH5α, DH5α Δ*acrAB*, and AG100A (Table 5.3). In each set of MIC experiments both the strain carrying the pBluescript-*mtrCDE*$_{His6}$ plasmid and the same strain carrying the empty vector pBluescript were assessed in parallel. MIC tests were only conducted without IPTG induction because the expression of the *mtrCDE* operon from pBluescript-*mtrCDE*$_{His6}$ is regulated by the T7 promoter, which requires T7 RNA polymerase for transcription. However, these strains lack T7 RNA polymerase, which is why IPTG induction was not used (Section 5.2.4). The MIC assays showed no increase in resistance to any of the three compounds for all of the *E. coli* strains carrying pBluescript-*mtrCDE*$_{His6}$ compared to the same strains carrying the empty vector, indicating a lack of all their activity (Table 5.6). Instead, in some cases cells carrying the pBluescript-*mtrCDE*$_{His6}$ plasmid were slightly more susceptible to these antimicrobials compared to the cells carrying empty vector likely impacting on the normal cell growth (Table 5.6).

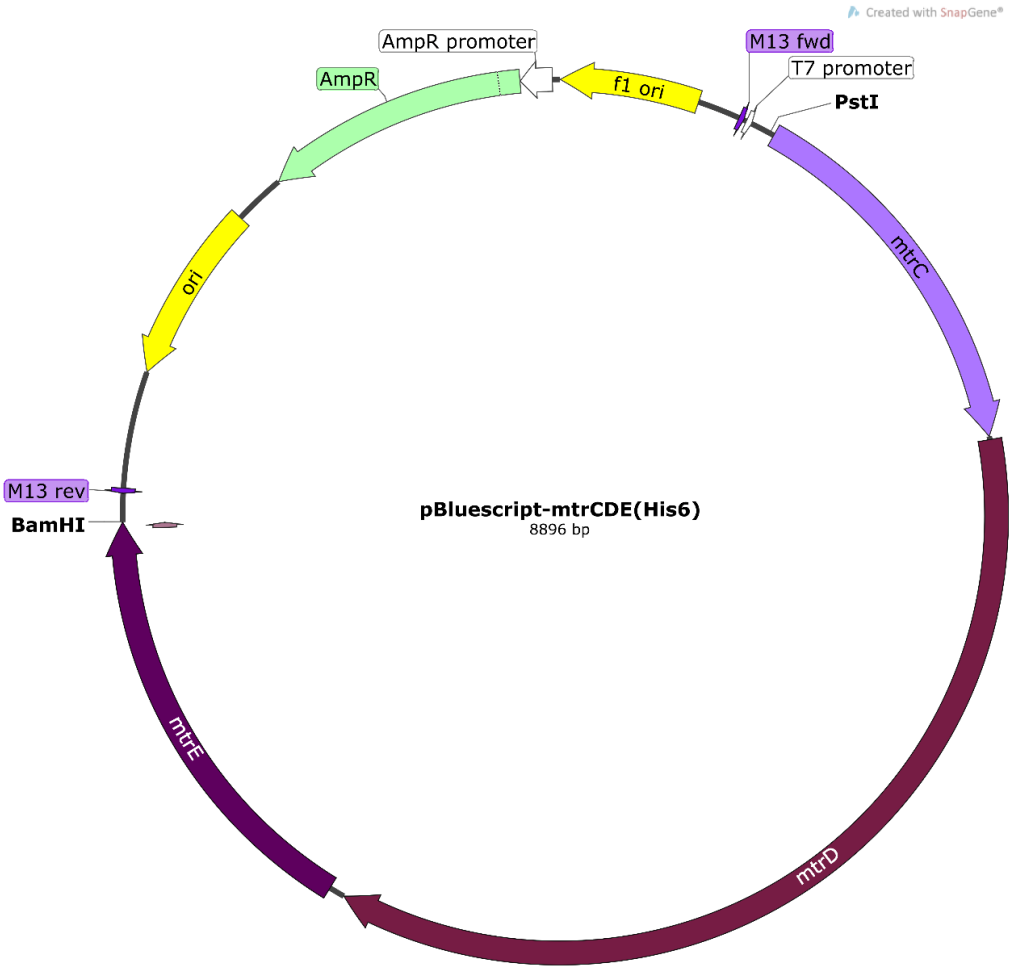

Figure 5.4: Map of the pBluescript-*mtrCDE*$_{His6}$ construct.

This is a map of the pBluescript-*mtrCDE*$_{His6}$ construct, where the recombinant *mtrC, mtrD,* and *mtrE* genes are coloured lavender, plum, and violet, respectively. The His6 affinity-tagged *mtrE* gene, which is the last gene in the operon, contains 1422 nucleotides and encodes the recombinant MtrE protein of 473 amino acids with a calculated molecular size of 51.2 kDa. The map was generated using SnapGene. The T7 promoter, *Pst*I and *Bam*HI sites, M13 forward and M13 reverse primers, ampicillin resistance (*bla* or Amp^R) ORF and its promoter, and pUC origin of replication (ori) are labelled.

5.3.4 Cloning of *mtrD* into the pGCC4 shuttle vector and expression in *E. coli*

A shuttle vector, such as pGCC4, provides a significant advantage for studying *N. gonorrhoeae* genes in their natural host (Dillard, 2011, Mehr and Seifert, 1997). It allows construction and propagation of genes in *E. coli*, which can then be incorporated into *N. gonorrhoeae*. The vector integrates genes

into the gonococcal chromosome between the *lctP* and *aspC* genes and places them under the control of the *lac* regulatory sequences, enabling inducible gene expression. Insertions between these genes do not affect gene expression or the gonococcal phenotype (Dillard, 2011, Mehr and Seifert, 1997). As a useful selectable marker for *N. gonorrhoeae*, pGCC4 contains *ermC* for ERY resistance (Dillard, 2011, Mehr and Seifert, 1997). Transforming *N. gonorrhoeae* and selecting for ERY resistance allows for selecting bacteria that have incorporated the constructed gene via double crossover recombination. For instance, the manipulation of the *mtrD* gene is easier in *E. coli* and can subsequently be introduced into the native host. Establishing a host-vector system is crucial for characterizing the resistance mechanisms employed by the MtrD efflux transporter. Modifying *mtrD* can be achieved in *E. coli*, while the function or structure of the WT or mutant MtrD proteins can be studied in *N. gonorrhoeae*. Consequently, we used the pGCC4 vector to construct a *mtrD* clone, as described in the next section.

5.3.4.1 Construction of the pGCC4-*mtrD*$_{His6}$ plasmid

The construction of a WT *mtrD* clone in the pGCC4 vector (pGCC4-*mtrD*$_{His6}$) is detailed in Section 2.7.4. The subsequent sections describe the expression of the WT MtrD protein from pGCC4-*mtrD*$_{His6}$, and the resistance conferred by this recombinant WT MtrD in *E. coli*.

5.3.4.2 Expression of MtrD from pGCC4-*mtrD*$_{His6}$

The *E. coli* BW25113(DE3) Δ*acrB* strain was transformed with the pGCC4-*mtrD*$_{His6}$ plasmid and separately with the pGCC4 empty vector and the transformed cells were selected for Kan^{R}. A representative colony from each transformation was grown in 200 ml batch cultures under both non-induced and induced conditions with IPTG, as described in section 5.2.6.

A whole-cell lysate was prepared from an aliquot of each culture and analysed via WB for recombinant MtrD protein expression, according to Section 5.2.6. The WB analysis confirmed the expression of recombinant MtrD protein in BW25113(DE3) Δ*acrB* cells under both IPTG-induced and non-induced conditions. However, a higher amount of protein was observed in the induced cells (Figure 5.3).

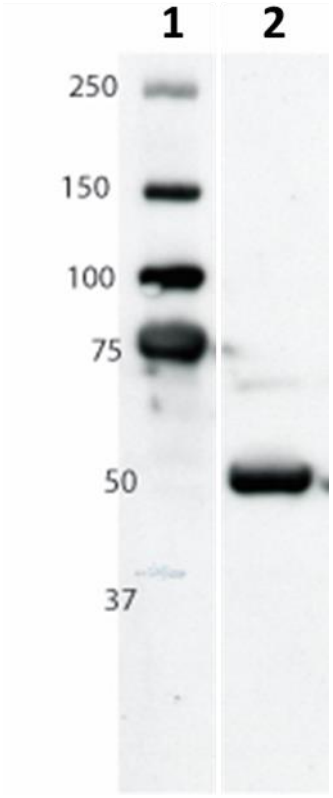

Figure 5.5: WB analysis demonstrating the expression of the MtrE protein in *E. coli* DH5α.

Proteins from the membrane fraction (10 µg total protein) of *E. coli* DH5α cells were isolated (Section 5.2.6) and separated by SDS-PAGE according to section 5.2.6. The transferred membrane was then probed with a 1:5000 dilution of anti-6xHis epitope tag (rabbit) antibody as described (Section 5.2.6). The predicted molecular weight of the full-length MtrE protein is 50.4 kDa (Delahay et al., 1997). Thus, the expression of MtrE was confirmed by the presence of a protein band at approximately 50 kDa using protein molecular mass standard (Precision Plus Protein Dual Colour; Bio-Rad), with the molecular masses of the standards indicated on the left in kDa. Lane 2 shows the membrane fraction from *E. coli* DH5α cells carrying the pBluescript-*mtrCDE*$_{His6}$ plasmid.

5.3.4.3 Antibiotic resistance capacity of *E. coli* BW25113(DE3) Δ*acrB* carrying the pGCC4-*mtrD*$_{His6}$ plasmid

The resistance of *E. coli* BW25113(DE3) Δ*acrB* cells harbouring pGCC4-*mtrD*$_{His6}$ was investigated against two known MtrD substrates, namely ERY and OXA. Resistance analysis was carried out by determining the MIC of BW25113(DE3) Δ*acrB* cells carrying (i) pGCC4-*mtrD*$_{His6}$ under uninduced and

(ii) induced conditions, as well as (iii) pGCC4 under uninduced and (iv) induced conditions, as described in Section 5.2.4. The results showed that the presence of the pGCC4-*mtrD*$_{His6}$ plasmid did not increase resistance to either ERY or OXA, irrespective of the induction conditions (Table 5.6).

5.3.5 Cloning of the *mtrD* gene into the pET21a vector

The pET vector system (Novagen) has long been used for the cloning and expression of recombinant proteins, including efflux transport proteins in *E. coli* (Rouquette-Loughlin et al., 2018a, Tsutsumi et al., 2019). One of the vectors in this series is pET21a (+), which contains the *lacUV5* promoter, allowing for controlled expression of the target gene cloned under regulation of a T7 promoter.

Recent advances in technology, such as styrene maleic acid lipid particles (SMALPs) solubilization and crystallography using nanodiscs, have significantly improved structural, biophysical, and functional studies of membrane proteins (Broadbent et al., 2022, Hardy et al., 2016, Laurence et al., 2022, Lyu et al., 2020, Pollock et al., 2018). These processes require large amount of pure, active protein. The pET vectors have been successfully used to overexpress many transporter proteins used in these studies. Thus, pET21a (+) expression vector was used to clone *mtrD* and to produce a high quantity of active MtrD protein for further characterisation.

5.3.5.1 Construction of an *mtrD* clone in pET21a expression vector

The *mtrD* gene was amplified using the MCNdeI-*mtrD* F and MCXhoI-*mtrD* R primers with *N. gonorrhoeae* FA19 chromosomal DNA as the template (Section 5.2.5, and Table 5.4) The primer sequences were adopted from Janganan et al with minor modifications (Janganan et al., 2011b). The MCNdeI-*mtrD* F primer contains an *Nde*I restriction site at the 5'-end and a sequence that anneals to 34 nucleotides downstream of and including the start codon of the *mtrD* gene. This primer design allows for the cloning of *mtrD* in front of the RBS of the pET21a vector. The MCXhoI-*mtrD* R primer contains an *Xho*I restriction site at the 5'-end, followed by a 32-nucleotide sequence that anneals to the end of the *mtrD* gene before its stop codon. This primer clones the *mtrD* gene in frame with a 6x histidine affinity tag sequence on the pET21a vector and at the 3'-terminus of the *mtrD* gene. The PCR amplified

NdeI-*mtrD*-XhoI fragment (3218 bp) was ligated into pET21a, which was digested with the same enzymes. Transformation of the ligation material into *E. coli* DH5α cells and selection on Amp plates produced several transformants (Section 5.2.5). PCR screening of transformation colonies using pET Upstream and T7 terminator primers (Table 5.4) and the extracted plasmids as template DNA resulted in one plasmid potentially bearing *mtrD*. Sequencing using pET Upstream, *mtrCDE*-SF4.1, *mtrCDE*-SR4.1 and T7 terminator primers confirmed integrity of the insert, resulting in pET21a-*mtrD*$_{His6}$ (Section 5.2.5; and Table 5.2 and Table 5.4).

5.3.5.2 Expression of MtrD protein from the pET21a-*mtrD*$_{His6}$ plasmid

We examined the expression of the MtrD protein in two strains of *E. coli*, BL21(DE3) and C43(DE3), where each strain was transformed separately with both the pET21a-*mtrD*$_{His6}$ plasmid and the control plasmid, pET21a (Sections 5.2.5 and 5.2.6). Batch cultures of 200 ml were prepared from each transformation, with or without IPTG induction (Section 5.2.6). Cellular membranes were isolated from each culture and assessed for MtrD protein expression by western blotting (Section 5.2.6). The WB analysis revealed that the recombinant MtrD protein was expressed only in cultures induced with IPTG in the BL21(DE3) and C43(DE3) strains carrying the pET21a-*mtrD*$_{His6}$ plasmid (Figure 5.6). The membrane fractions obtained from BL21(DE3)/ pET21a-*mtrD*$_{His6}$ cultures were used for the purification of MtrD, as described in the next section.

5.3.6 Purification of recombinant MtrD protein

In order to thoroughly characterise MtrD activity, it is necessary to obtain a highly purified protein suitable for various analytical techniques, such as isothermal calorimetry (ITC), surface plasmon resonance (SPR), liposome reconstitution, and crystallography studies. To achieve this, *E. coli* BL21(DE3) was utilised to overexpress MtrD, carrying the pET21a-*mtrD*$_{His6}$ plasmid as described in sections 5.2.5 and 5.2.6. A single, well-isolated colony from a pET21a-*mtrD*$_{His6}$ transformation plate was inoculated into 10 ml LB broth containing 100 µg/ml Amp and grown O/N. The following day, 200 ml of LB broth with Amp was inoculated at a 1/100 dilution ratio and incubated at 37° C with shaking at 200 rpm until the OD600 reached 0.6. The cultures were then

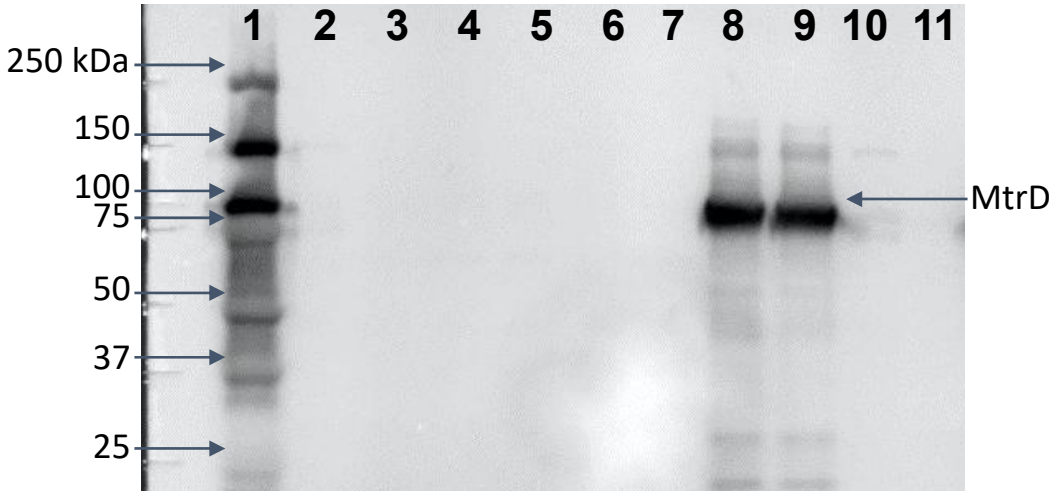

Figure 5.6: The expression of MtrD protein in different *E. coli* strains.

In Figure 4.6 (A), the expression of MtrD in different *E. coli* strains is shown through WB analysis. To do this, 10 µg of membrane fractions (total protein) from *E. coli* cells were separated by 12% SDS-PAGE, transferred to a PVDF membrane, and probed with a 1:5000 dilution of anti-6xHis epitope tag (rabbit) antibody (Section 5.2.6). The full-length MtrD protein has an expected molecular mass of approximately 114 kDa (Hagman et al., 1997), and therefore, the presence of a protein band at ~100 kDa, using a protein molecular mass standard (Lane 1; Precision Plus Protein Dual Colour; Bio-Rad) on the left in kDa, was used to assess the expression of MtrD. Each lane on the gel image is identified with a number that corresponds to the membrane sample loaded and are as follows: lane 2) BL21(DE3) Δ*acrAB*/pETDuet-*mtrCE-mtrD* induced with IPTG; lane 3) BW25113(DE3) Δ*acrAB*/pETDuet-*mtrCE-mtrD* induced with IPTG; lane 4) BL21(DE3) Δ*acrAB*/pETDuet-1 empty vector; lane 5) BW25113(DE3) *ΔacrAB*/pETDuet-1 empty vector; lane 6) BL21(DE3) Δ*acrAB*/pETDuet-*mtrCE* induced with IPTG; lane 7) BL21(DE3) Δ*acrAB*/pETDuet-*mtrC* induced with IPTG; lane 8) BL21(DE3)/pET21a-*mtrD*$_{His6}$ induced with IPTG; lane 9) C43(DE3)/pET21a-*mtrD*$_{His6}$ induced with IPTG; lane 10) BL21(DE3)/pET21a-*mtrD*$_{His6}$ with no IPTG induction; lane 11) C43(DE3)/pET21a-*mtrD*$_{His6}$ with no IPTG induction.

cooled to 25° C, and IPTG was added to a final concentration of 0.5 mM. After a further incubation period of 3-6 hours at 25° C, *E. coli* membrane fractions were prepared from these cultures (Section 5.2.6). The total protein concentration of each membrane fraction achieved was approximately 7

mg/ml, with the total volume of each sample being approximately 400 µl. The MtrD protein was subsequently purified using IMAC (Section 5.2.6), by taking a 100 µl aliquot of membrane fractions. Imidazole was added to a final concentration of 250 mM for elution of the nickel-bound proteins.

The SDS-PAGE analysis revealed a strong band present in the eluate and affinity matrix samples, slightly below 150 kDa, which is likely to be the MtrD protein (Figure 5.7 A; Lanes 4 and 5). To confirm whether the observed strong bands for the eluate and gel particle samples on the SDS-PAGE gel belong to the MtrD protein, the duplicate SDS-PAGE gel from the same experiment underwent WB analysis. The WB analysis showed two strong chemiluminescence bands at the same positions on the blot image, confirming the presence of the MtrD protein in the eluate and gel particles (Figure 5.7 B; lanes 4 and 5).

To further verify whether the observed protein bands for the eluate and gel particles samples on the SDS-PAGE gel belong to the purified MtrD protein in terms of their molecular weights, another aliquot of each of the first and second eluates was applied to a 12% pre-cast SDS-PAGE gel. This SDS-PAGE protein electrophoresis confirmed that the purified protein is located slightly above 100 kDa on the SDS-PAGE gel and likely belongs to the MtrD protein (Figure 5.8A, lanes 2 and 3).

To confirm the reproducibility of the method used for the purification of the MtrD protein expressed in BL21(DE3)/pET21a-*mtrD*$_{His6}$ membranes, another batch style purification was performed using the same reagents and method described in Section 5.2.6. However, one modification was made to the method, which included increasing the imidazole concentration in the equilibration/wash solution from 10 mM to 20 mM in order to reduce or remove nonspecific proteins that remained in eluates during the first attempt. The SDS-PAGE electrophoresis analysis showed that this batch style purification method successfully purified the recombinant MtrD protein from the *E. coli* membrane fractions with good quality in terms of purity as judged visually (Figure 5.8B).

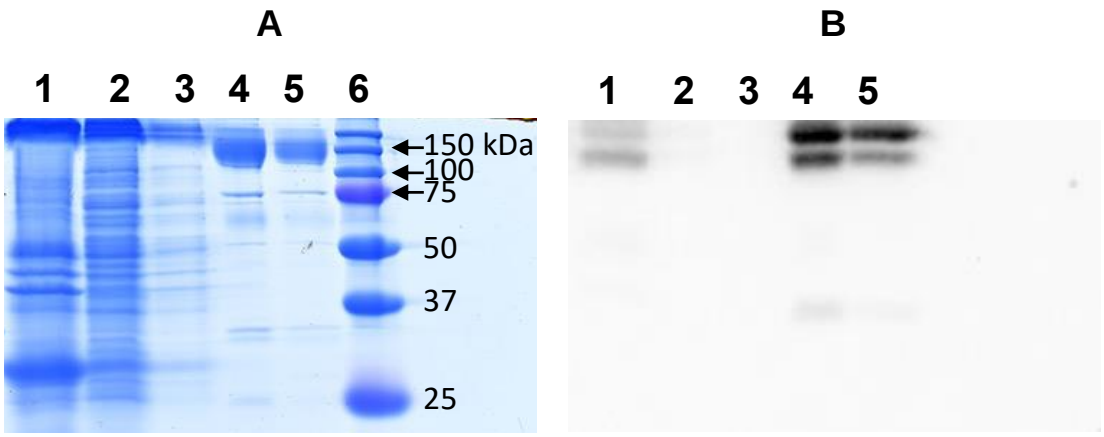

Figure 5.7: Purification of the MtrD protein from membrane fractions of *E. coli* BL21(DE3)/pET21a-*mtrD*His6 cells expressing MtrD.

(A) SDS-PAGE analysis of the purification process (Section 5.2.6) with lanes corresponding to: 1) insoluble material; 2) solubilised membrane proteins; 3) first wash solution; 4) first eluate; 5) gel particles after elution; and 6) protein molecular mass standards (Precision Plus Protein Dual Colour; Bio-Rad). Samples were loaded with 4x SDS loading buffer (1x in final concentration) into a 12% gel (Section 5.2.6), electrophoresed, and stained with Coomassie blue. The purified MtrD, identified by a strong band, appeared between 150 and 100 kDa standards (refer to predicted molecular mass in (Hagman et al., 1997).

(B) Western blot analysis confirmed MtrD purification using anti-6xHis epitope tag antibody (Section 5.2.6). Bands in Lanes 4 and 5, aligned with SDS-PAGE images (Figure 5.7 A), indicated MtrD presence between 100 and 150 kDa standards.

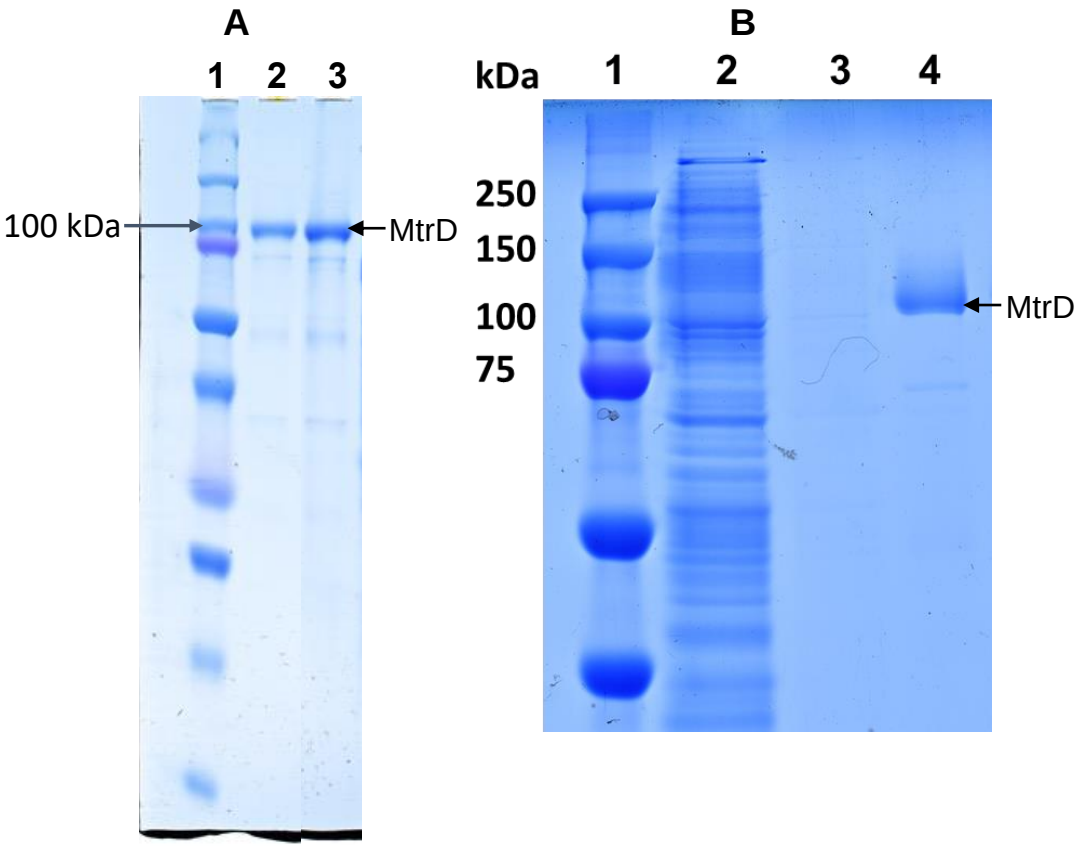

Figure 5.8: SDS-PAGE analysis of MtrD protein purification.

(A) Purification from *E. coli* BL21(DE3)/pET21a-*mtrD*$_{His6}$ cells involved loading 20 µl samples into an SDS-PAGE gel for the first and second eluates (Lanes 2 and 3). Bands slightly above the 100 kDa standard confirmed MtrD protein presence using 250 mM imidazole. (B) Reproducibility and efficiency were demonstrated using the modified method, with 20 µl samples loaded for supernatant (Lane 2), first wash solution (Lane 3), and first eluate (Lane 4). A strong band above the 100 kDa standard in Lane 4 indicated purified MtrD, with minimal nonspecific proteins. Precision Plus Protein Dual Colour served as the molecular mass standard (Lane 1 in each gel).

5.3.7 Cloning of the *mtrC*, *mtrD* and *mtrE* genes into pETDuet1 vector individually and in combinations

pETDuet-1 has two multiple cloning sites (MCS-1, and MCS-2) allowing for the cloning of two genes (Novy et al., 2002). Each MCS is preceded by a T7 promoter, a lac operator, and an RBS. This expression vector has been used successfully for cloning and co-expression in *E. coli* of efflux transporters composed of multiple genes (Esteves et al., 2021). The use of the pETDuet1 vector was considered as a cloning strategy to co-express all three proteins of the MtrCDE system simultaneously in *E. coli*.

5.3.7.1 Construction of the pETDuet-*mtrC* clone

The strategy for cloning the *mtrC*, *mtrD*, and *mtrE* genes into the pETDuet1 vector involved inserting the *mtrC* and *mtrE* genes into MCS-1 and the *mtrD* gene into MCS-2. The first step was to clone the *mtrC* gene into MCS-1.The *mtrC* gene was PCR amplified from *N. gonorrhoeae* FA19 chromosomal DNA using MCBamHI-*mtrC*-F and MCEcoRI-*mtrC*-SD-R primers (Table 5.4 and Section 5.2.5). The MCBamHI-*mtrC*-F primer contained a *Bam*HI restriction enzyme site at the 5'-end and a 30-nucleotide sequence at its 3'-end that annealed downstream of the *mtrC* start codon. This primer enabled the placement of *mtrC* in front of and in-frame with a sequence in the pETDuet-1 vector that contained a RBS, a start codon (ATG), and a 6x histidine amino acid affinity tag. The MCEcoRI-*mtrC*-SD-R primer contained an *Eco*RI recognition site at the 5'-end, followed by a 12-nucleotide Shine-Dalgarno sequence adapted from Chen et al. (1994), and a 21-nucleotide sequence at its 3'-end that annealed to the end of the *mtrC* gene (Chen et al., 1994). This Shine-Dalgarno sequence provided the RBS for *mtrE*, which was designed to be cloned downstream of *mtrC* in MCS-1 of the vector. After digestion with *Bam*HI and *Eco*RI enzymes, the PCR amplified *mtrC* gene and the pETDuet-1 vector were ligated by standard methods (Section 5.2.5). The ligation material was transformed into *E. coli* DH5α cells, and transformed cells were selected for resistance to Amp (Section 5.2.5). The pETDuet-*mtrC* construct was obtained by PCR screening of plasmids using PET Upstream and DuetDown1 primers and verified by sequencing using the same primers (Table 5.4 and Section 5.2.5). The details of the pETDuet-*mtrC* construct are shown in Figure 5.9.

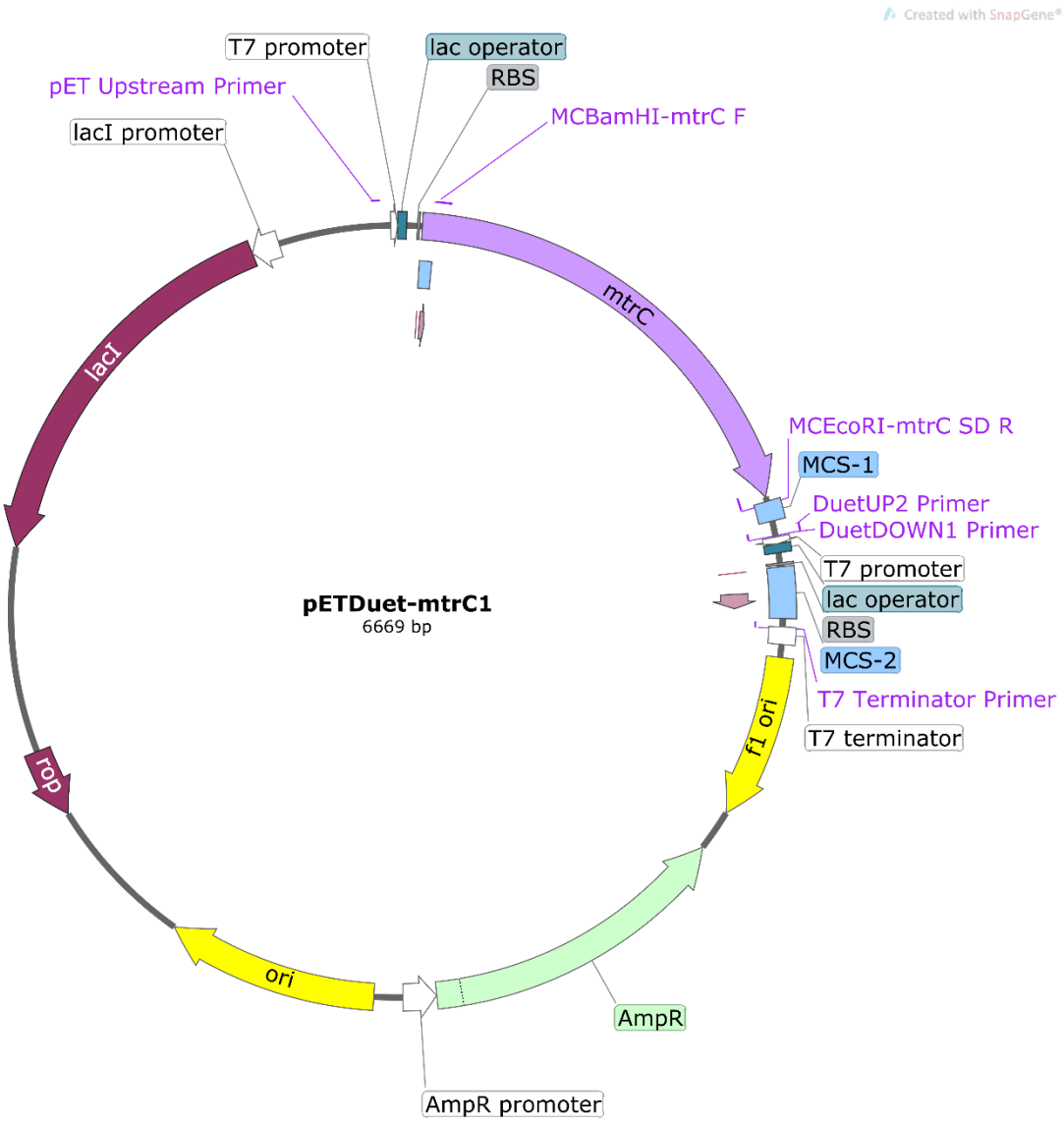

Figure 5.9: The map of pETDuet-*mtrC1* plasmid.

The pETDuet-*mtrC1* plasmid map was generated using the SnapGene program. The *mtrC* gene is labelled and coloured purple. This gene has been cloned into MCS-1 between *Bam*HI and *Eco*RI restrictions sites, using MCBamHI-*mtrC* F and MCEcoRI-*mtrC* SD R primers. The PET Upstream and DuetDown1 primers are also labelled and were used for PCR screening and sequencing of the insert.

5.3.7.2 Construction of the pETDuet-*mtrCE* plasmid

At the second step, the *mtrE* gene was cloned downstream of the *mtrC* gene in MCS-1 of the pETDuet-*mtrC* plasmid. To amplify the *mtrE* gene, the MCEcoRI-*mtrE* ATG F and MCHindIII-*mtrE* R primers were used, along with

N. gonorrhoeae FA19 chromosomal DNA as the template (Table 5.4). The MCEcoRI-*mtrE* ATG F primer has a sequence for the *Eco*RI re
the 5'-end, followed by a 24-nucleotide sequence that anneals to the beginning of the *mtrE* gene, immediately after and including its start codon. The MCHindIII-*mtrE* R primer has a sequence for the *Hind*III restriction site at the 5'-end, followed by a 31-nucleotide sequence that anneals to a sequence immediately upstream of the stop codon of the *mtrE* gene on the template. The PCR amplified *mtrE* gene (1413 bp) and pETDuet-*mtrC* plasmid were digested with *Eco*RI and *Hind*III enzymes and ligated by standard methods (Section 5.2.5). Ligation material was transformed into *E. coli* DH5α cells, and transformed cells were selected for resistance to Amp (Section 5.2.5). After extracting plasmids from transformation colonies, several were screened by PCR using MCBamHI-*mtrC*-F and MCHindIII-*mtrE* primers (Table 5.4). This led to the identification of two plasmids that contained the insert. Sequencing was then carried out using *mtrCDE*-SF2 and DuetDown1 primers to verify the insertion of the *mtrE* gene within the *Eco*RI and *Hind*III sites in the pETDuet-*mtrC* plasmid Table 5.4. This process resulted in the production of the pETDuet-*mtrCE* construct, which was confirmed by the sequencing data. The map of the pETDuet-*mtrCE* plasmid is shown in Figure 5.10.

5.3.7.3 Construction of the pETDuet-*mtrCE-mtrD* plasmid

At the third step, the *mtrD* gene was cloned into the MCS-2 site of the pETDuet-*mtrCE* plasmid. The MCNdeI-*mtrD*-F and MCKpnI-*mtrD*-R primers were used to amplify the *mtrD* gene, with *N. gonorrhoeae* FA19 chromosomal DNA as the template (Table 4.4). Standard methods were used to ligate the PCR product (3210 bp) and the pETDuet-*mtrCE* plasmid, which had been digested with *Nde*I and *Kpn*I enzymes and (Section 5.2.5). PCR colony screening was performed, and a few colonies were identified that carried a plasmid that was the same size as the pETDuet-*mtrCE* plasmid containing the insert. The insertion and integrity of the *mtrD* gene were confirmed in one of the screened plasmids producing the pETDuet-*mtrCE-mtrD* construct by sequencing using DuetUp2, *mtrCDE*-SF4.1, *mtrCDE*-SR4.1 and T7 terminator primers Figure 5.11.

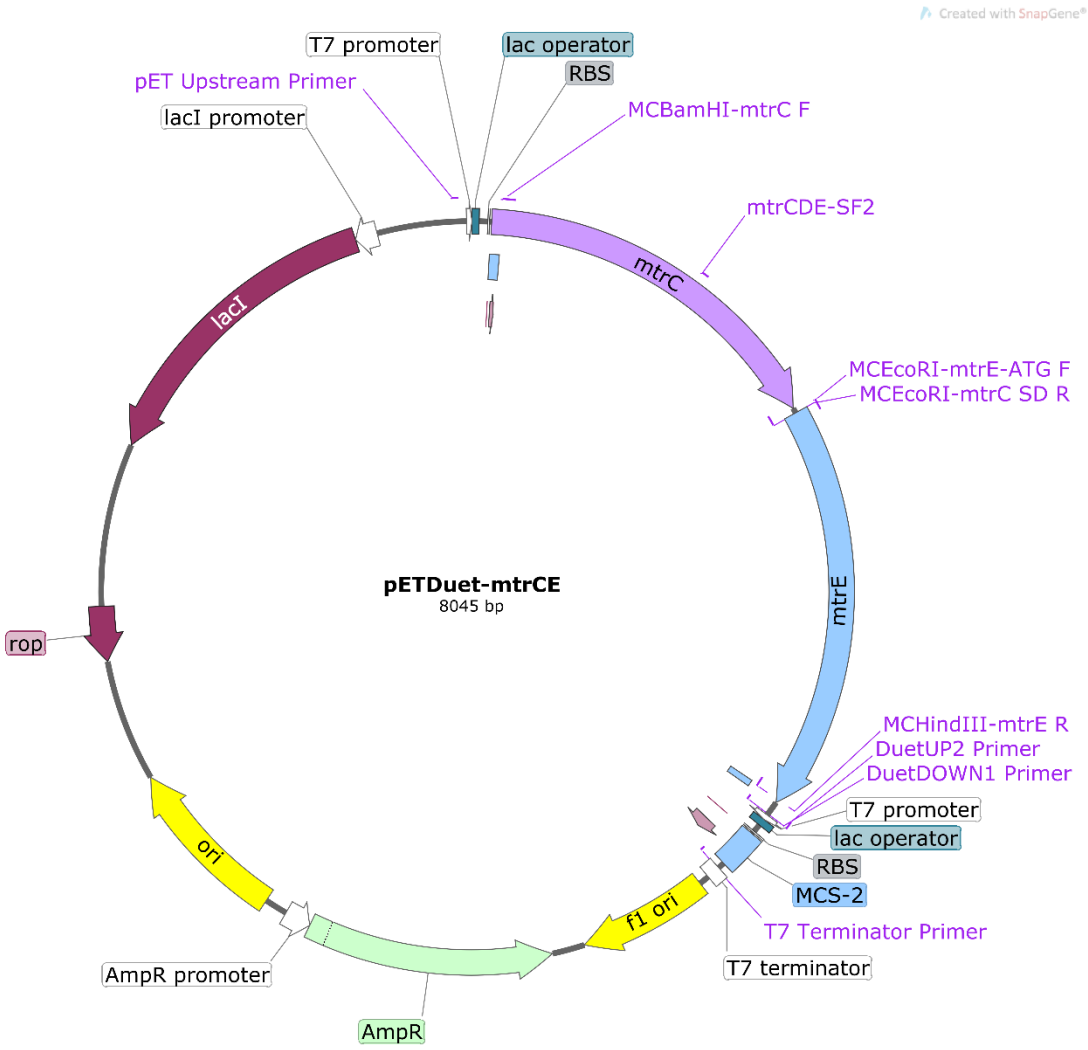

Figure 5.10: Map of pETDuet-*mtrCE* plasmid generated using SnapGene program.

The pETDuet-*mtrCE* plasmid map was generated using the SnapGene program. The *mtrC*, and *mtrE* genes are labelled, and coloured purple and blue, respectively. These two genes have been cloned into MCS-1 tandemly, with *mtrC* between *Bam*HI and *Eco*RI, and *mtrE* within *Eco*RI and *Hind*III restrictions sites. MCBamHI-*mtrC* F, MCEcoRI-*mtrC* SD R, MCEcoRI-*mtrE* ATG F and MCHindIII-*mtrE* R primers are labelled. MCBamHI-*mtrC* F, and MCEcoRI-*mtrC* SD R primers were used for cloning *mtrC*, and MCEcoRI-*mtrE* ATG F and MCHindIII-*mtrE* R primers were used for cloning *mtrE*. PET Upstream, *mtrCDE*-SF2, and DuetDown1 primers are labelled. These primers were used for sequencing of the inserts.

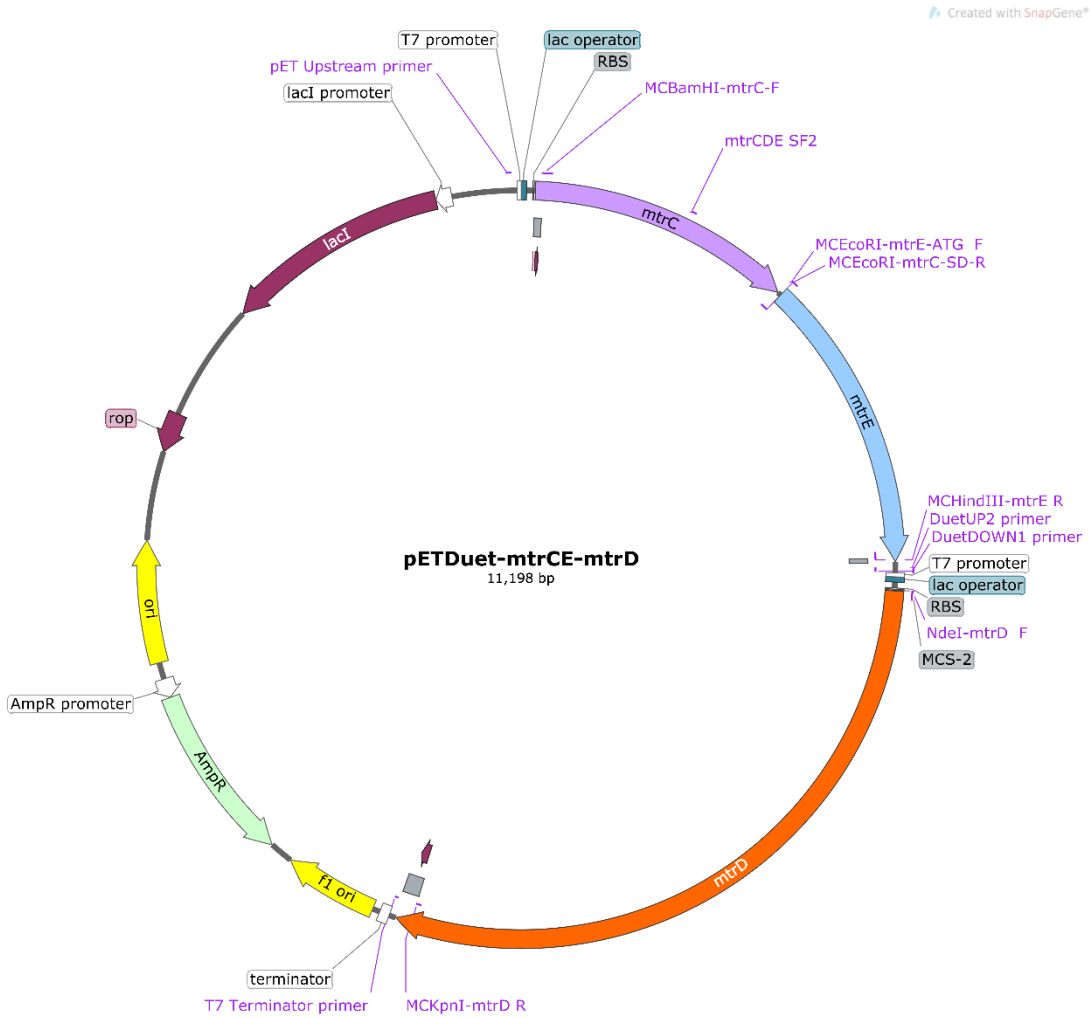

Figure 5.11: Map of the pETDuet-*mtrCE-mtrD* plasmid generated using the SnapGene program.

The *mtrD* gene was cloned into MCS-2 of the pETDuet-*mtrCE* construct between the *Nde*I and *Kpn*I restrictions sites. The MCNdeI-*mtrD*-F and MCKpnI-*mtrD*-R primers were used for cloning, and the DuetUp2, *mtrCDE*-SF4.1, *mtrCDE*-SR4.1 and T7 terminator primers were used for sequencing *mtrD* within the pETDuet-*mtrCE-mtrD* plasmid. These primers are labelled on the map, where the *mtrC*, *mtrE*, and *mtrD* genes are also labelled and coloured purple, blue, and orange, respectively. The position of the six histidine tag at the N-terminus of *mtrC* is shown as a small arrow below the *mtrC* gene.

The pETDuet-*mtrCE-mtrD* construction was designed to co-express the three protein components of the MtrCDE efflux pump system in *E. coli*, allowing for the assembly of a functional tripartite efflux pump to assess MtrD activities. To determine if the cloned genes were expressed and produced protein in *E.*

coli, the constructed plasmids (pETDuet-*mtrC*, pETDuet-*mtrCE* and pETDuet-*mtrCE-mtrD*) were transformed into two λ-DE3 lysogenised and *a*
strains: BL21(DE3) Δ*acrAB* and BW25113(DE3) Δ*acrAB* (Table 5.3). Protein expression was evaluated in 200 ml liquid cultures, induced with IPTG after growth reached an OD_{600} of 0.6, and incubated at 25° C for an additional 3-6 hours (Section 5.2.6). Cellular membranes from each culture were isolated and assessed for protein expression using SDS PAGE and WB analyses (Section 5.2.6).

In the SDS-PAGE gel, a distinct protein band was detected for *E. coli* BL21(DE3) Δ*acrAB* carrying the pETDuet-*mtrC* plasmid, which likely corresponds to MtrC, with a reported molecular mass of 42.7 kDa (Figure 5.12 B) (Hagman et al., 1995). However, MtrC was not detected in the WB image of this protein expression test, despite the incorporation of a 6x histidine affinity tag at the N-terminus of the recombinant MtrC protein. The detection of MtrE protein expression from the constructed plasmids was not expected, as the recombinant MtrE protein did not have a 6x histidine epitope tag on the protein. Although it is possible to detect the MtrD protein expression by WB analysis, this was not performed in this study due to time constraints. It is worth mentioning that the MtrD protein was cloned in-frame with the S-epitope tag on the the pETDuet plasmid at its C-terminus.

5.3.7.4 *E. coli* strains carrying the pETDuet-*mtrCE-mtrD* plasmid give resistance to MtrD substrates.

The constructed pETDuet-*mtrCE-mtrD* plasmid was investigated in various *E. coli* strains to express a functional MtrCDE efflux system and provide resistance to MtrD substrates. MICs for ET and NOV were determined using the micro-broth dilution method. However, due to time constraints, the disc diffusion method was used to determine susceptibilities to an additional six compounds (Section 5.2.4). IPTG was added to all assay culture media. These assays showed that *E. coli* strains BL21(DE3) Δ*acrAB*, BW25113(DE3) Δ*acrAB*, MC33.7 (Δ*acrAB*Δ*tolC*), and *E. coli* BW25113(DE3) Δ*tolC* carrying the pETDuet-*mtrCE-mtrD* plasmid gave resistance to ERY, CRO, NA, C, and TE compared to the same strains containing the pETDuet-1 empty vector

(Table 5.7). Additionally, the MC33.7 (Δ*acrAB*Δ*tolC*) and *E. coli* BW25113(DE3) Δ*tolC* strains both had 4-fold resistance to NOV, while the same strains had 2-, and 4-fold resistance to NOV, respectively (Table 5.7). These results indicate that the constructed pETDuet-*mtrCE-mtrD* plasmid can provide resistance to MtrD substrates in hypersensitive *E. coli* strains when grown under induction with IPTG.

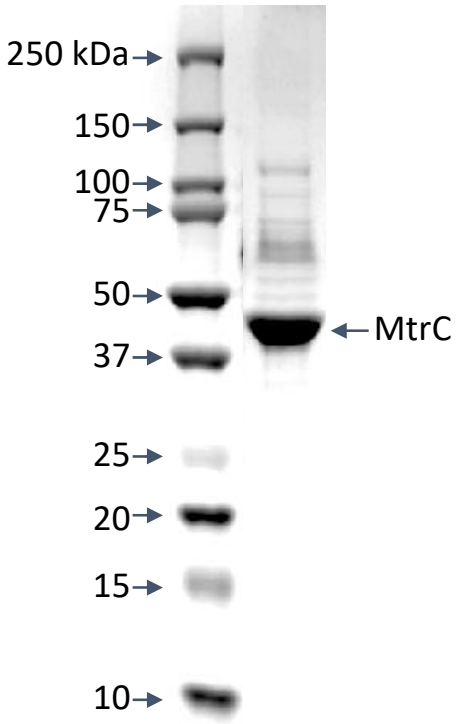

Figure 5.12: The expression of MtrC protein in *E. coli* BL21(DE3) Δ*acrAB* carrying pETDuet-*mtrC* plasmid.

The expression of MtrC protein in *E. coli* BL21(DE3) Δ*acrAB* carrying pETDuet-*mtrC* plasmid is demonstrated through SDS-PAGE analysis. Membrane fractions from *E. coli* cells were solubilized, separated by SDS-PAGE, and the gel was stained with Coomassie blue (Section 5.2.6). The MtrC lipoprotein, consisting of 412 amino acids, is reported to have a molecular mass of 42.7 kDa (Hagman et al., 1995). The expression of MtrC was confirmed by the presence of a distinct protein band in the SDS-PAGE gel between the protein molecular weight standards of 50 and 37, which are indicated on the left in kDa.

Table 5.7: Antibiotic susceptibility of *E. coli* strains expressing pETDuet-*mtrCE-mtrD* plasmid.

	Inhibition zone (mm)						MIC (µg/ml)	
Strain	**E[a]**	**CRO**	**NA**	**C**	**TE**	**CTX**	**ET**	**NOV**
BL21(DE3) Δ*acrAB*/pETDuet-mtrCE-*mtrD*	16.9	32.45	32.9	32.74	28.84	ND	ND	ND
BL21(DE3) Δ*acrAB*/pETDuet-1	20.19	41.17	39.88	39.36	34.68	ND	ND	ND
	(3.29)[b]	(8.72)	(6.98)	(6.4)	(5.84)			
BW25113(DE3) Δ*acrAB*/pETDuet-mtrCE-*mtrD*	15.58	23.87	14.85	25.18	25.87	ND	ND	ND
BW25113(DE3) Δ*acrAB*/pETDuet-1	21.82	37.02	19.69	35.76	30.05	ND	ND	ND
	(6.24)	(13.15)	(4.84)	(10.58)	(4.18)			
MC33.7(Δ*acrAB*Δ*tolC*)/pETDuet-mtrCE-*mtrD*	19.62	ND	ND	30.91	26.63	31.7	8	16
MC33.7(Δ*acrAB*Δ*tolC*)/pETDuet-1	24.55	ND	ND	38.8	31.32	37.1	4	4
	(4.93)			(7.89)	(4.69)	(5.4)	[2][c]	[4]
BW25113(DE3)Δ*tolC*/pETDuet-mtrCE-*mtrD*	18.1	ND	ND	29.28	25.58	28.21	16	8
BW25113(DE3)Δ*tolC*/pETDuet-1	24.97	ND	ND	36.84	31.94	37.04	4	2
	(6.87)			(7.56)	(6.36)	(8.83)	[4]	[4]

[a]Abbreviations: antibiotic discs; E, erythromycin 15 µg; CRO, ceftriaxone 30 µg; NA, nalidixic acid 30 µg; C, chloramphenicol 30 µg; TE, tetracycline 30 µg; CTX, Cefotaxime 5 µg; antimicrobial compounds; ET, ethidium; NOV, novobiocin

[b]The inhibition zone diameter difference between the strain containing pETDuet-1 and the corresponding strain containing the pETDuet-*mtrCE-mtrD* plasmid is given in millimetres (mm). The larger this value is, the more resistant the strain bearing pETDuet-*mtrCE-mtrD* plasmid is.

[c]The fold increase in resistance, as measure by MIC for *E. coli* strain expressing the pETDuet-*mtrCE-mtrD* plasmid compared to the same strain containing pETDuet-1 is given within brackets.

5.3.8 Construction of a bank of truncated *mtrD* clones to facilitate *mtrD* site-directed mutagenesis

The pGCC4-CL-*mtrD*$_{His6}$ plasmid (5.3.4.1) was initially used in this study to generate several *mtrD* mutants (Chapters 2, 3 and 4). However, due to the plasmid's large size (12,491 bp) and the PCR amplification method that used mutagenic primers in a linear PCR approach, creating these mutants proved to be difficult. To address this issue, the *mtrD* gene was modified to be mutated in shorter sequences, which were cloned individually into a small high copy number vector. The truncated sequences were then cloned into the pGCC4-CL-*mtrD*$_{His6}$ plasmid using the same restriction sites as those used for the cloning of each truncated sequence. This strategy enabled the truncation and cloning of the cysteine less *mtrD* gene, as four fragments of sizes 803 bp, 943 bp, 708 bp and 789 bp. It is worth mentioning that the pGCC4-CL-*mtrD*$_{His6}$ clone is a cysteine-less allele of *mtrD*, with cysteine 491 replaced with alanine.

At the first step, two unique restriction sites were identified, *Bsi*WI and *Fse*I, on the pGCC4-CL-*mtrD*$_{His6}$ plasmid that did not cut either pBluescript II or pGCC4 in the case of *Bsi*WI. Using these restriction sites, a 789 bp fragment that spans amino acids (V814-Y1067) of MtrD could be obtained. To clone this region into the pBluescript II vector, a pair of primers were designed that incorporated *Bsi*WI and *Fse*I sites (BsiWI-FseI) into the MCS of the pBluescript II vector within *Bam*HI and *Eco*RI sites. These primers, BsiWIFseI F and BsiWIFseI R, contained tandemly arranged sequences for *Bam*HI, *Bsi*WI, *Fse*I, and *Eco*RI sites (Table 5.4). The forward and reverse primers were annealed to each other, digested with *Bam*HI and *Eco*RI enzymes, and then ligated into the pBluescript II vector that was also digested with the same enzymes. The resulting transformants were screened by the restriction digestion method (Section 5.2.5), resulting in the pBluescript-BsiWIFseI plasmid. The integrity of the insert was confirmed by sequencing using the M13 Fw primer.

A fragment of DNA from *Bsi*WI and *Fse*I sites of *mtrD* from the pGCC4-CL-*mtrD*$_{His6}$ plasmid (BsiWI-*mtrD*-FseI) was obtained by digesting with *Bsi*WI and *Fse*I and gel-purification. This fragment was then ligated with BsiWI/FseI digested pBluescript, and following transformation and selection, transformation colonies screened using M13 Fw and M13 rev primers (Table

5.4). This screening produced the pBluescript-BsiWI-*mtrD*-FseI construct and the integrity of the insert was confirmed by sequencing using the M13 Fw primer (Table 5.4).

An additional allele of the CL-*mtrD*$_{His6}$ gene was created to incorporate two silent restriction sites (*Aat*II and *Sbf*I) in *mtrD* using the pGCC4-CL-*mtrD*$_{His6}$ plasmid in order to construct three additional separate truncated *mtrD* clones in pBluescript II from the remaining sequence of the *mtrD* gene. To achieve this, the cloning was designed to incorporate an *Aat*II site at a position 803 bp downstream of the *Pac*I site on the pGCC4-CL-*mtrD*$_{His6}$ plasmid. These two restriction sites were then used to clone the first 803 bp of the *mtrD* gene. Next, the *Sbf*I site was designed to be incorporated at 943 bp downstream of the *Aat*II site on CL-*mtrD*$_{His6}$ allowing cloning of the 943 bp sequence between *Aat*II and *Sbf*I. The *Bsi*WI site on CL-*mtrD*$_{His6}$ is located at 708 bp downstream of the *SbfI* site allowing cloning of the 703 bp sequence between *Sbf*I and *Bsi*WI sites.

A modified pBluescript II vector containing the four restriction enzyme sites (*Pac*I, *Aat*II, *Sbf*I, *Bsi*WI, and *Fse*I) within its MCS was produced after successful cloning of the first *mtrD* DNA fragment that spans amino acids (V814-Y1067) into the pBluescript II vector. This strategy complements the truncation strategy, making it possible to individually clone all four truncated sequences of the CL-*mtrD*$_{His6}$ gene into pBluescript II. A pair of homologous but reverse and complementary primers (MCSpBSK F and MCSpBSK R) were designed to incorporate a sequence that includes the *Bam*HI, *Pac*I, *Aat*II, *Sbf*I, *Bsi*WI, *Fse*I, and *Eco*RI restriction sites in the given order from 5' to 3' (Table 5.7). The forward and reverse primers were annealed together, and the resultant double-stranded DNA fragment (mMCSpBSK) was digested with *Bam*HI and *Eco*RI, as was pBluescript. These two DNA fragments were then ligated, resulting in the pBluescript-mMCS construct that contained, in its MCS, the newly inserted restriction sites in the order of *Pac*I, *Aat*II, *Sbf*I, *Bsi*WI, and *Fse*I. The integrity of this construct was confirmed by sequencing using M13 fw and M13 rev primers (Section 5.2.5, and Table 5.7).

5.4 Discussion

The MtrD protein of *N. gonorrhoeae* provides gonococcal cells an exceptional capability to resist toxic compounds that have antimicrobial activities (Ayala et al., 2022). This protection is achieved by expelling the compounds out of the cell before they can reach their targets. Although extensive research has been done on the AcrB protein from *E. coli*, which is an RND type efflux transporter similar to MtrD, it cannot provide information on the structure-function relationships of all RND pumps and the differences that can arise due to variations in host strains with distinctive inner and OM compositions. While molecular genetics and regulation aspects of the *mtrD* gene are well studied, there is limited information on the structure and efflux mechanisms of the MtrD protein (Sections 1.4 and 1.4.2). Chapters 2, 3 and 4 of this thesis contain insights into the mechanisms used by MtrD to mediate drug resistance. However, compared to AcrB, a real-time efflux assay for MtrD-mediated export is currently unavailable for analysis in either *Neisseria* or *E. coli*. Further knowledge or techniques in this area will advance our understanding of the transport activity mechanisms employed by MtrD.

To examine the expression and function of the MtrD protein, two *E. coli* mutants lacking the *acrAB* region, BL21(DE3) Δ*acrAB* and DH5α Δ*acrAB*, were created. By deleting the *acrAB* region from these strains, they became hypersusceptible to many antimicrobials and lack a functional AcrAB-TolC pump. These *E. coli* mutants are useful for characterising the MtrD protein without interference from the homologous adaptor protein, AcrA, or the RND pump, AcrB, which can potentially affect the analysis of MtrD in *E. coli.* The BL21(DE3) Δ*acrAB* strain can also be used for high-level expression of the MtrD protein with IPTG induction from plasmids that contain a T7 promoter behind the cloned gene. Moreover, these hypersusceptible Δ*acrAB E. coli* variants can aid in analysing other RND pump systems from different bacteria that may have overlapping substrates with the AcrAB system.

The *mtrD* gene was cloned and inserted into pBluescript II to create the construct pBluescript-*mtrD*$_{His6}$, which was then transformed into five different strains of *E. coli*. Among these strains were four λ-DE3 lysogenised strains ((BL21(DE3), BL21(DE3) Δ*acrB*, C43(DE3), and BW25113(DE3) Δ*acrB*) and

one non-λ-DE3 lysogenised strain (*E. coli* BW25113 (Δ*acrB* Δ*emrE* Δ*mdfA*::kan)). The resistance of the two hypersusceptible strains ((BW25113(DE3) Δ*acrB* and BW25113 (Δ*acrB* Δ*emrE* Δ*mdfA*::kan)), carrying the pBluescript-*mtrD*$_{His6}$ plasmid, to the MtrD substrate ERY was determined. Although MtrD was expressed in all five strains, including the two hypersusceptible strains, this did not lead to any resistance to ERY in either of the BW25113(DE3) Δ*acrB* or BW25113 (Δ*acrB* Δ*emrE* Δ*mdfA*::kan) strains, indicating that MtrD did not mediate any efflux activity (Table 5.6). Janganan et al. had previously observed a similar lack of resistance when they expressed recombinant MtrD protein in two hypersensitive *E. coli* strains (TG1 and KAM3) carrying a pACYC-MtrD plasmid (Janganan et al., 2011b). One possible explanation for this could be that the recombinant MtrD protein is unable to interact with the *E. coli* adaptor protein AcrA or the *E. coli* OM channel protein TolC *in vivo*. If this is the case, expression of the entire *mtrCDE* operon in *E. coli* might overcome this issue.

As an alternative approach to establishing a functional tripartite MtrCDE efflux pump in *E. coli*, the whole *mtrCDE* operon was cloned into the pBluescript II SK vector. The resulting pBluescript-*mtrCDE*$_{His6}$ plasmid was expressed in three non λ-DE3 lysogenised *E. coli* strains (DH5α, DH5α Δ*acrAB*, and AG100A), and expression confirmed by WB analysis. However, despite the expression of MtrE and indication of the expression of the entire efflux pump system, no increase in resistance to ERY, OXA or CV was observed. In fact, the expression of the MtrCDE efflux pump caused these strains to be more susceptible to the antibiotics. The reason for this unexpected observation could be that the expression of the efflux pump from the pBluescript-*mtrCDE*$_{His6}$ plasmid was not well-tuned, making the cells sick. This was supported by delayed growth and smaller colonies on LB medium compared to the growth of the same strains containing the control vector. Despite successful transformation of the plasmid into non λ-DE3 lysogenised *E. coli* strains, it was found to be lethal when transformed into λ-DE3 lysogenised *E. coli* strains, possibly due to toxicity from overexpression of the membrane proteins. The high copy number of the pBluescript II vector may have caused untuned expression of the MtrCDE pump efflux pump in *E. coli*, possibly leading to changes in the membrane permeability resulting in cell

death in the presence of Amp. Further growth curve analysis may be required to confirm this assumption. Additionally, reports from other researchers have highlighted the potential toxicity of overexpressing recombinant membrane proteins (Dumon-Seignovert et al., 2004, Hassan et al., 2009), which aligns with the observed lethality when the pBluescript-*mtrCDE*$_{His6}$ plasmid was transformed into λ-DE3 lysogenised *E. coli* strains. This toxicity may be attributed to the overexpression of membrane proteins, further suggesting the need for cautious modulation of expression levels for functional studies of efflux pump systems.

Because expression of MtrD from pBluescript-*mtrD*$_{His6}$ in *E. coli* did not result in any resistance to an MtrD substrate, the pGCC4-*mtrD*$_{His6}$ plasmid was used to investigate whether the lack of resistance to ERY in *E. coli* from pBluescript-*mtrD*$_{His6}$ was due to the vector or the host strain *E. coli*. This clone was developed early on in this study to create *mtrD* mutants in *E. coli* and mobilise them into *N. gonorrhoeae*. Results showed that the MtrD protein was expressed in the BW25113(DE3) Δ*acrB* cells carrying pGCC4-*mtrD*$_{His6}$ (Figure 5.3), however, no increased resistance to ERY or OXA was observed. In Chapter 2, it was shown that the expression of MtrD in *N. gonorrhoeae mtrD* deletion strains complemented with the WT *mtrD* gene using the pGCC4-*mtrD*$_{His6}$ plasmid provided full resistance to MtrD substrates (Section 2.5.2). These findings suggest that the pGCC4-*mtrD*$_{His6}$ plasmid supplies a fully functional MtrD protein if expressed in a suitable host strain. Additionally, the data revealed that the lack of resistance to ERY and OXA in the *E. coli* BW25113(DE3) Δ*acrB* strain expressing MtrD from the pGCC4-*mtrD*$_{His6}$ plasmid is likely due to MtrD not partnering with either one or both protein components of the *E. coli* AcrAB-TolC system, namely the AcrA and TolC proteins.

The MtrD protein was expressed in *E. coli* BL21(DE3) and C43(DE3) strains carrying the pET21a-*mtrD*$_{His6}$ plasmid. Batch-style purification of the MtrD protein resulted in reasonably strong chemiluminescence bands in the WB, indicating the presence of approximately 1.5 mg of purified protein per litre of the culture (Figure 5.8) and the presence of minimal non-specific protein bands in the Coomassie blue gel indicates the quality of the purification process. This level of protein expression suggests that the pET21a-*mtrD*$_{His6}$ plasmid is a

good candidate for obtaining the required protein levels for detailed analyses such as crystallography, SMALPs, SPR, or reconstitution in artificial membranes such as liposomes. Other investigators have also used the pET vector systems for cloning and overexpression of the MtrD protein and other RND efflux transporters (Du et al., 2020, Lyu et al., 2022, Reading et al., 2020, Zhang et al., 2023b). Additionally, the batch-style method developed in this study can be scaled up for large-scale affinity column purification to produce large quantities of the protein.

An alternative method for creating a functional MtrCDE efflux pump involved cloning the *mtrC*, *mtrD* and *mtrE* genes into the pETDuet-1 vector and expressing all three proteins in an *E. coli* host. The pETDuet-*mtrCE-mtrD* plasmid was successfully constructed and introduced into various *E. coli* strains, including BL21(DE3)/Δ*acrAB*, BW25113(DE3)/Δ*acrAB*, MC33.7 (Δ*acrAB*Δ*tolC*) and BW25113(DE3)Δ*tolC*. Antimicrobial susceptibility analysis showed that these strains exhibited resistance to multiple antibiotics and biocides known to be MtrD substrates, such as ERY, CRO, OXA, and ET (Section 2.5.1, and Table 5.7). Thus, pETDuet-*mtrCE-mtrD* construct is a useful tool for studying the microbiological and biochemical properties of the MtrD protein in a heterologous system.

The WB analysis did not detect expression of the MtrC protein from the pETDuet-*mtrCE-mtrD* plasmid or the two other plasmids (pETDuet-*mtrC*, pETDuet-*mtrCE*), which was unexpected given the 6x histidine amino acid affinity tag on the protein's N-terminus. However, a strong protein band corresponding to MtrC was visible on the SDS-PAGE gel. The 412 amino acid MtrC lipoprotein contains a bacterial signal peptidase II site located at positions 22-25 (Hagman et al., 1995), indicating that the leader sequence of the recombinant MtrC protein was likely removed by the *E. coli* signal peptidase II. As a result, the protein may not have retained the 6X histidine affinity tag incorporated in its N-terminus, rendering the cleaved MtrC protein undetectable by the anti-6x histidine affinity tag used in WB analysis.

Comparison of antimicrobial susceptibility results between MtrD expressed in *E. coli* and *N. gonorrhoeae* revealed that compounds such as CHL, TET, NA, and CRO are good substrates for the MtrD protein and that resistance to

these substances is more easily detectable in *E. coli* than in *N. gonorrhoeae* (Table 5.7). Differences in cell envelope composition between the two species are likely responsible for the observed differences in resistance levels. Thus, the *E. coli*/pETDuet-*mtrCE-mtrD* expression system offers a valuable tool for investigating MtrD-mediated resistance to specific substrates such as β-lactams, TET, and CHL. This is particularly useful because studying MtrD-mediated resistance to these compounds in *N. gonorrhoeae* is challenging due to the need to use gonococcal strains with mutations in other genes, such as *penA*, *penB tet*, and *chl*, as well as a high level of MtrD expression (Shafer and Folster, 2006, Sparling et al., 1975). Additionally, this system can facilitate undertaking real-time transport assays in *E. coli*. However, further future studies are required for a detailed microbiological and biochemical characterisation of MtrD in *E. coli*.

A modified pBluescript II vector, named pBSK-mMCS, was created. The vector's multiple cloning site now accommodates five new restriction sites, including *Pac*I, *Aat*II, *Sbf*I, *Bsi*WI, and *Fse*I. This alteration allows for the cloning of the *mtrD* gene as four short truncated sequences, enabling the construction of site-directed mutants of interest for the *mtrD* gene without the challenges of PCR mutagenesis using pGCC4-*mtrD*$_{His6}$ (12.5 kbp) as the template, which contains the whole *mtrD* gene. The new construct will result in a maximum construct size of approximately 3.9 kb, making it more manageable.

Moreover, the sequence containing the last 762 bp of the *mtrD* gene was successfully cloned into the pBSK-mMCS vector, resulting in the pBluescript-BsiWI-*mtrD*-FseI plasmid. These developments will aid in the construction of *mtrD* mutants and experimentally characterising this RND transporter, improving our understanding of the efflux mechanism of the MtrD and other RND transport proteins. This, in turn, may have implications for combating drug resistance in *N. gonorrhoeae*.

Overall, facilitating the analysis of the MtrD protein in *E. coli* is a critical step towards further characterising and understanding the efflux mechanism of MtrD and other RND transport proteins, potentially leading to innovative approaches for combating drug resistance in *N. gonorrhoeae*.

CHAPTER 6

DISCUSSION AND CONCLUSION

6.1 Using the MtrD protein of *Neisseria gonorrhoeae* as a strategy to address AMR

AMR is a pressing global issue that poses a significant threat to human health. With over 700,000 annual deaths attributed to AMR infections and a projected cost of $100tn between now and 2050, urgent action is required (O'Neill, 2016). The WHO has identified 12 families of antibiotic-resistant bacteria, including *N. gonorrhoeae*, which has developed almost all known mechanisms of AMR (WHO, 2017). As a sexually transmitted bacterium responsible for genital, rectal, and throat infections, *N. gonorrhoeae* poses a significant public health concern, particularly with the emergence and spread of multidrug and extensively drug-resistant strains such as H041, F89 and FC428 (Ohnishi et al., 2011b, Tang et al., 2023, Unemo et al., 2012).

Efflux mechanisms play a pivotal role in AMR by serving as the first line of defence for bacterial cells against harmful compounds, including antibiotics and host-derived cytotoxins (Section 1.3). By actively expelling these substances, efflux mechanisms not only confer resistance to bacteria but also collaborate with other AMR mechanisms. Furthermore, they afford bacteria a temporal window to acquire mutations in their genes, facilitating further resistance development (Section 1.3). Among the seven families/ superfamilies of efflux transporters identified, the RND transporters stand out due to their significant contributions to Gram-negative bacterial envelope barriers, their polyspecificity, and their ability to cooperate with other efflux transporters, thereby contributing to MDR (Section 1.3).

A crucial initial step in addressing AMR and developing strategies to inhibit proteins, including transporters that accomplish efflux, is to gain a detailed understanding of these transporters. A vast amount of knowledge on efflux-mediated drug resistance mechanisms has been acquired by studying a variety of efflux transporters from different families (Section 1.3). This includes understanding the energisation of efflux, transporter topology, structure, substrate binding sites, translocation pathways, geometry, and amino acid composition of drug binding sites, as well as interactions with substrates, functional transport mechanisms, and dynamics of transporter proteins. Moreover, insights have been gained into the interplay between transporters

and other partnering proteins in multicomponent systems, as well as inhibition mechanisms. Several paradigms, such as the alternating access mechanism or functional rotation mechanism, have been identified, extending our understanding of drug transport, even beyond efflux transporters. Notably, AcrB from *E. coli*, has significantly contributed to understanding MDR mediated by this family of proteins (Section 1.3.6.4.1). Furthermore, investigations into homologous RND transporters, such as MexB, MtrD, AdeB, AdeJ and CmeB, have also provided valuable insights into drug resistance (Lyu et al., 2020, Morgan et al., 2022, Murakami et al., 2006, Su et al., 2019, Zhang et al., 2023a, Zhang et al., 2023b). The study of diverse RND transporters is particularly crucial due to the sometimes subtle differences between these transporters (Section 1.3.6.4.1).

The MtrD protein is an important player in the resistance of *N. gonorrhoeae* to multiple antibiotics and natural antimicrobials (Ayala et al., 2022). This PhD research aimed to characterise structurally or functionally important residues or regions of the MtrD protein. In addition, this study explored dynamics of the MtrD protein that govern substrate recognition, binding and permeation, as well as with the hope of providing insights into the mechanisms of AMR and identifying potential targets for drug development. While sharing similarities with other HAE1 RNA transporters like AcrB and MexB, MtrD also exhibits distinct differences, e.g., in the composition of drug binding sites (Section 1.4.6). These disparities, albeit subtle, hint at potentially divergent mechanisms employed by MtrD in drug recognition and extraction, warranting further exploration.

This described studies endeavoured to pinpoint crucial residues or regions within the MtrD protein that dictate its structure and function, with a focus on understanding its dynamics governing substrate recognition, binding, and extrusion. Additionally, the study delves into the allosteric coupling between proton translocation and substrate efflux, aiming to elucidate the mechanisms underlying AMR and identify prospective targets for drug development. Moreover, the research introduces innovative methodologies aimed at facilitating the functional characterisation of MtrD. These collective efforts are directed towards combating drug resistance mediated by efflux transporters,

particularly RND pumps, thereby addressing a critical challenge in antimicrobial therapy.

6.2 Construction of a panel of isogenic *N. gonorrhoeae* derivatives for screening MtrD substrates and inhibitors

As discussed in Chapter 2, a site-directed mutagenesis system specific to analysing the MtrD export protein in its natural *N. gonorrhoeae* host was developed (Section 2.5.1 and 2.7.3). To achieve this, a highly discriminating *N. gonorrhoeae* strain to perform *in situ* analysis of MtrD activity was created. The well-characterised, antibiotic-sensitive FA19 strain (Sarubbi et al., 1974) was employed as the background strain and three isogenic FA19 derivatives (FA19Δ*mtrD*, FA19Δ*norM*, and FA19Δ*mtrD*Δ*norM*) and two KH15 (Hagman et al., 1995) isogenic derivatives (KH15Δ*mtrD* and KH15Δ*mtrD*Δ*norM*) were constructed using overlap extension PCR (Section 2.5.1 and 2.7.3). The NorM efflux pump of *N. gonorrhoeae* is recognised for its role in expelling various cationic toxic compounds, including CIP, ET, and ACR, with the latter two being shared substrates with MtrD (Rouquette-Loughlin et al., 2003). Therefore, to eliminate any potential interference from the unrelated NorM_NG multidrug efflux pump in evaluating MtrD function, the *norM* gene was also deleted.

The *N. gonorrhoeae* panel created in this study proved useful for screening MtrD or NorM substrates and inhibitors. Using this panel, 14 new MtrD substrates were identified and the two known RND inhibitors, NMP and PAβN, were classified as substrates for MtrD (Section 2.5.1). In addition, with exception of long-chain FAs, it was found that KH15Δ*mtrD*Δ*norM* can provide better discrimination when screening substrates compared to FA19Δ*mtrD*Δ*norM* (Section 2.5.1). This is reasonable since the MtrR transcriptional repressor of the *mtrCDE* operon, which is not expressed in KH15 due to a mutation in the *mtrR* promoter, is known to positively regulate the *farAB* genes that export FAs from the cell (Shafer et al., 2001), see Section 1.4.2. Thus, these data suggest that the constructed *N. gonorrhoeae* KH15Δ*mtrD*Δ*norM* strain can function as a good discriminative background strain for conducting analyses of *mtrD* mutants.

As discussed in Section 1.3.6.4.5, EPIs show promise in addressing antimicrobial drug resistance due to these transporters (Alenazy, 2022, Moir et al., 2021, Si et al., 2023). Currently, there are at least eight classes of core compounds being investigated for their ability to inhibit RND efflux pumps (Section 1.3.6.4.5) (Compagne et al., 2023). Advances in high-throughput screening of synthetic or commercially available compounds, as well as in silico screening methods combined with artificial intelligence, have led to the availability of several compound libraries (ChemDiv: The Chemistry of Cures, eurofins). Additionally, screening for potential EPI compounds from natural resources is ongoing, along with continuous optimisation of already discovered core compounds to enhance their inhibitory activities and reduce or eliminate adverse effects (Guo et al., 2023). The framework presented in this study serves as a valuable tool for evaluating both existing and novel compounds for their potential to inhibit MtrD in the future.

Given the polyspecific nature of HAE1 type RND transporters and the ongoing identification of their substrates, including physiological substrates, this panel of isogenic *N. gonorrhoeae* strains will aid in uncovering additional substrates in the future (Guo et al., 2023, Henderson et al., 2021, Plé et al., 2022, Zgurskaya et al., 2022). Furthermore, as demonstrated in Chapter 5, it was shown that expression of MtrD in *E. coli*, with various host-plasmid combinations, enables the facile detection of resistance to compounds such as CRO, CHL, or TET (Section 5.3.7.4). This detection proves challenging when using *N. gonorrhoeae* as the host strain with only *mtrD* removed. The development of this new *E. coli*-based MtrD expression system will facilitate further exploration of MtrD substrates or inhibitors in future studies.

In Chapter 2, a recombinant WT MtrD clone called pGCC4-*mtrD*$_{(His6)}$ was constructed based in the pGCC4 shuttle vector (Mehr and Seifert, 1998). This version used a MtrD cysteine-less variant which also encoded a 6-histidine tag that is useful in purification and localisation studies, pGCC4-CL*mtrD*$_{His6}$. It subsequently demonstrated the full functionality of both *mtrD* alleles in the *N. gonorrhoeae* KH15Δ*mtrD*Δ*norM* strain among others (Section 2.5.2 and 2.7.4). These plasmids allow for the construction and propagation of *mtrD* mutants in *E. coli* before mobilising them into *N. gonorrhoeae* (Mehr and Seifert, 1998). This system provides a valuable and dependable tool for evaluating the effects

of mutations in MtrD on efflux and resistance. This advancement is critical for future investigations on MtrD, as co-crystal structures of MtrD with Amp, ERY, CASP, colistin and LL-37 have revealed numerous residues involved in substrate interactions (Lyu et al., 2022, Lyu et al., 2020). Moreover, in Chapter 4 of this study, several residues - such as V640, A641, and S635 (Section 4.5.4) - were pinpointed, which our MD simulations suggest may play a role in facilitating substrate access to MtrD through CH1 or CH2 by interacting with the N917-P927 region. Future analyses could utilise this developed site-directed mutagenesis system to explore the functional significance of critical residues identified in co-crystallography studies and this study.

The extensive availability of whole genome sequences from gonococcal strains now enables the identification of critical amino acid changes in the MtrD efflux pump that may affect its activity. In this context, specific mutations in MtrD associated with reduced susceptibility or resistance to key antibiotics, including AZM, have been identified through the analysis of selected isolate subsets (Section 1.4). The newly developed site-directed mutagenesis system can serve as a valuable tool for functionally analysing these MtrD mutations in the future, providing deeper insights into their impact on efflux function and resistance.

The process of generating and analysing site-directed MtrD mutants in the future will be further facilitated by the introduction of a modified pBluescript II vector, named pBSK-mMCS in Chapter 5 (Section 5.3.8). This modified vector features an expanded multiple cloning site capable of accommodating five new restriction sites. These sites were specifically chosen to align with either incorporated or existing silent single-cut sites within *mtrD*, as cloned in the pGCC4 vector. This enhancement streamlines the cloning of *mtrD* fragments, simplifying the construction of site-directed mutants without the need for the more complex PCR mutagenesis approach typically required when using the larger pGCC4-*mtrD*$_{His6}$ template. With the advancements in gene synthesis technologies, this development offers an additional advantage in the construction of MtrD mutants at a reasonably low cost, bypassing the need for PCR amplification efforts.

A limitation of this host-vector system lies in the fact that although both ERY and AZM showed excellent MIC differentiation between the *mtrD* deleted derivative and its respective parental strain, the use of the ERY-resistance cassette present in pGCC4 as a selection marker precludes testing constructed MtrD mutant derivatives against these clinically important antibiotics (Section 2.5.2). In the future, overcoming this limitation will be possible either by utilising a gonococcal shuttle vector that employs a distinct antibiotic selection marker like CHL in pGCC6, or by substituting the selection marker in pGCC4 with an alternative antibiotic selection marker (Dillard, 2011).

The findings of this study hold great promise for future investigations into the resistance mechanisms of MtrD resulting from mutations in the *mtrD* gene. By developing a mutagenesis system, this study has provided a valuable tool for experimental exploration of these mechanisms. Moreover, the frequency of these mutations in clinical isolates of *N. gonorrhoeae* underscores the relevance of this study's results for understanding and addressing antibiotic resistance in this pathogen (Golparian et al., 2023b, Martin et al., 2023, Shafer, 2018, Thomas et al., 2019a).

6.3 Identification of functionally important residues in the MtrD efflux protein

MD simulations serve as a crucial tool in understanding both the drug binding properties and the structural dynamics governing the substrate efflux mechanism of RND transporters (Atzori et al., 2020, Vargiu and Nikaido, 2012). In Chapter 2, an MD simulation method was developed by the O'Mara group to explore the interaction of MtrD with its substrates. Using this protocol with the substrate PRO, valuable insights were gained into the substrate translocation pathway and the residues interacting with PRO. Notably, this investigation was conducted based on the apo MtrD structure available at the time. The simulation revealed notable features such as the PC1/PC2 cleft entrance, PBP and DBP, switch loop, and a group of 25 residues that interacted with PRO during its movement within the translocation pathway of MtrD. Intriguingly, six of these residues (F658, I660, V662, R714, K823, and S825) were subsequently identified in the later published cryo-EM structures of MtrD with Amp and ERY where they were found to interact with these drugs

and were proposed to contribute to drug selectivity and specificity (Lyu et al., 2020). Moreover, substitutions at position 823 have been identified as a result of acquiring mosaic alleles in *mtrD* from commensal *Neisseria* species, leading to decreased gonococcal susceptibility to macrolides (Wadsworth et al., 2018a). Rouquette-Loughlin et al. demonstrated that mosaic *mtrR* and *mtrD* genes, including the K823E substitution, play a crucial role in the emergence of AZM-resistant strains (Rouquette-Loughlin et al., 2018b). These findings are further supported by evidence demonstrating the importance of R714, an equivalent residue in AcrB (R717) and MexB (R716), in drug selectivity and as a hotspot for mutations in clinical isolates of RND pumps (Sajib et al., 2021, Trampari et al., 2023, Zwama and Nishino, 2021).

Out of the 25 identified residues by MD simulations, a subset contributes to the formation of either the PBP or DBP of MtrD. Several of these residues (S134, F176, F568, M570, F610, F612, F623, G671, R714 and E823) were subsequently found to interact with antimicrobials such as Amp, ERY, CASP, colistin, and LL-37 in co-crystal structures of MtrD with these compounds (Lyu et al., 2022, Lyu et al., 2020). Notably, except for F568, nine of these residues (underlined) are conserved in AcrB (Vargiu and Nikaido, 2012). This underscores the reliability of our MD simulations in studying MtrD interactions with substrates and its potential significance in future investigations of MtrD interactions with various substrates. Within this residue group, the phenylalanine cluster, R714, and K823, are particularly intriguing. Mutations at positions equivalent to 714 or 823 have been associated with gain of function and drug selectivity in other RND transporters (Trampari et al., 2023, Zwama and Nishino, 2021). Specifically, a K823E mutation has been linked to macrolide selectivity and is present in clinical strains of *N. gonorrhoeae* harbouring a mosaic-like *mtr* efflux pump locus, demonstrating reduced susceptibility to macrolides (Lyu et al., 2020, Rouquette-Loughlin et al., 2018b). The significance of the phenylalanine cluster will be elaborated on in the subsequent paragraphs.

The phenylalanine cluster (F136, F176, F610, F612, and F623) emerged as particularly interesting (Section 2.5.4), and its significance has been demonstrated in various RND transporters like AcrB, MexB, BpeF, Kp-AcrB, CmeB, AdeB, AdeJ and others (Kato et al., 2023, Morgan et al., 2022,

Murakami et al., 2006, Murakami et al., 2002, Nakashima et al., 2011, Su et al., 2019, Yamasaki et al., 2022, Yao et al., 2013, Zhang et al., 2023a, Zhang et al., 2023b). Similarly, in MtrD, its importance was confirmed through co-crystal structures with different compounds (Lyu et al., 2022, Lyu et al., 2020). Interestingly, aromatic side chains have been shown to contribute to the stabilisation of interactions with inducers in the binding pockets of transcriptional regulators AcrR, MtrR and QacR (Beggs et al., 2019, Peters et al., 2008, Routh et al., 2009). It's noteworthy that these residues contribute to forming a hydrophobic trap in MtrD, which is often considered the Achilles heel of RND efflux transporters (Aron and Opperman, 2018). Additionally, it was found that F612, located at the tip of the G-loop, enhanced the binding affinity of all eight docked compounds (Section 2.5.4), as confirmed by co-crystal structures of MtrD with antibiotics and antimicrobial peptides in later studies (Lyu et al., 2022, Lyu et al., 2020). The results obtained in this study underscore the significance of aromatic-aromatic interactions facilitated by phenylalanine residues in drug recognition, a shared feature among several HAE1 RND transporters (Athar et al., 2023). Furthermore, the findings emphasise the efficacy of the developed integrated approach, which incorporates MD simulations of PRO binding, molecular docking, and site-directed mutagenesis, to characterise MtrD's substrate binding (Chapter 2). This knowledge deepens our comprehension of the molecular mechanisms employed by RND transporters and their involvement in AMR in Gram-negative bacteria, including *N. gonorrhoeae*. This insight sets the stage for future research to explore molecular interactions between MtrD and its substrates, expanding beyond the scope of this study.

6.4 Coordination of substrate binding and protonation

In Chapter 3, the functionally rotating transport mechanism of the MtrD efflux pump was described. Through a combination of MD simulations and mutagenesis experiments, the coordination of substrate binding and protonation in driving the transition from symmetric to asymmetric conformations of MtrD was elucidated. The asymmetric conformation of the trimeric MtrD protein follows the functionally rotating transport mechanism

identified in other RND transporters (Murakami et al., 2006, Seeger et al., 2006, Zwama and Yamaguchi, 2018).

The critical role of the proton relay network, involving residues D405, D406, K948, N949, and T985, in mediating the transition between symmetric and asymmetric conformations of MtrD was identified. Protonation of D405/D406 in one monomer coupled with substrate binding in adjacent monomers led to asymmetry between the subunits, resulting in functional rotation of the transporter (Section 3.4.4). This transition to a functionally active trimer in MtrD upon protonation in one monomer follows previously described mechanism for AcrB (Matsunaga et al., 2018). This coordination between substrate binding and protonation highlights the dynamic nature of MtrD function and its adaptation to environmental cues.

The protonation of the relay network residues induced rotation of the transmembrane helices along the pseudosymmetrical axis, accompanied by the opening of the inter-monomeric gap between the extrusion and binding monomers (Section 3.4.5). These global conformational changes are crucial for substrate extrusion and are indicative of the functionally rotating transport mechanism in MtrD, following the same mechanism described for AcrB and other RND transporters (Jewel et al., 2020).

The synchronisation between local molecular binding events and large-scale conformational movements implied by the functionally rotating mechanism is a membrane transport paradigm that is being transferred to a wide array of unrelated prokaryotic and eukaryotic solute carrier families (Fairweather et al., 2021). The widespread application for this paradigm highlights the need for continued research into the full and dynamic transport cycle, which will require close collaboration between structural and computational biochemists.

6.5 Significance and impact of the N917-P927 region in MtrD

Located in TMS 9, the N917-P927 region represents a distinct characteristic of the MtrD pump that sets it apart from other RND pumps (Section 1.4.6.4) (Figure 4.2) (Bolla et al., 2014). Despite considerable protein sequence or

structural similarities among RND transporters, subtle structural disparities can yield significant functional implications. For instance, while the MexY efflux pump of *P. aeruginosa* provides resistance to GEN, this hydrophilic compound is not a substrate for MexB, AcrB or MtrD (Aires et al., 1999, Golparian et al., 2023a, Lau et al., 2014, Masuda et al., 2000). Additionally, the D13-9001 efflux pump inhibitor can inhibit AcrB and MexB but not MexY (Nakashima et al., 2013, Yamasaki et al., 2022). These phenotypic traits have been shown to be associated with structural differences (Dey et al., 2020, Nakashima et al., 2013). Hence, comprehending the mechanisms employed by individual RND efflux pumps is paramount, given its potential clinical implications for AMR and the design of rational drug or inhibitor strategies.

The positioning of the elongated N917-P927 helix and loop, along with the PC1/PC2 cleft, imply that this added structural characteristic could enhance the ability of the pump to efficiently transport substrates from the outer layer of the IM to the multidrug binding site located in the PD (Section 1.4.6.4). Analyses indicated that the N917-P927 sequence is essential for complete and efficient activity of the MtrD protein, as evidenced by the reduced resistance observed in the MtrD allele lacking this sequence when exposed to a range of MtrD substrates (Section 4.5.1). Positioned at the boundary between the membrane and the periplasm, various hypotheses were explored to elucidate the mechanism underlying the impact of N917-P927 on resistance. It was found that the mere presence of the protein backbone (via glycine substitution) or truncated side chains (via alanine substitution) is inadequate to generate a fully active MtrD variant (sections 4.5.2). Consequently, site-directed mutagenesis was used to investigate the role of each residue in this region individually. Results obtained highlight the importance of three key residues (N917, G924 and P927) for effective MtrD-mediated resistance against diverse substrates (Section 4.5.3). Through the replacement of these residues with different amino acids based on several hypotheses, it was concluded that: 1) the side-chain properties of asparagine at position 917 are essential for resistance; and 2) the backbone conformation at position 927, influenced by the presence of proline, is crucial for the efficient activity of MtrD (Section 4.5.3).

To identify the mechanisms by which the N917-P927 region influences MDR mediated by the MtrD protein, MD simulations were undertaken. Using simulations of the WT MtrD trimer unveiled distinct positioning of the N917-P927 region across protomers, in the A protomer it was located within the membrane at the periplasmic interface, while in the B and E protomers the region protruded above the membrane into the periplasm (Section 4.5.4). Over 500 ns simulations, dynamic changes were observed in the relative orientation of N917-P927, forming contacts with residues in the PD within the initial 50 ns (Section 4.5.4). Specifically, in the A protomer, N917-P927 remained close to the PC1 domain, narrowing the binding cleft entrance, while in the B protomer, similar interactions were observed. In contrast, the E protomer displayed interactions with residues on the PC2 side, physically hindering substrate entry (Section 4.5.4). These findings underscore the dynamic nature of the N917-P927 region and its crucial role in modulating substrate entry in the MtrD pump. Moreover, further MD simulations investigated the impact of introducing cysteine substitutions (N917C, G924C, and P927C) in a triple MtrD mutant, revealing protrusion of N917-P927 above the membrane interface in all protomers, hindering substrate entry (Section 4.5.4). Additionally, simulations of Δ(N917-P927) and 11G(917-927) MtrD mutants highlighted changes in the positioning of TMS 9 and loss of α-helical secondary structure, indicating destabilisation of the protein-lipid interface and potentially contributing to reduced activity observed in MIC analyses (Section 4.5.4 and 4.5.1).

These findings offer insights into the functioning of RND transporters and broader efflux mechanisms. The N917-P927 region likely plays a role in positioning and orienting MtrD within the gonococcal membrane, facilitating substrate access via the PC1/PC2 cleft. MD simulations comparing WT and mutant variants support this, showing hindered substrate entry in N917-P927 deletion and 11-glycine replacement mutants, as well as concurrent triple cysteine mutants. The role of the interaction between the CM and efflux pump proteins in modulating protein function has been previously described (Jodaitis et al., 2021, MacDermott-Opeskin et al., 2022, Sharom, 2014, Zang et al., 2021).

Another potential explanation is that mutations in the N917-P927 region could influence the conformational cycling of MtrD by affecting the movements

of PN2/PC1 and PN1/PC2 structural repeats during functional cycling. Additionally, MD simulations suggest that the N917-P927 region interacts with PC1 or PC2 in different protomers, further supporting this hypothesis. This coupling mechanism, involving proton translocation in TMD and substrate translocation in PD, has been described in AcrB, where a twist movement between the R1 and R2 repeats in TMD is transmitted to PD through coupling elements TMS 2 and TMS 8, leading to the displacement of PN2/PC1 structural subdomains on the rigid PN1/PC2. The interactions between the N917-P927 region and PC1 or PC2 in distinct protomers revealed in our MD simulations may strengthen this hypothesis (Oswald et al., 2016, Seeger et al., 2006, Tam et al., 2020).

Disturbances in the protein-lipid interface would also explain possible impact the interactions between MtrD and its substrates at the membrane-periplasm interface, affecting substrate capture via the IM entrance. The reduced resistance to multiple substrates observed in *N. gonorrhoeae* cells expressing the Δ(N917-P927) MtrD mutant compared to the WT parent confirms this idea (Section 4.5.1). These results are intriguing, as hydrophobic HAE-1 RND pump substrates are thought to interact with the IM-periplasm interface before they are captured and exported (Hagman et al., 1997, Nikaido, 1996, Nikaido et al., 1998). Furthermore, MD simulations of the Δ(N917-P927) MtrD mutant with the substrate PRO demonstrated that destabilisation of the protein-lipid interface in the region of TMS 9 could dysregulate substrate access to the binding cleft and closure of the substrate-binding pocket during the transport cycle, affecting substrate capture to the binding cleft (Section 4.5.5).

These findings underscore the need for further exploration into the molecular interactions between MtrD and the neisserial membrane. For instance, investigations similar to those elucidating how the interaction between AdeB and the *A. baumannii* membrane can affect drug susceptibility (Zang et al., 2021) or studies exploring how interactions between AcrZ and AcrB are influenced by the *E. coli* lipid environment and their impact on the resistance conferred by AcrB (Du et al., 2020, Qiu et al., 2018) are warranted.

Furthermore, the identification of residues responsible for regulating substrate intake through MD simulations of the WT and different N917-P927-region mutants, coupled with mutational examination, establishes a groundwork for employing the deep mutational scan technique in upcoming investigations, to achieve a more extensive insight into the structure-function profile of the MtrD protein (Meier et al., 2023).

6.6 Optimising overexpression of MtrD and MtrCDE in *E. coli*

Analysing the function of a bacterial protein is best done in its native host, but limitations exist when studying *Neisseria gonorrhoeae* due to its fastidious nature. Real-time efflux assays, commonly used to measure transport activity, can be performed in *E. coli*, but gonococcal cells quickly lose viability in buffer solutions (Elmros et al., 1976, Morse and Bartenstein, 1974). Additionally, difficulty in growing gonococci in liquid medium hinders overexpression of recombinant MtrD protein, which can instead be produced in *E. coli* for *in vitro* assays such as efflux and binding assays.

In this study an *E. coli* host and vector system was developed to optimally overexpress the active MtrD protein and the MtrCDE efflux system. However, since *E. coli* has several efflux systems, including the highly characterised AcrAB-TolC pump system, expressing MtrD in *E. coli* strains with their native AcrB may produce conflicting results in functional analyses or interfere with protein purification. Thus, the *acrAB* region from the *E. coli* chromosomes of BL21(DE3) and DH5α strains was deleted. The resulting *E. coli* strains are hypersusceptible to many hydrophobic antimicrobials (Section 5.3.1). This makes them useful for characterising the MtrD protein in *E. coli* without interference from the homologous adaptor protein AcrA or the RND pump AcrB. The BL21(DE3) Δ*acrAB* strain is particularly suitable for high-level expression of MtrD under T7 promoter regulation using plasmids such as pET systems. These hypersusceptible Δ*acrAB E. coli* variants can also facilitate the analysis of other RND pump systems from different bacteria that have similar substrates to the AcrAB system.

Despite successfully cloning the *mtrD* gene into the pBluescript vector, the resulting clone did not generate an operational efflux pump system in the *E.*

coli strains employed in this study (Section 5.3.2). Interestingly, the MtrD protein was expressed in various strains, including those with intact AcrAB-TolC and that with deleted *acrB* gene. One plausible explanation for this outcome is that the recombinant MtrD protein is unable to interact with the *E. coli* adaptor protein AcrA or the *E. coli* outer membrane channel protein TolC *in vivo*. Although this approach failed to produce active MtrD in *E. coli*, the *mtrD* clone generated through this method serves as a valuable plasmid for producing *mtrD* alleles in *E. coli*, facilitating the transformation of gonococci strains.

Therefore, an alternative approach was employed by cloning the *mtrCDE* operon into the pBluescript vector to produce an active MtrCDE efflux pump system in *E. coli* (Section 5.3.3). This cloned construct was successfully introduced into non-λ-DE3 lysogenized *E. coli* strains. However, despite expressing the MtrC, MtrD, and MtrE proteins in various non-λ-DE3 lysogenized *E. coli* strains using the pBluescript-*mtrCDE*$_{His6}$ construct, these strains failed to exhibit an active MtrCDE efflux pump system. One possible explanation for this lack of MtrCDE efflux activity is that the expression of the MtrCDE efflux system from the pBluescript plasmid was not properly regulated, resulting in cellular dysfunction. This hypothesis is supported by the observed delayed growth and smaller colonies on LB medium supplemented with ampicillin, compared to the growth of the same strains containing the control vector. Although this approach did not successfully produce an active MtrCDE system in *E. coli*, the *mtrCDE* clone generated through this method remains valuable as a plasmid for producing *mtrCDE* alleles in *E. coli*, facilitating the transformation of gonococcal strains.

The transformation of the pBluescript-*mtrCDE*$_{His6}$ plasmid into λ-DE3 lysogenized *E. coli* strains was determined to be lethal, possibly due to toxicity. It is probable that the high copy number vector, pBluescript, caused unregulated expression of the MtrCDE efflux pump in *E. coli*, resulting in alterations in membrane permeability and subsequent cell death in the presence of ampicillin. Additionally, reports from other researchers have highlighted the potential toxicity of overexpressing recombinant membrane proteins (Dumon-Seignovert et al., 2004, Hassan et al., 2009), which aligns with the observed lethality. This toxicity may be attributed to the

overexpression of membrane proteins, further suggesting the need for cautious modulation of expression levels for functional studies of efflux pump systems.

To investigate the reason behind the absence of MtrD substrate resistance in *E. coli* when expressing the MtrD protein from pBluescript-based clones, the pGCC4-*mtrD*$_{His6}$ plasmid was employed to differentiate between the vector and host strain effects. Initially developed to generate *mtrD* mutants in *E. coli* for transfer to *N. gonorrhoeae*, this clone successfully expressed the MtrD protein in BW25113(DE3) Δ*acrB* cells carrying pGCC4-*mtrD*$_{His6}$ (Section 5.3.4.2). However, no increased resistance to MtrD substrates was observed compared to the strain carrying the empty pGCC4 vector. In contrast, *N. gonorrhoeae mtrD* deletion strains complemented with WT *mtrD* gene using the same plasmid exhibited full MtrD substrate resistance. These results indicate that pGCC4-*mtrD*$_{His6}$ supplies a fully functional MtrD protein when expressed in a suitable host strain. Additionally, it suggests that the lack of resistance in *E. coli* BW25113(DE3) Δ*acrB* strain expressing MtrD from pGCC4-*mtrD*$_{His6}$ is likely due to MtrD's failure to interact with one or both protein components of the *E. coli* AcrAB-TolC system, specifically the AcrA and TolC proteins.

The pETDuet-1 vector was used to clone the *mtrC*, *mtrD*, and *mtrE* genes and express them in *E. coli*, creating the pETDuet-*mtrCE-mtrD* plasmid (Section 5.3.7). Various *E. coli* strains carrying this plasmid showed resistance to MtrD substrate antibiotics and biocides. Comparing antimicrobial susceptibility between *E. coli* and *N. gonorrhoeae*, it was found that *E. coli* exhibited greater resistance to certain compounds, likely due to differences in cell envelope composition. The *E. coli*/pETDuet-*mtrCE-mtrD* expression system is a valuable tool for studying MtrD-mediated resistance, particularly for specific substrates challenging to investigate in *N. gonorrhoeae*. Further research is needed for a detailed characterisation of MtrD in *E. coli*. Future studies can utilise this expression system to conduct real-time efflux assays, employing fluorescent MtrD substrates like ET, to further characterize MtrD-mediated efflux mechanisms. By examining the efflux kinetics, e.g., researchers can gain insights into the functioning of MtrD and its role in efflux processes.

6.7 Purification of MtrD protein

To achieve a high yield of MtrD protein for undertaking biophysical and biochemical studies, the *mtrD* gene was cloned into the expression vector pET21a (Section 5.3.5). The resulting pET21a-*mtrD*$_{His6}$ construct enabled expression of the MtrD protein in BL21(DE3) and C43(DE3) strains, two well-known *E. coli* derivatives used for over-expressing membrane proteins (Debruycker et al., 2020a, Dumon-Seignovert et al., 2004, Lyu et al., 2020, Miroux and Walker, 1996, Su et al., 2021, Yousefian et al., 2020). Subsequently, a batch-style purification method was utilised to isolate the MtrD protein from BL21(DE3) cells harbouring this pET21a-*mtrD*$_{His6}$ construct. Analyses demonstrated the successful production of a substantial quantity of high-quality MtrD protein using this approach (Section 5.3.6), underscoring the suitability of the pET21a-*mtrD*$_{His6}$ plasmid for generating sufficient protein quantities for subsequent investigations, including crystallography, SMALPs, SPR, or reconstitution in liposomes. This MtrD expression and purification system represents a valuable tool for further characterisation of the MtrD protein in future research endeavours.

6.8 Summary

In conclusion, the work described in this thesis has addressed the urgent need to combat AMR by focusing on the MtrD protein of *N. gonorrhoeae* as a potential target. AMR is a global health concern with significant mortality and economic implications. *N. gonorrhoeae*, as a sexually transmitted bacterium, poses a particular threat due to its multidrug and extensively drug-resistant strains. This body of work introduces an experimental tool for investigating substrates and potential inhibitors of MtrD, along with functional assessments of MtrD mutants. Moreover, it delves into the mechanisms underlying MtrD-mediated AMR by identifying functionally important residues or regions and elucidating interactions between MtrD and its substrates as well as functional mechanisms of this RND transporter. Previous research (Golparian et al., 2014, Hagman et al., 1995, Sparling et al., 1975), coupled with the findings presented here (Section 2.5.1), confirms the broad substrate specificity of the MtrD efflux pump. This study demonstrates that MDR mediated by MtrD can be elucidated through structural and functional relationship studies,

highlighting the role of the protein's structural nature in its polyspecificity. The combined use of *in silico* and experimental methods, including MD simulations, molecular docking, and site-directed mutagenesis, enables the identification of critical structural features that underlie the function of the protein in conferring resistance to diverse antimicrobials. Moreover, this integrated approach elucidates how subtle structural differences can impact protein function. These findings provide valuable insights into the mechanisms of drug binding and resistance in MtrD, enhancing our understanding of AMR.

Future research directions could focus on exploring how to inhibit the action of MtrD by investigating detailed interactions of currently available inhibitors with MtrD and designing new inhibitors using the *in silico* and experimental approach developed in this study. Additionally, the *N. gonorrhoeae* panel developed here offers potential for high-throughput screening of new antibiotics that circumvent efflux by MtrD or serve as inhibitors of MtrD, utilising the panel of isogenic isolates developed in this study.

CHAPTER 7

APPENDICES

7.1 Appendix A: Abbreviations

°C	Degree Celsius
µg	Microgram
µl	Microlitre
µM	Micromolar
A	Access (conformation)
Å	Angstrom
ACR	Acriflavine
Amp	Ampicillin
AMR	Antimicrobial resistance
AZM	Azithromycin
B	Binding (conformation)
BB	β-barrel
BC	Benzalkonium chloride
bp	Base pair
C	Chloramphenicol disc
CA	Capric acid
CDC	Centers for Disease Control and Prevention,
CFU	Colony forming unit
CH	Chlorhexidine
CHAPS	3-[(3-cholamidopropyl)dimethylammonio]-1-propanesulfonate
CHL	Chloramphenicol
CHO	Cholic acid
C_{in}	Inward-open
CIP	Ciprofloxacin
CM	Cytoplasmic membrane
C-out	Outward-open
CRO	Ceftriaxone
CST	Colistin
CV	Crystal violet
DBP	Distal drug-binding pocket
DHA	Drug/H+ antiporter
DNA	Deoxyribonucleic acid
DQ	Dequalinium

Dxc	deoxycholate
E	Erythromycin disc
E	Extrusion (conformation)
ERY	Erythromycin
ESC	Extended-spectrum cephalosporin
ET	Ethidium
FA	fatty acid
Fur	Ferric uptake regulator
FUS	fusidic acid
g	g-force
G	Guanine
GEN	Gentamicin
HAs	Hydrophobic antimicrobials
His_6	Six-histidine residue (His_6) affinity tag
HLH	Helix-loop-helix
HMMD	High molecular mass drug
HP	α-helical hairpin
HT	Hydrophobic trap
IM	Inner membrane
IMP	Inner membrane protein
IPTG	Isopropyl β-D-1-thiogalactopyranoside
Kan	Kanamycin
Kan^R	Kanamycin resistance
Kb	Kilo base
kDa	Kilo Dalton
L	Loose (conformation)
LB	Luria-Bertani
LDAO	n-dodecyl-N,N-dimethylamine-N-oxide
LIP	Lipoyl
LMMD	Low molecular mass drug
LPS	Lipopolysaccharides
MATE	Multidrug and toxic compound extrusion
MDR	Multidrug resistance
MFP	Membrane fusion protein
MFS	Major facilitator superfamily

mg	Milligram
MH	Mueller-Hinton
MIC	Minimum inhibitory concentration
ml	Millilitre
mm	Millimetre
mM	Millimolar
MRSA	Methicillin resistant *Staphylococcus aureus*
N-9	Nonoxynol-9
NCBI	National centre for biotechnology information
ng	Nanogram
nm	Nanometre
NMP	1-(1-naphtylmethyl)-piperazine
NOR	Norfloxacin
NOV	Novobiocin
O	Open (conformation)
O/N	Overnight
OD	Optical density
OM	Outer membrane
OMP	Outer membrane protein
ORF	Open reading frame
ori	Origin of replication
OXA	Oxacillin
PA	Palmitic acid
PAP	Periplasmic adaptor protein
PAβN	Phenylalanine arginine β-naphthylamide
PBP	Proximal drug-binding pocket
PBS	Phosphate buffered saline
PCR	Polymerase chain reaction
PD	Periplasmic domain
PEN	Benzylpenicillin
PFGE	Pulsed-field gel electrophoresis
PMB	Polymyxin B
PRO	Progesterone
psi	Pounds per square inch
PT	Pentamidine

PVDF	Polyvinylidene fluoride
R6G	rhodamine 6G
RIF	Rifampin
RNA	Ribonucleic acid
RND	Resistance-nodulation division
rpm	Rotations per minute
RT	Room temperature
SDS	Sodium dodecyl sulphate
SDS-PAGE	Sodium dodecyl sulphate polyacrylamide gel electrophoresis
SMP	Small multidrug protein
SMR	Small multidrug resistance
T	Thymine
T	Thymine
T	Tight (conformation)
TAE	Tris-base acetic acid ethylenediaminetetraacitic acid
TE	Tetracycline disc
TET	Tetracycline
TetR	Tetracycline resistance
TGC	Tigecycline
TM	Transmembrane domain
TMD-BP	TMD binding pocket
TMS	Transmembrane segment
TPP	tetraphenylphosphonium
TR	Triclosan
TTBS	Tween Tris-buffered saline
TW-80	Tween 80
TX-100	Triton X-100
V	Volt
v/v	Volume/volume
w/v	Weight/volume
WHO	World Health Organisation
WT	Wild-type

7.2 Appendix B: Paper 1: The role played by drug efflux pumps in bacterial multidrug resistance.

Essays in Biochemistry (2017) **61** 127–139
DOI: 10.1042/EBC20160064

Review Article

The role played by drug efflux pumps in bacterial multidrug resistance

Mohsen Chitsaz and Melissa H. Brown

School of Biological Sciences, Flinders University, Adelaide, South Australia, Australia

Correspondence: Melissa H. Brown (melissa.brown@flinders.edu.au)

Antimicrobial resistance is a current major challenge in chemotherapy and infection control. The ability of bacterial and eukaryotic cells to recognize and pump toxic compounds from within the cell to the environment before they reach their targets is one of the important mechanisms contributing to this phenomenon. Drug efflux pumps are membrane transport proteins that require energy to export substrates and can be selective for a specific drug or poly-specific that can export multiple structurally diverse drug compounds. These proteins can be classified into seven groups based on protein sequence homology, energy source and overall structure. Extensive studies on efflux proteins have resulted in a wealth of knowledge that has made possible in-depth understanding of the structures and mechanisms of action, substrate profiles, regulation and possible inhibition of many clinically important efflux pumps. This review focuses on describing known families of drug efflux pumps using examples that are well characterized structurally and/or biochemically.

Introduction

Antimicrobial resistance (AMR) is an increasingly serious global public health problem, where existing antibiotics are losing their effects and are no longer clinically useful. In 2014, WHO reported very high rates of resistance in common pathogenic bacteria such as *Escherichia coli*, *Klebsiella pneumoniae*, *Pseudomonas aeruginosa* and *Staphylococcus aureus*, where many of these organisms exhibit simultaneous resistance to multiple antimicrobials, a phenotype that is referred to as multidrug resistance (MDR) and can be attributable to a single or multiple resistance mechanisms [1]. These mechanisms that bacteria exploit to resist the toxic effects of antimicrobials can involve enzymatic modification or destruction of antimicrobials, target modification that moderates the affinity of target proteins for antimicrobials, and limitation of drug access to cellular targets mediated by both reduced influx and increased efflux of antimicrobials. Drug efflux, defined as recognition and expulsion of toxic compounds from within the cell to the external medium before they reach their targets, represents a major mechanism of drug resistance [2].

Drug efflux mechanisms involve energy-dependent efflux transport proteins, which are located in the cytoplasmic membrane (CM). They can be grouped into the following seven families/superfamilies based on protein sequence homology, overall protein structure, energy source (ATP hydrolysis or ion electrochemical gradient), substrate specificity and other properties. These families are: (i) the ATP-binding cassette (ABC) superfamily, members of which are primary active transporters that use the free energy of ATP hydrolysis to energize efflux; (ii) the resistance-nodulation division (RND) superfamily; (iii) the major facilitator superfamily (MFS); (iv) the multidrug and toxic compound extrusion (MATE) family; (v) the small multidrug resistance (SMR) family; (vi) the proteobacterial antimicrobial compound efflux (PACE) family and (vii) the *p*-aminobenzoyl-glutamate transporter (AbgT) family (Figure 1). The latter six groups are secondary active transporters that couple efflux with ion electrochemical membrane gradient as an energy source [3–5].

Received: 06 December 2016
Revised: 22 January 2017
Accepted: 24 January 2017

Version of Record published:
3 March 2017

© 2017 The Author(s). Published by Portland Press Limited on behalf of the Biochemical Society

Essays in Biochemistry (2017) 61 127–139
DOI: 10.1042/EBC20160064

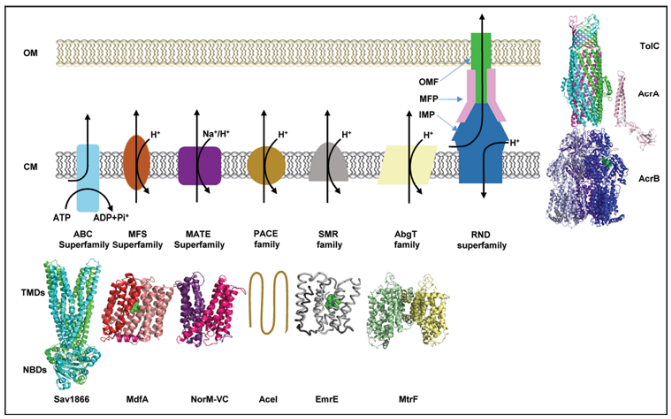

Figure 1. Schematic illustration of the seven families/superfamilies of multidrug transport proteins

Each group is shown by a distinct shape and highlighted with a different colour. Where available, a crystal structure of the functional unit or monomer of a representative protein of each group is shown in a similar colour to the corresponding diagram. Symmetric structures in proteins are visualized with different colours but in the same category of colours that matches the diagram's colours. Two crystal structures of the transporter contain a substrate that is represented as a green sphere. The CM and OM of Gram-negative bacteria are illustrated. The ABC superfamily (cyan rectangle), uses free energy of ATP hydrolysis catalysed by the NBDs of the transporter. The crystal structure of *S. aureus* Sav1866 (pdb: 2HYD), composed of a dimer (green and cyan), contains two TMDs and two NBDs and representing a functional unit of the ABC transporter is shown. Five singlet system secondary active transporter families/superfamilies: MFS, MATE, PACE, SMR and AbgT are shown by oval, rectangle, circle, chord and parallelogram shapes respectively. Crystal structures of the *E. coli* MFS MdfA (pdb: 4ZOW), *V. cholerae* MATE NorM (NorM_VC) (pdb: 3MKT), *E. coli* SMR EmrE (pdb: 3B5D) and *N. gonorrhoeae* AbgT MtrF (pdb: 4R1I) representative transport proteins are shown. A diagram containing four TMS representing the PACE family AceI transporter is also shown. The multicomponent RND superfamily system is shown by a diagram containing the CM-bound, MFP and OMF components, each highlighted by a different colour. Crystal structures of the *E. coli* AcrB (pdb: 2DRD) representing the integral CM protein, AcrA (pdb: 2F1M) the MFP and TolC (pdb: 2VDE) the OMF of an RND efflux system, are shown.

Drug efflux pumps are present in all bacterial species and other organisms. In bacteria, they play a key role not only in drug resistance but also in the movement of pathogenicity factors, e.g. by modulation of biofilm formation and possibly other physiological processes. They can also interact synergistically with other AMR mechanisms, the cumulative effects of which can result in AMR of clinical importance. Many efflux transporters can accommodate an extremely wide range of antimicrobial compounds (MDR efflux pumps), whereas others only export a specific substrate and its closely related derivatives. Both types are found in Gram-positive and Gram-negative bacteria and can contribute to clinical resistance. This review focuses on describing the known MDR export systems in bacteria and their affect on AMR.

The ABC superfamily

ABC transporters represent one of the largest superfamilies of proteins known in prokaryotes and eukaryotes involving both importers and exporters. Members of this superfamily translocate a wide range of substrates including sugars, amino acids, lipids and antimicrobial compounds. This substrate diversity reflects the numerous physiological roles that ABC transporters play in the cell, e.g. nutrient uptake, removal of waste and toxic products and export of cellular components such as cell wall polysaccharides [6]. LmrA from *Lactobacillus lactis* is a well-described ABC MDR efflux pump that exports a wide variety of substrates including antibiotics, toxic ions, lipids, antimicrobial peptides and antiseptics [7]. The *E. coli* MacB protein, another ABC MDR efflux pump, which are similar to RND pumps (described in the next section), functions together with its cognate membrane fusion protein (MFP) MacA and the outer membrane (OM) channel TolC, to confer resistance to macrolides [8]. The orthologous MacAB pump of *Neisseria*

© 2017 The Author(s). Published by Portland Press Limited on behalf of the Biochemical Society

Essays in Biochemistry (2017) **61** 127–139
DOI: 10.1042/EBC20160064

gonorrhoeae has also been shown to export multiple substrates including macrolides. Clinical isolates of *N. gonorrhoeae*, such as H041, have shown extensive resistance to extended-spectrum cephalosporins and the macrolide azithromycin and inactivation of MacAB renders the bacterium clinically susceptible to azithromycin according to MIC breakpoints indicating a key role of this pump in azithromycin resistance [9].

Solving the crystal structure of the *S. aureus* Sav1866 protein, which can transport structurally unrelated substrates such as ethidium, tetraphenylphosphonium and Hoechst 33342, marked one of the major steps in understanding ABC transporters at a structural and functional level (Figure 1) [10]. ABC transporters have a basic organization of two TMDs that contain the substrate translocation pathway and two nucleotide-binding domains (NBDs), which bind and hydrolyse ATP [10]. NBDs are highly conserved among ABC superfamily proteins and contain several motifs characteristic of this group of transporters. These include: the Walker A and B motifs, present in many nucleotide-binding proteins; motif C, specific to the ABC superfamily; and the stacking aromatic D-, H- and Q-loops and conserved sequences in loop regions that communicate conformational changes from the NBDs to the TMDs [6,11]. The functional unit of mammalian ABC transporters is a dimer, with each monomer containing two domains (TMD and NBD) contained in a single polypeptide. In bacterial transporters, however, each monomer is considered as a half transporter that is formed by the fusion of one TMD and one NBD, which are formed by separate polypeptides. In most ABC transporters, a functional transport complex is a homodimer, with each monomer containing six α-helical transmembrane segments (TMS) spanning the CM and 12 TMS in total per functional unit. Most ABC transporters follow this two-times-six TMS paradigm, albeit exceptions exist [12]. The structure of Sav1866 showed for the first time that TMS and NBD domains are connected via transmembrane helices and nucleotide binding is associated with dimerization [10].

A general model, referred to as conformational coupling, was proposed as the functional mechanism of ABC transporters. In this model, ATP-dependent conformational changes in the NBDs drive rearrangements of the TMS that enforces the link between transport and ATP hydrolysis and results in a transport mechanism often referred to as 'alternating access' [13]. This mechanism explains how the transport protein undergoes conformational changes, in which a central binding site located within a TMD is exposed alternately to the inside (inward-facing) or the outside (outward-facing) of the cell, but never simultaneously to both sides allowing the binding site alternating accessibility to each side of the membrane [13]. The current structural evidence obtained from several bacterial ABC transporters including Sav1866 [10], the lipid A and lipopolysaccharide transporter MsbA [14], BmrA from *Bacillus subtilis* and McjD from *E. coli*, indicate that these ABC exporters adopt an inward-facing conformation in the absence of nucleotide or when bound to ADP, and that they progress via an ATP-bound occluded transition state into the ATP-bound outward-facing conformation. Finally, the transporter is reset to the inward-facing conformation by dissociation of the NBD dimer mediated by ATP hydrolysis [13].

The RND superfamily

The RND superfamily represents a large ubiquitous group of efflux proteins that are found in prokaryotes, eukaryotes and archaea [15]. Of the eight families within this superfamily, one – the hydrophobic amphiphilic efflux 1 (HAE1) family, contains well-characterized, Gram-negative bacterial-specific RND transporters [15]. RND efflux pumps exhibit extensive topological similarity, usually with 12 TMS and two large hydrophilic periplasmic domains between TMS 1 and 2, and TMS 7 and 8 [15]. The N-terminal half of these RND transporters shares homology with the C-terminal half, suggesting an internal gene duplication event. RND integral membrane proteins function as part of a three-component system that includes two other proteins; the periplasmic adaptor protein belonging to the MFP family and the OM channel, belonging to the OM factor (OMF) family, that together form a functional tripartite efflux complex spanning the CM, the periplasm and the OM (Figure 1) [16]. RND transporters exhibit specificity mainly for hydrophobic and amphiphilic compounds, catalysing export of a wide spectrum of compounds including detergents, antibiotics, dyes, bile salts, fatty acids, biocides, isoflavonoids and aliphatic and aromatic organic solvents and capture their substrates preferentially from the periplasm [15].

The biochemically and structurally well-characterized *E. coli* AcrB protein is the prototype of RND efflux pumps. AcrB exports a large group of substrates including most antibacterial compounds. The X-ray crystal structure of AcrB without bound substrate was first reported in 2002, revealing a homotrimer [17]. Each monomer contained a large periplasmic domain and a TMD organized into 12 TMS, in addition to many subdomains and other structural features [17]. Further crystal structures of AcrB solved by three laboratories in 2006–2007 significantly advanced the understanding of the structure and function of RND pumps, in particular that each monomer has a unique conformation slightly different from that of its neighbours [18-20]. These three conformations correspond to three functional stages of the protein i.e. access, binding and extrusion that describe substrate binding and efflux by AcrB.

© 2017 The Author(s). Published by Portland Press Limited on behalf of the Biochemical Society

Essays in Biochemistry (2017) **61** 127–139
DOI: 10.1042/EBC20160064

AcrB co-crystallized with the substrates minocycline and doxorubicin identified a multisite drug binding (distal) pocket deep within the pore domain [18] and substrate molecules were only found in one monomer, called the binding monomer. The asymmetric crystal structure suggested that drugs are exported by a three-step functionally rotating mechanism, in which each monomer cycles through sequential conformations and substrates undergo ordered binding change [18]. Within the pore domain, crystal structures of AcrB bound to rifampicin and erythromycin identified an additional drug binding pocket [21] (the proximal pocket), which is hypothesized to accommodate and bind large substrates such as rifampicin. These two intramolecular substrate binding pockets are separated by a 'switch loop' that swings during conformational change from access to binding stages allowing substrates to move from the proximal site to the distal pocket [22]. Three entrances lead to and merge in the proximal pocket. Interestingly, it was shown that the hydrophobic parts of many compounds that can inhibit RND proteins (efflux pump inhibitors; EPIs), tightly bound to a site in the lower part of distal binding pocket known as the 'hydrophobic trap', thereby, distorting the shape of the rest of the pocket resulting in inhibition of efflux of typical substrates of AcrB [23]. A third drug-binding area was identified in the central cavity, from structures of AcrB bound to substrates such as ethidium. However, the significance of this drug-binding site could not be ascertained by site-directed mutagenesis [24,25]. It is believed that multisite multiple drug binding in AcrB follows the same principles elucidated by crystallographic studies of QacR, the soluble regulator of the multidrug efflux protein QacA [26]. The multisite-drug-oscillation hypothesis, which explains recognition of drugs with low-binding affinity to specific sites in the AcrB, is another possible multidrug recognition mechanism [27].

The energy requirements for substrate translocation originate from the proton motive force (PMF) [28], where four essential AcrB charged residues form a transmembrane proton-relay network involved in proton translocation [29]. A conformational cycling mechanism involving two remote alternating access sites within each AcrB monomer, one in the TMD for proton translocation and one for substrate translocation in the periplasmic domain, has been proposed [30].

AcrB operates as part of a tripartite system including AcrA and TolC (Figure 1); however, the stoichiometry of these three components in the functional complex is controversial. Based on individual crystal structures and cross-linking experiments, the docking stoichiometry of $AcrB_3$–$AcrA_3$–$TolC_3$ is a possible model of the tripartite assembly [27]. This model is challenged by electron microscopic images of the AcrAB–TolC complex obtained by Du et al. [31] as well as electron microscopic images of the native AcrAB–TolC, the MexAB–OprM and the interspecies AcrA–MexB–TolC complexes in nanodiscs [32]. These images indicate no direct interaction between the integral CM protein and the OM channel and suggested a 3:6:3 stoichiometry. It was previously shown that the small 49 amino acid AcrZ protein of *E. coli* interacts with AcrB to enhance the ability of the AcrAB–TolC pump system to export certain classes of substrates [33].

Expression of *acrAB* and *tolC* in *E. coli* is regulated at both local and global levels. The *acrAB* operon and the *tolC* gene are chromosomally encoded, and although in separate locations, their expression is often regulated by common mechanisms, involving repressors, activators, two-component systems and small RNAs. The *acrR* gene is divergently transcribed from *acrAB* and directly represses *acrAB* and its own expression [34]. Belonging to the TetR/QacR family of transcriptional regulators, AcrR functions as a dimeric two-domain molecule, in which the N-terminal region comprises the helix-turn-helix containing DNA-binding domain and the C-terminal region forms the dimerization and multidrug-binding domain [35,36]. AcrR, however, does not completely inhibit the expression of *acrAB*, allowing constitutive expression of the transporter and thus intrinsic MDR. Two other proteins are also involved in the regulation of *acrAB*. AcrS, a direct repressor of the AcrEF pump, also represses expression of other multidrug transporter genes including *acrAB* [37]. The quorum-sensing receptor SdiA, positively controls expression of *acrAB* likely by acting as a minor activator [38]. Furthermore, in terms of activation, three global regulators, MarA, SoxS and Rob also positively control expression of *acrAB* and *tolC* [39-42]. In addition, the two-component system EvgAS regulates expression of both *acrAB* and *tolC*, and a second two-component system, PhoPQ, regulates expression of *tolC* [43]. Furthermore, the small RNA RyeB, has been shown to be involved in controlling *acrAB* expression. Multiple regulatory systems controlling expression of RND pumps at local and global levels facilitate adaptation of host strains to diverse conditions [44].

There is overwhelming evidence that overexpression of RND pumps (and some exporters from other families) is significantly associated with MDR in antibiotic-resistant bacteria commonly isolated from humans and animals, where it can lead to resistance levels for multiple antibiotics at clinically significant levels. Many studies have shown this in MDR clinical isolates of *E. coli*, *K. pneumoniae*, *Salmonella enterica* serovar Typhimurium, *P. aeruginosa*, *Campylobacter jejuni*, *Acinetobacter baumannii* and other Gram-negative bacteria [45-48]. For example, *P. aeruginosa* that contains several RND pumps including MexAB-OprM, MexXY-OprM, MexCD-OprJ and MexEF-OprN, can export antibiotics used in current clinical settings such as fluoroquinolones, tetracycline, chloramphenicol and

© 2017 The Author(s). Published by Portland Press Limited on behalf of the Biochemical Society

some β-lactams [45]. In addition to these, an interesting study was recently performed in clinical isolates of *N. gonorrhoeae* that were extensively resistant to third generation cephalosporins (including ceftriaxone) and the macrolide azithromycin [9]. It was found that even in the presence of other mechanisms of drug resistance, deletion of the main RND pump, MtrCDE, from a number of these strains significantly reduced the MICs for many antibiotics (in particular ceftriaxone and azithromycin), below their clinical breakpoints [9].

The MFS

MFS transporters are also efflux proteins that are found ubiquitously in the membranes of all types of living organisms and compose the largest superfamily of secondary transporters. These proteins utilize the power in electrochemical gradients of either protons or sodium ions to transport amino acids, sugars, peptides and drugs, among others and can act as symporters, uniporters or antiporters. This superfamily is currently composed of 82 recognized subfamilies [49,50]. Many drug and multidrug transporters are classified within the MFS superfamily, with three drug/H^+ antiporter (DHA) families i.e. DHA1, DHA2 and DHA3, comprised exclusively of efflux transporters [5,51]. DHA1 and DHA3 families contain transport proteins that display 12 TMS and include several well-characterized MDR transporters such as MdfA and EmrD of *E. coli* and NorA of *S. aureus*. In contrast, members of the DHA2 family such as QacA/QacB and EmrB, contain 14 TMS [52]. It is believed that the most abundant MFS transporters i.e. 12-TMS proteins, have arisen from a single 2-TMS hairpin that triplicated, giving rise to a protein with 6 TMS that through a duplication event resulted in the formation of 12-TMS proteins [49]. Several superfamily and family specific amino acid sequences (motifs) within MFS transporters have been identified [5]. High conservation of these sequences/motifs within MFS members indicates that they are possibly involved in structural or functional roles. Motif A is known as the MFS-specific motif and structural analysis of the MFS transporter YjaR has demonstrated that residues contained in motif A sense and respond to protonation inside the central cavity [53].

Analyses of MFS transporters, including structures of MDR exporters EmrD and MdfA, have resulted in the following postulations: (i) MFS transporters generally function as monomers; (ii) they have a common structural architecture called the MFS-fold which comprises two domains, each consisting of bundles of six consecutive TMS organized into a pair of inverted '3 + 3' repeats; (iii) the N- and C-domains are related by a pseudo two-fold symmetry axis in the membrane plane and are linked by a long cytoplasmic loop or by two TMS and (iv) a membrane-embedded central cavity is present between these two domains, thus forming the substrate-transport pathway. In EmrD, this central cavity is quite large and surrounded by hydrophobic and aromatic side chains. This is in line with the more recent MdfA structure (Figure 1) that also possesses a central cavity of hydrophobic residues. In EmrD, the loops connecting TMS 4 and 5, and TMS 10 and 11 protrude into the cytoplasm and it is believed that they play a role in substrate recognition and capture [54].

Alternating access is the widely accepted mechanism of MFS substrate translocation, similar to that proposed for other transport proteins. Analyses of crystal structures of MFS transporters in multiple conformations (inward-open, occluded and outward-open) have enabled the elucidation of details of alternating access and energy-coupling mechanisms of MFS substrate transport translocation. These analyses suggested that the translocation pathway of the substrate follows the interface between the two six-helices, with the substrate binding pocket located halfway into the membrane [55]. A rocker-switch type of movement mechanism involving successive and concerted conformational changes of the two halves of the protein among inward-open, occluded and outward-open states alternately generate a pathway of access to either surface of the membrane. The transport coupling of MFS proteins occurs through sequential binding/releasing of substrate/counter-ion and this varies among family members [54,55].

Multiple MFS efflux transporters can be found in Gram-negative bacteria. In *E. coli* K-12, for example 70 MFS proteins have been identified, 15 of which may be considered drug efflux transporters. Some of these are present as tripartite systems, as in a similar fashion to the RND systems they use their cognate adaptor protein and the TolC channel. In *E. coli* for example, EmrB (occurring with the cognate adaptor EmrA) and EmrY (with EmrK) are believed to be involved in the efflux of uncouplers and other substrates. In contrast, MdfA is a singlet pump that has been studied extensively [44]. MdfA is known to confer resistance to a variety of structurally distinct cationic and zwitterionic lipophilic compounds, as well as to a number of electroneutral antibiotics of clinical importance [56]. MDR *E. coli* clinical strains have been shown to overexpress MdfA from plasmids and MdfA orthologues have been identified in several pathogenic bacterial species [56,57]. Recent structures of MdfA in complex with three different ligands identified and confirmed residues responsive to substrate binding in addition to confirming the recently ascribed role of D34 in substrate binding through protonation [57]. The plasmid encoded QacA MDR transporter is the best characterized 14-TMS MFS member. QacA specifies resistance to a range of structurally dissimilar organic cations, including monovalent cations, such as ethidium, benzalkonium and cetrimide and divalent cations, such as

© 2017 The Author(s). Published by Portland Press Limited on behalf of the Biochemical Society

Essays in Biochemistry (2017) **61** 127–139
DOI: 10.1042/EBC20160064

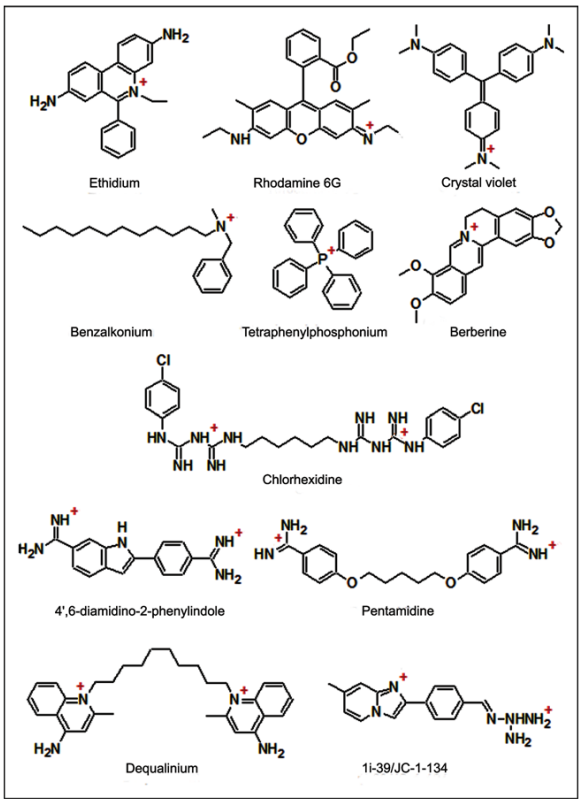

Figure 2. Representative substrates of the staphylococcal multidrug efflux protein QacA

QacA mediates resistance to an extensive range of monovalent and divalent cationic lipophilic compounds, which can be broadly classified as dyes, quaternary ammonium compounds, biguanidines, diamidines and guanylhydrazones. Chemical structures of a few examples of QacA substrates are displayed to illustrate the diversity of structures recognized, which have been identified as substrates of other pump systems. Six monovalent and five divalent cationic compounds are shown at the top and bottom of the picture respectively. Positive charges on each molecule are highlighted in red.

chlorhexidine, pentamidine and dequalinium (Figure 2). Interestingly, the highly homologous QacB can only efflux monovalent compounds; these two proteins differ by only seven residues [52,58-61].

Recently, a new mechanism of efflux by secondary transporters was described for MdfA[62]. Unlike QacA that can export both monovalent and divalent cationic substrates, MdfA was previously known to export only neutral or monovalent substrates by a mechanism involving the exchange of a single proton. However, it was shown later that by including an additional acidic residue, MdfA can catalyse efflux of divalent cations that have a unique architecture: two charged moieties that must be separated by a long linker [62]. Examples of these substrates, chlorhexidine and dequalinium, are shown in Figure 2. These two MFS transporters export this type of divalent cationic substrate in two successive transport cycles, where each cationic moiety is transported as if it were a separate substrate and involves

© 2017 The Author(s). Published by Portland Press Limited on behalf of the Biochemical Society

the exchange of two protons for one substrate molecule. It was proposed that secondary transporters can adopt a processive-like mode of action, thus expanding the substrate spectrum of multidrug transporters [62].

The MATE family

Over 1000 transport proteins are members of the MATE family and can be allocated into three subfamilies, which are further subdivided into 14 subfamilies [63]. These transporters use the membrane gradient of Na^+, H^+ or both, as an energy source for driving export of cationic compounds although the details of coupling mechanism is not fully understood yet. The NorM antiporter from *Vibrio parahaemolyticus* (NorM_VP) was the first MATE protein identified [64]. When expressed in *E. coli*, NorM_VP confers resistance to norfloxacin and ciprofloxacin, as well as structurally unrelated compounds like ethidium, kanamycin and streptomycin [64]. Other MATE members, including the *N. gonorrhoeae* NorM (NorM_NG), *E. coli* YdhE and *S. aureus* MepA proteins have been well characterized, with extensive substrate profiles [65,66].

Most proteins of the MATE family consist of 400–550 amino acids, with 12 TMS. They share ~45% similarity suggesting that they have common structural and functional features. NorM from *Vibrio cholerae* (NorM_VC) was the first member of the MATE family whose crystal structures were solved with and without substrate (rubidium) (Figure 1). These crystal structures showed that the membrane spanning protein is composed of two bundles of 6-TMS (TMS 1–6 and TMS 7–12) forming a large internal cavity that is open to the extracellular space (outward facing) [67]. These two halves have an intramolecular two-fold symmetry, suggesting that they have arisen due to a gene duplication. A cytoplasmic loop, also seen in the MFS transporters, connects these two halves. Two substrate passages, one from each side of the protein, are opened to the outer leaflet of the CM. In addition, a monocation-binding site was identified in the internal cavity suggesting that the outward facing conformation favours high affinity binding of monocations such as Na^+ and low affinity binding for substrates. The crystal structures of the Na^+-coupled NorM_NG in complex with three substrates, as well as Cs^+ (a Na^+ congener), were all solved in extracellular facing and drug-bound states [68]. These structures identified a multidrug-binding cavity containing four negatively charged residues and details of rearrangement of some TMS upon Na^+-induced drug export [68]. Structures and functional analyses of a MATE transporter from *Pyrococcus furiosus* in two distinct apo-form conformations and complexed with a norfloxacin derivative and three peptide inhibitors, showed that the protonation of Asp^{41} in the N-terminal part of the protein induces the bending of TMS 1, which in turn collapses the N-terminal part cavity, thereby extruding the substrate drug to the extracellular space [69].

The SMR family

The SMR family of transporters contain the smallest membrane transport proteins. This family can be divided into three subfamilies; the small multidrug pumps (SMP), paired small multidrug resistance pumps (PSMRs) and suppressors of *groEL* mutations (SUGs). Phylogenetic analysis of SMR family proteins identified two phylogenetic clusters, with only one of these containing proteins able to catalyse drug export [70]. This largest cluster is composed of the SMP proteins including QacC from *S. aureus* and EmrE from *E. coli*, two of the best characterized SMR family proteins.

SMR family proteins are highly hydrophobic and typically contain 100–150 amino acids constrained in four TMS. They are proton-coupled transporters that can confer low-level resistance to a variety of antimicrobial agents, including a number of biocides in addition to toxic lipophilic cations that function as DNA-intercalating agents. Additionally, SMR family proteins display regions of conservation with other larger transporters in the drug/metabolite efflux family [70]. The functional unit of SMP subfamily proteins is believed to be a homodimer. In contrast, members of the PSMR subfamily require simultaneous expression of two SMR gene copies co-located within the same operon that form a heteroligomer that can then actively extrude compounds. The most well-characterized PSMR proteins are EbrAB from *B. subtilis*. Structural and functional studies of this system have shown that these proteins form a heteroligomer where the two proteins are in opposite orientations [71].

The *E. coli* EmrE SMP protein is the prototype of all SMR proteins. It has been subjected to numerous studies by multiple laboratories analysing the biochemical and structural complexities of this protein. A number of structural approaches have been applied to EmrE including both solution and solid-state NMR, cryo-EM, spin-labelling EPR and X-ray diffraction. This 110-residue protein pumps out positively charged aromatic compounds such as ethidium, acriflavine, methyl viologen, benzalkonium, tetraphenylphosphonium, tetracycline, erythromycin and sulfadiazine. Like PSMR proteins, EmrE functions as a dimer, however, the organization of EmrE monomers in the membrane has been hotly contested. Current consensus is that the dual-topology protein EmrE has an asymmetrical arrangement where each protein monomer is in an antiparallel orientation. This dimeric EmrE exchanges two protons/substrate/transport

© 2017 The Author(s). Published by Portland Press Limited on behalf of the Biochemical Society

Essays in Biochemistry (2017) **61** 127–139
DOI: 10.1042/EBC20160064

cycle [72]. Site-directed mutagenic studies have shown that the antiport of drug and proton relies on a highly conserved negatively charged glutamate residue in the first TMS of SMR family proteins.

Substrate binding has been proposed to occur at the monomer–monomer interface, at the centre of the protein, from the inner leaflet of the CM and results in the movement of at least one TMS [73]. Similar to that determined for membrane transporters from other superfamilies (see above), the single site alternating access model has also been proposed for the mechanism of SMR proteins [74]. Thus, each state in the transport cycle is only open to one side of the membrane (outward-facing conformation) and only when a substrate or two protons are bound, does the protein interconvert to an inward-facing state.

The PACE and AbgT families

Recent studies have identified two new secondary active drug transporter families; the PACE family and the antimetabolite transporters forming the AbgT family (Figure 1). The first transport protein of the PACE family, AceI (Figure 1), was identified during a transcriptomic study in *A. baumannii* after a shock treatment with the biocide chlorhexidine was applied [75]. Although annotated as a hypothetical membrane protein, studies revealed that AceI conferred resistance to chlorhexidine via an active efflux mechanism. Bioinformatic analyses and subsequent functional assays have identified AceI homologues in a large number of species and the substrates of these transporters have been expanded to other synthetic biocides including benzalkonium, proflavine, acriflavine and dequalinium. PACE family members are small membrane proteins of ~150 residues and contain two tandem bacterial transmembrane pair (BTP; Pfam accession number PF05232) domains. To date, there are more than 750 protein sequences containing this domain listed in the Pfam database.

The latest family of MDR transporters is the AbgT family that is exemplified by the MtrF MDR protein of *N. gonorrhoeae* (Figure 1). Normally, this family contains proteins that act as importers, such as the AbgT (YdaH) protein of *E. coli* [76] that may be involved in the uptake of *p*-aminobenzoyl-glutamate, a precursor of folic acid biosynthesis [77,78]. Required for high-level hydrophobic AMR in *N. gonorrhoeae*, the MtrF protein was the first efflux transporter described in the AbgT family and acts in conjunction with the MtrCDE RND efflux system [79]. The YdaH protein of *Alcanivorax borkumensis*, a marine bacterium that uses oil hydrocarbons as its exclusive source of carbon and energy, was also recently identified to be a member of the AbgT family [4]. Crystal structures of both the *N. gonorrhoeae* MtrF and the *A. borkumensis* YdaH determined these two transporters assemble as dimers with architectures different from all other families of transporters. In both the proteins, the dimer forms a bowl-shaped structure with a solvent-filled basin extending from the cytoplasm midway through the membrane bilayer. Each monomer of MtrF and YdaH contains nine TMS and two hairpins. Further structural analyses combined with biochemical studies implied that both the MtrF and YdaH proteins are efflux pumps capable of producing resistance by exporting sulfonamide antimetabolites [4].

Control of efflux pumps

The flexible nature of drug efflux pump regulation enables bacteria to fine-tune expression of their systems to adapt to diverse environments [44]. This adaptation can occur either via conferring AMR or contributing to the bacterium's ability to invade and survive in host cells or specific host environments. As described above, the regulation of efflux pump expression can be controlled by local and global transcriptional regulators, modulators and two-component regulatory systems that involve different regulatory cascades and small RNA molecules. Mutations in the genes encoding these *trans*-acting regulatory elements can alter the expression levels of the efflux pumps sometimes with negative clinical outcomes [9,48]. For example in *E. coli* and other Enterobacteriaceae, mutations inactivating the local repressor *acrR* of *acrAB*, result in overexpression of this efflux pump and subsequent MDR [80–82]. Expression of AcrAB can also be increased by mutating *marR* and *soxR* as this can result in the enhanced production of the global activators, MarA and SoxS respectively, that also act on the AcrAB system.

Mutations in the regulatory sequences such as promoters can also increase the expression levels of efflux pumps and give rise to resistance with clinical importance. Called *cis*-acting regulatory elements, these important mechanisms of resistance are commonly identified in pathogenic bacteria. For example in clinical *N. gonorrhoeae* isolates, four *cis*-acting elements have been found associated with increased expression of the MtrCDE efflux system and MDR. These elements include: (i) a single bp deletion or a dinucleotide insertion within an inverted repeat in the *mtrR* promoter; (ii) a point mutation, located at 120-nts upstream of the *mtrC* start codon and (iii) a 153-bp insertion mutation in the *mtrR–mtrCDE* intervening region that is called Correia element [83]. Similarly, promoter mutations have been identified for the *S. aureus* NorA MFS MDR efflux pump, that result in overexpression of *norA* in clinical

© 2017 The Author(s). Published by Portland Press Limited on behalf of the Biochemical Society

strains. Additionally, clinical isolates of *Candida albicans* have been isolated that are azole resistant due to constitutively high-level expression of the ABC superfamily CDR1 and CDR2 pumps; a drug-responsive element sequence within their promoters was identified [84].

Since the discovery of efflux pump-mediated AMR, the development of EPIs as an effective strategy for combating AMR has been considered. These EPIs could promote the return of certain antibiotics into clinical practice and may also broaden the spectrum of antibiotics to cover Gram-negative bacteria that are naturally resistant to those antibiotics that act on Gram-positive bacteria [85]. It has been shown that EPIs significantly decrease the frequency of development of AMR mutants. In addition, inhibition of efflux would also have extra benefits of decreasing bacterial resistance to mediators of the innate immune response that are also substrates of efflux pumps and attenuating virulence of Gram-negative bacteria that is partly mediated by biofilm formation [86]. Many EPIs have been identified and characterized, including verapamil, reserpine, PAβN, NMP, D13-9001 and MBX2319. Some of these inhibitors are specific for an efflux pump whereas others inhibit the efflux activity of multiple proteins. Unfortunately, a number of EPIs have been shown to possess acute toxicity and prolonged accumulation in tissue cells [87]. Subsequently, no EPI has reached clinical use yet. This shows that the development of universal or even specific EPIs and/or drugs that bypass efflux pumps is not without problems. These challenges include: conversion of a lead compound to a new drug; formulation of effective combinational therapy; clinical trials; difficulties that are related to the nature of a molecule that can be used as an antibiotic or inhibitor in terms of physical and chemical properties; toxicity for humans and animals and identifying a molecule that can inhibit such flexible multispecific binding sites. Advances in science and technology have made it possible to identify and characterize many AMR-related efflux transporters and in particular develop an in-depth understanding of the structure and mechanisms of action of many of them as well as their interaction with a wide range of substrates. However, further progress in analyses of efflux transporters especially MDR-related systems is required to enable rational design of drugs or inhibitors in the future that could overcome to the current limitations.

Summary

- MDR efflux pumps are active transporters that mediate resistance to a broad range of structurally diverse drugs and are of increasing concern in chemotherapy of infections and cancer.
- Efflux pumps are widespread among bacteria and eukaryotes including those that are pathogens and can be grouped into the seven categories.
- Typical membrane structure (topology) of efflux pumps comprises 4, 6, 12 or 14 transmembrane spanning helices.
- Alternating access is the common mechanism used by many efflux systems to translocate substrates.
- Multidrug efflux pumps utilize one or more drug-binding pockets with multiple drug-binding sites to recognize and transport structurally diverse substrates.
- Regulation of efflux pump expression is typically controlled by the participation of several local and global transcriptional regulators, modulators and two-component regulatory systems that involve different regulatory pathways and mutations in expression control elements, such as promoters, also play a role.
- Several EPIs have been identified, however, none have progressed to clinical use yet.
- In-depth understanding of interaction of efflux pumps with antibiotics and efflux inhibitors will enable rational drug and inhibitor design.

© 2017 The Author(s). Published by Portland Press Limited on behalf of the Biochemical Society

Essays in Biochemistry (2017) **61** 127–139
DOI: 10.1042/EBC20160064

Funding

This work was supported by the National Health and Medical Research Council Australia Project Grant [grant number 1002670]; a Flinders Foundation Seeding Grant; a Weizmann-Australia Joint Research Program; and a Australian Government Research Training Program Scholarship (to M.C.). .

Competing interests

The authors declare that there are no competing interests associated with the manuscript.

Abbreviations

ABC, ATP-binding cassette; AMR, antimicrobial resistance; ATP, adenosine tri-phosphate; CM, cytoplasmic membrane; DHA, drug/H+ antiporter; EPI, efflux pump inhibitor; MATE, multidrug and toxic compound extrusion; MDR, multidrug resistance; MFP, membrane fusion protein; MFS, major facilitator superfamily; NBD, nucleotide-binding domain; NMP, NMP1-(1-naphthylmethyl)-piperazine; OM, outer membrane; OMF, OM factor; PAβN, phenylalanylarginine-β-naphthylamide; PACE, proteobacterial antimicrobial compound efflux; PDB, protein data bank; PSMR, paired small multidrug resistance pump; RND, resistance-nodulation division; SMP, small multidrug pump; SMR, small multidrug resistance; TMD, transmembrane domain; TMS, transmembrane segment; WHO, world health organization.

References

1 World Health Organization (2014) Antimicrobial resistance global report on surveillance: 2014 summary. Geneva, Switzerland
2 Holmes, A.H., Moore, L.S., Sundsfjord, A., Steinbakk, M., Regmi, S., Karkey, A. et al. (2016) Understanding the mechanisms and drivers of antimicrobial resistance. *Lancet* **387**, 176–187
3 Hassan, K.A., Liu, Q., Henderson, P.J. and Paulsen, I.T. (2015) Homologs of the *Acinetobacter baumannii* AceI transporter represent a new family of bacterial multidrug efflux systems. *MBio* **6**, e01982–14
4 .Delmar, J.A. and Yu, E.W. (2016) The AbgT family: a novel class of antimetabolite transporters. *Protein Sci.* **25**, 322–337
5 Paulsen, I.T., Brown, M.H. and Skurray, R.A. (1996) Proton-dependent multidrug efflux systems. *Microbiol. Rev.* **60**, 575–608
6 Rees, D.C., Johnson, E. and Lewinson, O. (2009) ABC transporters: the power to change. *Nat. Rev. Mol. Cell Biol.* **10**, 218–227
7 Poelarends, G.J., Mazurkiewicz, P. and Konings, W.N. (2002) Multidrug transporters and antibiotic resistance in *Lactococcus lactis*. *Biochim. Biophys. Acta* **1555**, 1–7
8 Kobayashi, N., Nishino, K. and Yamaguchi, A. (2001) Novel macrolide-specific ABC-type efflux transporter in *Escherichia coli*. *J. Bacteriol.* **183**, 5639–5644
9 Golparian, D., Shafer, W.M., Ohnishi, M. and Unemo, M. (2014) Importance of multidrug efflux pumps in the antimicrobial resistance property of clinical multidrug-resistant isolates of *Neisseria gonorrhoeae*. *Antimicrob. Agents Chemother.* **58**, 3556–3559
10 Dawson, R.J. and Locher, K.P. (2007) Structure of the multidrug ABC transporter Sav1866 from *Staphylococcus aureus* in complex with AMP-PNP. *FEBS Lett.* **581**, 935–938
11 Wilkens, S. (2015) Structure and mechanism of ABC transporters. *F1000Prime Rep.* **7**, 14
12 George, A.M. and Jones, P.M. (2013) An asymmetric post-hydrolysis state of the ABC transporter ATPase dimer. *PLoS ONE* **8**, e59854
13 van Veen, H.W. (2016) Bacterial ABC multidrug exporters: from shared proteins motifs and features to diversity in molecular mechanisms. In *ABC transporters-40 Years on* (George, A.M., ed.), pp. 37–51, Springer, Switzerland
14 Ward, A., Reyes, C.L., Yu, J., Roth, C.B. and Chang, G. (2007) Flexibility in the ABC transporter MsbA: alternating access with a twist. *Proc. Natl. Acad. Sci. U.S.A.* **104**, 19005–19010
15 Tseng, T.T., Gratwick, K., Kollman, J., Park, D., Nies, D., Goffeau, A. et al. (1999) The RND permease family: an ancient, ubiquitous and diverse family that includes human disease and development proteins. *J. Mol. Microbiol. Biotechnol.* **1**, 107–125
16 Nikaido, H. (2011) Structure and mechanism of RND-type multidrug efflux pumps. *Adv. Enzymol. Relat. Areas Mol. Biol.* **77**, 1–60
17 Murakami, S., Nakashima, R., Yamashita, E. and Yamaguchi, A. (2002) Crystal structure of bacterial multidrug efflux transporter AcrB. *Nature* **419**, 587–593
18 Murakami, S., Nakashima, R., Yamashita, E., Matsumoto, T. and Yamaguchi, A. (2006) Crystal structures of a multidrug transporter reveal a functionally rotating mechanism. *Nature* **443**, 173–179
19 Seeger, M.A., Schiefner, A., Eicher, T., Verrey, F., Diederichs, K. and Pos, K.M. (2006) Structural asymmetry of AcrB trimer suggests a peristaltic pump mechanism. *Science* **313**, 1295–1298
20 Sennhauser, G., Amstutz, P., Briand, C., Storchenegger, O. and Grutter, M.G. (2007) Drug export pathway of multidrug exporter AcrB revealed by DARPin inhibitors. *PLoS Biol.* **5**, e7
21 Nakashima, R., Sakurai, K., Yamasaki, S., Nishino, K. and Yamaguchi, A. (2011) Structures of the multidrug exporter AcrB reveal a proximal multisite drug-binding pocket. *Nature* **480**, 565–569
22 Eicher, T., Cha, H.J., Seeger, M.A., Brandstatter, L., El-Delik, J., Bohnert, J.A. et al. (2012) Transport of drugs by the multidrug transporter AcrB involves an access and a deep binding pocket that are separated by a switch-loop. *Proc. Natl. Acad. Sci. U.S.A.* **109**, 5687–5692
23 Nakashima, R., Sakurai, K., Yamasaki, S., Hayashi, K., Nagata, C., Hoshino, K. et al. (2013) Structural basis for the inhibition of bacterial multidrug exporters. *Nature* **500**, 102–106

© 2017 The Author(s). Published by Portland Press Limited on behalf of the Biochemical Society

24 Husain, F., Bikhchandani, M. and Nikaido, H. (2011) Vestibules are part of the substrate path in the multidrug efflux transporter AcrB of *Escherichia coli*. *J. Bacteriol.* **193**, 5847–5849
25 Yu, E.W., Aires, J.R., McDermott, G. and Nikaido, H. (2005) A periplasmic drug-binding site of the AcrB multidrug efflux pump: a crystallographic and site-directed mutagenesis study. *J. Bacteriol.* **187**, 6804–6815
26 Schumacher, M.A., Miller, M.C., Grkovic, S., Brown, M.H., Skurray, R.A. and Brennan, R.G. (2001) Structural mechanisms of QacR induction and multidrug recognition. *Science* **294**, 2158–2163
27 Yamaguchi, A., Nakashima, R. and Sakurai, K. (2015) Structural basis of RND-type multidrug exporters. *Front. Microbiol.* **6**, 327
28 Zgurskaya, H.I. and Nikaido, H. (1999) Bypassing the periplasm: reconstitution of the AcrAB multidrug efflux pump of *Escherichia coli*. *Proc. Natl. Acad. Sci. U.S.A.* **96**, 7190–7195
29 Guan, L. and Nakae, T. (2001) Identification of essential charged residues in transmembrane segments of the multidrug transporter MexB of *Pseudomonas aeruginosa*. *J. Bacteriol.* **183**, 1734–1739
30 Eicher, T., Seeger, M.A., Anselmi, C., Zhou, W., Brandstatter, L., Verrey, F. et al. (2014) Coupling of remote alternating-access transport mechanisms for protons and substrates in the multidrug efflux pump AcrB. *Elife* **3**, e03145
31 Du, D., Wang, Z., James, N.R., Voss, J.E., Klimont, E., Ohene-Agyei, T. et al. (2014) Structure of the AcrAB-TolC multidrug efflux pump. *Nature* **509**, 512–515
32 Daury, L., Orange, F., Taveau, J.C., Verchere, A., Monlezun, L., Gounou, C. et al. (2016) Tripartite assembly of RND multidrug efflux pumps. *Nat. Commun.* **7**, 10731
33 Hobbs, E.C., Yin, X., Paul, B.J., Astarita, J.L. and Storz, G. (2012) Conserved small protein associates with the multidrug efflux pump AcrB and differentially affects antibiotic resistance. *Proc. Natl. Acad. Sci. USA.* **109**, 16696–16701
34 Ma, D., Alberti, M., Lynch, C., Nikaido, H. and Hearst, J.E. (1996) The local repressor AcrR plays a modulating role in the regulation of *acrAB* genes of *Escherichia coli* by global stress signals. *Mol. Microbiol.* **19**, 101–112
35 Peters, K.M., Brooks, B.E., Schumacher, M.A., Skurray, R.A., Brennan, R.G. and Brown, M.H. (2011) A single acidic residue can guide binding site selection but does not govern QacR cationic-drug affinity. *PLoS ONE* **6**, e15974
36 Li, M., Gu, R., Su, C.C., Routh, M.D., Harris, K.C., Jewell, E.S. et al. (2007) Crystal structure of the transcriptional regulator AcrR from *Escherichia coli*. *J. Mol. Biol.* **374**, 591–603
37 Hirakawa, H., Takumi-Kobayashi, A., Theisen, U., Hirata, T., Nishino, K. and Yamaguchi, A. (2008) AcrS/EnvR represses expression of the acrAB multidrug efflux genes in *Escherichia coli*. *J. Bacteriol.* **190**, 6276–6279
38 Rahmati, S., Yang, S., Davidson, A.L. and Zechiedrich, E.L. (2002) Control of the AcrAB multidrug efflux pump by quorum-sensing regulator SdiA. *Mol. Microbiol.* **43**, 677–685
39 Barbosa, T.M. and Levy, S.B. (2000) Differential expression of over 60 chromosomal genes in *Escherichia coli* by constitutive expression of MarA. *J. Bacteriol.* **182**, 3467–3474
40 Alekshun, M.N. and Levy, S.B. (1997) Regulation of chromosomally mediated multiple antibiotic resistance: the mar regulon. *Antimicrob. Agents Chemother.* **41**, 2067–2075
41 McMurry, L.M., Oethinger, M. and Levy, S.B. (1998) Overexpression of *marA*, *soxS*, or *acrAB* produces resistance to triclosan in laboratory and clinical strains of *Escherichia coli*. *FEMS Microbiol. Lett.* **166**, 305–309
42 Kwon, H.J., Bennik, M.H., Demple, B. and Ellenberger, T. (2000) Crystal structure of the *Escherichia coli* Rob transcription factor in complex with DNA. *Nat. Struct. Biol.* **7**, 424–430
43 Eguchi, Y., Oshima, T., Mori, H., Aono, R., Yamamoto, K., Ishihama, A. et al. (2003) Transcriptional regulation of drug efflux genes by EvgAS, a two-component system in *Escherichia coli*. *Microbiology* **149**, 2819–2828
44 Li, X.Z., Plesiat, P. and Nikaido, H. (2015) The challenge of efflux-mediated antibiotic resistance in Gram-negative bacteria. *Clin. Microbiol. Rev.* **28**, 337–418
45 Poole, K. and Srikumar, R. (2001) Multidrug efflux in *Pseudomonas aeruginosa*: components, mechanisms and clinical significance. *Curr. Top. Med. Chem.* **1**, 59–71
46 Yoon, E.J., Balloy, V., Fiette, L., Chignard, M., Courvalin, P. and Grillot-Courvalin, C. (2016) Contribution of the Ade resistance-nodulation-cell division-type efflux pumps to fitness and pathogenesis of *Acinetobacter baumannii*. *MBio* **7**, e00697–16
47 Buckley, A.M., Webber, M.A., Cooles, S., Randall, L.P., La Ragione, R.M., Woodward, M.J. et al. (2006) The AcrAB-TolC efflux system of *Salmonella enterica* serovar Typhimurium plays a role in pathogenesis. *Cell. Microbiol.* **8**, 847–856
48 Piddock, L.J. (2006) Clinically relevant chromosomally encoded multidrug resistance efflux pumps in bacteria. *Clin. Microbiol. Rev.* **19**, 382–402
49 Reddy, V.S., Shlykov, M.A., Castillo, R., Sun, E.I. and Saier, M.H. (2012) The major facilitator superfamily (MFS) revisited. *FEBS J.* **279**, 2022–2035
50 Law, C.J., Maloney, P.C. and Wang, D.N. (2008) Ins and outs of major facilitator superfamily antiporters. *Annu. Rev. Microbiol.* **62**, 289–305
51 Saier, Jr., M.H., Beatty, J.T., Goffeau, A., Harley, K.T., Heijne, W.H., Huang, S.C. et al. (1999) The major facilitator superfamily. *J. Mol. Microbiol. Biotechnol.* **1**, 257–2579
52 Paulsen, I.T., Brown, M.H., Littlejohn, T.G., Mitchell, B.A. and Skurray, R.A. (1996) Multidrug resistance proteins QacA and QacB from *Staphylococcus aureus*: membrane topology and identification of residues involved in substrate specificity. *Proc. Natl. Acad. Sci. U.S.A.* **93**, 3630–3635
53 Jiang, D., Zhao, Y., Wang, X., Fan, J., Heng, J., Liu, X. et al. (2013) Structure of the YajR transporter suggests a transport mechanism based on the conserved motif A. *Proc. Natl. Acad. Sci. U.S.A.* **110**, 14664–14669
54 Yan, N. (2015) Structural biology of the major facilitator superfamily transporters. *Annu. Rev. Biophys.* **44**, 257–283
55 Du, D., van Veen, H.W., Murakami, S., Pos, K.M. and Luisi, B.F. (2015) Structure, mechanism and cooperation of bacterial multidrug transporters. *Curr. Opin. Struct. Biol.* **33**, 76–91

© 2017 The Author(s). Published by Portland Press Limited on behalf of the Biochemical Society

Essays in Biochemistry (2017) **61** 127–139
DOI: 10.1042/EBC20160064

56 Edgar, R. and Bibi, E. (1997) MdfA, an *Escherichia coli* multidrug resistance protein with an extraordinarily broad spectrum of drug recognition. *J. Bacteriol.* **179**, 2274–2280
57 Heng, J., Zhao, Y., Liu, M., Liu, Y., Fan, J., Wang, X. et al. (2015) Substrate-bound structure of the *E. coli* multidrug resistance transporter MdfA. *Cell Res.* **25**, 1060–1073
58 Rouch, D., Cram, D., Berardino, D., Littlejohn, T. and Skurray, R. (1990) Efflux-mediated antiseptic resistance gene *qacA* from *Staphylococcus aureus*: common ancestry with tetracycline- and sugar-transport proteins. *Mol. Microbiol.* **4**, 2051–2062
59 Mitchell, B.A., Paulsen, I.T., Brown, M.H. and Skurray, R.A. (1999) Bioenergetics of the staphylococcal multidrug export protein QacA. Identification of distinct binding sites for monovalent and divalent cations. *J. Biol. Chem.* **274**, 3541–3548
60 Xu, Z., O'Rourke, B.A., Skurray, R.A. and Brown, M.H. (2006) Role of transmembrane segment 10 in efflux mediated by the staphylococcal multidrug transport protein QacA. *J. Biol. Chem.* **281**, 792–799
61 Hassan, K.A., Skurray, R.A. and Brown, M.H. (2007) Active export proteins mediating drug resistance in staphylococci. *J. Mol. Microbiol. Biotechnol.* **12**, 180–196
62 Fluman, N., Adler, J., Rotenberg, S.A., Brown, M.H. and Bibi, E. (2014) Export of a single drug molecule in two transport cycles by a multidrug efflux pump. *Nat. Commun.* **5**, 4615
63 Omote, H., Hiasa, M., Matsumoto, T., Otsuka, M. and Moriyama, Y. (2006) The MATE proteins as fundamental transporters of metabolic and xenobiotic organic cations. *Trends Pharmacol. Sci.* **27**, 587–593
64 Morita, Y., Kodama, K., Shiota, S., Mine, T., Kataoka, A., Mizushima, T. et al. (1998) NorM, a putative multidrug efflux protein, of *Vibrio parahaemolyticus* and its homolog in *Escherichia coli*. *Antimicrob. Agents Chemother.* **42**, 1778–1782
65 Long, F., Rouquette-Loughlin, C., Shafer, W.M. and Yu, E.W. (2008) Functional cloning and characterization of the multidrug efflux pumps NorM from *Neisseria gonorrhoeae* and YdhE from *Escherichia coli*. *Antimicrob. Agents Chemother.* **52**, 3052–3060
66 McAleese, F., Petersen, P., Ruzin, A., Dunman, P.M., Murphy, E., Projan, S.J. et al. (2005) A novel MATE family efflux pump contributes to the reduced susceptibility of laboratory-derived *Staphylococcus aureus* mutants to tigecycline. *Antimicrob. Agents Chemother.* **49**, 1865–1871
67 He, X., Szewczyk, P., Karyakin, A., Evin, M., Hong, W.X., Zhang, Q. et al. (2010) Structure of a cation-bound multidrug and toxic compound extrusion transporter. *Nature* **467**, 991–994
68 Lu, M., Symersky, J., Radchenko, M., Koide, A., Guo, Y., Nie, R. et al. (2013) Structures of a Na+-coupled, substrate-bound MATE multidrug transporter. *Proc. Natl. Acad. Sci. U.S.A.* **110**, 2099–2104
69 Tanaka, Y., Hipolito, C.J., Maturana, A.D., Ito, K., Kuroda, T., Higuchi, T. et al. (2013) Structural basis for the drug extrusion mechanism by a MATE multidrug transporter. *Nature* **496**, 247–251
70 Bay, D.C. and Turner, R.J. (2009) Diversity and evolution of the small multidrug resistance protein family. *BMC Evol. Biol.* **9**, 140
71 Kikukawa, T., Miyauchi, S., Araiso, T., Kamo, N. and Nara, T. (2007) Anti-parallel membrane topology of two components of EbrAB, a multidrug transporter. *Biochem. Biophys. Res. Commun.* **358**, 1071–1075
72 Rotem, D. and Schuldiner, S. (2004) EmrE, a multidrug transporter from *Escherichia coli*, transports monovalent and divalent substrates with the same stoichiometry. *J. Biol. Chem.* **279**, 48787–48793
73 Tate, C.G., Ubarretxena-Belandia, I. and Baldwin, J.M. (2003) Conformational changes in the multidrug transporter EmrE associated with substrate binding. *J. Mol. Biol.* **332**, 229–242
74 Yerushalmi, H. and Schuldiner, S. (2000) A common binding site for substrates and protons in EmrE, an ion-coupled multidrug transporter. *FEBS Lett.* **476**, 93–97
75 Hassan, K.A., Jackson, S.M., Penesyan, A., Patching, S.G., Tetu, S.G., Eijkelkamp, B.A. et al. (2013) Transcriptomic and biochemical analyses identify a family of chlorhexidine efflux proteins. *Proc. Natl. Acad. Sci. U.S.A.* **110**, 20254–20259
76 Prakash, S., Cooper, G., Singhi, S. and Saier, Jr, M.H. (2003) The ion transporter superfamily. *Biochim. Biophys. Acta.* **1618**, 79–92
77 Carter, E.L., Jager, L., Gardner, L., Hall, C.C., Willis, S. and Green, J.M. (2007) *Escherichia coli abg* genes enable uptake and cleavage of the folate catabolite *p*-aminobenzoyl-glutamate. *J. Bacteriol.* **189**, 3329–3334
78 Hussein, M.J., Green, J.M. and Nichols, B.P. (1998) Characterization of mutations that allow *p*-aminobenzoyl-glutamate utilization by *Escherichia coli*. *J. Bacteriol.* **180**, 6260–6268
79 Veal, W.L. and Shafer, W.M. (2003) Identification of a cell envelope protein (MtrF) involved in hydrophobic antimicrobial resistance in *Neisseria gonorrhoeae*. *J. Antimicrob. Chemother.* **51**, 27–37
80 Okusu, H., Ma, D. and Nikaido, H. (1996) AcrAB efflux pump plays a major role in the antibiotic resistance phenotype of *Escherichia coli* multiple-antibiotic-resistance (Mar) mutants. *J. Bacteriol.* **178**, 306–308
81 Olliver, A., Valle, M., Chaslus-Dancla, E. and Cloeckaert, A. (2004) Role of an *acrR* mutation in multidrug resistance of *in vitro*-selected fluoroquinolone-resistant mutants of *Salmonella enterica* serovar Typhimurium. *FEMS Microbiol. Lett.* **238**, 267–272
82 Koutsolioutsou, A., Pena-Llopis, S. and Demple, B. (2005) Constitutive *soxR* mutations contribute to multiple-antibiotic resistance in clinical *Escherichia coli* isolates. *Antimicrob. Agents Chemother.* **49**, 2746–2752
83 Shafer, W.M., Yu, E.W., Rouquette-Loughlin, C., Golparian, D., Jerse, A.E. and Unemo, M. (2016) Efflux pumps in *Neisseria gonorrhoeae*: contributions to antimicrobial resistance and virulence. In *Efflux-Mediated Antimicrobial Resistance in Bacteria* (Li, X.-Z., Elkins, C.A. and Zgurskaya, H.I., eds), pp. 439–469, Springer, Switzerland
84 Coste, A.T., Crittin, J., Bauser, C., Rohde, B. and Sanglard, D. (2009) Functional analysis of *cis*- and *trans*-acting elements of the *Candida albicans CDR2* promoter with a novel promoter reporter system. *Eukaryot. Cell* **8**, 1250–1267
85 Lomovskaya, O. and Watkins, W. (2001) Inhibition of efflux pumps as a novel approach to combat drug resistance in bacteria. *J. Mol. Microbiol. Biotechnol.* **3**, 225–236

© 2017 The Author(s). Published by Portland Press Limited on behalf of the Biochemical Society

86 Baugh, S., Phillips, C.R., Ekanayaka, A.S., Piddock, L.J. and Webber, M.A. (2014) Inhibition of multidrug efflux as a strategy to prevent biofilm formation. *J. Antimicrob. Chemother.* **69**, 673–681
87 Lomovskaya, O., Warren, M.S., Lee, A., Galazzo, J., Fronko, R., Lee, M. et al. (2001) Identification and characterization of inhibitors of multidrug resistance efflux pumps in *Pseudomonas aeruginosa*: novel agents for combination therapy. *Antimicrob. Agents Chemother.* **45**, 105–116

© 2017 The Author(s). Published by Portland Press Limited on behalf of the Biochemical Society

7.3 Appendix C: Paper 2: Multidrug resistance in *Neisseria gonorrhoeae*: identification of functionally important residues in the MtrD efflux protein

AMERICAN SOCIETY FOR MICROBIOLOGY | mBio®

RESEARCH ARTICLE
Therapeutics and Prevention

Multidrug Resistance in *Neisseria gonorrhoeae*: Identification of Functionally Important Residues in the MtrD Efflux Protein

Mohsen Chitsaz,[a] Lauren Booth,[b] Mitchell T. Blyth,[b] Megan L. O'Mara,[b] Melissa H. Brown[a]

[a]College of Science and Engineering, Flinders University, Bedford Park, SA, Australia
[b]Research School of Chemistry, Australian National University, Canberra, ACT, Australia

ABSTRACT A key mechanism that *Neisseria gonorrhoeae* uses to achieve multidrug resistance is the expulsion of structurally different antimicrobials by the MtrD multidrug efflux protein. MtrD resembles the homologous *Escherichia coli* AcrB efflux protein with several common structural features, including an open cleft containing putative access and deep binding pockets proposed to interact with substrates. A highly discriminating *N. gonorrhoeae* strain, with the MtrD and NorM multidrug efflux pumps inactivated, was constructed and used to confirm and extend the substrate profile of MtrD to include 14 new compounds. The structural basis of substrate interactions with MtrD was interrogated by a combination of long-timescale molecular dynamics simulations and docking studies together with site-directed mutagenesis of selected residues. Of the MtrD mutants generated, only one (S611A) retained a wild-type (WT) resistance profile, while others (F136A, F176A, I605A, F610A, F612C, and F623C) showed reduced resistance to different antimicrobial compounds. Docking studies of eight MtrD substrates confirmed that many of the mutated residues play important nonspecific roles in binding to these substrates. Long-timescale molecular dynamics simulations of MtrD with its substrate progesterone showed the spontaneous binding of the substrate to the access pocket of the binding cleft and its subsequent penetration into the deep binding pocket, allowing the permeation pathway for a substrate through this important resistance mechanism to be identified. These findings provide a detailed picture of the interaction of MtrD with substrates that can be used as a basis for rational antibiotic and inhibitor design.

IMPORTANCE With over 78 million new infections globally each year, gonorrhea remains a frustratingly common infection. Continuous development and spread of antimicrobial-resistant strains of *Neisseria gonorrhoeae*, the causative agent of gonorrhea, have posed a serious threat to public health. One of the mechanisms in *N. gonorrhoeae* involved in resistance to multiple drugs is performed by the MtrD multidrug resistance efflux pump. This study demonstrated that the MtrD pump has a broader substrate specificity than previously proposed and identified a cluster of residues important for drug binding and translocation. Additionally, a permeation pathway for the MtrD substrate progesterone actively moving through the protein was determined, revealing key interactions within the putative MtrD drug binding pockets. Identification of functionally important residues and substrate-protein interactions of the MtrD protein is crucial to develop future strategies for the treatment of multidrug-resistant gonorrhea.

KEYWORDS *Neisseria gonorrhoeae*, multidrug resistance, efflux pumps, MtrCDE system, resistance-nodulation-division, molecular dynamics simulations, drug transport

Citation Chitsaz M, Booth L, Blyth MT, O'Mara ML, Brown MH. 2019. Multidrug resistance in *Neisseria gonorrhoeae*: identification of functionally important residues in the MtrD efflux protein. mBio 10:e02277-19. https://doi.org/10.1128/mBio.02277-19.

Editor Richard Gerald Brennan, Duke University School of Medicine

Copyright © 2019 Chitsaz et al. This is an open-access article distributed under the terms of the Creative Commons Attribution 4.0 International license.

Address correspondence to Melissa H. Brown, melissa.brown@flinders.edu.au.

This article is a direct contribution from Melissa H Brown, a Fellow of the American Academy of Microbiology, who arranged for and secured reviews by William Shafer, Emory University School of Medicine, and David Hooper, Massachusetts General Hospital.

Received 28 August 2019
Accepted 9 October 2019
Published 19 November 2019

Downloaded from http://mbio.asm.org/ on November 19, 2019 at FLINDERS UNIVERSITY OF SOUTH AUSTRALIA

The emergence of multidrug resistance (MDR) in bacteria is a global health problem that severely compromises effective treatment options, and efflux of antibiotics by membrane-bound transport proteins has been implicated as a key mechanism. In particular, in Gram-negative pathogens resistance-nodulation-division (RND) multidrug efflux systems represent the first line of defense for the cell. RND efflux systems constitute an inducible simultaneous MDR mechanism that acts against a broad spectrum of antibiotics and other antimicrobial agents. These tripartite protein complexes span the bacterial inner and outer membranes to provide a continuous drug efflux pathway.

The sexually transmitted pathogen *Neisseria gonorrhoeae* is unique among Gram-negative bacteria in that it contains a single RND efflux system to promote survival: the multiple transferable resistance (Mtr) system MtrCDE (1, 2). The MtrD efflux protein is embedded in the inner membrane and exports drugs from the periplasm and inner membrane to the MtrE outer membrane channel. MtrD contains the substrate binding sites and transduces the electrochemical energy required for drug export via a H^+/substrate antiporter mechanism (3). MtrD and MtrE are anchored together by the periplasmic MtrC to enable substrate efflux from the bacterium.

MtrD shares 48.9% sequence identity with the homologous *Escherichia coli* RND exporter AcrB, which has provided the structural basis for our understanding of RND exporters to date. It is well established that homologous proteins share common structural features. However, the unique amino acid sequence of each protein allows recognition and efflux of a distinct set of compounds required for survival of that specific bacterial species in its particular environment. Similar to AcrB, MtrD effluxes a wide spectrum of compounds, including detergents, antibiotics, dyes, bile salts, fatty acids, biocides, steroidal hormones, and aliphatic and host-derived cationic antimicrobial peptides (4, 5). Given that gonococci commonly infect mucosal sites bathed in fluids containing a number of these compounds, MtrCDE contributes to bacterial virulence as well as to antimicrobial resistance, enhancing colonization and disease development (5, 6).

In 2014, the crystal structure of MtrD was resolved to 3.53 Å, revealing an architecture similar to those of the homologous AcrB and MexB structures (7). Each MtrD monomer shows two pseudosymmetric halves and contains two domains: a transmembrane domain (TM), which is organized into 12 transmembrane α-helices embedded in the cytoplasmic membrane, and a large periplasmic domain that can be subdivided into a porter and a docking domain. The porter domain is composed of four subdomains, i.e., PN1, PN2, PC1, and PC2. In MtrD, PN1 makes up the central pore and stabilizes the trimeric organization, while PC1 and PC2 create a substrate binding cleft along the pseudosymmetric axis between the two halves of the porter domain. The docking domain is formed of two subdomains, DN and DC, that likely interact with MtrE in the outer membrane (7, 8).

Structures of AcrB bound to various substrates have identified two multidrug-binding sites within the binding cleft of the porter domain: the proximal (access) and distal (deep) binding pockets, which are separated by a so-called "switch loop" (9, 10). It is postulated that substrates first enter the access pocket of the binding cleft and then permeate into the deep binding pocket. The AcrB deep binding pocket is rich in phenylalanine residues, and many residues that have been identified as crucial to the export process (F136, F178, F610, F615, F617, and F628) are highly conserved between MexB and MtrD, suggesting that they play important and possibly similar roles in MtrD.

To date, MtrD, has not been cocrystallized with a substrate. Thus, the residues that comprise the MtrD substrate binding site(s) and whether the substrate binding residues common to RND proteins also play a role in MtrD efflux have not been ascertained. In this study, we established a site-directed mutagenesis system specific for analyzing the MtrD export protein in its natural host and, using this system, we identified 14 new MtrD substrates and experimentally explored the role of F136, F176, I605, F610, S611, F612, and F623 in MtrD-mediated multidrug resistance. To characterize the structural basis of substrate interactions with MtrD, we used a combination of long-timescale

Downloaded from http://mbio.asm.org/ on November 19, 2019 at FLINDERS UNIVERSITY OF SOUTH AUSTRALIA

TABLE 1 Antimicrobial resistance profiles of *Neisseria gonorrhoeae* strains for 11 compounds[a]

Strain or mutant	MIC (μg/ml)										
	Detergent					Antibiotic					
	N-9	TX-100	SDS	TW-80	CHAPS	RIF	NOV	ERY	AZM	CRO	OXA
N. gonorrhoeae FA19	64	128	16	64	2,048	0.03	0.25	0.25	0.125	0.0005	0.50
N. gonorrhoeae FA19 Δ*mtrD*	16	32	16	64	1,024	0.008	0.03	0.06	0.03	0.0005	0.06
N. gonorrhoeae FA19 Δ*norM*	64	128	16	64	2,048	0.03	0.25	0.25	0.125	0.0005	0.50
N. gonorrhoeae FA19 Δ*mtrD* Δ*norM*	16	32	16	64	1,024	0.008	0.03	0.06	0.03	0.0005	0.06
N. gonorrhoeae KH15	≥4,096	≥4,096	32	128	>2,048	0.125	1	2	0.50	0.001	4
N. gonorrhoeae KH15 Δ*mtrD*	16	32	16	64	1,024	0.008	0.03	0.06	0.03	0.0005	0.06
N. gonorrhoeae KH15 Δ*mtrD* Δ*norM*	16	32	16	64	1,024	0.008	0.03	0.06	0.03	0.0005	0.06
N. gonorrhoeae KH15 Δ*mtrD* Δ*norM*(*mtrD*)	≥4,096	≥4,096	32	128	>2,048	0.125	1	ND	ND	0.001	4

[a]All MIC data are representative of three or more independent experiments. Abbreviations: AZM, azithromycin; CHAPS, 3-[(3-cholamidopropyl)dimethylammonio]-1-propanesulfonate; CRO, ceftriaxone; ERY, erythromycin; N-9, nonoxynol-9; ND, not determined; NOV, novobiocin; OXA, oxacillin; RIF, rifampin; TW-80, Tween 80; TX-100, Triton X-100.

molecular dynamics (MD) simulations and docking studies. Long-timescale MD simulations of progesterone showed the spontaneous binding of progesterone to the access pocket of the binding cleft and its subsequent permeation past the switch loop and into the deep binding pocket. Docking studies of progesterone, nonoxynol-9, azithromycin, rifampin, ethidium, crystal violet, cholic acid, and the RND pump inhibitor phenylalanine arginine beta-naphthylamide (PAβN) indicated that several key residues play important nonspecific roles in the efflux of these substrates.

RESULTS

A highly discriminating *N. gonorrhoeae* strain for *in situ* analysis of MtrD activity. An expression and integration system was established in a *N. gonorrhoeae* host to analyze the function of wild-type (WT) MtrD and construct a set of isogenic mutants. This system has the advantage that it produces both cognate partner proteins of MtrD, i.e., MtrC and MtrE, allowing assembly of the active tripartite MtrCDE system in the neisserial membrane. This ensures that alterations in spectra and/or levels of resistance would be solely due to manipulation of MtrD. The well-characterized antibiotic-sensitive strain *N. gonorrhoeae* FA19 was selected as the background strain (11). As an initial step, three isogenic FA19 derivatives (FA19 Δ*mtrD*, FA19 Δ*norM*, and FA19 Δ*mtrD* Δ*norM* mutants) were created using overlap extension PCR (12). The NorM efflux pump of *N. gonorrhoeae* is known to expel a number of cationic toxic compounds, such as ciprofloxacin, ethidium, and acriflavine; the latter two compounds are substrates common with MtrD (13). Thus, to remove any contribution that the unrelated NorM multidrug efflux pump would have provided in the assessment of MtrD function, the MtrD derivatives were constructed in a strain in which *norM* was also deleted from the chromosome. To achieve a high level of discrimination for antimicrobial susceptibility assessments of MtrD, the isogenic FA19 derivate KH15 was also employed. This strain of *N. gonorrhoeae* has a single-base-pair deletion in the *mtrR* promoter that results in upregulation of the *mtrCDE* system and consequential increased levels of resistance (5). Hence, two KH15 isogenic derivatives (KH15 Δ*mtrD* and KH15 Δ*mtrD* Δ*norM* mutant strains) were also constructed using the same overlap extension PCR methodology. Sequencing of the complete *mtrRCDE* region of the KH15 Δ*mtrD* and KH15 Δ*mtrD* Δ*norM* strains confirmed deletion of the *mtrD* gene and ensured the integrity of the *mtrR/C* promoter region as well as that of the *mtrC* and the *mtrE* genes. Resistance profiles of the resulting strain set were determined for 33 compounds, which included 2 known RND pump inhibitors (Tables 1, 2, and 3).

Deletion of *mtrD* and *norM* from FA19 resulted in a (1.5-fold to 32-fold) reduction of the MICs for 25 of 31 of the tested compounds (Tables 1, 2, and 3), and 29 of 31 compounds showed reduced (1.5-fold to >256-fold) MIC levels in the KH15 strain background. SDS, Tween 80, capric acid, and ceftriaxone showed a decrease in resistance only in the KH15 background, probably due the higher level of *mtrCDE* expression in this strain than in strain FA19 (Tables 1 and 3). In fact, a 4-fold or greater reduction

Downloaded from http://mbio.asm.org/ on November 19, 2019 at FLINDERS UNIVERSITY OF SOUTH AUSTRALIA

TABLE 2 Antimicrobial resistance profiles of *Neisseria gonorrhoeae* strains for an additional 11 compounds[a]

	MIC (μg/ml)										
	Antibiotic						CAMP		Dye		
Strain or mutant	CHL	TET	PEN	TGC	CIP	GEN	CST	PMB	ET	CV	ACR
N. gonorrhoeae FA19	0.75	0.25	0.024	0.06	0.003	4	200	100	2	1	0.5
N. gonorrhoeae FA19 Δ*mtrD*	0.5	0.25	0.016	0.03	0.003	4	100	50	0.5	0.125	0.25
N. gonorrhoeae FA19 Δ*norM*	0.5	0.25	0.024	0.06	0.003	4	200	100	0.25	1	0.25
N. gonorrhoeae FA19 Δ*mtrD* Δ*norM*	0.5	0.25	0.016	0.03	0.0025	4	100	50	0.06	0.125	0.06
N. gonorrhoeae KH15	0.75	0.25	0.060	0.125	0.003	4	400	100	4	2	0.5
N. gonorrhoeae KH15 Δ*mtrD*	0.5	0.25	0.016	0.03	0.003	4	100	50	0.5	0.125	0.25
N. gonorrhoeae KH15 Δ*mtrD* Δ*norM*	0.5	0.25	0.016	0.03	0.0025	4	100	50	0.06	0.125	0.06
N. gonorrhoeae KH15 Δ*mtrD* Δ*norM*(*mtrD*)	>0.75	0.25	0.060	0.125	0.003	4	400	100	0.25	2	0.125

[a]All MIC data are representative of three or more independent experiments. Abbreviations: ACR, acriflavine; CHL, chloramphenicol; CIP, ciprofloxacin; CST, colistin; CV, crystal violet; ET, ethidium; GEN, gentamicin; PEN, benzylpenicillin; PMB, polymyxin B; TET, tetracycline; TGC, tigecycline.

in MICs was observed for 20 of 31 tested compounds for the KH15 derivatives, while this level of reduction of drug MICs in the FA19 background was observed for only 9 compounds. These data suggested that the KH15 Δ*mtrD* Δ*norM* strain can function as a good discriminative background strain for conducting analyses of *mtrD* mutants.

No change in resistance profiles was observed for the antibiotics tetracycline and gentamicin in strains with either *mtrD* or *norM* or both inactivated (Table 2). Although tetracycline has previously been identified as an MtrD substrate, this can be observed only in strains with concomitant mutations in multiple genes, including *mtrR*; these were not present in our background strain (14–16).

In addition to antimicrobial compounds, *N. gonorrhoeae* KH15 and derivatives were tested against two known RND pump inhibitors, PAβN and 1-(1-naphtylmethyl)-piperazine (NMP), for their resistance capacities. These assays showed decreased resistance of KH15 Δ*mtrD* and KH15 Δ*mtrD* Δ*norM* cells to PAβN and NMP, with 8-fold and 4-fold reductions in MICs, respectively (Table 3). Deletion of *norM* from the KH15Δ*mtrD* strain did not result in a further decrease of MIC for either compound. Thus, inactivation of *mtrD* in KH15 produced a decrease in resistance to 31 compounds, confirming the broad spectrum of antimicrobials that can be handled by this protein (Tables 1, 2, and 3).

Function can be restored in the *N. gonorrhoeae* KH15 Δ*mtrD* Δ*norM* derivative by reinsertion of *mtrD*. A procedure was established for introduction of *mtrD* derivatives, all containing a sequence encoding six C-terminal histidine residues ($mtrD_{His6}$) into the chromosome of the KH15 Δ*mtrD* Δ*norM* strain via the pGCC4 (*Neisseria* insertion complementation system [NICS]) shuttle vector. This system allows integration of an *mtrD* determinant into the *N. gonorrhoeae* chromosome between *aspC* and *lctP* and provides cells with a recombinant *mtrD* allele with its expression under *lac*

TABLE 3 Antimicrobial resistance profiles of *Neisseria gonorrhoeae* strains for 11 more compounds[a]

	MIC (μg/ml)										
	Bile acid	Fatty acid		Biocide					Hormone	Inhibitor	
Strain or mutant	CHO	CA	PA	BC	CH	TR	DQ	PT	PRO	NMP	PAβN
N. gonorrhoeae FA19	200	12.5	12.5	2	0.25	0.125	4	4	40	ND	ND
N. gonorrhoeae FA19 Δ*mtrD*	100	12.5	6.25	1	0.125	0.06	2	2	20	ND	ND
N. gonorrhoeae FA19 Δ*norM*	200	12.5	12.5	2	0.25	0.125	1	1	40	ND	ND
N. gonorrhoeae FA19 Δ*mtrD* Δ*norM*	100	12.5	6.25	1	0.125	0.06	1	1	20	ND	ND
N. gonorrhoeae KH15	400	25	100	4	0.5	0.25	16	8	80	256	512
N. gonorrhoeae KH15 Δ*mtrD*	100	12.5	6.25	1	0.125	0.06	1	2	20	64	128
N. gonorrhoeae KH15 Δ*mtrD* Δ*norM*	100	12.5	6.25	1	0.125	0.06	1	1	20	64	128
N. gonorrhoeae KH15 Δ*mtrD* Δ*norM*(*mtrD*)	400	25	ND	4	0.5	0.25	1	1	80	256	512

[a]All MIC data are representative of three or more independent experiments. Abbreviations: BC, benzalkonium; CA, capric acid; CH, chlorhexidine; CHO, cholic acid; DQ, dequalinium; NMP, 1-(1-naphtylmethyl)-piperazine; PA, palmitic acid; PAβN, phenylalanine arginine beta-naphthylamide; PRO, progesterone; PT, pentamidine; TR, triclosan.

Downloaded from http://mbio.asm.org/ on November 19, 2019 at FLINDERS UNIVERSITY OF SOUTH AUSTRALIA

promoter regulation (17). A pGCC4-$mtrD_{(His6)}$ clone was constructed and used for recombination of the WT *mtrD* allele into the *N. gonorrhoeae* KH15 Δ*mtrD* Δ*norM* chromosome, producing the KH15 Δ*mtrD* Δ*norM*($mtrD_{His6}$) strain. At the same time, the pGCC4 empty vector was also recombined to create an isogenic KH15 Δ*mtrD* Δ*norM*(NICS) strain that contained all the NICS elements, including the erythromycin resistance determinant present on the pGCC4 vector used for selection, and that could be utilized as a negative/background control. Western blotting confirmed expression and localization of the recombinant WT $MtrD_{His6}$ protein within isolated membranes of *N. gonorrhoeae* KH15 Δ*mtrD* Δ*norM*($mtrD_{His6}$) cells (see Fig. S1 in the supplemental material).

Complementation of the KH15 Δ*mtrD* Δ*norM* strain with $mtrD_{His6}$ restored resistance to WT levels fully for 24 compounds and partially for 4 compounds (Tables 1, 2, and 3). Partial complementation was seen for ethidium, acriflavine, dequalinium, and pentamidine, as the MICs were below those for the parental strain (Tables 2 and 3). This was expected, as these four compounds are substrates of both the MtrD and NorM multidrug efflux pumps. These data confirmed that the MtrCDE system is functional in the KH15 Δ*mtrD* Δ*norM*($mtrD_{His6}$) strain, offering a reliable system for analyzing incorporated site-directed MtrD mutants. Additionally, these data showed that the histidine-tagged MtrD protein in the KH15 Δ*mtrD* Δ*norM*($mtrD_{His6}$) strain provides resistance to a large number of MtrD substrates, allowing selection of a range of structurally different compounds for functional analysis of MtrD mutants. From these analyses, 11 compounds were chosen as representative compounds for subsequent MIC analysis of MtrD activity due to their high discrimination in MIC analysis and provide examples of a range of antimicrobials from different chemical classes. While both erythromycin and azithromycin demonstrated excellent MIC differentiation between the *mtrD* deletion strain and the corresponding parental strain, the use of the erythromycin resistance cassette present in pGCC4 as a selection marker precluded testing constructed MtrD mutant derivatives against these clinically important antibiotics.

Spontaneous uptake of progesterone identified from MD simulations. To investigate the interaction of MtrD with substrates, spontaneous binding simulations were performed with the substrate progesterone. In these simulations, 30 molecules of progesterone were randomly placed in the aqueous solution surrounding the MtrD porter and docking domains. In two of the three simulations (representing 700 ns of simulation time), progesterone randomly adsorbed to the protein via nonspecific interactions. In the remaining 200-ns replicate, a single molecule of progesterone entered the access pocket of the binding cleft, straddled the switch loop, and in the first 100 ns of the simulation interacted with the deep binding pocket, where it remained for the duration of the analysis. The time-dependent motion of progesterone within the binding cleft throughout the simulation is shown in Fig. 1. In the first 2 ns of the simulation, progesterone associated with the outer lip of the binding cleft in an upright orientation. Progesterone then rotated 90° to interact with the β-sheet residues from PC2 that line the binding cleft (Fig. 1, bottom panel, red) before moving into the MtrD access binding pocket, where it resided for the first 40 ns of the simulation (Fig. 1, bottom panel, green). After 40 ns of the simulation, progesterone moved further into the binding cleft, straddling the switch loop, before interacting with the deep binding pocket, where it remained for the rest of the 200-ns trajectory. Throughout the last 100 ns of the simulation, progesterone moved freely and changed orientation in the deep binding pocket, residing ~10 Å from the entrance of the binding cleft. From these simulations, 25 binding cleft residues were identified as being within 4 Å of progesterone throughout the simulation (Fig. 2). These residues include four phenylalanines (F174, F610, F612, and F623) that are conserved in both AcrB and MexB (Table 4; see also Fig. S2).

Docking of substrates to MtrD. The use of MD simulation studies is a computationally expensive approach for analysis of the interaction of MtrD with a range of substrates. Thus, to determine whether a simplified docking approach could give

Downloaded from http://mbio.asm.org/ on November 19, 2019 at FLINDERS UNIVERSITY OF SOUTH AUSTRALIA

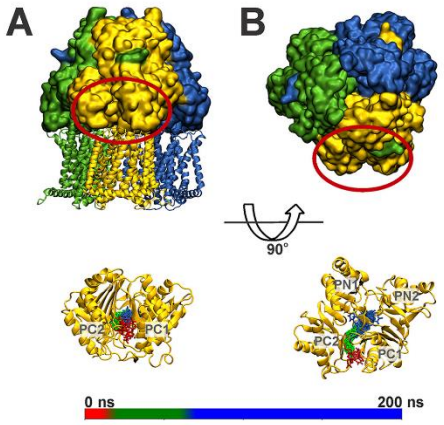

FIG 1 Progesterone binding in monomer B of the MtrD trimer shown as a (A) side view and (B) top view. Monomers A, B, and C of MtrD are colored green, gold, and blue, respectively. The periplasmic region of monomer B is circled in red. The lower panels show MtrD monomer B with the position of progesterone throughout the 200-ns simulation. Snapshots of progesterone taken every 10 ns are shown in licorice representation and colored according to simulation time. The scale bar gives the correlation between simulation time and progesterone color. The starting position of the progesterone molecule at 0 ns is shown in red, and the final position of progesterone at 200 ns, straddling the switch loop, is in blue.

insights into key MtrD residues in contact with substrates, flexible docking studies of progesterone were compared with MD simulations. Progesterone docked into the deep binding pocket of MtrD in several orientations, as shown in Fig. 2B, primarily interacting with F623, F612, F610, F176, and F136. A number of these residues were also high-

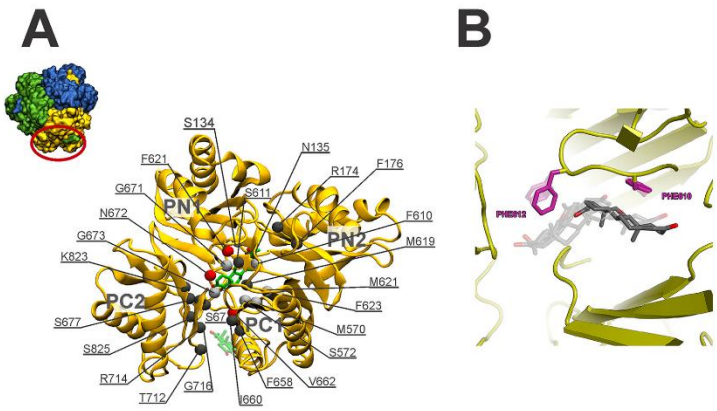

FIG 2 (A) Porter domain of MtrD viewed from the top, illustrating the residues implicated in binding of progesterone. Progesterone is drawn in licorice representation at 0 ns (washed out) and 200 ns. The Cα atoms of 25 residues most frequently within 4 Å of progesterone are drawn in van der Waals representation and colored as follows: red, >75% frequency; silver, >50% frequency; dark gray, >25% frequency. The inset shows a top view of the MtrD trimer with the periplasmic region of monomer B in gold. (B) The lowest-energy docked poses for progesterone in the access and deep pockets. F610 (magenta) plays the largest role in binding and transport of this substrate in the access pocket. F612 (magenta) plays the largest role in binding and transport of this substrate in the deep pocket.

Downloaded from http://mbio.asm.org/ on November 19, 2019 at FLINDERS UNIVERSITY OF SOUTH AUSTRALIA

TABLE 4 Residues belonging to binding pockets of MtrD and AcrB

Region	AcrB residues	MtrD residues from alignment[a]
Access pocket	79, 91, 134, 135, 292, 573, 575, 577, 617, 624, 662, 664, 666, 667, 668, 674, 676, 681, 717, 719, 826	79, 91, **134**, **135**, 290, **570**, **572**, 574, **612**, **619**, **658**, **660**, **662**, 663, 664, 670, **672**, 678, **714**, **716**, **823**
Deep binding pocket	46, 89, 128, 130, 134, 136, 176, 177, 178, 180, 273, 274, 276, 277, 290, 327, 573, 610, 612, 615, 617, 620, 628	46, 89, 128, 130, **134**, 136, **174**, 175, **176**, 178, 271, 272, 274, 275, 288, 325, **570**, 605, 607, **610**, **612**, 615, **623**

[a]MtrD residues implicated in binding progesterone in MD simulations are shown in bold; residues contributing to both the access and deep binding pockets are underlined.

lighted in MD simulations; for example, progesterone interacted with F612 for >90% of the simulation time, while F623 and F610 interacted with progesterone for >50% of the simulation time, and the interaction with F176 persisted for 25% of the simulation time.

Overall, docking studies and MD simulations of progesterone binding were in good agreement. Thus, we extended the procedure to dock a further six substrates and one inhibitor into the MtrD access and deep binding pockets. These compounds were the substrates nonoxynol-9, azithromycin, rifampin, ethidium, crystal violet, and cholic acid and the inhibitor PAβN. As stated previously, we were unable to test resistance to azithromycin for the MtrD mutants in our *in vivo* system. Thus, the ability to analyze the interaction of MtrD with azithromycin through *in silco* docking studies provides an example of the usefulness and versatility of this system. The lowest-energy docked poses revealed a set of common residues that appear to play a role in the binding and/or transport of these compounds (Fig. S3 to S6). Critically, a number of residues (F136, F176, F610, F612, and F623) were found to be implicated in substrate binding and are conserved in both the AcrB and MexB efflux proteins (Fig. S3 to S6). Site-directed mutagenesis was used to confirm their importance in MtrD-mediated resistance.

Site-directed mutagenesis identified six residues involved in MtrD-mediated resistance. Detailed knowledge of the interactions between substrates and amino acids that comprise drug binding sites within the porter domain of AcrB has been obtained by a variety of methods (18–20). Such studies identified, among others, a cluster of six phenylalanine residues (F136, F178, F610, F615, F617, and F628) that contribute to formation of the deep drug binding pocket and that are involved in substrate binding and recognition (9, 10). In MtrD, five of these phenylalanine residues are conserved (F136, F176, F610, F612, and F623) at similar locations, whereas F610 is an isoleucine in the corresponding position in MtrD (I605) (Fig. S2). Also included in our set of targets was S611, corresponding to G616 in AcrB (Fig. S2), which has been identified as playing a role in resistance (18, 21, 22). Thus, we were interested to learn whether these residues perform similar roles in the related RND transporter MtrD.

To facilitate later studies on the locations of substituted residues and on their inhibition (23), we initially generated a cysteineless variant of the *mtrD*$_{His6}$ clone in pGCC4 (pGCC4-CL*mtrD*$_{His6}$). This produced a MtrD C491A variant in which the sole cysteine residue at position 491 was replaced with alanine. When integrated into the KH15 Δ*mtrD* Δ*norM* background, the KH15 Δ*mtrD* Δ*norM*(CL*mtrD*$_{His6}$) strain had WT levels of resistance to all tested compounds (Table 5), and Western blot expression levels of the CL-MtrD$_{His6}$ protein in neisserial membranes were comparable to the expression level measured for WT MtrD$_{His6}$ (Fig. S1). As a result, the MtrD mutants described below were constructed in this pGCC4-CL*mtrD*$_{His6}$ derivative. Seven MtrD mutants (F136A, F176A, I605A, F610A, S611A, F612C, and F623C) were generated and individually recombined into the *N. gonorrhoeae* KH15 Δ*mtrD* Δ*norM* chromosome. Western blotting of isolated membranes from these bacteria confirmed expression of the MtrD mutant proteins at levels comparable to that determined for the CL-MtrD$_{His6}$ parent (Fig. S1).

Three MtrD mutants (F176A, F612C, and F623C) exhibited reduced resistance to all 11 compounds, indicating a significant and wide-ranging impact on resistance (Table 5). No resistance to ethidium, polymyxin B, progesterone, and dequalinium was

Downloaded from http://mbio.asm.org/ on November 19, 2019 at FLINDERS UNIVERSITY OF SOUTH AUSTRALIA

TABLE 5 *Neisseria gonorrhoeae* KH15 Δ*mtrD* Δ*norM* strain expressing MtrD derivatives

	MIC (μg/ml)[a]										
	Detergent		Antibiotic			CAMP	Dye		Bile acid	Hormone	Biocide
Mutation	N-9	TX-100	RIF	NOV	OXA	PMB	ET	CV	CHO	PRO	DQ
$MtrD_{His6}$[b]	≥4,096	≥4,096	0.125	1	4	100	0.25	2	400	80	1
CL-$MtrD_{His6}$	≥4,096	≥4,096	0.125	1	4	100	0.25	2	400	80	1
F136A	≥4,096	≥4,096	0.03	0.25	2	100	0.25	0.5	200	80	1
F176A	32	128	0.03	0.125	0.5	50	0.06	0.25	200	20	0.5
I605A	32	128	0.03	0.5	1	100	0.125	1	400	80	0.5
F610A	≥4,096	≥4,096	0.125	0.5	4	100	0.25	2	400	80	1
S611A	≥4,096	≥4,096	0.125	1	4	100	0.25	2	400	80	1
F612C	32	128	0.016	0.125	0.5	50	0.06	0.25	200	20	0.5
F623C	16	64	0.016	0.125	0.25	50	0.06	0.125	100	20	0.5
Negative control[c]	16	32	0.008	0.03	0.06	50	0.06	0.125	100	20	0.5

[a]All MIC data are representative of three or more independent experiments. Abbreviations: CAMP, cationic antimicrobial peptide; CHO, cholic acid; CV, crystal violet; DQ, dequalinium; ET, ethidium; N-9, nonoxynol-9; NOV, novobiocin; OXA, oxacillin; PMB, polymyxin B; PRO, progesterone; RIF, rifampin; TX-100, Triton X-100.
[b]Recombinant WT $MtrD_{His6}$.
[c]KH15 Δ*mtrD* Δ*norM* strain transformed with pGCC4 empty vector expressing no MtrD [KH15 Δ*mtrD* Δ*norM*(NICS) strain].

observed for any of the three mutants, and F623 showed only background levels of resistance to nonoxynol-9. They did retain a small degree of resistance to the other six compounds, namely, Triton X-100, rifampin, novobiocin, crystal violet, oxacillin, and cholic acid (Table 5). It is worth noting that the retention of this small degree of resistance is evidence that the complete loss of resistance that was seen for the group of four substrates was likely not due to complete misfolding of the mutant protein. These data suggest that the F176, F612, and F623 residues play important and widespread roles in MtrD-mediated multidrug resistance.

Replacement of residues in MtrD at positions 136, 605, and 610 differentially affected resistance to distinct compounds (Table 5). The MtrD F136A mutant showed reduced resistance to five compounds, while no changes in MICs were observed for six compounds (Table 5). Substitution of I605 with alanine reduced resistance to 8 of 11 tested compounds, with the WT resistance profile retained for only 3 compounds (Table 5). The effect of substitution of F610 was more limited, as MtrD F610A showed a reduction in resistance only to novobiocin, which was demonstrated by a consistent 2-fold reduction in MICs for this compound (Table 5). The MtrD S611A mutant was the only variant that retained a complete WT resistance profile with no change in MICs for any tested compound (Table 5).

DISCUSSION

Antibiotic resistance in *N. gonorrhoeae* is an effective survival strategy, as this bacterium has been successful in developing resistance to almost all antibiotics previously or currently used for treatment of gonorrhea. With the emergence and spread of gonococci strains that have shown resistance to the last options of empirical therapy, azithromycin and ceftriaxone, the problem has become more alarming. The limited discovery of new antibiotics during past 3 decades, particularly of those against Gram-negative bacteria, has intensified this concern. One of the mechanisms of drug resistance utilized by *N. gonorrhoeae* involves efflux pumps that enable the cells to keep interior levels of drugs below toxic levels. Recent reports have highlighted the importance of this mechanism of resistance by showing that *N. gonorrhoeae* can acquire mosaic drug efflux gene sequences from commensal *Neisseria* that can lead to low-level azithromycin resistance expressed by *N. gonorrhoeae* clinical isolates (24). Interestingly, the acquired mosaic-like sequence within *mtrD* in these isolates was found to increase MtrD activity, resulting in clinical resistance to azithromycin in the background of elevated expression of the MtrCDE efflux proteins.

To analyze in detail the MtrD pump component of the MtrCDE efflux system, a site-directed mutagenesis system specific for manipulation and analysis of this protein

Downloaded from http://mbio.asm.org/ on November 19, 2019 at FLINDERS UNIVERSITY OF SOUTH AUSTRALIA

in its natural host, *N. gonorrhoeae*, was established. Addition of a histidine tag on the C terminus of MtrD for monitoring expression levels and increasing the versatility of the system did not affect resistance (Tables 1, 2, and 3), making the $MtrD_{His6}$ protein advantageous for studying the effect of mutations on resistance to many important antibiotics, biocides, and human-derived antimicrobial peptides. Additionally, the cysteineless derivative of $MtrD_{His6}$ (CL-$MtrD_{His6}$) retained full activity compared to the corresponding parental $MtrD_{His6}$ protein, providing a reliable site-directed cysteine-scanning mutagenesis system for further analysis of MtrD (Table 5).

This study revealed that the MtrD efflux pump possesses an even wider substrate specificity than had previously been proposed (5, 15, 25) with the addition of 14 new substrates, including detergents (SDS, CHAPS (3-[(3-cholamidopropyl)dimethylammonio]-1-propanesulfonate), and Tween 80); antibiotics (tigecycline, novobiocin, ciprofloxacin, and pentamidine); biocides (dequalinium, benzalkonium, chlorhexidine, and triclosan); and a cationic polypeptide (colistin) as well as two efflux pump inhibitors PAβN and NMP (Tables 1, 2, and 3).

One of the interesting features of RND transporters is that they recognize and export a remarkably broad range of substrates from different chemical classes. This feature has been mainly attributed in AcrB to the existence of multiple pockets with each pocket containing multiple overlapping drug-binding sites within the porter domain as well as several entrances with specificity for different substrates (18, 26, 27), similarly to the substrate recognition mechanism first described for the multidrug binding protein QacR (28, 29). Additionally, the presence of multiple aromatic residues such as phenylalanine in a multisite substrate binding pocket that can act in a drug-specific manner has been reported previously for both QacR and AcrB (28). Similar features are apparent in the MtrD polyspecific RND efflux transporter. MD simulations of progesterone binding to MtrD identified 25 residues within the binding cleft that are implicated in progesterone binding (Table 4; see also Fig. 2A). This was in good agreement with docking results from analysis of progesterone, which identified a similar set of residues in contact with progesterone, including F176, F610, F612, and F623. Docking studies of a further six compounds also indicated that these five phenylalanine residues form key interactions with substrates in the access and deep binding pockets of MtrD. Mutational analyses of these five phenylalanine residues showed reduced resistance to various MtrD substrates, confirming the integral role that these aromatic residues play in MtrD drug binding and translocation.

Progesterone binding MD simulations of MtrD, docking analyses of eight compounds, and MIC analysis of F176A and F623C mutants showed that these residues, located in the region of MtrD corresponding to the deep binding pocket, have important functional roles in drug binding and resistance. This is similar to what has been ascribed to the homologous residues in AcrB, F178 and F628, which are involved in binding to drugs and RND efflux pump inhibitors (9, 26, 30–37).

F612 is a conserved residue located in the region corresponding to the AcrB switch loop (F617 in ArcB) that projects into the binding cleft cavity between the access and deep binding pocket. During the transition from the access conformation to the binding conformation of AcrB, movement of the switch loop allows high-molecular-mass (M_r > 600 dalton) substrates to move from the AcrB access pocket to the deep binding pocket (10, 38). Spontaneous binding of progesterone from MD simulations showed that Cα of F612 was within 4 Å of progesterone for >75% of the 200-ns simulation time (Table 4; see also Fig. 2A), while docking analyses confirmed that F612 is a contributor to binding affinity for all eight docked compounds (Fig. 2B; see also Fig. S3 to S6 in the supplemental material). Analysis of cells expressing the F612C MtrD mutant showed a significant reduction in resistance to all 11 tested compounds, confirming the importance of F612 in resistance afforded by MtrD (Table 5).

Like the homologous counterparts in AcrB (F136, F610, and F615), F136, I605, and F610 form part of the deep binding pocket and are involved in nonspecific drug binding of MtrD (Fig. S2) (9, 32, 37, 39). Our progesterone binding MD simulations showed that Cα of MtrD F610 was within 4 Å of progesterone for >50% of the

Downloaded from http://mbio.asm.org/ on November 19, 2019 at FLINDERS UNIVERSITY OF SOUTH AUSTRALIA

simulation time (Fig. 2A). Docking analyses identified F136 and F610 as contributors to the binding affinity for various compounds (Fig. 2B; see also Fig. S3 to S6), and the data were confirmed by MIC analysis of the corresponding MtrD mutant derivatives, even though the MIC for progesterone was unaffected in the F610A mutant. MIC data also suggest that I605, located in the distal region of the deep binding pocket, has a functionally important role in MtrD. However, analysis of the starting MtrD crystal structure and MD trajectories showed that, unlike the corresponding residue in AcrB (F610), I605 did not form part of the solvent-accessible cavity surface of the deep binding pocket in the MtrD crystal structure and thus did not interact with progesterone in either MD simulations or docking-based studies. The lack of correlation between the MIC data and the cocrystallography or MD simulation data is not uncommon in studies of these dynamic transporters, which undergo large-scale conformational changes during their transport cycle.

The use of MD simulations of progesterone binding in this study was found to be a successful approach for characterization of MtrD binding to a substrate. The predictive power of this method comes from a circumstantial finding of this study, which identified K823, located in the access pocket, as interacting with progesterone. In a recent study of a *N. gonorrhoeae* clinical isolate possessing a mosaic-like *mtr* efflux pump locus with reduced susceptibility to antimicrobials, mutation of K823 to glutamate (K823E) resulted in a gain-of-function impact on MtrD activity (40) suggesting an important functional role for this residue in MtrD drug translocation and confirming our assignment of this residue in substrate binding.

Characterization of antimicrobial efflux mechanisms in bacteria has helped understanding of the resources through which bacteria, including *N. gonorrhoeae*, are able to develop resistance against toxic compounds present in their environment, including those found naturally and antibiotics used for treatment of infections. In Gram-negative bacteria in particular, characterization of RND efflux pumps, including the gonoccocal MtrCDE system, has helped improve understanding of the main barrier for accumulation of antibiotics within cells at toxic levels. The detailed molecular, biochemical, structural and computational studies of RND pumps, including the *N. gonorrhoeae* MtrD protein, have provided new insights regarding determinations of operation/efflux mechanisms, substrate pathways, amino acid residues required for drug recognition and binding, and residues that are involved in other mechanisms of efflux operation such as energy coupling or interaction with partner proteins. These studies have also provided new insights regarding how some molecules interact with and inhibit RND pumps. New drugs that bypass efflux mechanisms are desperately needed for treatment of infections with highly resistant bacterial strains, especially of infections with Gram-negative bacteria. Identification of functionally important residues in MtrD represents a start for efforts aimed at gaining a better understanding of the transport mechanism(s) of the resistance-nodulation division family of multidrug transporters and at rationally based designing of antimicrobial drugs or efflux pump inhibitors.

MATERIALS AND METHODS

Bacterial strains, plasmids, and growth conditions. The bacterial strains and plasmids used in this study are listed in Table 6. Gonococci were grown on GC medium (Difco Laboratories, Detroit, MI) as previously described (41). The pGCC4 vector was used as the backbone in which *mtrD* mutants were constructed and then mobilized into *N. gonorrhoeae* (see below). Erythromycin was added into GC plates for selecting *N. gonorrhoeae* transformed with pGCC4 (0.5 μg/ml) or for replica plating for selection of *mtrD* deletions (0.06 μg/ml). Isopropyl-β-D-thiogalactopyranoside (IPTG) was used at a final concentration of 0.5 mM to induce *mtrD* expression in *N. gonorrhoeae* strains containing integrated *mtrD* constructs.

E. coli DH5α (42) was used in cloning experiments and for propagation of all pGCC4 vector-based constructs. *E. coli* cells were grown on LB agar or in LB broth (Oxoid; Thermo Fisher Scientific Australia Pty. Ltd.) with kanamycin (40 μg/ml) where required.

Molecular biology methods. Chromosomal DNA was isolated from *N. gonorrhoeae* cells by the use of a Wizard genomic DNA purification kit (Promega Co., USA) and plasmid DNA from *E. coli* using an Isolate II plasmid minikit (Bioline, Boston, USA) per the instructions of the manufacturers. Primers used in this study are listed in Table S1 in the supplemental material and were synthesized by GeneWorks (GeneWorks Pty. Ltd., Australia) or Integrated DNA Technologies. Bioline Velocity DNA polymerase was used in all cloning and mutagenesis procedures and Bioline Mango*Taq* DNA polymerase for screening

Downloaded from http://mbio.asm.org/ on November 19, 2019 at FLINDERS UNIVERSITY OF SOUTH AUSTRALIA

TABLE 6 Bacterial strains and plasmids used in this study

Strain or plasmid	Relevant genotypes or description[a]	Source or reference
Strains		
E. coli DH5α	*fhuA2* Δ(*argF-lacZ*)*U169 phoA glnV44* Φ80 Δ(*lacZ*)M15 *gyrA96 recA1 relA1 endA1 thi-1 hsdR17*	42
N. gonorrhoeae FA19	Antimicrobial sensitive	15
N. gonorrhoeae KH15	As FA19 but *mtrR*-171	5
N. gonorrhoeae FA19 Δ*mtrD*	As FA19 but Δ*mtrD*	This study
N. gonorrhoeae FA19 Δ*norM*	As FA19 but Δ*norM*	This study
N. gonorrhoeae FA19 Δ*mtrD* Δ*norM*	AS FA19 but Δ*mtrD* and Δ*norM*	This study
N. gonorrhoeae KH15 Δ*mtrD*	AS KH15 but Δ*mtrD*	This study
N. gonorrhoeae KH15 Δ*mtrD* Δ*norM*	AS KH15 but Δ*mtrD* and Δ*norM*	This study
N. gonorrhoeae KH15 Δ*mtrD* Δ*norM*(*mtrD*)	As KH15 Δ*mtrD* Δ*norM* but complemented with WT $mtrD_{6His}$	This study
Plasmids		
pGCC4	*Neisseria* insertion complementation system (NICS) vector; *lacI*, P_{lac}, Kan^r, Ery^r	17
pGCC4-$mtrD_{6His}$	*mtrD* cloned into PmeI and PacI sites of pGCC4 under the control of P_{lac} promoter with a 6His tag at the C terminus	This study
pGCC4-CL$mtrD_{His6}$	Cysteineless derivative of $mtrD_{His6}$ in pGCC4	This study
pGCC4-CL$mtrD_{His6}$(F136A)	Site-directed F136A MtrD mutant based on pGCC4-CL$mtrD_{His6}$	This study
pGCC4-CL$mtrD_{His6}$(F176A)	Site-directed F176A MtrD mutant based on pGCC4-CL$mtrD_{His6}$	This study
pGCC4-CL$mtrD_{His6}$(I605A)	Site-directed I605A MtrD mutant based on pGCC4-CL$mtrD_{His6}$	This study
pGCC4-CL$mtrD_{His6}$(F610A)	Site-directed F610A MtrD mutant based on pGCC4-CL$mtrD_{His6}$	This study
pGCC4-CL$mtrD_{His6}$(S611A)	Site-directed S611A MtrD mutant based on pGCC4-CL$mtrD_{His6}$	This study
pGCC4-CL$mtrD_{His6}$(F612C)	Site-directed F612C MtrD mutant based on pGCC4-CL$mtrD_{His6}$	This study
pGCC4-CL$mtrD_{His6}$(F623C)	Site-directed F6123C MtrD mutant based on pGCC4-CL$mtrD_{His6}$	This study

[a]Abbreviations: Ery^r, erythromycin resistance; Kan^r, kanamycin resistance.

PCRs (Bioline, Boston, MA, USA). All restriction digestion enzymes and T4 DNA ligase were from New England Biolabs (New England Biolabs Inc., Ipswich, MA, USA). Transformations into *N. gonorrhoeae* or *E. coli* cells were carried as described previously (42, 43). All sequencing was performed by Australian Genome Research Facility (AGRF; Australia).

Construction of unmarked *mtrD* and *norM* single and *mtrD*/*norM* double deletion strains. Two unmarked *mtrD* deletion strains (the FA19 Δ*mtrD* and KH15 Δ*mtrD* strains) were created by overlap extension PCR (12). Briefly, a 3,150-bp fusion DNA fragment that encompassed the *mtrD* gene was created by PCR using primers MtrD-Del-F2, MtrD-Ovl-R1, MtrD-Ovl-F2, and MtrD-Del-R2 (Table S1) and FA19 chromosomal DNA as the template. This two-step PCR removed *mtrD*, leaving only 177 bp before its stop codon. The PCR-amplified DNA was transformed into the FA19 and KH15 strains, and the resultant colonies were selected by analysis of susceptibility to erythromycin performed by replica plating on GC plates with or without erythromycin (0.06 μg/ml, 4-fold below MIC for FA19). Erythromycin was used as it is a known substrate of the MtrD protein, and sensitivity to erythromycin at a concentration below the MIC for FA19 could be used as evidence that the *mtrD* gene had been removed. Sequencing confirmed the removal of *mtrD* and the integrity of the flanking regions. The same method was used for creating the *N. gonorrhoeae* FA19 Δ*norM*, FA19 Δ*mtrD* Δ*norM*, and KH15 Δ*mtrD* Δ*norM* strains by deleting the *norM* gene from the respective progenitors. The NorM substrate ethidium (0.25 μg/ml for *norM*-only deletion and 0.06 μg/ml for *norM* and *mtrD* double deletion mutants) was used for selecting the *norM* knockout derivatives by replica plating.

Cloning of *mtrD* into pGCC4 and recombination into the neisserial chromosome. To recombine *mtrD* into the chromosome of the *N. gonorrhoeae* Δ*mtrD* knockout strains, the *mtrD* determinant was cloned into the pGCC4 shuttle vector behind the lac promoter. A PacI-*mtrD*-PmeI fragment was obtained by PCR amplification using FA19 chromosomal template DNA and PacI-*mtrD*-for and PmeI-*mtrD*-rev primers (Table S1). A sequence was also incorporated in the reverse primer, allowing addition of six histidine residues (His6) to act as an affinity tag at the C terminus of the protein. The resultant PCR product and vector were digested and cloned with PacI and PmeI, producing the *mtrD* clone called pGCC4-$mtrD_{(His6)}$.

The *mtrD* derivatives were recombined into the KH15 Δ*mtrD* Δ*norM* chromosome by transformation as previously described (43). The pGCC4 empty vector was also integrated into the KH15 Δ*mtrD* Δ*norM* chromosome, producing a NICS-only recombinant strain that could be utilized as a negative control by employment of the same methodology. KH15 Δ*mtrD* Δ*norM* recombinants were selected on GC plates containing erythromycin (0.5 μg/ml). A single purified transformant colony was subjected to PCR using SCRNG1 and MTRDSF5 primers (Table S1) for verification of $mtrD_{His6}$ integration between *lctP* and *aspC*.

Site-directed mutagenesis. The QuikChange site-directed mutagenesis method was used to individually replace the selected MtrD residues using the primers listed in Table S1. To aid in screening, a silent restriction site was incorporated into each primer pair where possible. Initially, a cysteineless derivative of MtrD was created by PCR amplification using C491A-F and C491A-R primers and pGCC4-$mtrD_{His6}$ as the template. The PCR cycling conditions were as follows: denaturation at 95°C for 5 min, followed by 30 cycles of 95°C for 20 s, 55°C for 1 min, 72°C for 8 min 30 s and then 72°C for 10 min.

Downloaded from http://mbio.asm.org/ on November 19, 2019 at FLINDERS UNIVERSITY OF SOUTH AUSTRALIA

Subsequent mutants (F136A, F176A, I605A, F610A, S611A, F612C, and F623C) were created using the pGCC4-CL*mtrD*$_{His6}$ construct as the template. The integrity of all constructs was verified by sequencing the whole *mtrD* gene followed by recombination of the gene into the *N. gonorrhoeae* KH15 Δ*mtrD* Δ*norM* chromosome.

Western blotting. Expression of MtrD proteins in KH15 Δ*mtrD* Δ*norM* membranes was analyzed by Western blotting using anti-6×His epitope tag (rabbit) antibody and peroxidase-conjugated anti-rabbit IgG (goat) antibody (Rockland) as primary and secondary antibodies, respectively. *N. gonorrhoeae* strains were grown at 37°C to an optical density at 600 nm (OD_{600}) of 0.6 in GC broth containing 0.5 mM IPTG. All membrane isolation and protein experiments were conducted on ice or at 4°C as previously described (44, 45). The total protein content in each sample was quantified using a Bio-Rad DC protein assay kit, and 10-μg samples were resolved on a 10% SDS-PAGE gel and transferred (44, 45). Membranes were scanned with a Bio-Rad ChemiDoc MP imaging system and analyzed using Image Lab software 6.0.1 (Bio-Rad). Mutant protein expression levels were compared to the WT protein expression level (see Fig. S1 in the supplemental material).

MIC analyses. MIC analyses of the *N. gonorrhoeae* strains used a previously reported agar dilution method (46) with modifications. MIC analyses were conducted using solid GC media supplemented with 0.5 mM IPTG and antimicrobial compounds. The MIC was determined as the lowest concentration of the antimicrobial compound required to fully inhibit bacterial growth. All MIC values shown are representative of results from three replicates.

Molecular dynamics simulations. The MtrD crystal structure (PDB identifier [ID]: 4MT1) was used for all simulations (7). The missing residues between residues 494 and 507, 671, and 672 were rebuilt; the N and C termini were capped with acetyl and amine groups, respectively; and the crystallographic symmetry operators were applied to rebuild the trimeric biological assembly (47). The MtrD trimer was embedded in an equilibrated *Neisserial* lipid bilayer containing 80% 1,2-dipalmitoyl-*sn*-glycero-3-phosphoethanolamine (DMPE) and 20% 1,2-dimyristoyl-sn-glycero-3-phospho-(1′-rac)-glycerol (DMPG) as described previously (48), using the Orientation of Membrane Proteins database to guide the orientation in the membrane (49). Thirty molecules of progesterone were inserted randomly in the solvent layer surrounding MtrD. The system was solvated with explicit water and 150 mM NaCl. Counter-ions were added to ensure the overall charge neutrality of the system.

All simulations were performed using GROMACS 2016.1 (50, 51) in conjunction with the GROMOS 54a7 forcefield (52) and a 2-fs time step. The simple point charge (SPC) water model (53) was used to describe the solvent water. The parameters used for the progesterone analyses, DMPE and DMPG, are available from the automated force field topology builder (ATB) (54). All simulations were performed under periodic boundary conditions in a hexagonal prism box. The dimensions of the box were chosen such that minimum distance of the protein to its periodic image was 3.5 nm.

The system was equilibrated over 10 ns, using a series of 2-ns simulations in the NPT (fixed number of atoms N, fixed pressure P, fixed temperature T) ensemble with progressively decreasing position restraint force constants of 500 kJ mol^{-1} nm^{-2}, 100 kJ mol^{-1} nm^{-2}, 50 kJ mol^{-1} nm^{-2}, 20 kJ mol^{-1} nm^{-2}, and 0 kJ mol^{-1} nm^{2} on the Cα atoms. The temperature of the simulations was maintained at 300 K using a Bussi velocity rescaling thermostat, with a coupling constant of 0.1 ps (55). The pressure coupling was semi-isotropic. The pressure was maintained at 1 bar using a Parrinello-Rahman barostat pressure coupling with a constant of 5 ps. The Particle Mesh Ewald (PME) method (56) was used to calculate electrostatic interactions with a cutoff at 1.4 nm. The LINCS algorithm (57) was used for bond constraints, and the SETTLE algorithm (58) was utilized to constrain waters. Three replicate simulations were performed, each 200 ns in length. To examine how changes in timescale influence the interaction with progesterone, the third simulation was extended to 500 ns in total, giving a total combined simulation time of 900 ns for the three replicates.

Docking studies. To identify the molecular interactions underlying the modified resistance profiles of our MtrD mutants, molecular docking of seven diverse MtrD substrates (progesterone, nonoxynol-9, azithromycin, rifampin, ethidium, crystal violet, and cholic acid) and the PAβN inhibitor was performed with AutoDock Vina V.1.1.2. United-atom representations of these substrates (with protonation states appropriate for pH 7.4) were docked to the repaired crystal structure of the MtrD trimer used to initialize the molecular dynamics simulations reported in this study. AutoDock Tools V.1.5.6 was used to determine two sets of grid parameters centered on the access and deep binding pocket cavities, respectively (Table S2). For each substrate, docked poses within the proposed access pocket or deep binding pocket were selected for analysis if the energy of a given pose was within 1 kcal/mol (inclusive) of the lowest-energy pose for a given substrate, with weighted energies obtained according to the default AutoDock Vina scoring function. Substrate amide bonds were allowed to rotate during docking. Residues comprising the putative access and deep binding pockets (Table 4) were made flexible during the docking procedure centered on the corresponding pocket. To identify the residues with the most significant binding interactions, approximate per-residue contributions to the binding affinity and energy breakdowns for each substrate were obtained by systematically removing each residue found within 8 Å of the lowest-scoring docked pose followed by (static) rescoring.

SUPPLEMENTAL MATERIAL

Supplemental material for this article may be found at https://doi.org/10.1128/mBio.02277-19.

FIG S1, DOCX file, 0.2 MB.

FIG S2, DOCX file, 0.2 MB.

Downloaded from http://mbio.asm.org/ on November 19, 2019 at FLINDERS UNIVERSITY OF SOUTH AUSTRALIA

FIG S3, DOCX file, 2.1 MB.
FIG S4, DOCX file, 2.4 MB.
FIG S5, DOCX file, 1.3 MB.
FIG S6, DOCX file, 0.4 MB.
TABLE S1, DOCX file, 0.02 MB.
TABLE S2, DOCX file, 0.02 MB.

ACKNOWLEDGMENTS

This work was supported by a Flinders Medical Research Foundation grant and was undertaken using resources from the National Computational Infrastructure (NCI), which is supported by the Australian Government. M.C. was supported by an Australian Government Research Training Program Scholarship.

We thank Stephen Fairweather for his help with figure compliance.

REFERENCES

1. Maness MJ, Sparling PF. 1973. Multiple antibiotic resistance due to a single mutation in *Neisseria gonorrhoeae*. J Infect Dis 128:321–330. https://doi.org/10.1093/infdis/128.3.321.
2. Hagman KE, Lucas CE, Balthazar JT, Snyder L, Nilles M, Judd RC, Shafer WM. 1997. The MtrD protein of *Neisseria gonorrhoeae* is a member of the resistance/nodulation/division protein family constituting part of an efflux system. Microbiology 143:2117–2125. https://doi.org/10.1099/00221287-143-7-2117.
3. Janganan TK, Bavro VN, Zhang L, Borges-Walmsley MI, Walmsley AR. 2013. Tripartite efflux pumps: energy is required for dissociation, but not assembly or opening of the outer membrane channel of the pump. Mol Microbiol 88:590–602. https://doi.org/10.1111/mmi.12211.
4. Shafer WM, Qu X, Waring AJ, Lehrer RI. 1998. Modulation of *Neisseria gonorrhoeae* susceptibility to vertebrate antibacterial peptides due to a member of the resistance/nodulation/division efflux pump family. Proc Natl Acad Sci U S A 95:1829–1833. https://doi.org/10.1073/pnas.95.4.1829.
5. Hagman KE, Pan W, Spratt BG, Balthazar JT, Judd RC, Shafer WM. 1995. Resistance of *Neisseria gonorrhoeae* to antimicrobial hydrophobic agents is modulated by the *mtrRCDE* efflux system. Microbiology 141:611–622. https://doi.org/10.1099/13500872-141-3-611.
6. Jerse AE, Sharma ND, Simms AN, Crow ET, Snyder LA, Shafer WM. 2003. A gonococcal efflux pump system enhances bacterial survival in a female mouse model of genital tract infection. Infect Immun 71:5576–5582. https://doi.org/10.1128/iai.71.10.5576-5582.2003.
7. Bolla JR, Su CC, Do SV, Radhakrishnan A, Kumar N, Long F, Chou TH, Delmar JA, Lei HT, Rajashankar KR, Shafer WM, Yu EW. 2014. Crystal structure of the *Neisseria gonorrhoeae* MtrD inner membrane multidrug efflux pump. PLoS One 9:e97903. https://doi.org/10.1371/journal.pone.0097903.
8. Lei HT, Chou TH, Su CC, Bolla JR, Kumar N, Radhakrishnan A, Long F, Delmar JA, Do SV, Rajashankar KR, Shafer WM, Yu EW. 2014. Crystal structure of the open state of the *Neisseria gonorrhoeae* MtrE outer membrane channel. PLoS One 9:e97475. https://doi.org/10.1371/journal.pone.0097475.
9. Murakami S, Nakashima R, Yamashita E, Matsumoto T, Yamaguchi A. 2006. Crystal structures of a multidrug transporter reveal a functionally rotating mechanism. Nature 443:173–179. https://doi.org/10.1038/nature05076.
10. Nakashima R, Sakurai K, Yamasaki S, Nishino K, Yamaguchi A. 2011. Structures of the multidrug exporter AcrB reveal a proximal multisite drug-binding pocket. Nature 480:565–569. https://doi.org/10.1038/nature10641.
11. Sarubbi FA, Blackman E, Sparling PF. 1974. Genetic mapping of linked antibiotic resistance loci in *Neisseria gonorrhoeae*. J Bacteriol 120:1284–1292.
12. Vallejo AN, Pogulis RJ, Pease LR. 1994. In vitro synthesis of novel genes: mutagenesis and recombination by PCR. PCR Methods Appl 4:S123–130. https://doi.org/10.1101/gr.4.3.S123.
13. Rouquette-Loughlin C, Dunham SA, Kuhn M, Balthazar JT, Shafer WM. 2003. The NorM efflux pump of *Neisseria gonorrhoeae* and *Neisseria meningitidis* recognizes antimicrobial cationic compounds. J Bacteriol 185:1101–1106. https://doi.org/10.1128/jb.185.3.1101-1106.2003.
14. Sarubbi F, Sparling PF, Blackman E, Lewis E. 1975. Loss of low-level antibiotic resistance in *Neisseria gonorrhoeae* due to env mutations. J Bacteriol 124:750–756.
15. Sparling PF, Sarubbi FAJ, Blackman E. 1975. Inheritance of low-level resistance to penicillin, tetracycline, and chloramphenicol in *Neisseria gonorrhoeae*. J Bacteriol 124:740–749.
16. Shafer WM, Folster JP. 2006. Towards an understanding of chromosomally mediated penicillin resistance in *Neisseria gonorrhoeae*: evidence for a porin-efflux pump collaboration. J Bacteriol 188:2297–2299. https://doi.org/10.1128/JB.188.7.2297-2299.2006.
17. Mehr IJ, Seifert HS. 1998. Differential roles of homologous recombination pathways in *Neisseria gonorrhoeae* pilin antigenic variation, DNA transformation and DNA repair. Mol Microbiol 30:697–710. https://doi.org/10.1046/j.1365-2958.1998.01089.x.
18. Zwama M, Yamasaki S, Nakashima R, Sakurai K, Nishino K, Yamaguchi A. 2018. Multiple entry pathways within the efflux transporter AcrB contribute to multidrug recognition. Nat Commun 9:124. https://doi.org/10.1038/s41467-017-02493-1.
19. Yamamoto K, Tamai R, Yamazaki M, Inaba T, Sowa Y, Kawagishi I. 2016. Substrate-dependent dynamics of the multidrug efflux transporter AcrB of *Escherichia coli*. Sci Rep 6:21909. https://doi.org/10.1038/srep21909.
20. Schuster S, Vavra M, Kern WV. 2016. Evidence of a substrate-discriminating entrance channel in the lower porter domain of the multidrug resistance efflux pump AcrB. Antimicrob Agents Chemother 60:4315–4323. https://doi.org/10.1128/AAC.00314-16.
21. Cha HJ, Muller RT, Pos KM. 2014. Switch-loop flexibility affects transport of large drugs by the promiscuous AcrB multidrug efflux transporter. Antimicrob Agents Chemother 58:4767–4772. https://doi.org/10.1128/AAC.02733-13.
22. Wehmeier C, Schuster S, Fahnrich E, Kern WV, Bohnert JA. 2009. Site-directed mutagenesis reveals amino acid residues in the *Escherichia coli* RND efflux pump AcrB that confer macrolide resistance. Antimicrob Agents Chemother 53:329–330. https://doi.org/10.1128/AAC.00921-08.
23. Hassan KA, Robinson KL, Smith AN, Gibson JH, Skurray RA, Brown MH. 2006. Glycine-rich transmembrane helix 10 in the staphylococcal tetracycline transporter TetA(K) lines a solvent-accessible channel. Biochemistry 45:15661–15669. https://doi.org/10.1021/bi0614380.
24. Shafer WM. 2018. Mosaic drug efflux gene sequences from commensal *Neisseria* can lead to low-level azithromycin resistance expressed by *Neisseria gonorrhoeae* clinical isolates. mBio 9:e01747-18. https://doi.org/10.1128/mBio.01747-18.
25. Golparian D, Shafer WM, Ohnishi M, Unemo M. 2014. Importance of multidrug efflux pumps in the antimicrobial resistance property of clinical multidrug-resistant isolates of *Neisseria gonorrhoeae*. Antimicrob Agents Chemother 58:3556–3559. https://doi.org/10.1128/AAC.00038-14.
26. Nakashima R, Sakurai K, Yamasaki S, Hayashi K, Nagata C, Hoshino K, Onodera Y, Nishino K, Yamaguchi A. 2013. Structural basis for the inhibition of bacterial multidrug exporters. Nature 500:102–106. https://doi.org/10.1038/nature12300.
27. Yamaguchi A, Nakashima R, Sakurai K. 2015. Structural basis of RND-type multidrug exporters. Front Microbiol 6:327. https://doi.org/10.3389/fmicb.2015.00327.

Downloaded from http://mbio.asm.org/ on November 19, 2019 at FLINDERS UNIVERSITY OF SOUTH AUSTRALIA

28. Schumacher MA, Miller MC, Grkovic S, Brown MH, Skurray RA, Brennan RG. 2001. Structural mechanisms of QacR induction and multidrug recognition. Science 294:2158–2163. https://doi.org/10.1126/science.1066020.
29. Grkovic S, Hardie KM, Brown MH, Skurray RA. 2003. Interactions of the QacR multidrug-binding protein with structurally diverse ligands: implications for the evolution of the binding pocket. Biochemistry 42:15226–15236. https://doi.org/10.1021/bi035447+.
30. Vargiu AV, Ramaswamy VK, Malloci G, Malvacio I, Atzori A, Ruggerone P. 31 January 2018, posting date. Computer simulations of the activity of RND efflux pumps. Res Microbiol https://doi.org/10.1016/j.resmic.2017.12.001.
31. Husain F, Nikaido H. 2010. Substrate path in the AcrB multidrug efflux pump of *Escherichia coli*. Mol Microbiol 78:320–330. https://doi.org/10.1111/j.1365-2958.2010.07330.x.
32. Schulz R, Vargiu AV, Collu F, Kleinekathofer U, Ruggerone P. 2010. Functional rotation of the transporter AcrB: insights into drug extrusion from simulations. PLoS Comput Biol 6:e1000806. https://doi.org/10.1371/journal.pcbi.1000806.
33. Takatsuka Y, Chen C, Nikaido H. 2010. Mechanism of recognition of compounds of diverse structures by the multidrug efflux pump AcrB of *Escherichia coli*. Proc Natl Acad Sci U S A 107:6559–6565. https://doi.org/10.1073/pnas.1001460107.
34. Vargiu AV, Ruggerone P, Opperman TJ, Nguyen ST, Nikaido H. 2014. Molecular mechanism of MBX2319 inhibition of *Escherichia coli* AcrB multidrug efflux pump and comparison with other inhibitors. Antimicrob Agents Chemother 58:6224–6234. https://doi.org/10.1128/AAC.03283-14.
35. Sjuts H, Vargiu AV, Kwasny SM, Nguyen ST, Kim HS, Ding X, Ornik AR, Ruggerone P, Bowlin TL, Nikaido H, Pos KM, Opperman TJ. 2016. Molecular basis for inhibition of AcrB multidrug efflux pump by novel and powerful pyranopyridine derivatives. Proc Natl Acad Sci U S A 113:3509–3514. https://doi.org/10.1073/pnas.1602472113.
36. Vargiu AV, Nikaido H. 2012. Multidrug binding properties of the AcrB efflux pump characterized by molecular dynamics simulations. Proc Natl Acad Sci U S A 109:20637–20642. https://doi.org/10.1073/pnas.1218348109.
37. Bohnert JA, Schuster S, Seeger MA, Fahnrich E, Pos KM, Kern WV. 2008. Site-directed mutagenesis reveals putative substrate binding residues in the *Escherichia coli* RND efflux pump AcrB. J Bacteriol 190:8225–8229. https://doi.org/10.1128/JB.00912-08.
38. Eicher T, Cha HJ, Seeger MA, Brandstatter L, El-Delik J, Bohnert JA, Kern WV, Verrey F, Grutter MG, Diederichs K, Pos KM. 2012. Transport of drugs by the multidrug transporter AcrB involves an access and a deep binding pocket that are separated by a switch-loop. Proc Natl Acad Sci U S A 109:5687–5692. https://doi.org/10.1073/pnas.1114944109.
39. Ababou A, Koronakis V. 2016. Structures of gate loop variants of the AcrB drug efflux pump bound by erythromycin substrate. PLoS One 11:e0159154. https://doi.org/10.1371/journal.pone.0159154.
40. Rouquette-Loughlin CE, Reimche JL, Balthazar JT, Dhulipala V, Gernert KM, Kersh EN, Pham CD, Pettus K, Abrams AJ, Trees DL, St Cyr S, Shafer WM. 2018. Mechanistic basis for decreased antimicrobial susceptibility in a clinical isolate of *Neisseria gonorrhoeae* possessing a mosaic-like *mtr* efflux pump locus. mBio 9:e02281-18. https://doi.org/10.1128/mBio.02281-18.
41. Kellogg DS, Jr, Peacock WL, Jr, Deacon WE, Brown L, Pirkle DI. 1963. *Neisseria gonorrhoeae*. I. Virulence genetically linked to clonal variation. J Bacteriol 85:1274–1279.
42. Hanahan D. 1983. Studies on transformation of *Escherichia coli* with plasmids. J Mol Biol 166:557–580. https://doi.org/10.1016/s0022-2836(83)80284-8.
43. Dillard JP. 2011. Genetic manipulation of *Neisseria gonorrhoeae*. Curr Protoc Microbiol Chapter 4:Unit4A 2. https://doi.org/10.1002/9780471729259.mc04a02s23.
44. Hassan KA, Xu Z, Watkins RE, Brennan RG, Skurray RA, Brown MH. 2009. Optimized production and analysis of the staphylococcal multidrug efflux protein QacA. Protein Expr Purif 64:118–124. https://doi.org/10.1016/j.pep.2008.11.009.
45. Hassan KA, Galea M, Wu J, Mitchell BA, Skurray RA, Brown MH. 2006. Functional effects of intramembranous proline substitutions in the staphylococcal multidrug transporter QacA. FEMS Microbiol Lett 263:76–85. https://doi.org/10.1111/j.1574-6968.2006.00411.x.
46. CLSI. 2012. Methods for dilution antimicrobial susceptibility tests for bacteria that grow aerobically: approved standard, 9th ed, vol 32. Clinical and Laboratory Standards Institute, Wayne, Pa.
47. Schrodinger LLC. 2010. The PyMOL molecular graphics system. Version 1:0. Schrodinger LLC, New York, NY.
48. Anandan A, Evans GL, Condic-Jurkic K, O'Mara ML, John CM, Phillips NJ, Jarvis GA, Wills SS, Stubbs KA, Moraes I, Kahler CM, Vrielink A. 2017. Structure of a lipid A phosphoethanolamine transferase suggests how conformational changes govern substrate binding. Proc Natl Acad Sci U S A 114:2218–2223. https://doi.org/10.1073/pnas.1612927114.
49. Lomize MA, Pogozheva ID, Joo H, Mosberg HI, Lomize AL. 2012. OPM database and PPM Web server: resources for positioning of proteins in membranes. Nucleic Acids Res 40:D370–D376. https://doi.org/10.1093/nar/gkr703.
50. Abraham MJ, Murtola T, Schulz R, Páll S, Smith JC, Hess B, Lindahl E. 2015. GROMACS: high performance molecular simulations through multi-level parallelism from laptops to supercomputers. SoftwareX 1:19–25. https://doi.org/10.1016/j.softx.2015.06.001.
51. Van Der Spoel D, Lindahl E, Hess B, Groenhof G, Mark AE, Berendsen HJ. 2005. GROMACS: fast, flexible, and free. J Comput Chem 26:1701–1718. https://doi.org/10.1002/jcc.20291.
52. Schmid N, Eichenberger AP, Choutko A, Riniker S, Winger M, Mark AE, van Gunsteren WF. 2011. Definition and testing of the GROMOS force-field versions 54A7 and 54B7. Eur Biophys J 40:843. https://doi.org/10.1007/s00249-011-0700-9.
53. Berendsen HJ, Postma JP, van Gunsteren WF, Hermans J. 1981. Interaction models for water in relation to protein hydration, p 331–342. *In* Pullman B, Intermolecular forces. Springer, New York, NY.
54. Malde AK, Zuo L, Breeze M, Stroet M, Poger D, Nair PC, Oostenbrink C, Mark AE. 2011. An automated force field topology builder (ATB) and repository: version 1.0. J Chem Theory Comput 7:4026–4037. https://doi.org/10.1021/ct200196m.
55. Bussi G, Donadio D, Parrinello M. 2007. Canonical sampling through velocity rescaling. J Chem Phys 126:14101. https://doi.org/10.1063/1.2408420.
56. Darden T, York D, Pedersen L. 1993. Particle mesh Ewald: an N· log (N) method for Ewald sums in large systems. J Chem Phys 98:10089–10092. https://doi.org/10.1063/1.464397.
57. Hess B, Bekker H, Berendsen HJ, Fraaije JG. 1997. LINCS: a linear constraint solver for molecular simulations. J Comput Chem 18:1463–1472. https://doi.org/10.1002/(SICI)1096-987X(199709)18:12<1463::AID-JCC4>3.3.CO;2-L.
58. Miyamoto S, Kollman PA. 1992. Settle: an analytical version of the SHAKE and RATTLE algorithm for rigid water models. J Comput Chem 13:952–962. https://doi.org/10.1002/jcc.540130805.

Downloaded from http://mbio.asm.org/ on November 19, 2019 at FLINDERS UNIVERSITY OF SOUTH AUSTRALIA

7.4 Appendix D: Paper 3: Coordination of substrate binding and protonation in the *Neisseria gonorrhoeae* MtrD efflux pump controls the functionally rotating transport mechanism.

ACS Infectious Diseases

pubs.acs.org/journal/aidcbc

Article

Coordination of Substrate Binding and Protonation in the *N. gonorrhoeae* MtrD Efflux Pump Controls the Functionally Rotating Transport Mechanism

Stephen J. Fairweather,[‖] Vrinda Gupta,[‖] Mohsen Chitsaz, Lauren Booth, Melissa H. Brown, and Megan L. O'Mara*

Cite This: *ACS Infect. Dis.* 2021, 7, 1833−1847

Read Online

ACCESS | Metrics & More | Article Recommendations | Supporting Information

Downloaded via FLINDERS UNIV on July 25, 2021 at 09:29:21 (UTC).
See https://pubs.acs.org/sharingguidelines for options on how to legitimately share published articles.

ABSTRACT: Multidrug resistance is a serious problem that threatens the effective treatment of the widespread sexually transmitted disease gonorrhea, caused by the Gram-negative bacterium *Neisseria gonorrhoeae*. The drug efflux pump primarily implicated in *N. gonorrhoeae* antimicrobial resistance is the inner membrane transporter MtrD, which forms part of the tripartite multiple transferable resistance (Mtr) CDE efflux system. A structure of MtrD was first solved in 2014 as a symmetrical homotrimer, and then, recently, as an asymmetrical homotrimer. Through a series of molecular dynamics simulations and mutagenesis experiments, we identify the combination of substrate binding and protonation states of the proton relay network that drives the transition from the symmetric to the asymmetric conformation of MtrD. We characterize the allosteric coupling between the functionally important local regions that control conformational changes between the access, binding, and extrusion states and allow for transition to the asymmetric MtrD conformation. We also highlight a significant rotation of the transmembrane helices caused by protonation of the proton relay network, which widens the intermonomeric gap that is a hallmark of the rotational transporter mechanism. This is the first analysis and description of the transport mechanism for the *N. gonorrhoeae* MtrD transporter and provides evidence that antimicrobial efflux in MtrD follows the functionally rotating transport mechanism seen in protein homologues from the same transport protein superfamily.

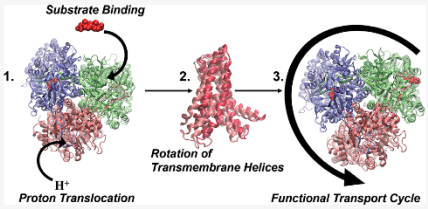

KEYWORDS: *Neisseria gonorrhoeae, antimicrobial resistance, efflux pumps, MtrD, molecular dynamics simulations, RND transporter*

The Gram-negative pathogenic bacterium *Neisseria gonorrhoeae* is the causative agent of the sexually transmitted disease gonorrhea, reported by the WHO to annually cause 78.3 million cases worldwide.[1] Although gonorrhea has been successfully treated with sulfonamides, β-lactams, and other antibiotics since the 1930s, cases of multidrug resistant gonorrhea have increased alarmingly in many regions.[2−5] Recent emergence of "super"-drug resistance to the current frontline therapy of dual cephalosporin and macrolide administration has led to fear of an emerging untreatable disease.[1−4,6,7]

In Gram-negative bacteria, resistance-nodulation-division (RND) multidrug efflux systems are a primary mechanism for the acquisition of multidrug resistance. *N. gonorrhoeae* possesses a single tripartite RND efflux system, the multiple transferable resistance (Mtr) CDE efflux system, composed of the inner membrane MtrD efflux protein, the outer membrane MtrE pore, and the periplasmic MtrC protein, which connects the two membrane-embedded components. Like other RND drug efflux systems, the inner membrane MtrD efflux protein uses a proton electromotive force to drive the efflux of substrate out of the periplasmic space and rid the organism of potentially harmful xenobiotics and antimicrobials.[8] The loss of MtrCDE encoding genes increases the susceptibility of *N. gonorrhoeae* to an array of antimicrobial molecules including dyes, detergents, bile salts, as well as host-derived antimicrobials, progesterone, fatty acids, aliphatic/cationic peptides, and multiple clinical antibiotics.[9,10] MtrCDE also plays a role in bacterial virulence by facilitating biofilm formation, which enhances colonization and disease progression *in vivo*.[1,11−15]

MtrD has over 40% protein sequence identity to other structurally well-characterized RND homologues, namely AcrB from *Escherichia coli*, MexB from *Pseudomonas aeruginosa*,[16] and AdeB from *Acinetobacter baumannii*[17] (Figure S1). The

Received: March 23, 2021
Published: May 13, 2021

ACS Publications © 2021 American Chemical Society

https://doi.org/10.1021/acsinfecdis.1c00149
ACS Infect. Dis. 2021, 7, 1833−1847

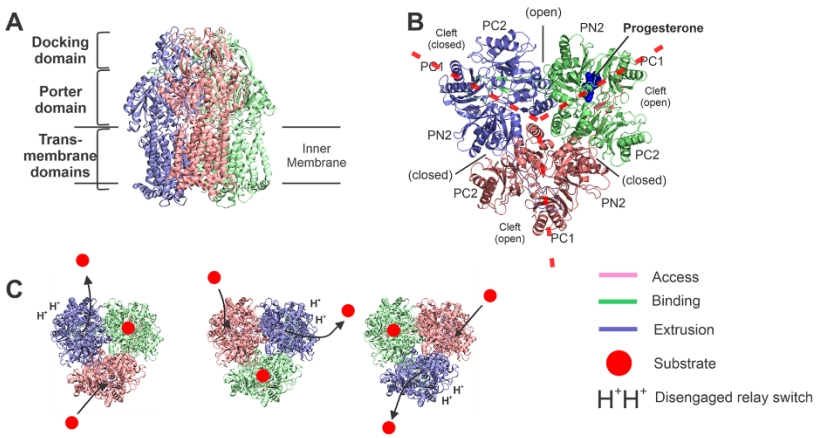

Figure 1. Asymmetric structure of MtrD and proposed transport cycle. (A) Side view and (B) top view of the asymmetric homotrimeric MtrD structure (PDB ID: 6VKT) showing key domains and subdomains, colored by access, binding, or extrusion conformation (transmembrane domains are hidden for clarity). Progesterone (blue VDW rendering) is shown in the binding conformation monomer (green) of the asymmetric structure. The axis of pseudosymmetry through each monomer is shown by a dashed red line. (C) The proposed asymmetric RND transport cycle alternates in a synchronized fashion through the access, binding, and extrusion conformations. The substrate binding configuration and protonation state of the three conformations are indicated by the presence of two protons (H^+) and substrate (red dot).

available MtrD structures[18,19] have the same overall architecture as other RND transporters. MtrD is a homotrimer, with each monomer organized into two large regions: an inner membrane transmembrane domain (TMD) containing 12 transmembrane (TM) α-helices immediately beneath a large periplasmic domain divided into the porter (PD) and docking domains (DD). The DD complexes with MtrC to link MtrD to the MtrE outer membrane channel (Figure 1A). Each MtrD monomer contains an axis of pseudosymmetry that extends longitudinally through the TMD, PD, and DD. The PD can be further divided into 4 subdomains (Figure 1B): PC1 and PC2 form the substrate binding cleft, while the PN1 and PN2 subdomains of each monomer combine to form part of the central pore of MtrD that stabilizes the trimeric structure. The highly conserved TMD proton relay network is responsible for the proton translocation needed for substrate efflux through the MtrCDE system. Despite the overall similarities to other RND protein structures, MtrD contains a unique, 11-residue insertion at the top of TM9 which extends into the periplasm.

Previous work on the MtrD homologue, AcrB, has provided a working paradigm of the RND transport cycle, in which trimeric RND efflux proteins adopt an asymmetric conformation with each of the three monomers in an "access", "binding", or "extrusion" state.[20−22] Substrate efflux depends on the synchronous cycling of the monomers through these three functional states (Figure 1C).[23,24] The transport cycle begins with the spontaneous binding of substrate in the proximal binding pocket of the access state (Figure 1B). During transition from the access to the binding state, substrate permeates along the binding pocket, ending in the distal (or deep) binding pocket. Finally, in the extrusion state, substrate is effluxed from the MtrD distal binding pocket, to the MtrE outer membrane channel.[16,25] These conformational states are coupled to changes in the protonation state of the TMD proton relay network, driven by the proton motive force across the inner membrane.

The proton relay network is highly conserved across all RND transporters and contains a network of titratable residues located on either side of the axis of pseudosymmetry to form a hydrogen bonding network. From structural comparison and sequence homology to AcrB, the MtrD residues D405 and D406 (TM 4), K948 and N949 (TM 10), and T985 (TM 11) form the putative proton relay network.[19,23,26−29] Previous studies have shown that the relay switch residues, corresponding to D405, D406, K948, and T985 in MtrD, have 100%, 77%, 65%, and 96% sequence identity across a reference set of 566 RND efflux pump sequences.[30] When considering only efflux pumps for which the role of one or more of these residues has been experimentally identified as important for substrate efflux, this conservation increases to 100%.[26,27,31−35] In AcrB, protonation of the D405 and/or D406 homologue residues via the uptake of protons leads to disengagement of the proton relay network and a global conformational change from the binding to the extrusion conformation.[20] Conversely, deprotonation of D405 and/or D406 engages the proton relay network and drives the monomer back into the access conformation.

The asymmetric MtrD cryo-EM structures (PDB ID: 6VKT, 6VKS)[19] each contain an access, binding, and extrusion monomer, with substrate bound in the distal binding pocket of the binding monomer. In comparison, in the earlier crystal structure (PDB ID: 4MT1),[18] all three monomers are in a symmetric conformation that does not align to the prototypical RND access, binding or extrusion states. Instead, each monomer has a mix of local features characteristic of the binding and extrusion states. A similar hybrid conformation

https://doi.org/10.1021/acsinfecdis.1c00149
ACS Infect. Dis. 2021, 7, 1833−1847

Table 1. *Neisseria gonorrhoeae* KH15Δ*mtrD*Δ*norM* Strain Expressing MtrD Derivatives

	MIC (μg/mL)[a]										
	detergent		antibiotic			CAMP	dye		bile acid	hormone	biocide
mutation	N-9	TX-100	RIF	NOV	OXA	PMB	ET	CV	CHO	PRO	DQ
CL-MtrD$_{His6}$(WT)[b]	≥4096	≥4096	0.125	1	4	100	0.25	2	400	80	1
D405C	16	32	0.008	0.03	0.06	50	0.06	0.125	100	20	0.5
negative control[c]	16	32	0.008	0.03	0.06	50	0.06	0.125	100	20	0.5

[a]All MIC data are representative of three or more independent experiments. Abbreviations: CAMP, cationic antimicrobial peptide; CHO, cholic acid; CV, crystal violet; DQ, dequalinium; ET, ethidium; N-9, nonoxynol-9; NOV, novobiocin; OXA, oxacillin; PMB, polymyxin B; PRO, progesterone; RIF, rifampicin and TX-100, Triton X-100. [b]Cysteine-less MtrD mutant representing wild-type resistance profile. [c]KH15Δ*mtrD*Δ*norM* strain transformed with the NICS section of the pGCC4 vector that does not express *mtrD*.

Table 2. MtrD Trimer Structures and Their Global/Local Conformational Characteristics

global structural characteristic			local conformation characteristic					
RND structure (PDB ID)	trimer structure	monomer conformation	cleft entrance	deep binding pocket	extrusion gate	proton relay network	substrate present	ref.
MtrD (4MT1)	symmetric	hybrid	open	open	closed	disengaged	no	18
MtrD (6VKS, 6VKT)	asymmetric	access	open	closed	closed	engaged	no	19
		binding	open	open	closed	engaged	yes	
		extrusion	closed	closed	open	disengaged	no	

with features from both the binding and extrusion states within the same monomer was also observed in a symmetric structure of the *A. baumannii* AdeB RND transporter.[17]

Here, we confirm the identity of the proton relay network residues in MtrD and investigate whether the symmetric MtrD structure will transition into an asymmetric state using a multiscale molecular dynamics (MD) simulation approach. Specifically, we examine whether simulations initiated from the symmetric MtrD structure sample states which correspond to the cryo-EM MtrD access, binding, and extrusion conformations. We show the symmetric MtrD homotrimer can only undergo coordinated conformational switching to the asymmetric state when the protonation state of the proton relay network residues is altered, and substrate is also present in the binding cleft of adjacent monomers. Protonation of the relay switch is allosterically coupled to conformational changes within the same and adjacent monomers of the MtrD homotrimer. In particular, relay switch protonation instigates a rotation of one-half of the TMD along the axis of pseudosymmetry, an event time-correlated with the opening of intramolecular distances between monomers, a hallmark feature of the functionally rotating efflux mechanism observed in other RND transporters.

■ RESULTS AND DISCUSSION

Characterization of the MtrD Proton Relay Network. The proton relay network of the MtrD homologues AcrB and MexB involves four strictly conserved residues that straddle the longitudinal axis of pseudosymmetry.[20,26,36] In MtrD, the corresponding residues are D405, D406 (TM 4), K948 (TM 10), and T985 (TM 11).[16,19] These residues are hypothesized to act as a proton relay via the formation of a hydrogen bonding network, where the protonation of D405 and/or D406 leads to the subsequent disengagement of D405 from K948.[19] To confirm the identity of the proton relay network through the impact of charge state on substrate efflux, D405 was mutated to cysteine by site-directed mutagenesis to disrupt the hypothesized proton transfer between D405 and K948 during the transport cycle. This residue was chosen because it was previously identified as being strictly conserved across a group of homologous RND efflux pumps.[30] Additionally, previous studies in AcrB and MexB have indicated that a single point mutation of this residue (D407 in AcrB/MexB) is sufficient to disrupt the bonding network amongst the proton relay residues and lead to a decrease in function.[26,31] A histidine-tagged cysteine-less allele of the *mtrD* gene (CL-*mtrD*$_{his6}$) that has been shown to express fully functional MtrD protein[16] (CL-MtrD$_{His6}$, referred to as the wild-type) was used as a backbone for constructing the D405C mutant. Analyses were conducted in *N. gonorrhoeae* KH15Δ*norM*Δ*mtrD* cells, which is a highly antimicrobial susceptible strain with both the *mtrD* and *norM* genes (encoding MtrD and NorM efflux pumps, respectively) removed and allows analysis of MtrD mutants in terms of resistance to the transporter substrates.[16] Resistance profiling of MtrD D405C in *N. gonorrhoeae* KH15Δ*norM*Δ*mtrD* showed no resistance to a panel of 11 previously identified MtrD substrates, exhibiting a resistance profile similar to that of the negative control expressing no MtrD (Table 1). For example, resistance to detergent nonoxynol-9, antibiotics rifampicin and oxacillin, and hormone progesterone was reduced 256-, 16-, 64-, and 4-fold, respectively, compared to that of the wild-type.

Protein expression levels of the D405C MtrD mutant present in *N. gonorrhoeae* KH15Δ*norM*Δ*mtrD*/CL-*mtrD*(D405C) were comparable to that of wild-type MtrD (Figure S2), indicating that the change in antimicrobial resistance was not due to a reduced amount of MtrD protein in the bacterial membrane but could be attributed to mutation of D405. These findings indicate the D405 residue is crucial for functional efflux in MtrD, thereby supporting its key role in the proton relay network.

Comparison of the MtrD Symmetric and Asymmetric Structures. The 2014 crystal structure of MtrD (PDB ID: 4MT1)[18] was solved at 3.53 Å resolution, with the three monomers adopting a symmetric hybrid conformation. On reconstruction of the crystallographic unit cell, crystallographic contacts between adjacent MtrD proteins were noted within the protein lattice (Figure S3). These protein−protein contacts may contribute to the observed hybrid conformation. In each monomer the transmembrane proton relay network residues

https://doi.org/10.1021/acsinfecdis.1c00149
ACS Infect. Dis. 2021, 7, 1833−1847

Table 3. RND Transport Residue Pairs Used to Determine Conformation States of MtrD During MD Simulations

local conformation characteristic	center of mass residues	"access" distance (Å)[a]	"binding" distance (Å)	"extrusion" distance (Å)
cleft entrance	PC1-PC2 domains	28.5 ± 1.76	30.09 ± 1.01	24.94 ± 0.25
binding pocket	F176-F610	7.14 ± 0.31	10.45 ± 0.35	6.98 ± 0.21
extrusion gate	Q124-Y755	5.51 ± 0.32	5.04 ± 0.18	12.15 ± 0.96
proton relay network	D406-K948	8.42 ± 0.60	7.84 ± 0.31	9.42 ± 0.32
	D405-K948	6.77 ± 0.65	6.58 ± 0.38	7.27 ± 0.20
	K948-N949	4.6 ± 0.19	4.74 ± 0.11	3.87 ± 0.15
	K948-T985	9.11 ± 0.59	10.00 ± 0.29	7.36 ± 0.16

[a]All distance values in angstroms are given as mean ± SD from the following RND multidrug efflux proteins: AcrB (PDB ID: 2GIF, 2HRT, 3AOB, 4DX5), MexB (PDB ID: 2V50, 6IIA), MtrD (PDB ID: 6VKS, 6VKT).

D405/D406, K948, and T985 were disengaged (Figure S4B), the entrance to the binding cleft and the binding pocket were open, and the substrate extrusion gate was closed (Figure S4C). Table 2 shows this hybrid conformation differs from the prototypical asymmetric access, binding, and extrusion conformations observed in the MtrD homologues, AcrB, MexB[20−22,37,38] and in the MtrD cryo-EM structures, resolved to 2.72 Å (PDB ID: 6VKT) and 3.02 Å (PDB ID: 6VKS).[19] Corresponding residue pair distances in the MtrD binding pocket, PC1-PC2 domains, extrusion gate, and proton relay network of the symmetrical hybrid and asymmetric MtrD structures are listed in Table 3.

Despite these conformational differences, the backbone RMSD between the symmetric MtrD and asymmetric MtrD structures over the whole trimer was less than 2 Å, indicating localized structural rearrangements rather than large-scale conformational changes distinguish the two (Figure S4D). However, these localized structural rearrangements from the symmetric to asymmetric structure could not be sampled in preliminary atomistic MD simulations. To enable the unbiased sampling of conformations not accessible in the time scale of unbiased atomistic simulations and identify whether the symmetric MtrD structure would spontaneously adopt an asymmetric conformation in coarse-grained MD simulations, triplicate 1 μs coarse-grained MD simulations were performed using the MARTINI 2.2P force-field with Gō potentials applied to the protein (GoMARTINI).[39]

In each replicate, the backbone RMSD was less than 4 Å from the starting MtrD structure, which lies within the thermal noise of simulation (Figure S5A).[40] In all simulations, the conformation of MtrD moved away from the symmetric MtrD crystal structure and developed asymmetries across the three monomers. Here, monomer B adopted a prototypical access conformation, while monomers A and C were in an intermediate conformation between access and extrusion. It is also important to note that the proton relay network was engaged in all three monomers, consistent with the access conformation, and as would be expected with D405 and D406 deprotonated in the coarse-grained model. To further investigate what MtrD conformation would be obtained from an atomistic MD system, the final frame of the coarse-grained replicate 1 trajectory was back-mapped to a united-atom conformation and energy minimized.[41]

Symmetric structures of AcrB and other RND efflux transporters, in which all three monomers adopt an access conformation in the absence of substrate and any changes to protonation state, have been proposed to represent a resting transporter state.[25] To determine whether the back-mapped MtrD would adopt a resting access conformation, simulations of MtrD were performed in the absence of substrate, with the proton relay network of each monomer deprotonated (Table 4 System 1, Figure 2A).

Table 4. MtrD Trimeric Binding Configurations Simulated[a]

simulation system	monomer A	monomer B	monomer C
System 1	$D405^-/D406^-$/no substrate	$D405^-/D406^-$/no substrate	$D405^-/D406^-$/no substrate
System 2	$D405^H/D406^H$/no substrate	$D405^-/D406^-$/no substrate	$D405^-/D406^-$/no substrate
System 3	$D405^H/D406^H$/no substrate	$D405^-/D406^-$/no substrate	$D405^-/D406^-$/ progesterone proximal
System 4	$D405^H/D406^H$/ progesterone distal	$D405^-/D406^-$/no substrate	$D405^-/D406^-$/ progesterone proximal
System 5	$D405^H/D406^H$/no substrate	$D405^-/D406^-$/ progesterone proximal	$D405^-/D406^-$/ progesterone distal

[a]$D405^-/D406^-$ refers to engaged and deprotonated relay network residues. $D405^H/D406^H$ refers to a disengaged and protonated relay network.

In the three replicate simulations, each MtrD monomer adopted an access conformation in 250 ns of simulation, consistent with the symmetric resting state observed for AcrB. Figure 2 shows residue pairs in the proton relay network were engaged, as expected with deprotonated D405 and D406 (Figure 2A). The average center of mass distances of the binding pockets (Figure 2C) and cleft entrances (Figure 2D) of all three monomers were also consistent with an access conformation. The opening of the extrusion gate of each monomer, given by the distance between Q124 and Y755 (Figure 2E), fluctuated throughout the simulation. The average distances from System 1 are summarized in Figure 2F.

On the basis of these distance measurements, the conformation of all three MtrD monomers corresponds most closely to the access conformation, albeit with a wider extrusion gate than observed for other RND access state monomers.[19,20]

Protonation of a Single MtrD Monomer Activates Extrusion Gate Opening. Many published asymmetric structures of RND efflux pumps contain bound substrate.[19−22,42] However, different monomer-specific combinations of substrate binding and protonation have been proposed to synchronize the functionally rotating transport mechanism of AcrB.[23,24,29,43,44] To characterize the order of events in the transport cycle, we varied the simulation conditions by changing the protonation state of the proton relay network and the location of docked substrate in the different monomers of the MtrD trimer. These different simulation conditions are summarized in Table 4.

https://doi.org/10.1021/acsinfecdis.1c00149
ACS Infect. Dis. 2021, 7, 1833−1847

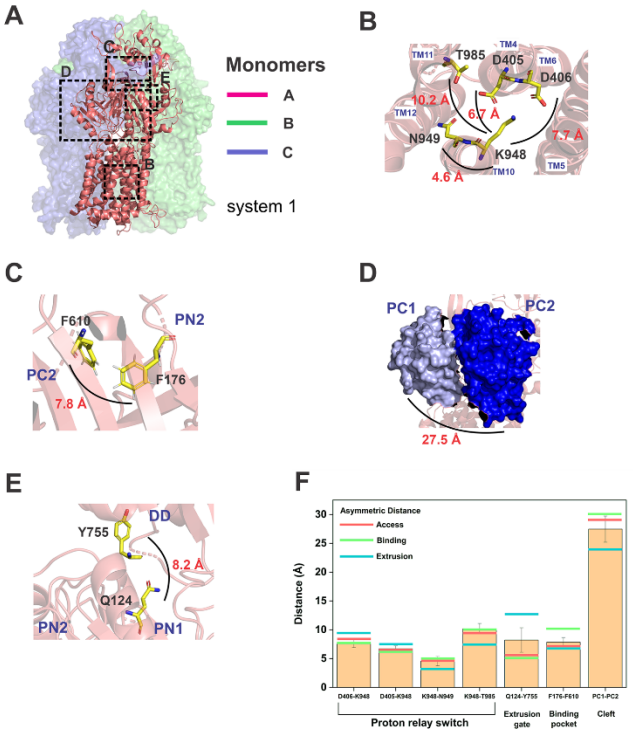

Figure 2. Apo MtrD homotrimer (System 1) simulation across 3 × 250 ns simulations. (A) The back-mapped MtrD homotrimer. Monomers are colored pink (monomer A), green (monomer B), or blue (monomer C). Monomer A is in cartoon, monomers B and C are rendered in transparent surface representation. The post simulation analysis focused on several regions of monomer A (dashed box inserts), including (B) the proton relay network, (C) the distal binding pocket, (D) the binding cleft entrance between PC1-PC2 subdomains, and (E) the extrusion gate. (F) Bar graph of the mean distances from the key regions shown in (B) to (D). Mean center of mass distances were calculated across all three monomers and all three 250 ns simulation repeats. Error bars show the SEM of the three repeat simulations. The corresponding distances from the access, binding, and extrusion states of published RND asymmetric structures (Table 3) are in red, green, and blue, respectively.

Systems 2 to 5 examined whether an asymmetric MtrD conformation could be captured within a 500 ns time frame in triplicate atomistic MD simulations. In Systems 2−5, residues D405 and D406 of the proton relay network were protonated in monomer A. System 3 also contained a single molecule of the substrate progesterone docked into the proximal binding pocket of the adjacent, anticlockwise monomer (monomer C), while Systems 4 and 5 contained two molecules of progesterone: one molecule each docked to monomer A and C (System 4) or to monomer B and C (System 5), as shown in Table 4. Progesterone was chosen as it is a known substrate of MtrD and has been demonstrated to permeate from the distal to the proximal MtrD binding pocket within the time scale sampled in atomistic MD simulations.[16] On the basis of previous structural data, the monomeric conformation of MtrD and its homologues can be characterized by three residue pair distances that accurately represent the discrete access, binding, and extrusion conformations of asymmetric structures: K948-T985 in the proton relay network, Q124-Y755 of the substrate extrusion gate, and F176-F610 of the MtrD binding cleft.[45−47] Distance distributions for these three residue pairs were assessed for each MtrD monomer across the combined 1500 ns of simulation for each system and compared with the prototypical asymmetric structure distances given in Table 3.

Initially protonation of D405 and D406 was carried out on monomer A alone (Table 4, System 2), with the hypothesis that this would lead to disengagement of the proton relay network to drive monomer A from a resting access-like conformation to an extrusion conformation; and induce the transition to a functional asymmetric trimer. In System 2, protonation of monomer A alone induced large changes in pairwise distances of the proton relay network. The distance distribution for K948-T985 in monomer A shows a wider distance distribution of 8−13 Å which, compared to the other

https://doi.org/10.1021/acsinfecdis.1c00149
ACS Infect. Dis. 2021, 7, 1833−1847

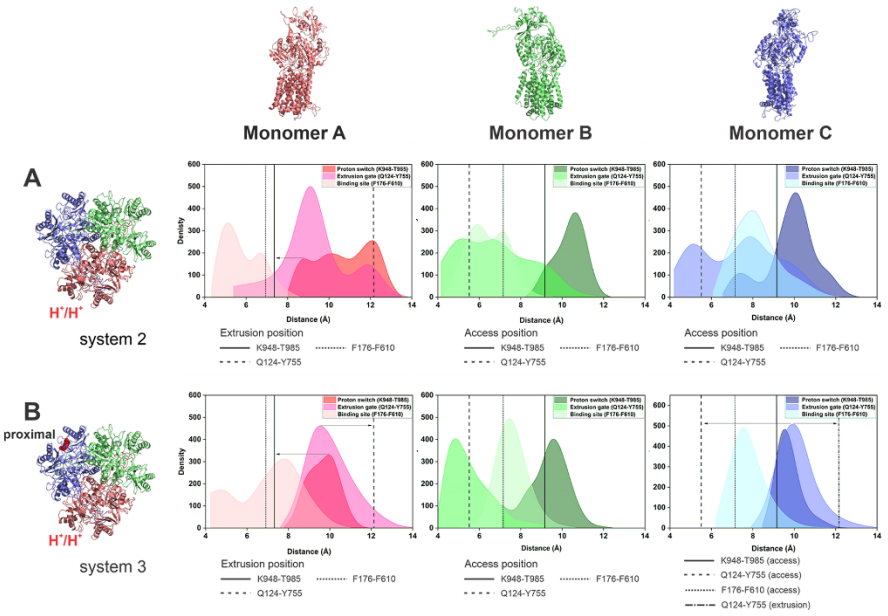

Figure 3. Distance distributions of functionally relevant residue pairs in different MtrD binding configurations from (A) System 2 and (B) System 3. The simulation configuration is displayed by the top-down view of the MtrD homotrimer at the left-hand side. In System 3, progesterone is shown in red. Each panel represents the residue pair center of mass distance for each monomer of the simulation system (top). The vertical lines represent the measured distances for the asymmetric configurations access, binding, and extrusion from a set of RND asymmetric structures (see Table 3). The horizontal arrows indicate the distance from the peak distance density for a given residue pair to the vertical lines corresponding to asymmetric structure average.

two nonprotonated monomers, approaches the fully disengaged distance of 7.36 Å (Figure 3A, LH panel).

The distance distribution displayed three peaks at 12.1, 10, and 8.2 Å, respectively, indicating protonation introduced instability at the relay switch. The extrusion gate Q124-Y755 also occupied two distance distribution peaks, one heavily occupied at 8.6 Å and a second smaller peak at 11.9 Å. This second peak corresponds to the distance present in the extrusion conformation of other RND asymmetric structures. The shift to the larger extrusion gate distance was coupled to a disengagement of the proton relay network in monomer A across all replicate simulations (Figure S6A). In both monomer B (Figure 3A, center panel) and monomer C (Figure 3A, right panel), the proton relay network and binding cleft distance distributions are consistent with an "access/binding" conformation. However, the extrusion gates of both monomer B and C displayed a broad distance distribution with multiple peaks, which do not closely align with any of the prototypical access, binding, or extrusion conformations. These results demonstrate protonation of a single MtrD monomer cannot induce complete transition to the MtrD asymmetric conformation but can couple protonation of the relay switch and opening of the extrusion gate within a single monomer.

Conformational Switching to Asymmetric MtrD Requires Coordinated Protonation and Substrate Binding in Two Separate Monomers. Numerous asymmetric structures of MtrD[19] and other RND transporters[20,21] have been solved with substrate in the binding pocket of one monomer. To investigate whether substrate is required to facilitate a conformational transition to the asymmetric MtrD, in System 3 a single molecule of progesterone was docked in the proximal binding pocket of monomer C, the monomer anticlockwise to the protonated monomer A (Figure 2A). In this binding configuration, the proton relay network of monomer A shows a narrower distribution density than System 2, with greater than 98% of K9498-T985 distances occupying a range from 11.0 to 8.0 Å (Figure 3B, left panel). Similar to System 2, the System 3 distance distribution approaches, but does not reach, the distance observed structurally in the fully disengaged proton relay network state (7.32 ± 0.16 Å, Table 3). Likewise, the monomer A extrusion gate distance displays a wider distribution than in the apo-MtrD simulation of System 1, with >95% of distances lying between 8 and 12.5 Å. As with System 2, fluctuations in extrusion gate distance of monomer A were allosterically coupled to fluctuations in the relay switch: the greater the disengagement of the relay switch (smaller distance) the

https://doi.org/10.1021/acsinfecdis.1c00149
ACS Infect. Dis. 2021, 7, 1833−1847

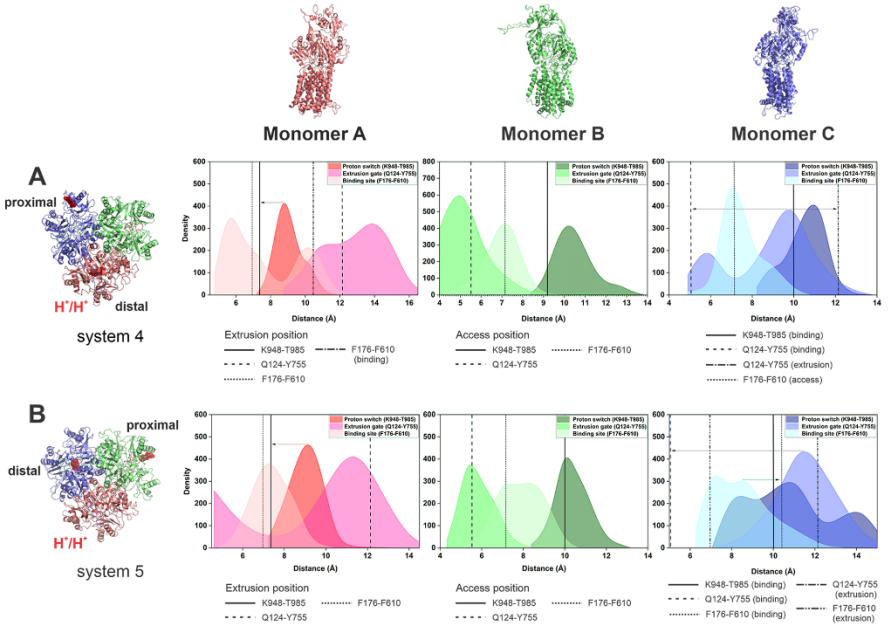

Figure 4. Distance distributions of functionally relevant residue pairs in the MtrD binding configurations from (A) System 4 and (B) System 5 (Table 4). The simulation configuration is displayed by the top-down view of the MtrD homotrimer at the left-hand side. Progesterone molecules are shown in red. Each panel represents the residue pair center of mass distance for each monomer of the simulation system (top). The vertical lines represent the measured distances for the asymmetric configurations access, binding, and extrusion from a set of RND asymmetric structures (see Table 3). The horizontal arrows indicate the distance from the peak distance density for a given residue pair to the vertical lines corresponding to asymmetric structure average.

greater the opening of the extrusion gate (Figure S6B). However, in contrast to System 2, the degree of fluctuations in both these regions is smaller, indicating the presence of progesterone has stabilized monomer A without allowing for the full transition to the extrusion conformation. The inter-residue distance pairs from monomer B and monomer C were largely stable across all simulations, displaying narrow distance distributions for all key functional regions, corresponding to the prototypical access distances (Figure 3B, center and right panel). These results show that in the presence of a single bound substrate molecule, the complete transition to an asymmetric conformation of MtrD is not readily sampled in the 500 ns time scale of the simulations. Recent MD work on AcrB has suggested that the conformational transition into an asymmetric functional RND state is accelerated when substrate is simultaneously bound to two monomers of the protein.[23,43]

To identify whether the docking of progesterone to multiple monomers would allow for the full transition to an asymmetric structure, progesterone was docked to two adjacent MtrD monomers (Figure 4).

Residues D405 and D406 of monomer A were again protonated. In System 4, progesterone was docked to the proximal binding pocket of monomer C, and to the distal binding pocket of the protonated monomer A (Figure 4A). In System 5, progesterone was docked to the distal pocket of monomer C and the proximal pocket of monomer B (Figure 4B). In System 4, the presence of two progesterone molecules induced a significant opening in the extrusion gate distance of the protonated monomer A toward a fully open state (Figure 4A and 4B, left panel). The two peaks of the extrusion gate distance distribution are centered at 10.8 and 13.9 Å, with >90% of the distances sampled lying between 10 and 15 Å. In addition, the K948-T985 proton relay network distance distribution adopts a single narrower peak at 8.6 Å. For System 5, the extrusion gate and proton relay network distance distribution displayed peaks at 11.8 and 8.9 Å, respectively. When compared to Systems 1 to 3, the distance distributions sampled in System 4 and 5 represent a large shift toward the extrusion conformation distances of the asymmetric structures in Table 3. Despite this trend, significant differences in the dynamics of monomer A are observed between System 4 and 5. In System 4, the opening of the extrusion gate and near-complete disengagement of the monomer A relay switch is accompanied by the opening of the binding cleft (Figure 4A, left panel). The changes between functionally relevant regions of monomer A in System 4 are coupled (Figure S7A), such

https://doi.org/10.1021/acsinfecdis.1c00149
ACS Infect. Dis. 2021, 7, 1833−1847

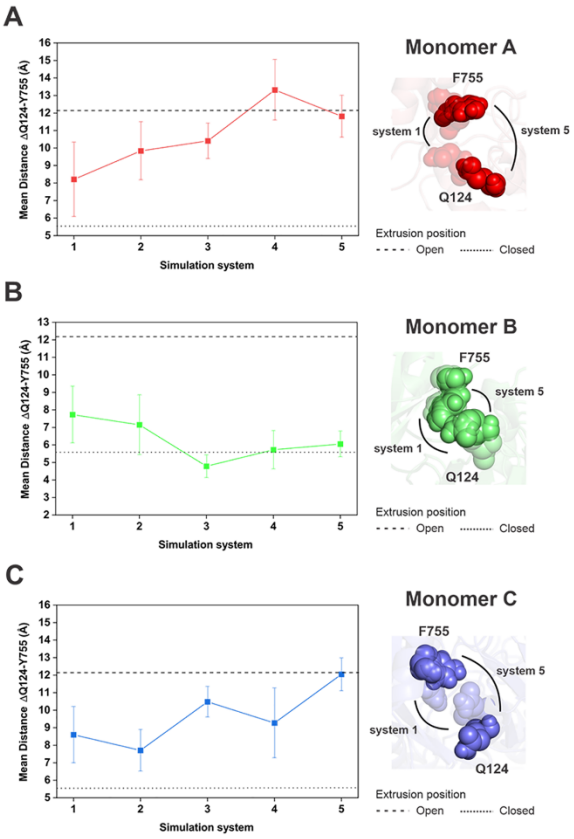

Figure 5. Extrusion gate distance of each MtrD monomer as an output of conformation. The extrusion gate distances across all simulation systems for (A) monomer A (protonated), (B) monomer B, and (C) monomer C. Residues pairs to the right of each figure show the average center of mass distances from simulation System 5 (solid spheres) and System 1 (transparent spheres) after alignment of the two structures.

that disengagement of the proton relay network accompanies opening of the extrusion gate, as was observed in Systems 2 and 3. Notably, the binding cleft distance distribution contains two peaks, at 5.8 and 10.2 Å, showing System 4 sampled both the closed and open binding cleft conformations in monomer A. In contrast, when progesterone was docked into the two nonprotonated monomers of System 5, the monomer A binding cleft remained in the closed extrusion conformation (Figure 4B, left panel, Figure S7B).

Overall, System 5 approaches an overall asymmetric MtrD conformation more closely than System 4. For example, in System 4, when progesterone is docked at the proximal binding pocket of monomer C, it does not adopt the prototypical MtrD asymmetric "binding" conformation, but instead adopts a "hybrid" conformation (Figure 4A, right panel). In contrast, monomer C of System 5 is consistent with the binding conformation (Figure 4B, right panel). In both Systems 4 and 5, monomer B adopts an "access" conformation (Figure 4A and 4B, center panels) as predicted by the rotational asymmetric model of transport (see Figure 1C). These simulations confirm that neither protonation of D405/D406 in the proton relay network, nor the presence of a single substrate molecule alone, is sufficient to induce full extrusion gate opening in MtrD within a 500 ns time scale over replicate simulations. When a single monomer is protonated, the binding of substrate in the two adjacent monomers (System 5) is required for the full transition to the functional asymmetric MtrD structure. Figure 5 plots the extrusion gate distance distributions from Systems 1 to 5. Although D405/D406 is always protonated, monomer A only adopted a full open

https://doi.org/10.1021/acsinfecdis.1c00149
ACS Infect. Dis. 2021, 7, 1833−1847

extrusion conformation in System 5 (Figure 5A), where progesterone is bound at the proximal binding pocket of monomer B and in the distal binding pocket of monomer C.

Here the proximally bound monomer B has a stable closed extrusion gate and adopts the access conformation (Figure 5B). The distally bound monomer C adopts the binding conformation (see Figure 4B, right panel), where opening of the binding pocket is coupled to a dynamic transition of the extrusion gate (Figure 5C and S7C).

Notably, complete disengagement of the proton relay network was not observed in any of the simulations, despite protonation of the proton relay network titratable aspartate residues. This could be due to one of several reasons. First, complete disengagement of the proton relay network may occur on time scales longer than those simulated in this study. Second, there is significant uncertainty of the exact proton stoichiometries involved in RND transporter proton translocation.[28,44,47,48] Thus, accelerated disengagement of the proton relay network may be driven by a proton stoichiometry not explored in this study.

Relay Network Protonation Drives the TM Helix Rotation in MtrD. The coupling of local conformational changes in MtrD to the large-scale conformational movements required for the functionally rotating transport cycle has not yet been resolved. Allosteric coupling between the extrusion gate and other regions, particularly between monomers A and C (Figure S7), suggests there is an overall coordination between subunits that must be reflected in these large-scale conformational changes. Other asymmetric RND transporter structures show a widening of the intermonomeric gap between the PN2 domain of the binding monomer and PC2 domain of the extrusion monomer (Figure 1B),[18−20] thus TMD rotation may form a significant step in the functionally rotating transporter mechanism of RND transporters. It has been suggested that this widening occurs due to rotation of one-half of protonated monomer's TMD with respect to the other along the 2-fold pseudosymmetrical axis (Figure 1B, red lines).[48,49] In the symmetric MtrD structure, the intermonomeric gap of 11.86 Å was largely consistent with the distances observed for resting or access conformations observed in other RND transporters (Table 5).

Protonation of D405 and D406 in monomer A (System 2) led to rotation of its TM helices along the pseudosymmetrical axis (Figure 6A), as measured by the angle between C_α atoms of the key proton relay network residues K948, T985, and D406. All three replicate simulations started with a D406-T985-K948 C_α angle between 53.7° and 54.9°. A rapid conformational change occurred in each replicate simulation (after ∼120 ns in replicate 1, ∼80 ns for replicate 2, and within the first 5 ns of replicate 3), characterized by a significant narrowing of the D406-T985-K948 C_α angle to stabilize at a mean angle of 43.6° ± 3.5°, 38.8° ± 2.5°, and 36.0° ± 2.3° in replicates 1, 2, and 3, respectively, throughout the remaining 400 ns of simulation.

In Figure 6B the initial (pink) and final (blue) frames of System 2 replicate 2 are superimposed to show the helical rotation about the pseudosymmetrical axis, resulting in a 16.0° change of the D406-T985-K948 C_α angle. The initial (pink) and final (blue) conformation of the monomer A relay switch D406-T985-K948 C_α angle is shown in Figure 6C and 6D, respectively. Previous work has identified the importance of water pathways throughout the MtrD homologue AcrB for the proton relay network and substrate permeation.[48,50,51] In our simulations, water solvation followed the pathways previously reported, with solvation of the periplasmic region of the protein from the periplasmic bulk water and solvation of the TMDs, including the proton relay network from the cytoplasmic bulk water. The permeation of water molecules from the cytoplasmic bulk water along the monomeric axis of pseudosymmetry to interact with the proton relay network was observed for all monomers. However, the greatest water density was observed in monomer C, the monomer anticlockwise to the protonated monomer (monomer A). This agrees with previous observations that the greatest water density, and the formation of more extensive water pathways occur in the binding monomer. Here the proposed protonation of D405 and/or D406 is hypothesized to occur in a transition state between the binding and extrusion monomers.[48,50,52] Water density in the TMD and the water pathways linking the TMD water density with the periplasmic water density are more limited in the access and extrusion monomers, as is reflected by the more restricted water pathways observed in monomers A and B of these simulations.

In contrast to the rotation of the TMD in the protonated monomer A, when D406 and D405 were deprotonated (charged) in all monomers of System 1, the rotation of the TMD did not change significantly (Figure 7A). The three 500 ns replicate simulations started with a D406-T985-K948 C_α angle of between 52.4° and 55.6°, which stabilized to a mean angle of 59.2° ± 2.9°, 55.6° ± 3.1°, 53.8° ± 2.5° across the final 400 ns of each replicate simulation. Figure 7B and 7C show that in replicate 2 of System 1 the K948-T985-D406 C_α angle between the starting and final structure changed by only 3° in monomer A, compared to a 16° rotation on protonation of D405 and D406. Similar changes were seen in the deprotonated monomers B and C of System 2, which showed only small helical rotations about the 2-fold pseudosymmetrical axis (Figure S8A and S8B).

The helical rotation observed upon protonation of monomer A in System 2 is time-correlated with a widening of the intermonomer distance between monomer A and C (Figure S9A). The increase in monomer A to C distance occurs rapidly following the start of simulations, and is coupled to a rapid helical rotation in the protonated monomer A. The distance

Table 5. Intermonomeric Distances (PN2-PC2) of RND Asymmetric Transporter Structures and MtrD MD Simulations

	PN2-PC2 distances (Å)		
MtrD structure	monomer A–monomer B (extrusion-access)	monomer B–monomer C (access-binding)	monomer C–monomer A (binding-extrusion)
Combined RND asymmetric structures[a]	16.19 ± 1.75	15.40 ± 1.40	31.0 ± 1.90
MtrD (4TM1)	11.86	11.86	11.86
System 1[b]	21.39 ± 2.84	21.31 ± 4.09	18.87 ± 1.73
System 2	21.21 ± 2.26	21.53 ± 2.86	26.98 ± 2.37
System 3	16.07 ± 2.14	20.60 ± 2.50	20.34 ± 2.43
System 4	21.96 ± 3.44	19.08 ± 2.94	20.29 ± 2.59
System 5	18.62 ± 4.24	18.96 ± 3.11	22.50 ± 2.84

[a]Calculated using the same structures used for Table 3 calculations. [b]Intermonomeric distances from all simulation systems are the mean ± SD of 3 × 500 ns repeats for each system, except for System 1 which underwent 3 × 250 ns repeats.

https://doi.org/10.1021/acsinfecdis.1c00149
ACS Infect. Dis. 2021, 7, 1833−1847

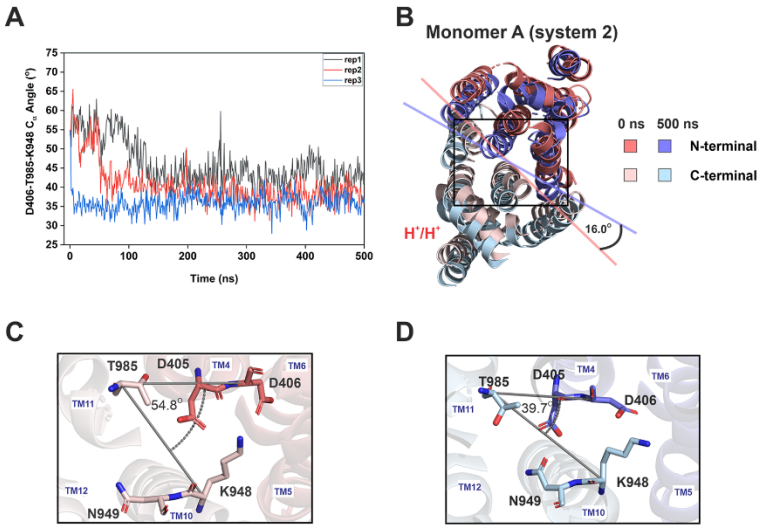

Figure 6. Protonation of a single monomer in MtrD causes rotation of TMD. The TMD is viewed as if looking from the cytoplasmic side of the membrane, i.e., from below. (A) The D406-T985-K948 C_α time-resolved angle values in the three replicates of simulation System 2, where only monomer A is protonated. (B) The ΔD406-T985-K948 C_α angle of the second replicate of System 2 shows a 16° rotation about the pseudosymmetrical axis of the TMD between the (C) initial and (D) last frames.

between the PC2 domain of protonated monomer A and PN2 domain of monomer C averages at 26.98 ± 2.37 Å across the three simulation replicates of System 2 (Table S, Figure S9B). By contrast, the intermonomeric distances in apo-MtrD (System 1) range from 21.39 ± 2.84 to 18.87 ± 1.73 (Table S, Figure S9C). The distances between the unprotonated monomers in System 2 were also smaller. These results suggest that protonation of D406 and D405 in the MtrD relay switch is the probable cause of the TMD helical rotation in the protonated monomer. We hypothesize that functional rotation of MtrD is driven by protonation leading to helical rotation and subsequent PC2-PN2 gap opening. Both the helical rotation and intermonomeric gap opening are proposed to be key for the functional rotational transport cycle for MtrD.

■ CONCLUSIONS

Our results indicate the MtrD inner membrane transporter from *N. gonorrhoeae* follows the functionally rotating transport mechanism identified in other RND inner membrane transporters.[20,21,53] We identify the conserved proton relay network in MtrD involves residues D405, D406, K948, N949, and T985. We show that protonation at D405/D406 and substrate binding in adjacent monomers drives asymmetry between monomers. Specifically, we demonstrate rotation of TM helices along the pseudosymmetrical axis and opening of intermolecular gap between the extrusion and binding monomers is only observed upon protonation of the relay network residues. We have validated these conclusions through highly conserved distance values from residue pairs in functionally relevant regions of multiple RND inner membrane transporter asymmetric structures (Table 3). The recent publication of the asymmetric structures of MtrD allowed for comparison between an inactive or resting symmetric conformation of the transporter and a functionally active one.[19]

Specifically, the System 5 simulations most closely approach the average distances observed in other asymmetric RND transporters. System 5 contains a single protonated monomer (relay network disengaged) and the remaining two monomers contain progesterone bound either in the distal binding site or the proximal binding site. However, simulation System 5 has two main differences that do not conform exactly to the static asymmetric RND transporter structures. Specifically, in the "binding" monomer C, the extrusion gate Q124-F755 residue distance is open; and the trimeric MtrD contains two progesterone molecules bound in both the binding and access monomers, at the proximal and distal binding sites, respectively. We suggest that these are related molecular events and represent the dynamic nature of the functionally rotating mechanism. Notably, the opening of the Q124-F755 extrusion gate in the "binding" monomer C does not occur in simulations that only include a single substrate molecule (System 3). Simulations involving different substrate stoichiometries and configurations in AcrB have also demonstrated the requirement for two substrates, synchronized in adjacent binding and access monomers, to instigate and accelerate full substrate extrusion.[23] The RND asymmetric structures, considered in isolation, suggest that a stable state is sufficient for continual cycling through the triconformational mechanism. Our results suggest that time-correlated molecular events

https://doi.org/10.1021/acsinfecdis.1c00149
ACS Infect. Dis. 2021, 7, 1833−1847

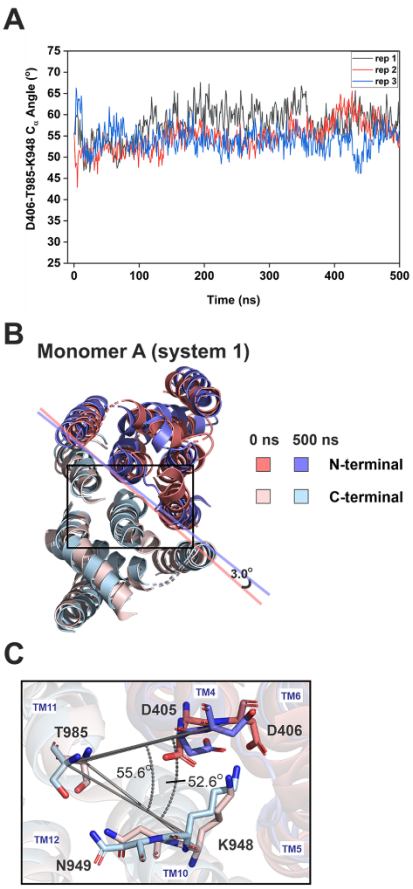

Figure 7. Rotation of TM domain helices does not occur in apo-MtrD simulations. The TM domains are viewed as if looking from the cytoplasmic side of the membrane, i.e., from below. The MtrD TM domains forming the proton relay network are viewed from the cytosolic side of the transporter. (A) The D406-T985-K948 C_α time-resolved angle values in the three replicates of simulation System 1, where no monomers are protonated or have substrate bound. (B) The ΔD406-T985-K948 C_α angle of the second replicate of System 1 shows a (C) 3° rotation about the pseudosymmetrical axis of the TM domains between the initial and last frames.

such as the binding and efflux of substrate drive the dynamic transitions of the transporter.

The rotation of the TMD about the pseudosymmetrical axis of the protonated monomer and the subsequent opening of the intermonomeric distance between the extrusion monomer and adjacent "binding" monomer are key global conformational changes resulting from protonation and which may be associated with substrate exit. Our results confirm, that for MtrD, both events occur only at the site of the protonated monomer, consistent with previous observations for TMD rotation in AcrB.[44] Indeed, thermodynamic calculations from simulations with protonation of AcrB D408 (homologous to D406 in MtrD) show that protonation at the relay network is the critical event for inducing large-scale substrate release and rotational conformational movements in the homotrimer and the larger tripartite RND complex.[44,49] It is notable, however, that the conformations in the proton relay network we observe in System 2 (in the absence of substrate) while instigate the requisite TM helical rotation and intermolecular distance asymmetries, do not reach the full disengaged "extrusion" state when compared to the recent asymmetric MtrD structures.[19] This is further evidence that a specific configuration and stoichiometry of substrate binding is ultimately required to induce full conformational transitioning.

These results imply that substrate extrusion is the rate-limiting step of the functionally rotating mechanism. The synchronization between local molecular binding events and large-scale conformational movements implied by the functionally rotating mechanism is a membrane transport paradigm that is being transferred to a wide array of unrelated prokaryotic and eukaryotic solute carrier families.[54] The widespread application for this paradigm highlights the need for continued research into the full and dynamic transport cycle, which will require close collaboration between structural and computational biochemists.

METHODS

System Details. *Simulation Setup.* The symmetric MtrD crystal structure, resolved to 3.53 Å (PDB ID: 4MT1), was used for all simulations.[18] The missing residues between residues 494 and 507, 671, and 672 were rebuilt and the N- and C-termini were capped with acetyl and amine groups, respectively. Crystallographic symmetry operators were applied to rebuild the trimeric biological assembly as previously described.[16] All simulations were carried out under periodic boundary conditions in a hexagonal prism box with semi-isotropic pressure coupling. The dimensions of the box were chosen such that minimum distance of the protein to its periodic image was 3.5 nm.

Coarse Grained Simulations. The GROMACS 2016.1 molecular dynamics (MD) engine[55] and the MARTINI2.2P force field[56] were used for all coarse-grained simulations. The repaired MtrD homotrimer was converted to a GoMARTINI coarse-grained model using the *go_martinize* package with Gō contacts of 9.414 kJ/mol.[59] The protein was embedded in a neisserial lipid bilayer containing 1-palmitoyl-2-palmitoleoyl-*sn*-glycero-3-phosphatidylethanolamine (PPPE) and 20% 1,2-dimyristoyl-sn-glycero-3-phosphoglycerol (DMPG) constructed using a custom version of the *insane* package.[57] The system was solvated with the MARTINI polarizable water model and a concentration of 150 mM NaCl was added for charge neutralization.[58]

The system was energy minimized using the steepest descent algorithm and equilibrated prior to production simulations. Equilibration was conducted for 5 ns at constant temperature and pressure. The temperature was maintained at 320 K using the Bussi thermostat[59] with a coupling constant of 1.0 ps. The pressure was maintained at 1 bar using a semi-isotropic Berendsen barostat with a compressibility of 3×10^{-4} bar^{-1}

https://doi.org/10.1021/acsinfecdis.1c00149
ACS Infect. Dis. 2021, 7, 1833−1847

and a coupling constant of 12 ps. Following equilibration, coarse-grained simulations were run for the system in triplicate for 1 μs. Temperature was maintained as described above, while semi-isotropic Parrinello−Rahman pressure coupling[60,61] was used to maintain a pressure of 1 bar with a compressibility of 3×10^{-4} bar^{-1} and a coupling constant of 12 ps. All simulations were conducted according to the recommended standard MARTINI configuration.[62]

Back-Mapping and Atomistic Simulations. Following the coarse-grained simulations, MtrD from the final frame of replicate 1 of the GoMARTINI simulations was back-mapped to united-atom coordinates using the *backward.py* program and protocol.[41] The protein was energy minimized using the steepest descent algorithm. The VMD cispeptide, chirality and Ramaplot plugins[63] were used to perform preliminary checks on the back-mapped structure. *Cis* peptide bonds not found in original MtrD structure were converted to the correct *trans* bonds with the VMD cispeptide plugin.[63]

The resulting MtrD back-mapped structure was used for all subsequent atomistic simulations. Five simulation regimes were carried out, as listed in Table 4. In summary these were as follows: an *apo* regime on the MtrD back-mapped structure with the fixed *cis* peptide bonds but no other changes; protonation of MtrD monomer A only; MtrD protonated in monomer A and progesterone in the proximal binding pocket of monomer C; and MtrD protonated in monomer A and progesterone in the proximal binding pocket of monomer C or B and distal binding pocket of monomer A or C, respectively. All simulations used the GROMOS 54a7 force field[64] and the GROMACS2016.1 and GROMACS2019.4 MD engines.[55] In System 2 to 5, residues D405 and D406 of the proton relay network were protonated in monomer A, as specified in Table 4. In System 3 to 5, progesterone was added to the substrate binding cleft of the specified monomer/s from Table 4 via structural alignment to bound progesterone from previous progesterone flooding simulations.[16]

In all simulations, the protein was embedded in our previously published *N. gonorrhoeae* membrane containing 80% 1-palmitoyl-2-palmitoleoyl-*sn*-glycero-3-phosphatidylethanolamine (PPPE), 20% 1,2-dimyristoyl-*sn*-glycero-3-phosphorylglycerol (DMPG) membrane.[65] This membrane composition was chosen to reflect the high percentage of PE lipids and phospholipids with short chain fatty acyl substituents in the *N. gonorrhoeae* membrane.[66] Each system was solvated with simple point charge (SPC) water,[67] and 150 mM NaCl was added for charge neutralization. United atom parameters for PPPE and DMPG were taken from Anandan et al.,[68] while parameters for progesterone were obtained from the Automated Topology Builder and Repository (ATB) (Molid: 1305).[69,70]

All systems were energy minimized using a steepest descent algorithm and subsequently equilibrated with decreasing restraints on the protein in six sequential 2 ns simulations (1000 kJ mol^{-1} nm^{-2}, 500 kJ mol^{-1} nm^{-2}, 100 kJ mol^{-1} nm^{-2}, 50 kJ mol^{-1} nm^{-2}, 10 kJ mol^{-1} nm^{-2}, and 0 kJ mol^{-1} nm^{-2} protein position restraints). The temperature was maintained at 300 K using the Bussi−Donadio−Parrinello velocity rescale thermostat and a coupling constant of 0.1 ps. Pressure was maintained at 1 bar using semi-isotropic pressure coupling, and in the equilibration simulations the Berendsen barostat was used with a 0.5 ps coupling constant and an isothermal compressibility of 4.5×10^{-5} bar^{-1}.

The coordinates from the final frame of each equilibrated system were used as the starting configuration for production simulations, performed in triplicate. All simulations were maintained at a constant temperature of 300 K as described above. In production simulations, the pressure was maintained at 1 bar using semi-isotropic pressure coupling with the Parrinello−Rahman barostat using a 5 ps coupling constant and an isothermal compressibility of 4.5×10^{-5} bar^{-1}. In System 1, production simulations were run for 250 ns per replicate, while Systems 2 to 5 were run for 500 ns per replicate. SETTLE was used to constrain the geometry of water molecules and LINCS was used to constrain the covalent bond lengths of the solute. The electrostatic interactions were calculated using the Particle Mesh Ewald summation, and noncovalent interactions were determined via the Verlet scheme with a 1.4 nm cutoff.[62]

Construction and Functional Analysis of an MtrD Site-Directed Mutant. Construction and functional analysis of site-directed *mtrD* mutants have been described previously.[16] The same methodology was used for construction and analysis of the MtrD D405C mutant in this study. Briefly, a pGCC4-Cl-$mtrD_{His6}$ clone, containing a fully functional histidine-tagged cysteine-less variant of the *mtrD* gene in the pGCC4 neisseria/*Escherichia coli* shuttle vector, was used as template DNA for PCR amplification using the primers D405C F (GGCATCGTGGTCTGTGACGCGATTGTG) and D405C R (CACAATCGCGTCACAGACCACGATGCC). Transformation into *E. coli* DH5α cells, colony screening using restriction enzyme digestion, and sequencing of the whole *mtrD* gene of the identified mutant confirmed the target amino acid change and integrity of the *mtrD* gene. The constructed MtrD D405C variant was reintroduced into the chromosome of the *N. gonorrhoeae* KH15Δ*norM*Δ*mtrD* strain,[16] a highly susceptible strain for analysis of MtrD pump substrates. The resultant strain, KH15Δ*norM*Δ*mtrD* (D405C), was evaluated for MtrD protein expression by Western blotting and its resistance profile determined by using a standard agar dilution method[71] against 11 representative MtrD substrates. To construct appropriate control strains, *N. gonorrhoeae* KH15Δ*norM*Δ*mtrD* was complemented with the recombinant wild-type ($MtrD_{His6}$) and cysteine-less (CL-$MtrD_{His6}$) alleles of the *mtrD* gene, and with the neisseria insertion complementation system (NICS) section of the pGCC4 vector that does not express *mtrD* and was used as a negative control.

Data Analysis. *Sequence Alignment.* Sequence alignment of the MtrD, AcrB, MexB, and AdeB protein sequence alignments was carried out using Clustal Omega[72] using the default settings and visualized using Jalview 2.11.1.4 software.[73]

Visual Analysis and Graphical Rendering of Protein Structures. For all graphical analysis of protein structures and simulations and all figure rendering VMD 1.9.3[74] and PyMOL2.3.1[75] were used. RMSD calculations were provided by the Align tool on VMD and the Alignment Plugin on PyMOL. The asymmetric structures of MtrD (PDB ID: 6VKS, 6VKT) were used along with additional RND family structures for comparison and validation of simulation conformations as detailed in Tables 2 and 3, in addition to structural alignment with the symmetrical MtrD structure (PDB ID: 4TM1). Alignment between MtrD symmetric and asymmetric structures was carried out using both Pymol and VMD protein backbone least-squares RMSD alignment algorithms Align and Multiseq.

https://doi.org/10.1021/acsinfecdis.1c00149
ACS Infect. Dis. 2021, 7, 1833−1847

Validation of Pre- and Postsimulation Protein Structures. The MtrD structures after each set of simulations were validated via the protein quality check WhatCheck to assess the quality of the structure[76] (see Table S1). WhatCheck provides Z-scores for a set of parameters, indicating the deviation from the average values as derived from a database of structures.

Distance and Density Calculations. Conformational changes within monomers were measured using the inter-residue distances across four key functional monomer regions: the (1) binding cleft entrance; (2) distal binding pocket; (3) extrusion gate; and (4) proton relay network. These regions were chosen as they are known to vary distinctly across the three asymmetric monomer conformations (Table 2). Distances were measured between the center of mass of the PC1 and PC2 subdomains for the cleft entrance; F176 and F610 in the distal binding pocket; Q124 and Y755 in the extrusion gate; and K948 and T985 of the proton relay network. Distances were measured over the combined trajectories of all three system replicates (1500 ns). Residue groups were chosen based on previously published analysis for the MtrD homologue, AcrB.[45−47] Density distribution of distances was obtained by binning the distance values for each system.

Simulation parameter files, the initial and final coordinates of the simulations, and key trajectories are available at https://github.com/OMaraLab/MtrD_Protonation.

■ ASSOCIATED CONTENT

Supporting Information

The Supporting Information is available free of charge at https://pubs.acs.org/doi/10.1021/acsinfecdis.1c00149.

Supplementary figures, original MD simulation trajectories, and back-mapping from coarse-grained to atomistic systems (PDF)

■ AUTHOR INFORMATION

Corresponding Author

Megan L. O'Mara − *Research School of Chemistry, The Australian National University, Canberra, ACT 0200, Australia*; Email: megan.omara@anu.edu.au

Authors

Stephen J. Fairweather − *Research School of Chemistry, The Australian National University, Canberra, ACT 0200, Australia; Research School of Biology, The Australian National University, Canberra, ACT 0200, Australia*

Vrinda Gupta − *Research School of Chemistry, The Australian National University, Canberra, ACT 0200, Australia*

Mohsen Chitsaz − *College of Science and Engineering, Flinders University, Bedford Park, SA 5042, Australia*

Lauren Booth − *Research School of Chemistry, The Australian National University, Canberra, ACT 0200, Australia*

Melissa H. Brown − *College of Science and Engineering, Flinders University, Bedford Park, SA 5042, Australia*

Complete contact information is available at: https://pubs.acs.org/10.1021/acsinfecdis.1c00149

Author Contributions

‖S.J.F. and V.G. are co-first-authors. S.J.F., V.G., M.H.B., and M.L.O. designed the research; V.G., S.J.F., M.C., and L.B. performed the MD simulations and bacterial experiments; S.J.F., V.G., M.C., M.H.B., and M.L.O. contributed to data analysis; S.J.F., V.G., M.C., M.H.B., and M.L.O contributed to writing the paper.

Notes

The authors declare no competing financial interest.

■ ACKNOWLEDGMENTS

The authors wish to thank Professor Edward Yu and his laboratory in the School of Medicine at Case Western Reserve University for supplying the asymmetric structures of MtrD PDB ID: 6VKS and 6VKT before they were made available on the RSCB PDB. The authors also wish to thank Dr. Katie Wilson, Mr. Hugo MacDermott-Opeskin, Ms. Lily Wang, and Mr. Richard Morris for valuable advice and discussion during the course of this research. This work was supported by a Flinders Foundation Seeding Grant, an Australian Government Research Training Program Scholarship (to M.C.), and an ANU Research School of Chemistry Honors Scholarship (to V.G.). The research was undertaken with the assistance of resources and services from the National Computational Infrastructure (NCI), which is supported by the Australian Government.

■ ABBREVIATIONS

DD, docking domain; Mtr, multiple transferable resistance; PD, porter domain; PDB, Protein Database; RND, resistance-nodulation-division; TM, transmembrane; TMD, transmembrane domain

■ REFERENCES

(1) Workowski, K. A., and Bolan, G. A. (2015) Sexually transmitted diseases treatment guidelines, 2015. *MMWR Recomm. Rep. 64* (Rr-03), 1−137.

(2) Bignell, C., Unemo, M., et al. (2013) 2012 European guideline on the diagnosis and treatment of gonorrhoea in adults. *Int. J. STD AIDS 24* (2), 85−92.

(3) Cámara, J., Serra, J., Ayats, J., Bastida, T., Carnicer-Pont, D., Andreu, A., and Ardanuy, C. (2012) Molecular characterization of two high-level ceftriaxone-resistant *Neisseria gonorrhoeae* isolates detected in Catalonia, Spain. *J. Antimicrob. Chemother. 67* (8), 1858−60.

(4) Smolarchuk, C., Wensley, A., Padfield, S., Fifer, H., Lee, A., and Hughes, G. (2018) Persistence of an outbreak of gonorrhoea with high-level resistance to azithromycin in England, November 2014-May 2018. *Euro. Surveill*, DOI: 10.2807/1560-7917.ES.2018.23.23.1800287.

(5) Fifer, H., Cole, M., Hughes, G., Padfield, S., Smolarchuk, C., Woodford, N., Wensley, A., Mustafa, N., Schaefer, U., Myers, R., Templeton, K., Shepherd, J., and Underwood, A. (2018) Sustained transmission of high-level azithromycin-resistant *Neisseria gonorrhoeae* in England: an observational study. *Lancet Infect. Dis. 18* (5), 573−581.

(6) Rasmussen, D. A., and Stadler, T. (2019) Coupling adaptive molecular evolution to phylodynamics using fitness-dependent birth-death models. *eLife*, DOI: 10.7554/eLife.45562.

(7) Unemo, M., Golparian, D., Nicholas, R., Ohnishi, M., Gallay, A., and Sednaoui, P. (2012) High-level cefixime- and ceftriaxone-resistant *Neisseria gonorrhoeae* in France: novel penA mosaic allele in a successful international clone causes treatment failure. *Antimicrob. Agents Chemother. 56* (3), 1273−80.

(8) Nikaido, H. (2018) RND transporters in the living world. *Res. Microbiol. 169* (7−8), 363−371.

(9) Shafer, W. M., Qu, X., Waring, A. J., and Lehrer, R. I. (1998) Modulation of *Neisseria gonorrhoeae* susceptibility to vertebrate antibacterial peptides due to a member of the resistance/

nodulation/division efflux pump family. *Proc. Natl. Acad. Sci. U. S. A.* 95 (4), 1829−33.
(10) Lee, E. H., and Shafer, W. M. (1999) The farAB-encoded efflux pump mediates resistance of gonococci to long-chained antibacterial fatty acids. *Mol. Microbiol.* 33 (4), 839−45.
(11) Kvist, M., Hancock, V., and Klemm, P. (2008) Inactivation of efflux pumps abolishes bacterial biofilm formation. *Appl. Environ. Microbiol.* 74 (23), 7376−82.
(12) Warner, D. M., Shafer, W. M., and Jerse, A. E. (2008) Clinically relevant mutations that cause derepression of the *Neisseria gonorrhoeae* MtrC-MtrD-MtrE Efflux pump system confer different levels of antimicrobial resistance and in vivo fitness. *Mol. Microbiol.* 70 (2), 462−78.
(13) Warner, D. M., Folster, J. P., Shafer, W. M., and Jerse, A. E. (2007) Regulation of the MtrC-MtrD-MtrE efflux-pump system modulates the in vivo fitness of *Neisseria gonorrhoeae*. *J. Infect. Dis.* 196 (12), 1804−12.
(14) Jerse, A. E., Sharma, N. D., Simms, A. N., Crow, E. T., Snyder, L. A., and Shafer, W. M. (2003) A gonococcal efflux pump system enhances bacterial survival in a female mouse model of genital tract infection. *Infect. Immun.* 71 (10), 5576−82.
(15) Spratt, B. G., Balthazar, J. T., Hagman, K. E., Pan, W., Judd, R. C., and Shafer, W. M. (1995) Resistance of *Neisseria gonorrhoeae* to antimicrobial hydrophobic agents is modulated by the mtrRCDE efflux system. *Microbiology* 141 (3), 611−622.
(16) Chitsaz, M., Booth, L., Blyth, M. T., O'Mara, M. L., and Brown, M. H. (2019) Multidrug Resistance in *Neisseria gonorrhoeae*: Identification of functionally important residues in the MtrD efflux protein. *mBio*, DOI: 10.1128/mBio.02277-19.
(17) Su, C.-C., Morgan, C. E., Kambakam, S., Rajavel, M., Scott, H., Huang, W., Emerson, C. C., Taylor, D. J., Stewart, P. L., Bonomo, R. A., and Yu, E. W. (2019) Cryo-Electron microscopy structure of an *Acinetobacter baumannii* multidrug efflux pump. *mBio* 10 (4), No. e01295-19.
(18) Bolla, J. R., Su, C. C., Do, S. V., Radhakrishnan, A., Kumar, N., Long, F., Chou, T. H., Delmar, J. A., Lei, H. T., Rajashankar, K. R., Shafer, W. M., and Yu, E. W. (2014) Crystal structure of the *Neisseria gonorrhoeae* MtrD inner membrane multidrug efflux pump. *PLoS One* 9 (6), No. e97903.
(19) Lyu, M., Moseng, M. A., Reimche, J. L., Holley, C. L., Dhulipala, V., Su, C. C., Shafer, W. M., and Yu, E. W. (2020) Cryo-EM atructures of a gonococcal multidrug efflux pump illuminate a mechanism of drug recognition and resistance. *mBio*, DOI: 10.1128/mBio.00996-20.
(20) Murakami, S., Nakashima, R., Yamashita, E., Matsumoto, T., and Yamaguchi, A. (2006) Crystal structures of a multidrug transporter reveal a functionally rotating mechanism. *Nature* 443 (7108), 173−9.
(21) Seeger, M. A., Schiefner, A., Eicher, T., Verrey, F., Diederichs, K., and Pos, K. M. (2006) Structural asymmetry of AcrB trimer suggests a peristaltic pump mechanism. *Science* 313 (5791), 1295−1298.
(22) Sennhauser, G., Amstutz, P., Briand, C., Storchenegger, O., and Grütter, M. G. (2006) Drug export pathway of multidrug exporter AcrB revealed by DARPin inhibitors. *PLoS Biol.* 5 (1), No. e7.
(23) Jewel, Y., Van Dinh, Q., Liu, J., and Dutta, P. (2020) Substrate-dependent transport mechanism in AcrB of multidrug resistant bacteria. *Proteins: Struct., Funct., Genet.* 88 (7), 853−864.
(24) Yao, X. Q., Kenzaki, H., Murakami, S., and Takada, S. (2010) Drug export and allosteric coupling in a multidrug transporter revealed by molecular simulations. *Nat. Commun.* 1, 117.
(25) Yamaguchi, A., Nakashima, R., and Sakurai, K. (2015) Structural basis of RND-type multidrug exporters. *Front. Microbiol.* 6, 327.
(26) Su, C. C., Li, M., Gu, R., Takatsuka, Y., McDermott, G., Nikaido, H., and Yu, E. W. (2006) Conformation of the AcrB multidrug efflux pump in mutants of the putative proton relay pathway. *J. Bacteriol.* 188 (20), 7290−6.
(27) Takatsuka, Y., and Nikaido, H. (2006) Threonine-978 in the transmembrane segment of the multidrug efflux pump AcrB of *Escherichia coli* is crucial for drug transport as a probable component of the proton relay network. *J. Bacteriol.* 188 (20), 7284−9.
(28) Yamane, T., Murakami, S., and Ikeguchi, M. (2013) Functional rotation induced by alternating protonation states in the multidrug transporter AcrB: all-atom molecular dynamics simulations. *Biochemistry* 52 (43), 7648−58.
(29) Yue, Z., Chen, W., Zgurskaya, H. I., and Shen, J. (2017) Constant pH molecular dynamics reveals how proton release drives the conformational transition of a transmembrane efflux pump. *J. Chem. Theory Comput.* 13 (12), 6405−6414.
(30) Takatsuka, Y., and Nikaido, H. (2006) Threonine-978 in the transmembrane segment of the multidrug efflux pump AcrB of *Escherichia coli* is crucial for drug transport as a probable component of the proton relay network. *J. Bacteriol.* 188 (20), 7284−9.
(31) Guan, L., and Nakae, T. (2001) Identification of essential charged residues in transmembrane segments of the multidrug transporter MexB of *Pseudomonas aeruginosa*. *J. Bacteriol.* 183 (5), 1734−9.
(32) Su, C. C., Long, F., Zimmermann, M. T., Rajashankar, K. R., Jernigan, R. L., and Yu, E. W. (2011) Crystal structure of the CusBA heavy-metal efflux complex of *Escherichia coli*. *Nature* 470 (7335), 558−62.
(33) Long, F., Su, C. C., Zimmermann, M. T., Boyken, S. E., Rajashankar, K. R., Jernigan, R. L., and Yu, E. W. (2010) Crystal structures of the CusA efflux pump suggest methionine-mediated metal transport. *Nature* 467 (7314), 484−8.
(34) Zhang, X., Wang, M. S., Liu, M. F., Zhu, D. K., Biville, F., Jia, R. Y., Chen, S., Sun, K. F., Yang, Q., Wu, Y., Zhao, X. X., Chen, X. Y., and Cheng, A. C. (2017) Contribution of RaeB, a putative RND-type transporter to aminoglycoside and detergent resistance in *Riemerella anatipestifer*. *Front. Microbiol.* 8, 2435.
(35) Su, C. C., Yin, L., Kumar, N., Dai, L., Radhakrishnan, A., Bolla, J. R., Lei, H. T., Chou, T. H., Delmar, J. A., Rajashankar, K. R., Zhang, Q., Shin, Y. K., and Yu, E. W. (2017) Structures and transport dynamics of a *Campylobacter jejuni* multidrug efflux pump. *Nat. Commun.* 8 (1), 171.
(36) Takatsuka, Y., and Nikaido, H. (2009) Covalently linked trimer of the AcrB multidrug efflux pump provides support for the functional rotating mechanism. *J. Bacteriol.* 191 (6), 1729−37.
(37) Nakashima, R., Sakurai, K., Yamasaki, S., Nishino, K., and Yamaguchi, A. (2011) Structures of the multidrug exporter AcrB reveal a proximal multisite drug-binding pocket. *Nature* 480 (7378), 565−9.
(38) Eicher, T., Cha, H. J., Seeger, M. A., Brandstätter, L., El-Delik, J., Bohnert, J. A., Kern, W. V., Verrey, F., Grütter, M. G., Diederichs, K., and Pos, K. M. (2012) Transport of drugs by the multidrug transporter AcrB involves an access and a deep binding pocket that are separated by a switch-loop. *Proc. Natl. Acad. Sci. U. S. A.* 109 (15), 5687−92.
(39) Poma, A. B., Cieplak, M., and Theodorakis, P. E. (2017) Combining the MARTINI and structure-based coarse-grained approaches for the molecular dynamics studies of conformational transitions in proteins. *J. Chem. Theory Comput.* 13 (3), 1366−1374.
(40) Maiorov, V. N., and Crippen, G. M. (1994) Significance of root-mean-square deviation in comparing three-dimensional structures of globular proteins. *J. Mol. Biol.* 235 (2), 625−34.
(41) Wassenaar, T. A., Pluhackova, K., Böckmann, R. A., Marrink, S. J., and Tieleman, D. P. (2014) Going backward: a flexible geometric approach to reverse transformation from coarse grained to atomistic models. *J. Chem. Theory Comput.* 10 (2), 676−90.
(42) Sennhauser, G., Bukowska, M. A., Briand, C., and Grütter, M. G. (2009) Crystal structure of the multidrug exporter MexB from *Pseudomonas aeruginosa*. *J. Mol. Biol.* 389 (1), 134−45.
(43) Wang, B., Weng, J., and Wang, W. (2015) Substrate binding accelerates the conformational transitions and substrate dissociation in multidrug efflux transporter AcrB. *Front. Microbiol.* 6, 302.

(44) Matsunaga, Y., Yamane, T., Terada, T., Moritsugu, K., Fujisaki, H., Murakami, S., Ikeguchi, M., and Kidera, A. (2018) Energetics and conformational pathways of functional rotation in the multidrug transporter AcrB. *eLife*, DOI: 10.7554/eLife.31715.
(45) Jewel, Y., Liu, J., and Dutta, P. (2017) Coarse-grained simulations of conformational changes in the multidrug efflux transporter AcrB. *Mol. BioSyst. 13* (10), 2006−2014.
(46) Schulz, R., Vargiu, A. V., Collu, F., Kleinekathöfer, U., and Ruggerone, P. (2010) Functional rotation of the transporter AcrB: insights into drug extrusion from simulations. *PLoS Comput. Biol. 6* (6), No. e1000806.
(47) Fischer, N., and Kandt, C. (2013) Porter domain opening and closing motions in the multi-drug efflux transporter AcrB. *Biochim. Biophys. Acta, Biomembr. 1828* (2), 632−41.
(48) Eicher, T., Seeger, M. A., Anselmi, C., Zhou, W., Brandstätter, L., Verrey, F., Diederichs, K., Faraldo-Gómez, J. D., and Pos, K. M. (2014) Coupling of remote alternating-access transport mechanisms for protons and substrates in the multidrug efflux pump AcrB. *eLife*, DOI: 10.7554/eLife.03145.
(49) Zhang, X. C., Liu, M., and Han, L. (2017) Energy coupling mechanisms of AcrB-like RND transporters. *Biophys Rep 3* (4), 73−84.
(50) Fischer, N., and Kandt, C. (2011) Three ways in, one way out: Water dynamics in the trans-membrane domains of the inner membrane translocase AcrB. *Proteins: Struct., Funct., Genet. 79* (10), 2871−2885.
(51) Vargiu, A. V., Ramaswamy, V. K., Malvacio, I., Malloci, G., Kleinekathöfer, U., and Ruggerone, P. (2018) Water-mediated interactions enable smooth substrate transport in a bacterial efflux pump. *Biochim. Biophys. Acta, Gen. Subj. 1862* (4), 836−845.
(52) Vargiu, A. V., Ramaswamy, V. K., Malvacio, I., Malloci, G., Kleinekathöfer, U., and Ruggerone, P. (2018) Water-mediated interactions enable smooth substrate transport in a bacterial efflux pump. *Biochim. Biophys. Acta, Gen. Subj. 1862* (4), 836−845.
(53) Zwama, M., and Yamaguchi, A. (2018) Molecular mechanisms of AcrB-mediated multidrug export. *Res. Microbiol. 169* (7−8), 372−383.
(54) Fairweather, S. J., Shah, N., and Bröer, S. (2020) Heteromeric solute carriers: function, structure, pathology and pharmacology. *Adv. Exp. Med. Biol. 21*, 13−127.
(55) Abraham, M. J., Murtola, T., Schulz, R., Páll, S., Smith, J. C., Hess, B., and Lindahl, E. (2015) GROMACS: High performance molecular simulations through multi-level parallelism from laptops to supercomputers. *SoftwareX 1−2*, 19−25.
(56) de Jong, D. H., Singh, G., Bennett, W. F., Arnarez, C., Wassenaar, T. A., Schäfer, L. V., Periole, X., Tieleman, D. P., and Marrink, S. J. (2013) Improved parameters for the Martini coarse-grained protein force field. *J. Chem. Theory Comput. 9* (1), 687−97.
(57) Wassenaar, T. A., Ingólfsson, H. I., Böckmann, R. A., Tieleman, D. P., and Marrink, S. J. (2015) Computational lipidomics with insane: a versatile tool for generating custom membranes for molecular simulations. *J. Chem. Theory Comput. 11* (5), 2144−55.
(58) Yesylevskyy, S. O., Schäfer, L. V., Sengupta, D., and Marrink, S. J. (2010) Polarizable water model for the coarse-grained MARTINI force field. *PLoS Comput. Biol. 6* (6), e1000810.
(59) Bussi, G., Donadio, D., and Parrinello, M. (2007) Canonical sampling through velocity rescaling. *J. Chem. Phys. 126* (1), 014101.
(60) Parrinello, M., and Rahman, A. (1981) ACS Catalysis. *J. Appl. Phys. 52* (12), 7182−7190.
(61) Parrinello, M., and Rahman, A. (1980) Crystal structure and pair potentials: a molecular-dynamics study. *Phys. Rev. Lett. 45* (14), 1196.
(62) de Jong, D. H., Baoukina, S., Ingólfsson, H. I., and Marrink, S. J. (2016) Martini straight: boosting performance using a shorter cutoff and GPUs. *Comput. Phys. Commun. 199*, 1−7.
(63) Schreiner, E., Trabuco, L. G., Freddolino, P. L., and Schulten, K. (2011) Stereochemical errors and their implications for molecular dynamics simulations. *BMC Bioinf. 12*, 190.
(64) Schmid, N., Eichenberger, A. P., Choutko, A., Riniker, S., Winger, M., Mark, A. E., and van Gunsteren, W. F. (2011) Definition and testing of the GROMOS force-field versions 54A7 and 54B7. *Eur. Biophys. J. 40* (7), 843.
(65) Anandan, A., Evans, G. L., Condic-Jurkic, K., O'Mara, M. L., John, C. M., Phillips, N. J., Jarvis, G. A., Wills, S. S., Stubbs, K. A., Moraes, I., Kahler, C. M., and Vrielink, A. (2017) Structure of a lipid A phosphoethanolamine transferase suggests how conformational changes govern substrate binding. *Proc. Natl. Acad. Sci. U. S. A. 114* (9), 2218−2223.
(66) Rahman, M. M., Kolli, V. S. K., Kahler, C. M., Shih, G., Stephens, D. S., and Carlson, R. W. (2000) The membrane phospholipids of *Neisseria meningitidis* and *Neisseria gonorrhoeae* as characterized by fast atom bombardment mass spectrometry. *Microbiology 146* (8), 1901−1911.
(67) Berendsen, H. J. C., Postma, J. P. M., van Gunsteren, W. F., and Hermans, J. (1981) Interaction models for water in relation to protein hydration. In *Intermolecular Forces: Proceedings of the Fourteenth Jerusalem Symposium on Quantum Chemistry and Biochemistry Held in Jerusalem, Israel, April 13−16, 1981* (Pullman, B., Ed.), pp 331−342, Springer Netherlands, Dordrecht. DOI: 10.1007/978-94-015-7658-1_21.
(68) Anandan, A., Evans, G. L., Condic-Jurkic, K., O'Mara, M. L., John, C. M., Phillips, N. J., Jarvis, G. A., Wills, S. S., Stubbs, K. A., Moraes, I., Kahler, C. M., and Vrielink, A. (2017) Structure of a lipid A phosphoethanolamine transferase suggests how conformational changes govern substrate binding. *Proc. Natl. Acad. Sci. U. S. A. 114* (9), 2218−2223.
(69) Koziara, K. B., Stroet, M., Malde, A. K., and Mark, A. E. (2014) Testing and validation of the Automated Topology Builder (ATB) version 2.0: prediction of hydration free enthalpies. *J. Comput.-Aided Mol. Des. 28* (3), 221−33.
(70) Malde, A. K., Zuo, L., Breeze, M., Stroet, M., Poger, D., Nair, P. C., Oostenbrink, C., and Mark, A. E. (2011) An Automated Force Field Topology Builder (ATB) and Repository: Version 1.0. *J. Chem. Theory Comput. 7* (12), 4026−37.
(71) Cockerill, F. R., Wikler, M. A., Alder, J., Dudley, M. N., Eliopoulos, G. M., Ferrro, M. J., Hardy, D. J., Hecht, D. W., Hindler, J. A., Patel, J. B., Powell, M., Swenson, J. M., Thomson, J. R. B., Traczewski, M. M., Turnidge, J. D., Weinstein, M. P., and Zimmer, B. L. (2012) Methods for dilution antimicrobial susceptibility tests for bacteria that grow aerobically; Approved Standard. *Clinical and Laboratory Standards Institute 32*, 88.
(72) Madeira, F., Park, Y. M., Lee, J., Buso, N., Gur, T., Madhusoodanan, N., Basutkar, P., Tivey, A. R. N., Potter, S. C., Finn, R. D., and Lopez, R. (2019) The EMBL-EBI search and sequence analysis tools APIs in 2019. *Nucleic Acids Res. 47* (W1), W636−W641.
(73) Waterhouse, A. M., Procter, J. B., Martin, D. M., Clamp, M., and Barton, G. J. (2009) Jalview Version 2−a multiple sequence alignment editor and analysis workbench. *Bioinformatics 25* (9), 1189−91.
(74) Humphrey, W., Dalke, A., and Schulten, K. (1996) VMD - Visual Molecular Dynamics. *J. Mol. Graphics 14*, 33.
(75) Schrodinger, LLC (2019) *PyMOL Molecular Graphics System*, Version 2.3.1.
(76) Hooft, R. W., Vriend, G., Sander, C., and Abola, E. E. (1996) Errors in protein structures. *Nature 381* (6580), 272.

https://doi.org/10.1021/acsinfecdis.1c00149
ACS Infect. Dis. 2021, 7, 1833−1847

7.5 Appendix E: Paper 4: A unique sequence is essential for efficient multidrug efflux function of the MtrD protein of *Neisseria gonorrhoeae*

AMERICAN SOCIETY FOR MICROBIOLOGY | mBio®

RESEARCH ARTICLE

A Unique Sequence Is Essential for Efficient Multidrug Efflux Function of the MtrD Protein of *Neisseria gonorrhoeae*

Mohsen Chitsaz,[a] Vrinda Gupta,[b] Benjamin Harris,[b] Megan L. O'Mara,[b] Melissa H. Brown[a]

[a]College of Science and Engineering, Flinders University, Bedford Park, SA, Australia
[b]Research School of Chemistry, Australian National University, Canberra, ACT, Australia

ABSTRACT Antimicrobial resistance in *Neisseria gonorrhoeae* has reached an alarming level, severely impacting the effective treatment of gonorrhea. Belonging to the resistance-nodulation-cell division (RND) superfamily of efflux transporters, the MtrD membrane protein of *N. gonorrhoeae* provides resistance to a broad range of antimicrobial compounds. A unique feature of MtrD is an 11-residue sequence (from N917 to P927 [N917-P927]) that connects transmembrane helices (TMS) 9 and 10; this sequence is not present in homologous RND proteins. This study explores the structural and functional roles of the N917-P927 region by means of mutant analysis and molecular dynamics simulations. We show that N917-P927 plays a key role in modulating substrate access to the binding cleft and influences the overall orientation of the protein within the inner membrane necessary for optimal functioning. Removal of N917-P927 significantly reduced MtrD-mediated resistance to a range of antimicrobials and mutations of three single amino acids impacted MtrD-mediated multidrug resistance. Furthermore, molecular dynamics simulations showed deletion of N917-P927 in MtrD may dysregulate access of the substrate to the binding cleft and closure of the substrate-binding pocket during the transport cycle. These findings indicate that N917-P927 is a key region for interacting with the inner membrane, conceivably influencing substrate capture from the membrane-periplasm interface and thus is essential for full multidrug resistance capacity of MtrD.

IMPORTANCE The historical sexually transmitted infection gonorrhea continues to be a major public health concern with an estimated global annual incidence of 86.9 million cases. *N. gonorrhoeae* has been identified by the World Health Organization as one of the 12 antimicrobial-resistant bacterial species that poses the greatest risk to human health. As the major efflux pump in gonococci, the MtrD transporter contributes to the cell envelope barrier in this organism and pumps antimicrobials from the periplasm and inner membrane, resulting in resistance. This study demonstrates that a unique region of the MtrD protein that connects TMS 9 and TMS 10 forms a structure that may interact with the inner membrane positioning TMS 9 and stabilizing the protein facilitating substrate capture from the inner membrane-periplasm interface. Analysis of mutants of this region identified that it was essential for MtrD-mediated multidrug resistance. Characterization of the structure and function of this unique local region of MtrD has implications for drug efflux mechanisms used by related proteins and is important knowledge for development of antibiotics that bypass efflux.

KEYWORDS RND protein, efflux pump, *Neisseria gonorrhoeae*, gonorrhea, multidrug resistance, MtrD protein, drug transport

With an estimated 86 million new cases of gonorrheal infections in adults in 2016 caused by *Neisseria gonorrhoeae*, the longstanding disease gonorrhea remains a serious global public health problem (1), primarily due to ability of the bacterium to develop or acquire resistance mechanisms to clinically relevant antibiotics (2). Export of antibiotics across the cellular membrane via efflux pumps is one of the most efficient mechanisms

Citation Chitsaz M, Gupta V, Harris B, O'Mara ML, Brown MH. 2021. A unique sequence is essential for efficient multidrug efflux function of the MtrD protein of *Neisseria gonorrhoeae*. mBio 12:e01675-21. https://doi.org/10.1128/mBio.01675-21.

Editor Richard Gerald Brennan, Duke University School of Medicine

Copyright © 2021 Chitsaz et al. This is an open-access article distributed under the terms of the Creative Commons Attribution 4.0 International license.

Address correspondence to Melissa H. Brown, melissa.brown@flinders.edu.au.

This article is a direct contribution from Melissa H. Brown, a Fellow of the American Academy of Microbiology, who arranged for and secured reviews by William Shafer, Emory University School of Medicine, and Michael Jennings, Griffith University.

Received 14 June 2021
Accepted 28 July 2021
Published 31 August 2021

Downloaded from https://journals.asm.org/journal/mbio on 18 March 2023 by 2001:8004:1680:11a3:f9e6:f3ec:ff34:a3ba.

used by *N. gonorrhoeae*, providing concomitant resistance to multiple antibiotics (3). Gonococci possess five drug efflux pump systems (4–6). Of these, the multiple transferrable resistance CDE (MtrCDE) system is the only transporter from the resistance-nodulation-cell division (RND) superfamily and is the most important efflux-mediated drug resistance mechanism (7, 8). Overexpression of MtrCDE imparts clinically significant levels of resistance to many important antibiotics used for treatment, such as β-lactams, and the currently used combined frontline treatment for gonorrhea of the third-generation cephalosporin ceftriaxone and macrolides such as azithromycin (4, 8–10). This can be mediated by *mtrR*, the transcriptional repressor of the *mtrCDE* operon (11, 12), through mutations in either *mtrR* or its promoter region (13–17) with the structural mechanism recently described (18). Furthermore, MtrCDE enables *N. gonorrhoeae* to persist in the presence of host-derived compounds, such as long-chain fatty acids, bile salts, hormones (e.g., progesterone) and cationic antimicrobial peptides that are found in human body sites frequently infected by *N. gonorrhoeae*, enhancing the ability of this pathogen to establish an infection or proliferate at mucosal surfaces (7, 19).

The MtrD component of the tripartite MtrCDE efflux system is a large protein of 1,067 amino acids, that, together with its closely related homologues (AcrB from *Escherichia coli* and MexB from *Pseudomonas aeruginosa*), belongs to the largely Gram-negative bacterial hydrophobe-amphiphile efflux-1 (HAE1) family of the RND superfamily (7, 20–22). The first crystal structure of MtrD revealed a homotrimer with symmetric monomers and an overall structure similar to those of homologous RND drug transporters (23). Each MtrD monomer has pseudosymmetric halves containing two domains: a transmembrane domain (TM) organized into 12 transmembrane α-helices (TMS) and a large periplasmic domain that can be subdivided into a porter domain and an MtrE docking domain (23). The porter domain is composed of four subdomains—PN1, PN2, PC1, and PC2—with three PN1 subdomains (one from each protomer) making up a central pore and stabilizing the trimeric organization. PC1 and PC2 create a cleft that opens to the periplasm likely allowing for periplasmic entry of substrates (23).

Recent cryo-electron microscopy (EM) structures of MtrD in complex with ampicillin and erythromycin revealed greater insight into the MtrD substrate translocation pathway and functional mechanism of drug efflux (24). In contrast to the first MtrD apo structure, these substrate-bound trimeric structures are asymmetric, similar to substrate-bound structures of AcrB and MexB (24–27). Each protomer adopts a distinct conformation resembling a three-step functionally rotating export cycle that is comprised of the access (A), binding (B), and extrusion (E) conformations (24–27). We recently described the functionally rotating transport mechanism of MtrD (28). As is the case for AcrB and MexB, the substrate permeation pathway through each MtrD protomer contains three possible entrance points, from the inner membrane (IM), from the periplasm, or via the central cavity (25–27, 29). Substrates then pass through the proximal and distal substrate recognition and binding sites and exit via the funnel-like channel within the MtrE docking domain (24–27, 29). The periplasmic entrance (also known as entrance channel 2 in AcrB) is located in the cleft formed between PC1 and PC2 and leads to the proximal pocket, likely collecting substrates found in the periplasm (25, 29, 30). Drugs that are partitioned in the membrane are expected to enter the pump via the IM entrance (also known as lateral entrance or entrance channel 1 in AcrB) that opens to the groove formed in the boundary between the TM and IM (25–27, 29). Surrounded by PN1, PN2, PC1, and PC2 β-sheets, the distal pocket is separated from the proximal pocket by a flexible switch loop or G-loop (29, 31, 32). These binding pockets are voluminous and formed by many hydrophobic, aromatic, polar, and charged residues (24–27, 29, 31). In the MtrD cryo-EM structures, ampicillin and erythromycin were both found in the distal pocket and only in the protomer adopting the binding conformation (24).

MtrD shares many, but not all, features with other bacterial HAE1 RND drug exporters (23, 27, 33). One of the unique features of MtrD is a sequence of 11 amino acids (N917 to P927 [N917-P927]) which is not present in homologous proteins. Using site-directed mutagenesis, molecular dynamics (MD) simulations, and resistance profiling,

Downloaded from https://journals.asm.org/journal/mbio on 18 March 2023 by 2001:8004:1680:11a3:f9e6:f3ee:ff34:a3ba.

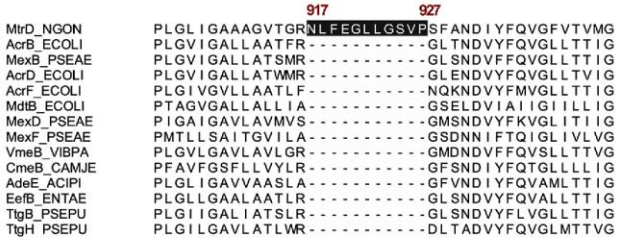

FIG 1 Protein sequences of selected members of RND proteins of the HAE1 family. Sequences were taken from the Transporter Classification Database (TCDB) (66, 67) and include MtrD of *N. gonorrhoeae* (Q51073), AcrB of *E. coli* (P31224), MexB of *P. aeruginosa* (P52002), AcrD of *E. coli* (P24177), AcrF of *E. coli* (P24181), MdtB of *E. coli* (P76398), MexD of *P. aeruginosa* (Q9HVI9), MexF of *P. aeruginosa* (Q9I0Y8), VmeB of *Vibrio parahaemolyticus* (Q2AAU3), CmeB of *Campylobacter jejuni* (AAL74245), AdeE of *Acinetobacter* sp. (Q8GKU1), EefB of *Enterobacter aerogenes* (Q8GC83), TtgB of *Pseudomonas putida* (O52248), and TtgH of *P. putida* (Q93PU4). Protein sequence alignment was performed using the NCBI protein blast tool and visualized using Ugene software. The N917-P927 sequence unique to MtrD is labeled in red.

we explore the role of the N917-P927 region in MtrD-mediated multidrug resistance. We found that this unique region is essential for full multidrug efflux and resistance capacity of MtrD since its removal rendered *N. gonorrhoeae* cells susceptible to many antimicrobials, and three individual residues within it in particular are important for drug resistance. In addition, we show that N917-P927 may influence the accessibility of substrates to the proximal binding pocket and stabilization of the protein within the IM required for optimal function. Furthermore, deletion of N917-P927 in MtrD may dysregulate the access of substrate to the binding cleft and the propagation of conformational changes to the substrate binding pocket during the transport cycle.

RESULTS

Removal of N917-P927 significantly reduced MtrD-mediated resistance. Bioinformatics analyses revealed that the N917-P927 sequence is unique to the MtrD protein (Fig. 1). In addition, analyses of whole-genome sequences available in the NCBI database revealed that this 11-amino-acid sequence (NLFEGLLGSVP) is 100% conserved among 739 *N. gonorrhoeae* genomes, including the two multidrug-resistant clinical isolates, H041 and F89, that are highly resistant to the extended-spectrum cephalosporins ceftriaxone and cefixime (34–36). Furthermore, the sequence is also conserved in *mtrD* within other pathogenic and commensal *Neisseria* species (data not shown). This sequence forms a short α-helix extending from TMS 9 and continues to a loop connecting TMS 9 and TMS 10 (Fig. 2A and B) positioned directly beneath the binding cleft entrance formed by PC1 and PC2 (Fig. 2C). In addition, this region is linked via the N terminus of TMS 9 to the groove formed between TMS 8 and TMS 9, which has been proposed to facilitate collection of substrates from the outer leaflet of the IM through the IM entrance (entrance 1) in AcrB (Fig. 2A and B) (23, 37). The spatial arrangement of the N917-P927 region suggests that this local structure may play a role in facilitation of substrate uptake during a functional cycle. Furthermore, the observed high conservation of the N917-P927 sequence suggests that this region of MtrD does not play a substrate-specific interaction that would have evolved under specific antibiotic pressure.

As an initial step in determining the role of N917-P927, the sequence encoding this region was deleted from *mtrD* by PCR mutagenesis using primers MTRD_LF1 and MTRD_LR1 (see Table S1 in the supplemental material) and pGCC4-CL-*mtrD*$_{His6}$ as the template DNA (38). The use of the pGCC4 vector allows for amplification of *E. coli*-based cloned *mtrD* or derivatives and subsequent integration of these determinants into the chromosome of a *N. gonorrhoeae* strain using a *Neisseria* insertion complementation system

Downloaded from https://journals.asm.org/journal/mbio on 18 March 2023 by 2001:8004:1680:11a3:f9e6:f3ee:ff34:a3ba.

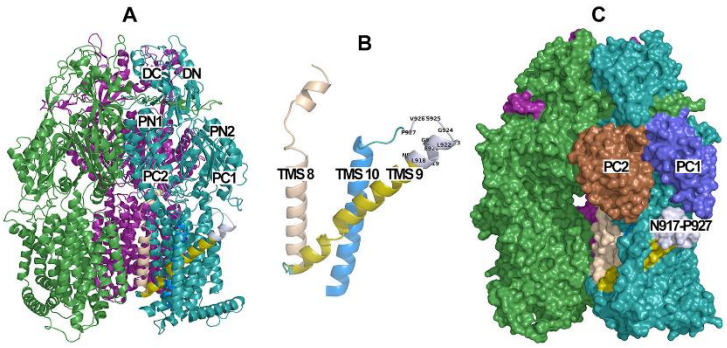

FIG 2 Secondary structure of the MtrD protein (PDB ID 6VKS). (A) Side view of the cryo-EM structure of the MtrD K823E variant. The three protomers are colored green (Access), teal (Binding), and magenta (Extrusion). The six subdomains of the porter domain are labeled in the B protomer. (B) Enhanced view of TMS 8 (beige), TMS 9 (gold), TMS 10 (marine blue), and N917-P927 (gray). (C) Surface representation of the K823E MtrD variant. Subdomains PC1 and PC2 in the binding protomer are shown in blue and russet, respectively. The position of the N917-P927 region at the bottom of the cleft opening between PC1 and PC2 is shown in gray.

(NICS) (39). This provides the gonococcal cells with a recombinant *mtrD* allele expressed under *lac* regulation (38, 39). Thus, the resultant construct, pGCC4-CL-$mtrD_{His6}$Δ(N917-P927), was recombined into the chromosome of *N. gonorrhoeae* strain KH15Δ*mtrD*Δ*norM*. This bacterial strain is a derivative of the *N. gonorrhoeae* KH15 strain known to bear a single bp deletion in the coinciding *mtrR* and *mtrC* promoter sequences, resulting in upregulation of the *mtrCDE* system and consequential increased levels of resistance to MtrD substrates (8). Since the NorM efflux pump shares some substrates in common with MtrD, the *N. gonorrhoeae* variant KH15Δ*mtrD*Δ*norM* with both the *norM* and *mtrD* efflux pumps deleted was constructed, producing a strain that was shown to be hypersusceptible to a broad range of MtrD-specific substrates (38, 40). Expression of recombinant wild-type (WT) *mtrD* from DNA integrated into this strain provided gonococcal cells with a fully functional MtrCDE efflux system mediating high levels of resistance to a broad range of antimicrobial compounds (38). Integration of the constructed CL-$mtrD_{His6}$Δ(N917-P927) mutant produced the strain KH15Δ*mtrD*Δ*norM*-CL-$mtrD_{His6}$Δ(N917-P927), which was confirmed by PCR using primers SCRNG1 and MTRDSF5 (see Table S1). SCRNG1 anneals to a location on the *N. gonorrhoeae* chromosome upstream of and outside the recombination site for the NICS of pGCC4 and MTRDSF5 anneals to the 3′ end of *mtrD* 167 bp upstream of its stop codon allowing verification of *mtrD* integration (38). Western blot analysis confirmed the presence of the MtrD Δ(N917-P927) deletion mutant protein in the membrane of KH15Δ*mtrD*Δ*norM*-CL-$mtrD_{His6}$Δ(N917-P927) cells at a level comparable with WT (see Fig. S1). It has been shown previously that addition of a histidine tag on the C terminus of MtrD for monitoring expression levels and increasing the versatility of the system does not affect protein expression and resistance (38). Therefore, any change in resistance profile of this mutant compared to WT could be attributed to the constructed Δ(N917-P927) deletion. Consequently, the KH15Δ*mtrD*Δ*norM*-$mtrD_{His6}$Δ(N917-P927) strain was tested for resistance against a panel of 10 compounds (listed in Table 1) using a standard MIC analysis method. These 10 compounds are known MtrD substrates and were selected because they give higher discrimination (≥4-fold difference in MIC) between the WT MtrD and the appropriate negative-control strain (KH15Δ*mtrD*Δ*norM* complemented with the NICS portion of the pGCC4 vector) (38). While the two macrolide antibiotics erythromycin and azithromycin are MtrD substrates with clinical importance, and our previous study has demonstrated excellent MIC differentiation between KH15Δ*mtrD*Δ*norM* and its parental strain KH15, the use of the erythromycin resistance cassette present in pGCC4 as a selection marker precluded testing constructed MtrD mutant derivatives against these antibiotics (38, 39). MIC analysis revealed that the deletion of N917-P927 did not totally abrogate but

Downloaded from https://journals.asm.org/journal/mbio on 18 March 2023 by 2001:8004:1680:11a3:f9e6:f3ee:f734:a3ba.

TABLE 1 Antimicrobial resistance of *N. gonorrhoeae* strain KH15Δ*mtrD*Δ*norM* expressing MtrD derivatives

	MIC (μg/ml)[a]									
	Detergent		Antibiotic			CAMP	Dye		Bile acid	Hormone
Mutation	N-9	TX-100	RIF	NOV	OXA	PMB	ET	CV	CHO	PRO
WT[b]	≥4,096	≥4,096	0.125	1	4	100	0.25	2	400	80
Δ(N917-P927)	64	128	0.03	0.5	2	50	0.125	1	300	40
N917C	32	64	0.015	0.25	1	50	0.06	0.5	300	40
L918C	≥4,096	≥4,096	0.125	1	4	100	0.25	2	400	80
F919C	≥4,096	≥4,096	0.125	1	4	100	0.25	2	400	80
E920C	≥4,096	≥4,096	0.06	1	4	100	0.25	1	300	80
G921C	≥4,096	≥4,096	0.125	1	4	100	0.25	2	400	80
L922C	≥4,096	≥4,096	0.125	1	2	100	0.25	2	400	80
L923C	≥4,096	≥4,096	0.125	1	4	100	0.25	2	400	80
G924C	32	64	0.015	0.25	2	50	0.06	0.5	200	40
S925C	≥4,096	≥4,096	0.125	1	4	100	0.25	2	400	80
V926C	≥4,096	≥4,096	0.125	1	4	100	0.25	2	400	80
P927C	32	64	0.03	0.25	1	50	0.06	0.5	300	40
11Ala	ND	32	ND	ND	0.06	ND	ND	ND	ND	ND
N917K	16	32	0.015	0.06	0.25	50	0.06	0.125	100	40
N917Q	32	64	0.015	0.25	0.5	50	0.06	0.5	200	40
N917S	64	128	0.06	1	2	75	0.125	1	300	80
P927G	≥4,096	≥4,096	0.125	1	4	100	0.25	2	400	80
Negative control[c]	16	32	0.008	0.03	0.06	50	0.06	0.125	100	20

[a]All MIC data are representative of three or more independent experiments. Abbreviations: CAMP, cationic antimicrobial peptide; CHO, cholic acid; CV, crystal violet; ET, ethidium; N-9, nonoxynol-9; NOV, novobiocin; OXA, oxacillin; PMB, polymyxin B; PRO, progesterone; RIF, rifampin; TX-100, Triton X-100; ND, not determined.
[b]Recombinant cysteine-less MtrD variant with a 6-histidine affinity tag at C terminus (CL-$MtrD_{His6}$).
[c]Strain KH15Δ*mtrD*Δ*norM* transformed with pGCC4 empty vector expressing no MtrD [KH15Δ*mtrD*Δ*norM* (NICS) strain].

reduced resistance to all 10 tested compounds from a minimum of 1.3-fold for cholic acid to a maximum of >128-fold for nonoxynol-9 (Table 1). These data indicate that the N917-P927 sequence is necessary for complete and efficient activity of the MtrD protein.

Integrity of the N917-P927 sequence is required for efficient efflux activity of the MtrD protein. To investigate whether the length or the specific residue composition of the N917-P927 sequence is an important factor for full function of the MtrD protein, the 11-amino-acid sequence was replaced with all alanines by site-directed mutagenesis using 11Ala F and 11Ala R primers (see Table S1) and pGCC4-CL-$mtrD_{His6}$(ΔN917-P927) as the template DNA. The resultant 11 alanine replacement mutant 11A(917-927) was integrated into the chromosome of the KH15Δ*mtrD*Δ*norM* strain, and PCR using the primers SCRNG1 and MTRDSF5 confirmed the existence of this mutant in the chromosome. Using Western analysis, cells expressing the *mtrD* mutant, were found to produce protein at a very low level, and MIC assays against Triton X-100 and oxacillin showed no resistance, exhibiting a resistance profile similar to that of the negative control (Table 1; see also Fig. S1). Thus, this mutant was not experimentally analyzed any further. A second mutant was similarly designed that replaced the N917-P927 sequence with a stretch of 11 glycine residues 11G(917-927). However, construction of this mutant was unsuccessful possibly due to lethality. Together, these data indicated that the presence of the protein backbone alone (glycine substitution) or truncated side chains (alanine substitution) is not sufficient to support production of a fully active MtrD variant.

Four residues in the N917-P927 region play an important role in MtrD activity. As mentioned above, the positioning of the N917-P927 region suggests it has structural and functional roles, e.g., by facilitation of substrate uptake during a functional cycle. Therefore, it was proposed that some residues in this region may be involved in mechanisms that help substrate uptake from the IM and are important for MtrD activity. To identify the functional importance of individual residues within this region, each of the 11 residues was individually substituted with cysteine; cysteine was selected to facilitate later studies on the location/inhibition of substituted residues (41) and allows characterization of properties such as charge, polarity, or hydrophobicity linked to the target residue side chain. The 11 mutants were generated by site-directed mutagenesis

Downloaded from https://journals.asm.org/journal/mbio on 18 March 2023 by 2001:8004:1680:11a3:f9e6:f3ee:ff34:a3ba.

using the primers listed in Table S1 and pGCC4-CL-*mtrD*$_{His6}$ as the template DNA. All 11 MtrD mutants were expressed in KH15Δ*mtrD*Δ*norM* cells at levels comparable to that of the WT, as judged by Western blotting (see Fig. S1), indicating that the amino acid substitutions did not affect MtrD protein stability and membrane insertion. MIC analyses revealed that cells expressing six of the MtrD mutants (L918C, F919C, G921C, L922C, L923C, S925C, and V926C) retained resistance profiles similar to that of the WT with no change in MICs for any of the 10 tested compounds (Table 1). In contrast, three MtrD mutants (N917C, G924C, and P927C) showed a reduction in resistance to all compounds with the greatest decrease (>128-fold) to the nonionic and amphiphilic surfactant Triton X-100 and the spermicide nonoxynol-9 (Table 1), demonstrating that these three residues are critical for efficient MtrD-mediated resistance against a broad range of substrates. In addition, mutation of a fourth residue (E920C), affected resistance to rifampin, crystal violet, and cholic acid (Table 1). These data raised questions about the possible role(s) played by these residues in the MtrD efflux process. Specifically, do they directly bind MtrD substrates or alternatively interact with neighboring residues to indirectly affect transport function through another mechanism, e.g., by altering the volume of the nearby substrate entrance? To address these questions, we conducted additional site-directed mutagenesis and MD simulations.

To ascertain the role played by N917, and to determine whether there were side chain requirements/limitations in this position, we aimed to replace the polar noncharged side chain of asparagine with amino acids of both similar and different side chain properties. N917 was replaced with two polar noncharged residues (glutamine and serine) and the positively charged lysine. In addition, replacement of asparagine with a negatively charged residue (aspartic acid) and an amphipathic and bulky amino acid (tryptophan) was attempted; however, construction of these two mutants was unsuccessful. Western blot analyses confirmed the expression of N917K, N917Q, and N917S proteins in the membranes of KH15Δ*mtrD*Δ*norM* cells expressing these mutant MtrD proteins at levels comparable to that of WT (see Fig. S1). Assays determined that resistance was not fully maintained by replacing N917 with either glutamine or serine although the N917S derivative mediated higher levels of resistance compared to the original N917C mutation (Table 1). These data indicate that side chain properties of asparagine are required at position 917. The MtrD N917K derivative exhibited reduced resistance to many of the tested compounds even more than that by the N917C mutation, with a resistance capacity for nonoxynol-9, Triton X-100, ethidium, cholic acid, and polymyxin B only at levels comparable to the negative control (Table 1).

We hypothesized that both G924 and P927 are residues required for optimal/efficient efflux function of MtrD through providing structural flexibility (glycine) or constraining backbone geometry (proline) within the loop region. Both proline and glycine are associated with a propensity to destabilize α-helices, promoting the formation of unstructured loops and modifying substrate capture from the IM. Interestingly, in the MtrD extrusion protomer, G924 is located at a position that corresponds to a break in the α-helix (Fig. 3). To test these hypotheses, we designed mutagenesis strategies to create the MtrD mutants G924P and P927G. Construction of the G924P mutant was not successful likely due to lethality in *E. coli* cells; however, the MtrD P927G derivative was obtained and shown to be expressed at a level comparable to that of WT (see Fig. S1). MIC analysis of MtrD P927G in KH15Δ*mtrD*Δ*norM* cells indicated that the proline at this position could be replaced by glycine since it retained full resistance capacity (Table 1). We postulate that this may be due to the backbone conformational flexibility of glycine, which allows it to adopt backbone dihedral conformations that span the region of the Ramachandran plot occupied by proline (42). Together, these data showed that N917, G924, and P927 play important roles in MtrD-mediated multidrug resistance.

Structural analysis and dynamics of the N917-P927 region. The ampicillin-bound cryo-EM structure of MtrD (PDB ID 6VKS) revealed that the conformation of the N917-P927 region at its N terminus is different in the A, B, and E protomers. In the A protomer the α-helix of TMS 9 is shorter than in the B and E protomers (Fig. 3A to C). In the

Downloaded from https://journals.asm.org/journal/mbio on 18 March 2023 by 2001:8004:1680:11a3:f9e6:f3ee:ff34:a3ba.

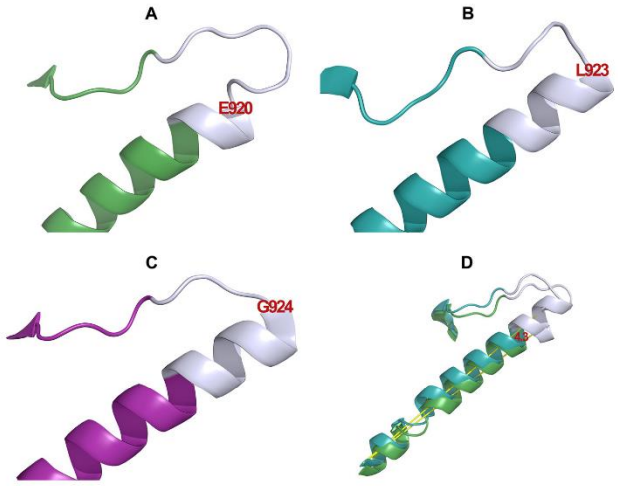

FIG 3 Secondary structure of the MtrD protein in complex with ampicillin (PDB ID 6VKS). The C terminus of TMS 9 and the N917-P927 is shown in cartoon representation. Each helix is colored according to its protomer: Access (green), Binding (teal), and Extrusion (magenta). N917-P927 is shown in gray in all pictures. (A) TMS 9 in the A protomer α-helix extends up to E920. (B) TMS 9 in the B protomer extends up to L923 forming two full turn α-helix turn in this region. (C) TMS 9 in the E protomer extends up to G924. (D) Superimposition of the A protomer and the B protomers (root mean square deviation of 1.6 Å). Residues 893 to 935 encompassing TMS 9 are shown in cartoon representation and the 4.3° angle formed between the C-alpha atoms of residues E920 and S893 is illustrated in yellow.

A protomer the TMS 9 α-helix extends to E920, while in the B protomer it extends to L923 and is further extended in the E protomer to G924 (Fig. 3A to C). These changes correspond to a change in the overall tilt angle of TMS 9 within the bilayer between these three conformations (Fig. 3D).

To better understand the impact of N917-P927 and the orientation of the TMS 9 helix on MtrD function, the ampicillin-bound cryo-EM structure of MtrD was embedded in a solvated neisserial membrane model (38) and MD simulations were carried out for 500 ns in triplicate (Fig. 4A). MD simulations were also performed on the Δ(N917-P927), 11G(917-927) variants, and an MtrD triple mutant (N917C/G924C/P927C), containing concurrent N917C, G924C, and P927C substitutions (Fig. 4B and C).

MD simulations of the WT MtrD trimer showed that N917-P927 of the A protomer lay within the membrane, positioned at the periplasmic membrane interface. In comparison, N917-P927 of the B and E protomers extended above the membrane into the periplasm (see Fig. S2A to C). The amino acid sequence of N917-P927 (NLFEGLLGSVP) is aliphatic, supporting its preferential location at the membrane-water interface.

In replicate 500-ns simulations of WT MtrD, the position and relative orientations of the TMS 9 extension, N917-P927, changed relative to the starting cryo-EM structure. In all three protomers of the cryo-EM structure, N917-P927 did not form close contacts with other regions of the protein. Within the first 50 ns of simulation, N917-P927 formed contacts with residues in the periplasmic domain, which differed between the A, B, and E protomers.

In the A protomer, N917-P927 remained close to the PC1 domain near the membrane interface. In particular, G924 was in close proximity to S635 from the PC1 domain, while P927 was positioned near to A641 (Fig. 5A). In the B protomer, N917-P927 interacted with the PC1 domain slightly higher in the binding pocket than in the A

Downloaded from https://journals.asm.org/journal/mbio on 18 March 2023 by 2001:8004:1680:11a3:f9e6:f3ee:ff34:a3ba.

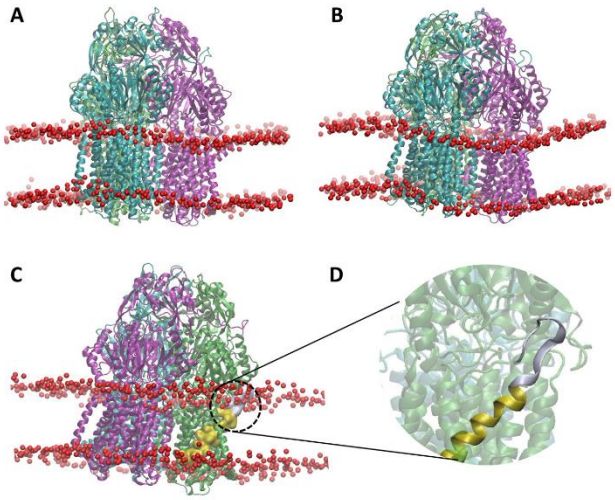

FIG 4 MD simulations showing the position of MtrD within the membrane. The three MtrD protomers are shown in ribbon representation and colored Access (green), Binding (teal), and Extrusion (magenta). The lipid phosphate head groups of the membrane are shown as red beads. (A to C) Positions of the WT trimer (A), Δ(N917-P927) trimer (B), and 11G(917-927) trimer (C) within the membrane. (D) Closeup view of the TMS 9 and N917-P927 regions in the Access protomer of the 11G (917-927) MtrD mutant. In panels C and D, TMS 9 is gold and N917-P927 is gray.

protomer and directly contacts it to form a protein-protein interface (Fig. 5B). In all three replicate simulations, the G924-P927 region formed protein-protein contacts in the vicinity of V640, A641, and S635. Compared to the A protomer, the change in position of N917-P927 effectively narrowed the binding cleft entrance and prevented the efficient entry of substrates (Fig. 5B). The precise nature of the contacts between G924-P927 and V640, A641 and S635 varied by replicate simulation. Notably, in one replicate simulation, the TMS 9 helical extension reoriented so that residues 917 to 927 adopted an elongated conformation in which G924 extended vertically into the base of the binding cleft to form a protein-protein contact with V640. In the remaining two replicate simulations, the conformation is less extreme. In all three replicate simulations, these interactions partially occluded the periplasmic binding cleft entrance. In the E protomer, N917 interacts with F929, while P927 interacts with T830 on the PC2 side of the binding cleft (Fig. 5C), protruding into the binding cleft to physically prevent substrate entry from both the periplasm and the IM substrate entrance.

MD simulations were then performed to assess the impact of the cysteine replacements at positions that were found to be important for MtrD function. Based on the underlying hypothesis that individual mutations within a protein are unlikely to perturb the overall secondary structure, a triple MtrD mutant, containing concurrent N917C, G924C, and P927C mutations (N917C/G924C/P927C) was developed. No steric clashes were observed in MtrD upon mutation of N917, G924, or P927 to cysteine. MD simulations showed that in contrast to the WT, for the triple mutant both the position and orientation of residues 917 to 927 in each protomer fluctuated and protruded above the membrane interface into the periplasm (see Fig. S3A to C). Interactions between the N917-P927 region and the rest of the protein are most altered in the A protomer of the triple cysteine mutant. In the A protomer, the N917-P927 loop extends to form a hairpin oriented into the binding cleft. Here, G924C interacts with V640 and A641 from the PC1 domain (Fig. 5D). This interaction extends further into the binding

Downloaded from https://journals.asm.org/journal/mbio on 18 March 2023 by 2001:8004:1680:11a3:f9e6:f3ee:f734:a3ba.

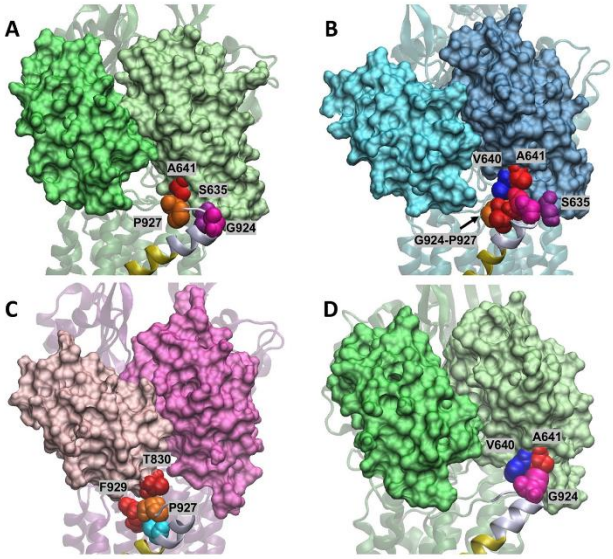

FIG 5 MD simulation analysis of interactions between the N917-P927 region and the MtrD periplasmic domain. TMS 9 is in gold and the N917-P927 region is in gray ribbon representation. Interactions are shown for the Access (green) (A), Binding (teal) (B), and Extrusion (magenta) (C) protomers in the WT MtrD protein and the Access (green) protomer (D) of the N917C/G924C/P927C triple mutant MtrD protein. The PC1 (right) and PC2 (left) domains are shown in surface representation. Interacting residues (labeled on the figure) are shown in Van der Waals (VDW) rendering and are colored by residue identity.

cleft than in simulations of WT MtrD, in which G924 interacts with S635 below the level of V640 and A641. The deeper penetration of G924C into the binding cleft entrance partially occluded the periplasmic entrance to the binding cleft. We hypothesize that this prevented the entry of some substrates through the proposed periplasmic entrance of the mutant MtrD A protomer. In the B protomer of the triple cysteine MtrD mutant, G924C interacts with S635 from the PC1 domain, anchoring N917-P927 at the lower right-hand entrance of the binding cleft. This interaction was also observed in the B protomer for the WT simulations but was more persistent throughout the simulations of the triple cysteine mutant. In the E protomer of the triple mutant, N917C formed contacts with F929, while P927C interacted with T830 on the PC2 side of the binding cleft, as was observed in the WT E protomer. We hypothesize that the P927C mutation decreases backbone dihedral angle constraints associated with the presence of proline, resulting in greater backbone mobility. The noticeable alteration in the positioning of the N917-P927 region in the A protomer of the triple cysteine mutant compared to the WT protein suggests the mutated residues N917, G924, and P927 play a key role in controlling substrate entry. The higher positioning of N917-P927 in the binding cleft of the triple cysteine mutant partially occluded the binding cleft entrance, preventing the entry of some substrates in the mutant MtrD A conformation. This restriction in substrate entry supports the decreased resistance profile experimentally observed upon mutation of these residues. Bioinformatics analysis of MtrD proteins in the NCBI database revealed that T830 and N929 are very highly conserved (100% amino acid identity), while S635 (63%), V640 (24%), and A641 (55%) are less conserved within *N. gonorrhoeae* strains. A similar homology trend is seen in MtrD present in strains of the closely related species *Neisseria meningitidis*. The conservation of these

Downloaded from https://journals.asm.org/journal/mbio on 18 March 2023 by 2001:8004:1680:11a3:f9e6:f3ee:f734:a3ba.

PC1/PC2 domain residues supports the MD simulations and the proposition that they inter-react with TMS 9 in MtrD efflux.

Simulations of the Δ(N917-P927) MtrD mutant showed the terminal region of TMS 9 was located at the periplasmic membrane-water interface in the A and B protomers and protruded slightly above the membrane into the periplasm in the E protomer (see Fig. S2D to F). Simulations of the Δ(N917-P927) MtrD protein, showed TMS 9 and TMS 10 did not associate with the periplasmic entrance to the binding cleft and a greater localized curvature in the membrane around MtrD was observed (Fig. 4A and B), suggesting that N917-P927 plays a role in the stability and orientation of MtrD within the membrane. Destabilization of the protein-lipid interface of MtrD upon deletion of N917-P927 supports the hypothesis that this region plays a key role in stabilizing MtrD within the membrane.

Simulations of the 11G(917-927) MtrD mutant show the 11G(917-927) region protruded above the membrane into the periplasm in the A and B protomers (see Fig. S3D and E). In the E protomer, 917-927Gly lay at the periplasmic membrane interface (see Fig. S3F). Consistent with the mutation to glycine, there was a loss of α-helical secondary structure in 11G(917-927) (Fig. 4D) across all three protomers. There was also a noticeable tilting of the 11G(917-927) MtrD mutant within the membrane during the 500-ns replicate MD simulations (Fig. 4C), again indicating a destabilization in the protein-lipid MtrD interface, as was seen in the Δ(N917-P927) mutant. The overall changes in the localization and stability of N917-P927 between the MtrD mutants may underpin the limited activity of the transporter seen in the MIC analyses.

Deletion of the N917-P927 region alters progesterone uptake. To investigate interaction of the Δ(N917-P927) MtrD mutant with substrates, spontaneous binding simulations were performed with the substrate progesterone. To increase the likelihood of observing spontaneous substrate binding, simulations were performed with the symmetric MtrD crystal structure (PDB ID 4MT1), containing all three protomers in the A conformation, using the same protocol as previously described (23, 38). Here, 30 molecules of progesterone were randomly placed in the solution surrounding the Δ(N917-P927) MtrD porter and docking domains and triplicate 200-ns MD simulations were performed. As observed in our previous simulations (38), progesterone adsorbed nonspecifically to the protein and membrane. In two of the three simulations, multiple molecules of progesterone entered the binding cleft in the region that would have been occupied by N917-P927 (Fig. 6) and bound to the proximal binding site. In both simulations, an initial progesterone molecule first entered the binding cleft and moved into the proximal binding site before a second progesterone molecule entered the binding cleft and formed stacking interactions with the first progesterone in the proximal binding site. No closure of the binding pocket was observed in the time frame of the simulation. We postulate that deletion of N917-P927 dysregulates the access of substrate to the MtrD binding cleft and the closure of the substrate binding pocket during the transport cycle.

DISCUSSION

In this study, we outline important features concerning multidrug export and resistance by the MtrD protein of *N. gonorrhoeae* involving the unique N917-P927 region. MtrD belongs to the RND superfamily of transport proteins, which in Gram-negative bacteria form one of the first line defense mechanisms against toxic chemicals, including antibiotics and host-derived antimicrobials. It has been shown that upregulation of MtrD, in synergy with other mechanisms of resistance, can result in highly drug-resistant strains of *N. gonorrhoeae* such as H041 and FC428 (35, 43, 44). One of the most interesting findings of this study is that the TMS 9 N917-P927 sequence is a unique dynamic region of MtrD that interacts with the membrane-periplasm interface and modulates drug access to the transporter during a functional cycle. Functional analysis of a set of MtrD mutants demonstrated that the N917-P927 region is essential for functional efflux and drug resistance capacity. In addition, MD simulations identified that

Downloaded from https://journals.asm.org/journal/mbio on 18 March 2023 by 2001:8004:1680:11a3:f9e6:f3ee:ff34:a3ba.

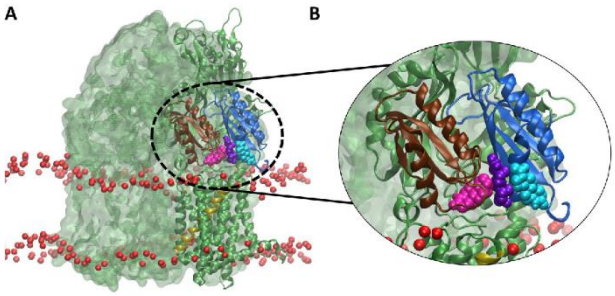

FIG 6 MD simulations of progesterone flooding of the Δ(N917-P927) mutant of MtrD (PDB ID 4MT1). Phosphate groups of the *N. gonorrhoeae* phospholipid inner membrane are shown as red beads. All three MtrD protomers are green, and TMS 9 is gold. The binding cleft of the PC1 domain is dark blue and the PC2 domain is brown. Three progesterone molecules (magenta, violet, and cyan) within the binding cleft entrance are shown in VDW representation. (A) Representative view showing multiple progesterone molecules in the MtrD binding cleft after 250 ns of the Δ(N917-P927) progesterone flooding simulation. (B) Magnification of the clustered progesterone molecules within the MtrD binding cleft.

this region may contribute to the positioning of the TMS 9 helix and stabilization of the protein within the neisserial IM, further facilitating efficient substrate capture.

Like AcrB, the MtrD substrate range is extremely broad and includes cationic, neutral, and anionic compounds (7, 45). Presence of a hydrophobic domain on the molecule or hydrophobicity *per se* seems to be a common feature of MtrD substrates (7, 45, 46) and suggests that they interact with the IM-periplasm interface before they are captured and exported by MtrD (45). Supporting this, RND transporters of the HAE1 family have been suggested to capture amphiphilic substrate molecules from the outer leaflet of the cytoplasmic membrane or from the membrane-periplasm interface (45, 47). Indeed, the recent MtrD crystal structures (PDB ID 6VKS and 6VKT) revealed two entrances; one from a periplasmic cleft and a second that opens to the outer leaflet of IM, both of which have been proposed as routes for hydrophobic substrate capture (24). The periplasmic end of the TMS 9 helix, including its N917-P927 region extension, is located at the membrane-periplasm boundary, such that mutations in this region are expected to impact on protein-lipid interactions in this area. As expected, MD simulations showed that deletion of the extension (ΔN917-P927) and replacement with a string of glycines [11G(917-927)] in MtrD resulted in destabilization of the protein-lipid interface and altered the positioning of MtrD within the membrane, supporting the hypothesis that this region plays a key role in stabilizing MtrD within the membrane. In addition, disturbances in the protein-lipid interface could also influence interactions with MtrD substrates at the membrane-periplasm interface and substrate capture via the IM entrance. This was supported by the reduced resistance to multiple substrates of *N. gonorrhoeae* cells expressing the Δ(N917-P927) MtrD mutant compared to the WT parent (Table 1). Furthermore, MD simulations of this deletion mutant with the substrate progesterone revealed that destabilization of the protein-lipid interface in the region of TMS 9 possibly impacts on substrate access to the binding cleft.

MtrD-mediated resistance to 10 selected substrates was significantly reduced by mutations to N917, G924, and P927. Their altered resistance profile could be attributed to changes in the position and relative orientation of the TMS 9 helix extension (N917-P927) during a transport cycle, since MD simulations of WT MtrD showed that the position and relative orientation of N917-P927 varies in the three protomers and involves interactions between N917, G924, and P927 with amino acids in the periplasmic domain. These variations would explain how access of hydrophobic substrates to the binding cleft entrance could be facilitated in the access protomer but efficiently prevented in the binding and extrusion protomers during a functional cycle.

In MD simulations of the N917C/G924C/P927C MtrD variant, both the position and the orientation of N917-P927 in each protomer fluctuated. In these simulations the

Downloaded from https://journals.asm.org/journal/mbio on 18 March 2023 by 2001:8004:1680:11a3:f9e6:f3ee:f034:a3ba.

interaction between N917-P927 and rest of the protein was most altered in the A protomer. Here, the N917-P927 region partially occluded the periplasmic substrate entrance to the binding cleft indicating that N917, G924, and P927 play a key role in substrate entry. It appears that reduced resistance capacity (Table 1) of the individual cysteine mutants (N917C, G924C, and P927C) is a result of altered interactions of these residues with rest of the protein impacting on correct positioning and orientation of N917-P927 in the membrane of *N. gonorrhoeae*, thereby limiting substrate access to MtrD. The first 50-ns simulations of WT MtrD revealed these important interactions. Mutations of N917, demonstrated that a positively charged polar amino acid was not tolerated in this position, since cells expressing the MtrD N917K mutant conferred resistance levels for compounds at levels only comparable to the negative control. Further analysis of the N917 asparagine side-chain demonstrated that neither glutamine nor serine (two polar noncharged residues) could compensate for asparagine, indicating that key features of asparagine are required for this position. Analysis of the residue requirement at position 927 showed that a glycine replacement in the P927G MtrD mutant still produced a fully functional protein. This supports the notion that the proline at 927 plays a structural role linked to MtrD stabilization in the IM and substrate capture from the IM-periplasm interface.

A comprehensive understanding of RND efflux pumps, which are a major contributor of antimicrobial resistance in Gram-negative bacteria, is central for combating bacterial infections, including those caused by multidrug-resistant strains of *N. gonorrhoeae*. Extensive genetic, biochemical, biophysical, and computational studies have hugely advanced our knowledge of efflux transporter systems and proteins, including the MtrCDE system of *N. gonorrhoeae*. A large body of knowledge already available with respect to the genetic aspects of the *mtrCDE* system (18), as well as the availability of crystal and cryo-EM structures of the MtrD protein in apo form (23) and in complex with drugs (24), has provided insights regarding the mechanisms used by this efflux pump to confer resistance against important antibiotics and other antimicrobials. Limited new antibiotics with activity against multidrug-resistant strains of Gram-negative pathogens have been discovered in the past 2 decades, even though they are desperately needed as this important public health problem continues to grow. Characterization of the structural and functional role of the unique N917-P927 region which connects TMS 9 and TMS 10 of MtrD provides insights concerning multidrug resistance afforded by this efflux pump. Moreover, it has revealed that subtle differences between RND transporters may have implications for drug efflux mechanisms and as such is important knowledge required to rationally design effective antibiotics or efflux pump inhibitors.

MATERIALS AND METHODS

Bacterial strains, plasmids, and growth conditions. The bacterial strains and plasmids used in this study are listed in Table 2. The background *N. gonorrhoeae* strain is based on a FA19 derivative, KH15 that overexpresses the MtrCDE complex due to a single-base-pair deletion in the promoter of the *mtrR* gene, whose product, the MtrR protein, negatively controls expression of the *mtrCDE* operon (8, 18). KH15Δ*mtrD*Δ*norM* is a derivative of KH15 (8) with the *mtrD* and *norM* genes removed and is a highly discriminating strain for antimicrobial resistance assays (38). pGCC4-CL-$mtrD_{His6}$ is a cysteine-less variant of *mtrD* (MtrD C491A) encoding a 6-histidine affinity tag at the C terminus (38). This fully functional *mtrD* derivative was used as a template for generating and mobilizing *mtrD* mutants into *N. gonorrhoeae*. Gonococci were grown on GC medium (Difco Laboratories, Detroit, MI) containing Kellogg's supplements I and II (48) at 37°C under 5% CO_2 or in GC broth (Difco Laboratories) containing Kellogg's supplements I and II and 0.048% (vol/vol) sodium bicarbonate at 37°C with shaking. *E. coli* DH5α (Invitrogen, Thermo Fisher Scientific Australia Pty, Ltd.) was used for propagation of all plasmid constructs and strains were grown on Luria-Bertani (LB) agar or in LB broth (Oxoid, Thermo Fisher Scientific Australia Pty, Ltd.). Antibiotics were added at the following concentrations: kanamycin at 40 μg/ml and erythromycin at 0.5 μg/ml. Isopropyl-β-D-thiogalactopyranoside (IPTG) at a final concentration of 0.5 mM was used to induce *mtrD* transcription in *N. gonorrhoeae* strains harboring pGCC4 vector constructs (39). Chemicals and antibiotics, if not specified, were from Sigma Chemicals (Sigma-Aldrich Pty, Ltd.).

Molecular biology methods. Plasmid DNA was isolated from *E. coli* cells using a Bioline Isolate II plasmid minikit (Bioline Meridian Bioscience, USA). Chromosomal DNA was isolated from *N. gonorrhoeae* cells by the use of a Wizard genomic DNA purification kit (Promega Co., USA). Primers used in this study are listed in Table S1 and were synthesized by Integrated DNA Technologies or Sigma-Aldrich. Bioline Velocity DNA polymerase was used in all PCR mutagenesis reactions and Bioline Mango*Taq* DNA polymerase for

Downloaded from https://journals.asm.org/journal/mbio on 18 March 2023 by 2001:8004:1680:11a3:f9e6:f3ee:ff34:a3ba.

TABLE 2 Bacterial strains and plasmids used in this study

Strain or plasmid	Relevant genotypes or description	Source or reference
Strains		
E. coli		
DH5α	*fhuA2* Δ(*argF-lacZ*)*U169 phoA glnV44* ϕ80 Δ(*lacZ*)M15 *gyrA96 recA1 relA1 endA1 thi-1 hsdR17*	65
N. gonorrhoeae		
KH15Δ*mtrD*Δ*norM*	KH15 is a derivative of the antibiotic-sensitive strain FA19 with a 1-bp deletion in the *mtrR* promoter with consequential *mtrCDE* upregulation and increased antibiotic resistance; has *mtrD* and *norM* genes inactivated	8, 38
Plasmids		
pGCC4	*Neisseria* insertion complementation system (NICS) vector; *lacI*, P_{lacI}; Kan^r Ery^r	39
pGCC4-CL*mtrD*$_{His6}$	Cysteine-less derivative of *mtrD*$_{His6}$ in pGCC4	38
N917C	N917C MtrD mutant based in pGCC4-CL*mtrD*$_{His6}$	This study
L918C	L918C MtrD mutant based in pGCC4-CL*mtrD*$_{His6}$	This study
F919C	F919C MtrD mutant based in pGCC4-CL*mtrD*$_{His6}$	This study
E920C	E920C MtrD mutant based in pGCC4-CL*mtrD*$_{His6}$	This study
G921C	G921C MtrD mutant based in pGCC4-CL*mtrD*$_{His6}$	This study
L922C	L922C MtrD mutant based in pGCC4-CL*mtrD*$_{His6}$	This study
L923C	L923C MtrD mutant based in pGCC4-CL*mtrD*$_{His6}$	This study
G924C	G924C MtrD mutant based in pGCC4-CL*mtrD*$_{His6}$	This study
S925C	S925C MtrD mutant based in pGCC4-CL*mtrD*$_{His6}$	This study
V926C	V926C MtrD mutant based in pGCC4-CL*mtrD*$_{His6}$	This study
P927C	P927C MtrD mutant based in pGCC4-CL*mtrD*$_{His6}$	This study
Δ(N917-P927)	917-927 deletion MtrD mutant based in pGCC4-CL*mtrD*$_{His6}$	This study
11A(917-927)	11Ala(917-927) insertion MtrD mutant based in pGCC4-CL*mtrD*$_{His6}$	This study
11G(917-927)	11Gly(917-927) insertion MtrD mutant based in pGCC4-CL*mtrD*$_{His6}$	This study
N917Q	N917Q MtrD mutant based in pGCC4-CL*mtrD*$_{His6}$	This study
N917S	N917S MtrD mutant based in pGCC4-CL*mtrD*$_{His6}$	This study
N917K	N917K MtrD mutant based in pGCC4-CL*mtrD*$_{His6}$	This study
P927G	P927G MtrD mutant based in pGCC4-CL*mtrD*$_{His6}$	This study

screening PCRs (Bioline, Boston, MA). All restriction digestion enzymes were from New England Biolabs (New England Biolabs, Inc., Ipswich, MA). Transformations into *N. gonorrhoeae* or *E. coli* cells were carried as described previously (38, 49). All sequencing was performed by the Australian Genome Research Facility.

Site-directed mutagenesis. The QuikChange site-directed mutagenesis method was used to construct *mtrD* mutants in the pGCC4-CL-*mtrD*$_{His6}$ plasmid using the primers listed in Table S1. To aid in screening, a silent restriction site was incorporated into each primer pair where possible (38). Integrity of *mtrD* constructs were verified by sequencing the whole insert and then recombined into the FA19 KH15Δ*mtrD*Δ*norM* chromosome (38). *N. gonorrhoeae* mutants were assessed for mutant MtrD protein production and their resistance profile.

Western blot analyses. Expression of MtrD mutant proteins in *N. gonorrhoeae* KH15Δ*mtrD*Δ*norM* membranes was determined by Western blotting as previously described, using anti-6×Histidine epitope tag (rabbit) antibody, and peroxidase-conjugated anti-rabbit IgG (goat) (Rockland antibodies and assays) as primary and secondary antibodies, respectively (38). Mutant protein expression levels were expressed as a percentage of the wild-type protein.

MIC analyses. Resistance profiles of the *N. gonorrhoeae* KH15Δ*mtrD*Δ*norM* strain expressing the MtrD mutants were determined by MIC analyses to a selected panel of 10 compounds using standard agar dilution method (38, 50) with modifications. MIC analyses were conducted using solid GC medium supplemented with 0.5 mM IPTG and increasing concentrations of antimicrobials (Table 1). The MIC was determined as the lowest concentration of the antimicrobial compound required to fully inhibit bacterial growth and was repeated at least three times.

MD simulations. The ampicillin-bound MtrD cryo-EM structure (PDB ID 6VKS) was used for the WT and mutant MtrD MD simulations (23). Ampicillin was removed prior to simulations. WT and mutant MtrD simulations were carried out on four protein models: WT, Δ(N917-P927), 11G(917-927), and a triple-cysteine-replacement mutant, with concurrent mutation of residues N917, G924, and P927 (N917C/G924C/P927C). All proline residues were assigned a *trans* isomerization, consistent with the conformation observed in the cryo-EM structures. Protein mutants were generated using the PyMOL Mutagenesis Wizard and SWISS-MODEL (51). All simulations were performed using GROMACS2019.4 (52, 53) and the united-atom GROMOS 54a7 force-field (54). The MtrD protein for each system was embedded in a neisserial IM model, consisting of a 4:1 ratio of 1-palmitoyl-2-palmitoleoyl-*sn*-glycero-3-phosphatidylethanolamine (PPoPE) and 1,2-dimyristoyl-*sn*-glycero-3-phosphatidylglycerol (DMPG). Systems were oriented in the *x-y* plane of an 18-nm × 18-nm × 19-nm box, solvated with the simple-point-charge water model (55), and charge neutralized with a physiological concentration of 150 mM NaCl. GROMOS parameters for PPoPE and DMPG were obtained from previously published membrane models (56), while

Downloaded from https://journals.asm.org/journal/mbio on 18 March 2023 by 2001:8004:1680:11a3:f9e6:f3ee:ff34:a3ba.

the parameters for ampicillin (Molid: 574595) were obtained from the Automated Topology Builder and Repository (ATB) (57, 58).

All systems were energy minimized using the steepest descent algorithm. Systems were equilibrated in a series of six sequential 2-ns simulations with progressively decreasing position restraints on the protein backbone atoms (force constants of 1,000, 500, 100, 50, 10, and 0 kJ mol $^{-1}$ nm $^{-2}$). The coordinates from the final equilibration frame were used as the starting coordinates for unrestrained production simulations performed in triplicate for each system. Production simulations were 500 ns for each system.

Simulations were performed using the NPT ensemble, with solute (protein/membrane) and solvent (ions/water) separately coupled to an external temperature bath of 310K. Temperature was held constant with a Bussi thermostat (τ_T = 0.1 ps) (59). Pressure was maintained via semi-isotropic pressure coupling to an external pressure bath at 100,000 Pa. The Berendsen barostat was used for equilibration simulations (τ_p = 0.5 ps and isothermal compressibility = 4.5×10^{-10} Pa $^{-1}$) (60). Production simulations employed the Parrinello-Rahman barostat (τ_p = 5 ps and isothermal compressibility = 4.5×10^{-10} Pa $^{-1}$) (61). Noncovalent interactions were determined via the Verlet scheme with a 1.4-nm cutoff (62). Electrostatic interactions were calculated using Particle Mesh Ewald (63), and covalent bonds were constrained using the LINCS algorithm (64).

Progesterone flooding simulations were conducted using the symmetric apo MtrD crystal structure (PDB 4MT1) (23). Flooding simulations were carried out as previously described (28), though with the protein being changed to a Δ(N917-P927) mutant of the symmetric crystal structure generated using SWISS-MODEL (51).

SUPPLEMENTAL MATERIAL

Supplemental material is available online only.

TABLE S1, DOCX file, 0.1 MB.

FIG S1, TIF file, 0.8 MB.

FIG S2, TIF file, 2.1 MB.

FIG S3, TIF file, 2.1 MB.

ACKNOWLEDGMENTS

This study was supported by a Flinders Medical Research Foundation Grant and was undertaken using resources from the National Computational Infrastructure (NCI), which is supported by the Australian Government. M.C. was supported by an Australian Government Research Training Program Scholarship.

REFERENCES

1. Wi T, Lahra MM, Ndowa F, Bala M, Dillon J-AR, Ramon-Pardo P, Eremin SR, Bolan G, Unemo M. 2017. Antimicrobial resistance in *Neisseria gonorrhoeae*: global surveillance and a call for international collaborative action. PLoS Med 14:e1002344. https://doi.org/10.1371/journal.pmed.1002344.
2. Lahra MM, Martin I, Demczuk W, Jennison AV, Lee K-I, Nakayama S-I, Lefebvre B, Longtin J, Ward A, Mulvey MR. 2018. Cooperative recognition of internationally disseminated ceftriaxone-resistant *Neisseria gonorrhoeae* strain. Emerg Infect Dis 24:735–740.
3. Shafer WM, Folster JP, Nicholas RA. 2010. Molecular mechanisms of antibiotic resistance expressed by the pathogenic *Neisseria*, p 245–267. *In* Genco CA, Wetzler L (ed), Neisseria: molecular mechanisms of pathogenesis. Caister Academic Press, Norfolk, UK.
4. Shafer WM, Yu EW, Rouquette-Loughlin C, Golparian D, Jerse AE, Unemo M. 2016. Efflux pumps in *Neisseria gonorrhoeae*: contributions to antimicrobial resistance and virulence, p 439–470. *In* Li X-Z, Elkins CA, Zgurskaya HI (ed), Efflux-mediated antimicrobial resistance in bacteria: mechanisms, regulation and clinical implications. Springer International Publishing, Cham, Switzerland. https://doi.org/10.1007/978-3-319-39658-3.
5. Prakash S, Cooper G, Singhi S, Saier MH, Jr. 2003. The ion transporter superfamily. Biochim Biophys Acta 1618:79–92. https://doi.org/10.1016/j.bbamem.2003.10.010.
6. Su C-C, Bolla JR, Kumar N, Radhakrishnan A, Long F, Delmar JA, Chou T-H, Rajashankar KR, Shafer WM, Yu EW. 2015. Structure and function of *Neisseria gonorrhoeae* MtrF illuminates a class of antimetabolite efflux pumps. Cell Rep 11:61–70. https://doi.org/10.1016/j.celrep.2015.03.003.
7. Hagman KE, Lucas CE, Balthazar JT, Snyder L, Nilles M, Judd RC, Shafer WM. 1997. The MtrD protein of *Neisseria gonorrhoeae* is a member of the resistance nodulation division protein family constituting part of an efflux system. Microbiology (Reading) 143(Pt 7):2117–2125. https://doi.org/10.1099/00221287-143-7-2117.
8. Hagman KE, Pan W, Spratt BG, Balthazar JT, Judd RC, Shafer WM. 1995. Resistance of *Neisseria gonorrhoeae* to antimicrobial hydrophobic agents is modulated by the *mtrRCDE* efflux system. Microbiology (Reading) 141(Pt 3):611–622. https://doi.org/10.1099/13500872-141-3-611.
9. Warner DM, Shafer WM, Jerse AE. 2008. Clinically relevant mutations that cause derepression of the *Neisseria gonorrhoeae* MtrC-MtrD-MtrE Efflux pump system confer different levels of antimicrobial resistance and *in vivo* fitness. Mol Microbiol 70:462–478. https://doi.org/10.1111/j.1365-2958.2008.06424.x.
10. Maness MJ, Sparling PF. 1973. Multiple antibiotic resistance due to a single mutation in *Neisseria gonorrhoeae*. J Infect Dis 128:321–330. https://doi.org/10.1093/infdis/128.3.321.
11. Beggs GA, Zalucki YM, Brown NG, Rastegari S, Phillips RK, Palzkill T, Shafer WM, Kumaraswami M, Brennan RG. 2019. Structural, biochemical, and *in vivo* characterization of MtrR-mediated resistance to innate antimicrobials by the human pathogen *Neisseria gonorrhoeae*. J Bacteriol 201:e00401-19. https://doi.org/10.1128/JB.00401-19.
12. Hoffmann KM, Williams D, Shafer WM, Brennan RG. 2005. Characterization of the multiple transferable resistance repressor, MtrR, from *Neisseria gonorrhoeae*. J Bacteriol 187:5008–5012. https://doi.org/10.1128/JB.187.14.5008-5012.2005.
13. Shafer WM, Balthazar JT, Hagman KE, Morse SA. 1995. Missense mutations that alter the DNA-binding domain of the MtrR protein occur frequently in rectal isolates of *Neisseria gonorrhoeae* that are resistant to faecal lipids. Microbiology (Reading) 141(Pt 4):907–911. https://doi.org/10.1099/13500872-141-4-907.
14. Zarantonelli L, Borthagaray G, Lee E-H, Shafer WM. 1999. Decreased azithromycin susceptibility of *Neisseria gonorrhoeae* due to *mtrR* mutations. Antimicrob Agents Chemother 43:2468–2472. https://doi.org/10.1128/AAC.43.10.2468.
15. Xia M, Whittington WL, Shafer WM, Holmes KK. 2000. Gonorrhea among men who have sex with men: outbreak caused by a single genotype of

Downloaded from https://journals.asm.org/journal/mbio on 18 March 2023 by 2001:8004:1680:11a3:f9e6:f3ee:ff34:a3ba.

erythromycin-resistant *Neisseria gonorrhoeae* with a single-base-pair deletion in the *mtrR* promoter region. J Infect Dis 181:2080–2082. https://doi.org/10.1086/315510.
16. Cousin SL, Jr, Whittington WLH, Roberts MC. 2003. Acquired resistance genes and the 1-bp deletion in the *mtrR* promoter in *Neisseria gonorrhoeae*. J Antimicrob Chemother 51:131–133. https://doi.org/10.1093/jac/dkg040.
17. Lindberg R, Fredlund H, Nicholas R, Unemo M. 2007. *Neisseria gonorrhoeae* isolates with reduced susceptibility to cefixime and ceftriaxone: association with genetic polymorphisms in *penA*, *mtrR*, *porB1b*, and *ponA*. Antimicrob Agents Chemother 51:2117–2122. https://doi.org/10.1128/AAC.01604-06.
18. Beggs GA, Ayala JC, Kavanaugh LG, Read TD, Hooks GM, Schumacher MA, Shafer WM, Brennan RG. 2021. Structures of *Neisseria gonorrhoeae* MtrR-operator complexes reveal molecular mechanisms of DNA recognition and antibiotic resistance-conferring clinical mutations. Nucleic Acids Res 49:4155–4170. https://doi.org/10.1093/nar/gkab213.
19. Shafer WM, Qu X, Waring AJ, Lehrer RI. 1998. Modulation of *Neisseria gonorrhoeae* susceptibility to vertebrate antibacterial peptides due to a member of the resistance/nodulation/division efflux pump family. Proc Natl Acad Sci U S A 95:1829–1833. https://doi.org/10.1073/pnas.95.4.1829.
20. Janganan TK, Bavro VN, Zhang L, Borges-Walmsley MI, Walmsley AR. 2013. Tripartite efflux pumps: energy is required for dissociation, but not assembly or opening of the outer membrane channel of the pump. Mol Microbiol 88:590–602. https://doi.org/10.1111/mmi.12211.
21. Tseng TT, Gratwick KS, Kollman J, Park D, Nies DH, Goffeau A, Saier MH, Jr. 1999. The RND permease superfamily: an ancient, ubiquitous and diverse family that includes human disease and development proteins. J Mol Microbiol Biotechnol 1:107–125.
22. Saier MH, Jr, Paulsen IT. 2001. Phylogeny of multidrug transporters. Semin Cell Dev Biol 12:205–213. https://doi.org/10.1006/scdb.2000.0246.
23. Bolla JR, Su CC, Do SV, Radhakrishnan A, Kumar N, Long F, Chou TH, Delmar JA, Lei HT, Rajashankar KR, Shafer WM, Yu EW. 2014. Crystal structure of the *Neisseria gonorrhoeae* MtrD inner membrane multidrug efflux pump. PLoS One 9:e97903. https://doi.org/10.1371/journal.pone.0097903.
24. Lyu M, Moseng MA, Reimche JL, Holley CL, Dhulipala V, Su CC, Shafer WM, Yu EW. 2020. Cryo-EM structures of a gonococcal multidrug efflux pump illuminate a mechanism of drug recognition and resistance. mBio 11:e.00996-20. https://doi.org/10.1128/mBio.00996-20.
25. Seeger MA, Schiefner A, Eicher T, Verrey F, Diederichs K, Pos KM. 2006. Structural asymmetry of AcrB trimer suggests a peristaltic pump mechanism. Science 313:1295–1298. https://doi.org/10.1126/science.1131542.
26. Sennhauser G, Amstutz P, Briand C, Storchenegger O, Grutter MG. 2007. Drug export pathway of multidrug exporter AcrB revealed by DARPin inhibitors. PLoS Biol 5:e7. https://doi.org/10.1371/journal.pbio.0050007.
27. Murakami S, Nakashima R, Yamashita E, Matsumoto T, Yamaguchi A. 2006. Crystal structures of a multidrug transporter reveal a functionally rotating mechanism. Nature 443:173–179. https://doi.org/10.1038/nature05076.
28. Fairweather SJ, Gupta V, Chitsaz M, Booth L, Brown MH, O'Mara ML. 2021. Coordination of substrate binding and protonation in the *Neisseria gonorrhoeae* MtrD efflux pump controls the functionally rotating transport mechanism. ACS Infect Dis 7:1833–1847. https://doi.org/10.1021/acsinfecdis.1c00149.
29. Nakashima R, Sakurai K, Yamasaki S, Nishino K, Yamaguchi A. 2011. Structures of the multidrug exporter AcrB reveal a proximal multisite drug-binding pocket. Nature 480:565–569. https://doi.org/10.1038/nature10641.
30. Yamaguchi A, Nakashima R, Sakurai K. 2015. Structural basis of RND-type multidrug exporters. Front Microbiol 6:327. https://doi.org/10.3389/fmicb.2015.00327.
31. Eicher T, Cha HJ, Seeger MA, Brandstatter L, El-Delik J, Bohnert JA, Kern WV, Verrey F, Grutter MG, Diederichs K, Pos KM. 2012. Transport of drugs by the multidrug transporter AcrB involves an access and a deep binding pocket that are separated by a switch-loop. Proc Natl Acad Sci U S A 109:5687–5692. https://doi.org/10.1073/pnas.1114944109.
32. Vargiu AV, Nikaido H. 2012. Multidrug binding properties of the AcrB efflux pump characterized by molecular dynamics simulations. Proc Natl Acad Sci U S A 109:20637–20642. https://doi.org/10.1073/pnas.1218348109.
33. Sennhauser G, Bukowska MA, Briand C, Grutter MG. 2009. Crystal structure of the multidrug exporter MexB from *Pseudomonas aeruginosa*. J Mol Biol 389:134–145. https://doi.org/10.1016/j.jmb.2009.04.001.
34. Unemo M, Golparian D, Nicholas R, Ohnishi M, Gallay A, Sednaoui P. 2012. High-level cefixime-and ceftriaxone-resistant *Neisseria gonorrhoeae* in France: novel *penA* mosaic allele in a successful international clone causes treatment failure. Antimicrob Agents Chemother 56:1273–1280. https://doi.org/10.1128/AAC.05760-11.
35. Ohnishi M, Saika T, Hoshina S, Iwasaku K, Nakayama S-I, Watanabe H, Kitawaki J. 2011. Ceftriaxone-resistant *Neisseria gonorrhoeae*. Emerg Infect Dis 17:148–149. https://doi.org/10.3201/eid1701.100397.
36. Zhang Z, Schwartz S, Wagner L, Miller W. 2000. A greedy algorithm for aligning DNA sequences. J Comput Biol 7:203–214. https://doi.org/10.1089/10665270050081478.
37. Pos KM. 2009. Drug transport mechanism of the AcrB efflux pump. Biochim Biophys Acta 1794:782–793. https://doi.org/10.1016/j.bbapap.2008.12.015.
38. Chitsaz M, Booth L, Blyth MT, O'Mara ML, Brown MH. 2019. Multidrug resistance in *Neisseria gonorrhoeae*: identification of functionally important residues in the MtrD efflux protein. mBio 10:e02277-19. https://doi.org/10.1128/mBio.02277-19.
39. Mehr IJ, Seifert HS. 1998. Differential roles of homologous recombination pathways in *Neisseria gonorrhoeae* pilin antigenic variation, DNA transformation, and DNA repair. Mol Microbiol 30:697–710. https://doi.org/10.1046/j.1365-2958.1998.01089.x.
40. Rouquette-Loughlin C, Dunham SA, Kuhn M, Balthazar JT, Shafer WM. 2003. The NorM efflux pump of *Neisseria gonorrhoeae* and *Neisseria meningitidis* recognizes antimicrobial cationic compounds. J Bacteriol 185:1101–1106. https://doi.org/10.1128/JB.185.3.1101-1106.2003.
41. Hassan KA, Robinson KL, Smith AN, Gibson JH, Skurray RA, Brown MH. 2006. Glycine-rich transmembrane helix 10 in the staphylococcal tetracycline transporter TetA(K) lines a solvent-accessible channel. Biochemistry 45:15661–15669. https://doi.org/10.1021/bi0614380.
42. Hollingsworth SA, Karplus PA. 2010. A fresh look at the Ramachandran plot and the occurrence of standard structures in proteins. Biomol Concepts 1:271–283. https://doi.org/10.1515/BMC.2010.022.
43. Nakayama S-I, Shimuta K, Furubayashi K-I, Kawahata T, Unemo M, Ohnishi M. 2016. New ceftriaxone-and multidrug-resistant *Neisseria gonorrhoeae* strain with a novel mosaic *penA* gene isolated in Japan. Antimicrob Agents Chemother 60:4339–4341. https://doi.org/10.1128/AAC.00504-16.
44. Golparian D, Rose L, Lynam A, Mohamed A, Bercot B, Ohnishi M, Crowley B, Unemo M. 2018. Multidrug-resistant *Neisseria gonorrhoeae* isolate, belonging to the internationally spreading Japanese FC428 clone, with ceftriaxone resistance and intermediate resistance to azithromycin, Ireland, August 2018. Euro Surveill 23. https://doi.org/10.2807/1560-7917.ES.2018.23.47.1800617.
45. Nikaido H. 1996. Multidrug efflux pumps of gram-negative bacteria. J Bacteriol 178:5853–5859. https://doi.org/10.1128/jb.178.20.5853-5859.1996.
46. Nikaido H, Basina M, Nguyen V, Rosenberg EY. 1998. Multidrug efflux pump AcrAB of *Salmonella* Typhimurium excretes only those β-lactam antibiotics containing lipophilic side chains. J Bacteriol 180:4686–4692. https://doi.org/10.1128/JB.180.17.4686-4692.1998.
47. Yao X-Q, Kimura N, Murakami S, Takada S. 2013. Drug uptake pathways of multidrug transporter AcrB studied by molecular simulations and site-directed mutagenesis experiments. J Am Chem Soc 135:7474–7485. https://doi.org/10.1021/ja310548h.
48. Kellogg DS, Jr, Peacock WL, Jr, Deacon WE, Brown L, Pirkle DI. 1963. *Neisseria gonorrhoeae*. I. Virulence genetically linked to clonal variation. J Bacteriol 85:1274–1279. https://doi.org/10.1128/jb.85.6.1274-1279.1963.
49. Dillard JP. 2011. Genetic manipulation of *Neisseria gonorrhoeae*. Curr Protoc Microbiol Chapter 4:Unit4A 2. https://doi.org/10.1002/9780471729259.mc04a02s23.
50. CLSI. 2012. Methods for dilution antimicrobial susceptibility tests for bacteria that grow aerobically: approved standard, 9th ed, vol 32. Clinical and Laboratory Standards Institute, Wayne, PA.
51. Waterhouse A, Bertoni M, Bienert S, Studer G, Tauriello G, Gumienny R, Heer FT, de Beer TAP, Rempfer C, Bordoli L, Lepore R, Schwede T. 2018. SWISS-MODEL: homology modeling of protein structures and complexes. Nucleic Acids Res 46:W296–W303. https://doi.org/10.1093/nar/gky427.
52. Lindahl E, Abraham M, Hess B, van der Spoel D. 2019. GROMACS 2019.4 source code. https://zenodo.org/record/3460414.
53. Abraham MJ, Murtola T, Schulz R, Páll S, Smith JC, Hess B, Lindahl E. 2015. GROMACS: high performance molecular simulations through multi-level parallelism from laptops to supercomputers. SoftwareX 1–2:19–25. https://doi.org/10.1016/j.softx.2015.06.001.
54. Schmid N, Eichenberger AP, Choutko A, Riniker S, Winger M, Mark AE, van Gunsteren WF. 2011. Definition and testing of the GROMOS force-field versions 54A7 and 54B7. Eur Biophys J 40:843–856. https://doi.org/10.1007/s00249-011-0700-9.

Downloaded from https://journals.asm.org/journal/mbio on 18 March 2023 by 2001:8004:1680:11a3:f9e6:f3ee:ff34:a3ba.

55. Berendsen HJ, Postma JP, van Gunsteren WF, Hermans J. 1981. Interaction models for water in relation to protein hydration, p 331–342. *In* Intermolecular forces. Springer, New York, NY.
56. Piggot TJ, Holdbrook DA, Khalid S. 2011. Electroporation of the *E. coli* and *S. aureus* membranes: molecular dynamics simulations of complex bacterial membranes. J Phys Chem B 115:13381–13388. https://doi.org/10.1021/jp207013v.
57. Malde AK, Zuo L, Breeze M, Stroet M, Poger D, Nair PC, Oostenbrink C, Mark AE. 2011. An automated force field topology builder (ATB) and repository: version 1.0. J Chem Theory Comput 7:4026–4037. https://doi.org/10.1021/ct200196m.
58. Koziara KB, Stroet M, Malde AK, Mark AE. 2014. Testing and validation of the Automated Topology Builder (ATB) version 2.0: prediction of hydration free enthalpies. J Comput Aided Mol Des 28:221–233. https://doi.org/10.1007/s10822-014-9713-7.
59. Bussi G, Donadio D, Parrinello M. 2007. Canonical sampling through velocity rescaling. J Chem Phys 126:014101. https://doi.org/10.1063/1.2408420.
60. Berendsen HJ, Postma J, van Gunsteren WF, DiNola A, Haak JR. 1984. Molecular dynamics with coupling to an external bath. J Chem Phys 81:3684–3690. https://doi.org/10.1063/1.448118.
61. Parrinello M, Rahman A. 1981. Polymorphic transitions in single crystals: a new molecular dynamics method. J Appl Phys 52:7182–7190. https://doi.org/10.1063/1.328693.
62. De Jong DH, Baoukina S, Ingólfsson HI, Marrink SJ. 2016. Martini straight: boosting performance using a shorter cutoff and GPUs. Comput Phys Commun 199:1–7. https://doi.org/10.1016/j.cpc.2015.09.014.
63. Darden T, York D, Pedersen L. 1993. Particle mesh Ewald: an N · log (N) method for Ewald sums in large systems. J Chem Phys 98:10089–10092. https://doi.org/10.1063/1.464397.
64. Hess B, Bekker H, Berendsen HJ, Fraaije JG. 1997. LINCS: a linear constraint solver for molecular simulations. J Comput Chem 18:1463–1472. https://doi.org/10.1002/(SICI)1096-987X(199709)18:12<1463::AID-JCC4>3.0.CO;2-H.
65. Hanahan D. 1983. Studies on transformation of *Escherichia coli* with plasmids. J Mol Biol 166:557–580. https://doi.org/10.1016/s0022-2836(83)80284-8.
66. Saier MH, Tran CV, Barabote RD. 2006. TCDB: the Transporter Classification Database for membrane transport protein analyses and information. Nucleic Acids Res 34:D181–D186. https://doi.org/10.1093/nar/gkj001.
67. Saier M. 20052020. Transporter classification database. http://www.tcdb.org/. Accessed 22 December 2020.

Downloaded from https://journals.asm.org/journal/mbio on 18 March 2023 by 2001:8004:1680:11a3:f9e6:f3ee:ff34:a3ba.

REFERENCES

Aas, F. E., Wolfgang, M., Frye, S., Dunham, S., Løvold, C. & Koomey, M. (2002). Competence for natural transformation in *Neisseria gonorrhoeae*: components of DNA binding and uptake linked to type IV pilus expression. *Molecular Microbiology,* 46**,** 749-60.

Ababou, A. & Koronakis, V. (2016). Structures of gate loop variants of the AcrB drug efflux pump bound by erythromycin substrate. *PLoS One,* 11**,** e0159154.

Abdali, N., Parks, J. M., Haynes, K. M., Chaney, J. L., Green, A. T., Wolloscheck, D., Walker, J. K., Rybenkov, V. V., Baudry, J., Smith, J. C. & Zgurskaya, H. I. (2017). Reviving antibiotics: efflux pump inhibitors that interact with AcrA, a membrane fusion protein of the AcrAB-TolC multidrug efflux pump. *ACS Infectious Diseases,* 3**,** 89-98.

Abraham, M. J., Murtola, T., Schulz, R., Páll, S., Smith, J. C., Hess, B. & Lindahl, E. (2015). GROMACS: High performance molecular simulations through multi-level parallelism from laptops to supercomputers. *SoftwareX,* 1-2**,** 19-25.

Abramson, J., Smirnova, I., Kasho, V., Verner, G., Iwata, S. & Kaback, H. R. (2003a). The lactose permease of *Escherichia coli*: overall structure, the sugar-binding site and the alternating access model for transport. *FEBS Letters,* 555**,** 96-101.

Abramson, J., Smirnova, I., Kasho, V., Verner, G., Kaback, H. R. & Iwata, S. (2003b). Structure and mechanism of the lactose permease of *Escherichia coli*. *Science,* 301**,** 610-5.

Adeolu, M. & Gupta, R. S. (2013). Phylogenomics and molecular signatures for the order *Neisseriales*: proposal for division of the order *Neisseriales* into the emended family *Neisseriaceae* and *Chromobacteriaceae* fam. nov. *Antonie Van Leeuwenhoek,* 104**,** 1-24.

Aires, J. R., Kohler, T., Nikaido, H. & Plesiat, P. (1999). Involvement of an active efflux system in the natural resistance of *Pseudomonas aeruginosa* to aminoglycosides. *Antimicrobial Agents and Chemotherapy,* 43**,** 2624-8.

Aires, J. R. & Nikaido, H. (2005). Aminoglycosides are captured from both periplasm and cytoplasm by the AcrD multidrug efflux transporter of *Escherichia coli*. *Journal of Bacteriology,* 187**,** 1923-9.

Akama, H., Kanemaki, M., Yoshimura, M., Tsukihara, T., Kashiwagi, T., Yoneyama, H., Narita, S., Nakagawa, A. & Nakae, T. (2004a). Crystal structure of the drug discharge outer membrane protein, OprM, of *Pseudomonas aeruginosa*: dual modes of membrane anchoring and occluded cavity end. *Journal of Biological Chemistry,* 279**,** 52816-9.

Akama, H., Matsuura, T., Kashiwagi, S., Yoneyama, H., Narita, S., Tsukihara, T., Nakagawa, A. & Nakae, T. (2004b). Crystal structure of the membrane fusion protein, MexA, of the multidrug transporter in *Pseudomonas aeruginosa*. *Journal of Biological Chemistry,* 279**,** 25939-42.

Alav, I., Bavro, V. N. & Blair, J. M. (2022). A role for the periplasmic adaptor protein AcrA in vetting substrate access to the RND efflux transporter AcrB. *Scientific Reports,* 12**,** 4752.

Alav, I., Kobylka, J., Kuth, M. S., Pos, K. M., Picard, M., Blair, J. M. A. & Bavro, V. N. (2021). Structure, assembly, and function of tripartite efflux and Type 1 secretion systems in Gram-negative bacteria. *Chemical Reviews,* 121**,** 5479-596.

Alekshun, M. N. & Levy, S. B. (1997). Regulation of chromosomally mediated multiple antibiotic resistance: the *mar* regulon. *Antimicrobial Agents and Chemotherapy,* 41**,** 2067-75.

Alenazy, R. (2022). Drug efflux pump inhibitors: a promising approach to counter multidrug resistance in Gram-negative pathogens by targeting AcrB protein from AcrAB-TolC multidrug efflux pump from *Escherichia coli*. *Biology,* 11**,** 1328.

Alguel, Y., Meng, C., Terán, W., Krell, T., Ramos, J. L., Gallegos, M.-T. & Zhang, X. (2007). Crystal structures of multidrug binding protein TtgR in complex with antibiotics and plant antimicrobials. *Journal of Molecular Biology,* 369**,** 829-40.

Allan-Blitz, L.-T., Fifer, H. & Klausner, J. D. (2024). Managing treatment failure in *Neisseria gonorrhoeae* infection: current guidelines and future directions. *The Lancet Infectious Diseases***,** DOI: https://doi.org/10.1016/S473-3099(24)00001-X.

Alting-Mees, M. A. & Short, J. M. (1989). pBluescript II: gene mapping vectors. *Nucleic Acids Research,* 17**,** 9494.

Ammerman, L., Mertz, S. B., Park, C. & Wise, J. G. (2021). Transport dynamics of MtrD: an RND multidrug efflux pump from *Neisseria gonorrhoeae*. *Biochemistry,* 60**,** 3098-113.

Anandan, A., Evans, G. L., Condic-Jurkic, K., O'Mara, M. L., John, C. M., Phillips, N. J., Jarvis, G. A., Wills, S. S., Stubbs, K. A. & Moraes, I. (2017). Structure of a lipid A phosphoethanolamine transferase suggests how conformational changes govern substrate binding. *Proceedings of the National Academy of Sciences of the United States of America,* 114**,** 2218-23.

Andersen, C., Koronakis, E., Bokma, E., Eswaran, J., Humphreys, D., Hughes, C. & Koronakis, V. (2002a). Transition to the open state of the TolC periplasmic tunnel entrance. *Proceedings of the National Academy of Sciences of the United States of America,* 99**,** 11103-8.

Andersen, C., Koronakis, E., Hughes, C. & Koronakis, V. (2002b). An aspartate ring at the TolC tunnel entrance determines ion selectivity and presents a target for blocking by large cations. *Molecular Microbiology,* 44**,** 1131-9.

Andersen, J. L., He, G.-X., Kakarla, P., Kc, R., Kumar, S., Lakra, W. S., Mukherjee, M. M., Ranaweera, I., Shrestha, U. & Tran, T. (2015). Multidrug efflux pumps from *Enterobacteriaceae*, *Vibrio cholerae* and *Staphylococcus aureus* bacterial food pathogens. *International Journal of Environmental Research and Public Health,* 12**,** 1487-547.

Anes, J., McCusker, M. P., Fanning, S. & Martins, M. (2015). The ins and outs of RND efflux pumps in *Escherichia coli*. *Frontiers in Microbiology,* 6**,** 587.

Aron, Z. & Opperman, T. J. (2018). The hydrophobic trap—the Achilles heel of RND efflux pumps. *Research in Microbiology,* 169**,** 393-400.

Athar, M., Gervasoni, S., Catte, A., Basciu, A., Malloci, G., Ruggerone, P. & Vargiu, A. V. (2023). Tripartite efflux pumps of the RND superfamily: what did we learn from computational studies? *Microbiology,* 169.

Atzori, A., Malloci, G., Cardamone, F., Bosin, A., Vargiu, A. V. & Ruggerone, P. (2020). Molecular interactions of carbapenem antibiotics with the multidrug efflux transporter AcrB of *Escherichia coli*. *International Journal of Molecular Sciences,* 21.

Atzori, A., Malloci, G., Prajapati, J. D., Basciu, A., Bosin, A., Kleinekathöfer, U., Dreier, J., Vargiu, A. V. & Ruggerone, P. (2019). Molecular interactions of cephalosporins with the deep binding pocket of RND-transporter AcrB. *The Journal of Physical Chemistry,* 123**,** 4625-35.

Ayala, J. C., Balthazar, J. T. & Shafer, W. M. (2022). Transcriptional regulation of the *mtrCDE* efflux pump operon: importance for *Neisseria gonorrhoeae* antimicrobial resistance. *Microbiology,* 168**,** 001231.

Baarda, B. I., Zielke, R. A., Jerse, A. E. & Sikora, A. E. (2018). Lipid-modified azurin of *Neisseria gonorrhoeae* is not surface exposed and does not interact with the nitrite reductase AniA. *Frontiers in Microbiology,* 9**,** 2915.

Banhart, S., Selb, R., Oehlmann, S., Bender, J., Buder, S., Jansen, K. & Heuer, D. (2021). The mosaic *mtr* locus as major genetic determinant of azithromycin resistance of *Neisseria gonorrhoeae* -Germany, 2018. *The Journal of Infectious Diseases,* 224**,** 1398-404.

Barbagallo, M., Di Martino, M. L., Marcocci, L., Pietrangeli, P., De Carolis, E., Casalino, M., Colonna, B. & Prosseda, G. (2011). A new piece of the *Shigella* pathogenicity puzzle: spermidine accumulationby silencing of the *speG* gene. *PLoS One,* 6**,** e27226.

Barbosa, T. M. & Levy, S. B. (2000). Differential expression of over 60 chromosomal genes in *Escherichia coli* by constitutive expression of MarA. *Journal of Bacteriology,* 182**,** 3467-74.

Barlow, D. & Phillips, I. (1978). Gonorrhoea in women: diagnostic, clinical, and laboratory aspects. *The Lancet,* 311**,** 761-4.

Baugh, S., Phillips, C. R., Ekanayaka, A. S., Piddock, L. J. & Webber, M. A. (2014). Inhibition of multidrug efflux as a strategy to prevent biofilm formation. *Journal of Antimicrobial Chemotherapy,* 69**,** 673-81.

Bavro, V. N., Pietras, Z., Furnham, N., Perez-Cano, L., Fernandez-Recio, J., Pei, X. Y., Misra, R. & Luisi, B. (2008). Assembly and channel opening in a bacterial drug efflux machine. *Molecular Cell,* 30**,** 114-21.

Bay, D. C., Rommens, K. L. & Turner, R. J. (2007). Small multidrug resistance proteins: A multidrug transporter family that continues to grow. *Biochimica et Biophysica Acta,* 1778**,** 1814-38.

Bay, D. C., Stremick, C. A., Slipski, C. J. & Turner, R. J. (2017). Secondary multidrug efflux pump mutants alter *Escherichia coli* biofilm growth in the presence of cationic antimicrobial compounds. *Research in Microbiology,* 168**,** 208-21.

Bay, D. C. & Turner, R. J. (2009). Diversity and evolution of the small multidrug resistance protein family. *BMC Evolutionary Biology,* 9**,** 140.

Bay, D. C. & Turner, R. J. 2016. Small multidrug resistance efflux pumps. *In:* LI, X.-Z., ELKINS, C. A. & ZGURSKAYA, H. I. (eds.) *Efflux-mediated antimicrobial resistance in bacteria: Mechanisms, regulation and clinical implications.* Adis Cham.

Beggs, G. A., Ayala, J. C., Kavanaugh, L. G., Read, Timothy D., Hooks, Grace M., Schumacher, Maria A., Shafer, William M. & Brennan, Richard G. (2021). Structures of *Neisseria gonorrhoeae* MtrR-operator complexes reveal molecular mechanisms of DNA recognition and antibiotic resistance-conferring clinical mutations. *Nucleic Acids Research,* 49**,** 4155-70.

Beggs, G. A., Zalucki, Y. M., Brown, N. G., Rastegari, S., Phillips, R. K., Palzkill, T., Shafer, W. M., Kumaraswami, M. & Brennan, R. G. (2019). Structural, biochemical, and *in vivo* characterization of MtrR-mediated resistance to innate antimicrobials by the human pathogen *Neisseria gonorrhoeae*. *Journal of Bacteriology,* 201**,** 1-15.

Benz, R., Maier, E. & Gentschev, I. (1993). TolC of *Escherichia coli* functions as an outer membrane channel. *Zentralblatt für Bakteriologie,* 278**,** 187-96.

Berendsen, H. J., Postma, J. P., van Gunsteren, W. F. & Hermans, J. 1981. Interaction models for water in relation to protein hydration. *In:* PULLMAN, B. (ed.) *Intermolecular Forces.* New York, NY: Springer.

Berendsen, H. J., Postma, J. v., van Gunsteren, W. F., DiNola, A. & Haak, J. R. (1984). Molecular dynamics with coupling to an external bath. *The Journal of Chemical Physics,* 81**,** 3684-90.

Bharatham, N., Bhowmik, P., Aoki, M., Okada, U., Sharma, S., Yamashita, E., Shanbhag, A. P., Rajagopal, S., Thomas, T. & Sarma, M. (2021). Structure and function relationship of OqxB efflux pump from Klebsiella pneumoniae. *Nature Communications,* 12**,** 5400.

Biswas, G., Sox, T., Blackman, E. & Sparling, P. (1977). Factors affecting genetic transformation of *Neisseria gonorrhoeae*. *Journal of Bacteriology,* 129**,** 983-92.

Blair, J., Zeth, K., Bavro, V. N. & Sancho-Vaello, E. (2022). The role of bacterial transport systems in the removal of host antimicrobial peptides in Gram-negative bacteria. *FEMS Microbiology Reviews,* 46**,** 1-28.

Blankson, G., Parhi, A. K., Kaul, M., Pilch, D. S. & LaVoie, E. J. (2019). Structure-activity relationships of potentiators of the antibiotic activity of clarithromycin against *Escherichia coli*. *European Journal of Medicinal Chemistry,* 178**,** 30-8.

Blight, M. A. & Holland, I. B. (1994). Heterologous protein secretion and the versatile *Escherichia coli* haemolysin translocator. *Trends In Biotechnology,* 12**,** 450-5.

Bohnert, J. A., Schuster, S., Seeger, M. A., Fahnrich, E., Pos, K. M. & Kern, W. V. (2008). Site-directed mutagenesis reveals putative substrate binding residues in the *Escherichia coli* RND efflux pump AcrB. *Journal of Bacteriology,* 190**,** 8225-9.

Bohnert, J. A., Schuster, S., Szymaniak-Vits, M. & Kern, W. V. (2011). Determination of real-time efflux phenotypes in *Escherichia coli* AcrB binding pocket phenylalanine mutants using a 1,2'-dinaphthylamine efflux assay. *PLoS One,* 6**,** e21196.

Bohnert, J. r. A. & Kern, W. V. (2005). Selected arylpiperazines are capable of reversing multidrug resistance in *Escherichia coli* overexpressing RND efflux pumps. *Antimicrobial Agents and Chemotherapy,* 49**,** 849-52.

Bolla, J.-M., Alibert-Franco, S., Handzlik, J., Chevalier, J., Mahamoud, A., Boyer, G., Kieć-Kononowicz, K. & Pagès, J.-M. (2011). Strategies for bypassing the membrane barrier in multidrug resistant Gram-negative bacteria. *FEBS Letters,* 585**,** 1682-90.

Bolla, J. R., Howes, A. C., Fiorentino, F. & Robinson, C. V. (2020). Assembly and regulation of the chlorhexidine-specific efflux pump AceI. *Proceedings of the National Academy of Sciences,* 117**,** 17011-8.

Bolla, J. R., Su, C. C., Do, S. V., Radhakrishnan, A., Kumar, N., Long, F., Chou, T. H., Delmar, J. A., Lei, H. T., Rajashankar, K. R., Shafer, W. M. & Yu, E. W. (2014). Crystal structure of the *Neisseria gonorrhoeae* MtrD inner membrane multidrug efflux pump. *PLoS One,* 9**,** e97903.

Bornhorst, J. A. & Falke, J. J. (2000). Purification of proteins using polyhistidine affinity tags. *Methods in enzymology,* 326**,** 245-54.

Boyer, P. D. (1997). The ATP synthase—a splendid molecular machine. *Annual Review of Biochemistry,* 66**,** 717-49.

Brawley, D. N., Sauer, D. B., Li, J., Zheng, X., Koide, A., Jedhe, G. S., Suwatthee, T., Song, J., Liu, Z. & Arora, P. S. (2022). Structural basis for inhibition of the drug efflux pump NorA from *Staphylococcus aureus*. *Nature Chemical Biology,* 18**,** 706-12.

Brill, S., Sade-Falk, O., Elbaz-Alon, Y. & Schuldiner, S. (2015). Specificity determinants in small multidrug transporters. *Journal of Molecular Biology,* 427**,** 468-77.

Bro-Jorgensen, A. & Jensen, T. (1973). Gonococcal pharyngeal infections. Report of 110 cases. *British Journal of Venereal Diseases,* 49**,** 491.

Broadbent, L., Depping, P., Lodé, A., Vaitsopoulou, A., Hardy, D., Ayub, H., Mitchell-White, J., Kerr, I. D., Goddard, A. D. & Bill, R. M. 2022. Detergent-free membrane protein purification using SMA polymer. *In:* ISABELLE, M.-V. (ed.) *Methods in Molecular Biology: Heterologous Expression of Membrane Proteins.* New York, U.S.A.: Springer.

Brow, M., Pesin, R. & Sutcliffe, J. (1985). The tetracycline repressor of pSC101. *Molecular Biology and Evolution,* 2**,** 1-12.

Brown, M. H., Paulsen, I. T. & Skurray, R. A. (1999). The multidrug efflux protein *NorM* is a prototype of a new family of transporters. *Molecular Microbiology,* 31**,** 394-5.

Brown, M. H. & Skurray, R. A. (2001). Staphylococcal multidrug efflux protein QacA. *Journal of Molecular Microbiology and Biotechnology,* 3**,** 163-70.

Buckley, A. M., Webber, M. A., Cooles, S., Randall, L. P., La Ragione, R. M., Woodward, M. J. & Piddock, L. J. (2006). The AcrAB-TolC efflux system of *Salmonella enterica* serovar Typhimurium plays a role in pathogenesis. *Cellular Microbiology,* 8**,** 847-56.

Burata, O. E., Macdonald, C. B., Kermani, A. A. & Stockbridge, R. (2021). Substrate recognition of the small multidrug resistance (SMR) family. *Biophysical Journal,* 120**,** 212a.

Burata, O. E., Yeh, T. J., Macdonald, C. B. & Stockbridge, R. B. (2022). Still rocking in the structural era: A molecular overview of the small multidrug resistance (SMR) transporter family. *Journal of Biological Chemistry,* 298**,** 102482.

Burley, S. K., Bhikadiya, C., Bi, C., Bittrich, S., Chen, L., Crichlow, G. V., Christie, C. H., Dalenberg, K., Di Costanzo, L. & Duarte, J. M. (2021). RCSB Protein Data Bank: powerful new tools for exploring 3D structures of biological macromolecules for basic and applied research and education in fundamental biology, biomedicine, biotechnology, bioengineering and energy sciences. *Nucleic Acids Research,* 49**,** D437-D51.

Bussi, G., Donadio, D. & Parrinello, M. (2007). Canonical sampling through velocity rescaling. *The Journal of Chemical Physics,* 126**,** 014101.

Cacciapuoti, A., Wegener, W. & Morse, S. (1978). Cell envelope of *Neisseria gonorrhoeae*: phospholipase activity and its relationship to autolysis. *Infection and Immunity,* 20**,** 418-20.

Cacciotto, P., Basciu, A., Oliva, F., Malloci, G., Zacharias, M., Ruggerone, P. & Vargiu, A. V. (2022). Molecular rationale for the impairment of the MexAB-OprM efflux pump by a single mutation in MexA. *Computational and Structural Biotechnology Journal,* 20**,** 252-60.

Cahoon, L. A. & Seifert, H. S. (2009). An alternative DNA structure is necessary for pilin antigenic variation in *Neisseria gonorrhoeae*. *Science,* 325**,** 764-7.

Callaghan, M. M., Heilers, J.-H., van der Does, C. & Dillard, J. P. 2017. Secretion of chromosomal DNA by the *Neisseria gonorrhoeae* Type IV secretion system. *In:* BACKERT, S. & GROHMANN, E. (eds.) *Type IV secretion in Gram-negative and Gram-Positive bacteria.* Cham: Springer International Publishing.

Carbonetti, N. H., Simnad, V. I., Seifert, H. S., So, M. & Sparling, P. F. (1988). Genetics of protein I of *Neisseria gonorrhoeae*: construction of hybrid porins. *Proceedings of the National Academy of Sciences of the United States of America,* 85**,** 6841-5.

Carter, E. L., Jager, L., Gardner, L., Hall, C. C., Willis, S. & Green, J. M. (2007). *Escherichia coli abg* genes enable uptake and cleavage of the folate catabolite *p*-aminobenzoyl-glutamate. *Journal of Bacteriology,* 189**,** 3329-34.

CDC (2007). Update to CDC's sexually transmitted diseases treatment guidelines, 2006: fluoroquinolones no longer recommended for treatment of gonococcal infections. MMWR Morb. Mortal. Wkly. Rep. 56**:**332-6.

CDC (2017a). *Gonorrhoea* [Online]. Centers for Disease Control and Prevention. Available: https://www.cdc.gov/std/stats17/gonorrhea.htm [Accessed 20/10/2020].

CDC (2017b). *STDs in men who have sex with men* [Online]. Centers for Disease Control and Prevention. Available: https://www.cdc.gov/std/stats17/msm.htm [Accessed 20/10/2020].

Cehovin, A., Simpson, P. J., McDowell, M. A., Brown, D. R., Noschese, R., Pallett, M., Brady, J., Baldwin, G. S., Lea, S. M. & Matthews, S. J. (2013). Specific DNA recognition mediated by a type IV pilin. *Proceedings of the National Academy of Sciences of the United States of America,* 110**,** 3065-70.

Cha, H. J., Muller, R. T. & Pos, K. M. (2014). Switch-loop flexibility affects transport of large drugs by the promiscuous AcrB multidrug efflux transporter. *Antimicrobial Agents and Chemotherapy,* 58**,** 4767-72.

ChemDiv: The Chemistry of Cures. Available: https://www.chemdiv.com/ [Accessed 14/04/2024 2024].

Chen, A. & Seifert, H. S. (2014). Saturating mutagenesis of an essential gene: a majority of the *Neisseria gonorrhoeae* major outer membrane porin (PorB) is mutable. *Journal of Bacteriology,* 196**,** 540-7.

Chen, H., Bjerknes, M., Kumar, R. & Jay, E. (1994). Determination of the optimal aligned spacing between the Shine–Dalgarno sequence and the translation initiation codon of *Escherichia coli* mRNAs. *Nucleic Acids Research,* 22**,** 4953-7.

Chen, I. & Dubnau, D. (2004). DNA uptake during bacterial transformation. *Nature Reviews Microbiology,* 2**,** 241-9.

Chen, S.-C., Yin, Y.-P., Dai, X.-Q., Unemo, M. & Chen, X.-S. (2014). Antimicrobial resistance, genetic resistance determinants for ceftriaxone and molecular epidemiology of *Neisseria gonorrhoeae* isolates in Nanjing, China. *Journal of Antimicrobial Chemotherapy,* 69**,** 2959-65.

Chen, S., Connolly, K. L., Rouquette-Loughlin, C., D'Andrea, A., Jerse, A. E. & Shafer, W. M. (2019). Could dampening expression of the *Neisseria gonorrhoeae mtrCDE*-encoded efflux pump be a strategy to preserve currently or resurrect formerly used antibiotics to treat gonorrhea? *mBio,* 10**,** e01576-19.

Chen, Z., Yang, H. & Pavletich, N. P. (2008). Mechanism of homologous recombination from the RecA–ssDNA/dsDNA structures. *Nature,* 453**,** 489-94.

Cho, H. & Kang, H. (2012). The PseEF efflux system is a virulence factor of *Pseudomonas syringae pv. syringae*. *The Journal of Microbiology,* 50**,** 79-90.

Chorev, D. S., Baker, L. A., Wu, D., Beilsten-Edmands, V., Rouse, S. L., Zeev-Ben-Mordehai, T., Jiko, C., Samsudin, F., Gerle, C. & Khalid, S. (2018). Protein assemblies ejected directly from native membranes yield complexes for mass spectrometry. *Science,* 362**,** 829-34.

Choudhury, H. G., Tong, Z., Mathavan, I., Li, Y., Iwata, S., Zirah, S., Rebuffat, S., Van Veen, H. W. & Beis, K. (2014). Structure of an antibacterial peptide ATP-binding cassette transporter in a novel outward occluded state. *Proceedings of the National Academy of Sciences,* 111**,** 9145-50.

Chung, Y. J. & Saier, M. H., Jr. (2001). SMR-type multidrug resistance pumps. *Current Opinion in Drug Discovery and Development,* 4**,** 237-45.

Chung, Y. J. & Saier, M. H., Jr. (2002). Overexpression of the *Escherichia coli sugE* gene confers resistance to a narrow range of quaternary ammonium compounds. *Journal of Bacteriology,* 184**,** 2543-5.

Clark, V. L., Campbell, L., Palermo, D., Evans, T. M. & Klimpel, K. (1987). Induction and repression of outer membrane proteins by anaerobic growth of *Neisseria gonorrhoeae*. *Infection and Immunity,* 55**,** 1359-64.

Claxton, D. P., Jagessar, K. L. & McHaourab, H. S. (2021). Principles of alternating access in multidrug and toxin extrusion (MATE) transporters. *Journal of Molecular Biology,* 433**,** 166959.

Claxton, D. P., Jagessar, K. L., Steed, P. R., Stein, R. A. & Mchaourab, H. S. (2018). Sodium and proton coupling in the conformational cycle of a MATE antiporter from *Vibrio cholerae*. *Proceedings of the National Academy of Sciences,* 115**,** E6182-E90.

CLSI. 2012. Methods for dilution antimicrobial susceptibility tests for bacteria that grow aerobically: approved standard. p.M07-A9. Clinical and Laboratory Standards Institute, Wayne, Pa.

Cockerill, F. R., Wikler, M. A., Alder, J., Dudley, M. N., Eliopoulos, G. M., Ferrro, M. J., Hardy, D. J., Hecht, D. W., Hindler, J. A., Patel, J. B., Powell, M., Swenson, J. M., Thomson, J. R. B., Traczewski, M. M., Turnidge, J. D., Weinstein, M. P. & Zimmer, B. L. (2012). Methods for dilution antimicrobial susceptibility tests for bacteria that grow aerobically; Approved Standard. *Clinical and Laboratory Standards Institute,* 32**,** 88.

Colclough, A. L., Alav, I., Whittle, E. E., Pugh, H. L., Darby, E. M., Legood, S. W., McNeil, H. E. & Blair, J. M. (2020). RND efflux pumps in Gram-negative bacteria; regulation, structure and role in antibiotic resistance. *Future Microbiology,* 15**,** 143-57.

Cole, J. A. (2012). Legless pathogens: how bacterial physiology provides the key to understanding pathogenicity. *Microbiology,* 158**,** 1402-13.

Cole, M. J., Day, M., Jacobsson, S., Amato-Gauci, A. J., Spiteri, G. & Unemo, M. (2022). The European response to control and manage multi-and extensively drug-resistant *Neisseria gonorrhoeae*. *Eurosurveillance,* 27**,** 2100611.

Collu, F., Vargiu, A. V., Dreier, J., Cascella, M. & Ruggerone, P. (2012). Recognition of imipenem and meropenem by the RND-transporter MexB studied by computer simulations. *Journal of the American Chemical Society,* 134**,** 19146-58.

Colmer, J. A., Fralick, J. A. & Hamood, A. N. (1998). Isolation and characterization of a putative multidrug resistance pump from *Vibrio cholerae*. *Molecular Microbiology,* 27**,** 63-72.

Coluccia, M., Béranger, A., Trirocco, R., Fanelli, G., Zanzi, F., Colonna, B., Grossi, M., Prosseda, G. & Pasqua, M. (2023). Role of the MDR efflux pump AcrAB in epithelial cell invasion by *Shigella flexneri*. *Biomolecules,* 13**,** 823.

Compagne, N., Vieira Da Cruz, A., Müller, R. T., Hartkoorn, R. C., Flipo, M. & Pos, K. M. (2023). Update on the discovery of efflux pump inhibitors

against critical priority Gram-negative bacteria. *Antibiotics,* 12**,** https://doi.org/10.3390/antibiotics12010180.

Cornelissen, C. N. & Hollander, A. (2011). TonB-dependent transporters expressed by *Neisseria gonorrhoeae*. *Frontiers in Microbiology,* 2**,** 117.

Cortez-Cordova, J. & Kumar, A. (2011). Activity of the efflux pump inhibitor phenylalanine-arginine *β*-naphthylamide against the AdeFGH pump of *Acinetobacter baumannii*. *International Journal of Antimicrobial Agents,* 37**,** 420-4.

Cousin, S. L., Jr, Whittington, W. L. H. & Roberts, M. C. (2003). Acquried resistance genes and the 1 bp deletion in the *mtrR* promoter in *Neisseria gonorrhoeae*. *Journal of Antimicrobial Chemotherapy,* 51**,** 131-3.

Craig, L., Pique, M. E. & Tainer, J. A. (2004). Type IV pilus structure and bacterial pathogenicity. *Nature Reviews Microbiology,* 2**,** 363-78.

Criss, A. K. & Seifert, H. S. (2012). A bacterial siren song: intimate interactions between *Neisseria* and neutrophils. *Nature Reviews Microbiology,* 10**,** 178-90.

Cuthbertson, L. & Nodwell, J. R. (2013). The TetR family of regulators. *Microbiology and Molecular Biology Reviews,* 77**,** 440-75.

Danaher, R. J., Levin, J. C., Arking, D., Burch, C. L., Sandlin, R. & Stein, D. C. (1995). Genetic basis of *Neisseria gonorrhoeae* lipooligosaccharide antigenic variation. *Journal of Bacteriology,* 177**,** 7275-9.

Dang, S., Sun, L., Huang, Y., Lu, F., Liu, Y., Gong, H., Wang, J. & Yan, N. (2010). Structure of a fucose transporter in an outward-open conformation. *Nature,* 467**,** 734-8.

Darby, E. M., Bavro, V. N., Dunn, S., McNally, A. & Blair, J. M. (2023). RND pumps across the genus *Acinetobacter*: AdeIJK is the universal efflux pump. *Microbial Genomics,* 9**,** 000964.

Darden, T., York, D. & Pedersen, L. (1993). Particle Mesh Ewald: An N· log (N) method for Ewald sums in large systems. *The Journal of Chemical Physics,* 98**,** 10089-92.

Darzynkiewicz, Z. M., Green, A. T., Abdali, N., Hazel, A., Fulton, R. L., Kimball, J., Gryczynski, Z., Gumbart, J. C., Parks, J. M. & Smith, J. C. (2019). Identification of binding sites for efflux pump inhibitors of the AcrAB-TolC component AcrA. *Biophysical Journal,* 116**,** 648-58.

Dashtbani-Roozbehani, A. & Brown, M. H. (2021). Efflux pump mediated antimicrobial resistance by *Staphylococci* in health-related environments: challenges and the quest for inhibition. *Antibiotics,* 10**,** 1-33.

Datsenko, K. A. & Wanner, B. L. (2000). One-step inactivation of chromosomal genes in *Escherichia coli* K-12 using PCR products. *Proceedings of the*

National Academy of Sciences of the United States of America, 97**,** 6640-5.

Daury, L., Orange, F., Taveau, J. C., Verchere, A., Monlezun, L., Gounou, C., Marreddy, R. K., Picard, M., Broutin, I., Pos, K. M. & Lambert, O. (2016). Tripartite assembly of RND multidrug efflux pumps. *Nature Communications,* 7**,** 10731.

Davidsen, T., Rødland, E. A., Lagesen, K., Seeberg, E., Rognes, T. & Tønjum, T. (2004). Biased distribution of DNA uptake sequences towards genome maintenance genes. *Nucleic Acids Research,* 32**,** 1050-8.

Dawson, R. J. & Locher, K. P. (2007). Structure of the multidrug ABC transporter Sav1866 from *Staphylococcus aureus* in complex with AMP-PNP. *FEBS Letters,* 581**,** 935-8.

Day, M., Pitt, R., Mody, N., Saunders, J., Rai, R., Nori, A., Church, H., Mensforth, S., Corkin, H. & Jones, J. (2022). Detection of 10 cases of ceftriaxone-resistant *Neisseria gonorrhoeae* in the United Kingdom, December 2021 to June 2022. *Eurosurveillance,* 27**,** 2200803.

De Angelis, F., Lee, J. K., O'Connell, J. D., 3rd, Miercke, L. J., Verschueren, K. H., Srinivasan, V., Bauvois, C., Govaerts, C., Robbins, R. A., Ruysschaert, J. M., Stroud, R. M. & Vandenbussche, G. (2010). Metal-induced conformational changes in ZneB suggest an active role of membrane fusion proteins in efflux resistance systems. *Proceedings of the National Academy of Sciences of the United States of America,* 107**,** 11038-43.

De Jong, D. H., Baoukina, S., Ingólfsson, H. I. & Marrink, S. J. (2016). Martini straight: Boosting performance using a shorter cutoff and GPUs. *Computer Physics Communications,* 199**,** 1-7.

De Jong, D. H., Singh, G., Bennett, W. F., Arnarez, C., Wassenaar, T. A., Schäfer, L. V., Periole, X., Tieleman, D. P. & Marrink, S. J. (2013). Improved parameters for the MARTINI coarse-grained protein force field. *Journal of Chemical Theory and Computation,* 9**,** 687-97.

Debruycker, V., Hutchin, A., Masureel, M., Ficici, E., Martens, C., Legrand, P., Stein, R. A., Mchaourab, H. S., Faraldo-Gómez, J. D. & Remaut, H. (2020a). An embedded lipid in the multidrug transporter LmrP suggests a mechanism for polyspecificity. *Nature Structural & Molecular Biology,* 27**,** 829-35.

Debruycker, V., Hutchin, A., Masureel, M., Ficici, E., Martens, C., Legrand, P., Stein, R. A., McHaourab, H. S., Faraldo-Gómez, J. D., Remaut, H. & Govaerts, C. (2020b). An embedded lipid in the multidrug transporter LmrP suggests a mechanism for polyspecificity. *Nature Structural & Molecular Biology,* 27**,** 829-35.

Dehio, C., Gray-Owen, S. D. & Meyer, T. F. (1998). The role of *neisserial* Opa proteins in interactions with host cells. *Trends in Microbiology,* 6**,** 489-95.

Delahay, R. M., Robertson, B. D., Balthazar, J. T., Shafer, W. M. & Ison, C. A. (1997). Involvement of the gonococcal MtrE protein in the resistance of *Neisseria gonorrhoeae* to toxic hydrophobic agents. *Microbiology,* 143 (Pt 7)**,** 2127-33.

Delmar, J. A. & Yu, E. W. (2016). The AbgT family: A novel class of antimetabolite transporters. *Protein Science,* 25**,** 322-37.

Dey, D., Kavanaugh, L. G. & Conn, G. L. (2020). Antibiotic substrate selectivity of *Pseudomonas aeruginosa* MexY and MexB efflux systems is determined by a Goldilocks affinity. *Antimicrobial Agents and Chemotherapy,* 64.

Dietrich, M., Bartfeld, S., Munke, R., Lange, C., Ogilvie, L. A., Friedrich, A. & Meyer, T. F. (2011). Activation of NF-KB by *Neisseria gonorrhoeae* is associated with microcolony formation and type IV pilus retraction. *Cellular Microbiology,* 13**,** 1168-82.

Dillard, J. P. (2011). Genetic manipulation of *Neisseria gonorrhoeae*. *Current Protocols in Microbiology,* Chapter 4**,** Unit4A 2.

Dinh, T., Paulsen, I. T. & Saier, M. H., Jr. (1994). A family of extracytoplasmic proteins that allow transport of large molecules across the outer membranes of Gram-negative bacteria. *Journal of Bacteriology,* 176**,** 3825-31.

Doerr, A. (2016). Single-particle cryo-electron microscopy: a brief overview of how to solve a macromolecular structure using single-particle cryo-electron microscopy (cryo-EM). *Nature Methods,* 13**,** 23-4.

Douafer, H., Andrieu, V., Phanstiel IV, O. & Brunel, J. M. (2019). Antibiotic adjuvants: make antibiotics great again! *Journal of Medicinal Chemistry,* 62**,** 8665-81.

Drew, D. & Boudker, O. (2016). Shared molecular mechanisms of membrane transporters. *Annual Review of Biochemistry,* 85**,** 543-72.

Du, D., Neuberger, A., Orr, M. W., Newman, C. E., Hsu, P. C., Samsudin, F., Szewczak-Harris, A., Ramos, L. M., Debela, M., Khalid, S., Storz, G. & Luisi, B. F. (2020). Interactions of a bacterial RND transporter with a transmembrane small protein in a lipid environment. *Structure,* 28**,** 625-34 e6.

Du, D., van Veen, H. W. & Luisi, B. F. (2015a). Assembly and operation of bacterial tripartite multidrug efflux pumps. *Trends in Microbiology,* 23**,** 311-9.

Du, D., Van Veen, H. W., Murakami, S., Pos, K. M. & Luisi, B. F. (2015b). Structure, mechanism and cooperation of bacterial multidrug transporters. *Current Opinion in Structural Biology,* 33**,** 76-91.

Du, D., Wang, Z., James, N. R., Voss, J. E., Klimont, E., Ohene-Agyei, T., Venter, H., Chiu, W. & Luisi, B. F. (2014). Structure of the AcrAB-TolC multidrug efflux pump. *Nature,* 509**,** 512-5.

Dumon-Seignovert, L., Cariot, G. & Vuillard, L. (2004). The toxicity of recombinant proteins in *Escherichia coli*: a comparison of overexpression in BL21(DE3), C41(DE3), and C43(DE3). *Protein Expression and Purification,* 37**,** 203-6.

Dutta, S., Morrison, E. A. & Henzler-Wildman, K. A. (2014). Blocking dynamics of the SMR transporter EmrE impairs efflux activity. *Biophysical Journal,* 107**,** 613-20.

Eda, S., Maseda, H. & Nakae, T. (2003). An elegant means of self-protection in Gram-negative bacteria by recognizing and extruding xenobiotics from the periplasmic space. *Journal of Biological Chemistry,* 278**,** 2085-8.

Edgar, R. & Bibi, E. (1997). MdfA, an *Escherichia coli* multidrug resistance protein with an extraordinarily broad spectrum of drug recognition. *Journal of Bacteriology,* 179**,** 2274-80.

Edgar, R. & Bibi, E. (1999). A single membrane-embedded negative charge is critical for recognizing positively charged drugs by the *Escherichia coli* multidrug resistance protein MdfA. *EMBO Journal,* 18**,** 822-32.

Edwards, J. L. & Apicella, M. A. (2004). The molecular mechanisms used by *Neisseria gonorrhoeae* to initiate infection differ between men and women. *Clinical Microbiology Reviews,* 17**,** 965-81.

Edwards, J. L., Shao, J. Q., Ault, K. A. & Apicella, M. A. (2000). *Neisseria gonorrhoeae* elicits membrane ruffling and cytoskeletal rearrangements upon infection of primary human endocervical and ectocervical cells. *Infection and Immunity,* 68**,** 5354-63.

Eguchi, Y., Oshima, T., Mori, H., Aono, R., Yamamoto, K., Ishihama, A. & Utsumi, R. (2003). Transcriptional regulation of drug efflux genes by EvgAS, a two-component system in *Escherichia coli*. *Microbiology,* 149**,** 2819-28.

Eicher, T., Cha, H. J., Seeger, M. A., Brandstatter, L., El-Delik, J., Bohnert, J. A., Kern, W. V., Verrey, F., Grutter, M. G., Diederichs, K. & Pos, K. M. (2012). Transport of drugs by the multidrug transporter AcrB involves an access and a deep binding pocket that are separated by a switch-loop. *Proceedings of the National Academy of Sciences of the United States of America,* 109**,** 5687-92.

Eicher, T., Seeger, M. A., Anselmi, C., Zhou, W., Brandstatter, L., Verrey, F., Diederichs, K., Faraldo-Gomez, J. D. & Pos, K. M. (2014). Coupling of remote alternating-access transport mechanisms for protons and substrates in the multidrug efflux pump AcrB. *Elife,* 3**,** e03145.

Eisinger, M. L., Nie, L., Dörrbaum, A. R., Langer, J. D. & Michel, H. (2018). The xenobiotic extrusion mechanism of the MATE transporter NorM_PS from *Pseudomonas stutzeri*. *Journal of Molecular Biology,* 430**,** 1311-23.

Elkins, C. A. & Nikaido, H. (2002). Substrate specificity of the RND-type multidrug efflux pumps AcrB and AcrD of *Escherichia coli* is determined predominantly by two large periplasmic loops. *Journal of Bacteriology,* 184**,** 6490-8.

Elmros, T., Sandström, G. & Burman, L. (1976). Autolysis of *Neisseria gonorrhoeae*: relation between mechanical stability and viability. *Sexually Transmitted Infections,* 52**,** 246-9.

Elsener, T. A., Jolley, K. A., Sanders, E., Maiden, M. C., Cehovin, A. & Tang, C. M. (2023). There are three major *Neisseria gonorrhoeae* β-lactamase plasmid variants which are associated with specific lineages and carry distinct TEM alleles. *Microbial Genomics,* 9**,** 001057.

Elwell, L. P., Roberts, M., Mayer, L. W. & Falkow, S. (1977). Plasmid-mediated beta-lactamase production in *Neisseria gonorrhoeae*. *Antimicrobial Agents and Chemotherapy,* 11**,** 528-33.

Erickson, J. D., Schafer, M., Bonner, T. I., Eiden, L. E. & Weihe, E. (1996). Distinct pharmacological properties and distribution in neurons and endocrine cells of two isoforms of the human vesicular monoamine transporter. *Proceedings of the National Academy of Sciences of the United States of America,* 93**,** 5166-71.

Erkens, G. B., Berntsson, R. P., Fulyani, F., Majsnerowska, M., Vujičić-Žagar, A., Ter Beek, J., Poolman, B. & Slotboom, D. J. (2011). The structural basis of modularity in ECF-type ABC transporters. *Nature Structural & Molecular Biology,* 18**,** 755.

Esteves, N. C., Porwollik, S., McClelland, M. & Scharf, B. E. (2021). The multidrug efflux system AcrABZ-TolC is essential for infection of *Salmonella typhimurium* by the flagellum-dependent bacteriophage Chi. *Journal of Virology,* 95**,** e00394-21.

eurofins *eurofins Discovery* [Online]. Available: https://www.eurofinsdiscovery.com/ [Accessed 14/04/2024 2024].

Eyre, D. W., Sanderson, N. D., Lord, E., Regisford-Reimmer, N., Chau, K., Barker, L., Morgan, M., Newnham, R., Golparian, D. & Unemo, M. (2018). Gonorrhoea treatment failure caused by a *Neisseria gonorrhoeae* strain with combined ceftriaxone and high-level azithromycin resistance, England, February 2018. *Eurosurveillance,* 23**,** 1800323.

Ezewudo, M. N., Joseph, S. J., Castillo-Ramirez, S., Dean, D., Del Rio, C., Didelot, X., Dillon, J.-A., Selden, R. F., Shafer, W. M. & Turingan, R. S. (2015). Population structure of *Neisseria gonorrhoeae* based on whole genome data and its relationship with antibiotic resistance. *PeerJ,* 3**,** e806.

Fairweather, S. J., Shah, N. & Bröer, S. (2021). Heteromeric solute carriers: function, structure, pathology and pharmacology. *Advances in Experimental Medicine and Biology,* 21**,** 13-127.

Fanelli, G., Pasqua, M., Prosseda, G., Grossi, M. & Colonna, B. (2023). AcrAB efflux pump impacts on the survival of adherent-invasive *Escherichia coli* strain LF82 inside macrophages. *Scientific Reports,* 13**,** 2692.

Feng, Z., Liu, D., Liu, Z., Liang, Y., Wang, Y., Liu, Q., Liu, Z., Zang, Z. & Cui, Y. (2020). Cloning and functional characterization of putative *Escherichia coli* ABC multidrug efflux transporter YddA. *Journal of Microbioloy & Biotechnology,* 30**,** 982-95.

Fifer, H., Saunders, J., Soni, S., Sadiq, S. T. & FitzGerald, M. (2020). 2018 UK national guideline for the management of infection with *Neisseria gonorrhoeae*. *International journal of STD & AIDS,* 31**,** 4-15.

Fischer, C. L. (2020). Antimicrobial activity of host-derived lipids. *Antibiotics,* 9**,** 75.

Fischer, N. & Kandt, C. (2011). Three ways in, one way out: water dynamics in the trans-membrane domains of the inner membrane translocase AcrB. *Proteins: Structure, Function, and Bioinformatics,* 79**,** 2871-85.

Fischer, N. & Kandt, C. (2013). Porter domain opening and closing motions in the multi-drug efflux transporter AcrB. *Biochimica et Biophysica Acta Biomembranes,* 1828**,** 632-41.

Fitzpatrick, A. W. P., Llabres, S., Neuberger, A., Blaza, J. N., Bai, X. C., Okada, U., Murakami, S., van Veen, H. W., Zachariae, U., Scheres, S. H. W., Luisi, B. F. & Du, D. (2017). Structure of the MacAB-TolC ABC-type tripartite multidrug efflux pump. *Nature Microbiology,* 2**,** 17070.

Fleming, D. T. & Wasserheit, J. N. (1999). From epidemiological synergy to public health policy and practice: the contribution of other sexually transmitted diseases to sexual transmission of HIV infection. *Sexually Transmitted Infections,* 75**,** 3-17.

Fluman, N., Adler, J., Rotenberg, S. A., Brown, M. H. & Bibi, E. (2014). Export of a single drug molecule in two transport cycles by a multidrug efflux pump. *Nature Communications,* 5**,** 4615.

Fluman, N., Cohen-Karni, D., Weiss, T. & Bibi, E. (2009). A promiscuous conformational switch in the secondary multidrug transporter MdfA. *Journal of Biological Chemistry,* 284**,** 32296-304.

Fluman, N., Ryan, C. M., Whitelegge, J. P. & Bibi, E. (2012). Dissection of mechanistic principles of a secondary multidrug efflux protein. *Molecular Cell,* 47**,** 777-87.

Folster, J. P., Dhulipala, V., Nicholas, R. A. & Shafer, W. M. (2007). Differential regulation of *ponA* and *pilMNOPQ* expression by the MtrR transcriptional regulatory protein in *Neisseria gonorrhoeae*. *Journal of Bacteriology,* 189**,** 4569-77.

Folster, J. P., Johnson, P. J., Jackson, L., Dhulipali, V., Dyer, D. W. & Shafer, W. M. (2009). MtrR modulates *rpoH* expression and levels of

antimicrobial resistance in *Neisseria gonorrhoeae*. *Journal of Bacteriology,* 191**,** 287-97.

Folster, J. P. & Shafer, W. M. (2005). Regulation of *mtrF* expression in *Neisseria gonorrhoeae* and its role in high-level antimicrobial resistance. *Journal of Bacteriology,* 187**,** 3713-20.

Fontaine, F., Fuchs, R. T. & Storz, G. (2011). Membrane localization of small proteins in *Escherichia coli*. *Journal of Biological Chemistry,* 286**,** 32464-74.

Foong, W. E., Wilhelm, J., Tam, H. K. & Pos, K. M. (2020). Tigecycline efflux in *Acinetobacter baumannii* is mediated by TetA in synergy with RND-type efflux transporters. *Journal of Antimicrobial Chemotherapy,* 75**,** 1135-9.

Ford, R. C. & Beis, K. (2019). Learning the ABCs one at a time: structure and mechanism of ABC transporters. *Biochemical Society Transactions,* 47**,** 23-36.

Fralick, J. A. (1996). Evidence that TolC is required for functioning of the Mar/AcrAB efflux pump of *Escherichia coli*. *Journal of Bacteriology,* 178**,** 5803-5.

Friedrich, A., Arvidson, C. G., Shafer, W. M., Lee, E.-H. & So, M. (2007). Two ABC transporter operons and the antimicrobial resistance gene *mtrF* are *pilT* responsive in *Neisseria gonorrhoeae*. *Journal of Bacteriology,* 189**,** 5399-402.

Frost, K. M., Charron-Smith, S. L., Cotsonas, T. C., Dimartino, D. C., Eisenhart, R. C., Everingham, E. T., Holland, E. C., Imtiaz, K., Kornowicz, C. J. & Lenhard, L. E. (2024a). Rolling the evolutionary dice: *Neisseria* commensals as proxies for elucidating the underpinnings of antibiotic resistance mechanisms and evolution in human pathogens. *Microbiology Spectrum***,** e03507-23.

Frost, K. M., Charron-Smith, S. L., Cotsonas, T. C., Dimartino, D. C., Eisenhart, R. C., Everingham, E. T., Holland, E. C., Imtiaz, K., Kornowicz, C. J., Lenhard, L. E., Lynch, L. H., Moore, N. P., Phadke, K., Reed, M. L., Smith, S. R., Ward, L. L. & Wadsworth, C. B. (2024b). Rolling the evolutionary dice: *Neisseria* commensals as proxies for elucidating the underpinnings of antibiotic resistance mechanisms and evolution in human pathogens. *Microbiology Spectrum,* 12**,** e03507-23.

Fudyk, T. C., Maclean, I. W., Simonsen, J. N., Njagi, E. N., Kimani, J., Brunham, R. C. & Plummer, F. A. (1999). Genetic diversity and mosaicism at the *por* locus of *Neisseria gonorrhoeae*. *Journal of Bacteriology,* 181**,** 5591-9.

Fujihira, E., Tamura, N. & Yamaguchi, A. (2002). Membrane topology of a multidrug efflux transporter, AcrB, in *Escherichia coli*. *Journal of Biochemistry,* 131**,** 145-51.

Fukuchi, J.-i., Kashiwagi, K., Yamagishi, M., Ishihama, A. & Igarashi, K. (1995). Decrease in cell viability due to the accumulation of spermidine in spermidine acetyltransferase-deficient mutant of *Escherichia coli*. *Journal of Biological Chemistry,* 270**,** 18831-5.

Galdiero, S., Falanga, A., Cantisani, M., Tarallo, R., Elena Della Pepa, M., D'Oriano, V. & Galdiero, M. (2012). Microbe-host interactions: structure and role of Gram-negative bacterial porins. *Current Protein and Peptide Science,* 13**,** 843-54.

Galimand, M., Gerbaud, G. & Courvalin, P. (2000). Spectinomycin resistance in *Neisseria* spp. due to mutations in 16S rRNA. *Antimicrobial Agents and Chemotherapy,* 44**,** 1365-6.

Gangaiah, D., Raterman, E. L., Wu, H., Fortney, K. R., Gao, H., Liu, Y., Jerse, A. E. & Spinola, S. M. (2017). Both MisR (CpxR) and MisS (CpxA) are required for *Neisseria gonorrhoeae* infection in a murine model of lower genital tract infection. *Infection and Immunity,* 85.

Garcia, Í. R., de Oliveira Garcia, F. A., Pereira, P. S., Coutinho, H. D. M., Siyadatpanah, A., Norouzi, R., Wilairatana, P., de Lourdes Pereira, M., Nissapatorn, V., Tintino, S. R. & Rodrigues, F. F. G. (2022). Microbial resistance: The role of efflux pump superfamilies and their respective substrates. *Life Sci,* 295**,** 120391.

Garvin, L. E., Bash, M. C., Keys, C., Warner, D. M., Ram, S., Shafer, W. M. & Jerse, A. E. (2008). Phenotypic and genotypic analyses of *Neisseria gonorrhoeae* isolates that express frequently recovered porB PIA variable region types suggest that certain P1a porin sequences confer a selective advantage for urogenital tract infection. *Infection and Immunity,* 76**,** 3700-9.

George, A. M. & Jones, P. M. (2013). An asymmetric post-hydrolysis state of the ABC transporter ATPase dimer. *PLoS One,* 8**,** e59854.

George, A. M. & Levy, S. B. (1983). Gene in the major cotransduction gap of the *Escherichia coli* K-12 linkage map required for the expression of chromosomal resistance to tetracycline and other antibiotics. *Journal of Bacteriology,* 155**,** 541-8.

Gerbase, A. C. & Zemouri, C. 2020. Global epidemiology of sexually transmitted infections in the twenty-first century: beyond the numbers. *In:* CRISTAUDO, A. & GIULIANI, M. (eds.) *Sexually transmitted infections: advances in understanding and management.* Gewerbestrasse, Switzerland: Springer.

Gerken, H. & Misra, R. (2004). Genetic evidence for functional interactions between TolC and AcrA proteins of a major antibiotic efflux pump of *Escherichia coli*. *Molecular Microbiology,* 54**,** 620-31.

Gernert, K. M., Seby, S., Schmerer, M. W., Thomas, J. C., Pham, C. D., St Cyr, S., Schlanger, K., Weinstock, H., Shafer, W. M. & Raphael, B. H. (2020). Azithromycin susceptibility of *Neisseria gonorrhoeae* in the USA

in 2017: a genomic analysis of surveillance data. *The Lancet Microbe,* 1**,** e154-64.

Gervasoni, S., Malloci, G., Bosin, A., Vargiu, A. V., Zgurskaya, H. I. & Ruggerone, P. (2022). Recognition of quinolone antibiotics by the multidrug efflux transporter MexB of *Pseudomonas aeruginosa*. *Physical Chemistry Chemical Physics,* 24**,** 16566-75.

Gianecini, R. A., Golparian, D., Zittermann, S., Litvik, A., Gonzalez, S., Oviedo, C., Melano, R. G., Unemo, M. & Galarza, P. (2019). Genome-based epidemiology and antimicrobial resistance determinants of *Neisseria gonorrhoeae* isolates with decreased susceptibility and resistance to extended-spectrum cephalosporins in Argentina in 2011–16. *Journal of Antimicrobial Chemotherapy,* 74**,** 1551-9.

Gianecini, R. A., Poklepovich, T., Golparian, D., Cuenca, N., Scocozza, L., Bergese, S., Canigia, L. F., Vilches, V., Elgart, M. J. L., Unemo, M., Campos, J. & Galarza, P. (2023). Sustained transmission of *Neisseria gonorrhoeae* strains with high-level azithromycin resistance (MIC ≥ 256 µg/mL) in Argentina, 2018 to 2022. *Microbiology Spectrum,* 11**,** e00970-23.

Gill, M., Simjee, S., Al-Hattawi, K., Robertson, B., Easmon, C. & Ison, C. (1998). Gonococcal resistance to β-lactams and tetracycline involves mutation in loop 3 of the porin encoded at the *penB* locus. *Antimicrobial Agents and Chemotherapy,* 42**,** 2799-803.

Gillings, M. R. (2017). Class 1 integrons as invasive species. *Current Opinion in Microbiology,* 38**,** 10-5.

Glavier, M., Puvanendran, D., Salvador, D., Decossas, M., Phan, G., Garnier, C., Frezza, E., Cece, Q., Schoehn, G. & Picard, M. (2020). Antibiotic export by MexB multidrug efflux transporter is allosterically controlled by a MexA-OprM chaperone-like complex. *Nature Communications,* 11**,** 4948.

Golparian, D., Jacobsson, S., Holley, C. L., Shafer, W. M. & Unemo, M. (2023a). High-level in vitro resistance to gentamicin acquired in a stepwise manner in *Neisseria gonorrhoeae*. *Journal of Antimicrobial Chemotherapy***,** dkad168.

Golparian, D., Rose, L., Lynam, A., Mohamed, A., Bercot, B., Ohnishi, M., Crowley, B. & Unemo, M. (2018). Multidrug-resistant *Neisseria gonorrhoeae* isolate, belonging to the internationally spreading Japanese FC428 clone, with ceftriaxone resistance and intermediate resistance to azithromycin, Ireland, August 2018. *Eurosurveillance,* 23.

Golparian, D., Shafer, W. M., Ohnishi, M. & Unemo, M. (2014). Importance of multidrug efflux pumps in the antimicrobial resistance property of clinical multidrug-resistant isolates of *Neisseria gonorrhoeae*. *Antimicrobial Agents and Chemotherapy,* 58**,** 3556-9.

Golparian, D., Vestberg, N., Södersten, W., Jacobsson, S., Ohnishi, M., Fang, H., Bhattarai, K. H. & Unemo, M. (2023b). Multidrug-resistant *Neisseria*

gonorrhoeae isolate SE690: mosaic penA-60.001 gene causing ceftriaxone resistance internationally has spread to the more antimicrobial-susceptible genomic lineage, Sweden, September 2022. *Eurosurveillance,* 28**,** 2300125.

Goodman, S. D. & Scocca, J. J. (1988). Identification and arrangement of the DNA sequence recognized in specific transformation of *Neisseria gonorrhoeae*. *Proceedings of the National Academy of Sciences of the United States of America,* 85**,** 6982-6.

Gorecki, K. & McEvoy, M. M. (2020). Phylogenetic analysis reveals an ancient gene duplication as the origin of the MdtABC efflux pump. *PLoS One,* 15**,** e0228877.

Goytia, M. & Wadsworth, C. B. (2022). Canary in the coal mine: How resistance surveillance in commensals could help curb the spread of AMR in pathogenic *Neisseria*. *mBio,* 13**,** e01991-22.

Grad, Y. H., Harris, S. R., Kirkcaldy, R. D., Green, A. G., Marks, D. S., Bentley, S. D., Trees, D. & Lipsitch, M. (2016). Genomic epidemiology of gonococcal resistance to extended-spectrum cephalosporins, macrolides, and fluoroquinolones in the United States, 2000–2013. *The Journal of Infectious Diseases,* 214**,** 1579-87.

Greener, T., Govenzenshy, D. & Zamir, A. (1993). A novel multicopy suppressor of a *groEL* mutation includes two nested open reading frames transcribed from different promoters. *EMBO Journal,* 12**,** 889-96.

Grimsey, E., Fais, C., Marshall, R., Ricci, V., Ciusa, M., Stone, J., Ivens, A., Malloci, G., Ruggerone, P. & Vargiu, A. 2020. Chlorpromazine and amitriptyline are substrates and inhibitors of the AcrB multidrug efflux pump. mBio 11: e00465-20.

Grinius, L., Dreguniene, G., Goldberg, E. B., Liao, C. H. & Projan, S. J. (1992). A staphylococcal multidrug resistance gene product is a member of a new protein family. *Plasmid,* 27**,** 119-29.

Grkovic, S., Hardie, K. M., Brown, M. H. & Skurray, R. A. (2003). Interactions of the QacR multidrug-binding protein with structurally diverse ligands: implications for the evolution of the binding pocket. *Biochemistry,* 42**,** 15226-36.

Guan, L. & Nakae, T. (2001). Identification of essential charged residues in transmembrane segments of the multidrug transporter MexB of *Pseudomonas aeruginosa*. *Journal of Bacteriology,* 183**,** 1734-9.

Gunn, J. S., Lim, K. B., Krueger, J., Kim, K., Guo, L., Hackett, M. & Miller, S. I. (1998). PmrA–PmrB-regulated genes necessary for 4-aminoarabinose lipid A modification and polymyxin resistance. *Molecular Microbiology,* 27**,** 1171-82.

Guo, T., Chen, Y., Chen, W., Semple, S. J., Gu, X., Polyak, S. W., Sun, G., Venter, H. & Ma, S. (2023). Design and synthesis of benzochromene

derivatives as AcrB inhibitors for the reversal of bacterial multidrug resistance. *European Journal of Medicinal Chemistry,* 249**,** 115148.

Guymon, L. F., Walstad, D. L. & Sparling, P. F. (1978). Cell envelope alterations in antibiotic-sensitive and-resistant strains of *Neisseria gonorrhoeae*. *Journal of Bacteriology,* 136**,** 391-401.

Hagman, K. E., Lucas, C. E., Balthazar, J. T., Snyder, L., Nilles, M., Judd, R. C. & Shafer, W. M. (1997). The MtrD protein of *Neisseria gonorrhoeae* is a member of the resistance nodulation division protein family constituting part of an efflux system. *Microbiology,* 143**,** 2117-25.

Hagman, K. E., Pan, W., Spratt, B. G., Balthazar, J. T., Judd, R. C. & Shafer, W. M. (1995). Resistance of *Neisseria gonorrhoeae* to antimicrobial hydrophobic agents is modulated by the *mtrRCDE* efflux system. *Microbiology,* 141**,** 611-22.

Hagman, K. E. & Shafer, W. M. (1995). Transcriptional control of the mtr efflux system of *Neisseria gonorrhoeae*. *Journal of Bacteriology,* 177**,** 4162-5.

Hamilton, H. L. & Dillard, J. P. (2006). Natural transformation of *Neisseria gonorrhoeae*: from DNA donation to homologous recombination. *Molecular Microbiology,* 59**,** 376-85.

Hanahan, D. (1983). Studies on transformation of *Escherichia coli* with plasmids. *Journal of Molecular Biology,* 166**,** 557-80.

Hancock, R. E. (1997). The bacterial outer membrane as a drug barrier. *Trends in Microbiology,* 5**,** 37-42.

Hardy, D., Bill, R. M., Jawhari, A. & Rothnie, A. J. (2016). Overcoming bottlenecks in the membrane protein structural biology pipeline. *Biochemical Society Transactions,* 44**,** 838-44.

Harley, K. T., Djordjevic, G. M., Tseng, T. T. & Saier, M. H. (2000). Membrane-fusion protein homologues in Gram-positive bacteria. *Molecular Microbiology,* 36**,** 516-7.

Harris, S. R., Cole, M. J., Spiteri, G., Sánchez-Busó, L., Golparian, D., Jacobsson, S., Goater, R., Abudahab, K., Yeats, C. A. & Bercot, B. (2018). Public health surveillance of multidrug-resistant clones of *Neisseria gonorrhoeae* in Europe: a genomic survey. *The Lancet Infectious Diseases,* 18**,** 758-68.

Harvey, H., Porat, N., Campbell, C., Jennings, M., Gibson, B., Phillips, N., Apicella, M. & Blake, M. (2000). Gonococcal lipooligosaccharide is a ligand for the asialoglycoprotein receptor on human sperm. *Molecular Microbiology,* 36**,** 1059-70.

Hassan, K. A., Galea, M., Wu, J., Mitchell, B. A., Skurray, R. A. & Brown, M. H. (2006a). Functional effects of intramembranous proline substitutions in the staphylococcal multidrug transporter QacA. *FEMS Microbiology Letters,* 263**,** 76-85.

Hassan, K. A., Jackson, S. M., Penesyan, A., Patching, S. G., Tetu, S. G., Eijkelkamp, B. A., Brown, M. H., Henderson, P. J. & Paulsen, I. T. (2013). Transcriptomic and biochemical analyses identify a family of chlorhexidine efflux proteins. *Proceedings of the National Academy of Sciences of the United States of America,* 110**,** 20254-9.

Hassan, K. A., Liu, Q., Elbourne, L. D., Ahmad, I., Sharples, D., Naidu, V., Chan, C. L., Li, L., Harborne, S. P. & Pokhrel, A. (2018). Pacing across the membrane: the novel PACE family of efflux pumps is widespread in Gram-negative pathogens. *Research in Microbiology,* 169**,** 450-4.

Hassan, K. A., Liu, Q., Henderson, P. J. & Paulsen, I. T. (2015). Homologs of the *Acinetobacter baumannii* AceI transporter represent a new family of bacterial multidrug efflux systems. *mBio,* 6**,** e01982–14.

Hassan, K. A., Maher, C., Elbourne, L. D., Henderson, P. J. & Paulsen, I. T. (2021). Increasing the PACE of characterising novel transporters by functional genomics. *Current Opinion in Microbiology,* 64**,** 1-8.

Hassan, K. A., Naidu, V., Edgerton, J. R., Mettrick, K. A., Liu, Q., Fahmy, L., Li, L., Jackson, S. M., Ahmad, I. & Sharples, D. (2019). Short-chain diamines are the physiological substrates of PACE family efflux pumps. *Proceedings of the National Academy of Sciences,* 116**,** 18015-20.

Hassan, K. A., Robinson, K. L., Smith, A. N., Gibson, J. H., Skurray, R. A. & Brown, M. H. (2006b). Glycine-rich transmembrane helix 10 in the staphylococcal tetracycline transporter TetA(K) lines a solvent-accessible channel. *Biochemistry,* 45**,** 15661-9.

Hassan, K. A., Souhani, T., Skurray, R. A. & Brown, M. H. (2008). Analysis of tryptophan residues in the staphylococcal multidrug transporter QacA reveals long-distance functional associations of residues on opposite sides of the membrane. *Journal of Bacteriology,* 190**,** 2441-9.

Hassan, K. A., Xu, Z., Watkins, R. E., Brennan, R. G., Skurray, R. A. & Brown, M. H. (2009). Optimized production and analysis of the staphylococcal multidrug efflux protein QacA. *Protein Expression and Purification,* 64**,** 118-24.

Hayashi, K., Nakashima, R., Sakurai, K., Kitagawa, K., Yamasaki, S., Nishino, K. & Yamaguchi, A. (2016). AcrB-AcrA fusion proteins that act as multidrug efflux transporters. *Journal of Bacteriology,* 198**,** 332-42.

He, X., Szewczyk, P., Karyakin, A., Evin, M., Hong, W.-X., Zhang, Q. & Chang, G. (2010). Structure of a cation-bound multidrug and toxic compound extrusion transporter. *Nature,* 467**,** 991-4.

Hearn, E. M., Gray, M. R. & Foght, J. M. (2006a). Mutations in the central cavity and periplasmic domain affect efflux activity of the resistance-nodulation-division pump EmhB from Pseudomonas fluorescens cLP6a. *Journal of Bacteriology,* 188**,** 115-23.

Hearn, E. M., Gray, M. R. & Foght, J. M. (2006b). Mutations in the central cavity and periplasmic domain affect efflux activity of the resistance-

nodulation-division pump EmhB from *Pseudomonas fluorescens* cLP6a. *Journal of Bacteriology,* 188**,** 115-23.

Hebeler, B. H. & Young, F. E. (1976). Mechanism of autolysis of *Neisseria gonorrhoeae*. *Journal of Bacteriology,* 126**,** 1186-93.

Helm, R. A. & Seifert, H. S. (2009). Pilin antigenic variation occurs independently of the RecBCD pathway in *Neisseria gonorrhoeae*. *Journal of Bacteriology,* 191**,** 5613-21.

Hemm, M. R., Paul, B. J., Schneider, T. D., Storz, G. & Rudd, K. E. (2008). Small membrane proteins found by comparative genomics and ribosome binding site models. *Molecular Microbiology,* 70**,** 1487-501.

Henderson, P. J., Maher, C., Elbourne, L. D., Eijkelkamp, B. A., Paulsen, I. T. & Hassan, K. A. (2021). Physiological functions of bacterial "multidrug" efflux pumps. *Chemical Reviews,* 121**,** 5417-78.

Heng, J., Zhao, Y., Liu, M., Liu, Y., Fan, J., Wang, X., Zhao, Y. & Zhang, X. C. (2015). Substrate-bound structure of the *Escherichia coli* multidrug resistance transporter MdfA. *Cell Research,* 25**,** 1060-73.

Hess, B., Bekker, H., Berendsen, H. J. & Fraaije, J. G. (1997). LINCS: a linear constraint solver for molecular simulations. *Journal of Computational Chemistry,* 18**,** 1463-72.

Hess, J., Wels, W., Vogel, M. & Goebel, W. (1986). Nucleotide sequence of a plasmid-encoded hemolysin determinant and its comparison with a corresponding chromosomal hemolysin sequence. *FEMS Microbiology Letters,* 34**,** 1-11.

Higashi, D. L., Lee, S. W., Snyder, A., Weyand, N. J., Bakke, A. & So, M. (2007). Dynamics of *Neisseria gonorrhoeae* attachment: microcolony development, cortical plaque formation, and cytoprotection. *Infection and Immunity,* 75**,** 4743-53.

Higashi, K., Ishigure, H., Demizu, R., Uemura, T., Nishino, K., Yamaguchi, A., Kashiwagi, K. & Igarashi, K. (2008). Identification of a spermidine excretion protein complex (MdtJI) in *Escherichia coli*. *Journal of Bacteriology,* 190**,** 872-8.

Higgins, M. K., Bokma, E., Koronakis, E., Hughes, C. & Koronakis, V. (2004). Structure of the periplasmic component of a bacterial drug efflux pump. *Proceedings of the National Academy of Sciences of the United States of America,* 101**,** 9994-9.

Hirakawa, H., Takumi-Kobayashi, A., Theisen, U., Hirata, T., Nishino, K. & Yamaguchi, A. (2008). AcrS/EnvR represses expression of the acrAB multidrug efflux genes in *Escherichia coli*. *Journal of Bacteriology,* 190**,** 6276-9.

Hirao, T., Sato, M., Shirahata, A. & Kamio, Y. (2000). Covalent linkage of polyamines to peptidoglycan in *Anaerovibrio lipolytica*. *Journal of Bacteriology,* 182**,** 1154-7.

Ho, H., Miu, A., Alexander, M. K., Garcia, N. K., Oh, A., Zilberleyb, I., Reichelt, M., Austin, C. D., Tam, C., Shriver, S., Hu, H., Labadie, S. S., Liang, J., Wang, L., Wang, J., Lu, Y., Purkey, H. E., Quinn, J., Franke, Y., Clark, K., Beresini, M. H., Tan, M. W., Sellers, B. D., Maurer, T., Koehler, M. F. T., Wecksler, A. T., Kiefer, J. R., Verma, V., Xu, Y., Nishiyama, M., Payandeh, J. & Koth, C. M. (2018). Structural basis for dual-mode inhibition of the ABC transporter MsbA. *Nature,* 557**,** 196-201.

Hobbs, E. C., Yin, X., Paul, B. J., Astarita, J. L. & Storz, G. (2012). Conserved small protein associates with the multidrug efflux pump AcrB and differentially affects antibiotic resistance. *Proceedings of the National Academy of Sciences of the United States of America,* 109**,** 16696-701.

Hoffmann, K. M., Williams, D., Shafer, W. M. & Brennan, R. G. (2005). Characterization of the multiple transferable resistance repressor, MtrR, from *Neisseria gonorrhoeae*. *Journal of Bacteriology,* 187**,** 5008-12.

Holler, J. G., Christensen, S. B., Slotved, H.-C., Rasmussen, H. B., Gúzman, A., Olsen, C.-E., Petersen, B. & Mølgaard, P. (2012). Novel inhibitory activity of the *Staphylococcus aureus* NorA efflux pump by a kaempferol rhamnoside isolated from *Persea lingue Nees*. *Journal of Antimicrobial Chemotherapy,* 67**,** 1138-44.

Holley, C. L., Dhulipala, V., Balthazar, J. T., Le Van, A., Begum, A. A., Chen, S.-C., Read, T. D., Matoga, M., Hoffman, I. F. & Golparian, D. (2022). A single amino acid substitution in elongation factor G can confer low-level gentamicin resistance in *Neisseria gonorrhoeae*. *Antimicrobial Agents and Chemotherapy,* 66**,** e00251-22.

Hollingsworth, S. A. & Karplus, P. A. (2010). A fresh look at the Ramachandran plot and the occurrence of standard structures in proteins. *Biomolecular Concepts,* 1**,** 271-83.

Holmes, A. H., Moore, L. S., Sundsfjord, A., Steinbakk, M., Regmi, S., Karkey, A., Guerin, P. J. & Piddock, L. J. (2016). Understanding the mechanisms and drivers of antimicrobial resistance. *Lancet,* 387**,** 176-87.

Holmes, K. K., Counts, G. W. & Beaty, H. N. (1971). Disseminated gonococcal infection. *Annals of Internal Medicine,* 74**,** 979-93.

Hooft, R. W., Vriend, G., Sander, C. & Abola, E. E. (1996). Errors in protein structures. *Nature,* 381**,** 272.

Hooks, G. M., Ayala, J. C., Holley, C. L., Dhulipala, V., Beggs, G. A., Perfect, J. R., Schumacher, M. A., Shafer, W. M. & Brennan, R. G. (2024). Hormonal steroids induce multidrug resistance and stress response genes in Neisseria gonorrhoeae by binding to MtrR. *Nature Communications,* 15**,** 1153.

Huang, H. & Hancock, R. (1996). The role of specific surface loop regions in determining the function of the imipenem-specific pore protein OprD of *Pseudomonas aeruginosa*. *Journal of Bacteriology,* 178**,** 3085-90.

Huang, Y., He, G., Tian, W., Li, D., Meng, L., Wu, D. & He, T. (2021). Genome-wide identification of MATE gene family in potato (*Solanum tuberosum* L.) and expression analysis in heavy metal stress. *Frontiers in Genetics,* 12**,** https://doi.org/10.3389/fgene.2021.650500.

Huang, Y., Lemieux, M. J., Song, J., Auer, M. & Wang, D.-N. (2003). Structure and mechanism of the glycerol-3-phosphate transporter from *Escherichia coli*. *Science,* 301**,** 616-20.

Humphrey, W., Dalke, A. & Schulten, K. (1996). VMD: visual molecular dynamics. *Journal of Molecular Graphics,* 14**,** 33-8.

Hung, L.-W., Kim, H.-B., Murakami, S., Gupta, G., Kim, C.-Y. & Terwilliger, T. C. (2013). Crystal structure of AcrB complexed with linezolid at 3.5 Å resolution. *Journal of Structural and Functional Genomics,* 14**,** 71-5.

Husain, F., Humbard, M. & Misra, R. (2004). Interaction between the TolC and AcrA proteins of a multidrug efflux system of *Escherichia coli*. *Journal of Bacteriology,* 186**,** 8533-6.

Husain, F. & Nikaido, H. (2010). Substrate path in the AcrB multidrug efflux pump of *Escherichia coli*. *Molecular Microbiology,* 78**,** 320-30.

Hussein, M. J., Green, J. M. & Nichols, B. P. (1998). Characterization of mutations that allow *p*-aminobenzoyl-glutamate utilization by *Escherichia coli*. *Journal of Bacteriology,* 180**,** 6260-8.

Hvorup, R. N., Winnen, B., Chang, A. B., Jiang, Y., Zhou, X. F. & Saier Jr, M. H. (2003). The multidrug/oligosaccharidyl-lipid/polysaccharide (MOP) exporter superfamily. *European Journal of Biochemistry,* 270**,** 799-813.

Imai, T., Miyashita, N., Sugita, Y., Kovalenko, A., Hirata, F. & Kidera, A. (2011). Functionality mapping on internal surfaces of multidrug transporter AcrB based on molecular theory of solvation: implications for drug efflux pathway. *The Journal of Physical Chemistry B,* 115**,** 8288-95.

Ito, S., Kusuhara, H., Kuroiwa, Y., Wu, C., Moriyama, Y., Inoue, K., Kondo, T., Yuasa, H., Nakayama, H. & Horita, S. (2010). Potent and specific inhibition of mMate1-mediated efflux of type I organic cations in the liver and kidney by pyrimethamine. *Journal of Pharmacology and Experimental Therapeutics,* 333**,** 341-50.

Jack, D. L., Yang, N. M. & Saier, M. H., Jr. (2001). The drug/metabolite transporter superfamily. *European Journal of Biochemistry,* 268**,** 3620-39.

Jackson, L. A., Ducey, T. F., Day, M. W., Zaitshik, J. B., Orvis, J. & Dyer, D. W. (2010). Transcriptional and functional analysis of the *Neisseria gonorrhoeae* Fur regulon. *Journal of Bacteriology,* 192**,** 77-85.

Jagessar, K. L., Claxton, D. P., Stein, R. A. & Mchaourab, H. S. (2020). Sequence and structural determinants of ligand-dependent alternating access of a MATE transporter. *Proceedings of the National Academy of Sciences,* 117**,** 4732-40.

Janganan, T. K., Bavro, V. N., Zhang, L., Borges-Walmsley, M. I. & Walmsley, A. R. (2013). Tripartite efflux pumps: energy is required for dissociation, but not assembly or opening of the outer membrane channel of the pump. *Molecular Microbiology,* 88**,** 590-602.

Janganan, T. K., Bavro, V. N., Zhang, L., Matak-Vinkovic, D., Barrera, N. P., Venien-Bryan, C., Robinson, C. V., Borges-Walmsley, M. I. & Walmsley, A. R. (2011a). Evidence for the assembly of a bacterial tripartite multidrug pump with a stoichiometry of 3:6:3. *Journal of Biological Chemistry,* 286**,** 26900-12.

Janganan, T. K., Zhang, L., Bavro, V. N., Matak-Vinkovic, D., Barrera, N. P., Burton, M. F., Steel, P. G., Robinson, C. V., Borges-Walmsley, M. I. & Walmsley, A. R. (2011b). Opening of the outer membrane protein channel in tripartite efflux pumps is induced by interaction with the membrane fusion partner. *The Journal of Biological Chemistry,* 286**,** 5484-93.

Jerse, A. E., Sharma, N. D., Simms, A. N., Crow, E. T., Snyder, L. A. & Shafer, W. M. (2003). A gonococcal efflux pump system enhances bacterial survival in a female mouse model of genital tract infection. *Infection and Immunity,* 71**,** 5576-82.

Jewel, Y., Liu, J. & Dutta, P. (2017). Coarse-grained simulations of conformational changes in the multidrug efflux transporter AcrB. *Molecular BioSystems,* 13**,** 2006-14.

Jewel, Y., Van Dinh, Q., Liu, J. & Dutta, P. (2020). Substrate-dependent transport mechanism in AcrB of multidrug resistant bacteria. *Proteins,* 88**,** 853-64.

Jia, R., Martens, C., Shekhar, M., Pant, S., Pellowe, G. A., Lau, A. M., Findlay, H. E., Harris, N. J., Tajkhorshid, E. & Booth, P. J. (2020). Hydrogen-deuterium exchange mass spectrometry captures distinct dynamics upon substrate and inhibitor binding to a transporter. *Nature Communications,* 11**,** 6162.

Jiang, D., Zhao, Y., Wang, X., Fan, J., Heng, J., Liu, X., Feng, W., Kang, X., Huang, B., Liu, J. & Zhang, X. C. (2013). Structure of the YajR transporter suggests a transport mechanism based on the conserved motif A. *Proceedings of the National Academy of Sciences of the United States of America,* 110**,** 14664-9.

Jodaitis, L., van Oene, T. & Martens, C. (2021). Assessing the Role of Lipids in the Molecular Mechanism of Membrane Proteins. *International Journal of Molecular Sciences,* 22.

Johnson, P. J. & Shafer, W. M. (2015). The transcriptional repressor, MtrR, of the *mtrCDE* efflux pump operon of *Neisseria gonorrhoeae* can also serve as an activator of “off target” gene (*glnE*) expression. *Antibiotics,* 4**,** 188-97.

Johnston, C., Martin, B., Fichant, G., Polard, P. & Claverys, J.-P. (2014). Bacterial transformation: distribution, shared mechanisms and divergent control. *Nature Reviews Microbiology,* 12**,** 181-96.

Jones, R. A., Jerse, A. E. & Tang, C. M. (2023). Gonococcal PorB: a multifaceted modulator of host immune responses. *Trends in Microbiology***,** DOI: https://doi.org/10.1016/j.tim.2023.10.002.

Jorgensen, J. H. & Turnidge, J. D. 2015. Antibacterial agents and susceptibility test methods. *In:* JORGENSEN, J. H. & PFALLER, M. A. (eds.) *Manual of Clinical Microbiology.* ASM Press.

Jurasz, J., Bagiński, M., Czub, J. & Wieczór, M. (2021). Molecular mechanism of proton-coupled ligand translocation by the bacterial efflux pump EmrE. *PLoS Computational Biology,* 17**,** e1009454.

Kaatz, G. W., McAleese, F. & Seo, S. M. (2005). Multidrug resistance in *Staphylococcus aureus* due to overexpression of a novel multidrug and toxin extrusion (MATE) transport protein. *Antimicrobial Agents and Chemotherapy,* 49**,** 1857-64.

Kakooza, F., Golparian, D., Matoga, M., Maseko, V., Lamorde, M., Krysiak, R., Manabe, Y. C., Chen, J. S., Kularatne, R., Jacobsson, S., Godreuil, S., Hoffman, I., Bercot, B., Wi, T., Unemo, M. & Group, o. b. o. t. W. S. (2023). Genomic surveillance and antimicrobial resistance determinants in *Neisseria gonorrhoeae* isolates from Uganda, Malawi and South Africa, 2015–20. *Journal of Antimicrobial Chemotherapy,* 78**,** 1982-91.

Kar, D., Pradhan, A. A., Dutta, A., Bhagavatula, L. & Datta, S. 2022. The multidrug and toxic compound extrusion (MATE) family in plants and their significance in metal transport. *In:* KUMAR, K. & SRIVASTAVA, S. (eds.) *Plant metal and metalloid transporters.* Singapore: Springer Nature Singapore.

Kato, T., Okada, U., Hung, L.-W., Yamashita, E., Kim, H.-B., Kim, C.-Y., Terwilliger, T. C., Schweizer, H. P. & Murakami, S. (2023). Crystal structures of multidrug efflux transporters from *Burkholderia pseudomallei* suggest details of transport mechanism. *Proceedings of the National Academy of Sciences,* 120**,** e2215072120.

Kazmier, K., Claxton, D. P. & McHaourab, H. S. (2017). Alternating access mechanisms of LeuT-fold transporters: trailblazing towards the promised energy landscapes. *Current Opinion in Structural Biology,* 45**,** 100-8.

Kellogg, D. S., Peacock, W. L., Deacon, W., Brown, L. & Pirkle, C. I. (1963). *Neisseria gonorrhoeae* I: virulence genetically linked to clonal variation. *Journal of Bacteriology,* 85**,** 1274-9.

Kerle, K., Mascola, J. & Miller, T. (1992). Disseminated gonococcal infection. *American Family Physician,* 45**,** 209.

Kermani, A. A., Burata, O. E., Koff, B. B., Koide, A., Koide, S. & Stockbridge, R. B. (2022). Crystal structures of bacterial small multidrug resistance transporter EmrE in complex with structurally diverse substrates. *Elife,* 11**,** e76766.

Kermani, A. A., Macdonald, C. B., Burata, O. E., Koff, B. B., Koide, A., Denbaum, E., Koide, S. & Stockbridge, R. B. (2020). The structural basis of promiscuity in small multidrug resistance transporters. *Nature Communications,* 11**,** 1-9.

Kermani, A. A., Macdonald, C. B., Gundepudi, R. & Stockbridge, R. B. (2018). Guanidinium export is the primal function of SMR family transporters. *Proceedings of the National Academy of Sciences,* 115**,** 3060-5.

Ketterer, M. R., Rice, P. A., Gulati, S., Kiel, S., Byerly, L., Fortenberry, J. D., Soper, D. E. & Apicella, M. A. (2016). Desialylation of *Neisseria gonorrhoeae* lipooligosaccharide by cervicovaginal microbiome sialidases: the potential for enhancing infectivity in men. *The Journal of Infectious Diseases,* 214**,** 1621-8.

Kikukawa, T., Miyauchi, S., Araiso, T., Kamo, N. & Nara, T. (2007). Anti-parallel membrane topology of two components of EbrAB, a multidrug transporter. *Biochemical and Biophysical Research Communications,* 358**,** 1071-5.

Kikukawa, T., Nara, T., Araiso, T., Miyauchi, S. & Kamo, N. (2006). Two-component bacterial multidrug transporter, EbrAB: Mutations making each component solely functional. *Biochimica et Biophysica Acta,* 1758**,** 673-9.

Kinana, A. D., Vargiu, A. V., May, T. & Nikaido, H. (2016). Aminoacyl β-naphthylamides as substrates and modulators of AcrB multidrug efflux pump. *Proceedings of the National Academy of Sciences,* 113**,** 1405-10.

Kinana, A. D., Vargiu, A. V. & Nikaido, H. (2013). Some ligands enhance the efflux of other ligands by the *Escherichia coli* multidrug pump AcrB. *Biochemistry,* 52**,** 8342-51.

Kirn, T. J., Lafferty, M. J., Sandoe, C. M. & Taylor, R. K. (2000). Delineation of pilin domains required for bacterial association into microcolonies and intestinal colonization by *Vibrio cholerae*. *Molecular Microbiology,* 35**,** 896-910.

Klein, E. J., Fisher, L. S., Chow, A. W. & Guze, L. B. (1977). Anorectal gonococcal infection. *Annals of Internal Medicine,* 86**,** 340-6.

Klenotic, P. A., Moseng, M. A., Morgan, C. E. & Yu, E. W. (2021). Structural and functional diversity of resistance-nodulation-cell division transporters. *Chemical Reviews,* 121**,** 5378–416.

Kline, K. A., Criss, A. K., Wallace, A. & Seifert, H. S. (2007). Transposon mutagenesis identifies sites upstream of the *Neisseria gonorrhoeae pilE*

gene that modulate pilin antigenic variation. *Journal of Bacteriology,* 189**,** 3462-70.

Kobayashi, N., Nishino, K. & Yamaguchi, A. (2001). Novel macrolide-specific ABC-type efflux transporter in *Escherichia coli*. *Journal of Bacteriology,* 183**,** 5639-44.

Kobayashi, N., Tamura, N., van Veen, H. W., Yamaguchi, A. & Murakami, S. (2014). β-Lactam selectivity of multidrug transporters AcrB and AcrD resides in the proximal binding pocket. *Journal of Biological Chemistry,* 289**,** 10680-90.

Kobylka, J., Kuth, M. S., Muller, R. T., Geertsma, E. R. & Pos, K. M. (2020). AcrB: a mean, keen, drug efflux machine. *Annals of the New York Academy of Sciences,* 1459**,** 38-68.

Kojima, S. & Nikaido, H. (2013). Permeation rates of penicillins indicate that *Escherichia coli* porins function principally as nonspecific channels. *Proceedings of the National Academy of Sciences of the United States of America,* 110**,** E2629-34.

Koomey, M. (1998). Competence for natural transformation in *Neisseria gonorrhoeae*: a model system for studies of horizontal gene transfer. *APMIS. Supplementum,* 84**,** 56-61.

Korkhov, V. M. & Tate, C. G. (2008). Electron crystallography reveals plasticity within the drug binding site of the small multidrug transporter EmrE. *Journal of Molecular Biology,* 377**,** 1094-103.

Koronakis, V., Sharff, A., Koronakis, E., Luisi, B. & Hughes, C. (2000). Crystal structure of the bacterial membrane protein TolC central to multidrug efflux and protein export. *Nature,* 405**,** 914-9.

Kowalczykowski, S. C. (2008). Snapshots of DNA repair. *Nature,* 453**,** 463-5.

Kowalczykowski, S. C. (2015). An overview of the molecular mechanisms of recombinational DNA repair. *Cold Spring Harbor Perspectives in Biology,* 7**,** a016410.

Koziara, K. B., Stroet, M., Malde, A. K. & Mark, A. E. (2014). Testing and validation of the Automated Topology Builder (ATB) version 2.0: prediction of hydration free enthalpies. *Journal of Computer-Aided Molecular Design,* 28**,** 221-33.

Krah, A., Huber, R. G., Zachariae, U. & Bond, P. J. (2020). On the ion coupling mechanism of the MATE transporter ClbM. *Biochimica et Biophysica Acta (BBA)-Biomembranes,* 1862**,** 183137.

Krishnamoorthy, G., Tikhonova, E. B., Dhamdhere, G. & Zgurskaya, H. I. (2013). On the role of TolC in multidrug efflux: the function and assembly of AcrAB-TolC tolerate significant depletion of intracellular TolC protein. *Molecular Microbiology,* 87**,** 982-97.

Krishnamoorthy, G., Wolloscheck, D., Weeks, J. W., Croft, C., Rybenkov, V. V. & Zgurskaya, H. I. (2016). Breaking the permeability barrier of *Escherichia coli* by controlled hyperporination of the outer membrane. *Antimicrobial Agents and Chemotherapy,* 60**,** 7372-81.

Kroll, J. S., Wilks, K. E., Farrant, J. L. & Langford, P. R. (1998). Natural genetic exchange between *Haemophilus* and *Neisseria*: intergeneric transfer of chromosomal genes between major human pathogens. *Proceedings of the National Academy of Sciences of the United States of America,* 95**,** 12381-5.

Kuo, K. M., Pang, Y. T., Lynch, D. L., Gumbart, J. C. & Zgurskaya, H. I. (2024). From closed to open: Exploring the conformational changes and influence of a biochemical inhibitor on efflux pump AcrAB-TolC. *Biophysical Journal,* 123**,** 485a.

Kuroda, T. & Tsuchiya, T. (2009). Multidrug efflux transporters in the MATE family. *Biochimica et Biophysica Acta (BBA)-Proteins and Proteomics,* 1794**,** 763-8.

Kusakizako, T., Miyauchi, H., Ishitani, R. & Nureki, O. (2020). Structural biology of the multidrug and toxic compound extrusion superfamily transporters. *Biochimica et Biophysica Acta (BBA)-Biomembranes,* 1862**,** 183154.

Kwon, H. J., Bennik, M. H., Demple, B. & Ellenberger, T. (2000). Crystal structure of the *Escherichia coli* Rob transcription factor in complex with DNA. *Nature Structural Biology,* 7**,** 424-30.

Laga, M., Meheus, A. & Piot, P. (1989). Epidemiology and control of gonococcal ophthalmia neonatorum. *Bulletin of the World Health Organization,* 67**,** 471.

Lahra, M. M., Hogan, T. R. & Armstrong, B. H. (2022). Australian Gonococcal Surveillance Programme Annual Report, 2021. Commun Dis Intell. 46.

Lahra, M. M., Martin, I., Demczuk, W., Jennison, A. V., Lee, K.-I., Nakayama, S.-I., Lefebvre, B., Longtin, J., Ward, A. & Mulvey, M. R. (2018). Cooperative recognition of internationally disseminated ceftriaxone-resistant *Neisseria gonorrhoeae* strain. *Emerging Infectious Diseases,* 24**,** 735-40.

Lambert, B. & LePecq, J. B. (1984). Effect of mutation, electric membrane potential, and metabolic inhibitors on the accessibility of nucleic acids to ethidium bromide in *Escherichia coli* cells. *Biochemistry,* 23**,** 166-76.

Lamers, R. P., Cavallari, J. F. & Burrows, L. L. (2013). The efflux inhibitor phenylalanine-arginine beta-naphthylamide (PAβN) permeabilizes the outer membrane of Gram-negative bacteria. *PLoS One,* 8**,** e60666.

Laskos, L., Ryan, C. S., Fyfe, J. A. & Davies, J. K. (2004). The RpoH-mediated stress response in *Neisseria gonorrhoeae* is regulated at the level of activity. *Journal of Bacteriology,* 186**,** 8443-52.

Lau, C. H., Hughes, D. & Poole, K. (2014). MexY-promoted aminoglycoside resistance in *Pseudomonas aeruginosa*: involvement of a putative proximal binding pocket in aminoglycoside recognition. *mBio,* 5**,** e01068.

Laurence, M. J., Carpenter, T. S., Laurence, T. A., Coleman, M. A., Shelby, M. & Liu, C. (2022). Biophysical characterization of membrane proteins embedded in nanodiscs using fluorescence correlation spectroscopy. *Membranes,* 12**,** 392.

Law, C. J., Maloney, P. C. & Wang, D.-N. (2008). Ins and outs of major facilitator superfamily antiporters. *Annual Review of Microbiology,* 62**,** 289.

Le, T. B., Schumacher, M. A., Lawson, D. M., Brennan, R. G. & Buttner, M. J. (2011). The crystal structure of the TetR family transcriptional repressor SimR bound to DNA and the role of a flexible N-terminal extension in minor groove binding. *Nucleic Acids Research,* 39**,** 9433-47.

Lee, E. H., Hill, S. A., Napier, R. & Shafer, W. M. (2006). Integration Host Factor is required for FarR repression of the *farAB*-encoded efflux pump of *Neisseria gonorrhoeae*. *Molecular Microbiology,* 60**,** 1381-400.

Lee, E. H., Rouquette-Loughlin, C., Folster, J. P. & Shafer, W. M. (2003). FarR regulates the *farAB*-encoded efflux pump of *Neisseria gonorrhoeae* via an MtrR regulatory mechanism. *Journal of Bacteriology,* 185**,** 7145-52.

Lee, E. H. & Shafer, W. M. (1999). The *farAB*-encoded efflux pump mediates resistance of gonococci to long-chained antibacterial fatty acids. *Molecular Microbiology,* 33**,** 839-45.

Lei, H. T., Chou, T. H., Su, C. C., Bolla, J. R., Kumar, N., Radhakrishnan, A., Long, F., Delmar, J. A., Do, S. V., Rajashankar, K. R., Shafer, W. M. & Yu, E. W. (2014). Crystal structure of the open state of the *Neisseria gonorrhoeae* MtrE outer membrane channel. *PLoS One,* 9**,** e97475.

Leung, Y. M., Holdbrook, D. A., Piggot, T. J. & Khalid, S. (2014). The NorM MATE transporter from *N. gonorrhoeae*: insights into drug and ion binding from atomistic molecular dynamics simulations. *Biophysical Journal,* 107**,** 460-8.

Lewinson, O., Adler, J., Poelarends, G. J., Mazurkiewicz, P., Driessen, A. J. & Bibi, E. (2003). The *Escherichia coli* multidrug transporter MdfA catalyzes both electrogenic and electroneutral transport reactions. *Proceedings of the National Academy of Sciences of the United States of America,* 100**,** 1667-72.

Lewinson, O., Padan, E. & Bibi, E. (2004). Alkalitolerance: a biological function for a multidrug transporter in pH homeostasis. *Proceedings of the National Academy of Sciences of the United States of America,* 101**,** 14073-8.

Lewis, J. S. & Bush, K. 2015. Antibacterial agents. *Manual of Clinical Microbiology, Eleventh Edition.* American Society of Microbiology.

Lewis, K. (1994). Multidrug resistance pumps in bacteria: variations on a theme. *Trends in Biochemical Sciences,* 19**,** 119-23.

Li, J., Zhang, H., Ning, J., Sajid, A., Cheng, G., Yuan, Z. & Hao, H. (2019). The nature and epidemiology of OqxAB, a multidrug efflux pump. *Antimicrobial Resistance & Infection Control,* 8**,** 1-13.

Li, M., Gu, R., Su, C. C., Routh, M. D., Harris, K. C., Jewell, E. S., McDermott, G. & Yu, E. W. (2007). Crystal structure of the transcriptional regulator AcrR from *Escherichia coli*. *Journal of Molecular Biology,* 374**,** 591-603.

Li, X., Lu, F., Trinh, M. N., Schmiege, P., Seemann, J., Wang, J. & Blobel, G. (2017). 3.3 Å structure of Niemann–Pick C1 protein reveals insights into the function of the C-terminal luminal domain in cholesterol transport. *Proceedings of the National Academy of Sciences of the United States of America,* 114**,** 9116-21.

Li, X. Z., Ma, D., Livermore, D. M. & Nikaido, H. (1994). Role of efflux pump(s) in intrinsic resistance of *Pseudomonas aeruginosa*: active efflux as a contributing factor to beta-lactam resistance. *Antimicrobial Agents and Chemotherapy,* 38**,** 1742-52.

Li, X. Z., Plesiat, P. & Nikaido, H. (2015). The challenge of efflux-mediated antibiotic resistance in Gram-negative bacteria. *Clinical Microbiology Reviews,* 28**,** 337-418.

Li, Y., Acharya, A., Yang, L., Liu, J., Tajkhorshid, E., Zgurskaya, H. I., Jackson, M. & Gumbart, J. C. (2023). Insights into substrate transport and water permeation in the mycobacterial transporter MmpL3. *Biophysical Journal,* 122**,** 2342-52.

Li, Y., Hopper, A., Overton, T., Squire, D. J., Cole, J. & Tovell, N. (2010). Organization of the electron transfer chain to oxygen in the obligate human pathogen *Neisseria gonorrhoeae*: roles for cytochromes c4 and c5, but not cytochrome c2, in oxygen reduction. *Journal of Bacteriology,* 192**,** 2395-406.

Lin, J., Michel, L. O. & Zhang, Q. (2002). CmeABC functions as a multidrug efflux system in *Campylobacter jejuni*. *Antimicrobial Agents and Chemotherapy,* 46**,** 2124-31.

Lindahl, E., Abraham, M., Hess, B. & van der Spoel, D. 2019. GROMACS 2019.4 Source Code.

Lindberg, R., Fredlund, H., Nicholas, R. & Unemo, M. (2007). *Neisseria gonorrhoeae* isolates with reduced susceptibility to cefixime and ceftriaxone: association with genetic polymorphisms in *penA*, *mtrR*, *porB*1b, and *ponA*. *Antimicrobial Agents and Chemotherapy,* 51**,** 2117-22.

Littlejohn, T. G., DiBerardino, D., Messerotti, L. J., Spiers, S. J. & Skurray, R. A. (1991). Structure and evolution of a family of genes encoding antiseptic and disinfectant resistance in *Staphylococcus aureus*. *Gene,* 101**,** 59-66.

Littlejohn, T. G., Paulsen, I. T., Gillespie, M. T., Tennent, J. M., Midgley, M., Jones, I. G., Purewal, A. S. & Skurray, R. A. (1992). Substrate specificity and energetics of antiseptic and disinfectant resistance in *Staphylococcus aureus*. *FEMS Microbiology Letters,* 95**,** 259-65.

Liu, G., Tang, C. M. & Exley, R. M. (2015). Non-pathogenic *Neisseria*: members of an abundant, multi-habitat, diverse genus. *Microbiology,* 161**,** 1297-312.

Liu, H., Zhang, Y., Wang, Y., Xie, X. & Shi, Q. (2021). The connection between Czc and Cad systems involved in cadmium resistance in *Pseudomonas putida*. *International Journal of Molecular Sciences,* 22**,** 9697.

Liu, Q., Hassan, K. A., Ashwood, H. E., Gamage, H. K., Li, L., Mabbutt, B. C. & Paulsen, I. T. (2018). Regulation of the *aceI* multidrug efflux pump gene in *Acinetobacter baumannii*. *Journal of Antimicrobial Chemotherapy,* 73**,** 1492-500.

Liyayi, I. K., Forehand, A. L., Ray, J. C. & Criss, A. K. (2023). Metal piracy by *Neisseria gonorrhoeae* to overcome human nutritional immunity. *PLoS Pathogens,* 19**,** e1011091.

Lo, H., Tang, C. M. & Exley, R. M. (2009). Mechanisms of avoidance of host immunity by *Neisseria meningitidis* and its effect on vaccine development. *The Lancet Infectious Diseases,* 9**,** 418-27.

Lobedanz, S., Bokma, E., Symmons, M. F., Koronakis, E., Hughes, C. & Koronakis, V. (2007). A periplasmic coiled-coil interface underlying TolC recruitment and the assembly of bacterial drug efflux pumps. *Proceedings of the National Academy of Sciences of the United States of America,* 104**,** 4612-7.

Locher, K. P. (2016). Mechanistic diversity in ATP-binding cassette (ABC) transporters. *Nature Structural & Molecular Biology,* 23**,** 487-93.

Lomize, M. A., Pogozheva, I. D., Joo, H., Mosberg, H. I. & Lomize, A. L. (2011). OPM database and PPM web server: resources for positioning of proteins in membranes. *Nucleic Acids Research,* 40**,** D370-D6.

Lomovskaya, O. & Bostian, K. A. (2006). Practical applications and feasibility of efflux pump inhibitors in the clinic—a vision for applied use. *Biochemical Pharmacology,* 71**,** 910-8.

Lomovskaya, O. & Lewis, K. (1992). *emr*, an *Escherichia coli* locus for multidrug resistance. *Proceedings of the National Academy of Sciences of the United States of America,* 89**,** 8938-42.

Lomovskaya, O., Warren, M. S., Lee, A., Galazzo, J., Fronko, R., Lee, M., Blais, J., Cho, D., Chamberland, S., Renau, T., Leger, R., Hecker, S., Watkins, W., Hoshino, K., Ishida, H. & Lee, V. J. (2001). Identification and characterization of inhibitors of multidrug resistance efflux pumps in *Pseudomonas aeruginosa*: Novel agents for combination therapy. *Antimicrobial Agents and Chemotherapy,* 45**,** 105-16.

Lomovskaya, O. & Watkins, W. (2001). Inhibition of efflux pumps as a novel approach to combat drug resistance in bacteria. *Journal of Molecular Microbiology and Biotechnology,* 3**,** 225-36.

Long, F., Rouquette-Loughlin, C., Shafer, W. M. & Yu, E. W. (2008). Functional cloning and characterization of the multidrug efflux pumps NorM from *Neisseria gonorrhoeae* and YdhE from *Escherichia coli*. *Antimicrobial Agents and Chemotherapy,* 52**,** 3052-60.

Long, F., Su, C.-C., Zimmermann, M. T., Boyken, S. E., Rajashankar, K. R., Jernigan, R. L. & Yu, E. W. (2010). Crystal structures of the CusA efflux pump suggest methionine-mediated metal transport. *Nature,* 467**,** 484-8.

Lopez, C. A., Travers, T., Pos, K. M., Zgurskaya, H. I. & Gnanakaran, S. (2017). Dynamics of intact MexAB-OprM efflux pump: focusing on the MexA-OprM interface. *Scientific Reports,* 7**,** 16521.

Lorenz, M. G. & Wackernagel, W. (1994). Bacterial gene transfer by natural genetic transformation in the environment. *Microbiological Reviews,* 58**,** 563-602.

Lu, M. (2016). Structures of multidrug and toxic compound extrusion transporters and their mechanistic implications. *Channels,* 10**,** 88-100.

Lu, M., Radchenko, M., Symersky, J., Nie, R. & Guo, Y. (2013a). Structural insights into H^+-coupled multidrug extrusion by a MATE transporter. *Nature Structural & Molecular Biology,* 20**,** 1310-7.

Lu, M., Symersky, J., Radchenko, M., Koide, A., Guo, Y., Nie, R. & Koide, S. (2013b). Structures of a Na^+-coupled, substrate-bound MATE multidrug transporter. *Proceedings of the National Academy of Sciences of the United States of America,* 110**,** 2099-104.

Lu, S. & Zgurskaya, H. I. (2013). MacA, a periplasmic membrane fusion protein of the macrolide transporter MacAB-TolC, binds lipopolysaccharide core specifically and with high affinity. *Journal of Bacteriology,* 195**,** 4865-72.

Lv, L., Wan, M., Wang, C., Gao, X., Yang, Q., Partridge, S. R., Wang, Y., Zong, Z., Doi, Y., Shen, J., Jia, P., Song, Q., Zhang, Q., Yang, J., Huang, X., Wang, M. & Liu, J. H. (2020). Emergence of a plasmid-encoded resistance-nodulation-division efflux pump conferring resistance to multiple drugs, including tigecycline, in *Klebsiella pneumoniae*. *mBio,* 11.

Lyon, B. R. & Skurray, R. (1987). Antimicrobial resistance of *Staphylococcus aureus*: genetic basis. *Microbiological Reviews,* 51**,** 88-134.

Lyu, M., Ayala, J. C., Chirakos, I., Su, C.-C., Shafer, W. M. & Yu, E. W. (2022). Structural basis of peptide-based antimicrobial inhibition of a resistance-nodulation-cell division multidrug efflux pump. *Microbiology Spectrum,* 10**,** e02990-22.

Lyu, M., Moseng, M. A., Reimche, J. L., Holley, C. L., Dhulipala, V., Su, C. C., Shafer, W. M. & Yu, E. W. (2020). Cryo-EM structures of a gonococcal multidrug efflux pump illuminate a mechanism of drug recognition and resistance. *mBio,* 11**,** e.00996-20.

Ma, D., Alberti, M., Lynch, C., Nikaido, H. & Hearst, J. E. (1996). The local repressor AcrR plays a modulating role in the regulation of *acrAB* genes of *Escherichia coli* by global stress signals. *Molecular Microbiology,* 19**,** 101-12.

Ma, D., Cook, D. N., Alberti, M., Pon, N. G., Nikaido, H. & Hearst, J. E. (1993). Molecular cloning and characterization of *acrA* and *acrE* genes of *Escherichia coli*. *Journal of Bacteriology,* 175**,** 6299-313.

Ma, D., Cook, D. N., Alberti, M., Pon, N. G., Nikaido, H. & Hearst, J. E. (1995). Genes *acrA* and *acrB* encode a stress-induced efflux system of *Escherichia coli*. *Molecular Microbiology,* 16**,** 45-55.

Ma, D., Cook, D. N., Hearst, J. E. & Nikaido, H. (1994). Efflux pumps and drug resistance in Gram-negative bacteria. *Trends in Microbiology,* 2**,** 489-93.

Ma, K. C., Mortimer, T. D. & Grad, Y. H. (2020a). Efflux pump antibiotic binding site mutations are associated with azithromycin nonsusceptibility in clinical *Neisseria gonorrhoeae* isolates. *mBio,* 11**,** 10.1128/mbio.01509-20.

Ma, K. C., Mortimer, T. D., Hicks, A. L., Wheeler, N. E., Sánchez-Busó, L., Golparian, D., Taiaroa, G., Rubin, D. H., Wang, Y. & Williamson, D. A. (2020b). Adaptation to the cervical environment is associated with increased antibiotic susceptibility in *Neisseria gonorrhoeae*. *Nature Communications,* 11**,** 1-11.

MacDermott-Opeskin, H. I., Gupta, V. & O'Mara, M. L. (2022). Lipid-mediated antimicrobial resistance: a phantom menace or a new hope? *Biophys Rev,* 14**,** 145-62.

Macdonald, C. B., Kermani, A. A. & Stockbridge, R. B. (2020). Overlapping substrate specificities in the small multidrug resistance (SMR) family of transporters. *Biophysical Journal,* 118**,** 130a.

Mackie, A. M., Hassan, K. A., Paulsen, I. T. & Tetu, S. G. (2014). Biolog phenotype microarrays for phenotypic characterization of microbial cells. *Environmental Microbiology: Methods and Protocols***,** 123-30.

Mahamoud, A., Chevalier, J., Alibert-Franco, S., Kern, W. V. & Pagès, J.-M. (2007). Antibiotic efflux pumps in Gram-negative bacteria: the inhibitor response strategy. *Journal of Antimicrobial Chemotherapy,* 59**,** 1223-9.

Mahlapuu, M., Håkansson, J., Ringstad, L. & Björn, C. (2016). Antimicrobial peptides: an emerging category of therapeutic agents. *Frontiers in Cellular and Infection Microbiology,* 6**,** 194.

Maier, B., Potter, L., So, M., Seifert, H. S. & Sheetz, M. P. (2002). Single pilus motor forces exceed 100 pN. *Proceedings of the National Academy of Sciences of the United States of America,* 99**,** 16012-7.

Maier, T. W., Zubrzycki, L. & Coyle, M. B. (1975). Genetic analysis of drug resistance in *Neisseria gonorrhoeae*: identification and linkage relationships of loci controlling drug resistance. *Antimicrobial Agents and Chemotherapy,* 7**,** 676-81.

Maiorov, V. N. & Crippen, G. M. (1994). Significance of root-mean-square deviation in comparing three-dimensional structures of globular proteins. *Journal of Molecular Biology,* 235**,** 625-34.

Malde, A. K., Zuo, L., Breeze, M., Stroet, M., Poger, D., Nair, P. C., Oostenbrink, C. & Mark, A. E. (2011). An automated force field topology builder (ATB) and repository: version 1.0. *Journal of Chemical Theory and Computation,* 7**,** 4026-37.

Malvacio, I., Buonfiglio, R., D'Atanasio, N., Serra, G., Bosin, A., Di Giorgio, F. P., Ruggerone, P., Ombrato, R. & Vargiu, A. V. (2019). Molecular basis for the different interactions of congeneric substrates with the polyspecific transporter AcrB. *Biochimica et Biophysica Acta (BBA)-Biomembranes,* 1861**,** 1397-408.

Mamelli, L., Amoros, J. P., Pages, J. M. & Bolla, J. M. (2003). A phenylalanine-arginine β-naphthylamide sensitive multidrug efflux pump involved in intrinsic and acquired resistance of *Campylobacter* to macrolides. *International Journal of Antimicrobial Agents,* 22**,** 237-41.

Maness, M. J. & Sparling, P. F. (1973). Multiple antibiotic resistance due to a single mutation in *Neisseria gonorrhoeae*. *Journal of Infectious Diseases,* 128**,** 321-30.

Maron, L. G., Pineros, M. A., Guimaraes, C. T., Magalhaes, J. V., Pleiman, J. K., Mao, C., Shaff, J., Belicuas, S. N. & Kochian, L. V. (2010). Two functionally distinct members of the MATE (multi-drug and toxic compound extrusion) family of transporters potentially underlie two major aluminum tolerance QTLs in maize. *The Plant Journal,* 61**,** 728-40.

Marsh, L. (2015). Strong ligand-protein interactions derived from diffuse ligand interactions with loose binding sites. *BioMed Research International,* 2015**,** 746980.

Marshall, R. L. & Bavro, V. N. (2020). Mutations in the TolC periplasmic domain affect substrate specificity of the AcrAB-TolC pump. *Frontiers in Molecular Biosciences,* 7**,** 166.

Martin, S. L., Mortimer, T. D. & Grad, Y. H. (2023). Machine learning models for *Neisseria gonorrhoeae* antimicrobial susceptibility tests. *Annals of the New York Academy of Sciences,* 1520**,** 74-88.

Masi, M., Refregiers, M., Pos, K. M. & Pages, J. M. (2017). Mechanisms of envelope permeability and antibiotic influx and efflux in Gram-negative bacteria. *Nature Microbiology,* 2**,** 17001.

Masuda, N. & Ohya, S. (1992). Cross-resistance to meropenem, cephems, and quinolones in *Pseudomonas aeruginosa*. *Antimicrobial Agents and Chemotherapy,* 36**,** 1847-51.

Masuda, N., Sakagawa, E., Ohya, S., Gotoh, N., Tsujimoto, H. & Nishino, T. (2000). Contribution of the MexX-MexY-OprM efflux system to intrinsic resistance in *Pseudomonas aeruginosa*. *Antimicrobial Agents and Chemotherapy,* 44**,** 2242-6.

Masuda, S., Terada, T., Yonezawa, A., Tanihara, Y., Kishimoto, K., Katsura, T., Ogawa, O. & Inui, K.-i. (2006). Identification and functional characterization of a new human kidney–specific H+/organic cation antiporter, Kidney-Specific Multidrug and Toxin Extrusion 2. *Journal of the American Society of Nephrology,* 17**,** 2127-35.

Matsumoto, Y., Hayama, K., Sakakihara, S., Nishino, K., Noji, H., Iino, R. & Yamaguchi, A. (2011). Evaluation of multidrug efflux pump inhibitors by a new method using microfluidic channels. *PLoS One,* 6**,** e18547.

Matsumura, K., Furukawa, S., Ogihara, H. & Morinaga, Y. (2011). Roles of multidrug efflux pumps on the biofilm formation of *Escherichia coli* K-12. *Biocontrol Science,* 16**,** 69-72.

Matsunaga, Y., Yamane, T., Terada, T., Moritsugu, K., Fujisaki, H., Murakami, S., Ikeguchi, M. & Kidera, A. (2018). Energetics and conformational pathways of functional rotation in the multidrug transporter AcrB. *Elife,* 7**,** e31715.

McAleese, F., Petersen, P., Ruzin, A., Dunman, P. M., Murphy, E., Projan, S. J. & Bradford, P. A. (2005). A novel MATE family efflux pump contributes to the reduced susceptibility of laboratory-derived *Staphylococcus aureus* mutants to tigecycline. *Antimicrobial Agents and Chemotherapy,* 49**,** 1865-71.

McCormack, W., Johnson, K., Stumacher, R., Donner, A. & Rychwalski, R. (1977). Clinical spectrum of gonococcal infection in women. *The Lancet,* 309**,** 1182-5.

McFarland, L., Mietzner, T., Knapp, J., Sandstrom, E., Holmes, K. & Morse, S. (1983). Gonococcal sensitivity to fecal lipids can be mediated by an Mtr-independent mechanism. *Journal of Clinical Microbiology,* 18**,** 121-7.

McMurry, L. M., Oethinger, M. & Levy, S. B. (1998). Overexpression of *marA*, *soxS*, or *acrAB* produces resistance to triclosan in laboratory and clinical strains of *Escherichia coli*. *FEMS Microbiology Letters,* 166**,** 305-9.

Mehr, I. J. & Seifert, H. S. (1997). Random shuttle mutagenesis: gonococcal mutants deficient in pilin antigenic variation. *Molecular Microbiology,* 23**,** 1121-31.

Mehr, I. J. & Seifert, H. S. (1998). Differential roles of homologous recombination pathways in *Neisseria gonorrhoeae* pilin antigenic variation, DNA transformation and DNA repair. *Molecular Microbiology,* 30**,** 697-710.

Meier, G., Thavarasah, S., Ehrenbolger, K., Hutter, C. A. J., Hürlimann, L. M., Barandun, J. & Seeger, M. A. (2023). Deep mutational scan of a drug efflux pump reveals its structure–function landscape. *Nature Chemical Biology,* 19**,** 440-50.

Mercante, A. D., Jackson, L., Johnson, P. J., Stringer, V. A., Dyer, D. W. & Shafer, W. M. (2012). MpeR regulates the mtr efflux locus in *Neisseria gonorrhoeae* and modulates antimicrobial resistance by an iron-responsive mechanism. *Antimicrobial Agents and Chemotherapy,* 56**,** 1491-501.

Merrick, R., Cole, M., Pitt, R., Enayat, Q., Ivanov, Z., Day, M., Sun, S., Sinka, K., Woodford, N., Mohammed, H. & Fifer, H. (2022). Antimicrobial-resistant gonorrhoea: the national public health response, England, 2013 to 2020. *Eurosurveillance,* 27**,** 2200057.

Merz, A. J., So, M. & Sheetz, M. P. (2000). Pilus retraction powers bacterial twitching motility. *Nature,* 407**,** 98-102.

Mikolosko, J., Bobyk, K., Zgurskaya, H. I. & Ghosh, P. (2006). Conformational flexibility in the multidrug efflux system protein AcrA. *Structure,* 14**,** 577-87.

Miller, R. D., Brown, K. E. & Morse, S. A. (1977). Inhibitory action of fatty acids on the growth of *Neisseria gonorrhoeae*. *Infection and Immunity,* 17**,** 303-12.

Miroux, B. & Walker, J. E. (1996). Over-production of proteins in *Escherichia coli*: mutant hosts that allow synthesis of some membrane proteins and globular proteins at high levels. *Journal of Molecular Biology,* 260**,** 289-98.

Mishima, H., Oshima, H., Yasuda, S. & Kinoshita, M. (2015). Statistical thermodynamics for functionally rotating mechanism of the multidrug efflux transporter AcrB. *The Journal of Physical Chemistry B,* 119**,** 3423-33.

Miyamae, S., Ueda, O., Yoshimura, F., Hwang, J., Tanaka, Y. & Nikaido, H. (2001). A MATE family multidrug efflux transporter pumps out fluoroquinolones in *Bacteroides thetaiotaomicron*. *Antimicrobial Agents and Chemotherapy,* 45**,** 3341-6.

Miyamoto, S. & Kollman, P. A. (1992). Settle: An analytical version of the SHAKE and RATTLE algorithm for rigid water models. *Journal of Computational Chemistry,* 13**,** 952-62.

Moir, D. T., Opperman, T. J., Aron, Z. D. & Bowlin, T. L. (2021). Adjunctive therapy for multidrug-resistant bacterial infections: type III secretion system and efflux inhibitors. *Drug Discovery Today,* 26**,** 2173-81.

Morgan, C. E., Glaza, P., Leus, I. V., Trinh, A., Su, C.-C., Cui, M., Zgurskaya, H. I. & Yu, E. W. (2021). Cryoelectron microscopy structures of AdeB illuminate mechanisms of simultaneous binding and exporting of substrates. *mBio,* 12**,** e03690-20.

Morgan, C. E., Zhang, Z., Bonomo, R. A. & Yu, E. W. (2022). An analysis of the novel fluorocycline TP-6076 bound to both the ribosome and multidrug efflux pump AdeJ from *Acinetobacter baumannii*. *mBio,* 13**,** e03732-21.

Morimyo, M., Hongo, E., Hama-Inaba, H. & Machida, I. (1992). Cloning and characterisation of the *mvrC* gene of *Escherichia coli* K12 which confers resistance against methyl viologen toxicity. *Nucleic Acids Research,* 20**,** 3159-65.

Morita, M., Shitan, N., Sawada, K., Van Montagu, M. C. E., Inzé, D., Rischer, H., Goossens, A., Oksman-Caldentey, K.-M., Moriyama, Y. & Yazaki, K. (2009). Vacuolar transport of nicotine is mediated by a multidrug and toxic compound extrusion (MATE) transporter in *Nicotiana tabacum*. *Proceedings of the National Academy of Sciences,* 106**,** 2447-52.

Morita, Y., Kataoka, A., Shiota, S., Mizushima, T. & Tsuchiya, T. (2000). NorM of Vibrio parahaemolyticus is an Na+-driven multidrug efflux pump. *Journal of Bacteriology,* 182**,** 6694-7.

Morita, Y., Kodama, K., Shiota, S., Mine, T., Kataoka, A., Mizushima, T. & Tsuchiya, T. (1998). NorM, a putative multidrug efflux protein, of *Vibrio parahaemolyticus* and its homolog in *Escherichia coli*. *Antimicrobial Agents and Chemotherapy,* 42**,** 1778-82.

Morita, Y., Nakashima, K.-i., Nishino, K., Kotani, K., Tomida, J., Inoue, M. & Kawamura, Y. (2016). Berberine is a novel type efflux inhibitor which attenuates the MexXY-mediated aminoglycoside resistance in *Pseudomonas aeruginosa*. *Frontiers in Microbiology,* 7**,** 1223.

Morona, R., Manning, P. & Reeves, P. (1983). Identification and characterization of the TolC protein, an outer membrane protein from *Escherichia coli*. *Journal of Bacteriology,* 153**,** 693-9.

Morrison, E. A., DeKoster, G. T., Dutta, S., Vafabakhsh, R., Clarkson, M. W., Bahl, A., Kern, D., Ha, T. & Henzler-Wildman, K. A. (2012). Antiparallel EmrE exports drugs by exchanging between asymmetric structures. *Nature,* 481**,** 45-50.

Morrison, E. A. & Henzler-Wildman, K. A. (2014). Transported substrate determines exchange rate in the multidrug resistance transporter EmrE. *Journal of Biological Chemistry,* 289**,** 6825-36.

Morse, S., Lysko, P., McFarland, L., Knapp, J., Sandstrom, E., Critchlow, C. & Holmes, K. (1982). Gonococcal strains from homosexual men have outer membranes with reduced permeability to hydrophobic molecules. *Infection and Immunity,* 37**,** 432-8.

Morse, S. A. (1979). *Neisseria gonorrhoeae*: physiology and metabolism. *Sexually Transmitted Diseases,* 6**,** 28-37.

Morse, S. A. & Bartenstein, L. (1974). Factors affecting autolysis of *Neisseria gonorrhoeae*. *Proceedings of the Society for Experimental Biology and Medicine,* 145**,** 1418-21.

Morse, S. A., Johnson, S. R., Biddle, J. W. & Roberts, M. C. (1986). High-level tetracycline resistance in *Neisseria gonorrhoeae* is result of acquisition of *Streptococcal tetM* determinant. *Antimicrobial Agents and Chemotherapy,* 30**,** 664-70.

Moseng, M. A., Lyu, M., Pipatpolkai, T., Glaza, P., Emerson, C. C., Stewart, P. L., Stansfeld, P. J. & Yu, E. W. (2021). Cryo-EM structures of CusA reveal a mechanism of metal-ion export. *mBio,* 12**,** 10.1128/mbio. 00452-21.

Moussatova, A., Kandt, C., O'Mara, M. L. & Tieleman, D. P. (2008). ATP-binding cassette transporters in *Escherichia coli*. *Biochimica et Biophysica Acta (BBA)-Biomembranes,* 1778**,** 1757-71.

Mulani, M. S., Kamble, E. E., Kumkar, S. N., Tawre, M. S. & Pardesi, K. R. (2019). Emerging strategies to combat ESKAPE pthogpens in the era of antimicrobial resistance: A review. *Frontiers in Microbiology,* 10**,** 539.

Müller, R. T., Travers, T., Cha, H.-j., Phillips, J. L., Gnanakaran, S. & Pos, K. M. (2017). Switch loop flexibility affects substrate transport of the AcrB efflux pump. *Journal of Molecular Biology,* 429**,** 3863-74.

Murakami, S. (2008). Multidrug efflux transporter, AcrB--the pumping mechanism. *Current Opinion in Structural Biology,* 18**,** 459-65.

Murakami, S., Nakashima, R., Yamashita, E., Matsumoto, T. & Yamaguchi, A. (2006). Crystal structures of a multidrug transporter reveal a functionally rotating mechanism. *Nature,* 443**,** 173-9.

Murakami, S., Nakashima, R., Yamashita, E. & Yamaguchi, A. (2002). Crystal structure of bacterial multidrug efflux transporter AcrB. *Nature,* 419**,** 587-93.

Murakami, S., Okada, U. & van Veen, H. W. (2020). Tripartite transporters as mechanotransmitters in periplasmic alternating-access mechanisms. *FEBS Letters,* 594**,** 3908-19.

Murphy, K. C. (1998). Use of bacteriophage λ recombination functions to promote gene replacement in *Escherichia coli*. *Journal of Bacteriology,* 180**,** 2063-71.

Muth, T. R. & Schuldiner, S. (2000). A membrane-embedded glutamate is required for ligand binding to the multidrug transporter EmrE. *EMBO Journal,* 19**,** 234-40.

Nagarathinam, K., Nakada-Nakura, Y., Parthier, C., Terada, T., Juge, N., Jaenecke, F., Liu, K., Hotta, Y., Miyaji, T. & Omote, H. (2018). Outward

open conformation of a Major Facilitator Superfamily multidrug/H^+ antiporter provides insights into switching mechanism. *Nature Communications,* 9**,** 1-9.

Nakashima, R., Sakurai, K., Yamasaki, S., Hayashi, K., Nagata, C., Hoshino, K., Onodera, Y., Nishino, K. & Yamaguchi, A. (2013). Structural basis for the inhibition of bacterial multidrug exporters. *Nature,* 500**,** 102-6.

Nakashima, R., Sakurai, K., Yamasaki, S., Nishino, K. & Yamaguchi, A. (2011). Structures of the multidrug exporter AcrB reveal a proximal multisite drug-binding pocket. *Nature,* 480**,** 565-9.

Nakayama, S.-i., Shimuta, K., Furubayashi, K.-i., Kawahata, T., Unemo, M. & Ohnishi, M. (2016). New ceftriaxone-and multidrug-resistant *Neisseria gonorrhoeae* strain with a novel mosaic *penA* gene isolated in Japan. *Antimicrobial Agents and Chemotherapy,* 60**,** 4339-41.

Naroditskaya, V., Schlosser, M. J., Fang, N. Y. & Lewis, K. (1993). An *E. coli* gene *emrD* is involved in adaptation to low energy shock. *Biochemical and Biophysical Research Communications,* 196**,** 803-9.

Neidig, A., Strempel, N., Waeber, N. B., Nizer, W. S. d. C. & Overhage, J. (2023). Knock-out of multidrug efflux pump MexXY-OprM results in increased susceptibility to antimicrobial peptides in *Pseudomonas aeruginosa*. *Microbiol Immunol,* 67**,** 422-7.

Nelson, J. W., Atilho, R. M., Sherlock, M. E., Stockbridge, R. B. & Breaker, R. R. (2017). Metabolism of free guanidine in bacteria ss regulated by a widespread riboswitch class. *Molecular Cell,* 65**,** 220-30.

Nie, L., Grell, E., Malviya, V. N., Xie, H., Wang, J. & Michel, H. (2016). Identification of the high-affinity substrate-binding site of the multidrug and toxic compound extrusion (MATE) family transporter from *Pseudomonas stutzeri*. *Journal of Biological Chemistry,* 291**,** 15503-14.

Nies, D. H., Nies, A., Chu, L. & Silver, S. (1989). Expression and nucleotide sequence of a plasmid-determined divalent cation efflux system from *Alcaligenes eutrophus*. *Proceedings of the National Academy of Sciences of the United States of America,* 86**,** 7351-5.

Nikaido, H. (1989). Outer membrane barrier as a mechanism of antimicrobial resistance. *Antimicrobial Agents and Chemotherapy,* 33**,** 1831-6.

Nikaido, H. (1994). Prevention of drug access to bacterial targets: permeability barriers and active efflux. *Science,* 264**,** 382-8.

Nikaido, H. (1996). Multidrug efflux pumps of Gram-negative bacteria. *Journal of Bacteriology,* 178**,** 5853-9.

Nikaido, H. (2000). How do exported proteins and antibiotics bypass the periplasm in Gram- negative bacterial cells? *Trends in Microbiology,* 8**,** 481-3.

Nikaido, H. (2003). Molecular basis of bacterial outer membrane permeability revisited. *Microbiology and Molecular Biology Reviews,* 67**,** 593-656.

Nikaido, H. (2011). Structure and mechanism of RND-type multidrug efflux pumps. *Advances in Enzymology and Related Areas of Molecular Biology,* 77**,** 1-60.

Nikaido, H. (2018). RND transporters in the living world. *Research in Microbiology,* 169**,** 363-71.

Nikaido, H., Basina, M., Nguyen, V. & Rosenberg, E. Y. (1998). Multidrug efflux pump AcrAB of *Salmonella typhimurium* excretes only those β-lactam antibiotics containing lipophilic side chains. *Journal of Bacteriology,* 180**,** 4686-92.

Nishino, K., Nikaido, E. & Yamaguchi, A. (2009). Regulation and physiological function of multidrug efflux pumps in *Escherichia coli* and *Salmonella*. *Biochimica et Biophysica Acta (BBA)-Proteins and Proteomics,* 1794**,** 834-43.

Nóbrega, C. S., Saraiva, I. H., Carreira, C., Devreese, B., Matzapetakis, M. & Pauleta, S. R. (2016). The solution structure of the soluble form of the lipid-modified azurin from *Neisseria gonorrhoeae*, the electron donor of cytochrome c peroxidase. *Biochimica et Biophysica Acta (BBA)-Bioenergetics,* 1857**,** 169-76.

Norrod, P. & Williams, R. P. (1979). Stability and viability of *Neisseria gonorrhoeae* in various solutions and buffers. *Applied and Environmental Microbiology,* 37**,** 293-7.

Novy, R., Yaeger, K., Held, D. & Mierendorf, R. (2002). Coexpression of multiple target proteins in *Escherichia coli*. *Innovations,* 15**,** 2.

O'Neill, J. 2016. Tackling drug-resistant infections globally: final report and recommendations. *The Review on Antimicrobial Resistance.* Wellcome Trust and HM Government, London.

O'Shea, R. & Moser, H. E. (2008). Physicochemical properties of antibacterial compounds: implications for drug discovery. *Journal of Medicinal Chemistry,* 51**,** 2871-8.

Obergfell, K. P. & Seifert, H. S. (2015). Mobile DNA in the pathogenic *Neisseria*. *Microbiology Spectrum,* 3**,** MDNA3-0015-2014.

Ohneck, E. A., Goytia, M., Rouquette-Loughlin, C. E., Joseph, S. J., Read, T. D., Jerse, A. E. & Shafer, W. M. (2015). Overproduction of the MtrCDE efflux pump in *Neisseria gonorrhoeae* produces unexpected changes in cellular transcription patterns. *Antimicrobial Agents and Chemotherapy,* 59**,** 724-6.

Ohneck, E. A., Zalucki, Y. M., Johnson, P. J., Dhulipala, V., Golparian, D., Unemo, M., Jerse, A. E. & Shafer, W. M. (2011). A novel mechanism of high-level, broad-spectrum antibiotic resistance caused by a single base pair change in *Neisseria gonorrhoeae*. *mBio,* 2.

Ohnishi, M., Golparian, D., Shimuta, K., Saika, T., Hoshina, S., Iwasaku, K., Nakayama, S., Kitawaki, J. & Unemo, M. (2011a). Is *Neisseria gonorrhoeae* initiating a future era of untreatable gonorrhea?: detailed characterization of the first strain with high-level resistance to ceftriaxone. *Antimicrobial Agents and Chemotherapy,* 55**,** 3538-45.

Ohnishi, M., Saika, T., Hoshina, S., Iwasaku, K., Nakayama, S.-i., Watanabe, H. & Kitawaki, J. (2011b). Ceftriaxone-resistant *Neisseria gonorrhoeae*, Japan. *Emerging Infectious Diseases,* 17**,** 148.

Okada, U. & Murakami, S. 2023. Structural and functional aspects of the macrolide efflux transporter, MacB-A tripartite ABC transporter. *Therapeutic Protein Targets for Drug Discovery and Clinical Evaluation: Bio-Crystallography and Drug Design.* World Scientific.

Okusu, H., Ma, D. & Nikaido, H. (1996). AcrAB efflux pump plays a major role in the antibiotic resistance phenotype of *Escherichia coli* multiple-antibiotic-resistance (Mar) mutants. *Journal of Bacteriology,* 178**,** 306-8.

Olesky, M., Hobbs, M. & Nicholas, R. A. (2002). Identification and analysis of amino acid mutations in Porin IB that mediate intermediate-level resistance to penicillin and tetracycline in *Neisseria gonorrhoeae*. *Antimicrobial Agents and Chemotherapy,* 46**,** 2811-20.

Olesky, M., Zhao, S., Rosenberg, R. L. & Nicholas, R. A. (2006). Porin-mediated antibiotic resistance in *Neisseria gonorrhoeae*: ion, solute, and antibiotic permeation through PIB proteins with *penB* mutations. *Journal of Bacteriology,* 188**,** 2300-8.

Omote, H., Hiasa, M., Matsumoto, T., Otsuka, M. & Moriyama, Y. (2006). The MATE proteins as fundamental transporters of metabolic and xenobiotic organic cations. *Trends in Pharmacological Sciences,* 27**,** 587-93.

Opperman, T. J., Kwasny, S. M., Kim, H. S., Nguyen, S. T., Houseweart, C., D'Souza, S., Walker, G. C., Peet, N. P., Nikaido, H. & Bowlin, T. L. (2014). Characterization of a novel pyranopyridine inhibitor of the AcrAB efflux pump of *Escherichia coli*. *Antimicrobial Agents and Chemotherapy,* 58**,** 722-33.

Ornik-Cha, A., Wilhelm, J., Kobylka, J., Sjuts, H., Vargiu, A. V., Malloci, G., Reitz, J., Seybert, A., Frangakis, A. S. & Pos, K. M. (2021). Structural and functional analysis of the promiscuous AcrB and AdeB efflux pumps suggests different drug binding mechanisms. *Nature Communications,* 12**,** 6919.

Orth, P., Schnappinger, D., Hillen, W., Saenger, W. & Hinrichs, W. (2000). Structural basis of gene regulation by the tetracycline inducible Tet repressor–operator system. *Nature Structural Biology,* 7**,** 215-9.

Oswald, C., Tam, H.-K. & Pos, K. M. (2016). Transport of lipophilic carboxylates is mediated by transmembrane helix 2 in multidrug transporter AcrB. *Nature Communications,* 7**,** 1-10.

Otsuka, M., Matsumoto, T., Morimoto, R., Arioka, S., Omote, H. & Moriyama, Y. (2005a). A human transporter protein that mediates the final excretion step for toxic organic cations. *Proceedings of the National Academy of Sciences,* 102**,** 17923-8.

Otsuka, M., Matsumoto, T., Morimoto, R., Arioka, S., Omote, H. & Moriyama, Y. (2005b). A human transporter protein that mediates the final excretion step for toxic organic cations. *Proceedings of the National Academy of Sciences of the United States of America,* 102**,** 17923-8.

Ovchinnikov, V., Stone, T. A., Deber, C. M. & Karplus, M. (2018). Structure of the EmrE multidrug transporter and its use for inhibitor peptide design. *Proceedings of the National Academy of Sciences of the United States of America,* 115**,** E7932-E41.

Padan, E., Kozachkov, L., Herz, K. & Rimon, A. (2009). NhaA crystal structure: functional–structural insights. *Journal of Experimental Biology,* 212**,** 1593-603.

Pal, C., Bengtsson-Palme, J., Kristiansson, E. & Larsson, D. J. (2015). Co-occurrence of resistance genes to antibiotics, biocides and metals reveals novel insights into their co-selection potential. *BMC Genomics,* 16**,** 1-14.

Palmer, G. H., Bankhead, T. & Seifert, H. S. (2016). Antigenic variation in bacterial pathogens. *Microbiology Spectrum,* 4.

Pan, W. & Spratt, B. G. (1994). Regulation of the permeability of the gonococcal cell envelope by the *mtr* system. *Molecular Microbiology,* 11**,** 769-75.

Pannek, S., Higgins, P. G., Steinke, P., Jonas, D., Akova, M., Bohnert, J. A., Seifert, H. & Kern, W. V. (2006). Multidrug efflux inhibition in *Acinetobacter baumannii*: comparison between 1-(1-naphthylmethyl)-piperazine and phenyl-arginine-β-naphthylamide. *Journal of Antimicrobial Chemotherapy,* 57**,** 970-4.

Pao, S. S., Paulsen, I. T. & Saier, M. H. (1998). Major facilitator superfamily. *Microbiology and Molecular Biology Reviews,* 62**,** 1-34.

Parrinello, M. & Rahman, A. (1980). Crystal structure and pair potentials: A molecular-dynamics study. *Physical Review Letters,* 45**,** 1196.

Parrinello, M. & Rahman, A. (1981a). ACS Catalysis. *Journal of Applied Physics,* 52**,** 7182-90.

Parrinello, M. & Rahman, A. (1981b). Polymorphic transitions in single crystals: A new molecular dynamics method. *Journal of Applied Physics,* 52**,** 7182-90.

Parsons, N. J., Patel, P. V., Tan, E. L., Andrade, J. R., Nairn, C. A., Goldner, M., Cole, J. A. & Smith, H. (1988). Cytidine 5′-monophospho-N-acetyl neuraminic acid and a low molecular weight factor from human blood cells induce lipopolysaccharide alteration in gonococci when conferring

resistance to killing by human serum. *Microbial Pathogenesis,* 5**,** 303-9.

Patel, C. N., Wortham, B. W., Lines, J. L., Fetherston, J. D., Perry, R. D. & Oliveira, M. A. (2006). Polyamines are essential for the formation of plague biofilm. *Journal of Bacteriology,* 188**,** 2355-63.

Paulsen, I. T., Brown, M. H., Dunstan, S. J. & Skurray, R. A. (1995). Molecular characterization of the staphylococcal multidrug resistance export protein QacC. *Journal of Bacteriology,* 177**,** 2827-33.

Paulsen, I. T., Brown, M. H., Littlejohn, T. G., Mitchell, B. A. & Skurray, R. A. (1996a). Multidrug resistance proteins QacA and QacB from *Staphylococcus aureus*: membrane topology and identification of residues involved in substrate specificity. *Proceedings of the National Academy of Sciences of the United States of America,* 93**,** 3630-5.

Paulsen, I. T., Brown, M. H. & Skurray, R. A. (1996b). Proton-dependent multidrug efflux systems. *Microbiological Reviews,* 60**,** 575-608.

Paulsen, I. T., Nguyen, L., Sliwinski, M. K., Rabus, R. & Saier, M. H., Jr. (2000). Microbial genome analyses: comparative transport capabilities in eighteen prokaryotes. *Journal of Molecular Biology,* 301**,** 75-100.

Paulsen, I. T., Park, J. H., Choi, P. S. & Saier, M. H., Jr. (1997). A family of Gram-negative bacterial outer membrane factors that function in the export of proteins, carbohydrates, drugs and heavy metals from Gram-negative bacteria. *FEMS Microbiology Letters,* 156**,** 1-8.

Paulsen, I. T. & Skurray, R. A. (1993). Topology, structure and evolution of two families of proteins involved in antibiotic and antiseptic resistance in eukaryotes and prokaryotes- an analysis. *Gene,* 124**,** 1-11.

Paulsen, I. T., Skurray, R. A., Tam, R., Saier, M. H., Turner, R. J., Weiner, J. H., Goldberg, E. B. & Grinius, L. L. (1996c). The SMR family: a novel family of multidrug efflux proteins involved with the efflux of lipophilic drugs. *Molecular Microbiology,* 19**,** 1167-75.

Pei, X.-Y., Hinchliffe, P., Symmons, M. F., Koronakis, E., Benz, R., Hughes, C. & Koronakis, V. (2011). Structures of sequential open states in a symmetrical opening transition of the TolC exit duct. *Proceedings of the National Academy of Sciences of the United States of America,* 108**,** 2112-7.

Perez, C., Gerber, S., Boilevin, J., Bucher, M., Darbre, T., Aebi, M., Reymond, J.-L. & Locher, K. P. (2015). Structure and mechanism of an active lipid-linked oligosaccharide flippase. *Nature,* 524**,** 433-8.

Peters, K. M., Brooks, B. E., Schumacher, M. A., Skurray, R. A., Brennan, R. G. & Brown, M. H. (2011). A single acidic residue can guide binding site selection but does not govern QacR cationic-drug affinity. *PLoS One,* 6**,** e15974.

Peters, K. M., Schuman, J. T., Skurray, R. A., Brown, M. H., Brennan, R. G. & Schumacher, M. A. (2008). QacR-cation recognition is mediated by a redundancy of residues capable of charge neutralization. *Biochemistry,* 47**,** 8122-9.

Peters, R. P., Chico, R. M., Rowley, J. & Low, N. (2022). Estimating the global burden of sexually transmitted infections. *The Lancet Infectious Diseases,* 22**,** 1112-3.

Petrova, A., Feodorova, Y., Miteva-Katrandzhieva, T., Petrov, M. & Murdjeva, M. (2019). First detected OXA-50 carbapenem-resistant clinical isolates *Pseudomonas aeruginosa* from Bulgaria and interplay between the expression of main efflux pumps, OprD and intrinsic AmpC. *Journal of Medical Microbiology,* 68**,** 1723-31.

Piddock, L. J. (2006a). Clinically relevant chromosomally encoded multidrug resistance efflux pumps in bacteria. *Clinical Microbiology Reviews,* 19**,** 382-402.

Piddock, L. J. (2006b). Multidrug-resistance efflux pumps - not just for resistance. *Nature Reviews Microbiology,* 4**,** 629-36.

Piggot, T. J., Holdbrook, D. A. & Khalid, S. (2011). Electroporation of the *E. coli* and *S. aureus* membranes: molecular dynamics simulations of complex bacterial membranes. *The Journal of Physical Chemistry B,* 115**,** 13381-8.

Płaczkiewicz, J., Gieczewska, K., Musiałowski, M., Adamczyk-Popławska, M., Bącal, P. & Kwiatek, A. (2023). Availability of iron ions impacts physicochemical properties and proteome of outer membrane vesicles released by *Neisseria gonorrhoeae*. *Scientific Reports,* 13**,** 18733.

Plé, C., Tam, H.-K., Vieira Da Cruz, A., Compagne, N., Jiménez-Castellanos, J.-C., Müller, R. T., Pradel, E., Foong, W. E., Malloci, G. & Ballée, A. (2022). Pyridylpiperazine-based allosteric inhibitors of RND-type multidrug efflux pumps. *Nature Communications,* 13**,** 115.

Pleininger, S., Indra, A., Golparian, D., Heger, F., Schindler, S., Jacobsson, S., Heidler, S. & Unemo, M. (2022). Extensively drug-resistant (XDR) *Neisseria gonorrhoeae* causing possible gonorrhoea treatment failure with ceftriaxone plus azithromycin in Austria, April 2022. *Eurosurveillance,* 27**,** 2200455.

Poelarends, G. J., Mazurkiewicz, P. & Konings, W. N. (2002). Multidrug transporters and antibiotic resistance in *Lactococcus lactis*. *Biochimica et Biophysica Acta,* 1555**,** 1-7.

Pollock, N. L., Lee, S. C., Patel, J. H., Gulamhussein, A. A. & Rothnie, A. J. (2018). Structure and function of membrane proteins encapsulated in a polymer-bound lipid bilayer. *Biochimica et Biophysica Acta (BBA)-Biomembranes,* 1860**,** 809-17.

Poma, A. B., Cieplak, M. & Theodorakis, P. E. (2017). Combining the MARTINI and structure-based coarse-grained approaches for the molecular

dynamics studies of conformational transitions in proteins. *Journal of Chemical Theory and Computation,* 13**,** 1366-74.

Poole, K. (2004). Efflux-mediated multiresistance in Gram-negative bacteria. *Clinical Microbiology and Infection,* 10**,** 12-26.

Poole, K., Heinrichs, D. E. & Neshat, S. (1993). Cloning and sequence analysis of an EnvCD homologue in *Pseudomonas aeruginosa*: regulation by iron and possible involvement in the secretion of the siderophore pyoverdine. *Molecular Microbiology,* 10**,** 529-44.

Poole, K. & Srikumar, R. (2001). Multidrug efflux in *Pseudomonas aeruginosa*: components, mechanisms and clinical significance. *Current Topics in Medicinal Chemistry,* 1**,** 59-71.

Porter, E., Ma, D. C., Alvarez, S. & Faull, K. F. (2015). Antimicrobial lipids: Emerging effector molecules of innate host defense. *World Journal of Immunology,* 5**,** 51-61.

Pos, K. M. (2009). Drug transport mechanism of the AcrB efflux pump. *Biochimica et Biophysica Acta,* 1794**,** 782-93.

Pournaras, S., Maniati, M., Spanakis, N., Ikonomidis, A., Tassios, P., Tsakris, A., Legakis, N. & Maniatis, A. (2005). Spread of efflux pump-overexpressing, non-metallo-β-lactamase-producing, meropenem-resistant but ceftazidime-susceptible *Pseudomonas aeruginosa* in a region with *bla*$_{VIM}$ endemicity. *Journal of Antimicrobial Chemotherapy,* 56**,** 761-4.

Powell, A. J., Tomberg, J., Deacon, A. M., Nicholas, R. A. & Davies, C. (2009). Crystal structures of penicillin-binding protein 2 from penicillin-susceptible and -resistant strains of *Neisseria gonorrhoeae* reveal an unexpectedly subtle mechanism for antibiotic resistance. *Journal of Biological Chemistry,* 284**,** 1202-12.

Prakash, S., Cooper, G., Singhi, S. & Saier, M. H., Jr. (2003). The ion transporter superfamily. *Biochimica et Biophysica Acta,* 1618**,** 79-92.

Prister, L. L., Yin, S., Cahoon, L. A. & Seifert, H. S. (2020). Altering the *Neisseria gonorrhoeae pilE* guanine quadruplex loop bases affects pilin antigenic variation. *Biochemistry,* 59**,** 1104-12.

Purewal, A. S. (1991). Nucleotide sequence of the ethidium efflux gene from *Escherichia coli*. *FEMS Microbiology Letters,* 66**,** 229-31.

Purewal, A. S., Jones, I. G. & Midgley, M. (1990). Cloning of the ethidium efflux gene from *Escherichia coli*. *FEMS Microbiology Letters,* 68**,** 73-6.

Qi, C., Di Minin, G., Vercellino, I., Wutz, A. & Korkhov, V. M. (2019). Structural basis of sterol recognition by human hedgehog receptor PTCH1. *Science Advances,* 5**,** eaaw6490.

Qian, L., McSheffrey, G. G., Gray-Owen, S. D., Zhang, J.-R. & Tang, Y.-W. 2024. Chapter 66 - *Neisseria gonorrhoeae*. *In:* TANG, Y.-W.,

HINDIYEH, M. Y., LIU, D., SAILS, A., SPEARMAN, P. & ZHANG, J.-R. (eds.) *Molecular Medical Microbiology (Third Edition).* Academic Press.

Qiu, W., Fu, Z., Xu, G. G., Grassucci, R. A., Zhang, Y., Frank, J., Hendrickson, W. A. & Guo, Y. (2018). Structure and activity of lipid bilayer within a membrane-protein transporter. *Proceedings of the National Academy of Sciences,* 115**,** 12985-90.

Quillin, S. J. & Seifert, H. S. (2018). *Neisseria gonorrhoeae* host adaptation and pathogenesis. *Nature Reviews Microbiology,* 16**,** 226-40.

Radchenko, M., Nie, R. & Lu, M. (2016). Disulfide cross-linking of a multidrug and toxic compound extrusion transporter impacts multidrug efflux. *Journal of Biological Chemistry,* 291**,** 9818-26.

Radding, C. M. (1981). Recombination activities of *Escherichia coli* RecA protein. *Cell,* 25**,** 3-4.

Rahmati, S., Yang, S., Davidson, A. L. & Zechiedrich, E. L. (2002). Control of the AcrAB multidrug efflux pump by quorum-sensing regulator SdiA. *Molecular Microbiology,* 43**,** 677-85.

Raisman, J. C., Fiore, M. A., Tomin, L., Adjei, J. K., Aswad, V. X., Chu, J., Domondon, C. J., Donahue, B. A., Masciotti, C. A. & McGrath, C. G. (2022). Evolutionary paths to macrolide resistance in a *Neisseria* commensal converge on ribosomal genes through short sequence duplications. *PLoS One,* 17**,** e0262370.

Ramaswamy, V. K., Vargiu, A. V., Malloci, G., Dreier, J. & Ruggerone, P. (2017). Molecular rationale behind the differential substrate specificity of bacterial RND multi-drug transporters. *Scientific Reports,* 7**,** 1-18.

Rathod, S., Dey, S., Pawar, S., Dhavale, R., Choudhari, P., Rajakumara, E., Mahuli, D., Bhagwat, D., Tamboli, Y. & Sankpal, P. (2023). Identification of potential biogenic chalcones against antibiotic resistant efflux pump (AcrB) via computational study. *Journal of Biomolecular Structure and Dynamics***,** 1-19.

Reading, E., Ahdash, Z., Fais, C., Ricci, V., Wang-Kan, X., Grimsey, E., Stone, J., Malloci, G., Lau, A. M. & Findlay, H. (2020). Perturbed structural dynamics underlie inhibition and altered efflux of the multidrug resistance pump AcrB. *Nature Communications,* 11**,** 1-11.

Reddy, V. S., Shlykov, M. A., Castillo, R., Sun, E. I. & Saier, M. H. (2012). The major facilitator superfamily (MFS) revisited. *FEBS Journal,* 279**,** 2022-35.

Rees, D. C., Johnson, E. & Lewinson, O. (2009). ABC transporters: the power to change. *Nature Reviews Molecular Cell Biology,* 10**,** 218-27.

Reimche, J. L., Clemons, A. A., Chivukula, V. L., Joseph, S. J., Schmerer, M. W., Pham, C. D., Schlanger, K., St Cyr, S. B., Kersh, E. N., Gernert, K. M. & Group, A.-R. W. (2023). Genomic analysis of 1710 surveillance-based *Neisseria gonorrhoeae* isolates from the USA in 2019 identifies

predominant strain types and chromosomal antimicrobial-resistance determinants. *Microbial Genomics,* 9**,** 1-24; https://doi.org/10.1099/mgen.0.001006.

Renau, T. E., Léger, R., Filonova, L., Flamme, E. M., Wang, M., Yen, R., Madsen, D., Griffith, D., Chamberland, S., Dudley, M. N., Lee, V. J., Lomovskaya, O., Watkins, W. J., Ohta, T., Nakayama, K. & Ishida, Y. (2003). Conformationally-restricted analogues of efflux pump inhibitors that potentiate the activity of levofloxacin in *Pseudomonas aeruginosa*. *Bioorganic and Medicinal Chemistry Letters,* 13**,** 2755-8.

Renau, T. E., Léger, R., Flamme, E. M., Sangalang, J., She, M. W., Yen, R., Gannon, C. L., Griffith, D., Chamberland, S., Lomovskaya, O., Hecker, S. J., Lee, V. J., Ohta, T. & Nakayama, K. (1999). Inhibitors of efflux pumps in *Pseudomonas aeruginosa* potentiate the activity of the fluoroquinolone antibacterial levofloxacin. *Journal of Medicinal Chemistry,* 42**,** 4928-31.

Retsema, J., Girard, A., Schelkly, W., Manousos, M., Anderson, M., Bright, G., Borovoy, R., Brennan, L. & Mason, R. (1987). Spectrum and mode of action of azithromycin (CP-62,993), a new 15-membered-ring macrolide with improved potency against Gram-negative organisms. *Antimicrobial Agents and Chemotherapy,* 31**,** 1939-47.

Riou, J., Althaus, C. L., Allen, H., Cole, M. J., Grad, Y. H., Heijne, J. C., Unemo, M. & Low, N. (2023). Projecting the development of antimicrobial resistance in *Neisseria gonorrhoeae* from antimicrobial surveillance data: a mathematical modelling study. *BMC Infectious Diseases,* 23**,** 252.

Roberts, M. C., Chung, W. O., Roe, D., Xia, M., Marquez, C., Borthagaray, G., Whittington, W. L. & Holmes, K. K. (1999). Erythromycin-resistant *Neisseria gonorrhoeae* and oral commensal *Neisseria* spp. carry known rRNA methylase genes. *Antimicrobial Agents and Chemotherapy,* 43**,** 1367-72.

Rogers, E. E., Wu, X., Stacey, G. & Nguyen, H. T. (2009). Two MATE proteins play a role in iron efficiency in soybean. *Journal of Plant Physiology,* 166**,** 1453-9.

Rohde, K. H. & Dyer, D. W. (2003). Mechanisms of iron acquisition by the human pathogens *Neisseria meningitidis* and *Neisseria gonorrhoeae*. *Frontiers in Bioscience,* 8**,** d1186-d218.

Rosenberg, E. Y., Ma, D. & Nikaido, H. (2000). AcrD of *Escherichia coli* is an aminoglycoside efflux pump. *Journal of Bacteriology,* 182**,** 1754-6.

Rotem, D., Steiner-Mordoch, S. & Schuldiner, S. (2006). Identification of tyrosine residues critical for the function of an ion-coupled multidrug transporter. *Journal of Biological Chemistry,* 281**,** 18715-22.

Rouquette-Loughlin, C., Dunham, S. A., Kuhn, M., Balthazar, J. T. & Shafer, W. M. (2003). The NorM efflux pump of *Neisseria gonorrhoeae* and

Neisseria meningitidis recognizes antimicrobial cationic compounds. *Journal of Bacteriology,* 185**,** 1101-6.

Rouquette-Loughlin, C., Stojiljkovic, I., Hrobowski, T., Balthazar, J. T. & Shafer, W. M. (2002). Inducible, but not constitutive, resistance of gonococci to hydrophobic agents due to the MtrC-MtrD-MtrE efflux pump requires TonB-ExbB-ExbD proteins. *Antimicrobial Agents and Chemotherapy,* 46**,** 561-5.

Rouquette-Loughlin, C. E., Balthazar, J. T., Hill, S. A. & Shafer, W. M. (2004). Modulation of the *mtrCDE*-encoded efflux pump gene complex of *Neisseria meningitidis* due to a Correia element insertion sequence. *Molecular Microbiology,* 54**,** 731-41.

Rouquette-Loughlin, C. E., Balthazar, J. T. & Shafer, W. M. (2005). Characterization of the MacA–MacB efflux system in *Neisseria gonorrhoeae*. *Journal of Antimicrobial Chemotherapy,* 56**,** 856-60.

Rouquette-Loughlin, C. E., Dhulipala, V., Reimche, J. L., Raterman, E., Begum, A. A., Jerse, A. E. & Shafer, W. M. (2018a). *cis*- and *trans*-acting factors influence expression of the *norM*-encoded efflux pump of *Neisseria gonorrhoeae* and levels of gonococcal susceptibility to substrate antimicrobials. *Antimicrobial Agents and Chemotherapy,* 62**,** e00821-18.

Rouquette-Loughlin, C. E., Reimche, J. L., Balthazar, J. T., Dhulipala, V., Gernert, K. M., Kersh, E. N., Pham, C. D., Pettus, K., Abrams, A. J. & Trees, D. L. (2018b). Mechanistic basis for decreased antimicrobial susceptibility in a clinical isolate of *Neisseria gonorrhoeae* possessing a mosaic-like *mtr* efflux pump locus. *mBio,* 9**,** e02281-18.

Rouquette-Loughlin, C. E., Zalucki, Y. M., Dhulipala, V. L., Balthazar, J. T., Doyle, R. G., Nicholas, R. A., Begum, A. A., Raterman, E. L., Jerse, A. E. & Shafer, W. M. (2017). Control of *gdhR* expression in *Neisseria gonorrhoeae* via autoregulation and a master repressor (MtrR) of a drug efflux pump operon. *mBio,* 8.

Rouquette, C., Harmon, J. B. & Shafer, W. M. (1999). Induction of the *mtrCDE*-encoded efflux pump system of *Neisseria gonorrhoeae* requires MtrA, an AraC-like protein. *Molecular Microbiology,* 33**,** 651-8.

Routh, M. D., Su, C. C., Zhang, Q. & Yu, E. W. (2009). Structures of AcrR and CmeR: Insight into the mechanisms of transcriptional repression and multi-drug recognition in the TetR family of regulators. *Biochimica et Biophysica Acta,* 1794**,** 844-51.

Rowley, J., Vander Hoorn, S., Korenromp, E., Low, N., Unemo, M., Abu-Raddad, L. J., Chico, R. M., Smolak, A., Newman, L. & Gottlieb, S. (2019). Chlamydia, gonorrhoea, trichomoniasis and syphilis: global prevalence and incidence estimates, 2016. *Bulletin of the World Health Organization,* 97**,** 548-62P.

Ruggerone, P., Murakami, S., M Pos, K. & Vargiu, A. V. (2013). RND efflux pumps: structural information translated into function and inhibition mechanisms. *Current Topics in Medicinal Chemistry,* 13**,** 3079-100.

Russell, A. (2002). Introduction of biocides into clinical practice and the impact on antibiotic-resistant bacteria. *Journal of Applied Microbiology,* 92**,** 121S-35S.

Russell, D. W. & Sambrook, J. 2001. *Molecular cloning: a laboratory manual,* Cold Spring Harbor, NY, Cold Spring Harbor Laboratory.

Rybenkov, V. V., Zgurskaya, H. I., Ganguly, C., Leus, I. V., Zhang, Z. & Moniruzzaman, M. (2021). The whole is bigger than the sum of its parts: drug transport in the context of two membranes with active efflux. *Chemical Reviews*.

Sadarangani, M., Pollard, A. J. & Gray-Owen, S. D. (2011). Opa proteins and CEACAMs: pathways of immune engagement for pathogenic *Neisseria*. *FEMS Microbiology Reviews,* 35**,** 498-514.

Saier, J. M. H. (2023). *Transporter Classification Databse* [Online]. The Saier Lab. Group @ UCSD in collaboration with the SDSC. Available: https://www.tcdb.org/ [Accessed 15/08/2023 2023].

Saier, M., Tam, R., Reizer, A. & Reizer, J. (1994). Two novel families of bacterial membrane proteins concerned with nodulation, cell division and transport. *Molecular Microbiology,* 11**,** 841-7.

Saier, M. H. (2000). A functional-phylogenetic classification system for transmembrane solute transporters. *Microbiology and Molecular Biology Reviews,* 64**,** 354-411.

Saier, M. H., Jr., Beatty, J. T., Goffeau, A., Harley, K. T., Heijne, W. H., Huang, S. C., Jack, D. L., Jahn, P. S., Lew, K., Liu, J., Pao, S. S., Paulsen, I. T., Tseng, T. T. & Virk, P. S. (1999). The major facilitator superfamily. *Journal of Molecular Microbiology and Biotechnology,* 1**,** 257-79.

Saier, M. H., Jr. & Paulsen, I. T. (2001). Phylogeny of multidrug transporters. *Seminars in Cell and Developmental Biology,* 12**,** 205-13.

Saier, M. H., Jr., Yen, M. R., Noto, K., Tamang, D. G. & Elkan, C. (2009). The Transporter Classification Database: recent advances. *Nucleic Acids Research,* 37**,** D274-8.

Saier, M. H., Reddy, V. S., Moreno-Hagelsieb, G., Hendargo, K. J., Zhang, Y., Iddamsetty, V., Lam, K. J. K., Tian, N., Russum, S., Wang, J. & Medrano-Soto, A. (2021). The Transporter Classification Database (TCDB): 2021 update. *Nucleic Acids Research,* 49**,** D461-d7.

Sajib, M. S., Tanmoy, A. M., Hooda, Y., Rahman, H., Andrews, J. R., Garrett, D. O., Endtz, H. P., Saha, S. K. & Saha, S. (2021). Tracking the emergence of azithromycin resistance in multiple genotypes of typhoidal salmonella. *mBio,* 12**,** 10.1128/mbio. 03481-20.

Sakurai, K., Yamasaki, S., Nakao, K., Nishino, K., Yamaguchi, A. & Nakashima, R. (2019). Crystal structures of multidrug efflux pump MexB bound with high-molecular-mass compounds. *Scientific Reports,* 9**,** 1-9.

Saleh, M., Bay, D. C. & Turner, R. J. (2018). Few conserved amino acids in the small multidrug resistance transporter EmrE influence drug polyselectivity. *Antimicrobial Agents and Chemotherapy,* 62**,** e00461-18.

Sambrook, J. & Russell, D. W. 2001. *Molecular cloning: a laboratory manual,* Cold Spring Harbor, N. Y., Cold Spring Harbor Laboratory Press.

Sarubbi, F., Sparling, P. F., Blackman, E. & Lewis, E. (1975). Loss of low-level antibiotic resistance in *Neisseria gonorrhoeae* due to *env* mutations. *Journal of Bacteriology,* 124**,** 750-6.

Sarubbi, F. A., Blackman, E. & Sparling, P. F. (1974). Genetic mapping of linked antibiotic resistance loci in *Neisseria gonorrhoeae*. *Journal of Bacteriology,* 120**,** 1284-92.

Sasatsu, M., Shima, K., Shibata, Y. & Kono, M. (1989). Nucleotide sequence of a gene that encodes resistance to ethidium bromide from a transferable plasmid in *Staphylococcus aureus*. *Nucleic Acids Research,* 17**,** 10103.

Satterwhite, C. L., Torrone, E., Meites, E., Dunne, E. F., Mahajan, R., Ocfemia, M. C. B., Su, J., Xu, F. & Weinstock, H. (2013). Sexually transmitted infections among US women and men: prevalence and incidence estimates, 2008. *Sexually Transmitted Diseases,* 40**,** 187-93.

Scherman, D. & Henry, J. P. (1984). Reserpine binding to bovine chromaffin granule membranes. Characterization and comparison with dihydrotetrabenazine binding. *Molecular Pharmacology,* 25**,** 113-22.

Schmid, N., Eichenberger, A. P., Choutko, A., Riniker, S., Winger, M., Mark, A. E. & van Gunsteren, W. F. (2011). Definition and testing of the GROMOS force-field versions 54A7 and 54B7. *European Biophysics Journal,* 40**,** 843-56.

Schneider, H., Griffiss, J. M., Williams, G. D. & Pier, G. B. (1982). Immunological basis of serum resistance of *Neisseria gonorrhoeae*. *Microbiology,* 128**,** 13-22.

Schneider, H., Hale, T., Zollinger, W., Seid, R., Hammack, C. & Griffiss, J. (1984). Heterogeneity of molecular size and antigenic expression within lipooligosaccharides of individual strains of *Neisseria gonorrhoeae* and *Neisseria meningitidis*. *Infection and Immunity,* 45**,** 544-9.

Schreiner, E., Trabuco, L. G., Freddolino, P. L. & Schulten, K. (2011). Stereochemical errors and their implications for molecular dynamics simulations. *BMC Bioinformatics,* 12**,** 190.

Schrodinger, LLC 2015. The PyMOL Molecular Graphics System, Version 1.8.

Schuldiner, S. (2014). Competition as a way of life for H^+-coupled antiporters. *Journal of Molecular Biology,* 426**,** 2539-46.

Schuldiner, S. (2018). The *Escherichia coli* effluxome. *Research in Microbiology,* 169**,** 357-62.

Schuldiner, S., Granot, D., Mordoch, S. S., Ninio, S., Rotem, D., Soskin, M., Tate, C. G. & Yerushalmi, H. (2001). Small is mighty: EmrE, a multidrug transporter as an experimental paradigm. *News in Physiological Sciences,* 16**,** 130-4.

Schulz, R., Vargiu, A. V., Collu, F., Kleinekathofer, U. & Ruggerone, P. (2010). Functional rotation of the transporter AcrB: insights into drug extrusion from simulations. *PLoS Computational Biology,* 6**,** e1000806.

Schulz, R., Vargiu, A. V., Ruggerone, P. & Kleinekathöfer, U. (2011). Role of water during the extrusion of substrates by the efflux transporter AcrB. *The Journal of Physical Chemistry B,* 115**,** 8278-87.

Schumacher, M. A., Miller, M. C., Grkovic, S., Brown, M. H., Skurray, R. A. & Brennan, R. G. (2001). Structural mechanisms of QacR induction and multidrug recognition. *Science,* 294**,** 2158-63.

Schumacher, M. A., Miller, M. C., Grkovic, S., Brown, M. H., Skurray, R. A. & Brennan, R. G. (2002). Structural basis for cooperative DNA binding by two dimers of the multidrug-binding protein QacR. *The EMBO Journal,* 21**,** 1210-8.

Schuster, S., Vavra, M. & Kern, W. V. (2016). Evidence of a substrate-discriminating entrance channel in the lower porter domain of the multidrug resistance efflux pump AcrB. *Antimicrobial Agents and Chemotherapy,* 60**,** 4315-23.

Schweizer, H. P. (2012). Understanding efflux in Gram-negative bacteria: opportunities for drug discovery. *Expert Opinion on Drug Discovery,* 7**,** 633-42.

Scott, C. & Ioannou, Y. (2004). The NPC1 protein: structure implies function. *Biochimica et Biophysica Acta (BBA)-Molecular and Cell Biology of Lipids,* 1685**,** 8-13.

Seeger, M. A., Diederichs, K., Eicher, T., Brandstatter, L., Schiefner, A., Verrey, F. & Pos, K. M. (2008). The AcrB efflux pump: conformational cycling and peristalsis lead to multidrug resistance. *Current Drug Targets,* 9**,** 729-49.

Seeger, M. A., Schiefner, A., Eicher, T., Verrey, F., Diederichs, K. & Pos, K. M. (2006). Structural asymmetry of AcrB trimer suggests a peristaltic pump mechanism. *Science,* 313**,** 1295-8.

Seeger, M. A., von Ballmoos, C., Verrey, F. & Pos, K. M. (2009). Crucial role of Asp408 in the proton translocation pathway of multidrug transporter AcrB: evidence from site-directed mutagenesis and carbodiimide labeling. *Biochemistry,* 48**,** 5801-12.

Seib, K. L., Jen, F. E.-C., Scott, A. L., Tan, A. & Jennings, M. P. (2017). Phase variation of DNA methyltransferases and the regulation of virulence and immune evasion in the pathogenic *Neisseria*. *Pathogens and Disease,* 75**,** ftx080.

Seib, K. L., Wu, H.-J., Kidd, S. P., Apicella, M. A., Jennings, M. P. & McEwan, A. G. (2006). Defenses against oxidative stress in *Neisseria gonorrhoeae*: a system tailored for a challenging environment. *Microbiology and Molecular Biology Reviews,* 70**,** 344-61.

Seifert, H. S. (2018). Above and beyond Watson and Crick: Guanine quadruplex structures and microbes. *Annual Review of Microbiology,* 72**,** 49-69.

Seifert, H. S. (2019). Location, location, location-commensalism, damage and evolution of the pathogenic *Neisseria*. *Journal of Molecular Biology,* 431**,** 3010-4.

Sennhauser, G., Amstutz, P., Briand, C., Storchenegger, O. & Grutter, M. G. (2007). Drug export pathway of multidrug exporter AcrB revealed by DARPin inhibitors. *PLoS Biology,* 5**,** e7.

Sennhauser, G., Bukowska, M. A., Briand, C. & Grutter, M. G. (2009a). Crystal structure of the multidrug exporter MexB from *Pseudomonas aeruginosa*. *Journal of Molecular Biology,* 389**,** 134-45.

Sennhauser, G., Bukowska, M. A., Briand, C. & Grütter, M. G. (2009b). Crystal structure of the multidrug exporter MexB from *Pseudomonas aeruginosa*. *Journal of Molecular Biology,* 389**,** 134-45.

Shafer, W. M. (2018). Mosaic drug efflux gene sequences from commensal *Neisseria* can lead to low-level azithromycin resistance expressed by *Neisseria gonorrhoeae* clinical isolates. *mBio,* 9**,** e01747-18.

Shafer, W. M., Balthazar, J. T., Hagman, K. E. & Morse, S. A. (1995). Missense mutations that alter the DNA-binding domain of the MtrR protein occur frequently in rectal isolates of *Neisseria gonorrhoeae* that are resistant to faecal lipids. *Microbiology,* 141**,** 907-11.

Shafer, W. M. & Folster, J. P. (2006). Towards an understanding of chromosomally mediated penicillin resistance in *Neisseria gonorrhoeae*: evidence for a porin-efflux pump collaboration. *Journal of Bacteriology,* 188**,** 2297-9.

Shafer, W. M., Folster, J. P. & Nicholas, R. A. 2010. Molecular mechanisms of antibiotic resistance expressed by the pathogenic *Neisseria*. *In:* GENCO, C. A. & WETZLER, L. (eds.) *Neisseria: Molecular Mechanisms of Pathogenesis.* Norfolk, UK: Caister Academic Press.

Shafer, W. M., Qu, X., Waring, A. J. & Lehrer, R. I. (1998). Modulation of *Neisseria gonorrhoeae* susceptibility to vertebrate antibacterial peptides due to a member of the resistance/nodulation/division efflux pump family. *Proceedings of the National Academy of Sciences of the United States of America,* 95**,** 1829-33.

Shafer, W. M., Veal, W. L., Lee, E.-H., Zarantonelli, L., Balthazar, J. T. & Rouquette, C. (2001). Genetic organization and regulation of antimicrobial efflux systems possessed by *Neisseria gonorrhoeae* and *Neisseria meningitidis*. *Journal of Molecular Microbiology and Biotechnology,* 3**,** 219-24.

Shafer, W. M., Yu, E. W., Rouquette-Loughlin, C., Golparian, D., Jerse, A. E. & Unemo, M. 2016. Efflux pumps in *Neisseria gonorrhoeae*: Contributions to antimicrobial resistance and virulence. *In:* LI, X.-Z., ELKINS, C. A. & ZGURSKAYA, H. I. (eds.) *Efflux-mediated antimicrobial resistance in bacteria.* Switzerland: Springer.

Shah, P. & Swiatlo, E. (2008). A multifaceted role for polyamines in bacterial pathogens. *Molecular Microbiology,* 68**,** 4-16.

Sharifi, S., Bakhshi, B. & Najar-peerayeh, S. (2021). Significant contribution of the CmeABC efflux pump in high-level resistance to ciprofloxacin and tetracycline in *Campylobacter jejuni* and *Campylobacter coli* clinical isolates. *Annals of Clinical Microbiology and Antimicrobials,* 20**,** 36.

Sharom, F. J. (2014). Complex interplay between the P-Glycoprotein multidrug efflux pump and the membrane: its role in modulating protein function. *Frontiers in Oncology,* 4**,** e00041.

Shi, X., Chen, M., Yu, Z., Bell, J. M., Wang, H., Forrester, I., Villarreal, H., Jakana, J., Du, D., Luisi, B. F., Ludtke, S. J. & Wang, Z. (2019). In situ structure and assembly of the multidrug efflux pump AcrAB-TolC. *Nature Communications,* 10**,** 2635.

Shome, S., Sankar, K. & Jernigan, R. L. (2021). Simulated drug efflux for the AbgT family of membrane transporters. *Journal of Chemical Information and Modeling,* 61**,** 5673-81.

Shvarev, D., Januliene, D. & Moeller, A. (2022). Frozen motion: how cryo-EM changes the way we look at ABC transporters. *Trends in Biochemical Sciences,* 47**,** 136-48.

Si, Z., Pethe, K. & Chan-Park, M. B. (2023). Chemical basis of combination therapy to combat antibiotic resistance. *JACS Au,* 3**,** 276-92.

Sierra, J. M., Fusté, E., Rabanal, F., Vinuesa, T. & Viñas, M. (2017). An overview of antimicrobial peptides and the latest advances in their development. *Expert Opinion on Biological Therapy,* 17**,** 663-76.

Silver, L. L. (2016). A Gestalt approach to Gram-negative entry. *Bioorganic & Medicinal Chemistry,* 24**,** 6379-89.

Sjuts, H., Vargiu, A. V., Kwasny, S. M., Nguyen, S. T., Kim, H. S., Ding, X., Ornik, A. R., Ruggerone, P., Bowlin, T. L., Nikaido, H., Pos, K. M. & Opperman, T. J. (2016). Molecular basis for inhibition of AcrB multidrug efflux pump by novel and powerful pyranopyridine derivatives. *Proceedings of the National Academy of Sciences of the United States of America,* 113**,** 3509-14.

Skerker, J. M. & Berg, H. C. (2001). Direct observation of extension and retraction of type IV pili. *Proceedings of the National Academy of Sciences of the United States of America,* 98**,** 6901-4.

Slipski, C. J., Jamieson, T. R., Lam, A., Shing, V. L., Bell, K., Zhanel, G. G. & Bay, D. C. (2019). Plasmid transmitted small multidrug resistant (SMR) efflux pumps differ in gene regulation and enhance tolerance to quaternary ammonium compounds (QAC) when grown as biofilms. *bioRxiv***,** 768630.

Smolarchuk, C., Wensley, A., Padfield, S., Fifer, H., Lee, A. & Hughes, G. (2018). Persistence of an outbreak of gonorrhoea with high-level resistance to azithromycin in England, November 2014–May 2018. *Eurosurveillance,* 23**,** 1800287.

Snyder, L. A., McGowan, S., Rogers, M., Duro, E., O'Farrell, E. & Saunders, N. J. (2007). The repertoire of minimal mobile elements in the *Neisseria* species and evidence that these are involved in horizontal gene transfer in other bacteria. *Molecular Biology and Evolution,* 24**,** 2802-15.

Song, W., Ma, L., Chen, R. & Stein, D. C. (2000). Role of lipooligosaccharide in Opa-independent invasion of *Neisseria gonorrhoeae* into human epithelial cells. *The Journal of Experimental Medicine,* 191**,** 949-60.

Sparling, P. F., Sarubbi, F. A. J. & Blackman, E. (1975). Inheritance of low-level resistance to penicillin, tetracycline, and chloramphenicol in *Neisseria gonorrhoeae*. *Journal of Bacteriology,* 124**,** 740-9.

Spence, J. M., Wright, L. & Clark, V. L. (2008). Laboratory maintenance of *Neisseria gonorrhoeae*. *Current Protocols in Microbiology,* 8**,** 4A. 1.-4A. 1.26.

Spencer-Smith, R., Roberts, S., Gurung, N. & Snyder, L. A. (2016). DNA uptake sequences in *Neisseria* gonorrhoeae as intrinsic transcriptional terminators and markers of horizontal gene transfer. *Microbial Genomics,* 2**,** 1-11.

Spoelstra, E. C., Westerhoff, H. V., Pinedo, H. M., Dekker, H. & Lankelma, J. (1994). The multidrug-resistance-reverser verapamil interferes with cellular P-glycoprotein-mediated pumping of daunorubicin as a non-competing substrate. *European Journal of Biochemistry,* 221**,** 363-73.

Srikhanta, Y. N., Dowideit, S. J., Edwards, J. L., Falsetta, M. L., Wu, H.-J., Harrison, O. B., Fox, K. L., Seib, K. L., Maguire, T. L. & Wang, A. H.-J. (2009). Phasevarions mediate random switching of gene expression in pathogenic *Neisseria*. *PLoS Pathog,* 5**,** e1000400.

St Cyr, S., Barbee, L., Workowski, K. A., Bachmann, L. H., Pham, C., Schlanger, K., Torrone, E., Weinstock, H., Kersh, E. N. & Thorpe, P. (2020). Update to CDC's treatment guidelines for gonococcal infection, 2020. *MMWR Morb Mortal Wkly Rep,* 69**,** 1911-6.

Stein, D. C. (1991). Transformation of *Neisseria gonorrhoeae*: physical requirements of the transforming DNA. *Canadian Journal of Microbiology,* 37**,** 345-9.

Steinmoen, H., Knutsen, E. & Håvarstein, L. S. (2002). Induction of natural competence in *Streptococcus pneumoniae* triggers lysis and DNA release from a subfraction of the cell population. *Proceedings of the National Academy of Sciences of the United States of America,* 99**,** 7681-6.

Stern, A., Brown, M., Nickel, P. & Meyer, T. F. (1986). Opacity genes in *Neisseria gonorrhoeae*: control of phase and antigenic variation. *Cell,* 47**,** 61-71.

Stevens, K., Zaia, A., Tawil, S., Bates, J., Hicks, V., Whiley, D., Limnios, A., Lahra, M. M. & Howden, B. P. (2015). *Neisseria gonorrhoeae* isolates with high-level resistance to azithromycin in Australia. *Journal of Antimicrobial Chemotherapy,* 70**,** 1267-8.

Story, R. M. & Steitz, T. A. (1992). Structure of the *recA* protein–ADP complex. *Nature,* 355**,** 374-6.

Studier, F. W. & Moffatt, B. A. (1986). Use of bacteriophage T7 RNA polymerase to direct selective high-level expression of cloned genes. *Journal of Molecular Biology,* 189**,** 113-30.

Su, C.-C., Bolla, J. R., Kumar, N., Radhakrishnan, A., Long, F., Delmar, J. A., Chou, T.-H., Rajashankar, K. R., Shafer, W. M. & Yu, E. W. (2015). Structure and function of *Neisseria gonorrhoeae* MtrF illuminates a class of antimetabolite efflux pumps. *Cell Reports,* 11**,** 61-70.

Su, C.-C., Long, F., Zimmermann, M. T., Rajashankar, K. R., Jernigan, R. L. & Yu, E. W. (2011). Crystal structure of the CusBA heavy-metal efflux complex of *Escherichia coli*. *Nature,* 470**,** 558-62.

Su, C.-C., Lyu, M., Morgan, C. E., Bolla, J. R., Robinson, C. V. & Edward, W. Y. (2021). A 'Build and Retrieve' methodology to simultaneously solve cryo-EM structures of membrane proteins. *Nature Methods,* 18**,** 69-75.

Su, C.-C., Morgan, C. E., Kambakam, S., Rajavel, M., Scott, H., Huang, W., Emerson, C. C., Taylor, D. J., Stewart, P. L. & Bonomo, R. A. (2019). Cryo-electron microscopy structure of an *Acinetobacter baumannii* multidrug efflux pump. *mBio,* 10**,** 01295-19.

Su, C. C., Li, M., Gu, R., Takatsuka, Y., McDermott, G., Nikaido, H. & Yu, E. W. (2006). Conformation of the AcrB multidrug efflux pump in mutants of the putative proton relay pathway. *Journal of Bacteriology,* 188**,** 7290-6.

Su, C. C., Rutherford, D. J. & Yu, E. W. (2007). Characterization of the multidrug efflux regulator AcrR from *Escherichia coli*. *Biochemical and Biophysical Research Communications,* 361**,** 85-90.

Su, C. C., Yin, L., Kumar, N., Dai, L., Radhakrishnan, A., Bolla, J. R., Lei, H. T., Chou, T. H., Delmar, J. A., Rajashankar, K. R., Zhang, Q., Shin, Y. K. & Yu, E. W. (2017). Structures and transport dynamics of a *Campylobacter jejuni* multidrug efflux pump. *Nature Communications,* 8**,** 171.

Sugawara, E. & Nikaido, H. (2014). Properties of AdeABC and AdeIJK efflux systems of *Acinetobacter baumannii* compared with those of the AcrAB-TolC system of *Escherichia coli*. *Antimicrobial Agents and Chemotherapy,* 58**,** 7250-7.

Sulavik, M. C., Houseweart, C., Cramer, C., Jiwani, N., Murgolo, N., Greene, J., DiDomenico, B., Shaw, K. J., Miller, G. H., Hare, R. & Shimer, G. (2001). Antibiotic susceptibility profiles of *Escherichia coli* strains lacking multidrug efflux pump genes. *Antimicrobial Agents and Chemotherapy,* 45**,** 1126-36.

Sun, J., Deng, Z. & Yan, A. (2014). Bacterial multidrug efflux pumps: mechanisms, physiology and pharmacological exploitations. *Biochemical and Biophysical Research Communications,* 453**,** 254-67.

Sunkavalli, A., McClure, R. & Genco, C. (2022). Molecular regulatory mechanisms drive emergent pathogenetic properties of *Neisseria gonorrhoeae*. *Microorganisms,* 10**,** 922.

Swanson, J. (1978). Studies on gonococcus infection. XII. Colony color and opacity varienats of gonococci. *Infection and Immunity,* 19**,** 320-31.

Swartzman, E., Silverman, M. & Meighen, E. (1992). The *luxR* gene product of *Vibrio harveyi* is a transcriptional activator of the *lux* promoter. *Journal of Bacteriology,* 174**,** 7490-3.

Swier, L. J., Slotboom, D.-J. & Poolman, B. (2016). ABC importers. *ABC transporters-40 Years on***,** 3-36.

Symmons, M. F., Bokma, E., Koronakis, E., Hughes, C. & Koronakis, V. (2009). The assembled structure of a complete tripartite bacterial multidrug efflux pump. *Proceedings of the National Academy of Sciences of the United States of America,* 106**,** 7173-8.

Tagliabue, A. & Rappuoli, R. (2018). Changing priorities in vaccinology: antibiotic resistance moving to the top. *Frontiers in Immunology,* 9**,** 1068.

Taipale, J., Cooper, M. K., Maiti, T. & Beachy, P. A. (2002). Patched acts catalytically to suppress the activity of Smoothened. *Nature,* 418**,** 892-7.

Takanashi, K., Shitan, N. & Yazaki, K. (2014). The multidrug and toxic compound extrusion (MATE) family in plants. *Plant Biotechnology,* 31**,** 417-30.

Takatsuka, Y., Chen, C. & Nikaido, H. (2010). Mechanism of recognition of compounds of diverse structures by the multidrug efflux pump AcrB of

Escherichia coli. *Proceedings of the National Academy of Sciences of the United States of America,* 107**,** 6559-65.

Takatsuka, Y. & Nikaido, H. (2006). Threonine-978 in the transmembrane segment of the multidrug efflux pump AcrB of *Escherichia coli* is crucial for drug transport as a probable component of the proton relay network. *Journal of Bacteriology,* 188**,** 7284-9.

Takatsuka, Y. & Nikaido, H. (2009). Covalently linked trimer of the AcrB multidrug efflux pump provides support for the functional rotating mechanism. *Journal of Bacteriology,* 191**,** 1729-37.

Tal, N. & Schuldiner, S. (2009). A coordinated network of transporters with overlapping specificities provides a robust survival strategy. *Proceedings of the National Academy of Sciences of the United States of America,* 106**,** 9051-6.

Tam, H.-K., Foong, W. E., Oswald, C., Herrmann, A., Zeng, H. & Pos, K. M. (2021). Allosteric drug transport mechanism of multidrug transporter AcrB. *Nature Communications,* 12**,** 3889.

Tam, H. K., Malviya, V. N., Foong, W. E., Herrmann, A., Malloci, G., Ruggerone, P., Vargiu, A. V. & Pos, K. M. (2020). Binding and transport of carboxylated drugs by the multidrug transporter AcrB. *Journal of Molecular Biology,* 432**,** 861-77.

Tamburrino, G., Llabrés, S., Vickery, O. N., Pitt, S. J. & Zachariae, U. (2017). Modulation of the *Neisseria gonorrhoeae* drug efflux conduit MtrE. *Scientific Reports,* 7**,** 1-10.

Tanaka, Y., Hipolito, C. J., Maturana, A. D., Ito, K., Kuroda, T., Higuchi, T., Katoh, T., Kato, H. E., Hattori, M. & Kumazaki, K. (2013). Structural basis for the drug extrusion mechanism by a MATE multidrug transporter. *Nature,* 496**,** 247-51.

Tang, K. & Zhao, H. (2023). Quinolone antibiotics: Resistance and therapy. *Infection and Drug Resistance***,** 811-20.

Tang, Y., Liu, X., Chen, W., Luo, X., Zhuang, P., Li, R. & Lin, X. (2023). Antimicrobial resistance profiling and genome analysis of the *penA*-60.001 *Neisseria gonorrhoeae* clinical isolates in China in 2021. *The Journal of Infectious Diseases,* 228**,** 792-9.

Tanihara, Y., Masuda, S., Sato, T., Katsura, T., Ogawa, O. & Inui, K.-i. (2007). Substrate specificity of MATE1 and MATE2-K, human multidrug and toxin extrusions/H^+-organic cation antiporters. *Biochemical Pharmacology,* 74**,** 359-71.

Tapsall, J. W. (2005). Antibiotic resistance in *Neisseria gonorrhoeae*. *Clinical Infectious Diseases,* 41**,** S263-S8.

Tapsall, J. W. (2009). *Neisseria gonorrhoeae* and emerging resistance to extended spectrum cephalosporins. *Current Opinion in Infectious Diseases,* 22**,** 87-91.

Tennent, J. M., Lyon, B. R., Midgley, M., Jones, G., Purewal, A. S. & Skurray, R. A. (1989). Physical and biochemical characterization of the *qacA* gene encoding antiseptic and disinfectant resistance in *Staphylococcus aureus*. *Microbiology,* 135**,** 1-10.

Terkelsen, D., Tolstrup, J., Johnsen, C. H., Lund, O., Larsen, H. K., Worning, P., Unemo, M. & Westh, H. (2017). Multidrug-resistant *Neisseria gonorrhoeae* infection with ceftriaxone resistance and intermediate resistance to azithromycin, Denmark, 2017. *Eurosurveillance,* 22**,** 17-00659.

Thakur, S. D., Levett, P. N., Horsman, G. B. & Dillon, J. R. (2018). Association of *Neisseria gonorrhoeae* genogroups and specific PBP2/MtrR/PorB mutation patterns with susceptibility to penicillin in a susceptible gonococcal population. *Journal of Antimicrobial Chemotherapy,* 73**,** 2682-6.

Thanabalu, T., Koronakis, E., Hughes, C. & Koronakis, V. (1998). Substrate-induced assembly of a contiguous channel for protein export from *Escherichia coli*: reversible bridging of an inner-membrane translocase to an outer membrane exit pore. *EMBO Journal,* 17**,** 6487-96.

Thanassi, D. G., Cheng, L. W. & Nikaido, H. (1997). Active efflux of bile salts by *Escherichia coli*. *Journal of Bacteriology,* 179**,** 2512-8.

Thomas, J. C., Kersh, E. N., Gernert, K. M., Shafer, W. M. & Raphael, B. H. (2020). Reply: Evidence of recent genomic evolution in gonococcal strains with decreased susceptibility to cephalosporins or azithromycin in the United States, 2014-2016. *The Journal of Infectious Diseases,* 221**,** 852-3.

Thomas, J. C., Seby, S., Abrams, A. J., Cartee, J., Lucking, S., Vidyaprakash, E., Schmerer, M., Pham, C. D., Hong, J., Torrone, E., Cyr, S. S., Shafer, W. M., Bernstein, K., Kersh, E. N. & Gernert, K. M. (2019a). Evidence of recent genomic evolution in gonococcal strains with decreased susceptibility to cephalosporins or azithromycin in the United States, 2014-2016. *The Journal of Infectious Diseases,* 220**,** 294-305.

Thomas, J. C., Seby, S., Abrams, A. J., Cartee, J., Lucking, S., Vidyaprakash, E., Schmerer, M., Pham, C. D., Hong, J., Torrone, E., Cyr, S. S., Shafer, W. M., Bernstein, K., Kersh, E. N., Gernert, K. M. & Group, A.-R. N. g. W. (2019b). Evidence of recent genomic evolution in gonococcal strains with decreased susceptibility to cephalosporins or azithromycin in the United States, 2014–2016. *The Journal of Infectious Diseases,* 220**,** 294-305.

Thompson, E. P., Wilkins, C., Demidchik, V., Davies, J. M. & Glover, B. J. (2009). An Arabidopsis flavonoid transporter is required for anther dehiscence and pollen development. *Journal of Experimental Botany,* 61**,** 439-51.

Tibazarwa, C., Wuertz, S., Mergeay, M., Wyns, L. & van Der Lelie, D. (2000). Regulation of the *cnr* cobalt and nickel resistance determinant of

Ralstonia eutropha (*Alcaligenes eutrophus*) CH34. *Journal of Bacteriology,* 182**,** 1399-409.

Tikhonova, E. B., Wang, Q. & Zgurskaya, H. I. (2002). Chimeric analysis of the multicomponent multidrug efflux transporters from Gram-negative bacteria. *Journal of Bacteriology,* 184**,** 6499-507.

Tikhonova, E. B., Yamada, Y. & Zgurskaya, H. I. (2011). Sequential mechanism of assembly of multidrug efflux pump AcrAB-TolC. *Chemistry & biology,* 18**,** 454-63.

Tikhonova, E. B. & Zgurskaya, H. I. (2004). AcrA, AcrB, and TolC of *Escherichia coli* form a stable intermembrane multidrug efflux complex. *Journal of Biological Chemistry,* 279**,** 32116-24.

Tomberg, J., Unemo, M., Davies, C. & Nicholas, R. A. (2010). Molecular and structural analysis of mosaic variants of penicillin-binding protein 2 conferring decreased susceptibility to expanded-spectrum cephalosporins in *Neisseria gonorrhoeae*: role of epistatic mutations. *Biochemistry,* 49**,** 8062-70.

Tønjum, T. & van Putten, J. 2017. *Neisseria*. *In:* COHEN, J., POWDERLY, W. G. & OPAL, S. M. (eds.) *Infectious Diseases (Fourth Edition).* Elsevier.

Törnroth-Horsefield, S., Gourdon, P., Horsefield, R., Brive, L., Yamamoto, N., Mori, H., Snijder, A. & Neutze, R. (2007). Crystal structure of AcrB in complex with a single transmembrane subunit reveals another twist. *Structure,* 15**,** 1663-73.

Trampari, E., Prischi, F., Vargiu, A. V., Abi-Assaf, J., Bavro, V. N. & Webber, M. A. (2023). Functionally distinct mutations within AcrB underpin antibiotic resistance in different lifestyles. *npj Antimicrobials and Resistance,* 1**,** 2.

Tseng, T. T., Gratwick, K. S., Kollman, J., Park, D., Nies, D. H., Goffeau, A. & Saier, M. H., Jr. (1999). The RND permease superfamily: an ancient, ubiquitous and diverse family that includes human disease and development proteins. *Journal of Molecular Microbiology and Biotechnology,* 1**,** 107-25.

Tsukazaki, T. (2018). Structure-based working model of SecDF, a proton-driven bacterial protein translocation factor. *FEMS Microbiology Letters,* 365.

Tsukazaki, T., Mori, H., Echizen, Y., Ishitani, R., Fukai, S., Tanaka, T., Perederina, A., Vassylyev, D. G., Kohno, T. & Maturana, A. D. (2011). Structure and function of a membrane component SecDF that enhances protein export. *Nature,* 474**,** 235-8.

Tsuruo, T., Iida, H., Tsukagoshi, S. & Sakurai, Y. (1981). Overcoming of vincristine resistance in P388 leukemia *in vivo* and *in vitro* through enhanced cytotoxicity of vincristine and vinblastine by verapamil. *Cancer Research,* 41**,** 1967-72.

Tsutsumi, K., Yonehara, R., Ishizaka-Ikeda, E., Miyazaki, N., Maeda, S., Iwasaki, K., Nakagawa, A. & Yamashita, E. (2019). Structures of the wild-type MexAB–OprM tripartite pump reveal its complex formation and drug efflux mechanism. *Nature Communications,* 10**,** 1520.

Tucker, A. T., Nowicki, E. M., Boll, J. M., Knauf, G. A., Burdis, N. C., Trent, M. S. & Davies, B. W. (2014). Defining gene-phenotype relationships in Acinetobacter baumannii through one-step chromosomal gene inactivation. *mBio,* 5**,** 10.1128/mbio. 01313-14.

Turlin, E., Heuck, G., Simões Brandão, M. I., Szili, N., Mellin, J., Lange, N. & Wandersman, C. (2014). Protoporphyrin (PPIX) efflux by the MacAB-TolC pump in *Escherichia coli*. *Microbiologyopen,* 3**,** 849-59.

Ubarretxena-Belandia, I., Baldwin, J. M., Schuldiner, S. & Tate, C. G. (2003). Three-dimensional structure of the bacterial multidrug transporter EmrE shows it is an asymmetric homodimer. *The EMBO Journal,* 22**,** 6175-81.

Ubukata, K., Itoh-Yamashita, N. & Konno, M. (1989). Cloning and expression of the *norA* gene for fluoroquinolone resistance in *Staphylococcus aureus*. *Antimicrobial Agents and Chemotherapy,* 33**,** 1535-9.

Unemo, M. (2020). Optimizations to keep gonorrhoea treatable and reduce antimicrobial resistance selection. *Nature Reviews Urology***,** 1-2.

Unemo, M., Bradshaw, C. S., Hocking, J. S., de Vries, H. J., Francis, S. C., Mabey, D., Marrazzo, J. M., Sonder, G. J., Schwebke, J. R. & Hoornenborg, E. (2017). Sexually transmitted infections: challenges ahead. *The Lancet Infectious Diseases,* 17**,** e235-e79.

Unemo, M., Del Rio, C. & Shafer, W. M. (2016). Antimicrobial resistance expressed by *Neisseria gonorrhoeae*: A major global public health problem in the 21st century. *Microbiology Spectrum,* 4.

Unemo, M., Golparian, D., Nicholas, R., Ohnishi, M., Gallay, A. & Sednaoui, P. (2012). High-level cefixime-and ceftriaxone-resistant *Neisseria gonorrhoeae* in France: novel *penA* mosaic allele in a successful international clone causes treatment failure. *Antimicrobial Agents and Chemotherapy,* 56**,** 1273-80.

Unemo, M., Lahra, M. M., Cole, M., Galarza, P., Ndowa, F., Martin, I., Dillon, J.-A. R., Ramon-Pardo, P., Bolan, G. & Wi, T. (2019a). World Health Organization Global Gonococcal Antimicrobial Surveillance Program (WHO GASP): review of new data and evidence to inform international collaborative actions and research efforts. *Sex Health,* 16**,** 412-25.

Unemo, M., Ross, J., Serwin, A., Gomberg, M., Cusini, M. & Jensen, J. (2020). 2020 European guideline for the diagnosis and treatment of gonorrhoea in adults. *International journal of STD & AIDS***,** 0956462420949126.

Unemo, M., Seifert, H. S., Hook, E. W., Hawkes, S., Ndowa, F. & Dillon, J.-A. R. (2019b). Gonorrhoea. *Nature Reviews Disease Primers,* 5**,** 1-23.

Unemo, M. & Shafer, W. M. (2014). Antimicrobial resistance in *Neisseria gonorrhoeae* in the 21st century: past, evolution, and future. *Clinical Microbiology Reviews,* 27**,** 587-613.

Upadhyay, N., Kar, D., Deepak Mahajan, B., Nanda, S., Rahiman, R., Panchakshari, N., Bhagavatula, L. & Datta, S. (2019). The multitasking abilities of MATE transporters in plants. *Journal of Experimental Botany,* 70**,** 4643-56.

Vallejo, A. N., Pogulis, R. J. & Pease, L. R. (1994). In vitro synthesis of novel genes: mutagenesis and recombination by PCR. *Genome Research,* 4**,** S123-30.

Vallet-Gely, I., Novikov, A., Augusto, L., Liehl, P., Bolbach, G., Péchy-Tarr, M., Cosson, P., Keel, C., Caroff, M. & Lemaitre, B. (2010). Association of hemolytic activity of *Pseudomonas entomophila*, a versatile soil bacterium, with cyclic lipopeptide production. *Applied and Environmental Microbiology,* 76**,** 910-21.

Van Der Spoel, D., Lindahl, E., Hess, B., Groenhof, G., Mark, A. E. & Berendsen, H. J. (2005). GROMACS: fast, flexible, and free. *Journal of Computational Chemistry,* 26**,** 1701-18.

Van Hal, S. J., Whiley, D. M., Le, T., Ray, S., Kundu, R. L., Kerr, E. & Lahra, M. M. (2023). Rapid expansion of *Neisseria gonorrhoeae* ST7827 clone in Australia, with variable ceftriaxone phenotype unexplained by genotype. *Journal of Antimicrobial Chemotherapy,* 78**,** 2203-8.

Van Veen, H. W. 2016. Bacterial ABC multidrug exporters: from shared proteins motifs and features to diversity in molecular mechanisms. *In:* GEORGE, A. M. (ed.) *ABC transporters-40 Years on.* Switzerland: Springer.

Varela, M. F., Sansom, C. E. & Griffith, J. K. (1995). Mutational analysis and molecular modelling of an amino acid sequence motif conserved in antiporters but not symporters in a transporter superfamily. *Molecular Membrane Biology,* 12**,** 313-9.

Vargiu, A. V., Collu, F., Schulz, R., Pos, K. M., Zacharias, M., Kleinekathofer, U. & Ruggerone, P. (2011). Effect of the F610A mutation on substrate extrusion in the AcrB transporter: explanation and rationale by molecular dynamics simulations. *Journal of the American Chemical Society,* 133**,** 10704-7.

Vargiu, A. V. & Nikaido, H. (2012). Multidrug binding properties of the AcrB efflux pump characterized by molecular dynamics simulations. *Proceedings of the National Academy of Sciences of the United States of America,* 109**,** 20637-42.

Vargiu, A. V., Ramaswamy, V. K., Malloci, G., Malvacio, I., Atzori, A. & Ruggerone, P. (2018a). Computer simulations of the activity of RND efflux pumps. *Research in Microbiology,* 169**,** 384-92.

Vargiu, A. V., Ramaswamy, V. K., Malvacio, I., Malloci, G., Kleinekathöfer, U. & Ruggerone, P. (2018b). Water-mediated interactions enable smooth substrate transport in a bacterial efflux pump. *Biochimica et Biophysica Acta (BBA)-General Subjects,* 1862**,** 836-45.

Vargiu, A. V., Ruggerone, P., Opperman, T. J., Nguyen, S. T. & Nikaido, H. (2014). Molecular mechanism of MBX2319 inhibition of *Escherichia coli* AcrB multidrug efflux pump and comparison with other inhibitors. *Antimicrobial Agents and Chemotherapy,* 58**,** 6224-34.

Veal, W. L., Nicholas, R. A. & Shafer, W. M. (2002). Overexpression of the MtrC-MtrD-MtrE efflux pump due to an *mtrR* mutation is required for chromosomally mediated penicillin resistance in *Neisseria gonorrhoeae*. *Journal of Bacteriology,* 184**,** 5619-24.

Veal, W. L. & Shafer, W. M. (2003). Identification of a cell envelope protein (MtrF) involved in hydrophobic antimicrobial resistance in *Neisseria gonorrhoeae*. *Journal of Antimicrobial Chemotherapy,* 51**,** 27-37.

Veal, W. L., Yellen, A., Balthazar, J. T., Pan, W., Spratt, B. G. & Shafer, W. M. (1998). Loss-of-function mutations in the *mtr* efflux system of *Neisseria gonorrhoeae*. *Microbiology,* 144 (Pt 3)**,** 621-7.

Verchere, A., Dezi, M., Adrien, V., Broutin, I. & Picard, M. (2015). In vitro transport activity of the fully assembled MexAB-OprM efflux pump from *Pseudomonas aeruginosa*. *Nature Communications,* 6**,** 6890.

Vergalli, J., Bodrenko, I. V., Masi, M., Moynie, L., Acosta-Gutierrez, S., Naismith, J. H., Davin-Regli, A., Ceccarelli, M., van den Berg, B., Winterhalter, M. & Pages, J. M. (2020). Porins and small-molecule translocation across the outer membrane of Gram-negative bacteria. *Nature Reviews Microbiology,* 18**,** 164-76.

Vergalli, J., Chauvet, H., Oliva, F., Pajović, J., Malloci, G., Vargiu, A. V., Réfrégiers, M., Ruggerone, P. & Pagès, J.-M. (2022). A framework for dissecting affinities of multidrug efflux transporter AcrB to fluoroquinolones. *Communications Biology,* 5**,** 1062.

Vermaas, J. V., Rempe, S. B. & Tajkhorshid, E. (2018). Electrostatic lock in the transport cycle of the multidrug resistance transporter EmrE. *Proceedings of the National Academy of Sciences*, 115, E7502-E11.

Vieira Da Cruz, A., Jiménez-Castellanos, J.-C., Börnsen, C., Van Maele, L., Compagne, N., Pradel, E., Müller, R. T., Meurillon, V., Soulard, D. & Piveteau, C. (2024). Pyridylpiperazine efflux pump inhibitor boosts in vivo antibiotic efficacy against *K. pneumoniae*. *EMBO Molecular Medicine,* 16**,** 93-111.

Vogt, A. D., Pozzi, N., Chen, Z. & Di Cera, E. (2014). Essential role of conformational selection in ligand binding. *Biophysical Chemistry,* 186**,** 13-21.

Wadsworth, C. B., Arnold, B. J., Sater, M. R. A. & Grad, Y. H. (2018a). Azithromycin resistance through interspecific acquisition of an

epistasis-dependent efflux pump component and transcriptional regulator in *Neisseria gonorrhoeae*. *mBio,* 9**,** e01419-18.

Wadsworth, C. B., Arnold, B. J., Sater, M. R. A. & Grad, Y. H. (2018b). Azithromycin Resistance through Interspecific Acquisition of an Epistasis-Dependent Efflux Pump Component and Transcriptional Regulator in Neisseria gonorrhoeae. *mBio,* 9**,** 10.1128/mbio.01419-18.

Wales, A. D. & Davies, R. H. (2015). Co-selection of resistance to antibiotics, biocides and heavy metals, and its relevance to foodborne pathogens. *Antibiotics,* 4**,** 567-604.

Walker, E., van Niekerk, S., Hanning, K., Kelton, W. & Hicks, J. (2023). Mechanisms of host manipulation by *Neisseria gonorrhoeae*. *Frontiers in Microbiology,* 14**,** 1119834.

Wandersman, C. & Delepelaire, P. (1990). TolC, an *Escherichia coli* outer membrane protein required for hemolysin secretion. *Proceedings of the National Academy of Sciences of the United States of America,* 87**,** 4776-80.

Wang-Kan, X., Rodríguez-Blanco, G., Southam, A. D., Winder, C. L., Dunn, W. B., Ivens, A. & Piddock, L. J. (2021). Metabolomics reveal potential natural substrates of AcrB in *Escherichia coli* and *Salmonella enterica* Serovar Typhimurium. *mBio*, 12, e00109-21.

Wang, B., Weng, J. & Wang, W. (2015). Substrate binding accelerates the conformational transitions and substrate dissociation in multidrug efflux transporter AcrB. *Frontiers in Microbiology,* 6**,** 302.

Wang, D., Hu, E., Chen, J., Tao, X., Gutierrez, K. & Qi, Y. (2013). Characterization of novel *ybjG* and *dacC* variants in *Escherichia coli*. *Journal of Medical Microbiology,* 62**,** 1728-34.

Wang, L., Johnson, Z. L., Wasserman, M. R., Levring, J., Chen, J. & Liu, S. (2020a). Characterization of the kinetic cycle of an ABC transporter by single-molecule and cryo-EM analyses. *Elife,* 9**,** e56451.

Wang, S. C., Davejan, P., Hendargo, K. J., Javadi-Razaz, I., Chou, A., Yee, D. C., Ghazi, F., Lam, K. J. K., Conn, A. M. & Madrigal, A. (2020b). Expansion of the Major Facilitator Superfamily (MFS) to include novel transporters as well as transmembrane-acting enzymes. *Biochimica et Biophysica Acta (BBA)-Biomembranes***,** 183277.

Wang, Y., Alenazy, R., Gu, X., Polyak, S. W., Zhang, P., Sykes, M. J., Zhang, N., Venter, H. & Ma, S. (2021). Design and structural optimization of novel 2H-benzo [h] chromene derivatives that target AcrB and reverse bacterial multidrug resistance. *European Journal of Medicinal Chemistry,* 213**,** 113049.

Wang, Y., Alenzy, R., Song, D., Liu, X., Teng, Y., Mowla, R., Ma, Y., Polyak, S. W., Venter, H. & Ma, S. (2020c). Structural optimization of natural product nordihydroguaretic acid to discover novel analogues as AcrB inhibitors. *Eur J Med Chem,* 186**,** 111910.

Wang, Z., Fan, G., Hryc, C. F., Blaza, J. N., Serysheva, II, Schmid, M. F., Chiu, W., Luisi, B. F. & Du, D. (2017). An allosteric transport mechanism for the AcrAB-TolC multidrug efflux pump. *Elife,* 6**,** e24905.

Ward, A., Reyes, C. L., Yu, J., Roth, C. B. & Chang, G. (2007). Flexibility in the ABC transporter MsbA: Alternating access with a twist. *Proceedings of the National Academy of Sciences of the United States of America,* 104**,** 19005-10.

Warner, D. M., Folster, J. P., Shafer, W. M. & Jerse, A. E. (2007). Regulation of the MtrC-MtrD-MtrE efflux-pump system modulates the in vivo fitness of *Neisseria gonorrhoeae*. *The Journal of Infectious Diseases,* 196**,** 1804-12.

Warner, D. M., Shafer, W. M. & Jerse, A. E. (2008). Clinically relevant mutations that cause derepression of the *Neisseria gonorrhoeae* MtrC-MtrD-MtrE Efflux pump system confer different levels of antimicrobial resistance and *in vivo* fitness. *Molecular Microbiology,* 70**,** 462-78.

Wassenaar, T. A., Ingólfsson, H. I., Böckmann, R. A., Tieleman, D. P. & Marrink, S. J. (2015). Computational lipidomics with insane: A versatile tool for generating custom membranes for molecular simulations. *Journal of Chemical Theory and Computation,* 11**,** 2144-55.

Wassenaar, T. A., Pluhackova, K., Böckmann, R. A., Marrink, S. J. & Tieleman, D. P. (2014). Going backward: a flexible geometric approach to reverse transformation from coarse grained to atomistic models. *Journal of Chemical Theory and Computation,* 10**,** 676-90.

Waterhouse, A., Bertoni, M., Bienert, S., Studer, G., Tauriello, G., Gumienny, R., Heer, F. T., de Beer, T. A. P., Rempfer, C. & Bordoli, L. (2018). SWISS-MODEL: homology modelling of protein structures and complexes. *Nucleic Acids Research,* 46**,** W296-W303.

Webber, A., Ratnaweera, M., Harris, A., Luisi, B. F. & Ntsogo Enguéné, V. Y. (2022). A model for allosteric communication in drug transport by the AcrAB-TolC tripartite efflux pump. *Antibiotics,* 11**,** 1-21.

Weeks, J. W., Celaya-Kolb, T., Pecora, S. & Misra, R. (2010). AcrA suppressor alterations reverse the drug hypersensitivity phenotype of a TolC mutant by inducing TolC aperture opening. *Molecular Microbiology,* 75**,** 1468-83.

Wehmeier, C., Schuster, S., Fahnrich, E., Kern, W. V. & Bohnert, J. A. (2009). Site-directed mutagenesis reveals amino acid residues in the *Escherichia coli* RND efflux pump AcrB that confer macrolide resistance. *Antimicrobial Agents and Chemotherapy,* 53**,** 329-30.

Wetzler, L., Blake, M., Barry, K. & Gotschlich, E. (1992). Gonococcal porin vaccine evaluation: comparison of Por proteosomes, liposomes, and blebs isolated from *rmp* deletion mutants. *Journal of Infectious Diseases,* 166**,** 551-5.

WHO (2017). *WHO publishes list of bacteria for which new antibiotics are urgently needed* [Online]. Available: https://www.who.int/news-room/detail/27-02-2017-who-publishes-list-of-bacteria-for-which-new-antibiotics-are-urgently-needed [Accessed 14/06/2020].

WHO (2021). Global progress report on HIV, viral hepatitis and sexually transmitted infections, 2021: accountability for the global health sector strategies 2016–2021: actions for impact.1-108.

Wi, T., Lahra, M. M., Ndowa, F., Bala, M., Dillon, J.-A. R., Ramon-Pardo, P., Eremin, S. R., Bolan, G. & Unemo, M. (2017). Antimicrobial resistance in *Neisseria gonorrhoeae*: Global surveillance and a call for international collaborative action. *PLOS Medicine,* 14**,** e1002344.

Wiegand, I., Hilpert, K. & Hancock, R. E. (2008). Agar and broth dilution methods to determine the minimal inhibitory concentration (MIC) of antimicrobial substances. *Nature Protocols,* 3**,** 163-75.

Wilke, M. S., Heller, M., Creagh, A. L., Haynes, C. A., McIntosh, L. P., Poole, K. & Strynadka, N. C. (2008). The crystal structure of MexR from *Pseudomonas aeruginosa* in complex with its antirepressor ArmR. *Proceedings of the National Academy of Sciences,* 105**,** 14832-7.

Wilkens, S. (2015). Structure and mechanism of ABC transporters. *F1000Prime Reports* 7**,** 1-9.

Williams, E., Seib, K. L., Fairley, C. K., Pollock, G. L., Hocking, J. S., McCarthy, J. S. & Williamson, D. A. (2024). *Neisseria gonorrhoeae* vaccines: a contemporary overview. *Clinical Microbiology Reviews***,** e00094-23.

Woods, J., Dempsey, J., Kawula, T., Barritt, D. & Cannon, J. (1989). Characterization of the neisserial lipid-modified azurin bearing the H. 8 epitope. *Molecular Microbiology,* 3**,** 583-91.

Workowski, K. A., Bachmann, L. H., Chan, P. A., Johnston, C. M., Muzny, C. A., Park, I., Reno, H., Zenilman, J. M. & Bolan, G. A. (2021). Sexually transmitted infections treatment guidelines, 2021. *MMWR Recommendations and Reports,* 70**,** 1.

World Health Organisation (WHO). 2012. Global action plan to control the spread and impact of antimicrobial resistance in *Neisseria gonorrhoeae*. Geneva, Switzerland: WHO.

Wu, C., Wynne, S. A., Thomas, N. E., Uhlemann, E.-M., Tate, C. G. & Henzler-Wildman, K. A. (2019). Identification of an alternating-access dynamics mutant of EmrE with impaired transport. *Journal of Molecular Biology,* 431**,** 2777-89.

Xia, M., Whittington, W. L., Shafer, W. M. & Holmes, K. K. (2000). Gonorrhea among men who have sex with men: outbreak caused by a single genotype of erythromycin-resistant *Neisseria gonorrhoeae* with a single- base pair deletion in the *mtrR p*romoter region. *Journal of Infectious Diseases,* 181**,** 2080-2.

Xu, Y., Lee, M., Moeller, A., Song, S., Yoon, B. Y., Kim, H. M., Jun, S. Y., Lee, K. & Ha, N. C. (2011). Funnel-like hexameric assembly of the periplasmic adapter protein in the tripartite multidrug efflux pump in Gram-negative bacteria. *Journal of Biological Chemistry,* 286**,** 17910-20.

Yamaguchi, A., Nakashima, R. & Sakurai, K. (2015). Structural basis of RND-type multidrug exporters. *Frontiers in Microbiology,* 6**,** 327.

Yamamoto, K., Tamai, R., Yamazaki, M., Inaba, T., Sowa, Y. & Kawagishi, I. (2016). Substrate-dependent dynamics of the multidrug efflux transporter AcrB of *Escherichia coli*. *Scientific Reports,* 6**,** 21909.

Yamanaka, H., Kobayashi, H., Takahashi, E. & Okamoto, K. (2008). MacAB is involved in the secretion of *Escherichia coli* heat-stable enterotoxin II. *Journal of Bacteriology,* 190**,** 7693-8.

Yamane, T., Murakami, S. & Ikeguchi, M. (2013). Functional rotation induced by alternating protonation states in the multidrug transporter AcrB: all-atom molecular dynamics simulations. *Biochemistry,* 52**,** 7648-58.

Yamasaki, S., Koga, N., Zwama, M., Sakurai, K., Nakashima, R., Yamaguchi, A. & Nishino, K. (2022). Spatial characteristics of the efflux pump MexB determine inhibitor binding. *Antimicrobial Agents and Chemotherapy,* 66**,** e00672-22.

Yan, A., Guan, Z. & Raetz, C. R. (2007). An undecaprenyl phosphate-aminoarabinose flippase required for polymyxin resistance in *Escherichia coli*. *Journal of Biological Chemistry,* 282**,** 36077-89.

Yan, N. (2015). Structural biology of the major facilitator superfamily transporters. *Annual Review of Biophysics,* 44**,** 257-83.

Yang, H. B., Hou, W. T., Cheng, M. T., Jiang, Y. L., Chen, Y. & Zhou, C. Z. (2018). Structure of a MacAB-like efflux pump from *Streptococcus pneumoniae*. *Nature Communications,* 9**,** 196.

Yao, H., Shen, Z., Wang, Y., Deng, F., Liu, D., Naren, G., Dai, L., Su, C.-C., Wang, B. & Wang, S. (2016). Emergence of a potent multidrug efflux pump variant that enhances *Campylobacter* resistance to multiple antibiotics. *mBio,* 7**,** 10.1128/mbio. 01543-16.

Yao, X.-Q., Kimura, N., Murakami, S. & Takada, S. (2013). Drug uptake pathways of multidrug transporter AcrB studied by molecular simulations and site-directed mutagenesis experiments. *Journal of the American Chemical Society,* 135**,** 7474-85.

Yao, X. Q., Kenzaki, H., Murakami, S. & Takada, S. (2010). Drug export and allosteric coupling in a multidrug transporter revealed by molecular simulations. *Nature Communications,* 1**,** 117.

Yardeni, E. H., Mishra, S., Stein, R. A., Bibi, E. & Mchaourab, H. S. (2020). The multidrug transporter MdfA deviates from the canonical model of

alternating access of MFS transporters. *Journal of Molecular Biology,* 432**,** 5665-80.

Yen, M. R., Chen, J. S., Marquez, J. L., Sun, E. I. & Saier, M. H. (2010). Multidrug resistance: phylogenetic characterization of superfamilies of secondary carriers that include drug exporters. *Membrane Transporters in Drug Discovery and Development: Methods and Protocols***,** 47-64.

Yerushalmi, H., Lebendiker, M. & Schuldiner, S. (1995). EmrE, an *Escherichia coli* 12-kDa multidrug transporter, exchanges toxic cations and H^+ and is soluble in organic solvents. *Journal of Biological Chemistry,* 270**,** 6856-63.

Yerushalmi, H. & Schuldiner, S. (2000a). A common binding site for substrates and protons in EmrE, an ion-coupled multidrug transporter. *FEBS Letters,* 476**,** 93-7.

Yerushalmi, H. & Schuldiner, S. (2000b). An essential glutamyl residue in EmrE, a multidrug antiporter from *Escherichia coli*. *Journal of Biological Chemistry,* 275**,** 5264-9.

Yesylevskyy, S. O., Schäfer, L. V., Sengupta, D. & Marrink, S. J. (2010). Polarizable water model for the coarse-grained MARTINI force field. *PLoS Computational Biology,* 6.

Yin, Y., He, X., Szewczyk, P. & Chang, G. (2006). Structure of the multidrug transporter EmrD from *Escherichia coli*. *Science,* 312**,** 741-4.

Yoneyama, H., Maseda, H., Kamiguchi, H. & Nakae, T. (2000). Function of the membrane fusion protein, MexA, of the MexA, B-OprM efflux pump in *Pseudomonas aeruginosa* without an anchoring membrane. *Journal of Biological Chemistry,* 275**,** 4628-34.

Yonezawa, A. & Inui, K. i. (2011). Importance of the multidrug and toxin extrusion MATE/SLC47A family to pharmacokinetics, pharmacodynamics/toxicodynamics and pharmacogenomics. *British Journal of Pharmacology,* 164**,** 1817-25.

Yoon, E. J., Balloy, V., Fiette, L., Chignard, M., Courvalin, P. & Grillot-Courvalin, C. (2016). Contribution of the Ade resistance-nodulation-cell division-type efflux pumps to fitness and pathogenesis of *Acinetobacter baumannii*. *mBio,* 7**,** e00697-16.

Yoshida, K.-i., Nakayama, K., Ohtsuka, M., Kuru, N., Yokomizo, Y., Sakamoto, A., Takemura, M., Hoshino, K., Kanda, H. & Nitanai, H. (2007). MexAB-OprM specific efflux pump inhibitors in *Pseudomonas aeruginosa*. Part 7: highly soluble and in vivo active quaternary ammonium analogue D13-9001, a potential preclinical candidate. *Bioorganic & Medicinal Chemistry,* 15**,** 7087-97.

Yousefian, N., Ornik-Cha, A., Poussard, S., Decossas, M., Berbon, M., Daury, L., Taveau, J.-C., Dupuy, J.-W., Đorđević-Marquardt, S. & Lambert, O. (2020). Structural characterization of the EmrAB-TolC efflux complex

from *E. coli*. *Biochimica et Biophysica Acta (BBA)-Biomembranes,* 1863**,** 183488.

Yu, E. W., Aires, J. R., McDermott, G. & Nikaido, H. (2005). A periplasmic drug-binding site of the AcrB multidrug efflux pump: A crystallographic and site-directed mutagenesis study. *Journal of Bacteriology,* 187**,** 6804-15.

Yu, E. W., McDermott, G., Zgurskaya, H. I., Nikaido, H. & Koshland, D. E., Jr. (2003). Structural basis of multiple drug-binding capacity of the AcrB multidrug efflux pump. *Science,* 300**,** 976-80.

Yue, Z., Chen, W., Zgurskaya, H. I. & Shen, J. (2017). Constant pH molecular dynamics reveals how proton release drives the conformational transition of a transmembrane efflux pump. *Journal of Chemical Theory and Computation,* 13**,** 6405-14.

Zakrzewska, S., Mehdipour, A. R., Malviya, V. N., Nonaka, T., Koepke, J., Muenke, C., Hausner, W., Hummer, G., Safarian, S. & Michel, H. (2019). Inward-facing conformation of a multidrug resistance MATE family transporter. *Proceedings of the National Academy of Sciences,* 116**,** 12275-84.

Zalucki, Y. M., Dhulipala, V. & Shafer, W. M. (2012). Dueling regulatory properties of a transcriptional activator (MtrA) and repressor (MtrR) that control efflux pump gene expression in *Neisseria gonorrhoeae*. *mBio,* 3**,** e00446-12.

Zang, M., MacDermott-Opeskin, H., Adams, F. G., Naidu, V., Waters, J. K., Carey, A. B., Ashenden, A., McLean, K. T., Brazel, E. B., Jiang, J. H., Panizza, A., Trappetti, C., Paton, J. C., Peleg, A. Y., Koper, I., Paulsen, I. T., Hassan, K. A., O'Mara, M. L. & Eijkelkamp, B. A. (2021). The Membrane Composition Defines the Spatial Organization and Function of a Major Acinetobacter baumannii Drug Efflux System. *mBio,* 12**,** e0107021.

Zarantonelli, L., Borthagaray, G., Lee, E.-H. & Shafer, W. M. (1999). Decreased azithromycin susceptibility of *Neisseria gonorrhoeae* due to *mtrR* mutations. *Antimicrobial Agents and Chemotherapy,* 43**,** 2468-72.

Zarantonelli, L., Borthagaray, G., Lee, E. H., Veal, W. & Shafer, W. M. (2001). Decreased susceptibility to azithromycin and erythromycin mediated by a novel *mtr(R)* promoter mutation in *Neisseria gonorrhoeae*. *Journal of Antimicrobial Chemotherapy,* 47**,** 651-4.

Zechini, B. & Versace, I. (2009). Inhibitors of multidrug resistant efflux systems in bacteria. *Recent Patents on Anti-Infective Drug Discovery,* 4**,** 37-50.

Zgurskaya, H. I., Adamiak, J. W. & Leus, I. V. (2022). Making sense of drug-efflux transporters in the physiological environment. *Current Opinion in Microbiology,* 69**,** 102179.

Zgurskaya, H. I., Krishnamoorthy, G., Ntreh, A. & Lu, S. (2011). Mechanism and function of the outer membrane channel TolC in multidrug

resistance and physiology of enterobacteria. *Frontiers in Microbiology,* 2**,** 189.

Zgurskaya, H. I., Malloci, G., Chandar, B., Vargiu, A. V. & Ruggerone, P. (2021). Bacterial efflux transporters' polyspecificity – a gift and a curse? *Current Opinion in Microbiology,* 61**,** 115-23.

Zgurskaya, H. I. & Nikaido, H. (1999). Bypassing the periplasm: reconstitution of the AcrAB multidrug efflux pump of *Escherichia coli*. *Proceedings of the National Academy of Sciences of the United States of America,* 96**,** 7190-5.

Zgurskaya, H. I. & Nikaido, H. (2000). Cross-linked complex between oligomeric periplasmic lipoprotein AcrA and the inner-membrane-associated multidrug efflux pump AcrB from *Escherichia coli*. *Journal of Bacteriology,* 182**,** 4264-7.

Zgurskaya, H. I. & Rybenkov, V. V. (2020). Permeability barriers of Gram-negative pathogens. *Annals of the New York Academy of Sciences,* 1459**,** 5-18.

Zgurskaya, H. I., Weeks, J. W., Ntreh, A. T., Nickels, L. M. & Wolloscheck, D. (2015). Mechanism of coupling drug transport reactions located in two different membranes. *Frontiers in Microbiology,* 6**,** 100.

Zgurskaya, H. I., Yamada, Y., Tikhonova, E. B., Ge, Q. & Krishnamoorthy, G. (2009). Structural and functional diversity of bacterial membrane fusion proteins. *Biochimica et Biophysica Acta,* 1794**,** 794-807.

Zhang, B., Li, J., Yang, X., Wu, L., Zhang, J., Yang, Y., Zhao, Y., Zhang, L., Yang, X., Yang, X., Cheng, X., Liu, Z., Jiang, B., Jiang, H., Guddat, L. W., Yang, H. & Rao, Z. (2019). Crystal structures of membrane transporter MmpL3, an anti-TB drug target. *Cell,* 176**,** 636-48 e13.

Zhang, G., Meredith, T. C. & Kahne, D. (2013). On the essentiality of lipopolysaccharide to Gram-negative bacteria. *Current Opinion in Microbiology,* 16**,** 779-85.

Zhang, H., Zhu, H., Pan, Y., Yu, Y., Luan, S. & Li, L. (2014). A DTX/MATE-type transporter facilitates abscisic acid efflux and modulates ABA sensitivity and drought tolerance in *Arabidopsis*. *Molecular plant,* 7**,** 1522-32.

Zhang, X. C., Liu, M. & Han, L. (2017). Energy coupling mechanisms of AcrB-like RND transporters. *Biophysics Reports,* 3**,** 73-84.

Zhang, Y., Rosado-Lugo, J. D., Datta, P., Sun, Y., Cao, Y., Banerjee, A., Yuan, Y. & Parhi, A. K. (2022). Evaluation of a conformationally constrained indole carboxamide as a potential efflux pump inhibitor in *Pseudomonas aeruginosa*. *Antibiotics,* 11**,** 716. https://doi.org/10.3390/antibiotics11060716.

Zhang, Z., Lizer, N., Wu, Z., Morgan, C. E., Yan, Y., Zhang, Q. & Yu, E. W. (2023a). Cryo-electron microscopy structures of a *Campylobacter*

multidrug efflux pump reveal a novel mechanism of drug recognition and resistance. *Microbiology Spectrum,* 11**,** e01197-23.

Zhang, Z., Ma, C., Pornillos, O., Xiu, X., Chang, G. & Saier, M. H., Jr. (2007). Functional characterization of the heterooligomeric EbrAB multidrug efflux transporter of *Bacillus subtilis*. *Biochemistry,* 46**,** 5218-25.

Zhang, Z., Morgan, C. E., Bonomo, R. A. & Yu, E. W. (2021). Cryo-EM determination of eravacycline-bound structures of the ribosome and the multidrug efflux pump AdeJ of *Acinetobacter baumannii*. *mBio,* 12**,** 10.1128/mbio. 01031-21.

Zhang, Z., Morgan, C. E., Bonomo, R. A. & Yu, E. W. (2023b). Cryo-EM structures of the *Klebsiella pneumoniae* AcrB multidrug efflux pump. *mBio***,** e00659-23.

Zhang, Z., Morgan, C. E., Cui, M. & Yu, E. W. (2023c). Cryo-EM structures of AcrD illuminate a mechanism for capturing aminoglycosides from its central cavity. *mBio,* 14**,** e03383-22.

Zhang, Z., Schwartz, S., Wagner, L. & Miller, W. (2000). A greedy algorithm for aligning DNA sequences. *Journal of Computational Biology,* 7**,** 203-14.

Zhu, Y.-G., Zhao, Y., Li, B., Huang, C.-L., Zhang, S.-Y., Yu, S., Chen, Y.-S., Zhang, T., Gillings, M. R. & Su, J.-Q. (2017). Continental-scale pollution of estuaries with antibiotic resistance genes. *Nature Microbiology,* 2**,** 1-7.

Zhu, Y., He, L., Liu, Y., Zhao, Y. & Zhang, X. C. (2019). smFRET probing reveals substrate-dependent conformational dynamics of *E. coli* multidrug MdfA. *Biophysical Journal,* 116**,** 2296-303.

Zomot, E., Yardeni, E. H., Vargiu, A. V., Tam, H.-K., Malloci, G., Ramaswamy, V. K., Perach, M., Ruggerone, P., Pos, K. M. & Bibi, E. (2018). A new critical conformational determinant of multidrug efflux by an MFS transporter. *Journal of Molecular Biology,* 430**,** 1368-85.

Zuo, Z., Wang, B., Weng, J. & Wang, W. (2015). Stepwise substrate translocation mechanism revealed by free energy calculations of doxorubicin in the multidrug transporter AcrB. *Scientific Reports,* 5**,** 13905.

Zwama, M. & Nishino, K. (2021). Ever-adapting RND efflux pumps in Gram-negative multidrug-resistant pathogens: A race against time. *Antibiotics (Basel),* 10.

Zwama, M. & Nishino, K. (2022). Proximal binding pocket Arg717 substitutions in *Escherichia coli* AcrB cause clinically relevant divergencies in resistance profiles. *Antimicrobial Agents and Chemotherapy,* 66**,** e02392-21.

Zwama, M. & Yamaguchi, A. (2018). Molecular mechanisms of AcrB-mediated multidrug export. *Research in Microbiology,* 169**,** 372-83.

Zwama, M., Yamasaki, S., Nakashima, R., Sakurai, K., Nishino, K. & Yamaguchi, A. (2018). Multiple entry pathways within the efflux transporter AcrB contribute to multidrug recognition. *Nature Communications,* 9**,** 124.